

# UNIVERSITY LILLE 1 - SCIENCES AND TECHNOLOGIES

Doctoral School: SCIENCES DE LA MATIÈRE, DU RAYONNEMENT ET DE L'ENVIRONNEMENT

## PhD Thesis

For the degree of Doctor of the University Lille 1 Sciences and Technologies

Speciality: **Molécules et Matière Condensée**

Presented and defended by

**Romain GUITARD**

### **Oxidation of omega-3 oils and preservation by natural phenolic antioxidants**

PhD Thesis under the supervision of:

Pr. Jean-Marie AUBRY and Pr. Véronique NARDELLO-RATAJ

Defense on **October 28<sup>th</sup> 2016**

#### Members of the jury:

<i>Reviewers</i>	Pr. Olivier DANGLES Pr. Véronique CHEYNIER	University of Avignon INRA Montpellier
<i>Supervisors</i>	Pr. Jean-Marie AUBRY Pr. Véronique NARDELLO-RATAJ	ENSCL University of Lille 1
<i>Examiners</i>	Dr. Andreas MENZEL Dr. Emmanuelle VULLIET	CARGILL company CNRS, University of Lyon



# ACKNOWLEDGEMENTS

---

The work described in this PhD thesis has been fulfilled in the CISCO research group which is part of the UCCS lab at the University of Lille 1, Sciences and Technologies under the supervision of Prof. Jean-Marie Aubry and Prof. Véronique Nardello-Rataj. Additionally, this PhD thesis was part of an industrial project financed by the CARGILL company under the direction of Dr. Andreas Menzel and Dr. Erik Hagestuen. I would like to express my honest thanks to them for having welcomed me in their laboratories and teams, and for having given me the opportunity to work on this interesting project.

First and foremost, I would like to express my most sincere gratitude to my supervisors, Prof. Jean-Marie Aubry and Prof. Véronique Nardello-Rataj, who supervised my thesis during the last three years. Thank you for guiding my work in an ambitious way and having faith in my work and decisions. Especially the helpful improvements during the creation of the manuscript were well appreciated. I would like to thank deeply my industrial supervisors Dr. Andreas Menzel and Dr. Erik Hagestuen for their scientific advices, helpful discussions and your welcome in the USA.

I am grateful to the jury members, the reviewers Prof. Oliver Dangles and Prof. Véronique Cheynier, and the examiners Dr. Andreas Menzel and Dr. Emmanuelle Vulliet, for having accepted to take their time and to bring their experience to evaluate this manuscript.

I would like to express my sincere gratitude to Dr. Emmanuelle Vulliet for her welcome in the research team TRACES of ISA. I also convey my special acknowledge to Barbara Giroud and Audrey Buleté for skillfully training myself to the UPLC-MS/MS apparatus. My appreciation is extended to people from Cargill: Gregg Perri for his invaluable assistance for the Rancimat analyses and Brian Gutrie for our inspiring discussions.

My special thanks go to Dr. Raphaël Lebeuf for his expertise in the synthesis of new antioxidants, Prof. Jean-François Paul and Dr. Loïc Leclercq for their advice on molecular modeling and Dr. Christel Pierlot for sharing his time during the transfer of scientific knowledge to students.

I would like to express my sincere gratitude to my colleagues and friends of the lab for sharing this special atmosphere and their extraordinary support. I will always remember Laura Dubrulle as my PetroOxy lover, Maxime Royer as my Clash of Clans collaborator, Maxime Nollet as my favorite yellow M&M's, Valentin Goussard and his special laugh, Benjamin Pacaud and his famous "Pacaunade", Florian Laubé and his large pliers, Estelle Illous as the best Pokemon trainer, Benjamin Joossen and his enormous jokes, Mike Ortega Vaz and his football debriefings, Corentine Mainguy and her delicious traditional "galettes bretonnes", Bingyu Yang and her Chinese professionalism, Andrea Mühlbauer and her German strictness, Thomas Lukowicz and the poor nationalmannschaft, Jesus Fermin Ontiveros and Roberto Company for our Spanish conversations, Delphine Blondé with her "foof-mobile", Bing Hong for his special Chinese food, Adrien Benazzouz and his unbelievable anecdotes, Laurianne Moity with her celebrity gossips, and all the student apprentices present in the lab during the last three years. Moreover, I would like to thank Maeva, Antoine, Loïc, Barbara, Aurélie, Camille, Alexandre, Martin, Alexandra and Audrey for all the great times spent in Lyon. It is truly my honor to corporate and share the joy with them.

Finally, I would like to express my deepest thanks to my family, especially my mother, father and sister and to my family-in-law for their inestimable support. And very special thanks go to Laure, thank you infinitely for everything, especially for giving me strength and incredible encouragement in hard times.

# ABSTRACT

---

Omega-3 has been known as essential fatty acids to health since the 30s but related studies have been multiplied at an accelerated rate only since the 80s. They are particularly sensitive to oxygen because of their numerous bis-allylic hydrogens. This oxidative degradation leads to a deterioration of their organoleptic and nutraceutical properties. Protecting omega-3 oils against oxidation is then crucial and requires the addition of highly effective antioxidants but safe for consumers.

As regards to the complex mechanism occurring in the degradation of polyunsaturated fatty acids (PUFAs), it is a relevant challenge to detect and identify traces of oxidation products in oxidized oils. For this purpose, electrospray ionization mass spectrometry (ESI-MS) appears as the most suitable technique. By screening a series of cations, we could show that  $\text{Cs}^+$  allows a remarkable selective and sensitive ionization of intact hydroperoxides which are the primary oxidation products formed in the oxidation process. A specific detection into a fatty acid methyl ester (FAME) matrix discriminating hydroperoxides at the nanomole level was possible. Separation and chemical structure identification of mixture of hydroperoxides could be obtained by liquid chromatography coupled to tandem mass spectrometry LC-MS/MS.

In order to prevent oxidative degradation, antioxidants are commonly introduced into foods. Synthetic phenolic antioxidants such as butylated hydroxytoluene (BHT) and butylated hydroxyanisole (BHA) are widely used but, due to an increased safety concern from the consumer side, there is a strong push to replace them by natural alternatives. In this context, we focused on natural phenolic antioxidants. In a first time, quantum chemical calculation was used to determine the Bond Dissociation Enthalpies (BDEs) of 70 phenolic antioxidants providing a scale of predictive activity. From a mechanism viewpoint, the radical hydrogen atom transfer (HAT) mechanism implies the hydrogen transfer from phenols to peroxy radicals  $\text{ROO}^\bullet$ . It is shown that the corresponding kinetic rate constants ( $k$ ) are strongly correlated to the BDEs. The autoxidation of omega-3 FAMES in the presence of the phenols was also kinetically investigated. The efficiency of phenolic antioxidants can be predicted with thermodynamic, kinetic and stoichiometric parameters highlighting the structural requirements for obtaining effective antioxidants.

Synergistic and antagonistic effects of mixtures of antioxidants, which are often observed but rarely understood, were also investigated since they can allow a better inhibition of the oxidative degradation. BDEs and the relative concentrations of the primary antioxidant (*i.e.*  $\alpha$ -tocopherol) and co-antioxidant are the key parameters responsible for synergistic effects. The mechanisms of synergy involve the transfer of hydrogen atoms  $\text{H}^\bullet$  from the co-antioxidants and then from their radicals and dimers to the primary phenoxy radical (*i.e.* the tocopheroxy radical) leading to the regeneration of the antioxidant. On the contrary, some co-antioxidants give radicals which are able to degrade the primary antioxidant explaining the antagonist effect. Finally, polar environments suppress the regeneration of some primary antioxidants and impede synergies.

**Keywords:** Omega-3, Mass spectrometry, Hydroperoxide, Phenolic antioxidant, BDE,  $\text{DPPH}^\bullet$ , Autoxidation, Synergy

# RÉSUMÉ

---

Les oméga-3 sont reconnus comme étant des acides gras essentiels pour la santé depuis les années 30 et les recherches se sont intensifiées depuis 1980. Les oméga-3 sont particulièrement sensibles à l'oxygène en raison de leurs nombreux atomes d'hydrogène allyliques. Cette dégradation oxydante mène à une détérioration de leurs propriétés organoleptique et nutraceutique. Il est donc crucial de les protéger contre l'oxydation par l'ajout d'antioxydants très efficaces, mais sans danger pour les consommateurs.

Au vu des mécanismes complexes se produisant lors de la dégradation d'acides gras polyinsaturés (AGPI), c'est un véritable challenge de détecter et identifier des traces de produits oxydés dans les huiles. Pour cela, la spectrométrie de masse couplée à une ionisation par électronébulisation (ESI-MS) apparaît être la technique la plus appropriée. Grâce au criblage d'une série de cations, nous avons montré que  $\text{Cs}^+$  permet une remarquable ionisation sélective et sensible d'hydroperoxydes intacts identifiés comme étant les produits d'oxydation primaires. Une détection spécifique au sein d'une matrice d'ester méthylique d'acide gras discriminant les hydroperoxydes au niveau nanomolaire a été possible. La séparation et l'identification des structures chimiques d'un mélange complexe d'hydroperoxydes peuvent être effectuées par chromatographie liquide couplée à la spectrométrie de masse tandem (LC-MS/MS).

Afin de retarder l'oxydation, des antioxydants sont couramment introduits dans les aliments. Les antioxydants phénoliques synthétiques, tels que l'hydroxytoluène butylé (BHT) et l'hydroxyanisole butylé (BHA), sont largement utilisés mais suscitent la méfiance des consommateurs. La tendance actuelle est donc de les remplacer par des composés naturels. Dans ce contexte, nous nous sommes concentrés sur les antioxydants phénoliques naturels. Tout d'abord, une échelle de réactivité prédictive basée sur le calcul d'énergie de dissociation (BDE) des liaisons phénoliques a été établie pour 70 antioxydants par modélisation moléculaire. Concernant la réactivité, le mécanisme radicalaire (HAT) implique le transfert d'atomes d'hydrogène des phénols aux radicaux peroxydes  $\text{ROO}^\bullet$ . Il a été montré que les constantes cinétiques correspondantes ( $k$ ) sont fortement corrélées aux BDEs des liaisons phénoliques. Les cinétiques d'autoxydation des oméga-3 en présence de phénols ont également été étudiées. L'efficacité des antioxydants phénoliques peut être prédite par les paramètres thermodynamiques, cinétiques et stœchiométriques mettant en évidence les structures chimiques des phénols performants.

Les effets synergiques et antagonistes des mélanges d'antioxydants, souvent observés mais rarement compris, ont également été étudiés car ils peuvent permettre une meilleure inhibition de l'oxydation. De cette façon, les BDEs des liaisons phénoliques et les concentrations relatives en antioxydant primaire (*i.e.*  $\alpha$ -tocophérol) et co-antioxydant sont démontrées comme étant les principaux paramètres gouvernant les effets synergiques. Les mécanismes de synergie impliquent le transfert d'hydrogène  $\text{H}^\bullet$  des co-antioxydants puis de leurs radicaux et dimères aux radicaux phénoxydes primaires (*i.e.* le radical tocophéroxyde) conduisant à la régénération de l'antioxydant. Au contraire, certains co-antioxydants forment des radicaux capables de dégrader l'antioxydant primaire expliquant l'effet antagoniste. Les environnements polaires suppriment la régénération de certains antioxydants primaires et empêchent ainsi les synergies.

**Mots-clés :** Oméga-3, Spectrométrie de masse, Hydroperoxyde, Antioxydant phénolique, BDE, DPPH $^\bullet$ , Autoxydation, Synergie

# TABLE OF CONTENTS

---

Acknowledgements.....	iii
Abstract.....	iv
Résumé.....	v
Table of Contents.....	vi
List of Abbreviations and Symbols.....	ix
General Introduction.....	1
<b>Chapter 1. Peroxidation of (Poly)unsaturated Fatty Acids and Analyzes of Oxidized Lipids: A Literature Survey.....</b>	<b>9</b>
1. Introduction.....	10
2. Autoxidation and photooxidation of unsaturated fatty acids.....	11
2.1 Autoxidation of unsaturated fatty acids by ground state oxygen $^3\text{O}_2$ .....	12
2.1.1 General mechanism of autoxidation.....	12
2.1.2 Autoxidation of unsaturated fatty acids by ground state oxygen.....	15
2.2 Photosensitized oxidation of unsaturated fatty acids by singlet oxygen $^1\text{O}_2$ .....	18
2.2.1 Formation and reactivity of singlet oxygen $^1\text{O}_2$ .....	18
2.2.2 Photooxidation of (poly)unsaturated fatty acids by singlet oxygen.....	22
2.3 Degradation of fatty acid peroxides.....	27
2.3.1 Initiation of $\text{LOO}^\bullet$ and $\text{LO}^\bullet$ radicals.....	27
2.3.2 Propagation of peroxy ( $\text{LOO}^\bullet$ ) and alkoxy ( $\text{LO}^\bullet$ ) radicals.....	27
2.4 Factors affecting the oxidation of oils.....	31
3. Separation and analyzes of fatty acids and oxidized lipids.....	33
3.1 Separation and analyzes of non-oxidized lipids.....	33
3.1.1 Nuclear Magnetic Resonance (NMR).....	33
3.1.2 Gas Chromatography (GC).....	33
3.1.3 High Performance Liquid Chromatography (HPLC).....	34
3.2 Separation and analysis of lipid oxidation products.....	38
3.2.1 TBARS, FOX and Iodometric assays.....	38
3.2.2 Fourier Transform Infrared Spectroscopy (FTIR).....	39
3.2.3 Nuclear Magnetic Resonance (NMR).....	39
3.2.4 Gas Chromatography (GC).....	39
3.2.5 High Performance Liquid Chromatography (HPLC).....	40
4. Conclusion.....	45
<b>Chapter 2. Preparation of Hydroperoxides by Singlet Oxygenation and Mass Spectrometry Investigations.....</b>	<b>47</b>
1. Introduction.....	48
2. Preparation of lipids and terpenes hydroperoxides by singlet oxygenation.....	48
2.1 Choice of the investigated lipids and terpenes, the singlet oxygenation process and the analytical techniques.....	48
2.2 Singlet oxygenation of terpenoids.....	51
2.2.1 LC-UV analyses of hydroperoxides and their structural identification by NMR.....	51
2.2.2 Analysis of hydroperoxides by $^1\text{H}$ and $^{13}\text{C}$ NMR.....	53

2.3	Lipid hydroperoxides from singlet oxygenation.....	57
2.4	Kinetic approaches and singlet oxygen quenching activity.....	61
2.5	Conclusion .....	65
3.	Mass spectrometry investigations of (poly)unsaturated terpenes, FAMES, hydroperoxides and peroxide compounds.....	66
3.1	Influence of various ions on the detection of FAMES and hydroperoxides by MS .....	66
3.1.1	Direct Liquid Injection Mass Spectrometry (DLI-MS) analysis of FAMES .....	67
3.1.2	Direct Liquid Injection Mass Spectrometry (DLI-MS) analysis of hydroperoxides ....	69
3.1.3	Competition between FAMES and hydroperoxide ionizations .....	69
3.2	Selective detection of hydroperoxides and peroxides with Cs <sup>+</sup> by ElectroSpray Ionization Mass Spectrometry (ESI-MS).....	73
3.3	Liquid chromatography - ElectroSpray Ionization and Coordination IonSpray Mass Spectrometry (LC-MS and LC-MS/MS) .....	80
3.3.1	Terpenoids and related hydroperoxides .....	81
3.3.2	FAMES of linseed oil and peroxides.....	85
3.4	Formation of peroxyhemiacetals during the oxidation of edible oils .....	95
3.5	Conclusion .....	98
<b>Chapter 2. Experimental Part.....</b>		<b>99</b>
<b>Chapter 3. Preservation of Omega-3 oils by Natural Phenolic Antioxidants: Thermodynamic, Kinetic and Oxidative Investigations.....</b>		<b>127</b>
1.	Introduction.....	128
2.	Literature survey on the measuring of the antioxidant power.....	129
2.1	Measurement of substrate consumption or formation of oxidation products .....	129
2.1.1	Inhibited Oxygen Uptake method (IOU).....	129
2.1.2	Quantification of oxidized products by UV spectrometry.....	130
2.1.3	Headspace of hexanal and oxidized products in biological systems.....	131
2.1.4	Measuring of hydroperoxides during the oxidation of lipids.....	131
2.2	Experimental methods for the detection of free radicals.....	131
2.2.1	Electron Paramagnetic Resonance spectroscopy (EPR) .....	131
2.2.2	2,2-Diphenyl-1-picrylhydrazil radical (DPPH <sup>*</sup> ) scavenging test .....	132
2.3	Selected tests to determine the antioxidant power of phenols .....	132
3.	Thermodynamic properties of phenolic antioxidants.....	133
3.1	Definition of BDE, IP and pK <sub>a</sub> parameters.....	133
3.2	Determination of the antioxidant power with BDE calculation .....	135
3.2.1	Substituent effects on BDEs .....	135
3.2.2	Determination of BDEs for phenolic antioxidants: scale of reactivity .....	140
3.2.3	Solvent effects on BDEs.....	154
3.2.4	Ionization Potential (IP) and stability of phenols .....	158
3.2.5	pK <sub>a</sub> and acidity of phenols .....	161
3.3	Conclusion .....	163
4.	Experimental determinations of the efficiency of phenolic antioxidants.....	164
4.1	Selection of phenolic antioxidant studied.....	164
4.2	DPPH <sup>*</sup> or 2,2-diphenyl-1-picrylhydrazil radical test .....	165
4.2.1	Principles .....	165
4.2.2	Kinetic rate constants of hydrogen transfer in apolar aprotic solvent: scale of reactivity of phenolic antioxidants.....	170
4.2.3	Kinetic Solvent Effects (KSEs) on the reactivity of phenolic antioxidants .....	172

4.2.4	Stoichiometric number $\sigma_{\text{exp}}$ of phenolic antioxidants .....	176
4.2.5	Conclusion .....	187
4.3	Antioxidant activity of phenolic compounds against the oxidation of omega-3 oils .....	187
4.3.1	RapidOxy® analyses .....	188
4.3.2	Rancimat experiments.....	197
4.3.3	Conclusion .....	200
5.	Conclusions.....	200
<b>Chapter 3. Experimental Part .....</b>		<b>203</b>
<b>Chapter 4. Synergy Between Phenolic Antioxidants For Food Applications.....</b>		<b>227</b>
1.	Introduction.....	228
2.	Literature survey .....	229
2.1	Regeneration of the primary antioxidant by the co-antioxidant(s) .....	231
2.2	Kinetic approaches .....	235
2.3	Conclusion .....	237
3.	Synergy between $\alpha$ -tocopherol and co-antioxidants as well as other phenolic mixtures for the preservation of omega-3 oils .....	237
3.1	Methods and approaches to study synergies between antioxidants .....	238
3.1.1	Initial reaction rates of mixtures ( $V_{i \text{ Mix}}$ ) .....	239
3.1.2	Stoichiometric numbers ( $\sigma_{\text{Mix}}$ ) .....	240
3.2	Synergistic behaviors in apolar aprotic solvents .....	241
3.2.1	Reaction of $\alpha$ -tocopherol .....	242
3.2.2	Synergism with reactive monophenols and catechol derivatives .....	244
3.2.3	Super synergism with ascorbic and carnosic acids, hydroquinone and pyrogallol derivatives .....	251
3.2.4	Additivity with poorly reactive monophenols.....	254
3.3	Kinetic Solvent Effects (KSEs) on synergism .....	254
3.3.1	Hydrogen Bond Acceptor (HBA) solvents.....	254
3.3.2	Preservation of omega-3 oils against oxidation by mixture of phenols.....	258
3.3.3	Influence of polar protic medium.....	262
4.	Conclusion .....	266
<b>Chapter 4. Experimental Part .....</b>		<b>269</b>
<b>General Conclusions and Prospects .....</b>		<b>283</b>
<b>References .....</b>		<b>295</b>

# LIST OF ABBREVIATIONS AND SYMBOLS

---

## Fatty acids

<b>ALA</b>	Alpha-linolenic acid
<b>DHA</b>	Docosahexaenoic acid
<b>EPA</b>	Eicosapentaenoic Acid
<b>FAME</b>	Fatty Acid Methyl Ester
<b>LA</b>	Linoleic Acid
<b>MUFAs</b>	Monounsaturated Fatty Acids
<b>n-3, <math>\omega</math>-3</b>	Omega-3
<b>n-6, <math>\omega</math>-6</b>	Omega-6
<b>n-9, <math>\omega</math>-9</b>	Omega-9
<b>PUFAs</b>	Polyunsaturated Fatty Acids

## Analytical techniques

<b>APCI-MS</b>	Atmospheric Pressure Chemical Ionization - Mass Spectrometry
<b>APT</b>	Attached-Proton Test
<b>CID</b>	Collision-Induced Dissociation
<b>CIS-MS</b>	Coordination IonSpray - Mass Spectrometry
<b>CL</b>	ChemiLuminescence
<b>Cps</b>	Coups
<b>DPPH<sup>•</sup> test</b>	2,2-diphenyl-1-picrylhydrazyl radical test
<b>DLI</b>	Direct Liquid Injection
<b>EPR</b>	Electron Paramagnetic Resonance
<b>ESI-MS</b>	ElectroSpray Ionization - Mass Spectrometry
<b>ESP</b>	Electron Spin Resonance
<b>FOX</b>	Ferrous Oxidation of Xylenol
<b>FTIR</b>	Fourier Transform Infrared Spectroscopy
<b>GC-FID</b>	Gas Chromatography - Flame Ionization Detector
<b>GC-MS</b>	Gas Chromatography - Mass Spectrometry
<b>HPLC</b>	High Performance Liquid Chromatography
<b>IOU</b>	Inhibited Oxygen Uptake
<b>LC-MS</b>	Liquid Chromatography - Mass Spectrometry
<b>LC-MS/MS</b>	Liquid chromatography coupled to tandem mass spectrometry
<b>MALDI-TOF</b>	Matrix Assisted Laser Desorption Ionization - Time-Of-Flight
<b>MRM</b>	Multiple Reaction Monitoring
<b>NMR</b>	Nuclear Magnetic Resonance
<b>ReqEPR</b>	Radical Equilibrium Electron Paramagnetic Resonance
<b>pCEC</b>	Pressure-assisted Capillary ElectroChromatography
<b>SIR</b>	Single Ion Recorded
<b>TBARS</b>	Thiobarbituric Acid Reactive Substances
<b>TLC</b>	Thin Layer Chromatography
<b>UPLC</b>	Ultra Performance Liquid Chromatography

## Molecular modeling

<b>B3LYP</b>	Becke, Lee-Yang-Parr
<b>BDE</b>	Bond Dissociation Enthalpy
<b>DFT</b>	Density functional Theory
<b>IP</b>	Ionization Potential
<b>MM</b>	Molecular Mechanisms
<b>UFF</b>	Universal Force Field
<b>ZPE</b>	Zero Point Energy

### Antioxidants, co-antioxidants and related radicals

<b>BHA</b>	Butylated hydroxyanisole
<b>BHT</b>	Butylated hydroxytoluene
<b>EC</b>	Epicatechin
<b>ECG</b>	Epicatechin gallate
<b>EGC</b>	Epigallocatechin
<b>EGCG</b>	Epigallocatechin gallate
<b>GTO</b>	Green tea polyphenols
<b>NDGA</b>	Nordihydroguaiaretic acid
<b>PG</b>	Propyl gallate
<b>PY</b>	Pyrogallol
<b>TBHQ</b>	Tert-butylhydroquinone
<b>TOH</b>	$\alpha$ -tocopherol
<b>VC</b>	Vitamin C
<b>ArOH</b>	Phenol
<b>AH<sub>2</sub></b>	Antioxidant
<b>AH<sup>•</sup></b>	Phenoxy radical of the antioxidant, tocopheroxyl radical
<b>A<sup>•</sup></b>	Final oxidation product of the antioxidant
<b>CoAH<sub>2</sub></b>	Co-antioxidant
<b>CoAH<sup>•</sup></b>	Phenoxy radical of the co-antioxidant
<b>QH<sub>2</sub></b>	Hydroquinone
<b>QH<sup>•</sup></b>	semiquinone radical of the hydroquinone
<b>Q</b>	Quinone

### Kinetic rate constants

<b><i>k</i><sub>Antiox</sub></b>	Kinetic rate constants of inhibition by the antioxidant
<b><i>k'</i><sub>Antiox</sub></b>	Kinetic rate constants of inhibition by the antioxidant radical
<b><i>k</i><sub>CoAntiox</sub></b>	Kinetic rate constants of inhibition by the co-antioxidants
<b><i>k'</i><sub>Coantiox</sub></b>	Kinetic rate constants of inhibition by the co-antioxidant radical
<b><i>k</i><sub>Dism</sub></b>	Kinetic rate constants of dismutation
<b><i>k</i><sub>Dimer</sub></b>	Kinetic rate constants of dimerization
<b><i>k</i><sub>Decomp</sub></b>	Kinetic rate constants of decomposition
<b><i>k</i><sub>Mix</sub></b>	Kinetic rate constants of mixture of phenols
<b><i>k</i><sub>Syn</sub></b>	Kinetic rate constants of synergy
<b><i>k</i><sub>p</sub></b>	Kinetic rate constant of the propagation stage
<b><i>k</i><sub>inh</sub></b>	Kinetic rate constant of the inhibition stage
<b><i>K</i><sub>r</sub></b>	Equilibrium constant of hydrogen transfer between antioxidant and co-antioxidant
<b><i>k</i><sub>d</sub></b>	Kinetic rate constant of the radiative deactivation of <sup>1</sup> O <sub>2</sub> with the solvent
<b><i>k</i><sub>r</sub></b>	Kinetic rate constant of the chemical reaction of <sup>1</sup> O <sub>2</sub> with a substrate
<b><i>k</i><sub>q</sub></b>	Kinetic rate constant of the physical non-radiative deactivation of <sup>1</sup> O <sub>2</sub>

### Autoxidation, photooxidation and oxidized species

<b><sup>1</sup>O<sub>2</sub></b>	Singlet oxygen
<b><sup>3</sup>O<sub>2</sub></b>	Ground state oxygen
<b><math>\beta</math></b>	Foot reactivity index
<b>O<sub>2</sub><sup>•-</sup></b>	Superoxide anion
<b>S</b>	Sensitizer
<b>ROS</b>	Reactive Oxygen Species
<b>LH</b>	Unsaturated lipid
<b>L<sup>•</sup></b>	Alkyl radical
<b>LO<sup>•</sup></b>	Alcoxyl radical
<b>LOO<sup>•</sup>, ROO<sup>•</sup></b>	Peroxyl radical
<b>LOOH, R(OO)<sub>1</sub></b>	Hydroperoxide
<b>R(OO)<sub>2</sub></b>	Dihydroperoxide, di-peroxide
<b>R(OO)<sub>3</sub></b>	Tri-peroxide

## Solvents

<b>ACN, CH<sub>3</sub>CN</b>	Acetonitrile
<b>C<sub>6</sub>H<sub>6</sub></b>	Benzene
<b>CD<sub>3</sub>CN</b>	Deuterated acetonitrile
<b>CD<sub>3</sub>COCD<sub>3</sub></b>	Deuterated acetone
<b>CH<sub>2</sub>Cl<sub>2</sub></b>	Dichloromethane
<b>CH<sub>3</sub>COCH<sub>3</sub></b>	Acetone
<b>CH<sub>3</sub>OH</b>	Methanol
<b>D<sub>2</sub>O</b>	Deuterated water
<b>EtOAc</b>	Ethyl acetate
<b>EtOH</b>	Ethanol
<b>H<sub>2</sub>O</b>	Water

## Other compounds and parameters

<b>AAPH</b>	2,2'-azobis(2-amidinopropane)dihydrochloride
<b>AIBN</b>	Azobisisobutyronitrile
<b>EDG</b>	Electron-Donating Group
<b>EDTA</b>	Ethylenediaminetetraacetic acid
<b>EWG</b>	Electron-Withdrawing Group
<b>FOK</b>	pseudo-First Order Kinetic
<b>HAT</b>	Hydrogen Atom Transfer
<b>HBA</b>	Hydrogen Bond Acceptor
<b>KSE</b>	Kinetic Solvent Effect
<b>LDL</b>	Low Density Lipoprotein
<b>MDA</b>	Malondialdehyde
<b>MPTZ</b>	1,9-dimethylphenothiazine
<b>SET-PT</b>	Sequential Electron Transfer – Proton Transfer
<b>SPLET</b>	Sequential Proton Loss Electron Transfer
<b>SOK</b>	Second Order Kinetic
<b>α</b>	Regeneration coefficient
<b>β</b>	Abraham's parameter
<b>ε</b>	Dielectric constant
<b>E°</b>	Reduction potential
<b>σ<sub>exp</sub></b>	Stoichiometric number
<b>σ<sub>Mix</sub></b>	Stoichiometric number of mixture of phenols
<b>τ, IP</b>	Induction period
<b>R<sub>ox</sub></b>	Oxidation rate
<b>OSI</b>	Oxidation Stability Index



# GENERAL INTRODUCTION

---

Omega-3 fatty acids capture the attention of scientists and studies have been multiplied in recent decades, highlighting their virtues and indispensable role to the body. In this introduction, we shall briefly mention the discovery of omega-3 and their biological properties. Then, we shall raise the oxidative degradation of omega-3 issue, which is a crucial problem in food and biological fields. Finally, the major challenges of this project will be highlighted as well as the strategy developed during the thesis.

- *Omega-3 as essential fatty acids*

By the early 1800s<sup>1</sup>, researches conducted by a French scientist, Michel-Eugène Chevreul, concluded that some fats are essential for the proper functioning of the body. This important observation is the premise of the future discoveries about omega-3. In 1923, US scientists Burr and Evans identified these fats as polyunsaturated fatty acids (PUFAs) and named these molecules Vitamin F because they are essential substances.<sup>2</sup> In 1930, Burr distinguished two families of essential fatty acids: omega-3 from  $\alpha$ -linolenic acid and omega-6 from linoleic acid. These fatty acids have both the prefix “lin” because they were extracted from the linseed.<sup>3</sup> Since this classification, researchers were more and more interested in these fatty acids and discoveries were multiplying.

The British physiologist Hugh Sinclair, noticed that Eskimos population has the highest consumption of fats rich in essential fatty acids, a weak cholesterol level and no Western infectious disease.<sup>4</sup> The first link between cardiovascular disease and omega-3 was established in 1970 by Dr. Jorn Dyeberg, a Danish epidemiologist.<sup>5</sup> Moreover, the Danish doctor Bernhard Lauritz Frederik Bang highlighted that the rapid decrease of heart disease and mortality percentage in Norway were linked to dietary changes (more fish, less meat).<sup>6</sup> Also in the 70s, a study conducted by Professor Ancel Keys reveal the benefits of the famous Cretan diet rich in omega-3.<sup>7</sup> Other data suggest that Japanese longevity is also due to their high fish consumption.<sup>8</sup> The explanation of the link between deficiency in essential fatty acids and symptoms of this deficit were highlighted firstly by Bergstrom<sup>9</sup>, Samuelsson<sup>10</sup> and Vane<sup>11</sup> (**Fig. I.1**).



**Figure I.1: Bergstrom, Samuelsson and Vane received the Nobel Prize in Physiology or Medicine 1982 for their discoveries concerning prostaglandins and related biologically active substances<sup>12</sup>**

They observed that omega-3 and omega-6 fatty acids are converted in the body into many important physiological molecules such as prostaglandins which act at the cell level. Called “cell mediators”, prostaglandins regulate all sorts of effects (*i.e.* immunity or inflammation) and allow interaction between our cells. The Nobel Prize in Physiology or Medicine 1982 was awarded jointly to these 3 scientists for their discoveries concerning prostaglandins and related biologically active substances.

In the 90s, several studies confirmed all the observations and hypothesis made by these researchers. Indeed, when omega-3 diets are prescribed, the rate of heart attacks and cardiovascular deaths decrease significantly. The “Lyon” study, led by Dr. Michel de Lorgeril<sup>13</sup>, was one of the most convincing demonstrations.<sup>14</sup> Nevertheless, omega-3 virtues are not limited to cardiovascular field.<sup>15</sup> As observed by Cretan and Japanese diet, these essential nutrients reduce also mortality. Other investigators affirmed the interest of omega-3 in reducing the risk of some cancers<sup>16</sup>, mental illness<sup>17</sup> such as depression<sup>18</sup>, bipolar disorder<sup>19</sup>, stress<sup>20</sup> or Alzheimer’s disease<sup>21</sup>. They shown also interest of omega-3 diet in the decrease of triglyceride level<sup>22</sup> and a better development of the fetus and child<sup>23</sup> (Fig. I.2).

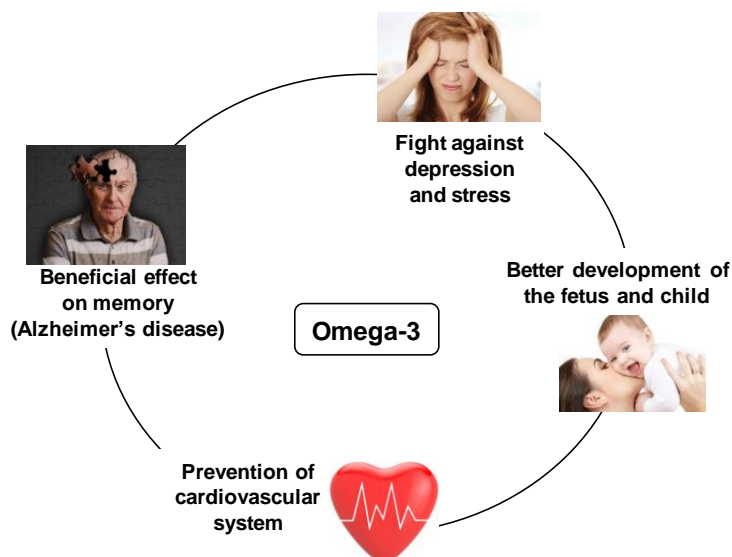


Figure I.2: Main virtues of omega-3 fatty acids<sup>24-27</sup>

As a definition, fatty acids which have one or more double bond are named respectively mono-unsaturated (MUFAs) and poly-unsaturated (PUFAs) fatty acids.<sup>28</sup> PUFAs are then classified into two groups: omega-3 and omega-6. This classification is based on the position of the first double bond on the carbon chain. Thus, omega-3 ( $n-3$  or  $\omega-3$ ) has their first double bond located at the 3<sup>rd</sup> carbon as for  $\alpha$ -linolenic acid (18:3,  $\omega-3$ , ALA) (Fig. I.3A). However, the family of omega-6 ( $n-6$ ,  $\omega-6$ ) fatty acids has their first double bond located at the 6<sup>th</sup> carbon from the methyl end (18:2,  $\omega-6$ , LA) (Fig. I.3B).

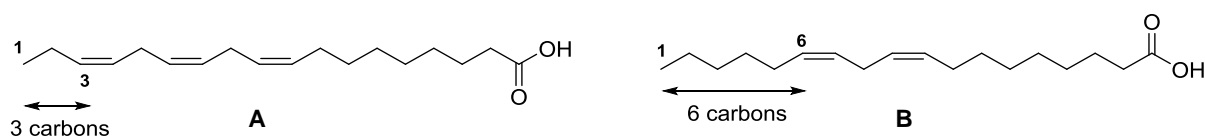


Figure I.3: Typical chemical structure of essential omega-3 ( $\alpha$ -linolenic acid) and omega-6 (linoleic acid) fatty acids

The main omega-3 fatty acids found in food are  $\alpha$ -linolenic acid (18:3, ALA), eicosapentaenoic acid (20:5, EPA) and docosahexaenoic acid (22:6, DHA) (Table I.1).<sup>29</sup> The numbers in parentheses mean that these 3 fatty acids have respectively 3, 5 and 6 double bonds in the carbon chain consisting of 18, 20 and 22 carbon atoms respectively. All these double bond are in the “cis” configuration. Actually, if there were in the “trans” configuration, omega-3 fatty acids would not be useful to the organism.

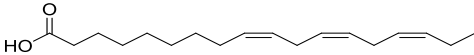
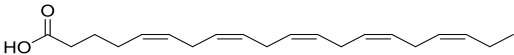
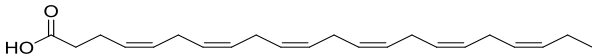
Major food $\omega$ -3 fatty acids	Chemical structures
$\alpha$ -Linolenic acid (18:3, ALA)	
Eicosapentaenoic acid (20:5, EPA)	
Docosahexaenoic acid (22:6, DHA)	

Table I.1: Three major food  $\omega$ -3 fatty acids:  $\alpha$ -linolenic acid (ALA), eicosapentaenoic acid (EPA) and docosahexaenoic acid (DHA)<sup>30</sup>

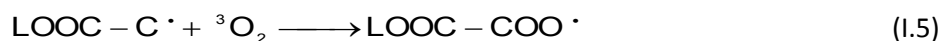
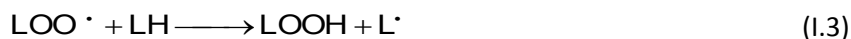
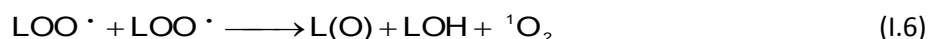
ALA is the precursor for the enzymatic synthesis of other important fatty acids but our body cannot produce it. It is, therefore, essential in our diet.<sup>29</sup> There are many sources of omega-3, which can be separated into the food of animal and plant origins.<sup>31</sup> The consumption of plants with high level of omega-3 in the form of vegetable oils is strongly recommended. Rapeseed (9 %), soya (7 %) and nuts (13 %) oils have significant ratios of omega-3 fatty acids but linseed oil is the richest vegetable source of ALA (53 %).<sup>32</sup> Since our body barely synthesizes EPA and DHA, it is imperative that food also bring these two essential fatty acids. Fatty fish are key food, especially salmon, mackerel and herring.<sup>33</sup> Furthermore, some algae produce derivatives of omega-3. In recent times, there are farm animals “naturally” enriched in omega-3 in order to increase their nutritional value and combined ALA, EPA and DHA all together.<sup>34</sup>

The recommended dietary intakes for omega-3 takes into account the consumption of another essential fatty acid named the linoleic acid, which is part of the omega-6 family. Indeed, the over consumption of omega-6 competes with omega-3 which cannot play its role properly. Professionals of health and nutrition agree to advice a ratio of 1/5 between  $\alpha$ -linolenic (omega-3) and linoleic (omega-6) acids.

- *Critical oxidation of omega-3 oils*

Omega-3 fatty acids are essential for the organism. Nevertheless, given their chemical structures rich in double bounds and their numerous bis-allylic hydrogens, they are particularly sensitive to oxygen and are therefore subject to oxidative degradation leading to a deterioration of their organoleptic and nutraceutical properties. The food degradation is often the result of a complex oxidation process which depends on many factors.<sup>35</sup> Oxidation reactions, whose key players are reactive oxygen species (ROS) and peroxy radicals, are studied since many years because they are involved in many biological process and in the degradation of various products such as food<sup>36, 37</sup>, polymers<sup>38</sup> and cosmetics<sup>39</sup>.

Unsaturated lipids (LH) are prone to autoxidation which takes place in three main steps. The first one is the initiation step which consists, at high temperature (> 60 °C), of the formation of lipidic radical which could go with the loss of a hydrogen atom under the action of metal traces, light or heat (**Eq. I.1**). Moreover, traces of hydroperoxides are always present in oils. Nevertheless, as they are instable compounds, they are fragmented into peroxy (LOO<sup>\*</sup>) and alcoxyl (LO<sup>\*</sup>) radicals which could also initiate the oxidation process by reacting with lipid (LH). The resulting lipid radical (L<sup>\*</sup>) reacts with ground state oxygen (<sup>3</sup>O<sub>2</sub>) in a second step to form a peroxy radical (LOO<sup>\*</sup>) (**Eq. I.2**). During the propagation stage, LOO<sup>\*</sup> reacts with LH to form fatty acid hydroperoxides (LOOH) which are the primary products of autoxidation (**Eqs I.3 to I.5**). In a third step, *i.e* the termination step, two radicals react together to form non-radical products (**Eqs I.6 to I.8**).<sup>40, 41</sup>

*Initiation**Propagation**Termination*

Alcoyl ( $\text{LO}\cdot$ ) and peroxy ( $\text{LOO}\cdot$ ) radicals formed during the oxidation process are reactive intermediates and are further degraded giving new oxidized products such as alcohols, aldehydes and ketones. Finally, cyclisation mechanisms are also involved in the formation of hydroperoxy cyclic and bis-cyclic peroxides.<sup>42</sup>

- *Main challenges of the thesis*

As regards to the complex mechanisms involved in the degradation of polyunsaturated fatty acids (PUFAs), it is of the utmost importance to have a method able to detect primary oxidation products generated during the first steps of the process. Nevertheless, the direct detection of hydroperoxides by gas chromatography (GC) is tricky because of their thermal sensitivity and low concentration in oils. While there is a large variety of analytical techniques able to detect pre-derivatized peroxides species<sup>43</sup>, there are few methods for detecting hydroperoxides themselves<sup>44, 45</sup>. Consequently, it is a relevant challenge to develop an analytical method for this type of thermo-sensitive compound present as traces in oxidized oils.

To minimize the oxidative degradation, food industrials have to anticipate this problem by optimizing the conditions of oil storage. They could avoid light, heat and also incorporate into the formulations additives named antioxidants. These precautions ensure to consumers a better prevention of the oxidative rancidity of fats and an extension of the shelf life of many food stuffs. As defined by Becker *et al.*, food antioxidants are “substances that, in small quantities, are able to prevent or greatly retard the oxidation of easily oxidizable materials such as fats”.<sup>46</sup> Antioxidants play their protective roles at different steps of the oxidation process according to various mechanisms. Depending on the Reactive Oxygen Species (ROS) involved, there are two families of antioxidants: **1)** the “primary” antioxidants or chain-breaking antioxidants which scavenge free radicals and stop the radical chain reactions and **2)** the “secondary” antioxidants or preventive antioxidants which interact in prevention on the chemical species which may play a role during the oxidative degradation (**Fig. I.4**).<sup>47, 48</sup>

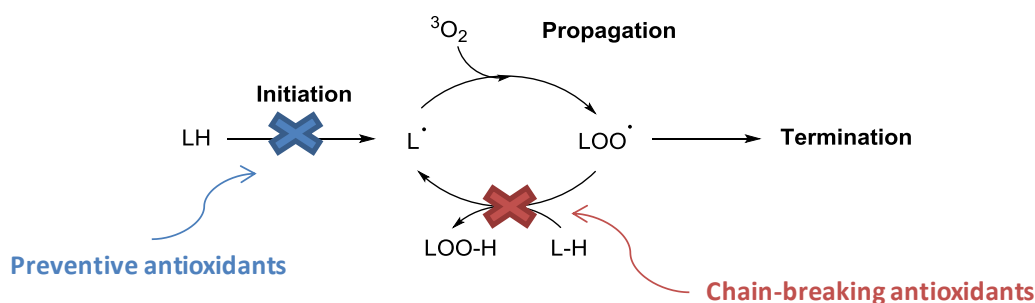


Figure 1.4: Mechanisms of inhibition of oil oxidation by primary and secondary antioxidants

Nevertheless, theoretical methods or experimental investigations are rarely combined and always made on few antioxidants. Therefore, based on literature, it is difficult to compare the effects of a large range of natural phenolic antioxidants during the protection of the same substrate and highlight the required conditions to enhance the inhibition of oxidation. In this context, CARGILL funded this PhD thesis in order to develop structure-activity relationships and highlights the best antioxidants for the protection of edible oils rich in omega-3.

Food producers are also interested to rationalize and anticipate the effectiveness of mixtures of antioxidants, which have major interests: **1)** the best inhibition of oxidative degradation in food and **2)** the reduction of the quantity of potentially toxic antioxidant in the final product. Combinations of two types of phenolic antioxidants were examined to assess synergistic effects by scientists in many publications<sup>49</sup>. The best example of synergistic effect is found between  $\alpha$ -tocopherol (vitamin E) and ascorbic acid (vitamin C) in heterogeneous system (Fig. 1.5).<sup>50, 51</sup>

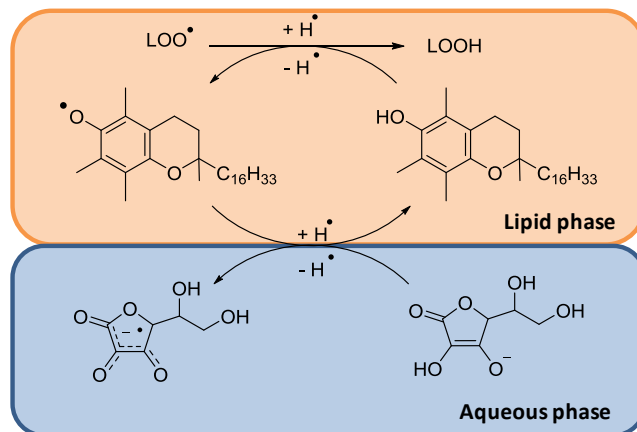


Figure 1.5: Regeneration of  $\alpha$ -tocopherol by ascorbic acid in heterogeneous system<sup>50, 51</sup>

There is a considerable literature related to the antioxidant power of mixture of phenols for the protection of fats in the human body and in food products.<sup>52</sup> Nevertheless, few of them are focused on the enhancement of the protective power of omega-3 oil against oxidation. Finally, mechanisms of synergistic effect between phenolic antioxidants are not fully understood. The elucidation of synergistic phenomena is therefore a major scientific challenge for researchers and industrial partners in the field of edible oil rich in omega-3.

- *Strategy and thesis organization*

The **chapter 1** presents a bibliographic analysis of the literature on the oxidation degradation of fatty acids and highlights the factors influencing the oxidation of oils. It also describes the analytical techniques available for the detection of fatty acid hydroperoxides.

Then, the **chapter 2** is focused on the photochemical preparation and the analysis of hydroperoxides derived from various model molecules. The oxidation of PUFAs by ground state oxygen ( $^3\text{O}_2$ ) is much slower than the photooxidation process with excited singlet oxygen ( $^1\text{O}_2$ ). As an example, methyl linoleate reacts 500 times faster with  $^1\text{O}_2$  than with  $^3\text{O}_2$ . Moreover, the required experimental conditions (*i.e.* long reaction time and/or high temperature) for oxidation with  $^3\text{O}_2$  lead to a degradation of hydroperoxides. Therefore, the fatty acid methyl esters (FAMES) related to linseed oil such as methyl linolenate ( $\omega$ -3), methyl linoleate ( $\omega$ -6) and methyl oleate ( $\omega$ -9) as well as terpenoid molecules (*i.e.* citronellol caprate and geraniol caprate) in the same range of molecular weight as FAMES were photooxidized (**Table I.2**). A combination of chromatographic analyses, titration of hydroperoxides and NMR investigations was undertaken to follow the photooxidation of substrates and a kinetic analysis of the singlet oxygenation is detailed.

Substrate	Chemical structure
Methyl oleate	
Methyl linoleate	
Methyl linolenate	
Citronellol caprate	
Geraniol caprate	

**Table I.2:** Chemical structures of model substrates oxidized with photochemically generated singlet oxygen ( $^1\text{O}_2$ )

These analytical methods allow detecting hydroperoxides but do not provide a detailed picture of the chemical structures. Consequently, we resort to the ElectroSpray Ionization Mass Spectrometry (ESI-MS) which is particularly appropriate for the analysis of thermo-sensitive hydroperoxides without derivatization. This work is made possible thanks to the collaboration with the TRACES research team of the "Institut des Sciences Analytiques" (ISA, Lyon).

Many scientists are studying on the inhibition of oxidation of organic compounds with phenols either natural or synthetic.<sup>52</sup> The choice of antioxidants for a given application is based on their antioxidant capacity, availability, cost and toxicity. The ubiquitous synthetic antioxidants are currently the butylated hydroxytoluene (BHT), butylated hydroxyanisole (BHA), propyl gallate (PG) and *tert*-butylhydroquinone (TBHQ) (**Fig I.6**).

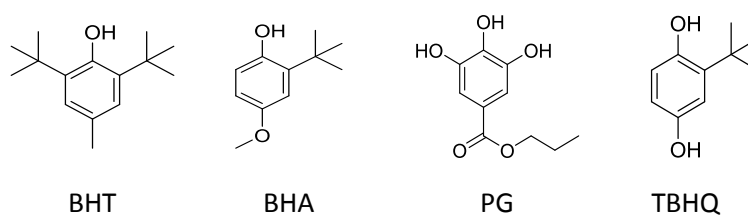


**Figure I.6:** Main synthetic phenolic antioxidants: BHT (butylated hydroxytoluene), BHA (butylated hydroxyanisole), PG (propyl gallate) and TBHQ (*tert*-butylhydroquinone)

These phenols have always alkyl substituents in order to improve their effectiveness as well as their oil and fat solubility. For toxicity reasons, some acceptable antioxidants in the field of polymers are no longer tolerated when products are intended to be ingested. In recent years, the biological effects of BHT and BHA have been extensively studied since these compounds are subjected to controversy.<sup>53</sup> Because of safety problems highlighted for synthetic antioxidants and a growing distrust of consumers, there is a strong pressure for searching for natural alternatives. In this context, industries are turning increasingly to natural conservators.  $\alpha$ -Tocopherol is the most widely used natural antioxidant as it is very effective and can be introduced in food in higher concentrations compared to BHA and BHT due to its low toxicity.<sup>54</sup> Nevertheless, as regards to the fast degradation of omega-3 fatty acids, oils and food producers are looking for even more powerful natural antioxidants. Based on these considerations, the **chapter 3** is devoted to study the antioxidant properties of a large number of natural and synthetic phenols with respect to the protection of omega-3 oils combining theoretical and experimental approaches.

In order to be more and more effective in the extension of the shelf life of omega-3 oils with a minimum amount of natural antioxidants, CARGILL is strongly interested in synergistic phenomena. Indeed, the **chapter 4** is focused on the elucidation of mechanisms which explain synergistic effects between phenolic antioxidants. Experiments have been focused on  $\alpha$ -tocopherol as primary antioxidant combined with other phenols as co-antioxidants. Complementary thermodynamic and kinetic approaches have been employed and the most efficient couples of phenols for the protection of omega-3 oil against oxidation are highlighted.

# CHAPTER 1. PEROXIDATION OF (POLY)UNSATURATED FATTY ACIDS AND ANALYZES OF OXIDIZED LIPIDS: A LITERATURE SURVEY

---

## 1. Introduction

Lipid peroxidation is a general phenomenon that occurs in the presence of oxygen. This paramagnetic uncoupled electron pair oxygen is named triplet oxygen  $^3\text{O}_2$  and is involved in oxidation pathways. A higher energy state of oxygen was discovered by Herzberg in 1934 using spectroscopy and he reported this oxygen as singlet oxygen. In its singlet state,  $^1\text{O}_2$  is involved in photooxidation processes as demonstrated by Foote and Wexler.<sup>55</sup> With its two states, oxygen is in charge of mainly degradation processes of (poly)unsaturated hydrocarbons rich in electron and more particularly in the oxidation of lipids, polyunsaturated fatty acids, terpenes and polymers. Nevertheless, triplet and singlet oxygen have not the same oxidation power as regards to the unsaturated compounds. Indeed, the oxidation rate of singlet oxygen with oils is higher than that of triplet oxygen because of a lower activation energy.<sup>56</sup>

All lipids containing unsaturated fatty acids such as vegetable oils, fish oils, animal fats, cell membranes and lipoproteins are concerned by the lipid peroxidation. In recent decades, the mechanistic study of lipid peroxidation has known a renewed interest because of the implication of lipid peroxidation in the field of nutrition. These oxidation reactions are formed by either triplet oxygen or singlet oxygen. The diradical triplet oxygen was extensively studied during the last 70 years whereas the non radical singlet oxygen oxidation of food has been only investigated during the last 30 years.<sup>56</sup>

On one hand, lipid oxidation in food is a serious issue for the food industries which offer more and more highly unsaturated fatty acids such as those of omega-3 ( $\omega$ -3) extremely sensitive to oxidation. Indeed, oxidation of food lipids causes the degradation of color and organoleptic properties such as rancidity, vitamin loss or toxicity because of the products of lipid peroxidation (peroxides, aldehydes, ketones...).<sup>47</sup> The mechanisms involved are complex and depend on different parameters such as light, traces of metals, temperature, concentrations, medium polarity.... They differ in the nature of the radical involved, the products of oxidation formed and the kinetics of the substrate degradation.<sup>48</sup> On the other hand, lipid peroxidation<sup>48</sup> can also take place *in vivo* because cell membranes are particularly rich in polyunsaturated fatty acids (30 to 50%) with the presence of phospholipids. The lipoperoxidation of the membranes alters their functionality such as the permeability and fluidity which have important impact on the cell apoptosis.<sup>57</sup> Moreover, many other diseases are related to the lipid peroxidation such as neurodegenerative diseases (*i.e.* Alzheimer and Parkinson), cardiovascular diseases (CVD) and low-density lipoprotein (LDL) peroxidation.

The understanding of these phenomena was possible thanks to concerted efforts of universities, industries and governments.<sup>58</sup> This results in an intense literature about the mechanisms of lipid oxidation. These mechanisms of oxidation are developed thanks to the separation and analysis of oxidized lipids by various methods. Nevertheless, it is difficult to obtain a complete knowledge of the chemical structures of a mixture of lipid peroxides. Thus, engineers have to monitor the food composition to ensure the quality and safety of edible products. In that way, some relevant methods are set up and Fatty Acid Methyl Esters (FAMES) analysis becomes a crucial technique for determining the total content of food.<sup>59</sup>

Therefore, the oxidation of (poly)unsaturated fatty acids has been studied to assess the state of progress especially for oleic ( $\omega$ -9), linoleic ( $\omega$ -6) and linolenic ( $\omega$ -3) acids. Their generic mechanisms of oxidation are developed whether it is with ground state oxygen  $^3\text{O}_2$  or with singlet oxygen  $^1\text{O}_2$ . Moreover, the degradation of fatty acid peroxides and the factors affecting the oxidation of oils which are drastic parameters are also investigated on this literature survey. Finally, this literature

search is focused on the different analytic methods able to separate and analyze FAMES and respective oxidized products.

## 2. Autoxidation and photooxidation of unsaturated fatty acids

Fatty acids are ubiquitous in the nature as attested by the amount of references (593 500) found in the Scifinder® database. Food chemistry (43 %) and biochemistry (39 %) are the two major sectors highlighted by the term of “unsaturated fatty acids”. The areas of cosmetic and detergency, pharmacology and toxicology are less concerned by these molecules (**Fig. 1.1**). This survey reveals that unsaturated fatty acids have been strongly studied because of their nutritional quality and their highly oxidability in food and in the human body. In the case of food chemistry, the main investigations are related to oxidation (49 %) and antioxidants (21 %).

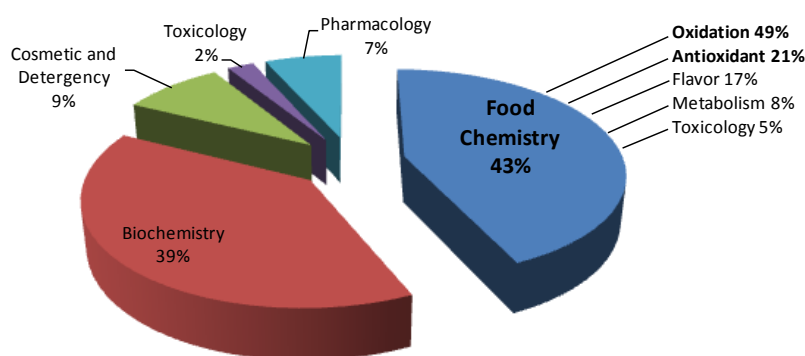


Figure 1.1: Main study areas of unsaturated fatty acids with the Scifinder® database

Oleic acid ( $\omega$ -9), linoleic acid ( $\omega$ -6), arachidonic acid ( $\omega$ -6) and then linolenic acid ( $\omega$ -3) are the most largely reported fatty acids.<sup>60</sup> The literature survey of these compounds highlights their omnipresence in vivo notably in cell membranes. Unsaturated fatty acids are also present in oils in the form of triglycerides. The oxidative stability of oils is represented by their resistance to oxidation during their storage and the production of food.<sup>61</sup> It is primordial to determine the oil quality and lifetime because off-flavor compounds can be released making the oil unsatisfactory to consumers and industrials.<sup>62</sup> Moreover, the oxidation of unsaturated fatty acids can produce toxic compounds (*i.e.* 4-hydroxy-2-alkenals<sup>63, 64</sup>) and polymers<sup>65</sup>. Two different mechanisms are responsible for the oxidation of edible oils: **1**) autoxidation *via* ground state oxygen  $^3\text{O}_2$  and **2**) photosensitized oxidation *via* singlet oxygen  $^1\text{O}_2$ . This singlet oxidation is not the main oxidative pathway and it is rarely considered. However, it can initiate the oxidative degradation which is followed then by the autoxidation process.

The autoxidation and singlet photooxidation of methyl oleate (C18:1), linoleate (C18:2) and linolenate (C18:3) (**Table 1.1**) are reported in numerous publications. The oxidation of oils is also affected by various factors such as light or heat, the composition of fatty acids, traces of metals and the presence of enzymes. This is why industrials are carrying out researches to delay the oxidation of oils.

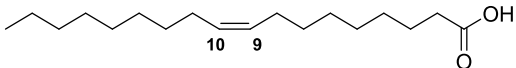
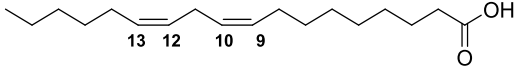
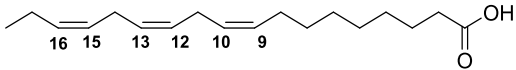
Name	Chemical structure
Oleic acid (C18:1)	
Linoleic acid (C18:2)	
$\alpha$ -Linolenic acid (C18:3)	

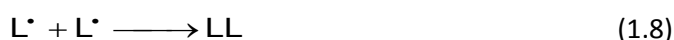
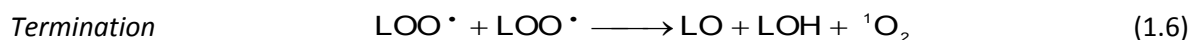
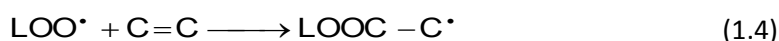
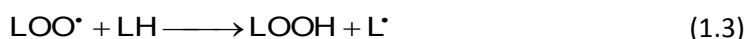
Table 1.1: Chemical structures of oleic acid (C18:1), linoleic acid (C18:2) and  $\alpha$ -linolenic acid (C18:3)

## 2.1 Autoxidation of unsaturated fatty acids by ground state oxygen $^3\text{O}_2$

The oxidation of unsaturated fatty acids results in the combination of the substrate with ground state oxygen  $^3\text{O}_2$ . More precisely,  $^3\text{O}_2$  reacts following a catalytic radical mechanism named autoxidation.

### 2.1.1 General mechanism of autoxidation

The main compounds subjected to autoxidation *via* a radical pathway are unsaturated compounds.<sup>66</sup> Unsaturated lipids (LH), in the presence of oxygen  $^3\text{O}_2$ , are prone to oxidation which takes place in three main steps.<sup>36</sup> The first one is the initiation step which consists, at high temperature ( $> 60\text{ }^\circ\text{C}$ ), of the formation of lipidic radical which could go with the loss of a hydrogen atom under the action of metal traces, light or heat (**Eq. 1.1**). Moreover, traces of hydroperoxides are always present in oils. Nevertheless, as they are instable compounds, they are fragmented into peroxy ( $\text{LOO}^\bullet$ ) and alcoxyl ( $\text{LO}^\bullet$ ) radicals which could also initiate the oxidation process by reacting with lipid (LH). The resulting lipid radical ( $\text{L}^\bullet$ ) reacts with oxygen in a second step to form a peroxy radical  $\text{LOO}^\bullet$  (**Eq. 1.2**). During the propagation stage,  $\text{LOO}^\bullet$  reacts with LH to form fatty acid hydroperoxides ( $\text{LOOH}$ ) which are the primary products of autoxidation (**Eqs. 1.3 to 1.5**). In a third step, *i.e.* the termination step, two radicals react together to form non-radical products (**Eqs. 1.6 to 1.8**).<sup>41</sup>



The instability and the reactivity of hydroperoxides are responsible for their decomposition into various secondary products, some of which catalyze the oxidative process and make more complex the study of the mechanisms.<sup>66</sup> The hypothetical autoxidation of unsaturated fatty acids represented as a function of time includes firstly a lag time or initiation step followed by a rapid accumulation of hydroperoxides (propagation step). Then, the hydroperoxides are decomposed and form several

different types of molecules which become important; *i.e.* compounds with the same chain length as lipid (non-volatiles end-products as peroxides), dimers and volatiles compounds (**Fig. 1.2**).

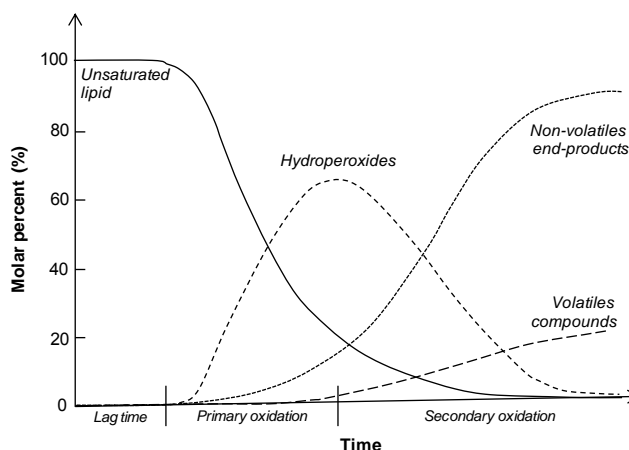


**Figure 1.2:** Autoxidation of unsaturated lipids and formation of hydroperoxides, non-volatiles end-products and volatiles compounds as a function of time<sup>66</sup>

In most cases, the autoxidation is considered as a spontaneous reaction but it is not really the case. Indeed,  $^3\text{O}_2$  cannot react directly with the double bonds of the unsaturated fatty acids according to the Wigner's rule of spin conservation: transitions between terms of the same multiplicity are spin-allowed, while transitions between terms of different multiplicity are spin-forbidden.<sup>67</sup> On one hand, ground state oxygen in its triplet state ( $^3\text{O}_2$ ) displays two electrons with parallel spins in two separated  $\pi^*$  orbitals<sup>68</sup> as presented in **figure 1.3**.

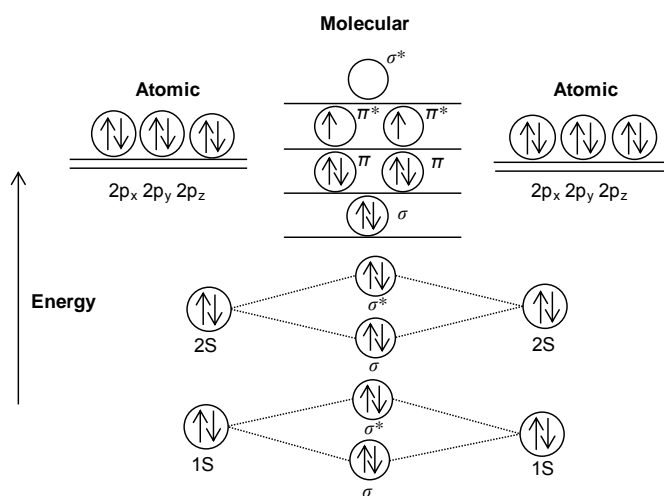


**Figure 1.3:** Electronic configuration of triplet oxygen  $^3\text{O}_2$ <sup>35</sup>

In another hand, the double bond is into a singlet state and has two electrons with opposite spins in the same orbital. In order to allow the reaction between both of them, another element has to interact. It must either shift dioxygen into a singlet state ( $^1\text{O}_2$ ) or abstract one electron or  $\text{H}^*$  from the unsaturated compound. The energy to abstract on hydrogen atom from an organic compound depends on the position of the hydrogen on the chemical structure. The allylic hydrogen is more labile than the vinylic hydrogen. Moreover, it is extremely labile when it is bis-allylic as for linoleic and  $\alpha$ -linolenic acids. The ability to abstract hydrogen is correlated with a low Bond Dissociation Enthalpy (BDE). BDEs are strongly dependant on the method of calculation used. As there is not one publication dealing with the comparative BDEs of targeted molecules, our DFT method B3LYP/6-

311++G(2d,2p)//B3LYP/6-311G(d,p) is used to calculate the BDEs of saturated and unsaturated patterns (Table 1.2).

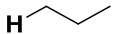
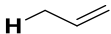
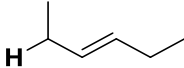
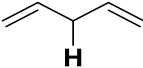
Substrate					
BDE (kcal.mol <sup>-1</sup> )	106.9	97.5	97.0	73.5	65.3

Table 1.2: Bond Dissociation Enthalpies of various C-H bonds calculated by the DFT method B3LYP/6-311++G(2d,2p)//B3LYP/6-311G(d,p) in vacuum

Lipid radicals of unsaturated compounds can also be formed through UV radiations. Indeed, at a wavelength below 400 nm, the energy of photons activates the scission of the L-H bond ( $E_a \sim 94.4$  kcal.mol<sup>-1</sup>) forming lipid radicals ( $L^\bullet$ ). This formation of lipid radicals  $L^\bullet$  is also enhanced by heating.<sup>69</sup> Consequently, the mechanism of the lipid radical formation is indirect. Moreover, there is a homolytic scission of some hydroperoxides leading to free initiators (*i.e.*  $LO^\bullet$  and  $HO^\bullet$ ) which are able to abstract hydrogens on lipid molecules and form lipid radicals ( $L^\bullet$ ).

After the generation of lipid radicals ( $L^\bullet$ ), there is the propagation step which is a complex stage. Indeed, this radical chain mechanism includes **1**) the radical coupling with oxygen (Eq. 1.9), **2**) the atom or group transfers (Eq. 1.10), **3**) fragmentation (Eq. 1.11), **4**) rearrangement (Eq. 1.12) and **5**) cyclisation (Eq. 1.13).<sup>70</sup> In the case of the rearrangement and cyclisation steps, small unsaturated patterns are used for a better understanding of mechanisms.

1) Radical coupling



2) Atom transfer



3) Fragmentation



4) Rearrangement



4) Cyclisation



The process of autoxidation of lipid is stopped by the termination step. Therefore, the reaction of two radicals together produces a non-reactive species, which end the radical process. This decreases the number of reacting chains. It is obvious that these latter reactions only happen when the concentration of lipids [LH] is becoming low.

### 2.1.2 Autoxidation of unsaturated fatty acids by ground state oxygen

The autoxidation of oleic ( $\omega$ -9), linoleic ( $\omega$ -6) and linolenic ( $\omega$ -3) acids or FAMES derivatives is developed in this section. They all form hydroperoxides as primary oxidation products which react then with ground state oxygen  $^3\text{O}_2$  leading to secondary oxidation products.<sup>68</sup>

#### Autoxidation of oleic acid ( $\omega$ -9)

The autoxidation mechanism of oleic acid starts with the abstraction of the allylic hydrogen located on the C<sub>8</sub> and C<sub>11</sub> carbons. This produces two allylic radicals in which electrons are delocalized through a system of 3 carbons.<sup>71</sup> The radicals formed react with  $^3\text{O}_2$  at the end-positions leading to a mixture of 4 hydroperoxides isomers: 8-, 9-, 10- and 11-hydroperoxides (**Fig. 1.4**).<sup>36, 72, 73</sup>

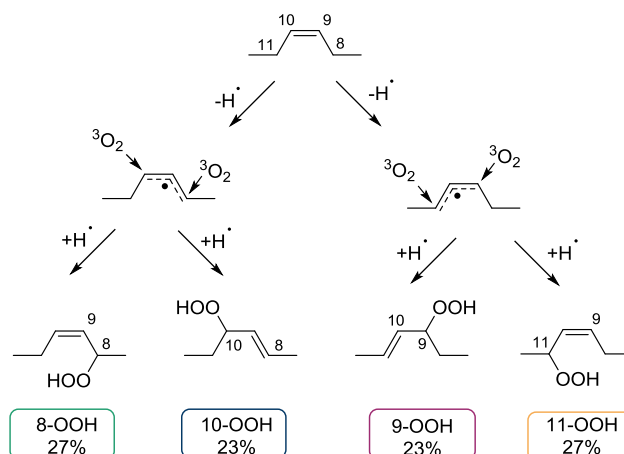


Figure 1.4: Autoxidation mechanism of oleic acid and formation of six hydroperoxides isomers<sup>36</sup>

Recent studies based on GC-MS and HPLC analyses demonstrate that the outer hydroperoxides (8- and 11-hydroperoxides, 27%) are formed in consistently higher amounts than the inner hydroperoxides (9- and 10-hydroperoxides, 23%). This results from a better reactivity of  $^3\text{O}_2$  with the radical located on the C<sub>8</sub> and C<sub>11</sub> positions.<sup>74</sup> It is explained by a rearrangement of the peroxy radical which influences the composition of the hydroperoxide mixtures (**Fig. 1.5**).<sup>75</sup> Moreover, as reported by Garwood et al., the isomeric distribution of hydroperoxides changes when the mixture is heated.<sup>76</sup>

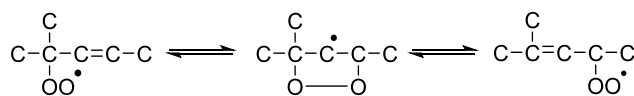


Figure 1.5: Rearrangement of allylic hydroperoxides

In highly oxidized oleic acid, there is the formation of saturated epoxy compounds, allylic ketones, saturated and mono-unsaturated dihydroperoxides (**Fig. 1.6**) as described by Frankel.<sup>36</sup>

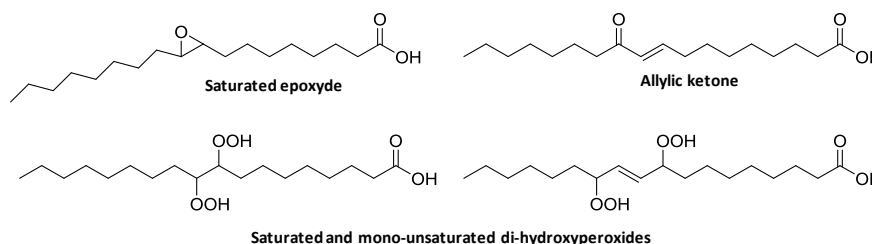


Figure 1.6: Highly oxidized oleic acid by ground state oxygen  $^3\text{O}_2$  and formation of saturated epoxy, allylic ketone, saturated and mono-unsaturated dihydroperoxides<sup>36</sup>

- *Autoxidation of linoleic acid ( $\omega$ -6)*

In the case of *di*-unsaturated fatty acids, the hydrogen abstraction from the bis-allylic methylene group on the C<sub>11</sub> position produces a delocalized pentadienyl radical.<sup>36, 77</sup> This radical reacts with <sup>3</sup>O<sub>2</sub> at the two terminal positions producing an equal mixture<sup>74, 78</sup> of conjugated 9- and 13-hydroperoxides isomers with *trans*, *cis*-configurations (**Fig. 1.7**)<sup>70, 71, 79</sup> as shown by LC, GC-MS and NMR.<sup>80</sup> The formation of 9- and 13- hydroperoxides is favored by the conjugated diene system. Moreover, the 11-hydroperoxide is not detected because it is formed in too small quantity or it is unstable.<sup>81</sup>

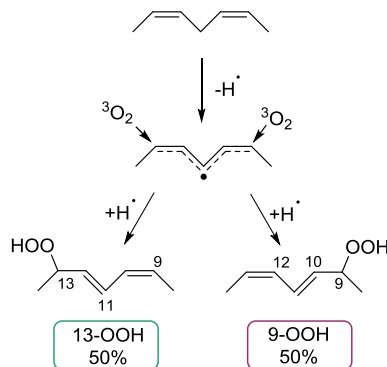


Figure 1.7: Formation of 9- and 13-hydroperoxides by autoxidation of linoleic acid<sup>36</sup>

Mono-hydroperoxides of linoleic acid could then react with <sup>3</sup>O<sub>2</sub> and form secondary oxidation products such as epoxy-hydroperoxides, keto-hydroperoxides, di-hydroperoxides and hydroperoxy epidioxides<sup>82</sup> as represented by the **figure 1.8**.<sup>68, 83, 84</sup>

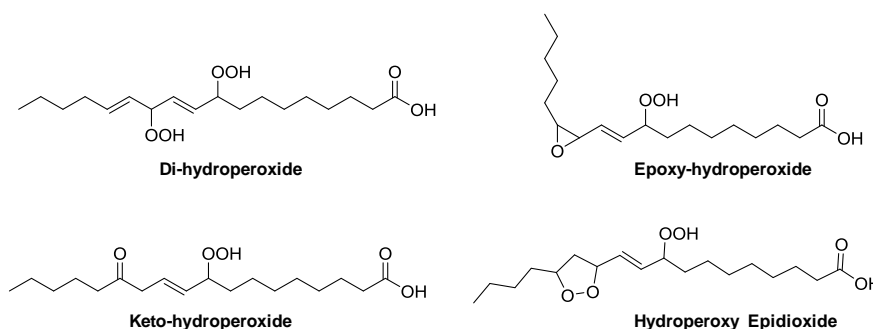


Figure 1.8: Formation of secondary oxidation products from autoxidation of linoleic acid mono-hydroperoxides with <sup>3</sup>O<sub>2</sub>

- *Autoxidation of  $\alpha$ -linolenic acid ( $\omega$ -3)*

Concerning the *tri*-unsaturated fatty acids such as  $\alpha$ -linolenic acid or its FAME derivatives, the bis-allylic hydrogens located at the C<sub>11</sub> and C<sub>14</sub> positions are abstracted leading to the formation of two pentadienyl radicals.<sup>73</sup> These two delocalized radicals react at the end-positions with <sup>3</sup>O<sub>2</sub> producing a mixture of 9-, 12-, 13- and 16- conjugated diene-triene hydroperoxide isomers (**Fig. 1.9**).<sup>36, 85</sup>

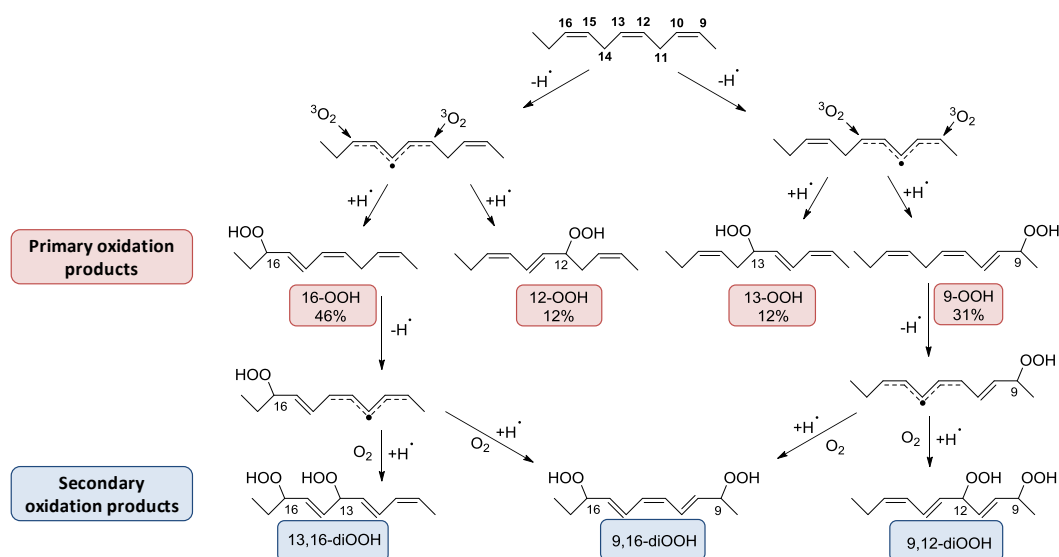


Figure 1.9: Autoxidation pathway of  $\alpha$ -linolenic acid and formation of 4 mono-hydroperoxides and 3 di-hydroperoxides<sup>36</sup>

Various investigation techniques as NMR, LC<sup>74</sup> and GC-MS with derivatization of hydroperoxides<sup>43</sup> showed that significantly higher proportion of the outer 9- and 16-hydroperoxides are obtained. There are various arguments to explain this phenomenon: **1)** the steric factor of C<sub>12</sub> and C<sub>13</sub> internal radicals, **2)** the internal isomers 12- and 13- hydroperoxides are decomposed more quickly than the 9- and 16- isomers and **3)** the homoallylic structure of the internal isomers allows a cyclisation to form hydroperoxy cyclic peroxides.<sup>71, 73</sup>

As for linoleic acid, secondary oxidation products have also been identified.<sup>36</sup> The abstraction of the bis-allylic hydrogen from mono-hydroperoxides produces another time two pentadienyl radicals. The reaction of these radicals with  $^3\text{O}_2$  forms the 9,12- and 13,16-di-hydroperoxides with conjugated diene-triene configuration and the 9,16-di-hydroperoxides with conjugated triene system (Fig. 1.9). Moreover, a multiple of secondary oxidation products are then obtained as di- and tri- oxygenated compounds including epoxy-hydroperoxides and ketohydroperoxides as represented by the figure 1.10.<sup>36</sup>

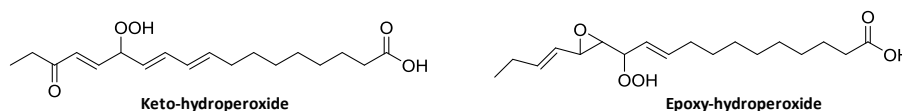


Figure 1.10: Example of secondary oxidation products obtained from the autoxidation of  $\alpha$ -linolenic acid mono-hydroperoxides

Finally, GC-MS, LC-MS and NMR analyses highlight that unsaturated fatty acids composed by more than two double bonds are prone to form cyclic peroxides.<sup>36, 86, 87</sup> It is the case for the autoxidation of  $\alpha$ -linolenic acid (Fig. 1.11).

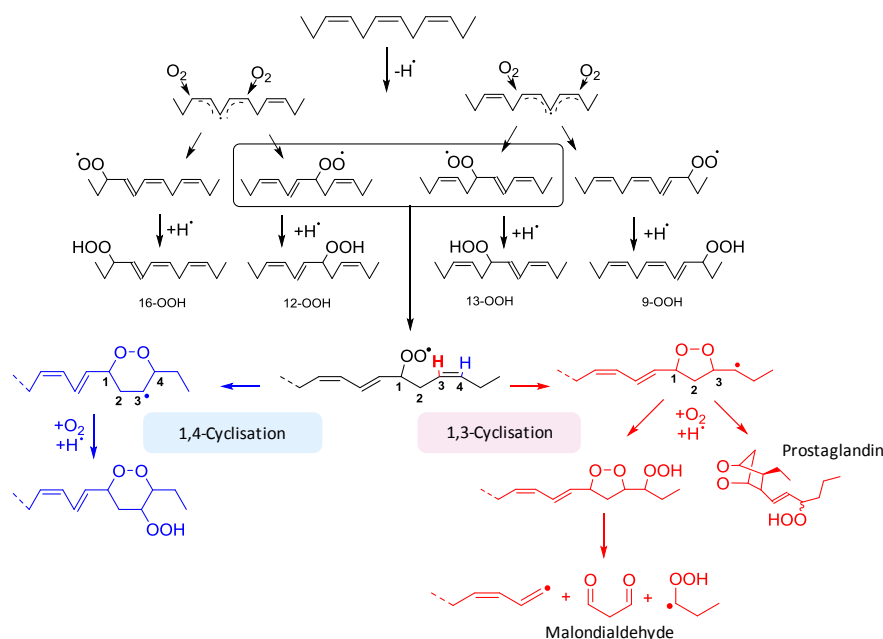


Figure 1.11: Autoxidation of  $\alpha$ -linolenic acid and formation of cyclic peroxides as secondary oxidation products<sup>35, 88</sup>

The mechanisms are based on the 1,3- and 1,4-cyclizations of the internal 12- and 13-hydroperoxyl radicals.<sup>43, 71</sup> This results respectively in the formation of 5- and 6-membered rings.<sup>89</sup> These hydroperoxy cyclic peroxides could then be subjected to a second cyclisation leading to bicycloendoperoxides structurally related to prostaglandins.<sup>82, 90, 91</sup>

## 2.2 Photosensitized oxidation of unsaturated fatty acids by singlet oxygen $^1O_2$

### 2.2.1 Formation and reactivity of singlet oxygen $^1O_2$

Photochemistry affords the reaction between oxygen and double bonds, by changing the oxygen from its triplet state to a singlet state or by abstracting one electron on the substrate to oxidize. Visible light ( $\lambda > 400$  nm) does not provide enough energy to generate directly lipid radicals<sup>68</sup> as already explained for ground state oxygen. Nevertheless, the light can be absorbed by the sensitizers which reach an excited state. Then, this energy is transferred to double bonds to generate free radicals *via* a reaction of electron transfer (Type I, **Eq. 1.14**). Moreover, the energy can also be transferred to ground state oxygen leading to the formation of singlet oxygen which can then react with the double bonds of unsaturated fatty acids according to a non-radical process (Type II, **Eq. 1.15**). The type II pathway is a reaction of oxygenation which is 1500 times faster than the reaction involving oxygen in its triplet state.<sup>92</sup>



- *Formation of singlet oxygen via photochemical reaction*

The sensitizer (S, such as chlorophylls, porphyrins and phthalocyanins) does not participate in the reaction. In its excited state,  $^3S^*$  promotes the oxidation by the way of the type I and type II mechanisms. The type I mechanism involves the abstraction of one hydrogen or a transfer of electron between the excited sensitizer and the substrate, leading to the formation of a free radical.

This radical reacts with oxygen and forms active species as the radical superoxide anion  $O_2^{\bullet -}$ <sup>93</sup> or initiates a radical chain reaction.<sup>94</sup>

Following a type II mechanism,  $^1O_2$  is generated *via* the transfer of energy from  $^3S^*$  to the oxygen molecule.<sup>95</sup> One molecule of sensitizer could product from  $10^3$  to  $10^5$  molecules of singlet oxygen before degradation.<sup>96</sup> These two mechanisms are competitive and are part of the photooxidation process (**Fig. 1.12**).

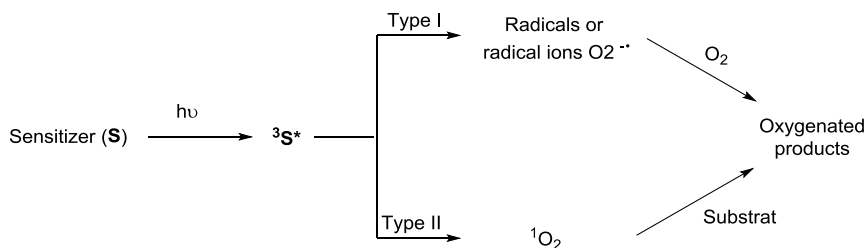


**Figure 1.12: Photooxidation by the Type I and type II mechanisms**

By the way of photochemistry, singlet oxygen is produced with the combination of light and sensitizer.<sup>93</sup> The Jablonski diagram, illustrated by **figure 1.13**, models the order of the energy levels and the photophysical levels involved during the photooxidation.<sup>97</sup>

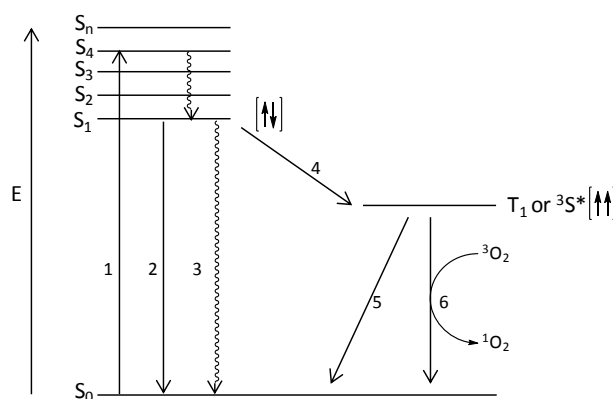


**Figure 1.13: Modified Jablonski diagram describing the photophysical processes: 1) absorption, 2) fluorescence, 3) internal conversion, 4) inter-conversion, 5) phosphorescence, 6) formation of singlet oxygen  $^1O_2$  with transfer of energy from the T1 state of the photosensitizer to the triplet oxygen  $^3O_2$** <sup>97</sup>

With a UV or visible specific wavelength, the photosensitizer in its ground state  $S_0$ , absorbs a photon of energy and reaches its excited state  $S_n$  (1). This excited state could be subjected to a transition without radiation between two states with the same multiplicity called the internal conversion (3) to come back to the ground state ( $S_0$ ) or keep an excited state with a lowest energy characteristic of a more stable state ( $S_1$ ). This excited state has a short lifetime and could follow two steps of transition. The first one is to come back to the ground state delivering the absorbed energy (2): this is fluorescence. The second one is a non-radiatif relaxation occurring during the intersystem crossing (4) towards the first excited triplet state  $T_1$  (or  $^3S^*$ ). This transition, causing the change of multiplicity from the anti-parallel spins to the parallel spins is forbidden but an appropriate photosensitizer allows this transition. The excited state  $T_1$  has a long lifetime and its reaction with ground state oxygen ( $^3O_2$ ) leads to a modification of the spin providing an excited singlet state of oxygen ( $^1O_2$ ) characterized by its proper electronic configuration (**Fig. 1.14**). Finally, the photosensitizer comes back to its ground state (6). This excited state of the oxygen reacts directly with unsaturated compounds to form hydroperoxides without intermediate radicals. Starting from

$T_1$ , the photosensitizer could also come back to its ground state by a radiatif descent named the phosphorescence (5).<sup>93, 97, 98</sup>

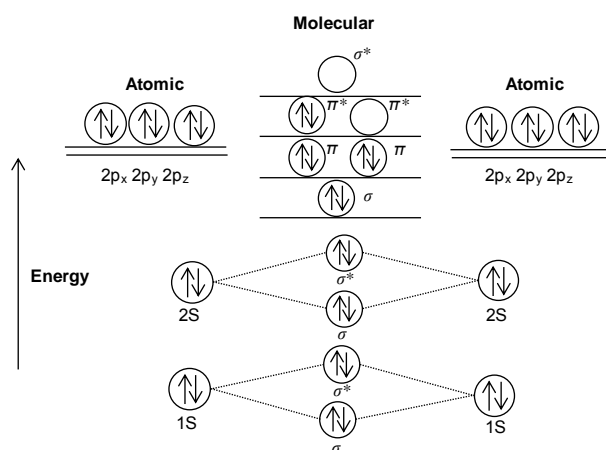


Figure 1.14: Electronic configuration  $2p\pi$  antibonding orbital of singlet oxygen  $^1O_2$ <sup>35</sup>

The choice of the sensitizer is primordial. Indeed, it was shown that benzophenone used as sensitizer boost the formation of epoxides to the detriment of hydroperoxides.<sup>99</sup> It is noteworthy that singlet oxygen can also be formed chemically through various processes such as the disproportionation of hydrogen peroxide as reported by Aubry in 1985. The excited state of oxygen is obtained by a hydrogen peroxide/molybdate system.<sup>100-103</sup>

- *Reactivity of singlet oxygen with unsaturated compounds*

$^1O_2$  is deactivated to return to its ground state. Three phenomena allow this transition to its triplet state: **1)** the radiative deactivation by the solvent with emission of photons following a kinetic rate constant  $k_d$ , **2)** the chemical deactivation by reacting with a substrate leading to oxygenated compound following a kinetic rate constant  $k_r$  and **3)** the physical non-radiative deactivation with a transfer of energy to another molecule without altering the chemical structure of these molecule and following a kinetic rate constant  $k_q$  (Fig. 1.15).

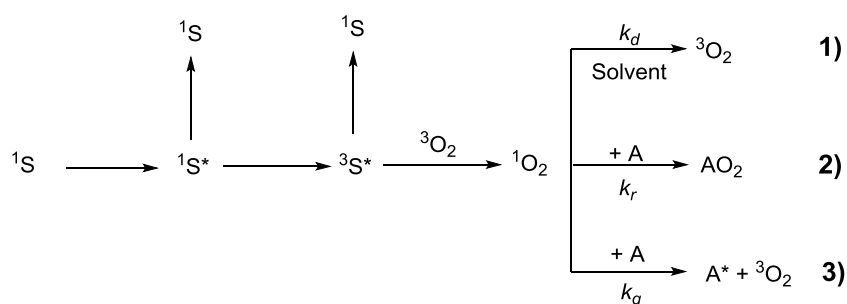


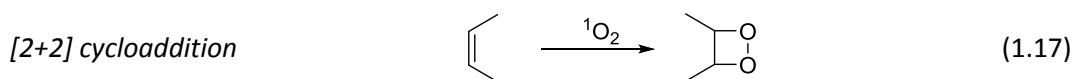
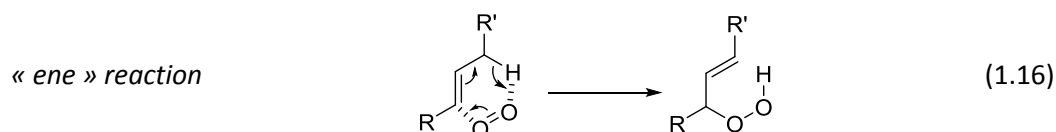
Figure 1.15: 3 ways of deactivation of singlet oxygen<sup>56, 104, 105</sup>

The competition between the pathways 1 and 2 is defined by the Foote coefficient  $\beta$  corresponding to the  $k_d/k_r$  ratio.<sup>105</sup> Singlet oxygen has a lifetime from  $10^{-6}$  to  $10^{-3}$  seconds in solution depending on the solvent (Table 1.3).<sup>106</sup> Deuterated solvents increase the singlet oxygen lifetime ( $\tau$   $^1O_2$ ) and favor a faster photooxidation.<sup>106-108</sup>

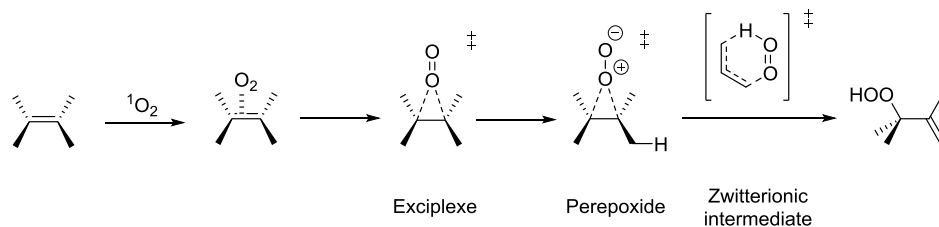
Solvent	Singlet oxygen lifetime $\tau$ $^1\text{O}_2$ ( $\mu\text{s}$ )
Water ( $\text{H}_2\text{O}$ )	$3.0 \pm 0.2$
Methanol ( $\text{CH}_3\text{OH}$ )	$10 \pm 0.1$
Benzene ( $\text{C}_6\text{H}_6$ )	$26.7 \pm 1.3$
Acetone ( $\text{CH}_3\text{COCH}_3$ )	$46.5 \pm 2.0$
Acetonitrile ( $\text{CH}_3\text{CN}$ )	$54.4 \pm 1.3$
Deuterated acetonitrile ( $\text{CD}_3\text{CN}$ )	$600 \pm 33$
Deuterated acetone ( $\text{CD}_3\text{COCD}_3$ )	$690 \pm 2.0$

Table 1.3: Lifetime of singlet oxygen ( $\zeta$   $^1\text{O}_2$ ) in various classic and deuterated solvents<sup>106-108</sup>

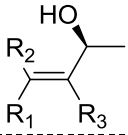
$^1\text{O}_2$  reacts with the double bonds rich in electrons leading to the formation of hydroperoxides (via “ene” reaction), dioxetane (via [2+2] cycloaddition) and endoperoxides (via [4+2] cycloaddition) as represented by equations 1.16 to 1.18.<sup>56, 109-112</sup>



During the “ene” reaction which is faster than the cyclization reactions, there is the addition of singlet oxygen and the abstraction of the hydrogen onto the  $\pi$  system of the olefin<sup>111, 113</sup> involving the shift of the double bond (Fig. 1.16).<sup>114</sup>

Figure 1.16: Detailed mechanism of the « ene » reaction highlighting the intermediates of reaction<sup>113, 115</sup>

$^1\text{O}_2$  is able to abstract the hindered hydrogens on the olefin.<sup>113</sup> Nardello *et al.* have determined by flash photolysis the kinetic rate constants of photooxidation ( $k_r + k_q$ ) and the value of the Foote coefficient  $\beta$  for a series of allylic alcohols (Table 1.4)<sup>116</sup> proving this tendency. This phenomenon is known as the “cis effect” and was described for the first time by Foot.<sup>115</sup>

			$(k_r + k_q)^*$ $10^4 \times \text{M}^{-1} \cdot \text{s}^{-1}$	$\beta = k_d / k_r^{**} \text{ (M)}$
R <sub>1</sub>	R <sub>2</sub>	R <sub>3</sub>		
CH <sub>3</sub>	CH <sub>3</sub>	H	2.4	0.43
H	CH <sub>3</sub>	CH <sub>3</sub>	14	0.074
CH <sub>3</sub>	H	CH <sub>3</sub>	18	0.058
CH <sub>3</sub>	CH <sub>3</sub>	CH <sub>3</sub>	320	0.0032

\*  $\text{CD}_3\text{OD}$  as solvent, tetraphenylporphine sulfonate as sensitizer\*\*  $\text{CH}_2\text{Cl}_2$  as solventTable 1.4: Kinetic rate constants ( $k_r + k_q$ ) and Foote coefficient  $\beta$  determined by flash photolysis for the photooxidation of allylic alcohols<sup>116</sup>

As regards to the unsaturated fatty acids, the both sites of the double bonds have the same steric hindrance, that's why the amount of the two hydroperoxides formed is equal.<sup>35</sup> The factors affecting the formation of hydroperoxides are: **1)** the temperature, **2)** the solvent, **3)** the amount of sensitizers and **4)** the intensity of the light.<sup>117</sup> These parameters influence the regio- and stereoselectivity of the reactions between singlet oxygen and unsaturated compounds.<sup>113</sup> The photooxidation with  $^1\text{O}_2$  depends also on the number and the sort of double bonds (conjugated or not). Indeed, kinetic rate constants related to the reaction of  $^1\text{O}_2$  with oleic, linoleic and linolenic acids are 0.7, 1.3 and 1.9 x  $10^{-5} \text{ M}^{-1} \cdot \text{s}^{-1}$  respectively.<sup>94</sup>

### 2.2.2 Photooxidation of (poly)unsaturated fatty acids by singlet oxygen

Unsaturated fatty acids in nature may be oxidized by light in the presence of a dye such as chlorophyll.<sup>36</sup> Singlet oxygen reacts with methyl linoleate 500 times faster than with ground state oxygen. Indeed,  $^1\text{O}_2$  plays an important role in the oxidation process.<sup>92, 118</sup>  $^1\text{O}_2$  reacts with each isolated double bond to provide two equivalent hydroperoxides. The photooxidation of oleic, linoleic and linolenic acids or FAMES is described in this following part.<sup>119</sup>

#### ▪ Photooxidation of oleic acid ( $\omega$ -9)

The photooxidation of oleic acid or FAMES provides an equivalent mixture of the 9- and 10-hydroperoxides with the allylic trans-double bond<sup>36, 71, 120</sup> as represented in **figure 1.17**.<sup>74, 121</sup>

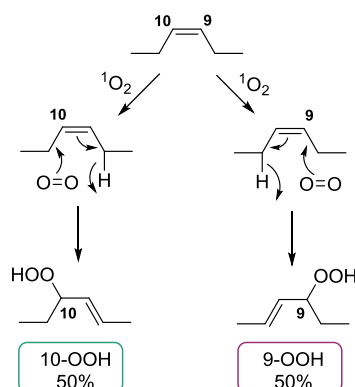


**Figure 1.17: Mechanism of photooxidation of the oleic acid**<sup>36</sup>

Frankel *et al.* reported the quantification of hydroperoxides obtained from the photooxidation and autoxidation of methyl oleate<sup>36</sup> as indicated in **table 1.5**. The autoxidation of C18:1 leads to the 8-, 9-, 10- and 11-hydroperoxides whereas its photooxidation gives only the 9- and 10-hydroperoxides.

Isomeric Hydroperoxides			
Autoxidation of methyl oleate			
8-OOH	9-OOH	10-OOH	11-OOH
27%	23%	23%	27%
Photooxidation of methyl oleate			
	9-OOH	10-OOH	
	50%	50%	

**Table 1.5: Comparison between the amounts of mono-hydroperoxides obtained during the autoxidation and photooxidation of methyl oleate**<sup>36</sup>

▪ Photooxidation of linoleic acid ( $\omega$ -6)

The photooxidation of linoleic acid produces a mixture of 4 isomeric hydroperoxides as primary photooxidation products<sup>71</sup>: two conjugated diene hydroperoxides as for autoxidation (9- and 13-hydroperoxides) and two unconjugated 10- and 12-hydroperoxides which differ from the autoxidation (**Fig. 1.18**).<sup>74, 122, 123</sup>

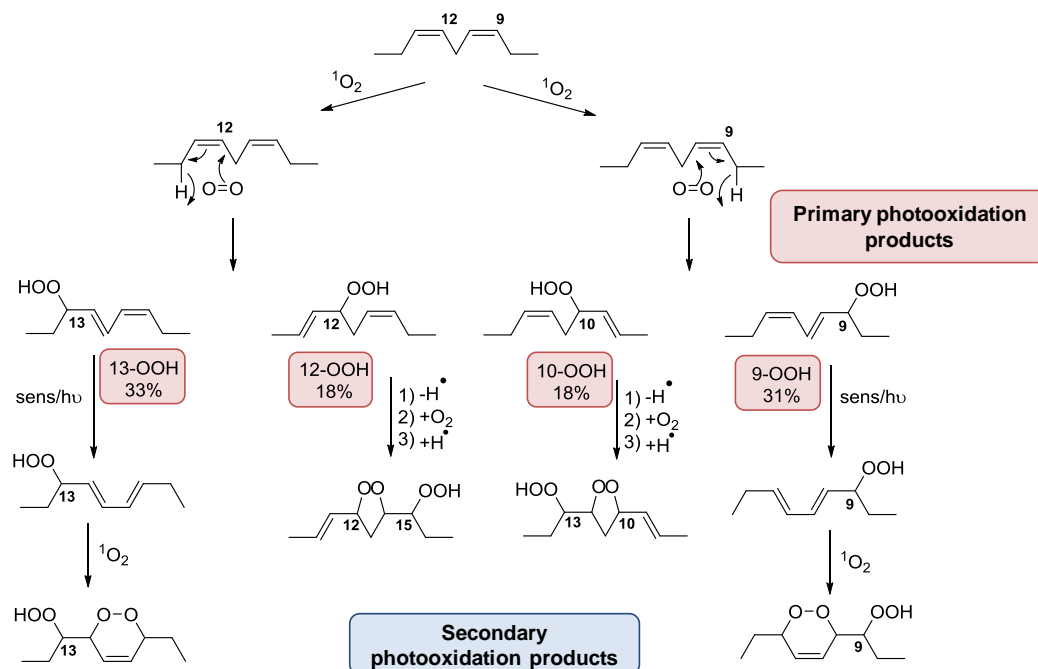


**Figure 1.18: Mechanism of photooxidation of linoleic acid and formation of hydroperoxides as primary photooxidation products and internal cyclic peroxides (epidioxides, endoperoxides) as secondary oxidation products**<sup>36, 71</sup>

As regards to the formation of hydroperoxides, it will be expected a statistical distribution but is not the case. The ratio of conjugated and non-conjugated hydroperoxides is 2:1. The internal hydroperoxides (10- and 12-OOH) are formed in significantly lower amount than the external hydroperoxides (13- and 9-OOH). This is due to the fact that internal hydroperoxides have a homoallylic structure which allows an easy 1,3-cyclisation to form hydroperoxy cyclic peroxides<sup>36, 120, 124</sup> which is a side radical reaction with ground state oxygen (**Fig. 1.18**). Moreover, there is also the formation of 6-membered cyclic peroxides *via* 1,4-cyclisation of the conjugated diene system found on the terminal mono-hydroperoxides. Before this cyclisation, the *trans,cis*-diene system is isomerized into the *trans,trans* configuration by the sensitizer and light (**Fig. 1.18**).<sup>125</sup> This 1,4-cyclisation is less favorable than the 1,3-cyclisation as regards to the amount of each monohydroperoxide. This reveals that the 1,3-cyclisation of the internal 10- and 12-mono-hydroperoxides *via* a radical mechanism prevails over the 1,4-cycloaddition of singlet oxygen on the terminal 9- and 13-mono-hydroperoxides.

Frankel *et al.* reported the quantification of hydroperoxides obtained from the photooxidation and autoxidation of methyl linoleate (**Table 1.6**).<sup>36</sup> The autoxidation process gives only the 9- and 13-hydroperoxides in equivalent amount whereas the photooxidation process leads to the four isomeric 9-, 10-, 12- and 13-hydroperoxides.

Isomeric Hydroperoxides			
<b>Autoxidation of methyl linoleate</b>			
9-OOH	13-OOH		
50%	50%		
<b>Photooxidation of methyl linoleate</b>			
9-OOH	10-OOH	12-OOH	13-OOH
31%	18%	18%	33%

Table 1.6: Comparison between the amount of monohydroperoxides obtained during the autoxidation and photooxidation of methyl linoleate<sup>36</sup>

The formation of the 8,13- and 9,14-di-hydroperoxides can be explained by two possible mechanisms (Fig. 1.19). On one hand, these di-hydroperoxides could be free radical side products obtained *via* the abstraction of the hydrogen located on the C<sub>8</sub> and C<sub>14</sub> conjugated diene system. By the same mechanism, the 12,13- and 9,10-di-hydroperoxides are expected from the internal monohydroperoxides. Nevertheless, they are not obtained because the delocalized radical is not formed. On the other hand, they could be also obtained from the hydrogen abstraction on the C<sub>8</sub> or C<sub>14</sub> position of the 6-membered epoxide followed by a loss of oxygen and a rearrangement of the double bonds.<sup>36, 126</sup>

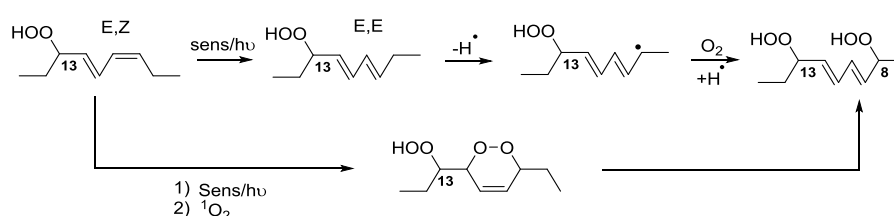


Figure 1.19: Formation of di-hydroperoxides by two possible mechanisms

#### ▪ Photooxidation of linolenic acid ( $\omega$ -3)

The photooxidation of the tri-unsaturated fatty acids such as  $\alpha$ -linolenic acid leads to the formation of six isomer hydroperoxides<sup>121</sup>: the 9-, 12- 13- and 16-isomers are the same as in the autoxidation pathway whereas the 10- and 15-isomers are different (Fig. 1.20).<sup>74, 120, 127</sup> Frankel *et al.* also reported the quantification of hydroperoxides obtained from the photooxidation and autoxidation of methyl linolenate (Table 1.7).<sup>36</sup>

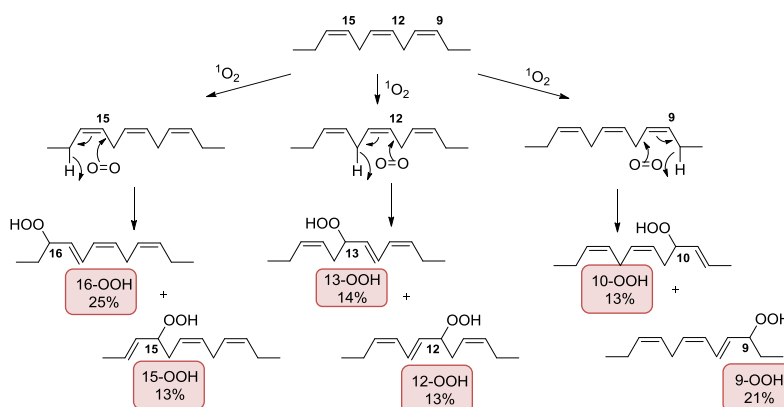


Figure 1.20: Photooxidation of methyl linolenate by singlet oxygen  $^1\text{O}_2$ <sup>36</sup>

Isomeric Hydroperoxides					
<b>Autoxidation of methyl linolenate</b>					
9-OOH	12-OOH	13-OOH	16-OOH		
30%	12%	12%	46%		
<b>Photooxidation of methyl linolenate</b>					
9-OOH	10-OOH	12-OOH	13-OOH	15-OOH	16-OOH
21%	12%	13%	14%	13%	25%

Table 1.7: Comparison between the amounts of mono-hydroperoxides obtained during the autoxidation and photooxidation of methyl linolenate<sup>36</sup>

Accordingly to the “ene” addition of  $^1\text{O}_2$ , a statistical distribution of mono-hydroperoxides is expected. However, it is not the case.<sup>71, 123</sup> The external 9- and 16- hydroperoxides are in higher amount than the other internal hydroperoxides.<sup>36</sup> As for methyl linoleate, the uneven distribution is due to the homoallylic structure of the internal hydroperoxides leading to the formation of hydroperoxy cyclic peroxides *via* a 1,3-cyclisation (Fig. 1.21).<sup>120</sup>

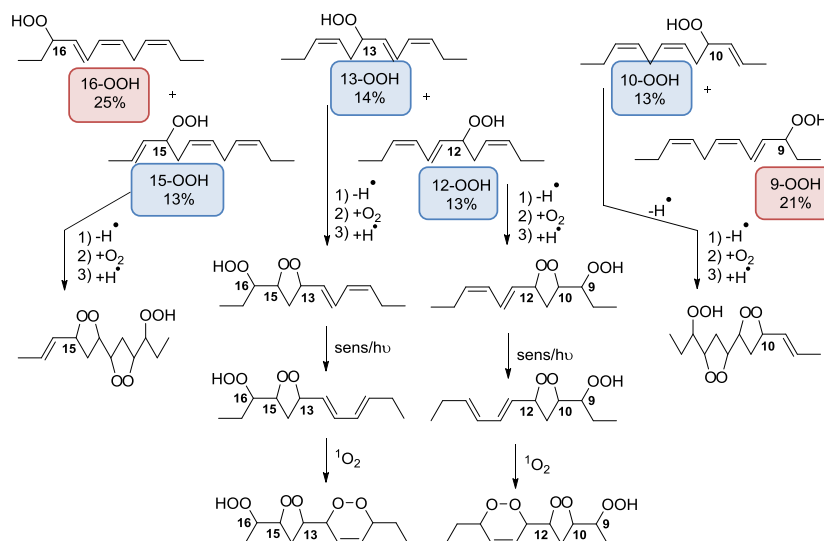


Figure 1.21: 1,3-cyclisation of internal hydroperoxides leading to cyclic and bis-cyclic endoperoxides<sup>36, 71, 119</sup>

The major amount of cyclic hydroperoxides derived from the 12- and 13-mono-hydroperoxides has been also identified during the autoxidation methyl linolenate.<sup>128</sup> These cyclic peroxides are obtained *via* a side radical mechanism. Due to their large number of unsaturations, the cyclic peroxides could react again by side radical reactions leading to hydroperoxy bis-cyclic peroxides composed by two 5-membered cyclic peroxides.<sup>119, 128</sup> Moreover, as regards to the cyclic peroxides obtained from the 12- and 13-hydroperoxides, the *trans,cis*-diene system is isomerized into the *trans,trans* configuration by the sensitizer and light. After that, there is the “ene” addition on  $^1\text{O}_2$  leading to the formation of the 6-membered cyclic peroxide (Fig. 1.21).<sup>42</sup>

Moreover, the 6-membered hydroperoxy epidioxides may be formed by the 1,4-cycloaddition to the conjugated 1,3-diene system of the terminal 9- and 16-mono-hydroperoxides.<sup>71</sup> The *trans, cis* diene configuration of the mono-hydroperoxides is firstly changed into a *trans,trans* configuration before the cycloaddition of  $^1\text{O}_2$  by the sensitizer (Fig. 1.22).<sup>42</sup>

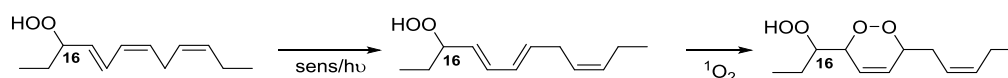


Figure 1.22: Formation of 6-membered cyclic peroxides *via* 1,4-cycloaddition of  $^1\text{O}_2$

The higher proportion found for the 5-membered than for the 6-membered cyclic peroxides shows that the radical cyclisation of the 10-, 12-, 13- and 15-hydroperoxides prevails on the 1,4-cycloaddition of  $^1\text{O}_2$  to the outer 9- and 16-hydroperoxides isomers (Table 1.8).<sup>126, 128</sup>

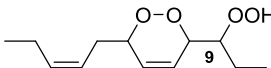
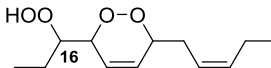
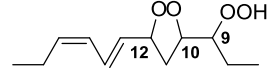
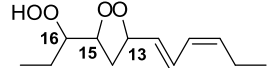
Chemical Structures of hydroperoxy cyclic peroxide	Mass Percentage
Non-reactive monohydroperoxides	30%
	12%
	17%
	26%
	15%
Non identified compounds	15%

Table 1.8: Chemical structures and quantification of hydroperoxy epidioxides of photooxidized methyl linolenate<sup>126, 128</sup>

Di-hydroperoxides are also detected as major secondary products of methyl linolenate photooxidation.<sup>128</sup> The 9,12-, 13,16- and 9,16-dihydroperoxides (in green) are synthesized from the 9- and 16-hydroperoxides as depicted in figure 1.23. The same radical mechanism used for the formation of di-hydroperoxides during the autoxidation of methyl linolenate is proposed.<sup>36, 120</sup> However, the other di-hydroperoxides identified as 1,3-disubstituted (*i.e.* 13,15- and 10,13-dihydroperoxides) and 1,7-disubstituted (*i.e.* 9,15- and 10,16-dihydroperoxides) compounds are presumed to come from the photooxidation of the corresponding mono-hydroperoxides using  $^1\text{O}_2$  and sensitizer.<sup>74</sup> Nevertheless, authors are not dealing with tri-hydroperoxide compounds.

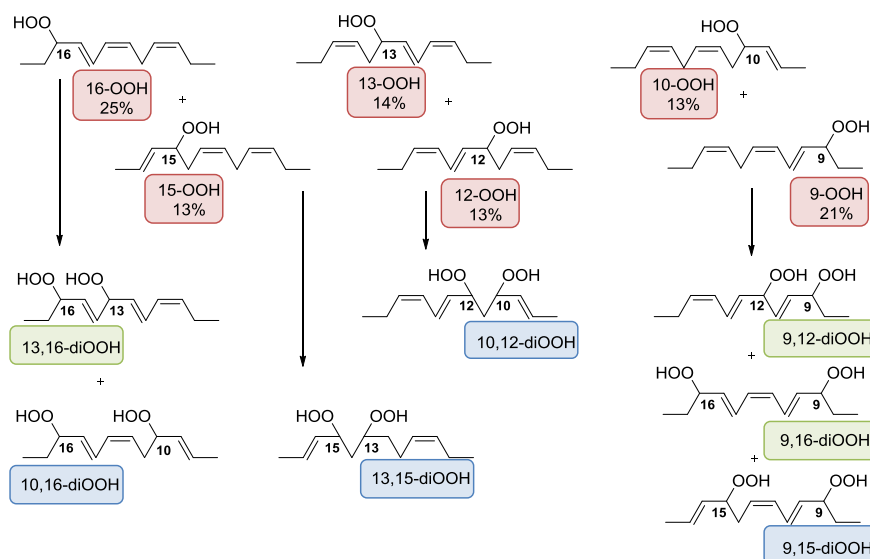


Figure 1.23: Formation of di-hydroperoxydes from methyl linolenate photooxidation<sup>36, 128</sup>

## 2.3 Degradation of fatty acid peroxides

The decomposition of lipid hydroperoxides leads to the formation of a lot of oxidized compounds *via* a crucial complex process. It is interesting to focus on this phenomenon because it is responsible for biological effects and in the change of the taste of foods.<sup>73</sup>

### 2.3.1 Initiation of LOO<sup>•</sup> and LO<sup>•</sup> radicals

Hydroperoxides are the primary oxidation products of unsaturated fatty acids. They are relatively stable but, in the presence of metals<sup>129</sup> or heat, they are decomposed into alkoxy radicals (LO<sup>•</sup>) and peroxy radicals (LOO<sup>•</sup>) leading to aldehydes, ketones, alcohols, acids and small hydrocarbons. This decomposition is due to the homolytic cleavage of the O-O bond leading to the formation of LO<sup>•</sup> and <sup>•</sup>OH radicals. The activation energy of this cleavage is about 46 kcal.mol<sup>-1</sup> and it is lower than that of the O-H related to the formation of the LOO<sup>•</sup> radical.<sup>35</sup> The alkoxy radical could be then subjected to homolytic  $\beta$ -scission of the C-C bond (**Fig. 1.24**). Electronic rearrangements, addition of other radicals or transfer of hydrogen allow the formation of secondary oxidation products with, in most of cases, lower molecular weight (*i.e.* aldehydes, ketones and alcohols).

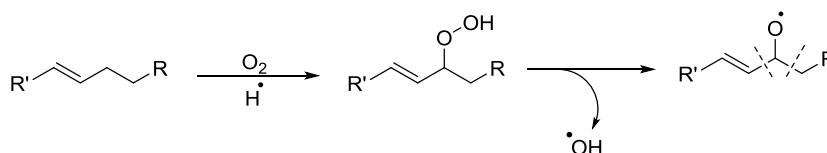


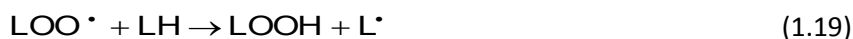
Figure 1.24: Decomposition of hydroperoxides and formation of alkoxy and hydroxyl radicals<sup>35</sup>

### 2.3.2 Propagation of peroxy (LOO<sup>•</sup>) and alkoxy (LO<sup>•</sup>) radicals

Hydroperoxides are subjected to scission because the alkoxy radical LO<sup>•</sup> is more reactive ( $k = 10^7 - 10^8 \text{ L.mol}^{-1}.\text{s}^{-1}$ )<sup>68, 130</sup> than the peroxy radical LOO<sup>•</sup> ( $k = 62 \text{ L.mol}^{-1}.\text{s}^{-1}$ ) for the H-abstraction from LH.<sup>68, 131</sup> There are different major mechanisms related to the radical propagation. The mechanism or propagation is influenced by the structure of the double bonds, solvent and temperature.

- *Atom transfer and hydrogen abstraction*

The abstraction of hydrogen is the first step of the classical chain radical mechanisms. The abstraction of H<sup>•</sup> by the alkoxy radical (LO<sup>•</sup>) is very fast ( $k = 10^7 - 10^8 \text{ L.mol}^{-1}.\text{s}^{-1}$ ) but less selective than by the peroxy radical (LOO<sup>•</sup>).<sup>130</sup> The initial radical formed on fatty acids transfers its unpaired electron to the other unsaturated lipid molecule by the abstraction of hydrogen. This process works indefinitely until the termination step (**Eqs. 1.19** and **1.20**).



The factors affecting the kinetic rate constants of hydrogen abstraction by the radicals are: **1**) the availability of the hydrogen on the target molecule, **2**) the structure of the radical and **3**) the solvent.<sup>132</sup> The relative rate of the hydrogen abstraction by the alkoxy radical (LO<sup>•</sup>) is proportional to the number of allylic and bis-allylic hydrogens of unsaturated fatty acids (**Table 1.9**).<sup>68</sup>

Fatty acid	$10^{-6} \times k \text{ (L.mol}^{-1}.\text{s}^{-1}\text{)}$
Oleic (C18:1)	3.8
Linoleic (C18:2)	8.3
$\alpha$ -Linolenic (C18:3)	13
Arachidonic (C20:4)	20.5

Table 1.9: Kinetic rate constants of hydrogen abstraction on polyunsaturated fatty acids by t-BuO<sup>•</sup> in apolar solvent, the reactivity of LO<sup>•</sup> is equal to that of t-BuO<sup>•</sup> <sup>68</sup>

The hydrogen abstraction is favored in apolar aprotic solvents or when there is a high concentration of lipids. In protic solvents<sup>133</sup> or with low lipid concentration, the hydrogen abstraction is in competition with internal rearrangements and scissions.<sup>134-136</sup> In fact, with other sources of hydrogens in solution, a competitive hydrogen abstraction leads to the reduction of the radical and the end of the propagation.<sup>137</sup> The increase of temperature improves the kinetic rate constants of hydrogen abstraction whatever the solvent. For example, the abstraction of H<sup>•</sup> by LOO<sup>•</sup> is lower than 1.0 L.M<sup>-1</sup>.s<sup>-1</sup> and increases to 10<sup>3</sup> - 10<sup>4</sup> L.M<sup>-1</sup>.s<sup>-1</sup> at 65 °C.<sup>138</sup> Nevertheless, it is difficult to get accurate values because the cyclisation rate of LOO<sup>•</sup> increases with the temperature compared to the hydrogen abstraction.

- Fragmentation by  $\alpha$ - and  $\beta$ -scissions

Figure 1.25 points out that  $\alpha$ - and  $\beta$ -scissions are the two sorts of possible scissions. It depends on the cleavage location on the alkyl chain compared to the hydroperoxide location. There is the transformation of alcoxyl radical (LO<sup>•</sup>) into more polar products (*i.e.* alcohols, aldehydes and ketones)<sup>36</sup> thanks to a transition state which influences the transformation of LO<sup>•</sup>.

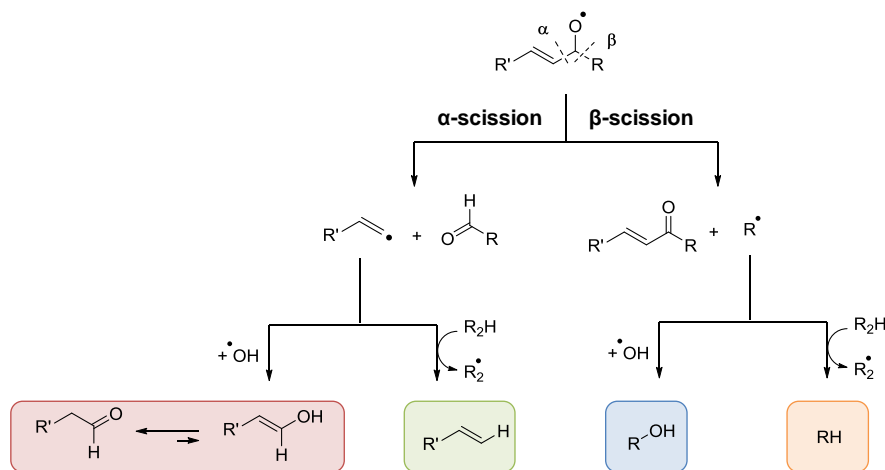


Figure 1.25:  $\alpha$ - and  $\beta$ -scissions of the alcoxyl radicals of unsaturated fatty acids<sup>36</sup>

The mechanism of scission is faster in polar solvents. The reaction made in an aqueous solution is 10 to 100 times faster than in apolar solvents.<sup>68</sup> Water and protic solvents stabilize the transition state and the carbonyl products. With that, the solvation and intramolecular hydrogen bondings are favored and lead to the decrease of the dissociation energy providing the rupture of the bond.<sup>134-136, 139, 140</sup> The scission is also increased when lipids are diluted in apolar solvents. Indeed, this reduces the competition with the abstraction of hydrogens.

The propagation step is favored with the increase of double bonds on substrates<sup>138</sup> and with high temperature in which the scissions of the radicals is improved.<sup>68</sup> The cleavage of hydroperoxides is

not important at 60 °C but become an essential factor of the propagation at a temperature higher than 100 °C.<sup>141</sup>

Most of the radicals products obtained from the scissions are recombined into non-radical products thanks to the abstraction of hydrogen in the solution. Unsaturated fragments, especially conjugated diene systems, are still available to oxidation and contribute to the radical chain reaction. The cleavage of all the radicals leads to the formation of complex mixtures where carbonyl compounds and free radicals, such as aldehydes, alkanes and oxo-esters are gathered.<sup>142</sup>

#### ▪ Cyclisation

The internal recombination or cyclisation is obtained with the 1,3-addition of the peroxy radical on the closed double bond at the  $\beta$ -position. This results in the formation of a 5-membered cycle with a radical located on the  $\gamma$ -carbon of the starting double bond. This radical reacts with oxygen and then with lipids leading to the final hydroperoxy cyclic peroxide (**Fig. 1.26**).<sup>68</sup>

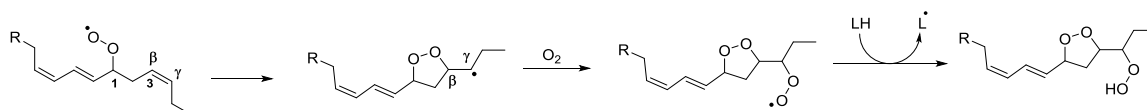


**Figure 1.26:** Formation of a 5-membered cycle from the 13-hydroperoxide of linolenic acid during photooxidation<sup>68</sup>

The intramolecular cyclisation is 4 to 6 times faster than the  $\beta$ -scission as regards to the unsaturated fatty acids. Indeed, the 5-membered cycle is formed with a kinetic rate ( $k \approx 10^3 \text{ s}^{-1}$ ) higher than that of the O-O bond dissociation ( $k \approx 27 - 430 \text{ s}^{-1}$ ) and that of the hydrogen abstraction ( $k \approx 1 - 400 \text{ s}^{-1}$ ).<sup>138, 143</sup> Therefore, this cyclisation process is particularly suitable for the highly unsaturated fatty acid (*i.e.* linoleic and linolenic acids).

The cyclisation of  $\text{LOO}^\bullet$  *via* a 1,4-addition at the  $\gamma$ -carbon of the double bond leads to the formation of a 6-membered cycle (**Fig. 1.27**). The reaction of the radical formed with oxygen and lipid leads to the formation of hydroperoxy cyclic peroxide. Nevertheless, this reaction of cyclisation is less favorable ( $k \sim 10 \text{ s}^{-1}$ )<sup>70, 90</sup> compared to the formation of the 5-membered cycle ( $k \sim 10^3 \text{ s}^{-1}$ ).

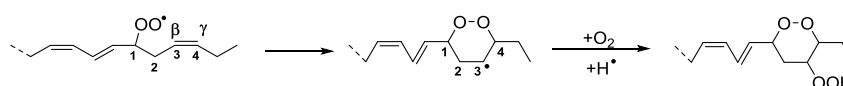


**Figure 1.27:** Formation of a 6-membered cycle from the 12-hydroperoxide of linoleic acid during autoxidation<sup>70, 90</sup>

The alkoxy radical ( $\text{LO}^\bullet$ ) is also subjected to 1,2-addition into a nearby double bond in order to form epoxides and epoxyallylic radicals (**Fig. 1.28**).<sup>68</sup> It is a fast reaction and becomes predominant in aprotic solvents, with low concentration of lipids<sup>144</sup>, at room temperature<sup>145-147</sup> and with low oxygen pressure.<sup>141, 144</sup> The cyclisation of the alkoxy radicals ( $\text{LO}^\bullet$ ) is stereospecific. Indeed, the configuration of the end-product is defined by the configuration of the radical  $\text{LO}^\bullet$ .

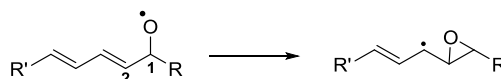


**Figure 1.28:** Formation of an epoxide and the respective epoxyallylic radical<sup>68</sup>

Some factors such as the solvent, lipid concentration, level of oxidation and temperature have an impact on the cyclisation or the propagation of the radical chain. For example, low oxygen pressure favors the cyclisation process.<sup>144</sup> In aprotic solvents and diluted solutions at temperature room, the abstraction of external hydrogen is limited and the cyclisation dominate. The increase of the

temperature leads to an improvement of hydrogen transfer and cleavages, which become the vector of the propagation.<sup>141</sup> These mechanisms of cyclisation could be activated by traces of metals (*i.e.* iron and copper) and the competition between the propagation and the cyclisation mechanisms leads to a mixture of products.<sup>89, 148</sup>

- *Addition on a double bond and cross-linkage*

When the abstraction of hydrogen is limited, radicals react directly with non-oxidized lipid molecules leading to cross-linkage process.<sup>149</sup> The factors which control the cross-linkage of radicals with double bonds are: **1)** the strength of the resulting bond, **2)** the steric hindrance and **3)** the polar effects.<sup>150</sup> The double bonds in the trans configuration offset the steric hindrance and improve the addition of peroxy radicals.<sup>151</sup>

The addition of  $\text{LOO}^\bullet$  increases with the temperature, level of oxidation<sup>152</sup> and polarity of solvents.<sup>152</sup> Dimers are mainly composed by C-O-O-C bonds at low temperature but they are changed into C-C and C-O-C links with the increase of the temperature. At 40 °C, the peroxy radicals ( $\text{LOO}^\bullet$ ) could react with double bonds leading to more than 90% of dimerization. The addition of the alcoxyl radical ( $\text{LO}^\bullet$ ) is more complicated. It is favored by the absence of allylic hydrogens, conjugation and *cis*-configuration of the double bonds (**Fig. 1.29**).<sup>68</sup>

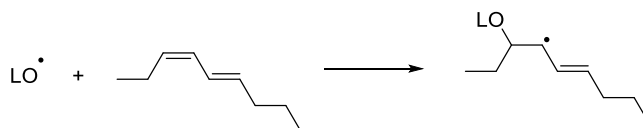
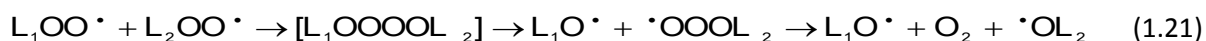


**Figure 1.29:** Cross-linkage: addition of the  $\text{LO}^\bullet$  radical on the double bond in *cis* configuration<sup>68</sup>

As described in **figure 1.29**, the addition of a radical into a double bond leads to the formation of another radical. The radical chain propagation is favored thanks to three ways of reaction: **1)** the elimination of the alcoxyl radical and formation of epoxide, **2)** the addition of another  $\text{LOOH}$  to carry on the polymerization and **3)** the abstraction of hydrogen to spread the radical chain and form a hydroperoxide stable dimer.

- *Dismutation or radical recombination of  $\text{LOO}^\bullet$*

The radical recombination is known to be a termination step. Nevertheless, some mechanisms are involved in the propagation step leading to the formation of new radical species. This reaction happens more often with peroxy radicals ( $\text{LOO}^\bullet$ , **Eqs. 1.21** and **1.22**).<sup>68</sup> The reaction of dismutation takes place in oxidized lipids or in aprotic solvents. In polar solvents and in aqueous solutions,  $\beta$ -scissions are favored and the kinetic rates of  $\text{LOO}^\bullet$  decomposition is increased. With that, the reaction of dismutation becomes preferentially a reaction of termination than a reaction of propagation.

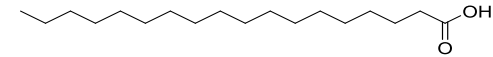
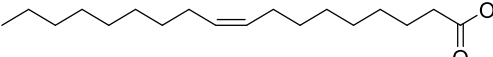
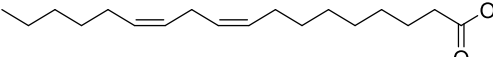
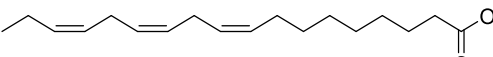


## 2.4 Factors affecting the oxidation of oils

The oxidation of oils by either ground state oxygen or singlet oxygen is influenced by various factors such as **1)** their fatty acid composition, **2)** temperature and light, **3)** concentration and electronic configuration of oxygen ( $^3\text{O}_2$  or  $^1\text{O}_2$ ), **5)** traces of metals and **6)** presence of enzymes. All these factors are primordial and their study becomes inevitable. Nevertheless, it is complex to distinguish the effect of each factor because their impacts are simultaneous.

### ▪ Fatty acid composition of oils

A high number of unsaturations in fatty acids leads to a fast rate of oxidation.<sup>153</sup> Indeed, as reported in **table 1.10**, the hydrogen abstraction by a free radical is easier in the case of  $\alpha$ -linolenic acid than for linoleic and oleic acids because of their two, one and zero bis-allylic hydrogens respectively. Therefore, the oxidation rate and the amount of the primary oxidation compounds formed depend on the chemical structures of oils.<sup>154, 155</sup> As reported by Vever-Bizet *et al.*, tri-unsaturated fatty acid ( $\alpha$ -linolenic acid) is photooxidized faster than di-unsaturated fatty acid (linoleic acid) and then than mono-unsaturated fatty acid (oleic acid) and saturated compound (stearic acid).<sup>156</sup>

Fatty acid	Chemical structure	$10^{-4} \times$ Oxidation rate ( $\text{M}^{-1} \cdot \text{s}^{-1}$ )
Stearic acid (C18:0)		1.2
Oleic acid (C18:1)		5.3
Linoleic acid (C18:2)		7.3
$\alpha$ -Linolenic acid (C18:3)		10.4

**Table 1.10: Photooxidation rate of saturated, mono, di- and tri-unsaturated fatty acids**<sup>156</sup>

### ▪ Temperature and light

The autoxidation of oil increases with the improvement of the temperature.<sup>66, 157</sup> Moreover, a low UV wavelength is more critical on oils than UV with high wavelength because unsaturations could be changed into radicals by abstraction of hydrogen as expressed by the **table 1.11**.<sup>68</sup>

Bond	C=C	O-H	C-H	C-O	C-C	C-N	O-O
Wavelength (nm)	195	257	289	331	342	390	759

**Table 1.11: UV wavelengths necessary for the cleavage of typical bonds**<sup>68</sup>

### ▪ Concentration and type of oxygen

The oxidation of oil starts when the three main components are put together (*i.e.* oil, oxygen and catalysts). High concentration of oxygen leads to a stronger oxidation.<sup>158</sup> For example, Min and Wen described that the rate constant for oxygen disappearance in soybean oil containing 8.5 ppm of dissolved water is three times higher than that for oil containing only 2.5 ppm of dissolved oxygen.

The strong effect of dissolved oxygen in the oxidation of oils is improved with the increase of the temperature, the presence of light or traces of metals.<sup>66</sup>

The oxidation rate between oil and oxygen depends on the type of oxygen. Indeed,  $^1\text{O}_2$  is more reactive than  $^3\text{O}_2$  because it can react directly with lipid whereas ground state oxygen react just with the lipid radical  $\text{L}^\bullet$ . As described by Rawls and Van Santen, methyl linoleate reacts faster with singlet oxygen (1450 time faster) than with ground state oxygen.<sup>92</sup>

- *Free fatty acids*

Free fatty acids are minor components in oil. They are more sensitive to oxidation than esterified fatty acids. Indeed, given the lipophilic behavior of the oil, the free fatty acids are not well solubilized because of their acid function and are concentrated to the oil surface.<sup>35</sup> The surface tension decreases and conversely, the diffusion of oxygen increases leading to a stronger oxidation of oils.<sup>159</sup>

- *Metal ions as catalyst of oxidation*

The metals with redox potentials are the most important initiators of the oxidation of oils, food and biological systems. Indeed, they are ubiquitous, actives and only traces of metals are sufficient to catalyze the oxidation. Only compounds capable to transfer one electron to oils and dioxygen play a role in the catalysis of oxidation (*i.e.* cobalt, iron, copper, manganese and vanadium). Indeed, they are involved in the Fenton reaction which produces hydroxyl radicals leading to a fast oxidation process. However, metal ions which transfer two electrons (*i.e.*  $\text{Sn}^{2+}$  and  $\text{Tl}^{2+}$ ) are not active.<sup>160</sup> Copper increases about 50 times the decomposition of hydroperoxides and hydrogen peroxide than ferrous ions  $\text{Fe}^{2+}$  which, in turn, are 1000 times more active than ferric ions  $\text{Fe}^{3+}$ .<sup>68</sup> The rate constant of oils oxidation is increased by the presence of metals because they reduce the activation energy of the initiation step from 104 to 63 kJ/mol.<sup>35</sup>

The mechanisms related to the catalysis of oxidation are very complex and depend on various factors such as: **1)** the metal and complex formed, **2)** the chelating agent, **3)** the redox potential of metal and complexes formed, **4)** the solvent and **5)** the availability of oxygen and hydroperoxides formed. There is two kind of oxidation by metals: **1)** the direct initiation by metals with high valence electrons allowing the formation of alkyl radicals by electron abstraction of a double bond<sup>68</sup> and **2)** the indirect initiation *via* hypervalent complexes metal-oxygen<sup>161</sup> which catalyze the introduction of oxygen into the C-H bonding leading to the formation of epoxides, ketones and alcohols.

- *Enzymes as catalysts of oxidation*

The enzymes are proteins used in small concentration which catalyze a reaction without modification of them.<sup>162</sup> They can react selectively with only one compound in a complex mixture. Their classifications are based on six categories.<sup>162</sup> Some of them play an important role in the oxidation of lipids (*i.e.* lipoxygenase and hydroperoxide liase). They can either oxidize fatty acids into hydroperoxides or catalyze the degradation of hydroperoxides.

Nevertheless, their actions are influenced by some parameters such as: **1)** the pH of the solution (they are more efficient between 5 and 9), **2)** the temperature (it is optimal in a range from 40 to 50 °C) and **3)** the concentration of enzymes and substrates.

- *Antioxidants*

Edible oils naturally contain antioxidants as  $\alpha$ -tocopherol, flavonoids, carotenoids, phenolic compounds and sterols. These compounds are present in minor amount but they play an important role in the stability of oils.<sup>163</sup> They are also deliberately added to oils in order to increase their stability against oxidation. The antioxidants are capable to enhance the induction period and lower the kinetics of oxidation. They trap the free radicals, reduce metals and deactivate singlet oxygen.<sup>164</sup> The study of the mechanism and the impact of a large number of natural and synthetic phenolic antioxidants will be discussed at the chapter 3.

### 3. Separation and analyzes of fatty acids and oxidized lipids

This part deals with the main techniques used to analyze and separate the food components. Moreover, as oxidized lipids have a strong impact on the degradation of food organoleptic properties, we focused on the analytical techniques applied for the separation of oxidized lipids.

#### 3.1 Separation and analyzes of non-oxidized lipids

##### 3.1.1 Nuclear Magnetic Resonance (NMR)

Proton and carbon nuclear magnetic resonance ( $^1\text{H}$  NMR and  $^{13}\text{C}$  NMR) spectroscopy is used to identify non-oxidized food lipids as entire natural glyceride oils.<sup>165</sup> This technique could be useful not only for the identification, but also for the quantification of oil components such as fatty acids and fatty acid esters.<sup>165-168</sup> A lot of publications are dedicated to the quantification *via*  $^1\text{H}$  NMR of omega-3 fatty acid<sup>169, 170</sup> such as docosahexaenoic acid (DHA).<sup>171</sup>  $^{13}\text{C}$  NMR is a rapid and non-invasive method to determine the composition of oils thanks to the relative intensities of methylenic, vinylic and ester carboxyl resonances.<sup>172</sup> As an example, Siddiqui *et al.* attributed vinylic and allylic carbon resonances to the DHA and EPA present in fish oil.<sup>173</sup>

##### 3.1.2 Gas Chromatography (GC)

Triglycerides are converted into methyl ester derivatives (FAMES) before analysis by gas chromatography (GC). GC of FAMES is the most popular approach for the identification of fatty acids in natural materials. Gas chromatography with flame ionization detector (FID) is used to determine the percentage contribution of FAMES to the fatty acid profile in food<sup>174</sup> *via* the comparison with identical retention times of standards.<sup>175, 176</sup> Nevertheless, because of the large structural variety of fatty acids, coelutions are unavoidable. Moreover, *cis/trans* isomers of polyunsaturated fatty acids are not separated leading to important errors.

In order to improve the selectivity of GC analysis, an Electron Ionization Mass Spectrometry (EI-MS) can be used as detector.<sup>177</sup> Low fatty acid content could be analyzed and this method was recommended for the peak identification of FAMES and determination of their relative abundance.<sup>176</sup> Daughters obtained from the fragmentation of various FAMES (*i.e.* stearic, oleic, linoleic and  $\gamma$ -linolenic acids) allow to identify the parent compounds using the Selected Ion Recording mode (SIR).<sup>177</sup>

Nevertheless, the position of the double bonds is usually not directly available. Moreover, GC analysis has some drawbacks: **1)** the presence of heat-labile compounds affects the quantification of

FAMES, **2**) the polyunsaturated carbon chain of fatty acids may undergo structural changes and decomposition under high temperature, **3**) it is not possible to collect the separated fractions for further analysis and **4**) it frequently requires derivatizations step being time-consuming.<sup>178, 179</sup> For these reasons, analytical methods involving liquid chromatography (LC) are more often investigated nowadays.

### 3.1.3 High Performance Liquid Chromatography (HPLC)

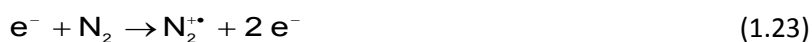
#### ▪ UV detection

FAMES are strongly UV-absorbing at 234 nm because of double bonds. The absorbance depends on the number of double bonds. Carvalho *et al.* and Di Nicola *et al.* described the chromatographic analysis of mono-, di-, tri-acylglycerides and FAMES by LC-UV analysis.<sup>174, 180</sup>

Even if this analytical method has satisfactory repeatability, it has an important drawback. In fact, all the unsaturated compounds present in the analyzed mixture (*i.e.* polyterpenes, polyphenolic antioxidants) are also detected. Moreover, saturated compounds (*i.e.* methyl palmitate and stearate) do not absorb in UV region, making them invisible to UV detection. Consequently, LC is more often coupled to mass spectrometry.

#### ▪ Atmospheric Pressure Chemical (APCI) and ElectroSpray (ESI) Ionizations mass spectrometry

Coupled with atmospheric pressure chemical ionization (APCI) mass spectrometry, liquid chromatography becomes a relevant technique of separation<sup>181</sup>. It is a soft ionization technique but not as soft as ElectroSpray ionization (ESI) because charged ions are not generated in APCI source and it operates at high temperature (350 - 550 °C).<sup>182</sup> This technique is used preferentially to analyze small, thermally stable polar and non polar compounds. Indeed, this ionization technique could be used for the analysis of FAMES but not for hydroperoxides. The electrons ionize nitrogen (**Eq. 1.23**) in the source and the ionized nitrogen reacts with the molecules of solvent. Charged solvent species are formed through a series of gas-phase reactions (**Eqs. 1.24 to 1.25**) and the analytes (M) are finally ionized (**Eq. 1.26**)<sup>182</sup>.



The gas-phase reactions of acetonitrile and unsaturated FAMES in the APCI source provide  $[M+C_3H_5N]^{+\bullet}$  adducts and their fragmentation leads to unambiguous localization of double bonds. Vrkoslav *et al.* make the difference between methyl oleate (FAME, 18:1, n-9) and methyl vaccinate (FAME, 18:1, n-7).<sup>183</sup> Even if the molecular peaks are the same, the fragmentation of parent adducts implies the formation of specific daughters (**Fig. 1.30**). Moreover, they separated FAMES of blackcurrant oil and identified unsaturated FAMES not seen by GC/MS.<sup>183</sup>

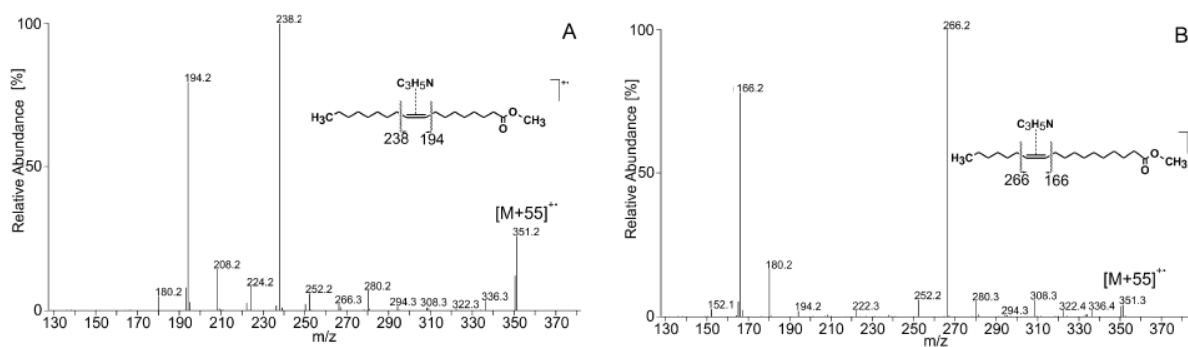


Figure 1.30: APCI MS/MS spectrum of the  $[M+55]^{+}$  adduct of methyl oleate (FAME, 18:1, n-9) (A) and methyl vaccinate (FAME, 18:1, n-7) (B)<sup>183</sup>

LC-ESI-MS (Electrospray Ionization) is also used for the analysis of FAMES. ESI is one of the most important ionization techniques for the coupling of liquid chromatography to a mass spectrometer. The solvent of charged droplets is evaporated leading to a reduction of their diameter. Continuous depletion and fission of droplets by “Coulomb explosion” lead to the concentration of charges and analytes in a drop. For example, adducts formed with  $\text{Na}^+$  (Eq. 1.27) are then transferred to the mass quadrupole for analysis.<sup>182</sup>



This technique is particularly suitable for polar organic compounds that cannot be analyzed by gas chromatography such as hydroperoxides.

▪ *Chemical Ionization and Collision-Induced Decomposition (CID) mass spectrometry*

The analysis of molecular adducts by addition of alkali ions to a molecule *via* chemical ionization (CI) has been first proposed by Hodges and Beauchamp.<sup>184</sup> The binding energy  $D(\text{B}-\text{M})^+$  also called enthalpy of the reaction ( $\Delta H$ ) of a Lewis base (B) to an alkali ion ( $\text{M}^+$ ) must be large enough to allow a significant stable population of the complex formed (Eq. 1.28).

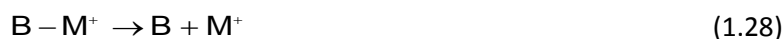


Table 1.12 points out the thermodynamic data (enthalpy  $\Delta H^\circ$ , entropy  $\Delta S^\circ$  and free energy  $\Delta G^\circ$ ) related to the equation 1.28. Hodges and Beauchamp showed that the enthalpy ( $\Delta H^\circ$ ) and free energy ( $\Delta G^\circ$ ) decrease from  $\text{Li}^+$  to  $\text{Cs}^+$ . Consequently,  $\text{Li}^+$  is the preferred alkali ion reagent compared to  $\text{Na}^+$ ,  $\text{K}^+$ ,  $\text{Rb}^+$  and  $\text{Cs}^+$  for the chemical ionization of samples.<sup>184</sup> Therefore, the complexation of  $\text{Li}^+$  with  $\text{H}_2\text{O}$  is favored instead of the reverse reaction.

M	$\Delta H^\circ$ <sup>a</sup>	$\Delta S^\circ$ <sup>b</sup>	$\Delta G^\circ$ <sup>a</sup>
$\text{Li}^+$	34.0	23.0	25.5
$\text{Na}^+$	24.0	21.5	17.6
$\text{K}^+$	17.9	21.6	11.4
$\text{Rb}^+$	15.9	21.2	9.6
$\text{Cs}^+$	13.7	19.4	7.9

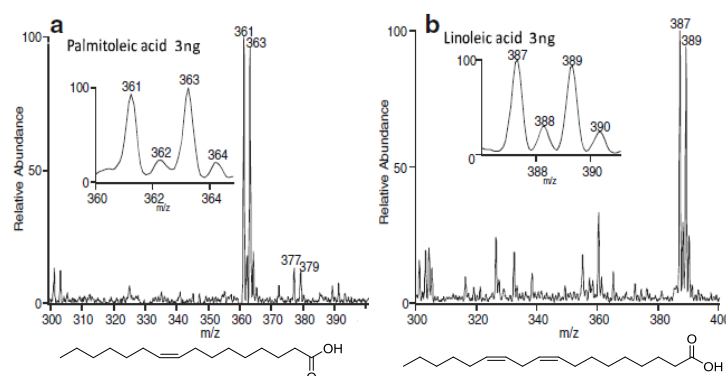
<sup>a</sup>kcal.mol<sup>-1</sup>, <sup>b</sup>J/K

Table 1.12: Thermodynamic data for the process  $\text{B}-\text{M}^+ \rightarrow \text{B} + \text{M}^+$  where  $\text{B} = \text{H}_2\text{O}$

The relative binding energies of several molecules toward  $\text{Li}^+$  have been determined by trapped ion cyclotron resonance techniques and highlight that a wide range of compounds including alkenes have a sufficiently large binding energies with  $\text{Li}^+$  to be detectable at low concentrations.<sup>185</sup> Coupled with liquid chromatography, collision-induced decomposition (CID) analysis is a relevant method to analyze fatty alcohols, FAMES and acids *via* the formation of complexes with alkali ions characterized by typical fragmentations.<sup>186</sup> Indeed, the decomposition of metal ion complexes produces significantly more information than the decomposition of  $[\text{M}+\text{H}]^+$ .

▪ *Coordination IonSpray Mass Spectrometry (CIS-MS)*

Coordinating ions able to form charged complexes with analytes may be used to analyze unsaturated compounds. These complexes are detected by mass spectrometry with Direct Liquid Injection (DLI). This new technique is called Coordination-IonSpray Mass Spectrometry (CIS).<sup>187</sup> While olefins and polyolefins (*i.e.* terpenes, vitamins, unsaturated fatty acids and steroids) are detected with poor sensitivity with ESI-MS, CIS analysis enhances the mass signals. Bayer *et al.* showed that unsaturated compounds form highly stable  $\pi$  or  $\pi$ -allyl complexes with metals such as copper ( $\text{Cu}^{\text{I}}$ ), nickel ( $\text{Ni}^{\text{II}}$ ), palladium ( $\text{Pd}^{\text{II}}$ ), platinum ( $\text{Pt}$ ) and silver ( $\text{Ag}^{\text{I}}$ ).<sup>187</sup> This improves their detection and enhance their mass signal compared to the analysis without coordinate ions.<sup>188</sup> Silver ion adducts can be easily identify in a MS spectrum due to the natural isotopic abundance of silver (52:48) characterized by the doublet isotopic pattern of  $[\text{M}+\text{Ag}^{107}]^+$  and  $[\text{M}+\text{Ag}^{109}]^+$  (**Fig. 1.31**).<sup>127</sup>



**Figure 1.31:** Mass spectra of silver adducts using a solvent spray of  $\text{MeOH}:\text{H}_2\text{O}$  doped with  $5.5 \mu\text{g}/\text{mL}$  of  $\text{AgNO}_3$  for a) 3 ng of palmitoleic acid and b) 3 ng of linoleic acid<sup>188</sup>

Direct coupling of separation methods such as liquid chromatography with CIS-MS is a new applicable analytical method. The complexes are formed after the separation and before entry into the ion source.<sup>189</sup> Bayer *et al.* described the separation of unsaturated FAMES by pressure-assisted capillary electrochromatography (pCEC) coupled with CIS-MS for the detection of silver complexes.<sup>187, 190</sup> Moreover, Medvedovici *et al.* developed the analysis of jojoba oil by the same methodology.<sup>191</sup> Neither APCI nor ESI ionizations with mobile phase additives (*i.e.* formic acid, acetic acid and ammonium formate) provided ions but excellent ionization was obtained by post-column injection of  $\text{Ag}^+$ .<sup>191</sup>

- “Argentation” chromatography

Based on the selectivity of coordination between silver ion and double bonds, new analytical techniques called “argentation” chromatography appears and improve the analysis and separation of lipids.<sup>192</sup> Thin-layer chromatography (TLC) has been used with a modification of layers by silver nitrate or with a silver nitrate solution as eluent.<sup>193</sup> As an example, Scholfield *et al.* analyzed linseed oil methyl ester *via* a resin of column treated with silver nitrate.<sup>194</sup>

Ghebreyessus *et al.* developed a method dedicated to the modification of fatty acid composition of oils in order to create new properties.<sup>195</sup> Indeed, some vegetable oils are composed by highly unsaturated fatty acid (*i.e.* linolenic acid) and are prone to oxidation which reduces their application as cooking oils. Moreover, saturated fatty acids are unsuitable when the oils are dedicated for drying. In that way, *via* a solid-phase extractant  $\text{AgNO}_3/\text{SiO}_2$ , the composition of the final FAMES mixture is different from the starting crude (**Fig. 1.32**).

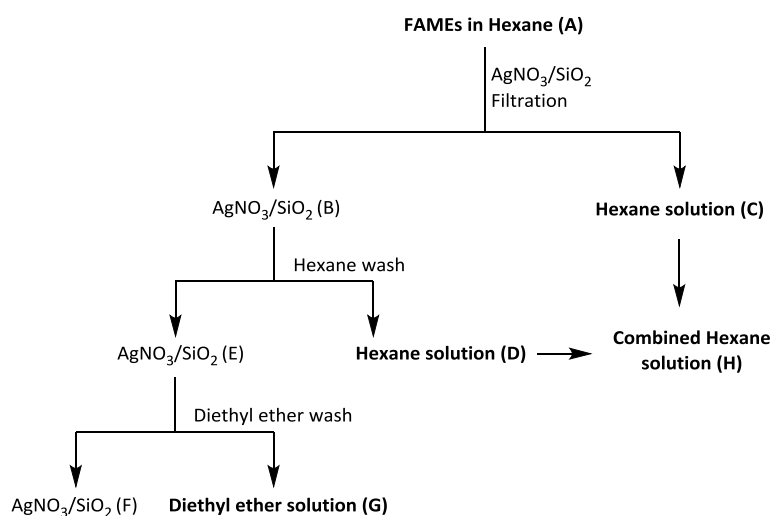


**Figure 1.32: General procedure of FAMES extraction<sup>195</sup>**

Saturated (*i.e.* palmitate and stearate) and monounsaturated (*i.e.* oleate) FAMES are firstly extracted with hexane eluent (**H**) because they are not or weakly coordinate with silver ion due to their low number of unsaturations. Polyunsaturated FAMES (*i.e.* linoleate and linolenate) are more coordinated with silver ion and are not eluted with non polar solvent but rather with polar eluent (diethyl ether **G**). The diethyl ether fraction is enriched with polyunsaturated compound whereas the hexane fraction contain most of saturated and monounsaturated FAMES (**Table 1.13**).

FAMES	Hexane fraction H (wt%)	Diethyl ether fraction G (wt%)
16 :0	6.8	0.0
18 :0	3.5	0.0
18 :1	78.2	35.0
18 :2	9.8	43.1
18 :3	1.7	21.6
18 :2/18 :1 ratio	0.13	1.2

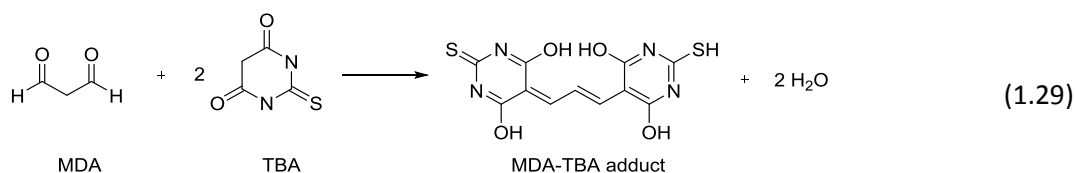
**Table 1.13: FAMES composition (wt%) of the hexane (H) and diethyl ether (G) fraction from an extraction of methyl canolate with 2.0 g of 20%  $\text{AgNO}_3/\text{SiO}_2$ <sup>195</sup>**

### 3.2 Separation and analysis of lipid oxidation products

Many different oxidized products (*i.e.* hydroperoxides, cyclic peroxides, volatile organic compounds, epoxides) are obtained by autoxidation and/or photooxidation of lipids. They are responsible of the loss of organoleptic properties and nutraceutical effect of food. Therefore, the identification and the quantification of these oxidized lipids is a relevant challenge in order to evaluate the advancement of oil degradation and fight against their formation.<sup>196</sup> The most effective methods used by authors are described in the following part.

#### 3.2.1 TBARS, FOX and Iodometric assays

The Thiobarbituric Acid Reactive Substances (TBARS) assay is one of the most frequently methods used to assess lipid peroxidation. This test is usually performed by heating a lipid oxidized mixture and thiobarbituric acid (TBA) in an acidic medium. TBA reacts with malondialdehyde (MDA) and form a red pigment which has a maximum of absorption at 532 nm.<sup>127</sup> This test measures the MDA present in the sample, which is issue from the decomposition of some primary and secondary peroxidized lipid (**Eq. 1.29**). Lenz *et al.* analyzed the oxidation of low density lipoprotein (LDL) and showed a decrease of linoleate and arachidonate content which go along with an increase of TBAR substances and hydroperoxides.<sup>197</sup>



The ferrous oxidation of xylenol (FOX) assay was developed by Wolff *et al.* to detect the hydroperoxides formed from lipid oxidation.<sup>198</sup> Hydroperoxides react with an excess of ferrous ion ( $\text{Fe}^{2+}$ ) in the presence of the xylenol orange dye (XO) (**Fig. 1.33**).

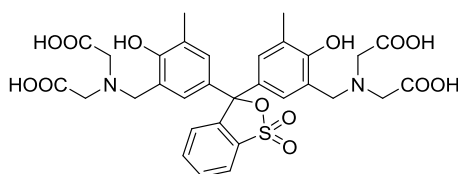
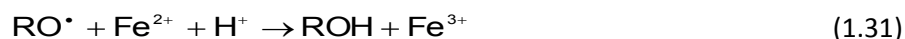


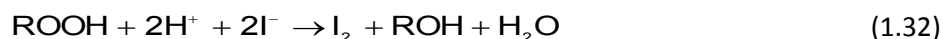
Figure 1.33: Chemical structure of the xylenol orange dye (XO)

The amount of the ferric iron ( $\text{Fe}^{3+}$ ) generated is measured as the Fe-XO complex form at 560 nm (**Eqs. 1.30** and **1.31**).<sup>199</sup> This method finds its application on the study of linoleic acid<sup>200</sup>, LDL<sup>201</sup> and edible oils<sup>202</sup> oxidations.



Nevertheless, both of TBARS and FOX assays are non specific methods of hydroperoxides and caution is recommended when the analysis of oxidized biomolecules as endoperoxides are undertaken.<sup>203</sup>

The iodometric titration is based on the reaction of hydroperoxides with an excess of iodide ions ( $\text{I}^-$ ) in acetic medium (**Eq. 1.32**). The  $\text{I}_2$  generated is titrated by a sodium thiosulfate solution with starch (**Eq. 1.33**).<sup>204</sup>



The method has a good specificity and exact 1/1 stoichiometry between the amount of peroxide reacting and iodine produced, allowing the quantification of hydroperoxides.<sup>205</sup> The reaction of ROOR peroxides and 4-membered cyclic peroxides follow analogous pathways (Eq. 1.34).<sup>204</sup>

However, the limits of this iodometric titration are well known, namely, a low sensibility and selectivity with the apparition of side reactions such as: **1)** addition of iodine on lipid double bonds, **2)** oxidation of iodine by dissolved oxygen and **3)** variable reactivity of hydroperoxides. Accordingly, these 3 assays are too simple to elucidate the chemical structure of complex mixtures of peroxides.

### 3.2.2 Fourier Transform Infrared Spectroscopy (FTIR)

Fourier Transform Infrared Spectroscopy (FTIR) is a simple and rapid method to follow the oxidation of oils and fats. It provides information on the characteristics, composition and/or chemical changes taking place in oils. The oxidative state of oil can be defined in terms of hydroperoxides, alcohol percents and total carbonyl content.<sup>206, 207</sup> The progressive increase of O-H stretching vibration of hydroperoxides with time goes along with a decrease of C-H and CH<sub>2</sub> stretching vibration of *cis* double bonds. This loss of *cis* double bond is largely attributed to an oxygen uptake effect. Moreover, the formation of hexanal and 2-hexenal during the oxidation process could be shown by characteristic absorptions in the carbonyl region at 1750 – 1650 cm<sup>-1</sup>.<sup>206, 207</sup>

### 3.2.3 Nuclear Magnetic Resonance (NMR)

It is possible to follow the oxidation change of food by monitoring the formation of primary and secondary oxidation products by proton (<sup>1</sup>H NMR) and carbon (<sup>13</sup>C NMR) nuclear magnetic resonance.<sup>208-210</sup> For example, compared to the original spectrum of sunflower oil, there is a decrease of the proportion of olefinic, bis-allylic and allylic protons.<sup>211, 212</sup> Hydroperoxide functions and *Z,E* or *E,E* conjugated dienic systems formed could be also identified. Indeed, signals near 8.4 ppm are due to the presence of labile proton from hydroperoxides. Moreover, there is the apparition of signals related to protons of some secondary oxidation compounds (*i.e.* aldehydes) in the spectral region between 9.4 and 9.8 ppm.

The oxidation products of edible oils can also be analyzed by <sup>13</sup>C NMR which provides insight into the nature of lipid mixtures. Saeed *et al.* identified the peaks of the carbon atom carrying the hydroxyl groups (87 ppm)<sup>213</sup> with derivatization of hydroperoxides whereas intact hydroperoxides can be also analyzed as revealed by Pajunen *et al.*<sup>214</sup>

### 3.2.4 Gas Chromatography (GC)

The measurement of oxidized species by GC-MS has been widely developed *via* chemical ionization in the negative ion mode due to its superior sensitivity and specificity.<sup>215</sup> However, hydroperoxides are thermally instable. Indeed, separation and chemical derivatizations steps are required before the GC-MS analysis. Allylic hydroperoxides<sup>42, 72, 76, 80, 83, 85, 119-123, 125, 216</sup> and secondary oxidation products<sup>42, 71, 82, 87, 91, 119, 125, 126, 217</sup> from (poly)unsaturated FAMES are largely analyzed thanks

to: **1**) reduction to the corresponding alcohols with sodium borohydride ( $\text{NaBH}_4$ )<sup>42, 72, 76, 80, 83, 85, 216</sup>, potassium iodide (KI)<sup>72, 80, 85, 216</sup> or tin chloride ( $\text{SnCl}_2$ )<sup>82, 91</sup>, **2**) catalytic hydrogenation to saturated hydroxyl-esters<sup>83, 85, 87, 119, 121, 123, 125, 217</sup> and **3**) silylation after reduction leading to trimethylsilane (TMS) derivatives<sup>42, 72, 80, 82, 83, 87, 91, 119, 122, 125, 126, 216, 217</sup>. Nevertheless, it is a laborious work and mass spectrometry is more often coupled with liquid chromatography for the analysis of oxidized lipids.

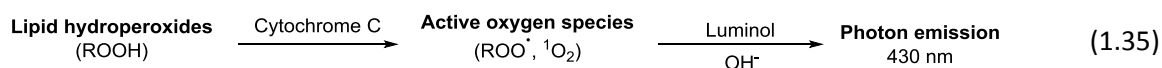
### 3.2.5 High Performance Liquid Chromatography (HPLC)

#### ▪ UV detection

The assessment of the lipid peroxidation *via* liquid chromatography and UV detection has been realized by the measurement of conjugated diene of lipid hydroperoxides. Kenar *et al.* developed a LC-UV method at 234 nm to identify and separate hydroperoxides obtained from the autoxidation of cholesteryl linoleate.<sup>218</sup> However, as for the identification of FAMES by LC-UV, this method is limited by the interfering compounds with the same UV absorption.

#### ▪ Luminol chemiluminescence detection (CL)

A specific detection discriminating hydroperoxides at the picomole<sup>219</sup> level from hydroxyl and non-oxidized compounds has been developed by Miyazawa *et al.* *via* luminol chemiluminescence detection (CL) coupled to liquid chromatography.<sup>220</sup> They reported the analysis of methyl linoleate<sup>219</sup>, arachidonic acid<sup>219</sup>, cholesterol<sup>219</sup> and phosphatidylcholine<sup>220</sup> hydroperoxides with a CL-LC method in which a cytochrome c/luminol mixture was used as hydroperoxide specific CL reagent. Hydroperoxides react with cytochrome C and active oxygen species. Then, luminol is oxidized under alkaline conditions and CL is emitted (Eq. 1.35).<sup>219</sup>



#### ▪ $\text{Ag}^+$ Coordination Ion Spray Mass Spectrometry (CIS-MS)

As discussed previously, Bayer *et al.* reported the use of coordinating ions to ionize highly electrophilic compounds such as FAMES, terpenes, aromatics and vitamins.<sup>187</sup> This analytical technique is also a powerful tool for the analysis of intact peroxide mixtures.<sup>44</sup>

Direct liquid injection (DLI) is one of the most frequently used techniques to analyze lipid oxidized products since it just requires a mass spectrometer without separating method. Havrilla *et al.* analyzed cholesteryl linoleate monohydroperoxide in the form of  $[\text{M}+\text{Ag}]^+$  adduct.<sup>44</sup> The collision induced dissociation (CID) experiment on this adducts gives fragment ions related to a loss of water and hexanal.<sup>44</sup> Moreover, Yin *et al.* analyzed the oxidation mixture of eicosapentaenoic acid (EPA) methyl ester and pointed out the formation of adducts between  $\text{Ag}^+$  and 5-mono-hydroperoxide ( $m/z$  455/457), monocyclic peroxide ( $m/z$  487/489), bicyclic endoperoxides ( $m/z$  519-521) and tricyclic peroxide ( $m/z$  551/553) (Fig. 1.34).<sup>221</sup>

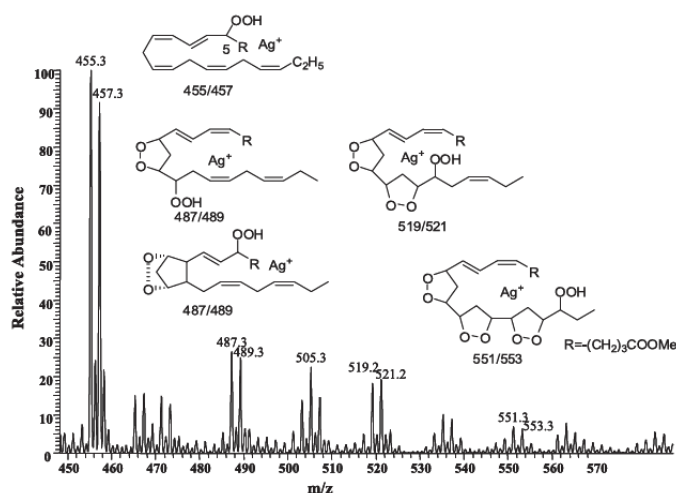


Figure 1.34: Direct liquid injection (DLI) analysis of an oxidized mixture of EPA methyl ester using  $\text{Ag}^+$  CIS-MS method<sup>221</sup>

Collision Induced Dissociation (CID) experiments allow identifying different oxidized products which have the same precursor ion. The fragmentation patterns of monocyclic peroxide (**Fig. 1.35a**) and bicyclic endoperoxides (**Fig. 1.35b**) are quite different even though they have the same precursor ion at 487/489 m/z.

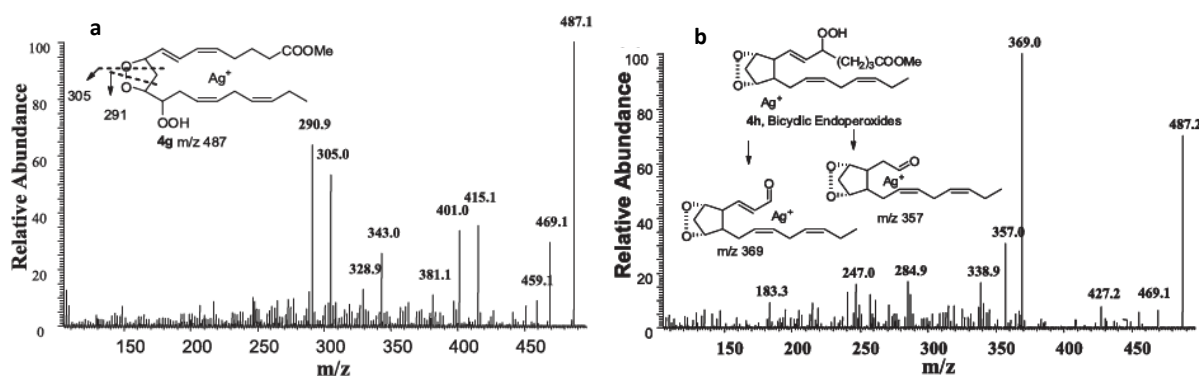


Figure 1.35: CID analysis of an oxidized mixture of EPA methyl ester using  $\text{Ag}^+$  CIS-MS, a) monocyclic peroxide (m/z 487), b) bicyclic endoperoxides (m/z 487)<sup>221</sup>

It was suggested that the fragmentation pattern observed is due to the Hock fragmentation of the silver ion hydroperoxide complex (**Fig. 1.36**). It affords an unambiguous information about the position of hydroperoxide on linoleate chain.<sup>44</sup>

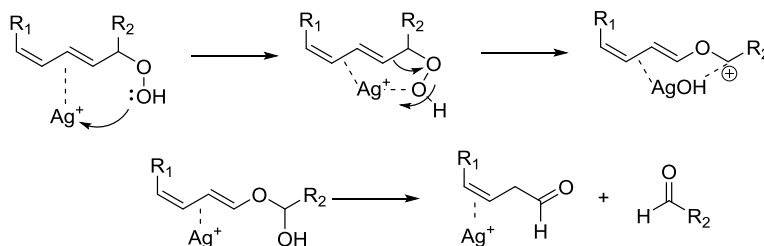


Figure 1.36: Hock fragmentation of a diene hydroperoxide promoted by silver ion<sup>44</sup>

LC coupled with  $\text{Ag}^+$  coordination ion spray-mass spectrometry (LC- $\text{Ag}^+$  CIS-MS) is made possible by post-column injection of the coordinate ion. It is a combination of powerful normal-phase separation techniques with detection methods that provide unambiguous structural information of complex peroxide compounds. Havrilla *et al.* pointed out that the Multiple Reaction Monitoring (MRM) mode, which is a specific parent-to-daughter mass conversion, clearly distinguishes the 9-

hydroperoxide from the 13-hydroperoxide.<sup>44</sup> Yin *et al.* have characterized the different diastereoisomers obtained from the oxidation of 5-mono-hydroperoxide of EPA methyl ester.<sup>221</sup> The precursor ions of interest are selected in the first MS quadrupole which are fragmented in the second quadrupole.

▪ *Electrospray Ionization mass spectrometry (ESI-MS)*

Electrospray ionization Mass Spectrometry (ESI-MS) has been widely used to study the lipid oxidation due to its sensitivity and specificity.<sup>222</sup> Tandem MS/MS technique enables the characterization of oxidation products when CID experiments are set up without liquid chromatography separation.<sup>127</sup>

Authors investigated the formation of  $[M+NH_4]^+$  adducts for the identification of fatty acid hydroperoxides<sup>223</sup>, hydroperoxy cyclic peroxides and di-hydroperoxides of methyl linoleate, linolenate<sup>224</sup> and diacyl peroxides.<sup>225</sup> Nevertheless, in the absence of alkali metals, CID of protonated hydroperoxide produced no fragment ions or very little fragmentation.<sup>223</sup> Ito *et al.* showed that in the presence of alkali metals, especially sodium, CID of hydroperoxide isomers leads to structure-diagnostic fragment ions that were useful to elucidate the hydroperoxy group position.<sup>226</sup>

Some differentiations are pointed out between various ions. Very intense fragment ions were observed with sodium compared to lithium or potassium adducts.<sup>226</sup> Moreover, Kohler and Leary published that the most significant increase in abundance of the carbohydrate adduct ionization is obtained with  $Li^+$ , which approximately 70 times more abundant than the corresponding  $[M+H]^+$ .<sup>227</sup> The affinity for alkali metal with larger ionic radius as potassium ( $K^+$ ), rubidium ( $Rb^+$ ) and cesium ( $Cs^+$ ) was sharply dropped compared to lithium ( $Li^+$ ) and sodium ( $Na^+$ ) (Fig. 1.37).

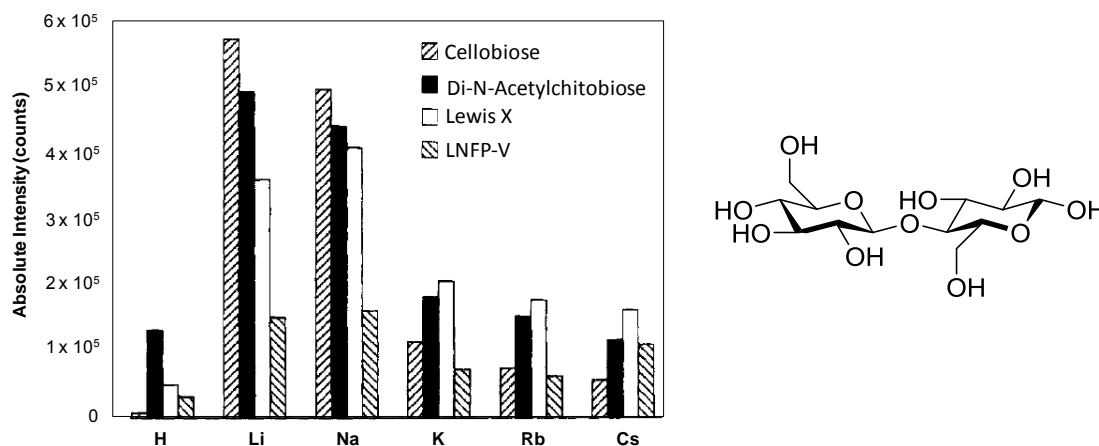


Figure 1.37: Abundance of the carbohydrate-metal complexes with  $Li^+$ ,  $Na^+$ ,  $K^+$ ,  $Rb^+$  and  $Cs^+$  and chemical structure of cellobiose<sup>227</sup>

Then, transitions are used to separate hydroperoxides contained in a crude mixture *via* LC-MS/MS method in multiple reaction monitoring (MRM) mode. 13-9Z,11E hydroperoxides of linoleic acid are separated into their different enantiomers R and S thanks to the addition of sodium acetate which improves the mass signal and fragmentations.<sup>226</sup>

The MRM mode is a powerful technique to characterize oxidized lipids. **Tables 1.14, 1.15 and 1.16** gathers all the identified products resulting from the thermal decomposition<sup>36, 68, 73</sup> of oxidized methyl oleate, linoleate and linolenate obtained *via* mechanisms of scission.<sup>68</sup> These structures could help us to identify and characterize mono-hydroperoxides by fragmentation on mass spectrometry.

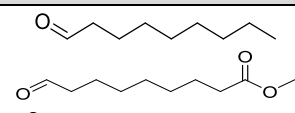
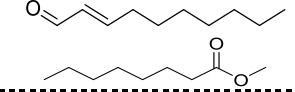
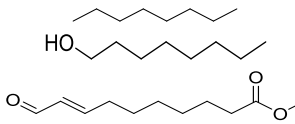
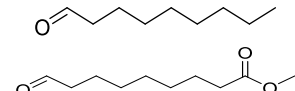
ROOH	Scission	Products	Chemical structures
<b>Methyl oleate (C18:1, <math>\omega</math>-9)</b>			
9-OOH 50%	$\alpha$	Nonanal Methyl 9-oxononanoate	
	$\beta$	2-decenal Methyl octanoate	
-----			
10-OOH 50%	$\alpha$	Octane 1-octanol Methyl 10-oxo-8-decenoate	
	$\beta$	Nonanal Methyl 9-oxononanoate	

Table 1.14: Products formed during the scission of hydroperoxides of methyl oleate obtained by photooxidation<sup>36, 68, 73,</sup>  
228

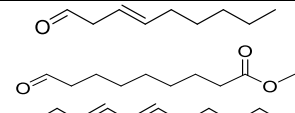
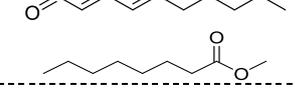
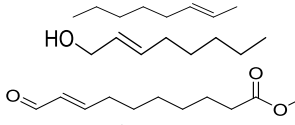
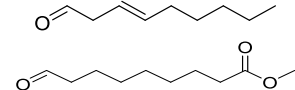
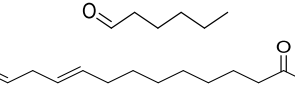
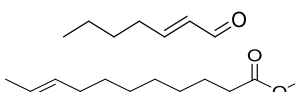
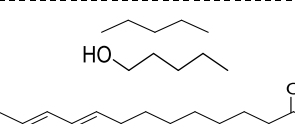
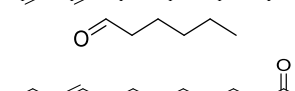
ROOH	Scission	Products	Chemical structures
<b>Methyl linoleate (C18:2, <math>\omega</math>-6)</b>			
9-OOH 31%	$\alpha$	3-nonenal Methyl 9-oxononanoate	
	$\beta$	2,4-decadienal Methyl octanoate	
-----			
10-OOH 18%	$\alpha$	2-octene 2-octen-1-ol Methyl 10-oxo-8-decenoate	
	$\beta$	3-nonenal Methyl 9-oxononanoate	
-----			
12-OOH 18%	$\alpha$	Hexanal Methyl 12-oxo-9-dodecenoate	
	$\beta$	2-heptenal Methyl 9-undecenoate	
-----			
13-OOH 33%	$\alpha$	Pentane 1-pentanol Methyl 13-oxo-9,11-tridecadienoate	
	$\beta$	Hexanal Methyl 12-oxo-9-dodecenoate	

Table 1.15: Products formed during the scission of hydroperoxides of methyl linoleate obtained by photooxidation<sup>36, 68, 73,</sup>  
228

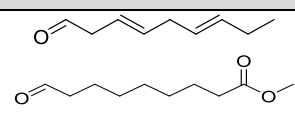
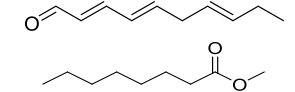
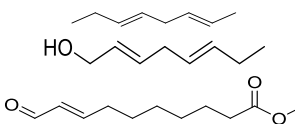
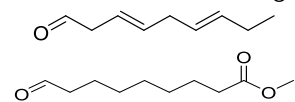
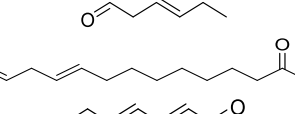
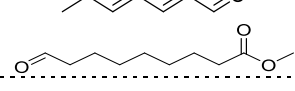
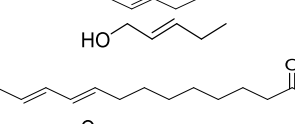
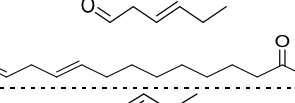
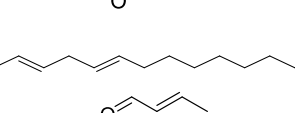
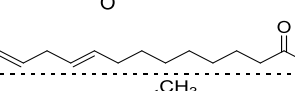
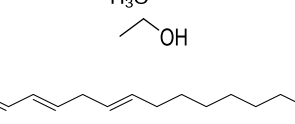
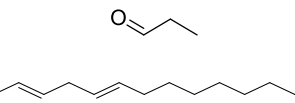
ROOH	Scission	Products	Chemical structures
<b>Linolenic acid (C18:3, <math>\omega</math>-3)</b>			
9-OOH 21%	$\alpha$	3,6-nonadienal Methyl 9-oxononanoate	
	$\beta$	2,4,7-decatrienal Methyl octanoate	
10-OOH 13%	$\alpha$	2,5-octadiene 2,5-octadien-1-ol Methyl 10-oxo-8-decenoate	
	$\beta$	3,6-nonedial Methyl 9-oxononanoate	
12-OOH 13%	$\alpha$	3-hexenal Methyl 12-oxo-9-dodecenoate	
	$\beta$	2,4-heptadienal Methyl 9-undecenoate	
13-OOH 14%	$\alpha$	2-Pentene 2-penten-1-ol Methyl 13-oxo-9,11-tridecadienoate	
	$\beta$	3-hexenal Methyl 12-oxo-9-dodecenoate	
15-OOH 13%	$\alpha$	Propional Methyl 15-oxo-9,12-pentadecadienoate	
	$\beta$	2-butenal Methyl 9,12-butadecadienoate	
16-OOH 25%	$\alpha$	Ethane Ethanol Methyl 16-oxo-9,12,14-hexadecatrienoate	
	$\beta$	Propional Methyl 15-oxo-9,12-pentadecadienoate	

Table 1.16: Products formed during the scission of hydroperoxides of methyl linolenate obtained by photooxidation<sup>36, 68, 73, 228</sup>

A lot of 5- and 6-membered oxidized compounds are also obtained from oxidized unsaturated fatty acids. Frankel studied the importance of these oxidized compounds in 1984.<sup>229</sup> He highlighted that thermal decomposition of these cyclic peroxides leads to volatiles compounds. The main cleavage is obtained between the -OOH group and the cycle leading to aldehydes and esters formations whereas the cleavage of the cycle implies the formation of aldehydes and unsaturated esters.<sup>36</sup> The cleavage on the other side of the -OOH group forms hydrocarbons and ester with small chain (Fig. 1.38).

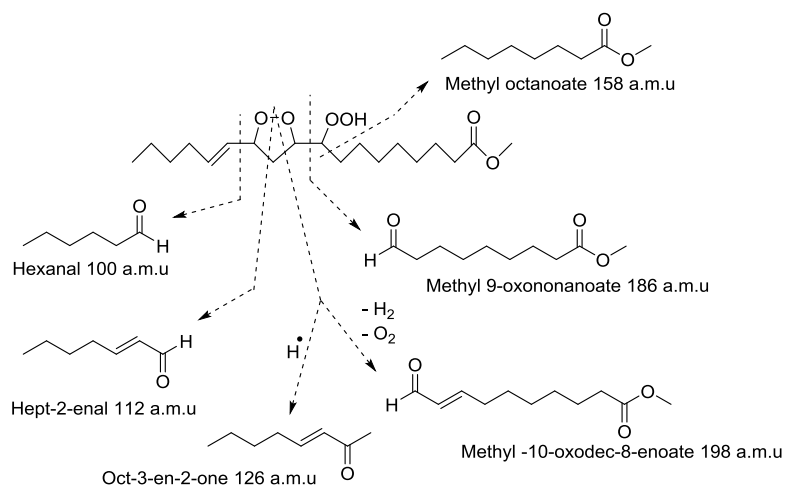


Figure 1.38: Example of the thermal decomposition of secondary cyclic oxidation compound of methyl linoleate<sup>36</sup>

## 4. Conclusion

The problematic of the degradation of food and the deterioration of their organoleptic properties are current concerns and a lot of research works address these issues. The studies dealing with autoxidation lead to the determination of the precursors of rancidity. In this way,  $\alpha$ -linolenic acid has been highlighted as the main fatty acid responsible for the deterioration of vegetable oils because of its large number of bis-allylic hydrogens.<sup>73</sup> Moreover, the origin of oxidation and the different physical or chemical pathways are abundant. **Figure 1.39** summarizes the oxidation of oils, from the initiation step to the variety of oxidized products formed.

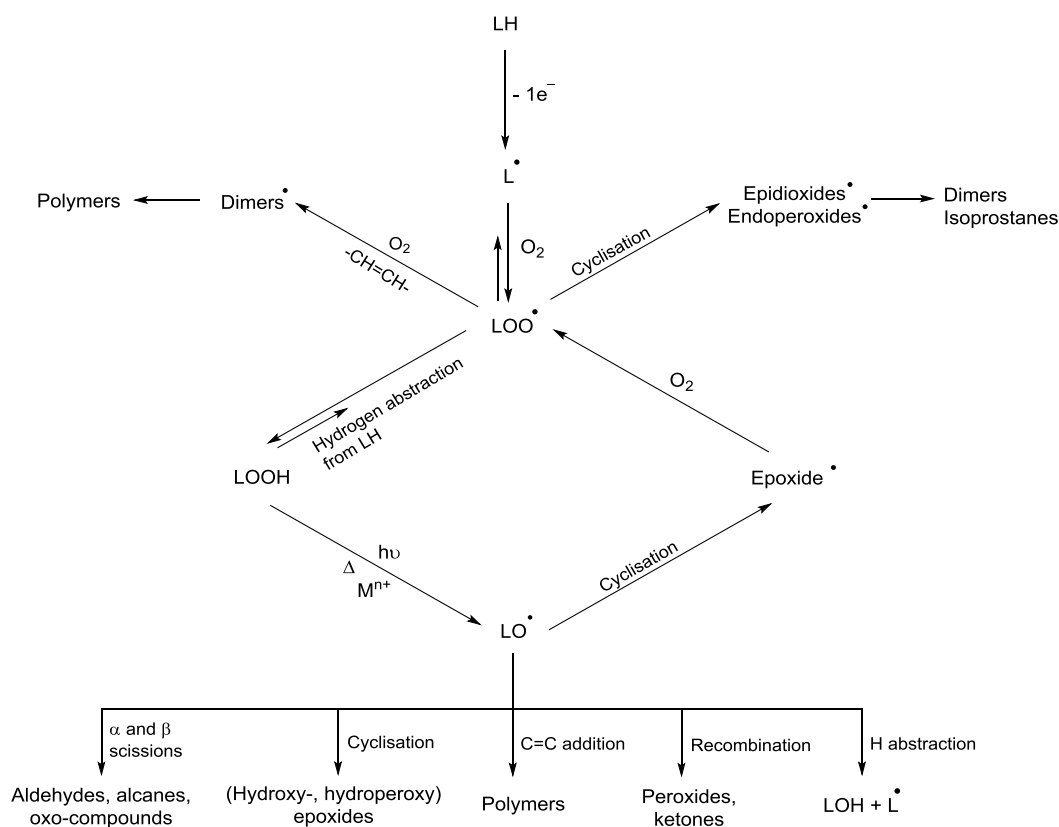


Figure 1.39: General scheme of the multiple reaction ways for the oxidation of unsaturated lipids<sup>68</sup>

There are numerous possible degradations of unsaturated fatty acids by oxygen ( $^1\text{O}_2$  or  $^3\text{O}_2$ ). Because of that, the oxidation of oils becomes an important subject of studies and the protection of oils is now a necessity. All the factors affecting the oxidation of oils such as temperature, light or the kind of oils used have to be taken into account during the studies of this phenomenon. Moreover, some catalytic metal complexes and photosensitizers naturally present in the plants are factors which influence the oxidation and the deterioration of oils. In this way, the nature provides some efficient inhibitors such as natural phenolic antioxidant which are studied in **chapters 3** and **4**.

Most publications related to the analyses of FAMES and oxidized derivatives are focused on 3 types of analytical techniques: **1)** derivatizations and reduction of hydroperoxides before analysis by GC-MS<sup>43, 230, 231</sup>, **2)** LC separation coupled with UV detection<sup>174</sup> and **3)** direct analysis *via* mass spectrometry.<sup>181, 183</sup> Nevertheless, only few of them studied the influence of alkali ions for the detection of oxidized lipid derivatives by ESI-MS method. Moreover, LC-Ag<sup>+</sup> CIS-MS technique is a new interesting powerful method still barely used for the detection of oxidized omega-3 oils.

In that way, lipid hydroperoxides were prepared by the photooxidation of the prevalent FAMES (methyl oleate, linoelate and linolenate) found in the linseed oil rich in omega-3. Moreover, the singlet oxygenation of terpenes derivatives was undertaken in order to work on tri-substituted double bonds which change the reactivity towards  $^1\text{O}_2$ . The hydroperoxides of terpenes have also been synthesized because they are crucial allergenic compounds in fragrances and need to be analyzed to quantify their presence in formulations. The photooxidation was the smooth technique used to synthesized hydroperoxides in a short time and avoid their degradation. The hydroperoxides obtained have been analyzed and characterized first by non-damaged techniques (*i.e.* iodometric titration of hydroperoxides and LC-UV). The peroxides isolated from the reaction media have been also characterized by  $^1\text{H}$  and  $^{13}\text{C}$  NMR and a kinetic modeling study based on the disappearance of substrates was undertaken. Finally, peroxides formed by photooxidation have been analyzed by mass spectrometry coupled with liquid chromatography separation *via* collaboration with the TRACES research team of the "Institut des Sciences Analytiques" (ISA, Lyon). The **chapter 2** of this manuscript is completely dedicated to the preparation of hydroperoxides by photooxidation and their analyses.

# CHAPTER 2. PREPARATION OF HYDROPEROXIDES BY SINGLET OXYGENATION AND MASS SPECTROMETRY INVESTIGATIONS

---

## 1. Introduction

A complete knowledge on the chemical structures of a lipid peroxide mixtures is difficult to obtain as discussed in the chapter 1. Accordingly, it is a great challenge to separate and analyze traces of these oxidized products without pre-reduction or derivatization. That is why (poly)unsaturated Fatty Acid Methyl Esters (FAMES) of linseed oil (*i.e.* methyl stearate, oleate, linoleate and linolenate) composed of di-substituted double bonds were oxidized by the way of the smooth singlet oxygenation (5 °C) to get non-degraded hydroperoxides. Moreover, (poly)unsaturated terpene (*i.e.* limonene) and terpenoids (*i.e.* linalool, citronellol, citronellol caprate and geraniol caprate) were photooxidized in order to study on tri-substituted double bonds which have a higher reactivity towards  $^1\text{O}_2$ . The hydroperoxides of terpenes were also studied because they are problematic allergenic compounds in fragrances and it is important to quantify them in formulations. By using non-degradative analytical techniques (*i.e.* titration of hydroperoxides, LC-UV separation and NMR analyses), kinetic studies on the singlet oxidation of (poly)unsaturated compounds followed by a structural investigation of peroxide could be completed.

Hydroperoxides were then analyzed by ElectroSpray Ionization (ESI) and Coordination IonSpray (CIS) mass spectrometry and separated by LC-MS/MS. The increase in molecular weight of terpenic alcohols (*i.e.* citronellol and geraniol) is obtained with the grafting of a decanoate part in order to facilitate mass spectrometry (MS) analysis. Indeed, peaks corresponding to light terpenes ( $\text{MW} \approx 160 \text{ g}\cdot\text{mol}^{-1}$ ) are located in the background signal which makes the MS analysis more complicated. The influence of various ions on the metal adducts formation during the mass spectrometry analysis of (poly)unsaturated FAMES and related peroxides has been also studied *via* Direct Liquid Injection (DLI) mass spectrometry. The goal of this study is was to enhance selectively the ionization of hydroperoxides in order to be able to detect traces of peroxides into an oxidized oil system. The possible formation of peroxyhemiacetals during the oxidation of edible oils was finally investigated by reacting hydroperoxides with aldehydes since it has been shown recently that such unusual peroxide is formed in fragrances. This work was made possible by the collaboration with the TRACES research team of the "Institut des Sciences Analytiques" (ISA, Lyon).

## 2. Preparation of lipids and terpenes hydroperoxides by singlet oxygenation

### 2.1 Choice of the investigated lipids and terpenes, the singlet oxygenation process and the analytical techniques

Most terpenoids and lipids contain electron-rich double bonds capable of reacting with ground state oxygen *via* a radical reaction leading to the formation of several hydroperoxides as the first stage of oxidation. As ground state oxygen is in a triplet state ( $^3\text{O}_2$ ), its reactions with ground state organic compounds (singlet state) are generally slow at room temperature since it is a spin-forbidden process according to Wigner's rule. However, these radical reactions can be accelerated by heat, UV light, radical initiators but under such harsh conditions, hydroperoxides are partially decomposed giving secondary oxidation products.

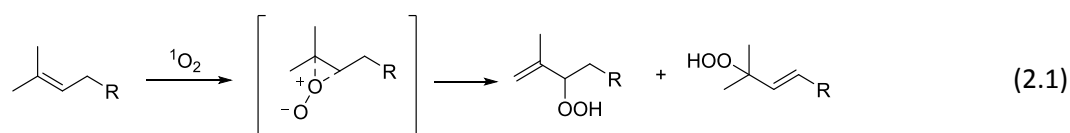
The goal of this study was to develop a method capable of detecting directly traces of hydroperoxides without any pre-derivatization steps. Therefore, we turned to singlet oxygenation to get access to intact hydroperoxides. A series of saturated and (poly)unsaturated terpenoids and FAMES have thus been photochemically peroxidized by singlet oxygen at 5 °C in order to preserve the

integrity of the formed hydroperoxides (**Table 2.1**). Three terpenoids as oil model with no, one or two double bonds have been studied. In order to well mimic the weight of (poly)unsaturated FAMES for better mass spectrometry analyses, derivatives of 3,7-dimethyl-1-octanol, citronellol and geraniol were synthesized by esterification with decanoyl chloride. Therefore, the synthesized 3,7-dimethyloctyl decanoate, citronellol caprate and geraniol caprate were photooxidized. The FAMES of the three main fatty acids found in linseed oil (*i.e.* oleic, linoleic and  $\alpha$ -linolenic acids) were also photooxidized. Finally, the photooxidation of  $\alpha$ -terpinene was also undertaken because it reacts very quickly with  $^1\text{O}_2$  and will be used as a reference for kinetic studies.

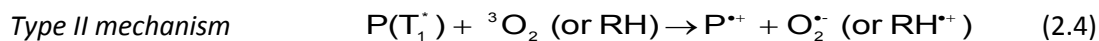
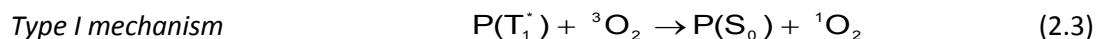
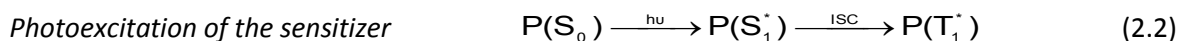
Substrate	Chemical structure
Methyl stearate	
Methyl oleate	
Methyl linoleate	
Methyl linolenate	
3,7-Dimethyloctyl decanoate	
Citronellol caprate	
Geraniol caprate	
$\alpha$ -terpinene	

**Table 2.1: Chemical structures of photooxidized substrates analyzed by mass spectrometry (MS)**

It is well documented that excited singlet oxygen ( $^1\text{O}_2$ ) readily reacts with electron-rich olefins containing allylic hydrogen according to a non-radical process called Schenck ene-reaction. Oxygen is inserted into the allylic C-H bond and there is a migration of the double bond. The reaction of  $^1\text{O}_2$  with polyisoprenic substrates does not exhibit regioselectivity and mixtures of secondary and tertiary allylic hydroperoxides are obtained (**Eq. 2.1**).



Singlet oxygen is generated *via* indirect photochemical excitation of  $^3\text{O}_2$  in the presence of specific photosensitizers. It is a very versatile method because a wide range of solvents can be used at low temperatures if required. In the photochemical process, the photosensitizer (P) absorbs visible light giving the singlet excited state ( $S_1^*$ ) which is converted into triplet excited state ( $T_1^*$ ) after the intersystem crossing (ISC) (**Eq. 2.2**). As the lifetime of the  $T_1^*$  state is much longer ( $\mu\text{s}$  -  $\text{ms}$ ) than that of the  $S_1^*$  state ( $\text{ps}$  -  $\text{ns}$ ), it can react with  $^3\text{O}_2$  which is converted into  $^1\text{O}_2$  *via* a spin-allowed energy transfer (**Eq. 2.3**). This process is defined as a type I mechanism and competes with the type II mechanism involving a hydrogen atom abstraction or electron transfer between  $T_1^*$  and oxygen or the organic substrate leading to the formation of various free radicals (*i.e.* superoxide radical anion  $\text{O}_2^{\cdot-}$ ) (**Eq. 2.4**).



The photosensitized oxidations of substrates (0.03 M) were carried out at 5 °C in methanol with Rose Bengal (5 mg/mL, structure given in **figure 2.1**) as a sensitizer by irradiation with a sodium lamp while maintaining a continuous bubbling of O<sub>2</sub>. The experimental apparatus is illustrated in **figure 2.1**.

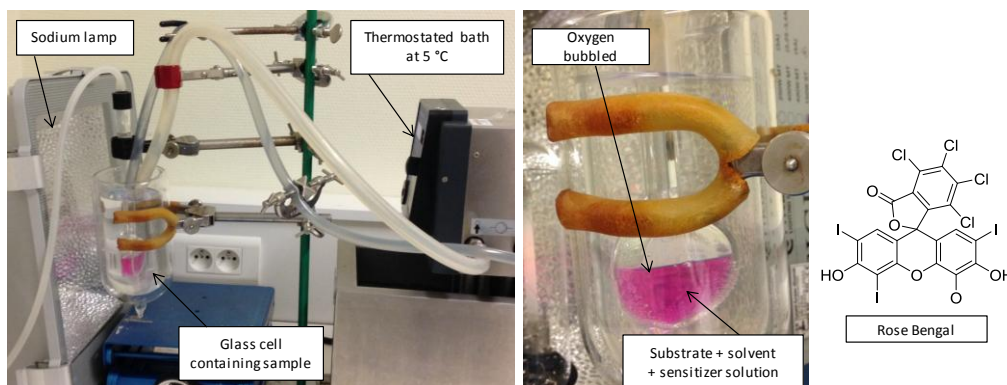
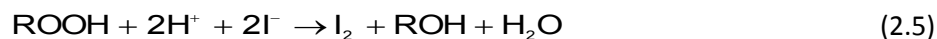


**Figure 2.1: Experimental apparatus for the formation of hydroperoxides by singlet oxygenation**

The evaluation of the progress of the photooxidation was monitored by iodometric titration of hydroperoxides. The titration is based on the reaction of hydroperoxides with an excess of iodide ions (I<sup>-</sup>) in acetic medium (**Eq. 2.5**). Then, I<sub>2</sub> generated is titrated by a sodium thiosulfate solution (**Eq. 2.7**).<sup>204</sup>



When the equivalence point is reached, the amount of substance of hydroperoxides ( $n_{ROOH}$ ) is obtained with the following equation (**Eq. 2.8**):

$$n_{I_2} = 0.5 \times [Na_2S_2O_3] \times V_{eq} = n_{ROOH} \quad (2.8)$$

Therefore, the resulting concentration of hydroperoxides  $[ROOH]_t$  is obtained with the **equation 2.9**.

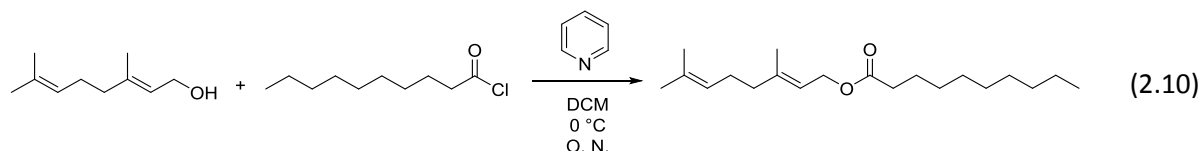
$$[ROOH]_t = \frac{0.5 \times [Na_2S_2O_3] \times V_{eq}}{V_0} \quad (2.9)$$

$[ROOH]_t$  and  $[Na_2S_2O_3]$  are the respective concentrations of total hydroperoxides and pentahydrate thiosulfate solutions,  $V_{eq}$  and  $V_0$  represent respectively the volume of Na<sub>2</sub>S<sub>2</sub>O<sub>3</sub> added at the equivalence point and the initial volume of hydroperoxides solution added. The method has the advantages of a good specificity and exact 1/1 stoichiometry between the amount of peroxide reacting and iodine produced, allowing the quantification of the hydroperoxides.<sup>205</sup> The reaction of ROOR peroxides and 4-membered cyclic peroxides follow analogous pathways (**Eq. 2.6**).<sup>204</sup>

Moreover, LC-UV at a wavelength of 205 nm was also used to follow the disappearance of the unsaturated substrates and the formation of unsaturated photooxidized compounds (*i.e.* hydroperoxides and peroxide compounds). Finally, hydroperoxides isolated from the reaction media were then characterized by  $^1\text{H}$  and  $^{13}\text{C}$  NMR in order to elucidate their chemical structures.

## 2.2 Singlet oxygenation of terpenoids

The three main terpenoids studied were synthesized from the 3,7-dimethyl-1-octanol, citronellol and geraniol as starting material *via* an esterification process using decanoyl chloride and pyridine (Eq. 2.10).



The photooxidation of the three-main synthesized terpenoids (*i.e.* 3,7-dimethyloctyl decanoate, citronellol caprate and geraniol caprate) has been monitored by LC-UV spectrometry and all the conceivable hydroperoxides formed have been taken into consideration. The main hydroperoxide patterns have been then described by  $^1\text{H}$  and  $^{13}\text{C}$  NMR.

### 2.2.1 LC-UV analyses of hydroperoxides and their structural identification by NMR

The LC-UV analysis of the photooxidized 3,7-dimethyloctyl decanoate confirms our thinking. Indeed, the absence of double bond is unfavorable for the photooxidation process. Consequently, saturated compounds are not oxidized by singlet oxygen.

Figure 2.2 shows the LC-UV chromatograms related to the photooxidation of citronellol and geraniol caprate. Di-hydroperoxides  $\text{R}(\text{OO})_2$  are much more polar than mono-hydroperoxides  $\text{R}(\text{OO})_1$  which are in turn more polar than substrates. With a reversed-phase chromatography, the more polar compounds are firstly obtained followed by the less polar substrates. The chromatogram for the photooxidized citronellol caprate (Fig. 2.2A) points out the formation of only mono-hydroperoxides. Moreover, the figure 2.2B shows the formation of mono- and di-hydroperoxides during the singlet oxygenation of geraniol caprate.

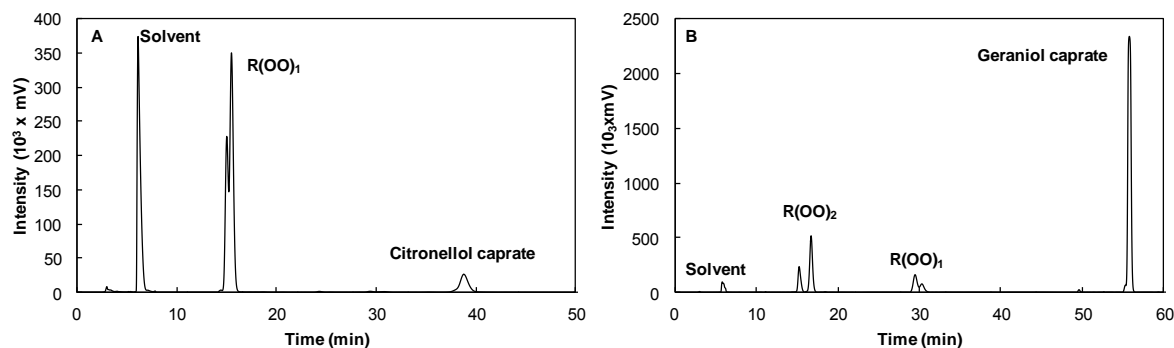


Figure 2.2: LC chromatograms obtained for the singlet oxygenation of citronellol caprate (A) and geraniol caprate (B), formation of mono- and di-hydroperoxides ( $\text{R}(\text{OO})_1$  and  $\text{R}(\text{OO})_2$  respectively)

Citronellol caprate exhibits one double bond whereas geraniol caprate has two unsaturations. Their respective singlet oxygenation leads to the possible formation of 3 mono-hydroperoxides and 9 mono-hydroperoxides with 18 di-hydroperoxides (Table 2.2) shown in figure 2.3.<sup>232</sup>

Number of -OOH	Citronellol caprate	Geraniol caprate
R(OO) <sub>1</sub>	3	9
R(OO) <sub>2</sub>	-	18

Table 2.2: Number of differentiable isomeric mono- and di-hydroperoxides (R(OO)<sub>1</sub> and R(OO)<sub>2</sub> respectively) using a non-chiral analytical method

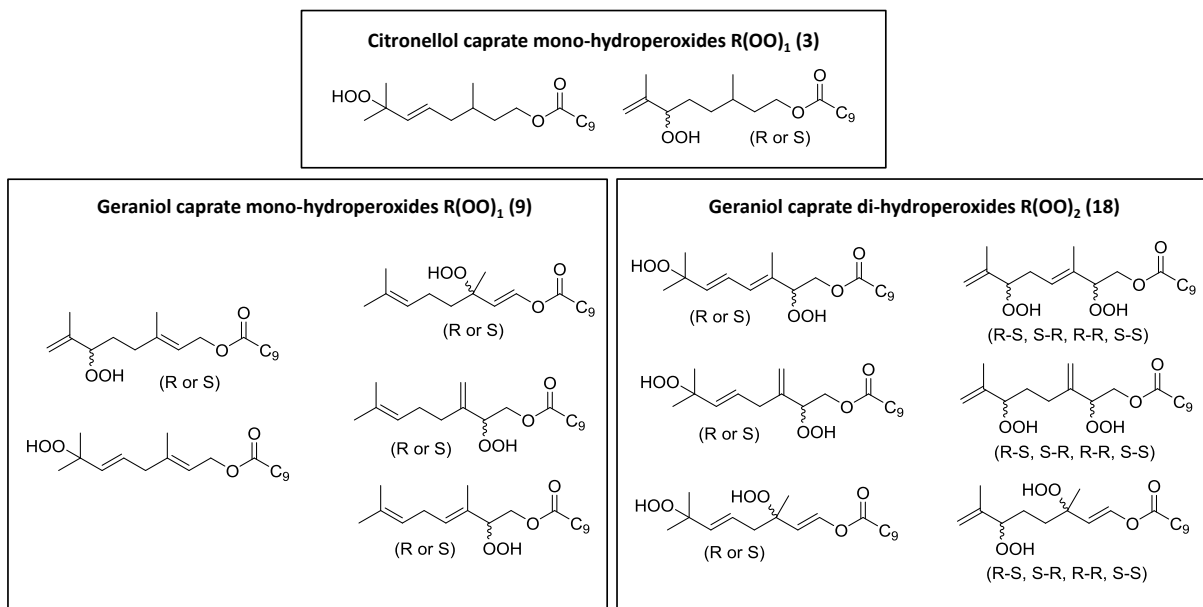


Figure 2.3: Molecular structure of all the possible *mono-* and *di-*hydroperoxides (R(OO)<sub>1</sub> and R(OO)<sub>2</sub> respectively) that may be obtained by singlet oxygenation of citronellol caprate and geraniol caprate

Each mono-hydroperoxide isomer formed still bears one or two double bonds which can further react with singlet oxygen. However, depending on their chemical structures (*i.e.* methyl substitution degree of the remaining double bond, conjugation or not, hydroperoxyl function in  $\alpha$ -position), they will kinetically react differently with singlet oxygen. The singlet oxygenation of citronellol caprate and geraniol caprate leads to mono-hydroperoxides constituted by di-substituted double bonds, which are less reactive than the starting tri-substituted ones (Fig. 2.4). Tanielian showed also that tri-alkylated olefins are about 150 times more reactive than dialkylated olefins.<sup>233</sup> Moreover, these disubstituted double bonds have a hydroperoxyl function in  $\alpha$ -position which makes them further less reactive.<sup>234</sup>

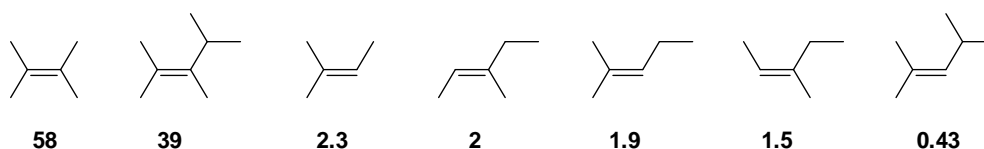
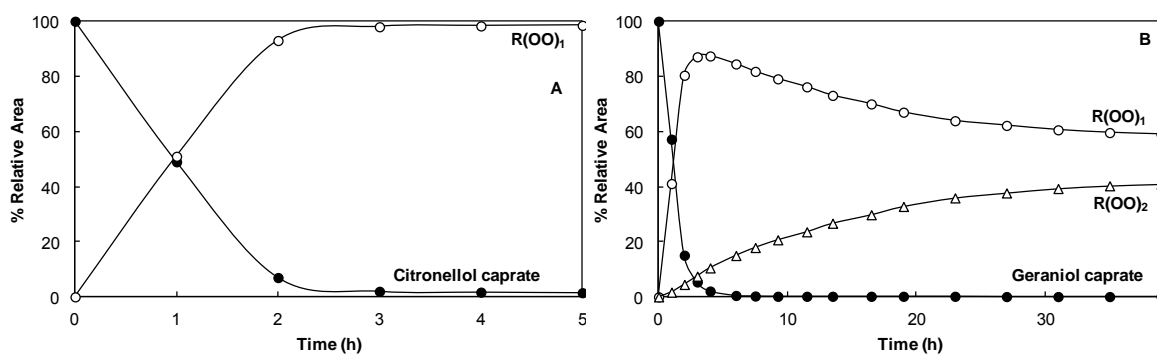


Figure 2.4: Relative rate constants of olefin with singlet oxygen ( $k \times 10^{-6} \text{ L mol}^{-1} \text{ s}^{-1}$ )<sup>234</sup>

The remaining double bonds of final mono- and di-hydroperoxides are less electron-rich and do not further react with singlet oxygen under our experimental conditions. As regards to the photooxidation of the geraniol caprate, the 2,3 double bond with the allylic decanoate function is substantially less reactive than the 6,7 double bond substituted by three alkyl groups. Indeed, the 6,7 double bond is a more electron-rich olefin with the electron-donating groups (*i.e.* alkyl functions) whereas the 2,3 double bond is more deficient in electron because of the electron-withdrawing group (*i.e.* ester function). Consequently, mono- hydroperoxides are generated firstly at a high

kinetic rate<sup>104</sup> whereas the formation of di-hydroperoxides starts very slowly compared to that of mono-hydroperoxides (**Fig. 2.5**).



**Figure 2.5:** LC-UV monitoring of the photooxidation of citronellol caprate (**A**) and geraniol caprate (**B**), % relative areas of the different peaks obtained (● starting material, ○ R(OO)<sub>1</sub> and △ R(OO)<sub>2</sub>) vs the photooxidation time

The second addition of singlet oxygen is made possible by the intermediary of the mono-hydroperoxide with a trisubstituted double bond. Terminal double bonds are so no reactive by singlet oxygenation. Finally, there is a stabilization of the relative percentage of mono-hydroperoxide (60 %) and di-hydroperoxides (40 %). The formation of mono-hydroperoxide and a mixture of mono- with di-hydroperoxides during the singlet oxygenation of citronellol caprate and geraniol caprate respectively have been reinforced by the ESI-MS analysis. The results of mass spectrometry are largely developed in the appropriate part dedicated (see paragraph 3).

### 2.2.2 Analysis of hydroperoxides by <sup>1</sup>H and <sup>13</sup>C NMR

<sup>1</sup>H and <sup>13</sup>C NMR analyses have been performed on the complex mixture containing all the mono-hydroperoxides (2) and all the mono- (9) and di- (18) hydroperoxides obtained during the singlet oxygenation of citronellol caprate and geraniol caprate respectively. Nevertheless, the determination of the proportion of each hydroperoxide of geraniol caprate was not possible as regards to the numerous isomers obtained. <sup>1</sup>H and <sup>13</sup>C NMR APT spectrum related to the unsaturated hydroperoxide moiety of the molecules are described below. The entire NMR descriptions are developed in the experimental section.

The <sup>1</sup>H NMR analysis of the photooxidized citronellol caprate allows us to describe the mono-hydroperoxides obtained and highlights the two structural isomer **1A** and **1B** (**Fig. 2.6**). The hydrogens of the hydroperoxide groups are distinguished with respective <sup>1</sup>H NMR chemical shift at 7.71 and 8.10 ppm. Moreover, with an asymmetric center (\*), it is possible to differentiate the two diastereoisomers with the small separation of the B peak. Finally, the vinylic hydrogens (C<sub>1</sub>-C<sub>2</sub> and D<sub>1</sub>-D<sub>2</sub>) and the hydrogen (E) situated on the carbon bearing the hydroperoxide function could also be identified as represented on the **figure 2.6**. The integration of the peak E which characterizes the isomer **2A** highlights the isomeric ratio of 0.53(1A) / 0.47 (2A).

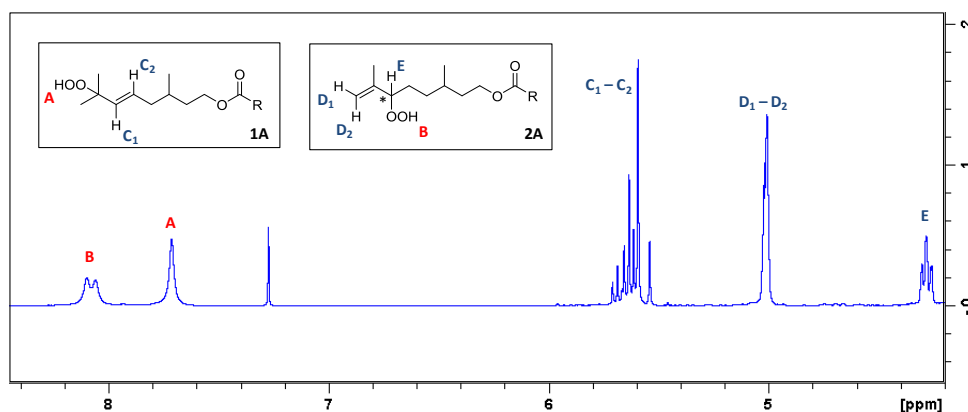


Figure 2.6: Part of the  $^1\text{H}$  NMR spectrum of the photooxidized citronellol caprate

The  $^{13}\text{C}$  NMR analysis of the photooxidized citronellol caprate is another proof of the formation of the two structural isomer **1A** and **1B** (Fig. 2.7).

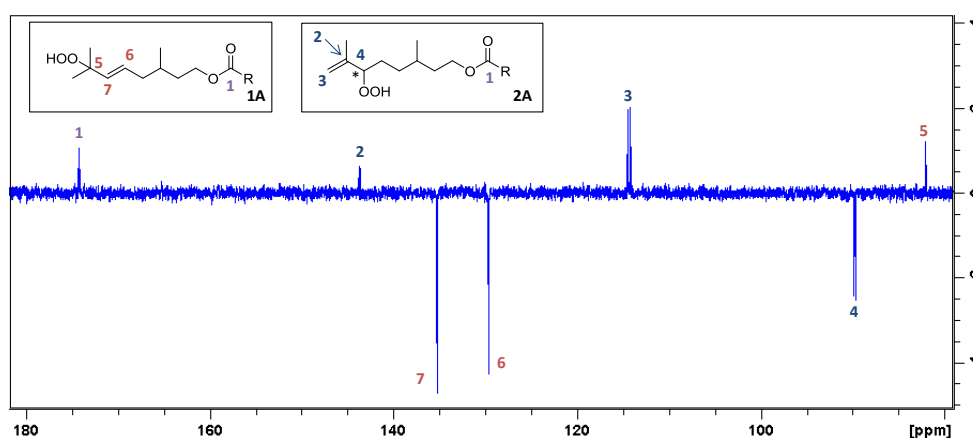


Figure 2.7: Part of the  $^{13}\text{C}$  NMR APT spectrum of the photooxidized citronellol caprate

This APT spectrum is presented “upside-down” with CH and  $\text{CH}_3$  peaks “down” and quaternary and  $\text{CH}_2$  peaks “up”. The two different carbons (4 and 5) bearing the hydroperoxide function are distinguished by this method which confirms our finding. Moreover, carbons related to the olefin function for both compounds (6-7 and 2-3) have not the same chemical shift and could be attributed as described by figure 2.7. The two structural units A and B (*i.e.* tertiary and secondary end-chain hydroperoxides) highlighted by the investigation of the  $^1\text{H}$  and  $^{13}\text{C}$  NMR spectra of photooxidized citronellol caprate are gathered with their main respective chemical shifts ( $\delta$ ) on the Table 2.3.

N°	Name of $\text{R}(\text{OO})_1$	Patterns	Chemical shift $\delta$ (ppm)	
			$^1\text{H}$ (300 MHz)	$^{13}\text{C}$ (300 MHz)
A	Tertiary end-chain		$\text{H}_{1-6}$ : 6H, s, 1.34 ppm $\text{H}_{3-4}$ : 2H, m, 5.50-5.72 ppm	$\text{C}_2$ : C, 82.1 ppm $\text{C}_3$ : CH, 135.2 ppm $\text{C}_4$ : CH, 129.6 ppm
B	Secondary end-chain		$\text{H}_1$ : 2H, m, 4.98-5.05 ppm $\text{H}_3$ : 1H, m, 4.24-4.33 ppm $\text{H}_6$ : 3H, s, 1.73 ppm	$\text{C}_1$ : $\text{CH}_2$ , 114.4 ppm $\text{C}_2$ : C, 143.6 ppm $\text{C}_3$ : CH, 89.8 ppm

Table 2.3:  $^1\text{H}$  and  $^{13}\text{C}$  NMR characteristics of the 2 main hydroperoxides patterns, A: tertiary end-chain hydroperoxide and B: secondary end-chain hydroperoxide

The investigation of the  $^1\text{H}$  NMR spectrum related to the photooxidation of geraniol caprate is more complicated to exploit because of the large number of mono- and di-hydroperoxides obtained. Nevertheless, it is possible to highlight the 5 characteristic hydrogens of the various hydroperoxides formed which are found into 4 main structural units (Fig. 2.8).

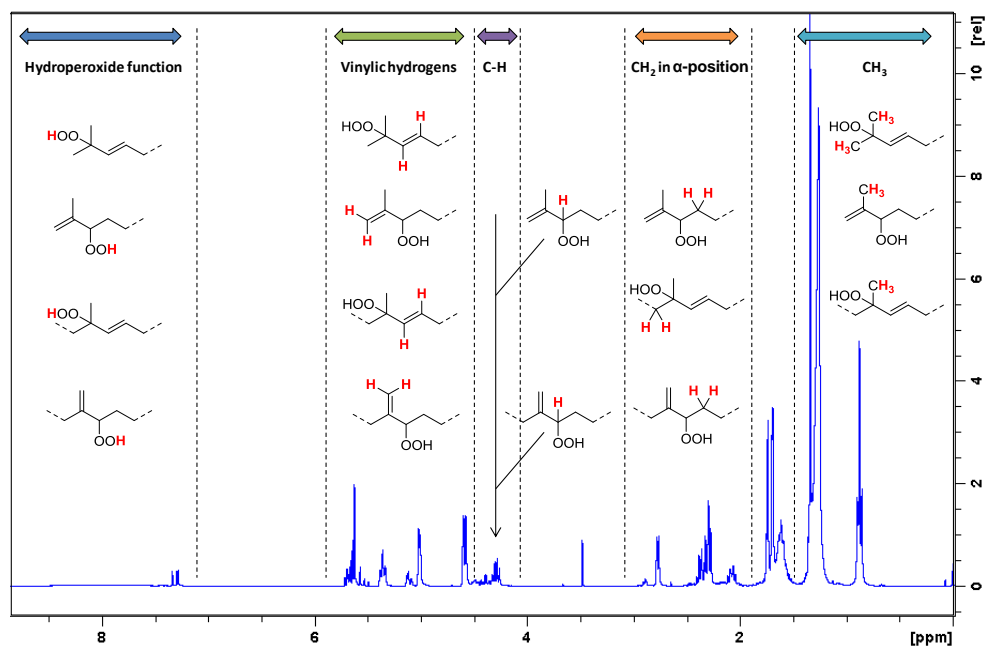


Figure 2.8:  $^1\text{H}$  NMR spectrum of the photooxidized geraniol caprate

Indeed, hydroperoxide functions are obtained at the termination site of the molecule (end-chain hydroperoxides) or closed to the decanoyl ester group (internal hydroperoxides). Tertiary and secondary hydroperoxides are mostly characterized by hydrogens from the hydroperoxide function at high chemical shift ( $\delta > 7$  ppm) in the form of thin or large peaks. Moreover, as hydroperoxides are labile function, their hydrogens can be located at different part of the spectrum. The thin peak located at 3.48 ppm could also represent the hydrogen of the hydroperoxide group. Vinyllic hydrogens are then less polar than those of hydroperoxide functions and are located between 5 and 6 ppm. Their chemical shift depends on the neighborhood of the hydrogens situated at the *cis* and *trans* position. Moreover, the C-H function characterizes the tertiary hydroperoxides. Indeed, in this case, the carbon which bears the hydroperoxide function is also described by the hydrogen located on the same carbon. Only two structural units are impacted by this characterization. The chemical shift of this hydrogen is situated between 4 and 5 ppm.  $\text{CH}_2$  functions located at the  $\alpha$ -position of the hydroperoxide groups are characterized by multiplet between 2 and 3 ppm. They are more deshielded than classical  $\text{CH}_2$  located under 2 ppm. Finally,  $\text{CH}_3$  functions closed to hydroperoxide groups are more deshielded than the same function situated at the end of apolar tail ( $\delta = 0.87$  ppm). Their signals are huge singlet located between 1.2 and 1.4 ppm.

The  $^{13}\text{C}$  APT NMR analysis of the photooxidized geraniol caprate works on the same reasoning of the  $^{13}\text{C}$  NMR spectrum of the photooxidized citronellol caprate (Fig. 2.9).

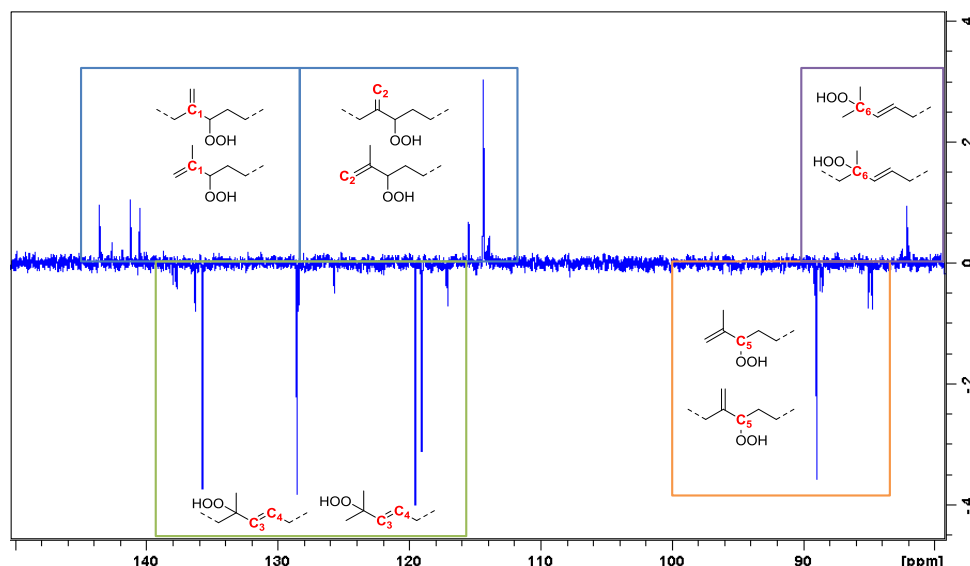


Figure 2.9:  $^{13}\text{C}$  APT NMR spectrum of the photooxidized geraniol caprate

Secondary internal and end-chain hydroperoxides are characterized by the quaternary ( $\text{C}_1$ ,  $130 < \delta$  (ppm)  $< 150$ ) and secondary ( $\text{C}_2$ ,  $110 < \delta$  (ppm)  $< 130$ ) carbons related to the olefin group. Moreover, the carbon bearing the hydroperoxide function ( $\text{C}_5$ ,  $85 < \delta$  (ppm)  $< 90$ ) is also a characteristic probe of secondary hydroperoxides. On the other hand, tertiary internal and end-chain hydroperoxides are highlighted by quaternary carbons bearing the  $-\text{OOH}$  function and a methyl group ( $\text{C}_6$ ,  $\delta = 82$  ppm). Furthermore,  $\text{C}_3$  and  $\text{C}_4$  carbons forming the other olefin part ( $115 < \delta$  (ppm)  $< 140$ ) and which are situated “down” on the spectrum, also define tertiary hydroperoxides.

The four main structural units A, B, C and D (*i.e.* tertiary and secondary end-chain or internal hydroperoxides) pointed out by the investigation of the  $^1\text{H}$  and  $^{13}\text{C}$  NMR spectra of photooxidized geraniol caprate are gathered in **table 2.4** with their main respective chemical shifts ( $\delta$ ). The tertiary (A) and secondary (B) end-chain hydroperoxides obtained for the photooxidized citronellol caprate have similar chemical shifts than for the photooxidized geraniol caprate.

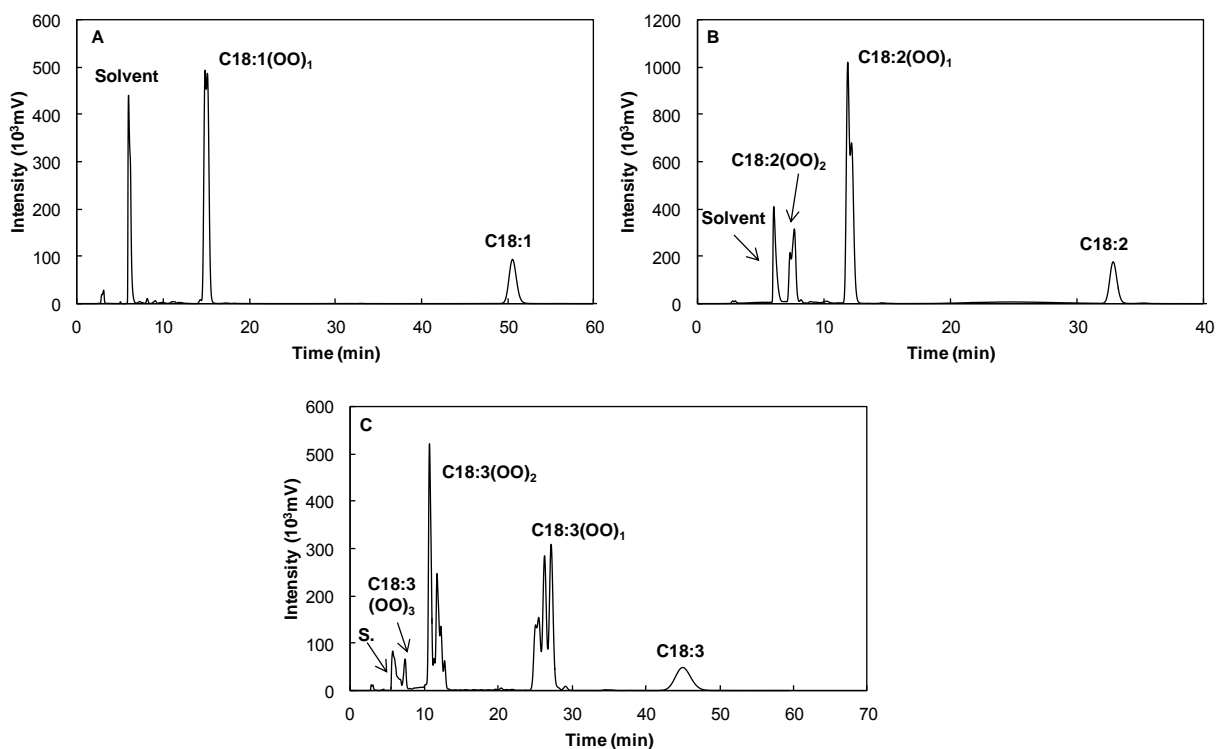
N°	Name of $\text{R}(\text{OO})_1$	Patterns	Chemical shift $\delta$ (ppm)	
			$^1\text{H}$ (300 MHz)	$^{13}\text{C}$ (300 MHz)
A	Tertiary end-chain		$\text{H}_{1-6}$ : 6H, bs, 1.33 ppm $\text{H}_{3-4}$ : 2H, m, 5.49-5.72 ppm	$\text{C}_2$ : C, 82.1 ppm $\text{C}_3$ : CH, 135.7 ppm $\text{C}_4$ : CH, 128.5 ppm
B	Secondary end-chain		$\text{H}_1$ : 2H, m, 4.91-5.20 ppm $\text{H}_3$ : 1H, m, 4.20-4.48 ppm $\text{H}_4$ : 2H, m, 2.70-2.96 ppm $\text{H}_6$ : 2H, s, 1.34 ppm	$\text{C}_1$ : $\text{CH}_2$ , 114.3 ppm $\text{C}_2$ : C, 143.7 ppm $\text{C}_3$ : CH, 88.9 ppm
C	Tertiary internal		$\text{H}_1$ : 2H, m, 2.24-2.41 ppm $\text{H}_{3-4}$ : 2H, m, 5.00-5.15 ppm $\text{H}_6$ : 3H, bs, 1.33 ppm	$\text{C}_2$ : C, 82.1 ppm $\text{C}_3$ : CH, 136.3 ppm $\text{C}_4$ : CH, 125.7 ppm
D	Secondary internal		$\text{H}_3$ : 1H, m, 4.20-4.48 ppm $\text{H}_4$ : 2H, m, 2.70-2.96 ppm $\text{H}_6$ : 2H, s, 4.54-4.63 ppm	$\text{C}_2$ : C, 142.7 ppm $\text{C}_3$ : CH, 85.0 ppm $\text{C}_6$ : $\text{CH}_2$ , 115.5 ppm

Table 2.4:  $^1\text{H}$  and  $^{13}\text{C}$  NMR characteristics of the 4 main hydroperoxides patterns, A: tertiary end-chain hydroperoxide, B: secondary end-chain hydroperoxide, C: tertiary internal hydroperoxide and D: secondary internal hydroperoxide

### 2.3 Lipid hydroperoxides from singlet oxygenation

Based on the structural investigation of photooxidized terpenoids (*i.e.* citronellol caprate and geraniol caprate) by the way of chromatographic and NMR analyses, FAMES hydroperoxides used as food oxidized species models have been synthesized and analyzed. The three (poly)unsaturated fatty acids found in linseed oil were studied separately under their FAMES forms. The photooxidation of methyl oleate, linoleate and linolenate was monitored by LC-UV spectrometry and iodometric titration. A structural investigation of all conceivable hydroperoxides formed was examined thanks to the large literature survey. The main hydroperoxide patterns for mono-hydroperoxides and more peroxidized substrates were then described by  $^1\text{H}$  and  $^{13}\text{C}$  NMR.

**Figure 2.10** points out the LC-UV chromatograms related to the singlet oxygenation of FAMES linseed oil (*i.e.* methyl oleate, linoleate and linolenate).



**Figure 2.10:** LC-UV chromatograms ( $\lambda = 205\text{ nm}$ ) obtained during the singlet oxygenation of methyl oleate (A, C18:1), linoleate (B, C18:2) and linolenate (C, C18:3), formation of mono-hydroperoxides (C18:1(OO)<sub>1</sub>, C18:2(OO)<sub>2</sub> and C18:3(OO)<sub>3</sub>), di-peroxides (C18:2(OO)<sub>2</sub> and C18:3(OO)<sub>3</sub>) and tri-peroxides (C18:3(OO)<sub>3</sub>)

#### ▪ Methyl oleate hydroperoxides

As reported by Frankel *et al.*, the photooxidation of methyl oleate (C18:1) leads to the formation of 9- and 10-hydroperoxides (C18:1(OO)<sub>1</sub>) as the same ratio (50/50) (**Fig. 2.11**).<sup>36</sup> The mono-hydroperoxides peak obtained is in fact divided into two identical closed peaks if the polarity of the eluent is increased.

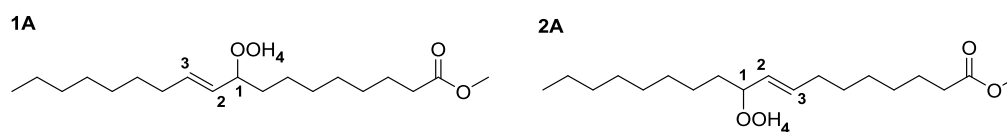


**Figure 2.11:** Molecular structure of all *mono-* hydroperoxides (C18:1(OO)<sub>1</sub>) that may be obtained by singlet oxygenation of methyl oleate

$^1\text{H}$  and  $^{13}\text{C}$  NMR experiments show this equimolar proportion (Fig. 2.12). Indeed, the hydroperoxide is characterized by the hydrogen ( $\text{H}_1$ ,  $\delta = 4.26$  ppm) linked to the carbon bearing the hydroperoxide function. Moreover, the two isomers are characterized by the vinylic hydrogens  $\text{H}_2$  ( $\delta = 5.78$  ppm) and  $\text{H}_3$  ( $\delta = 5.38$  ppm). As 1 hydrogen  $\text{H}_1$  is associated to 1 hydrogen  $\text{H}_2$  and 1 hydrogen  $\text{H}_3$ , we assumed that the isomeric ratio between these two hydroperoxides is 1/1. The carbon bearing these hydrogens are easily found on the  $^{13}\text{C}$  carbon spectrum. The hydroperoxide titration points out a progressive increase of the hydroperoxidation and exhibits a plateau which corresponds to a total hydroperoxyl function concentration equal to  $35 \text{ mmol.L}^{-1}$ .

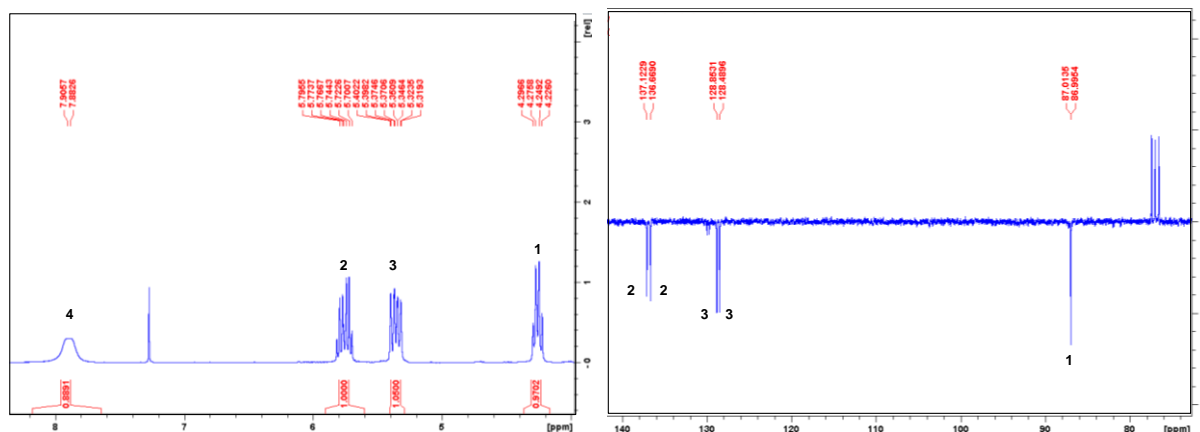


Figure 2.12:  $^1\text{H}$  and  $^{13}\text{C}$  NMR spectra of photooxidized methyl oleate  $\text{C18:1(OO)}_1$

Table 2.5 highlights the NMR characterization of the structural unit A (*i.e.* secondary hydroperoxide) related to the hydroperoxides from methyl oleate.

N°	Name of ROOH	Pattern	Chemical shift $\delta$ (ppm)	
			$^1\text{H}$ (300 MHz)	$^{13}\text{C}$ (300 MHz)
A	Secondary internal		$\text{H}_1$ : 1H, m, 4.26 ppm $\text{H}_2$ : 1H, m, 5.78 ppm $\text{H}_3$ : 1H, m, 5.38 ppm $\text{H}_4$ : 1H, m, 7.90 ppm	$\text{C}_1$ : CH, 87.0 ppm $\text{C}_2$ : CH, 137.0 ppm $\text{C}_3$ : CH, 129.0 ppm

Table 2.5:  $^1\text{H}$  and  $^{13}\text{C}$  NMR characteristics of the main hydroperoxides pattern A

▪ *Methyl linoleate and linolenate peroxides*

The mixture of hydroperoxides from photooxidized methyl linoleate ( $\text{C18:2}$ ) and methyl linolenate ( $\text{C18:3}$ ) are much more complex to investigate in detail because of their two and three unsaturations respectively. The molecular structure of all the possible peroxides obtained during the photooxidation of  $\text{C18:2}$  and  $\text{C18:3}$  are represented in figures 2.13 and 2.14 respectively. LC-UV chromatograms highlight the formation of mono-hydroperoxides ( $\text{C18:2(OO)}_1$  and  $\text{C18:3(OO)}_1$ ) and di-peroxide ( $\text{C18:2(OO)}_2$  and  $\text{C18:3(OO)}_2$ ) in both cases. Nevertheless, only the singlet oxygenation of  $\text{C18:3}$  leads to the formation of tri-peroxide  $\text{C18:3(OO)}_3$ .

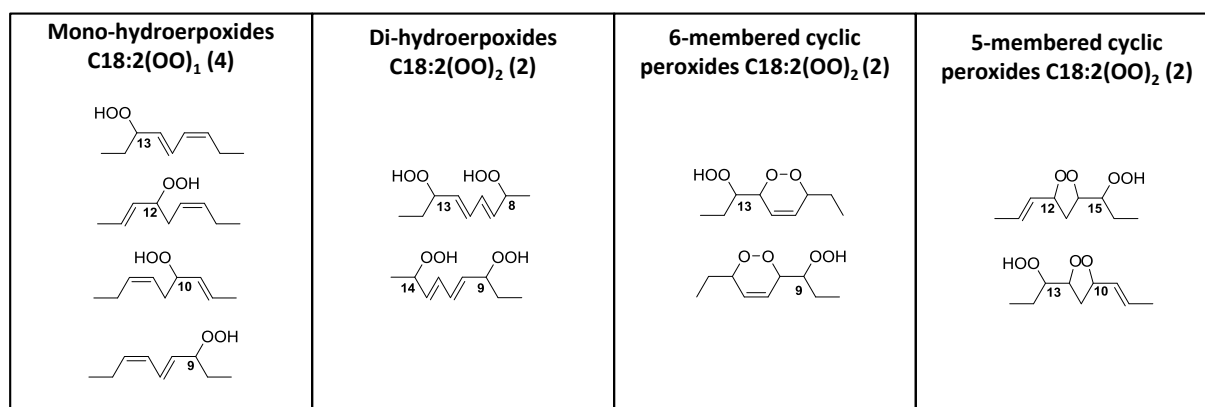


Figure 2.13: Molecular structure of all the possible *mono*- and *di*-hydroperoxides (C18:2(OO)<sub>1</sub> and C18:2(OO)<sub>2</sub>), 6- and 5-membered cyclic peroxides (C18:2(OO)<sub>2</sub>) that may be obtained by singlet oxygenation of methyl linoleate (C18:2)

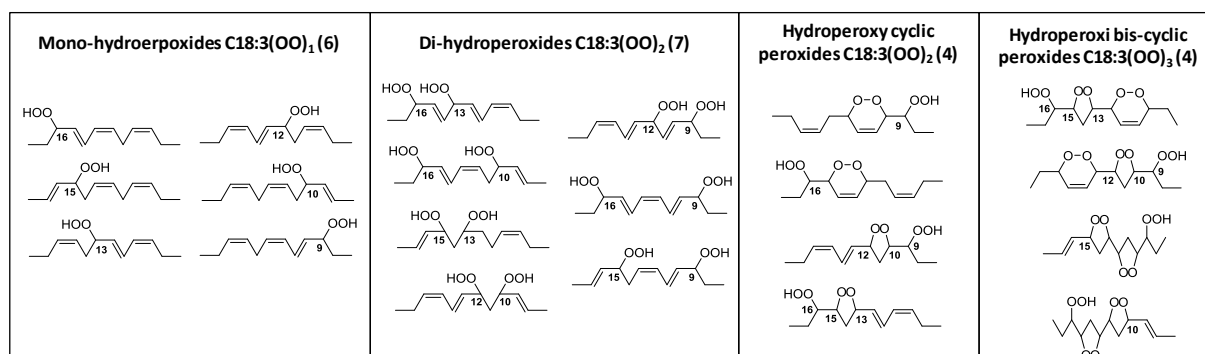


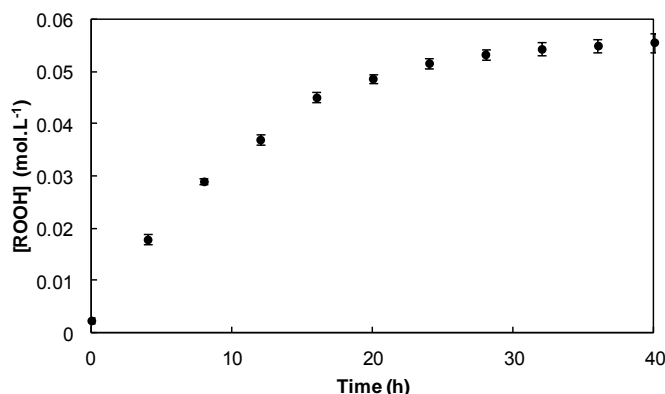
Figure 2.14: Molecular structure of all the possible *mono*- and *di*-hydroperoxides (C18:3(OO)<sub>1</sub> and C18:3(OO)<sub>2</sub>), 6- and 5-membered cyclic peroxides (C18:3(OO)<sub>2</sub>) and hydroperoxy bis-cyclic peroxides (C18:3(OO)<sub>3</sub>) that may be obtained by singlet oxygenation of methyl linolenate (C18:3)

As discussed before, authors were focused on the structural elucidation of peroxides obtained from the singlet oxygenation of these two FAMEs. The photooxidation of methyl linoleate and linolenate produces a respective mixture of 4 (Fig. 2.13) and 6 isomeric (Fig. 2.14) mono-hydroperoxides as primary photooxidation products.<sup>71</sup> The other oxidation steps are much more complicated than for the photooxidation of geraniol caprate. Indeed, the internal hydroperoxides have a homoallylic structure which allows an easy 1,3-cyclisation to form 5-membered hydroperoxy cyclic peroxides by a radical mechanism with ground state oxygen <sup>3</sup>O<sub>2</sub> categorized as free radical side reactions.<sup>36, 120, 124</sup> Other oxidation products result from the [4 + 2] cycloaddition of <sup>1</sup>O<sub>2</sub> leading to the formation of 6-membered hydroperoxy cyclic peroxides. Based on the amount of each mono-hydroperoxide, authors reveal that 1,3-cyclisation by a radical mechanism of the internal mono-hydroperoxides prevails over the 1,4-cycloaddition of singlet oxygen on the outer mono-hydroperoxides. It is possible that di-hydroperoxides are also obtained. They could be obtained through a pentadienyl radical as for the autoxidation pathway or they are presumed to come from the photooxidation of the corresponding mono-hydroperoxides with singlet oxygen and sensitizer.<sup>74</sup> Finally, only in the case of methyl linolenate, the hydroperoxy cyclic peroxides could again react by radical mechanism leading to the hydroperoxy bis-cyclic peroxides formations which are composed by two 5-membered or 5- and 6-membered cyclic peroxides.<sup>119, 128</sup>

As regards to the complex mixtures obtained for the photooxidized methyl linoleate and linolenate, <sup>1</sup>H and <sup>13</sup>C NMR experiments are too difficult to interpret without separation of each oxidized species. Nevertheless, NMR analyses give information on the disappearance of the substrates and the formation of key structural parameters such as hydrogens from the hydroperoxyl

and olefin functions, and from the tertiary carbon bearing the hydroperoxyl function.  $^1\text{H}$  and  $^{13}\text{C}$  NMR spectra are described in the experimental part.

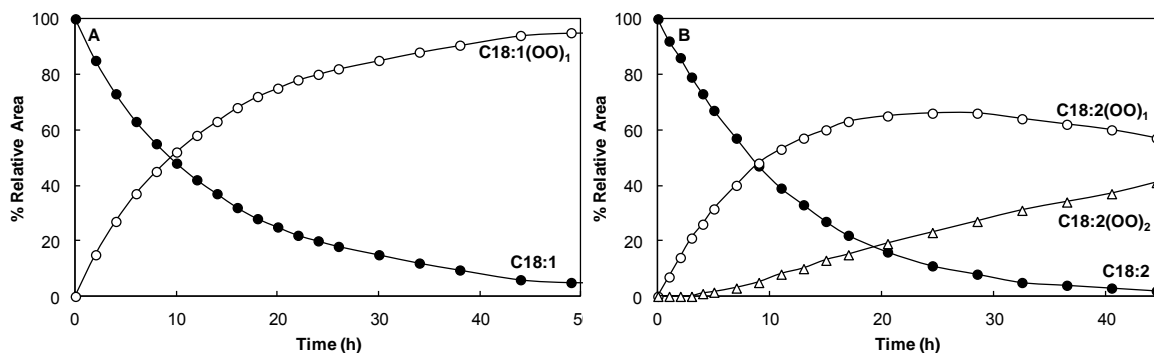
The hypothesis of the formation of hydroperoxy cyclic peroxides is supported by hydroperoxide titration during the reaction of singlet oxygenation (**Fig. 2.15**).



**Figure 2.15:** Formation of hydroperoxides during the singlet oxygenation of methyl linolenate (C) detected by LC-UV at  $\lambda = 205 \text{ nm}$

Indeed, it indicated a progressive increase of the peroxidation confirming the formation of more and more peroxidized FAMES. Moreover, it also exhibits a stationary state which corresponds to a total hydroperoxyl function concentration equal to  $55 \text{ mmol.L}^{-1}$  for the photooxidation of methyl linolenate.

**Figure 2.16** reports the evolution of the relative intensities for the LC peak vs the irradiation time for the photooxidation of methyl oleate (A), linoleate (B) and linolenate (C). As soon as the photooxidation has started, mono-hydroperoxides (ROOH) are formed whereas di-peroxides and tri-peroxides are not obtained. Then, as the photooxidation proceeds, di-peroxides appear first before the formation of tri-peroxides whereas the less peroxidized compounds starts disappearing. This highlights that mono-hydroperoxides are used to get di-peroxides compounds which are in turn dedicated to the formation of tri-peroxides compounds. On one hand, **figure 2.16B** points out that, in the case of the methyl linoleate photooxidation, there are finally 57 % of mono-hydroperoxides ( $\text{C18:2(OO)}_1$ ), 41 % of di-peroxides compounds ( $\text{C18:2(OO)}_2$ ) with only 2 % of resulting starting material ( $\text{C18:2}$ ). On the other hand, the singlet oxygenation of methyl linolenate leads to 18% of mono-hydroperoxides ( $\text{C18:3(OO)}_1$ ), 70 % of di-peroxides ( $\text{C18:3(OO)}_2$ ) and 12 % of tri-peroxides ( $\text{C18:3(OO)}_3$ ) (**Fig. 2.16C**).



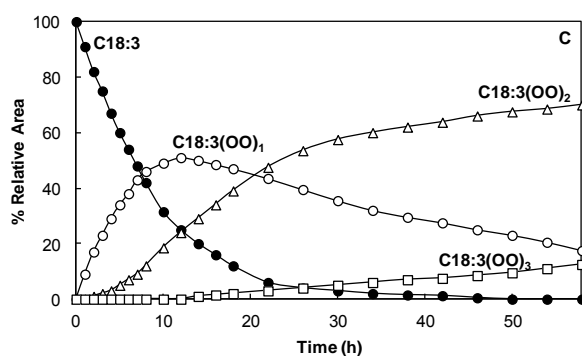


Figure 2.16: Relative intensities of LC-UV peaks of the substrates (●, FAMES), mono-hydroperoxides (○  $R(OO)_1$ ), di-peroxides (△,  $R(OO)_2$ ) and tri-peroxides (□,  $R(OO)_3$ ) obtained during the singlet oxygenation of methyl oleate (A, C18:1), methyl linoleate (B, C18:2) and methyl linolenate (C, C18:3)

- Peroxides from FAMES of linseed oil

The photooxidation of FAMES of linseed oil was undertaken with the same method. Figure 2.17 shows the LC chromatogram obtained and the relative area of each substrate and peroxides detected.

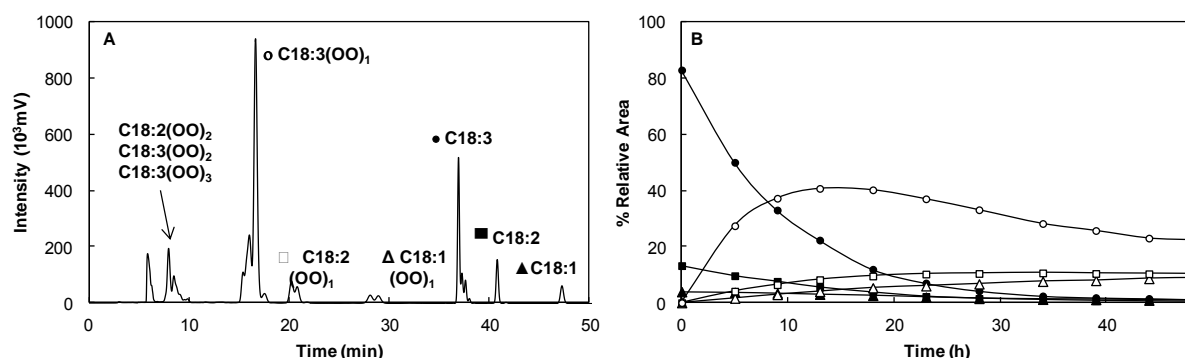


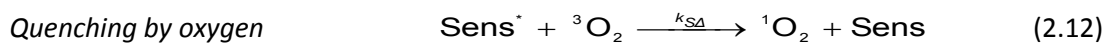
Figure 2.17: (A) LC-UV chromatograms ( $\lambda = 205$  nm) obtained during the singlet oxygenation of FAMES of linseed oil and (B) relative intensities of LC-UV peaks of the substrates (● C18:3, ■ C18:2, ▲ C18:1) and respective mono-hydroperoxides (○  $R(OO)_1$  from C18:3, □  $R(OO)_1$  from C18:2 and △  $R(OO)_1$  from C18:1)

Our LC method allows the separation of the respective mono-hydroperoxides ( $R(OO)_1$ ) from C18:3, C18:2 and C18:1. Nevertheless, it was not possible to separate the different di- and tri-peroxide compounds from C18:3 and C18:2. Based on the UV detection, LC-UV analysis is not a relevant method to separate and identify complex mixture of peroxides.

## 2.4 Kinetic approaches and singlet oxygen quenching activity

The disappearance of substrates could be modeled *via* a kinetic approach as developed by Caminade *et al.*<sup>235</sup> The first step of the photooxidation process is the photoexcitation of the sensitizer (*i.e.* rose bengal) by the sodium lamp (Eq. 2.11). Through its reaction with ground-state oxygen, the excited sensitizer forms singlet oxygen ( $^1O_2$ ,  $^1\Delta_g$ ) which is the lowest excited state of oxygen (Eq. 2.12). Singlet oxygen could be deactivated to return to its ground-state through chemical reaction and physical quenching by the substrate or the solvent. The chemical quenching by the substrate (M) leads to an oxygenated product with a kinetic rate constant  $k_r$  (Eq. 2.13). Then, the non-radiative physical deactivation occurs through a transfer of energy from singlet oxygen ( $^1O_2$ ) to the substrate

(M) with a kinetic rate constant  $k_q$  (Eq. 2.14). Finally, there is the non-radiative deactivation of  $^1\text{O}_2$  by the solvent leading to the formation of ground-state oxygen ( $^3\text{O}_2$ ) according a kinetic rate constant  $k_d$  (Eq. 2.15).



The variation of the singlet oxygen ( $^1\text{O}_2$ ) concentration is obtained by the **equation 2.16** where  $(d[{}^1\text{O}_2]/dt)_f$  is related to the formation of singlet oxygen by the sensitizer,  $-k_d[{}^1\text{O}_2]$  correspond to the deactivation of singlet oxygen by the solvent and  $-(k_r + k_q)[{}^1\text{O}_2][\text{M}]$  comes from the chemical reaction and physical quenching of  $^1\text{O}_2$  by the substrate M.

$$\frac{d[{}^1\text{O}_2]}{dt} = \left(\frac{d[{}^1\text{O}_2]}{dt}\right)_f - k_d[{}^1\text{O}_2] - (k_r + k_q)[{}^1\text{O}_2][\text{M}] \quad (2.16)$$

The **equation 2.17** is then obtained thanks to the pseudo-steady state approximation applied to singlet oxygen  $^1\text{O}_2$ .

$$\frac{d[{}^1\text{O}_2]}{dt} = 0 \quad [{}^1\text{O}_2] = \left(\frac{d[{}^1\text{O}_2]}{dt}\right)_f \times \frac{1}{k_d + (k_r + k_q)[\text{M}]} \quad (2.17)$$

On the other hand, the variation of the substrate (M) concentration through the chemical reaction is described by **equation 2.18**. The combination of **equations 2.17 and 2.18** leads to the **equation 2.19**.

$$\frac{d[\text{M}]}{dt} = -k_r [{}^1\text{O}_2][\text{M}] \quad (2.18)$$

$$\frac{d[\text{M}]}{dt} = -\left(\frac{d[{}^1\text{O}_2]}{dt}\right)_f \times \frac{k_r [\text{M}]}{k_d + (k_r + k_q)[\text{M}]} \quad (2.19)$$

The integration between 0 and t of the last equation leads to the **equations 2.20 and 2.21** where  $V_f$  represents the formation rate of singlet oxygen.

$$\frac{k_d}{k_r} \int_0^t \frac{d[\text{M}]}{[\text{M}]} + \frac{k_r + k_q}{k_r} \int_0^t d[\text{M}] = -V_f \int_0^t dt \quad (2.20)$$

$$\frac{k_d}{k_r} [\text{Ln}(\text{M})]_0^t + \frac{k_r + k_q}{k_r} [\text{M}]_0^t = -V_f [t]_0^t \quad (2.21)$$

The final **equations 2.22 and 2.23** introduce 2 relevant parameters: the Foote reactivity index  $\beta = k_d / (k_r + k_q)$  and the parameter  $\gamma = k_r / (k_r + k_q)$  related to the efficiency of the singlet oxygenation process.

$$\frac{k_d}{k_r + k_q} \text{Ln} \frac{[\text{M}]_0}{[\text{M}]_t} + [\text{M}]_0 - [\text{M}]_t = \frac{k_r}{k_r + k_q} V_f t \quad (2.22)$$

$$\beta \text{Ln} \frac{[\text{M}]_0}{[\text{M}]_t} + [\text{M}]_0 - [\text{M}]_t = \gamma V_f t \quad (2.23)$$

The kinetic rate constant  $k_d$  related to the deactivation of  $^1\text{O}_2$  by solvent molecules depends on the solvent used. Indeed,  $k_d$  is equal to the reciprocal of the singlet oxygen lifetime in the solvent of the study (Eq. 2.24).

$$k_d = \frac{1}{\tau_\Delta} \quad (2.24)$$

In deuterated solvents, the singlet oxygen lifetime ( $\tau_\Delta$ ) is much longer than in protonated solvents which allows faster photooxidations (Table 2.6).<sup>106-108</sup> As photooxidation reactions are carried out into methanol ( $\text{CH}_3\text{OH}$ ), the value of  $k_d$  used to model the kinetic rate of photooxidation is equal to  $1 \times 10^5 \text{ s}^{-1}$ .

Solvent	$\tau_\Delta$ ( $\mu\text{s}$ )	$k_d$ ( $\text{s}^{-1}$ )
Water ( $\text{H}_2\text{O}$ )	$2.0 \pm 0.2$	$5 \times 10^5$
Methanol ( $\text{CH}_3\text{OH}$ )	$10 \pm 0.1$	$1 \times 10^5$
Benzene ( $\text{C}_6\text{H}_6$ )	$26.7 \pm 1.3$	$3.7 \times 10^4$
Acetonitrile ( $\text{CH}_3\text{CN}$ )	$54.4 \pm 1.3$	$1.8 \times 10^4$
Deuterated water ( $\text{D}_2\text{O}$ )	$68.1 \pm 2.5$	$1.5 \times 10^4$
Deuterated benzene ( $\text{C}_6\text{D}_6$ )	$550 \pm 11$	$1.8 \times 10^3$
Deuterated acetonitrile ( $\text{CD}_3\text{CN}$ )	$600 \pm 33$	$1.6 \times 10^3$

Table 2.6: Lifetime of singlet oxygen ( $\tau^1\text{O}_2$ ) in various classic and deuterated solvents<sup>106-108</sup>

The  $V_f$  parameter represents the rate of formation for singlet oxygen cumulated in the time of photooxidation when there is a complete and fast consumption of  $^1\text{O}_2$  by chemical reaction. Therefore,  $V_f$  is obtained for the fastest photooxidized substrate. This situation is attained when there is no physical quenching ( $k_q = 0$ ,  $\gamma = 1$ ) and negligible deactivation of  $^1\text{O}_2$  by the solvent ( $\beta = 0$ ,  $k_d \ll k_r + k_q$ ) (Eq. 2.25).

$$[\text{M}]_0 - [\text{M}]_t = V_f t \quad (2.25)$$

The substrate used as reference in our study is  $\alpha$ -terpinene as it reacts very quickly with singlet oxygen through a pure chemical process ( $k_r[\text{M}] \gg k_d$  and  $k_q[\text{M}]$ ) via 2+4 cycloaddition. Consequently, as  $\alpha$ -terpinene ( $M_0 = 3 \times 10^{-2} \text{ mol.L}^{-1}$ ) is completely consumed ( $[\text{M}]_t = 0 \text{ mol.L}^{-1}$ ) after 15 min of photooxidation, the formation rate of singlet oxygen ( $V_f$ ) is calculated by the equation 2.26 and it is equal to  $2 \times 10^{-3} \text{ M.min}^{-1}$ .

$$V_f = \frac{[\text{M}]_0}{t} \quad (2.26)$$

Figure 2.18 shows the substrate disappearance during the photooxidation of  $\alpha$ -terpinene (•), citronellol caprate (•), geraniol caprate (•), methyl linolenate (•), methyl linoleate (•) and methyl oleate (•). The final equation 2.23 is used to model the kinetic rate of the substrate disappearance and their respective kinetic curves are obtained. We showed that the kinetic curves well fit the experimental points.

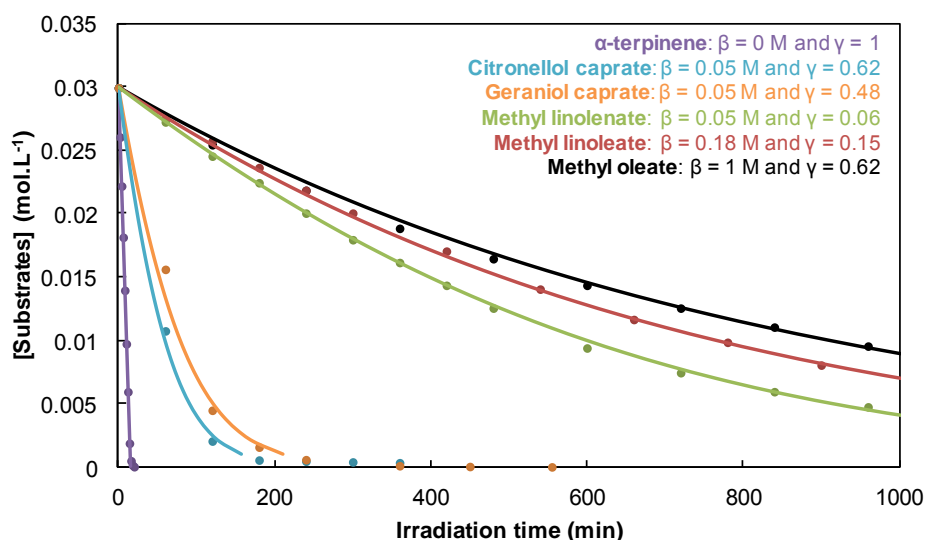


Figure 2.18: Monitoring of the substrate disappearance ( $\alpha$ -terpinene  $\bullet$ , citronellol caprate  $\bullet$ , geraniol caprate  $\bullet$ , methyl linolenate  $\bullet$ , methyl linoleate  $\bullet$  and methyl oleate  $\bullet$ ) during their respective photooxidation, modeling of the kinetic rate of disappearance through the equation 2.23

Table 2.7 gathers the  $\gamma$  and  $\beta$  parameters with the respective  $(k_r + k_q)$  and  $k_r$  values related to all the substrates studied.

Substrates	$\gamma = k_r / (k_r + k_q)$	$\beta = k_d / (k_r + k_q)$ (mol.L <sup>-1</sup> )	$k_r + k_q$ (M <sup>-1</sup> .s <sup>-1</sup> )	$k_r$ (M <sup>-1</sup> .s <sup>-1</sup> )
$\alpha$ -Terpinene	1	0	/	/
Citronellol caprate	0.65	0.05	$2.0 \times 10^6$	$1.30 \times 10^6$
Geraniol caprate	0.51	0.05	$2.0 \times 10^6$	$1.02 \times 10^6$
Methyl linolenate	0.06	0.05	$2.0 \times 10^6$	$1.20 \times 10^5$
Methyl linoleate	0.15	0.18	$5.5 \times 10^5$	$8.25 \times 10^4$
Methyl oleate	0.58	1	$1.0 \times 10^5$	$5.80 \times 10^4$

Table 2.7:  $\gamma$ ,  $\beta$  and  $(k_r + k_q)$  parameters obtained for the photooxidation of substrates

First of all, 3 categories of substrates are highlighted.  $\alpha$ -Terpinene is the most reactive substrate towards  $^1\text{O}_2$  leading to the fast formation of endoperoxide. This singlet oxygenation is characterized by extreme values for  $\gamma$  and  $\beta$  parameters leading to a pure chemical quenching of  $^1\text{O}_2$  with the substrate (M) and negligible physical quenching by the substrate and the solvent. Indeed,  $\gamma = 1$  highlights that  $k_r = (k_r + k_q)$  and therefore, there is not physical quenching ( $k_q = 0$ ). Moreover,  $\beta = 0$  shows that the kinetic rate constant of chemical reaction ( $k_r$ ) and chemical quenching ( $k_q$ ) are much higher than that of the deactivation of  $^1\text{O}_2$  by the solvent ( $k_d$ ) (Eq. 2.27).

$$k_d \ll (k_r + k_q)[M] \quad (2.27)$$

As there is not physical quenching ( $k_q = 0$ ), the equation 2.27 becomes the equation 2.28.

$$k_d \ll k_r [M] \quad (2.28)$$

Citronellol caprate and geraniol caprate have the same Foote coefficient ( $\beta = 0.05$ ) and therefore the same  $(k_r + k_q)$  parameter ( $2.0 \times 10^6 \text{ M}^{-1}.\text{s}^{-1}$ ). Nevertheless, the difference results in their respective  $\gamma$  parameter which is higher for citronellol caprate (0.65) than for geraniol caprate (0.51). Consequently, the kinetic reactivity  $k_r$  related to the chemical reaction between substrate and  $^1\text{O}_2$  is higher for citronellol caprate ( $1.30 \times 10^6 \text{ M}^{-1}.\text{s}^{-1}$ ) than for geraniol caprate ( $1.02 \times 10^6 \text{ M}^{-1}.\text{s}^{-1}$ ). Conversely, this highlights a higher physical quenching ( $k_q$ ) for the geraniol caprate photooxidation.

Terpenoids and FAMES are easily identifiable as two different groups of compounds. Indeed, the linear carbon chains of the three FAMES (*i.e.* methyl oleate, linoleate and linolenate) allow just the reaction of singlet oxygen with di-substituted olefins whereas the reactions of terpenoids (*i.e.* citronellol and geraniol caprate) support the reaction of  $^1\text{O}_2$  with tri-substituted olefins. As mentioned before, trisubstituted olefins terpenoids are more reactive than di-substituted ones (FAMES) in agreement with our kinetic curves (Fig. 2.18). Moreover, the reactivity of tri-unsaturated substrates (methyl linolenate) towards  $^1\text{O}_2$  is faster than for di-unsaturated FAME (methyl linoleate) and than for mono-unsaturated FAME (methyl oleate). Indeed, kinetic rate constants  $k_r$  and  $(k_r + k_q)$  are respectively higher for the singlet oxygenation of methyl linolenate ( $1.20 \times 10^5 \text{ M}^{-1}\cdot\text{s}^{-1}$ ,  $2.0 \times 10^6 \text{ M}^{-1}\cdot\text{s}^{-1}$ ) than methyl linoleate ( $8.25 \times 10^4 \text{ M}^{-1}\cdot\text{s}^{-1}$ ,  $5.5 \times 10^5 \text{ M}^{-1}\cdot\text{s}^{-1}$ ) which is in turn more reactive than methyl oleate ( $5.80 \times 10^4 \text{ M}^{-1}\cdot\text{s}^{-1}$ ,  $1.0 \times 10^5 \text{ M}^{-1}\cdot\text{s}^{-1}$ ). Surprisingly, the kinetic rate constant  $k_q$  is about 50 times higher in the case of methyl linolenate compared to methyl linoleate. This is probably due to the large number of unsaturation for peroxides from methyl linolenate which lead to a deactivation of  $^1\text{O}_2$  as for carotenoids. Figure 2.19 illustrates the reactivity of each substrate vs the kinetic rate constants of chemical reaction ( $k_r$ ).

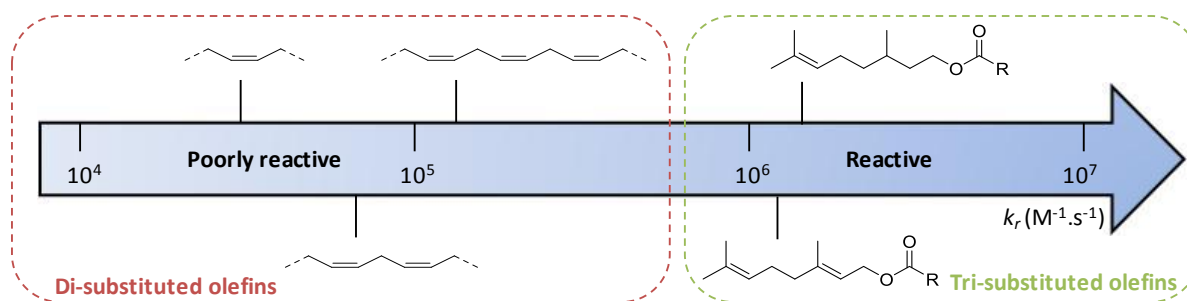


Figure 2.19: Scale of reactivity of di- (*i.e.* methyl oleate, linoleate and linolenate) and tri- (*i.e.* citronellol and geraniol caprate) substituted olefins towards singlet oxygen based on their chemical reactivity ( $k_r$ ) with  $^1\text{O}_2$

## 2.5 Conclusion

The singlet oxygenation of terpenoids and FAMES leads to complex mixtures of hydroperoxide isomers and peroxides. The singlet oxygenation is a simple and smooth method to get intact hydroperoxides and peroxides compounds at low temperature (5 °C) which are then used as food oxidized models. Compared to autoxidation, this method allows obtaining both faster and more selectively hydroperoxides.

LC-UV analyses can differentiate the different degrees of oxidation compounds (*i.e.* mono-hydroperoxides, di- and tri-peroxides) providing interesting kinetic information. The reactivity of tri-substituted olefins towards  $^1\text{O}_2$  is much higher than that with di-substituted olefins as seen from the respective kinetic curves of terpenoids (*i.e.* geraniol and citronellol caprate) and FAMES (*i.e.* methyl oleate, linoleate and linolenate) disappearance. It is a convenient method for the detection of products but the separation of hydroperoxides is not complete. Indeed, the LC-UV method is pointed out as not efficient for the separation of different regioisomers of hydroperoxides and complex mixture of peroxides. Moreover, this technique does not lead to a chemical structure elucidation of compounds.

NMR investigation is an effective method to analyze the peroxides obtained by photooxidation. Indeed, the isomeric ratio between two mono-hydroperoxides can be calculated on a simple photooxidized compound. Moreover, it is possible to identify the characteristic patterns of secondary

and tertiary internal and end-chain hydroperoxides. Nevertheless, it is complex to characterize traces of oxidized compounds and identify each hydroperoxides into a complex oxidized mixture.

LC-UV and NMR analyses have shown some limits and do not allow a complete separation and a full chemical structure elucidation of complex mixture of peroxides. Consequently, we turned to mass spectrometry to confirm the nature of various peroxides detected, improve their separation and specifically analyse traces of hydroperoxides.

### 3. Mass spectrometry investigations of (poly)unsaturated terpenes, FAMES, hydroperoxides and peroxide compounds

In the previous paragraphs (see the paragraph 2), we showed that the direct analysis of traces of FAMES hydroperoxides (< 1 %) through classical methods was not satisfactory. Thus, GC-MS requires a high temperature leading to the decomposition of hydroperoxide if it is not pre-silylated or pre-reduced.  $^1\text{H}$  and  $^{13}\text{C}$  NMR are not sensitive to detect traces of targeted compounds and are unsuitable for the analysis of complex mixtures without preliminary separation. LC-UV respects the integrity of hydroperoxides but it is not efficient for the separation of different regioisomers of hydroperoxides and complex mixture of peroxides.

Further to these difficulties, we have undertaken an analytical study in order to develop a new method able to exalt the selective detection of hydroperoxides and minimize their decomposition. The underlying idea was to analyse by direct liquid injection mass spectrometry (DLI-ESI-MS) some solutions of FAMES and related hydroperoxides on which different cations were added in order to found the one which has the highest affinity for peroxides and the lowest affinity for double bonds and ester functions also contained in oxidized FAMES. Series of classical ( $\text{H}^+$ ,  $\text{NH}_4^+$ ,  $\text{Na}^+$ ,  $\text{Li}^+$  and  $\text{Ag}^+$ ) or more unusual ( $\text{K}^+$ ,  $\text{Rb}^+$ ,  $\text{Cs}^+$ ,  $\text{Be}^{2+}$ ,  $\text{Ca}^{2+}$  and  $\text{Ba}^{2+}$ ) cations associated to the acetate counterion have been tested. The counterion could lead to a suppression of signals during the electrospray ionization. Indeed, the counterions with strong conductivity are responsible for a sharp decrease of the intensity of mass peaks. Therefore, due to its low conductivity, acetate is the relevant counterion. Then, Liquid chromatography coupled to tandem mass spectrometry (LC-MS/MS) was employed to separate complex mixtures of hydroperoxides. Finally, the hypothetical peroxyhemiacetals which could be produced through secondary reactions between hydroperoxides and aldehydes is searched in oxidized edible oils since it has been shown recently that such unusual peroxide is formed in fragrances. This work is made possible by the collaboration with the TRACES research team of the "Institut des Sciences Analytiques" (ISA, Lyon).

#### 3.1 Influence of various ions on the detection of FAMES and hydroperoxides by MS

The impact of alkali metal ( $\text{H}^+$ ,  $\text{Li}^+$ ,  $\text{Na}^+$ ,  $\text{K}^+$  and  $\text{Cs}^+$ ), alkaline earth metal ( $\text{Be}^{2+}$ ,  $\text{Ca}^{2+}$  and  $\text{Ba}^{2+}$ ), transition metal ( $\text{Ag}^+$ ) and non-metallic ( $\text{NH}_4^+$ ) ions has been studied by Direct Liquid Injection (DLI) mass spectrometry analysis of FAMES and mono-hydroperoxide of methyl oleate ( $\text{C}_{18}:1(\text{OO})_1$ ). The various adducts formed between substrates (M) and ions ( $\text{X}^+$ ) are identified in the form of  $[\text{M}+\text{X}]^+$  at specified m/z values. The experimental part gathered all the  $[\text{M}+\text{X}]^+$  m/z data and absolute intensity of each adducts formed.

### 3.1.1 Direct Liquid Injection Mass Spectrometry (DLI-MS) analysis of FAMES

Figure 2.20 shows the absolute intensity of adducts formed between FAMES (*i.e.* methyl stearate, oleate, linoleate and linolenate) and monovalent ions (*i.e.*  $\text{NH}_4^+$ ,  $\text{H}^+$ ,  $\text{Li}^+$ ,  $\text{Na}^+$ ,  $\text{K}^+$ ,  $\text{Rb}^+$ ,  $\text{Cs}^+$  and  $\text{Ag}^+$ ).

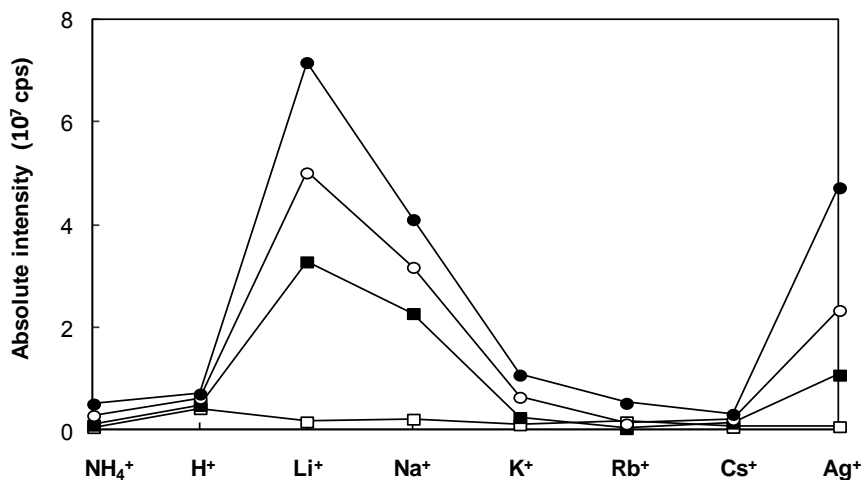


Figure 2.20 Absolute intensity of peaks observed through ionization of methyl stearate (□), methyl oleate (■), methyl linoleate (○) and methyl linolenate (●) ( $[\text{FAMES}] = 10^{-6} \text{ mol.L}^{-1}$ ) with each separate cations  $\text{H}^+$ ,  $\text{NH}_4^+$ ,  $\text{Li}^+$ ,  $\text{Na}^+$ ,  $\text{K}^+$ ,  $\text{Rb}^+$ ,  $\text{Cs}^+$  and  $\text{Ag}^+$  ( $[\text{ions}] = 10^{-3} \text{ mol.L}^{-1}$ ) during Direct Liquid Injection (DLI) ESI-MS in ion-positive mode (ES+) (solvent:  $\text{H}_2\text{O}/\text{MeOH}$  50/50 v:v)

First of all, there is almost no ionization of saturated FAME (methyl stearate, C18:0) whatever the ion used whereas (poly)unsaturated FAMES are readily ionized. Therefore, we assume that the double bond is ionized instead of the ester group. Moreover, in any case, the ionization is stronger for methyl linolenate (C18:3) than for methyl linoleate (C18:2) which is in turn more intense than for methyl oleate (C18:1). Accordingly, the more FAMES are unsaturated, the higher is the ionization.

$\text{NH}_4^+$  and  $\text{H}^+$  are not effective for ionizing substrates although the concentration of these ions is 1000 times higher than for FAMES. The most significant increase in intensity is observed with  $\text{Li}^+$ . Indeed, the signal of the  $[\text{M}+\text{Li}]^+$  adduct is found to be approximately 10 times higher than the corresponding  $[\text{M}+\text{H}]^+$  signal. Then, a sharp drop in affinity is found when alkali metals of larger ionic radius ( $\text{Na}^+$ ,  $\text{K}^+$ ,  $\text{Rb}^+$  and  $\text{Cs}^+$ ) are used (Table 2.8). All the FAMES investigated suffer a gradual decline in affinity with an increasing MW of the alkali metals. The smallest is the cation, the stronger is the interaction with double bonds due to electrostatic field. It is essential to note that FAMES are almost not ionized by  $\text{Cs}^+$ . The same behavior was found by Kohler and Leary with the LC-MS/MS analyses of carbohydrates with post column addition of metal chloride.<sup>227</sup>

Alkali metal ion	$\text{Li}^+$	$\text{Na}^+$	$\text{K}^+$	$\text{Rb}^+$	$\text{Cs}^+$
Ionic radius (pm)	76	102	138	152	167

Table 2.8: Atomic radius (pm) of alkali metals ions ( $\text{Li}^+$ ,  $\text{Na}^+$ ,  $\text{K}^+$ ,  $\text{Rb}^+$ ,  $\text{Cs}^+$  and  $\text{Fr}^+$ )

As described first by Bayer *et al*,  $\text{Ag}^+$  enhances the ionization of unsaturated compounds *via* coordination of  $\text{Ag}^+$  to double bonds leading to stable  $\pi$  complexes.<sup>187</sup> The two silver isotopes  $^{107}\text{Ag}$  and  $^{109}\text{Ag}$  are present in a ratio of approximately 1:1 and adducts formed with FAMES and hydroperoxides provide distinctive doublets in mass spectrometry (Fig. 2.21).

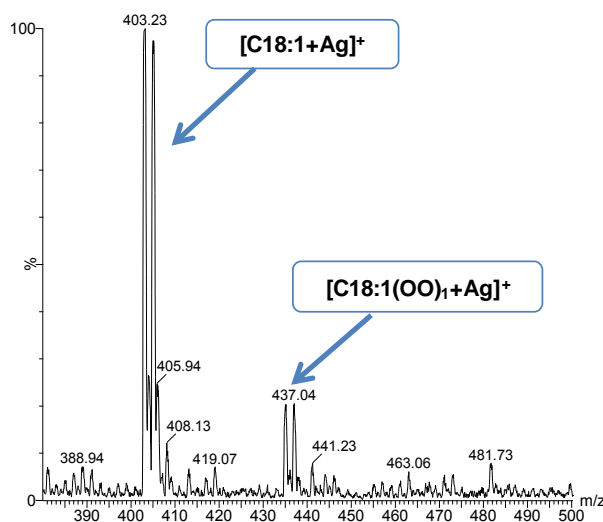


Figure 2.21: CIS-MS spectrum of a mixture of methyl oleate C18:1 and its mono-hydroperoxide C18:1(OO)<sub>1</sub> ( $10^{-6}$  M) with Ag<sup>+</sup> ( $10^{-3}$  M) in ion-positive mode (ES+) (solvent: H<sub>2</sub>O/MeOH 50/50 v:v)

As expected, the saturated methyl stearate (C18:0) does not form silver ion adduct. In contrast, the binding ability of esters to Ag<sup>+</sup> increases with the number of double bonds (C18:3 > C18:2 > C18:1 and C18:0 ≈ 0). Seal *et al.* observed the same behavior of Ag<sup>+</sup> with cholesterol esters (C20:0, C20:1, C20:2, C20:3 and C20:4).<sup>45</sup>

The same tendency is obtained by analyzing equimolar mixture of methyl oleate, linoleate and linolenate ([C18:1] = [C18:2] = [C18:3] =  $10^{-6}$  mol.L<sup>-1</sup>). As an example, **figure 2.22** shows a stronger affinity of Li<sup>+</sup> and Na<sup>+</sup> for 3 double bonds (C18:3) than for two (C18:2) and one (C18:1) unsaturations.

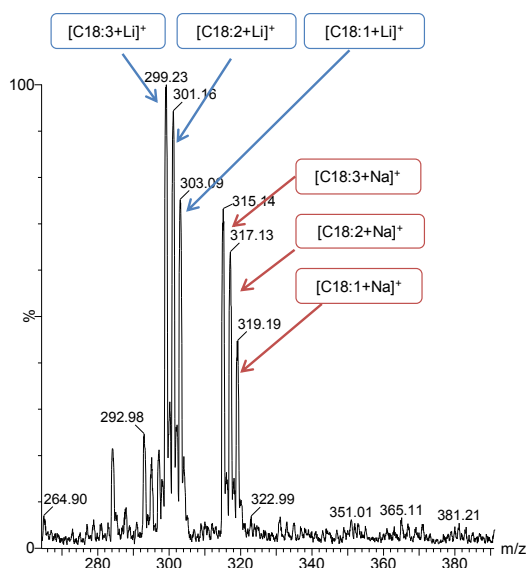
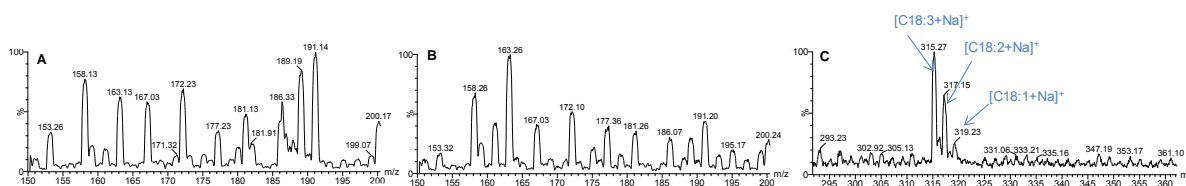


Figure 2.22: DLI-ESI-MS spectrum of an equimolar mixture of FAMES ([C18:1] = [C18:2] = [C18:3] =  $10^{-6}$  M) with Li<sup>+</sup> ( $10^{-5}$  M) and natural occurrence of Na<sup>+</sup> in ion-positive mode (ES+) (solvent: H<sub>2</sub>O/MeOH 50:50 v:v)

There is no ionization of substrates by alkaline earth metal divalent ions Be<sup>2+</sup>, Ca<sup>2+</sup> and Ba<sup>2+</sup>. FAMES remain on the [M+Na]<sup>+</sup> form because of the Na<sup>+</sup> cations are naturally present in the LC-MS system. Moreover, as they are divalent cations, the resulting mass peak of adducts is divided by two ([M+X]<sup>+</sup>/2). It is a real disadvantage because the mass peak could be located on the background which is more complex to analyze. **Figure 2.23** shows the DLI mass spectrometry analysis of equimolar mixture of FAMES mixed with Ca<sup>2+</sup>. The predicted mass peaks [M+Ca]<sup>+</sup>/2 (m/z = 168 for

C18:1, 167 for C18:2 and 166 for C18:3) are not obtained and the mass spectrum is equivalent to that of the blank composed by methanol and water. After all, FAMES are still well ionized by  $\text{Na}^+$ .



**Figure 2.23:** DLI-ESI-MS spectra in ion-positive mode (ES+) of an equimolar mixture of FAMES ([C18:1] = [C18:2] = [C18:3] =  $10^{-6}$  M) with  $\text{Ca}^{2+}$  acetate ( $10^{-3}$  M), mass range from  $m/z = 150$  to  $200$  for  $[\text{M}+\text{Ca}]^{2+}$  visualization (A), blank spectrum (B) and mass range from  $m/z = 300$  to  $360$  for  $[\text{M}+\text{Na}]^+$  visualization (C) (solvent:  $\text{H}_2\text{O}/\text{MeOH}$  50/50 v:v)

### 3.1.2 Direct Liquid Injection Mass Spectrometry (DLI-MS) analysis of hydroperoxides

**Figure 2.24** shows the absolute intensity of adducts  $[\text{C18:1}(\text{OO})_1+\text{X}]^+$  formed between mono-hydroperoxide C18:1(OO)<sub>1</sub> and 8 different monovalent ions (X).

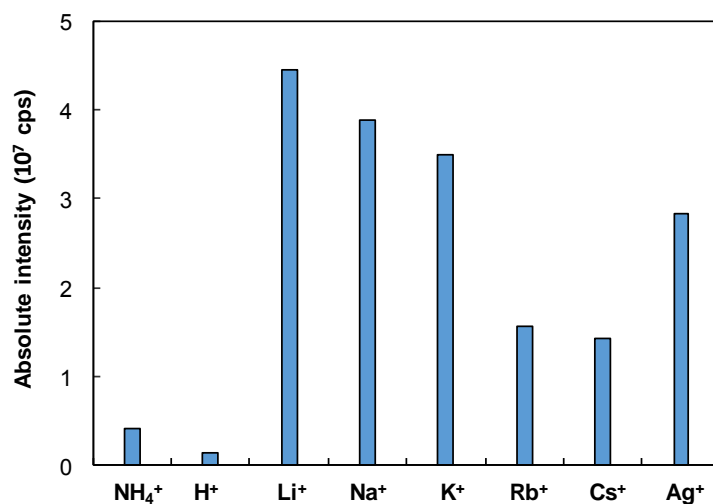


**Figure 2.24:** Absolute intensity of peaks observed through ionization of C18:1(OO)<sub>1</sub> ( $10^{-6}$  M) with each separate  $\text{NH}_4^+$ ,  $\text{H}^+$ ,  $\text{Li}^+$ ,  $\text{Na}^+$ ,  $\text{K}^+$ ,  $\text{Rb}^+$ ,  $\text{Cs}^+$ , and  $\text{Ag}^+$  acetates during Direct Liquid Injection (DLI) ESI-MS in ion-positive mode (ES+) (solvent:  $\text{H}_2\text{O}/\text{MeOH}$  50/50 v:v)

As for FAMES, mono-hydroperoxide ionization shows a gradual decline in affinity with increasing MW of alkali metals. Indeed, strongest ionization is obtained with  $\text{Li}^+$  followed by  $\text{Na}^+$ ,  $\text{K}^+$ ,  $\text{Rb}^+$  and  $\text{Cs}^+$ . C18:1(OO)<sub>1</sub> strongly binds to  $\text{Ag}^+$  giving the  $[\text{C18:1}(\text{OO})_1+\text{Ag}]^+$  adducts. Finally,  $\text{H}^+$  and  $\text{NH}_4^+$  only afford a weak ionization of C18:1(OO)<sub>1</sub>. Moreover, there is still no ionization of hydroperoxide by alkaline earth metal divalent ions  $\text{Be}^{2+}$ ,  $\text{Ca}^{2+}$  and  $\text{Ba}^{2+}$  since they remain on the  $[\text{M}+\text{Na}]^+$  form. Therefore,  $\text{Li}^+$  is the most promising monovalent ion to enhance the detection of pure hydroperoxides.

### 3.1.3 Competition between FAMES and hydroperoxide ionizations

**Figure 2.25** shows the absolute intensity of adducts formed between equimolar mixture of methyl oleate hydroperoxide (C18:1(OO)<sub>1</sub>) and methyl oleate (C18:1) with 6 different monovalent cations (Table S2.5). The goal of this study is to enhance the MS signal of hydroperoxides compared to that of FAMES through a specific ionization of hydroperoxide. In order to compare the effectiveness of different ions with regard to this criterion, the ratios  $R = \text{C18:1}(\text{OO})_1/\text{C18:1}$  of peaks intensities are calculated for each ion added at  $10^{-4}$  M.

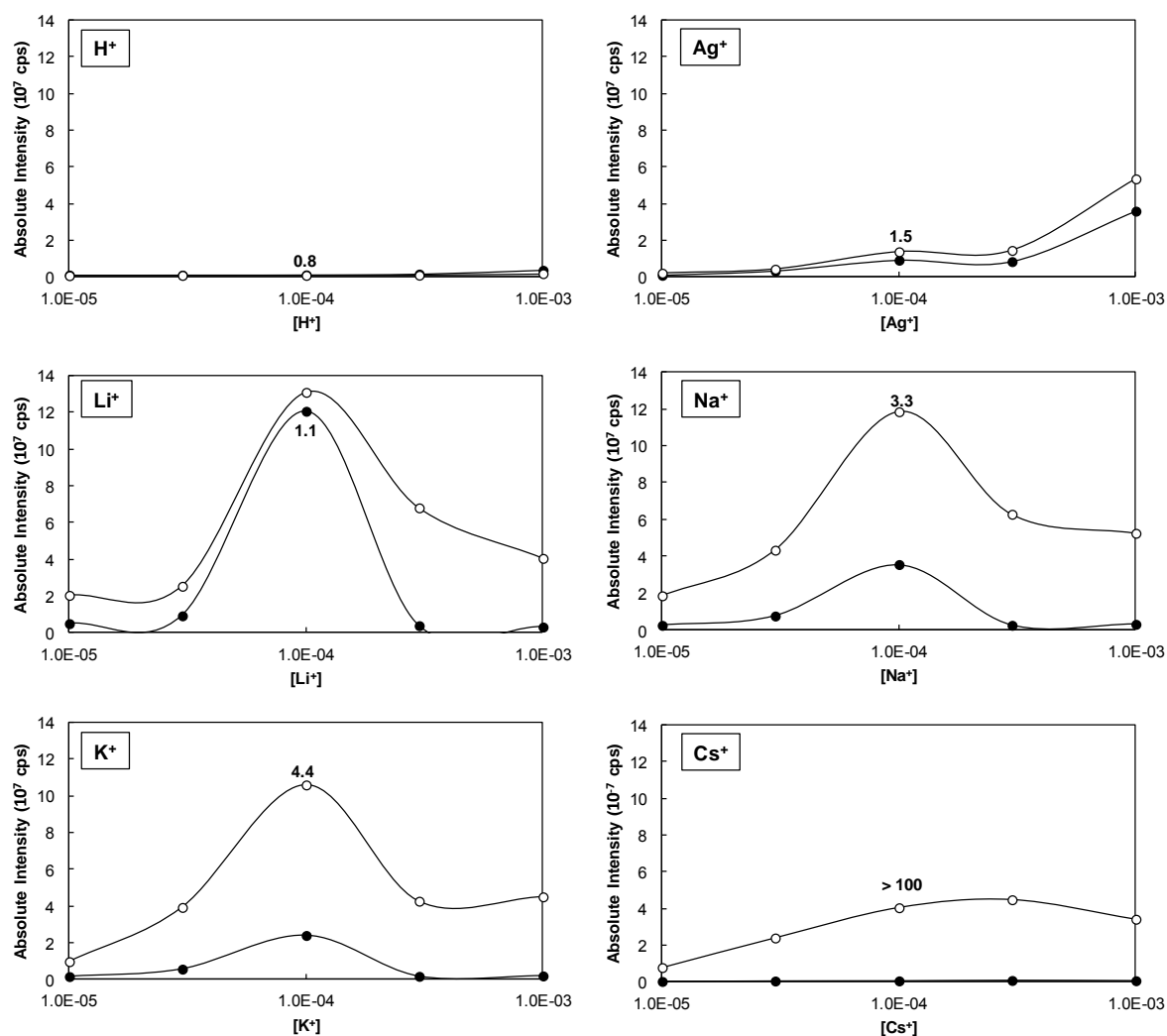


Figure 2.25: Absolute intensity of peaks observed through ionization of an equimolar mixture of  $C18:1(OO)_1$  ( $\circ$ ,  $10^{-6}$  M) and  $C18:1$  ( $\bullet$ ,  $10^{-6}$  M) with  $H^+$ ,  $Ag^+$ ,  $Li^+$ ,  $Na^+$ ,  $K^+$  and  $Cs^+$  acetates at various concentration during Direct Liquid Injection (DLI) ESI-MS in ion-positive mode (ES+) (solvent:  $H_2O/MeOH$  50/50 v:v), the ratios  $R = C18:1(OO)_1/C18:1$  of peaks intensities are indicated above the curves for  $[ion] = 10^{-4}$  M

$H^+$  shows a greater ionization of  $C18:1$  than  $C18:1(OO)_1$ . The ratio  $C18:1(OO)_1/C18:1$  of peaks intensities is lower than 1.0 whereas it is higher than one for the other cations ( $C18:1(OO)_1/C18:1 > 1.0$ ). This is probably due to the degradation of  $[R(OO)_1+H]^+$  adduct into epoxide and alcohol as described by Karlberg *et al.*<sup>236</sup> Added to the low absolute intensities of peaks,  $H^+$  is not an appropriate ion for the selective ionization of hydroperoxides. Given the  $C18:1(OO)_1/C18:1$  intensity ratios obtained with  $Ag^+$ , we see that it has approximately the same affinity for  $C18:1$  than  $C18:1(OO)_1$ . This is due to the presence of one double bond in both substrates. Accordingly,  $Ag^+$  enhances the mass signal of  $C18:1(OO)_1$  but also that of  $C18:1$  which is not in favor of a selective ionization of hydroperoxides.  $Li^+$ ,  $Na^+$  and  $K^+$  show a maximum of ionization at  $10^{-4}$  mol.L $^{-1}$  and then there is an inhibition of the signal at high concentration of ions. Even if these 3 ions reveal a strong ionization of  $C18:1(OO)_1$ , the ratios  $C18:1(OO)_1/C18:1$  are lower than 5 with  $[ions] < 10^{-4}$  mol.L $^{-1}$ . Consequently, they can be used for the ionization of FAMES and hydroperoxides but these 3 alkaline ions are not convenient for a specific ionization of  $C18:1(OO)_1$ . It is worth to notice  $Cs^+$  does not form any adducts with  $C18:1$  whereas ionization takes place with  $C18:1(OO)_1$  since the ratio  $C18:1(OO)_1/C18:1$  is higher than 100. Finally, it is clear that  $Cs^+$  is the most effective alkaline cation with regard to the selective ionization of hydroperoxides.

Figure 2.26 illustrates the comparison between the absolute intensity of the peaks obtained for C18:1(OO)<sub>1</sub> and C18:1 adducts with each ion (10<sup>-4</sup> mol.L<sup>-1</sup>) and results are compared with the main bisector (dotted line).

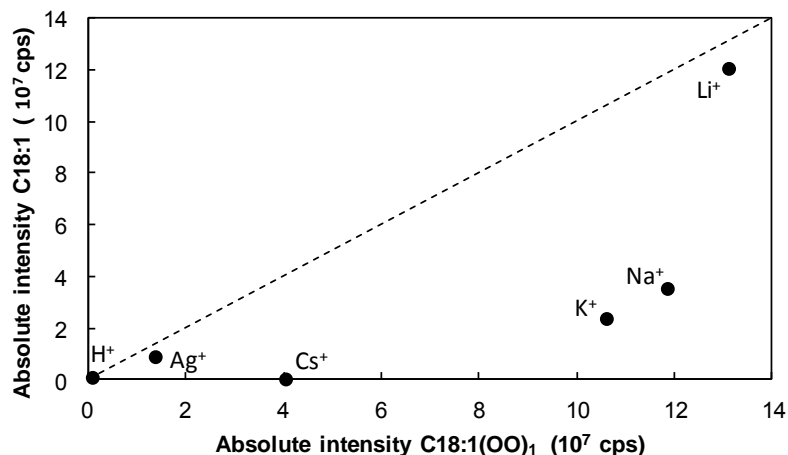
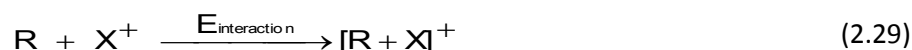


Figure 2.26: Comparison of the absolute intensity of peaks observed through ionization of an equimolar mixture of C18:1(OO)<sub>1</sub> and C18:1 ([C18:1(OO)<sub>1</sub>] = [C18:1] = 10<sup>-6</sup> M) with H<sup>+</sup>, Ag<sup>+</sup>, Li<sup>+</sup>, Na<sup>+</sup>, K<sup>+</sup> and Cs<sup>+</sup> acetates ([ion] = 10<sup>-4</sup> mol.L<sup>-1</sup>) during Direct Liquid Injection (DLI) ESI-MS in ion-positive mode (ES+) (solvent: H<sub>2</sub>O/MeOH 50/50 v:v)

This figure shows that H<sup>+</sup> is not at all efficient to enhance the ionization of C18:1 and C18:1(OO)<sub>1</sub> whereas Li<sup>+</sup> and Ag<sup>+</sup> ionize both compounds with the same efficiency. Na<sup>+</sup> and K<sup>+</sup> exhibit a higher affinity for C18:1(OO)<sub>1</sub> but they still ionize significantly C18:1. Cs<sup>+</sup> is highlighted as the most relevant monovalent ion for inducing a highly selective ionization of hydroperoxides. The ionization of target compounds by cations can be rationalized by molecular modeling (Gaussian software) through DFT calculation from equations 2.29 to 2.31. The studied substrate, ions and adducts are modeled by DFT computations by putting the ion closed to the targeted function. The energy of interaction between substrate and ion is given by the difference between the enthalpy of formation of adduct and those of substrate and ion.



$$E_{\text{interaction}} = H_f^0([R + X]^+) - H_f^0(R) - H_f^0(X^+) \quad (2.30)$$

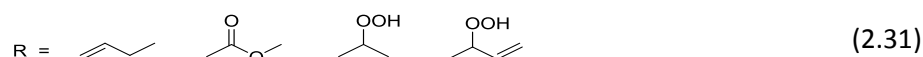


Figure 2.27 shows the molecular modeling of targeted adducts formed between unsaturated carbon chain, ester, saturated and unsaturated hydroperoxides with Cs<sup>+</sup>.

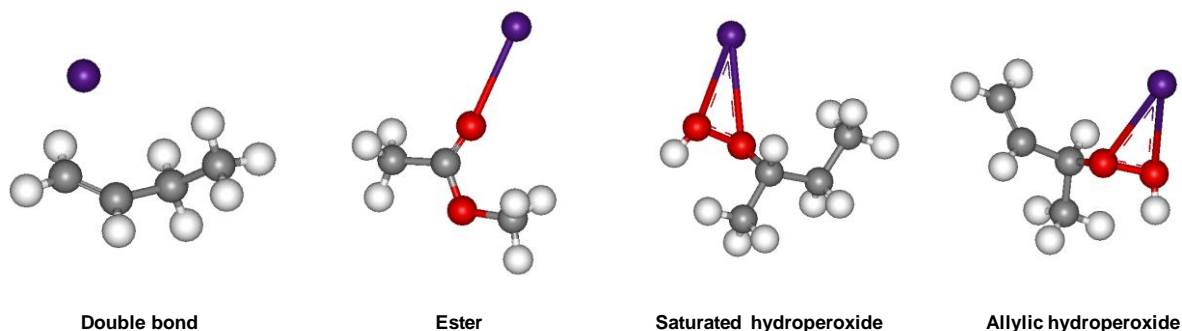


Figure 2.27: Molecular modeling with DFT calculation of adducts formed between all the investigated molecules (R) and Cs<sup>+</sup>

The same model has also been constructed with  $\text{Na}^+$ ,  $\text{Li}^+$ ,  $\text{K}^+$  and  $\text{Ag}^+$ . The energies and distances related to the interaction between analytes and cations are gathered in **table 2.9**.

	$E_{\text{interaction}}$ ( $\text{kcal.mol}^{-1}$ ) and distance ( $\text{\AA}$ )				
	$\text{Li}^+$	$\text{Na}^+$	$\text{K}^+$	$\text{Cs}^+$	$\text{Ag}^+$
<b>Double bond</b>	-28.1 2.34 $\text{\AA}$	-20.1 2.69 $\text{\AA}$	-12.2 3.17 $\text{\AA}$	-8.5 3.63 $\text{\AA}$	-44.4 2.32 $\text{\AA}$
<b>Ester</b>	-45.1 1.76 $\text{\AA}$	-32.0 2.11 $\text{\AA}$	-22.9 2.55 $\text{\AA}$	-16.8 2.93 $\text{\AA}$	-40.5 2.16 $\text{\AA}$
<b>Hydroperoxide</b>	-45.5 1.91 $\text{\AA}$	-32.8 2.27 $\text{\AA}$	-22.5 2.72 $\text{\AA}$	-16.4 3.16 $\text{\AA}$	-40.2 2.28 $\text{\AA}$
<b>Allylic hydroperoxide</b>	-49.3	-35.9	-24.2	-18.0	-49.4

**Table 2.9:** Energies ( $\text{kcal.mol}^{-1}$ , in black) and distances ( $\text{\AA}$ , in red) related to the interactions between analytes (R) and monovalent cations ( $\text{H}^+$ ,  $\text{Li}^+$ ,  $\text{Na}^+$ ,  $\text{K}^+$ ,  $\text{Cs}^+$  and  $\text{Ag}^+$ )

The lowest energies are related to the most stable adducts. As regards to alkali metal ions,  $\text{Li}^+$  forms the most stable adducts. As expected, this is correlated with its lowest atomic radius and distance to the targeted molecule. Therefore, it is the most relevant cation to enhance the ionization of hydroperoxides. Then, the energy of interaction decreases following the increase of the atomic radius of cations ( $\text{Li}^+ < \text{Na}^+ < \text{K}^+ < \text{Cs}^+$ ). All the cations studied have the same interaction with ester and hydroperoxyl functions which is not in agreement with our experimental results showing almost no ionization of methyl stearate. The cation  $\text{Ag}^+$  shows the strongest affinity for double bonds as experimentally well described by Bayer *et al.* with the formation of charged stable  $\pi$  complexes.<sup>187</sup> Given the low energies of interaction,  $\text{Ag}^+$  is also a relevant ion for the ionization of esters and hydroperoxides. Surprisingly, the allylic hydroperoxide adducts formed with all the ions are more stable than those built with saturated hydroperoxide ( $E_{\text{allylic hydroperoxide}} < E_{\text{hydroperoxide}}$ ) (**Fig. 2.28**).

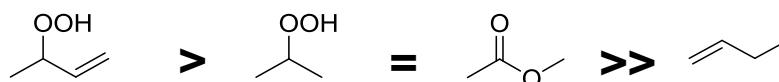


**Figure 2.28:** Decreasing affinity of metal alkali ions ( $\text{H}^+$ ,  $\text{Li}^+$ ,  $\text{Na}^+$ ,  $\text{K}^+$  and  $\text{Cs}^+$ ) for targeted molecules (allylic hydroperoxide, hydroperoxide, ester and double bond)

The cations  $\text{Li}^+$ ,  $\text{Na}^+$ ,  $\text{K}^+$  and  $\text{Ag}^+$  are not relevant for the selective detection of hydroperoxides given the low energies of interaction ( $< -10 \text{ kcal.mol}^{-1}$ ) with double bonds and also hydroperoxides. However, the higher energy of interaction ( $> -10 \text{ kcal.mol}^{-1}$ ) of  $\text{Cs}^+$  with double bonds points out its weak affinity for unsaturated compounds. Added to this its higher affinity for allylic hydroperoxides ( $E_{\text{interaction}} = -18.0 \text{ kcal.mol}^{-1}$ ), we assumed that  $\text{Cs}^+$  could selectively ionize allylic ROOH which is in agreement with our ESI-MS experiments.

The highly selective ionization of allylic hydroperoxides with  $\text{Cs}^+$  can be extremely helpful for detecting very small amount of hydroperoxides found in fragrances and fats during the first steps of oxidative degradation by oxygen.

### 3.2 Selective detection of hydroperoxides and peroxides with Cs<sup>+</sup> by ElectroSpray Ionization Mass Spectrometry (ESI-MS)

Terpenes are ubiquitous in cosmetics and perfumes for their pleasant scent. Nevertheless, they are easily oxidized with O<sub>2</sub> leading to the formation of allergenic hydroperoxides.<sup>237</sup> The oxidation of (poly)unsaturated fatty acids (PUFAs) leads to the formation of hydroperoxides (primary oxidation products) and cyclic peroxides (secondary oxidation products) which are responsible of the deterioration of the organoleptic properties (taste, odor, color) of food.<sup>238</sup>

Therefore, the development of an analytical method is crucial for the determination and quantification of these peroxides. TBARS<sup>127</sup>, FOX<sup>198</sup> and iodometric<sup>205</sup> assays are used to assess lipid peroxidation. However, the limits of these assays are well known, namely, a low sensibility and selectivity. Then, FTIR method provides information on the characteristics, composition and/or chemical changes taking place in oils.<sup>206, 207</sup> <sup>1</sup>H and <sup>13</sup>C NMR can monitor the formation of primary and secondary oxidation products.<sup>208-210</sup> The measurement of oxidized species in food<sup>215</sup> and fragrance<sup>239</sup> by GC-MS has been widely developed *via* chemical ionization. However, hydroperoxides are thermally unstable. Indeed, separation and chemical derivatizations steps are required before the GC-MS analysis of hydroperoxides<sup>43, 72, 76, 83, 85, 120, 122, 239, 240</sup> and secondary oxidation products<sup>71, 82, 87, 91, 119, 217</sup> from (poly)unsaturated FAMES and terpenes. Nevertheless, it is a laborious work and liquid chromatography is now considered as the most effective method to separate and identify intact peroxides.

The assessment of the lipid peroxidation *via* liquid chromatography and UV detection has been realized by the measurement of conjugated diene of lipid hydroperoxides.<sup>218</sup> However, this method is limited by the interfering compounds with the same UV absorption. A specific detection discriminating hydroperoxides from hydroxyl and non-oxidized compounds has been developed by Miyazawa *et al.* *via* luminol chemiluminescence detection (CL) coupled to liquid chromatography.<sup>219, 220</sup> Mass spectrometry is a much more powerful and informative tool for the analysis of hydroperoxides. Indeed, ElectroSpray ionization Mass Spectrometry (ESI-MS) has been widely used to study lipid oxidation due to its sensitivity and specificity.<sup>222</sup> Karlberg *et al.* evaluated the ionization techniques for mass spectrometric detection of hydroperoxides from terpenes and pointed out that [M+H]<sup>+</sup> adducts are well detected.<sup>236</sup> Nevertheless, hydroperoxides are degraded during this experiment because of their dehydration of into epoxide. Moreover, m/z adducts are located in the background where a lot of low molecular weight contaminate the mass spectrum which complicate the analysis.

The strategy of using a metal cation to generate complexes of olefins that can be analyzed by "Coordination Ion-Spray MS" was described by Bayer *et al.* in 1999.<sup>187</sup> In that study, the Ag<sup>+</sup> cation was used to enhance the MS detection of (poly)unsaturated compounds such as olefins, polyolefins and aromatic substrates (*i.e.* vitamins, carotenoids, polystyrenes, terpenes and unsaturated fatty acids) through the formation of charged stable  $\pi$  complexes (Fig. 2.29).

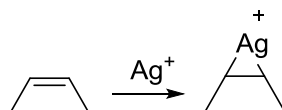


Figure 2.29: Formation of stable  $\pi$  complexes between silver (Ag<sup>+</sup>) and unsaturated compounds

This analytical technique is also a powerful tool for the analysis of peroxide mixtures without pre-derivatization. Havrilla *et al.* analyzed cholesteryl linoleate monohydroperoxide in the form of [M+Ag]<sup>+</sup> adduct.<sup>44</sup> Moreover, Yin *et al.* analyzed the oxidation mixture of eicosapentaenoic acid (EPA)

methyl ester and pointed out the formation of adducts between  $\text{Ag}^+$  and 5-mono-hydroperoxide, monocyclic peroxide, bicyclic endoperoxides and tricyclic peroxide.<sup>221</sup> Nevertheless, due the strong coordination between  $\text{Ag}^+$  and double bonds, the adducts gives fragment ions related to a loss of water and hexanal.<sup>44</sup> As described by Porter *et al.*, the ionization of mono-hydroperoxides from methyl linoleate with  $\text{Ag}^+$  also leads to the Hock fragmentation into aldehydes.<sup>241</sup> Therefore, a part of hydroperoxides is cleaved during the CIS-MS analysis.

The studies have been extended to the alkaline metal cation series ( $\text{Li}^+$ ,  $\text{Na}^+$ ,  $\text{K}^+$ ,  $\text{Rb}^+$  and  $\text{Cs}^+$ ) and comparison of ionization have been made. Kohler and Leary published that the most significant increase in abundance of the carbohydrate adduct ionization is obtained with  $\text{Li}^+$ , which approximately 70 times more abundant than the corresponding  $[\text{M}+\text{H}]^+$ .<sup>227</sup> The affinity for alkali metal with larger ionic radius as potassium ( $\text{K}^+$ ), rubidium ( $\text{Rb}^+$ ) and cesium ( $\text{Cs}^+$ ) was sharply dropped compared to lithium ( $\text{Li}^+$ ) and sodium ( $\text{Na}^+$ ). However, many fragment ions were observed with sodium compared to lithium or potassium adducts.<sup>226</sup>

$\text{Cs}^+$  has already been used to ionize different types of analytes namely poly(ethylene)glycols, phospholipids and carbohydrates. The advantages related to its use have been highlighted.<sup>242</sup> Bogan and Agnes studied the cationization of poly(ethylene glycol) by alkali metal ions including  $\text{Cs}^+$  and showed that the highest resolution of mass peaks is obtained for  $\text{Cs}^+$  and the lowest for  $\text{Na}^+$ .<sup>243</sup> Schiller *et al.* used the matrix-assisted laser desorption and ionization time-of-flight mass spectrometry (MALDI-TOF MS) for the analysis of phospholipids. In biological sample, various cations are present (*i.e.*  $\text{H}^+$ ,  $\text{Na}^+$ ,  $\text{K}^+$ ) which formed different adducts with analytes leading to a considerable peak overlap. The problem of peaks assignment can be overcome by the addition of  $\text{Cs}^+$  due to the large shift of the molecular mass. Kaufman *et al.* pointed out that the MALDI-MS analysis of copolymers can be difficult because of the interferences made by some cations (*i.e.*  $\text{Na}^+$  and  $\text{K}^+$ ). In that way, the addition of  $\text{Cs}^+$  provides the elimination of possible interference.<sup>244</sup> Rogatski *et al.* developed a sensitive LC-MS/MS method for the quantitative analysis of carbohydrate from human plasma through the formation of  $[\text{M}+\text{Cs}]^+$  adducts.<sup>245</sup> Cesium is the preferred monoisotopic cation involved in the formation of adducts as its large mass coupled to the analyte raises the  $m/z$  out of the background where a lot of low molecular weight contaminate the mass spectrum. Finally, large cations as  $\text{Cs}^+$  have lower affinities with carbohydrate compared to smaller cations ( $\text{Li}^+$  and  $\text{Na}^+$ ) due to electrostatic field. Therefore, while there is a significant decomposition of carbohydrate with  $\text{Li}^+$  and  $\text{Na}^+$  due to their high coordination affinity,  $[\text{M}+\text{Cs}]^+$  adducts preferentially undergo a cation elimination without carbohydrate dissociation. However, the ESI-MS analysis of hydroperoxides and peroxides was never tested through the ionization with  $\text{Cs}^+$  although the specific features of  $\text{Cs}^+$  should preserve the integrity of the peroxide function.

- *Ionization with  $\text{Cs}^+$  and suppression of fragmentation into epoxide and alcohol*

Besides the increase of the  $m/z$  of adducts leading to a shift of peaks of small molecules ( $\text{MW} < 200 \text{ g}\cdot\text{mol}^{-1}$ ) out of the background,  $\text{Cs}^+$  improves the selective ionization of intact hydroperoxides without fragmentation of the  $[\text{R}(\text{OO})_1+\text{Cs}]^+$  adduct. The ionization of an equimolar mixture of citronellol ( $\text{MW} = 156 \text{ g}\cdot\text{mol}^{-1}$ ) and its hydroperoxide ( $\text{MW} = 188 \text{ g}\cdot\text{mol}^{-1}$ ) has been studied with  $\text{H}^+$ ,  $\text{Na}^+$ ,  $\text{Li}^+$ ,  $\text{Cs}^+$  and  $\text{Ag}^+$ . **Figure 2.30** shows the DLI-ESI-MS spectra with  $\text{H}^+$ ,  $\text{Na}^+$  and  $\text{Cs}^+$ .

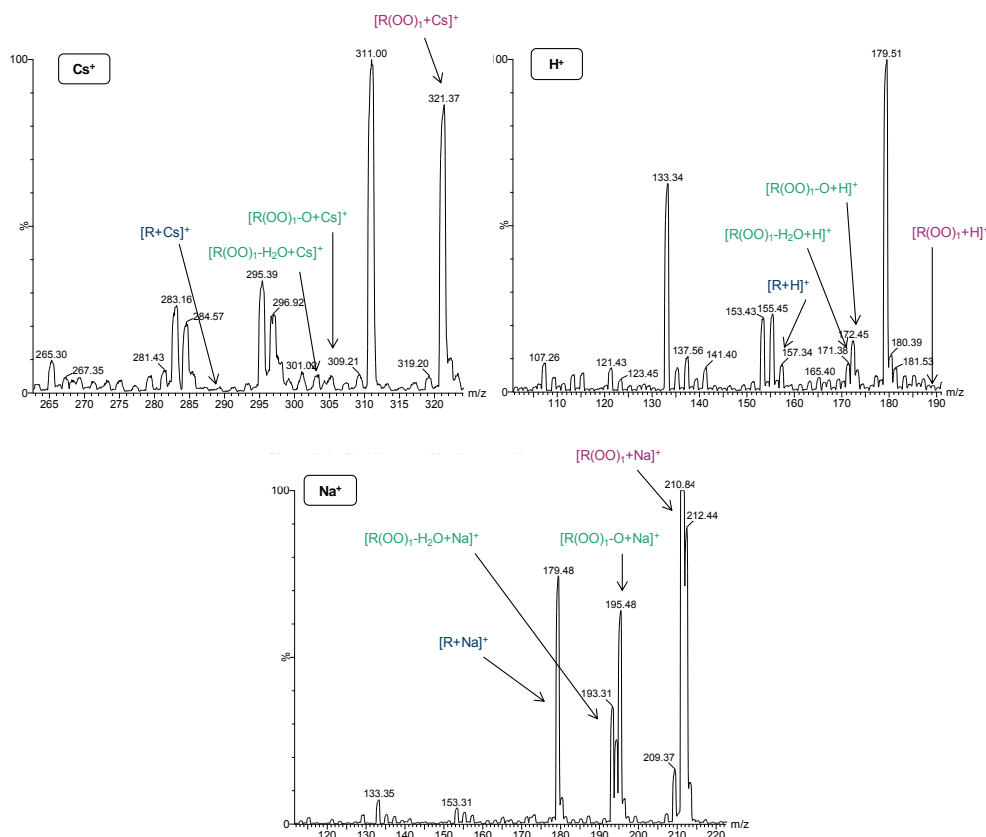


Figure 2.30: DLI-ESI-MS spectra in ion-positive mode (ES+) of an equimolar mixture of citronellol and hydroperoxides ( $[R] = [R(OO)_1] = 4 \times 10^{-6} \text{ M}$ ) with  $\text{Cs}^+$ ,  $\text{H}^+$  and  $\text{Ag}^+$  ( $[\text{ion}] = 10^{-4} \text{ M}$ ) (solvent:  $\text{H}_2\text{O}/\text{MeOH}$  50/50 v:v)

Table 2.10 gathers the resulting (epoxide)/(epoxide + hydroperoxides) and (alcohol)/(alcohol + hydroperoxides) percentage ratios obtained during the ionization of the equimolar mixture of citronellol and hydroperoxides with ions. These ratios represent the dehydration of hydroperoxides into epoxides or enones ( $-\text{H}_2\text{O}$ ,  $-18 \text{ m/z}$ ) and the formation of alcohol ( $-\text{O}$ ,  $-16 \text{ m/z}$ ) (Fig. 2.31).

Ions	Epoxide or Enone	Alcohol
	$-\text{H}_2\text{O}$ E / (E + H) %	$-\text{O}$ A / (A + H) %
$\text{H}^+$	75	81
$\text{Li}^+$	50	50
$\text{Na}^+$	31	42
$\text{Cs}^+$	9	6
$\text{Ag}^+$	50	50

Table 2.10: (epoxide)/(epoxide + hydroperoxides) and (alcohol)/(alcohol + hydroperoxides) percentage ratios obtained during the ionization of the equimolar mixture of citronellol and hydroperoxides ( $[R] = [R(OO)_1] = 4 \times 10^{-6} \text{ M}$ ) with  $\text{H}^+$ ,  $\text{Na}^+$ ,  $\text{Li}^+$ ,  $\text{Cs}^+$  and  $\text{Ag}^+$  ( $[\text{ion}] = 10^{-4} \text{ M}$ ), E = epoxide, A = alcohol and H = hydroperoxide

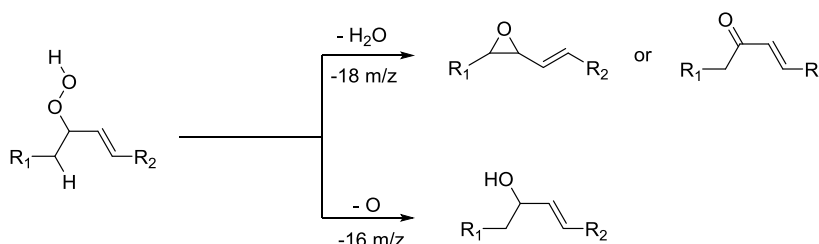
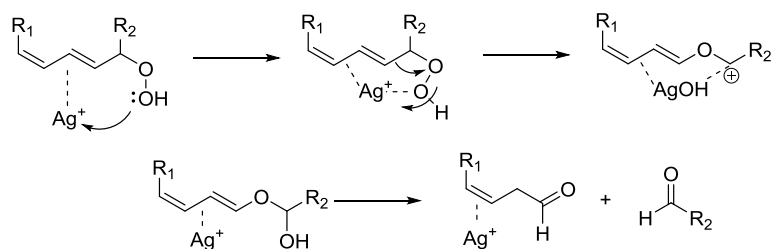


Figure 2.31: Fragmentation of hydroperoxides into epoxides or enones ( $-\text{H}_2\text{O}$ ) and alcohol ( $-\text{O}$ )<sup>246</sup>

As expected, with the lowest E/(E+H) and A/(A+H) ratios, Cs<sup>+</sup> allows the non-degradative ionization of hydroperoxides with almost no cleavage into epoxide and alcohol. Conversely, in our conditions of ionization, H<sup>+</sup>, Li<sup>+</sup>, Na<sup>+</sup> and Ag<sup>+</sup> lead to the strong fragmentation of R(OO)<sub>1</sub>. Moreover, the [R(OO)<sub>1</sub>+H]<sup>+</sup> adduct was almost not detected because it is easily fragmented. We showed previously that large cations as Cs<sup>+</sup> have lower affinities with hydroperoxides compared to smaller cations (Li<sup>+</sup> and Na<sup>+</sup>) due to electrostatic field. Therefore, while there is a decomposition of hydroperoxides into epoxide and alcohol with H<sup>+</sup>, Li<sup>+</sup>, Na<sup>+</sup> and Ag<sup>+</sup> due to their high coordination affinity, [M+Cs]<sup>+</sup> adducts preferentially undergo a cation elimination (-Cs<sup>+</sup>, -133 a.m.u) without hydroperoxide dissociation.

▪ *Ionization with Cs<sup>+</sup> and suppression of the Hock fragmentation into aldehyde*

The Hock fragmentation of hydroperoxides catalyzed by silver (Ag<sup>+</sup>) could be an advantage since it affords an unambiguous information about the position of hydroperoxide on linoleate chain (**Fig. 2.32**).<sup>44</sup> However, this reaction must be avoided when the goal is to detect intact hydroperoxides.



**Figure 2.32:** Hock fragmentation of a diene hydroperoxide promoted by silver ion<sup>44</sup>

Indeed, as pointed out by Porter *et al.*, the ionization of mono-hydroperoxides from methyl linoleate C18:2(OO)<sub>1</sub> with Ag<sup>+</sup> leads to the fragmentation into aldehydes as shown on **figure 2.33**.<sup>241</sup>

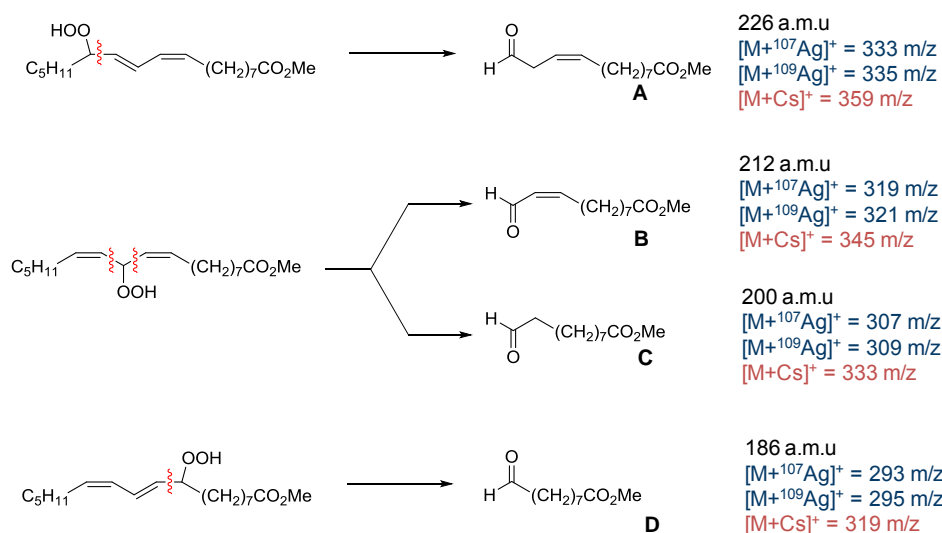


**Figure 2.33:** Hock fragmentation of mono-hydroperoxides from methyl linoleate (C18:2(OO)<sub>1</sub>) and m/z characterization of aldehydes adducts formed with <sup>107</sup>Ag<sup>+</sup> ([M+<sup>107</sup>Ag]<sup>+</sup>) and Cs<sup>+</sup> ([M+Cs]<sup>+</sup>)<sup>241</sup>

The DLI-ESI-MS analysis of the photooxidized methyl linoleate points out the formation of mono- and di- hydroperoxides ([C18:2(OO)<sub>1</sub>+<sup>107</sup>Ag]<sup>+</sup> and C18:2(OO)<sub>2</sub>+<sup>107</sup>Ag]<sup>+</sup> respectively, **Figure 2.34**). As expected, without adding conditions of fragmentation (0 eV), these hydroperoxides undergoes the dehydration into epoxide (C18:2(OO)<sub>1</sub>-H<sub>2</sub>O+<sup>107</sup>Ag]<sup>+</sup> and C18:2(OO)<sub>2</sub>-H<sub>2</sub>O+<sup>107</sup>Ag]<sup>+</sup>) and the Hock's fragmentation into aldehydes (A+<sup>107</sup>Ag]<sup>+</sup>, [C+<sup>107</sup>Ag]<sup>+</sup> and [D+<sup>107</sup>Ag]<sup>+</sup>). Then, it is shown that the

resulting fragmentation (10 eV) of the characteristic adduct of mono-hydroperoxide ( $[\text{C}18:2(\text{OO})_1+^{107}\text{Ag}]^+$  at 433 m/z) favors these fragmentations.

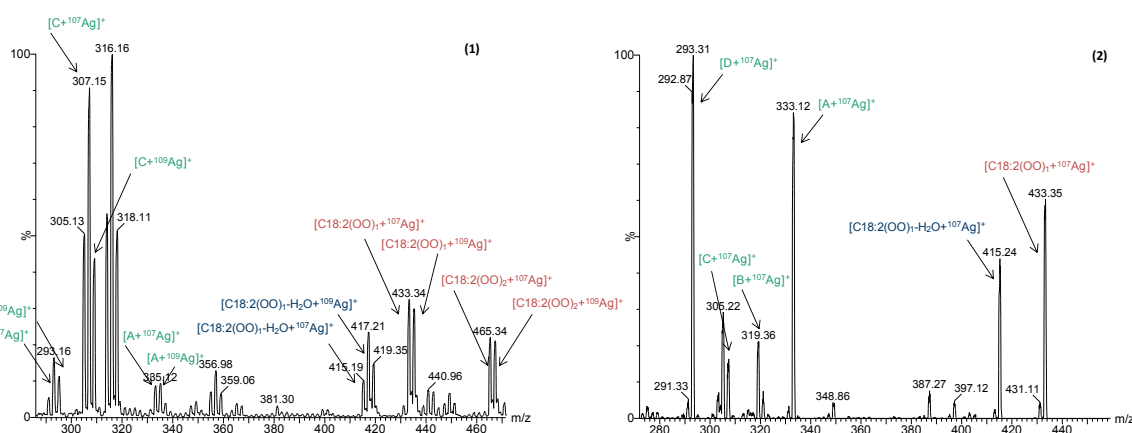


Figure 2.34: DLI-ESI-MS spectra in ion-positive mode (ES+) of mono- and di-hydroperoxides from methyl linoleate ( $4 \times 10^{-6}$  M,  $\text{C}18:2(\text{OO})_1$  and  $\text{C}18:2(\text{OO})_2$  respectively) with  $\text{Ag}^+$  ( $10^{-4}$  M) without condition of fragmentation (1, 0 eV) and under 10 eV (2), fragmentation into epoxide ( $[\text{C}18:2(\text{OO})_1-\text{H}_2\text{O}+^{107}\text{Ag}]^+$  and  $[\text{C}18:2(\text{OO})_2-\text{H}_2\text{O}+^{107}\text{Ag}]^+$ ) and aldehydes ( $[\text{A}+^{107}\text{Ag}]^+$ ,  $[\text{B}+^{107}\text{Ag}]^+$ ,  $[\text{C}+^{107}\text{Ag}]^+$  and  $[\text{D}+^{107}\text{Ag}]^+$ ) (solvent:  $\text{H}_2\text{O}/\text{MeOH}$  50/50 v:v)

Conversely, the DLI-ESI-MS analysis of the same mixture with  $\text{Cs}^+$  shows the ionization of intact hydroperoxides without dehydration or fragmentation into aldehyde (Fig. 2.35). The resulting fragmentation (10 eV) of the characteristic adduct of mono-hydroperoxide ( $[\text{C}18:2(\text{OO})_1+\text{Cs}]^+$  at m/z = 459) does not change anything.

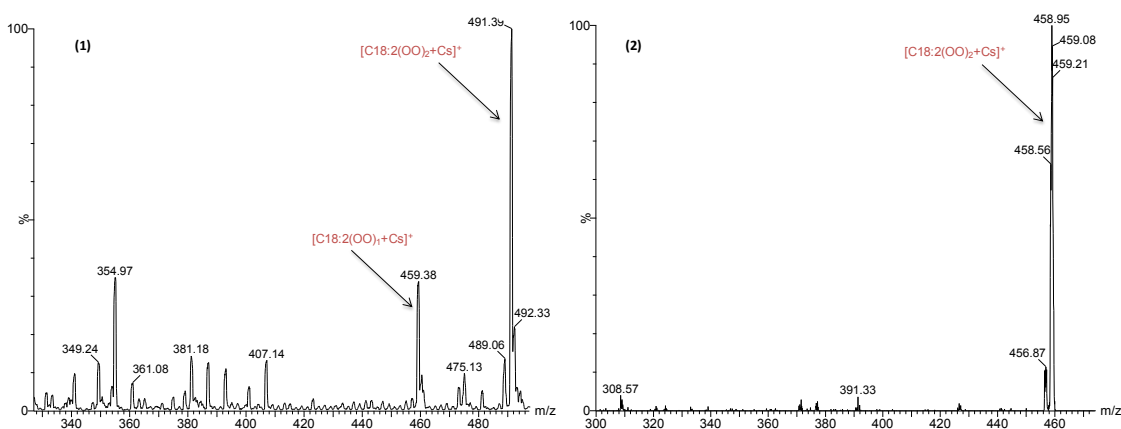


Figure 2.35: DLI-ESI-MS spectra in ion-positive mode (ES+) of mono- and di-hydroperoxides from methyl linoleate ( $4 \times 10^{-6}$  M,  $\text{C}18:2(\text{OO})_1$  and  $\text{C}18:2(\text{OO})_2$  respectively) with  $\text{Cs}^+$  ( $10^{-4}$  M) without condition of fragmentation (1, 0 eV) and under 10 eV (2) (solvent:  $\text{H}_2\text{O}/\text{MeOH}$  50/50 v:v)

While there is a decomposition of hydroperoxides into aldehyde fragments with  $\text{Ag}^+$  due to its high coordination affinity,  $[\text{M}+\text{Cs}]^+$  adducts preferentially undergo a cation elimination ( $-\text{Cs}^+$ , -133 a.m.u). Consequently,  $\text{Cs}^+$  is the highly effective cation for the ionization of hydroperoxides without fragmentation.

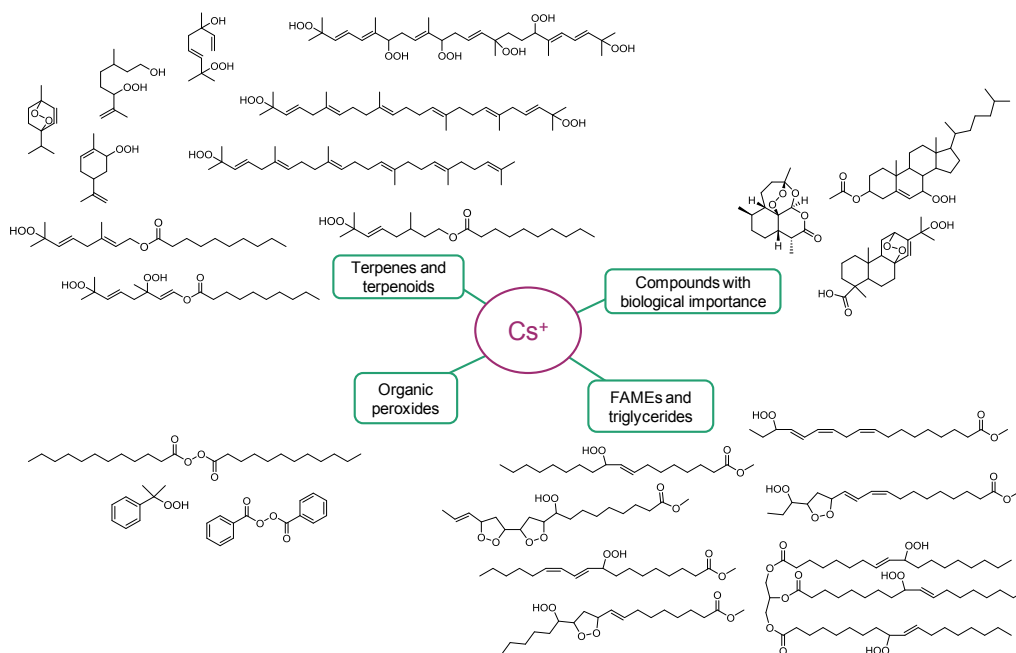
- *Ionization with  $\text{Cs}^+$  and suppression of the peak overlap*

$\text{Cs}^+$  shows another important advantage compared to the use of  $\text{Ag}^+$ . Indeed, the ionization of complex mixture of hydroperoxides with silver leads to the overlapping of peaks due to the isotopic profile of  $\text{Ag}^+$  which complicates the detection. For example, as regards to the complex oxidized



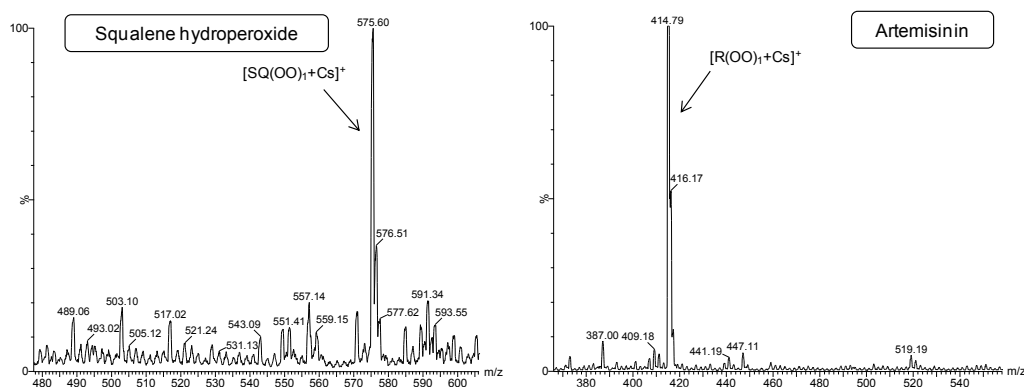
- ESI-MS analysis with  $\text{Cs}^+$  for a large scope of hydroperoxides and peroxides

Based on the advantages given by  $\text{Cs}^+$  during ESI-MS analysis, a large range of hydroperoxides and peroxides from terpenes (*i.e.*  $\alpha$ -terpinene, limonene, citronellol, linalool and squalene), terpenoids (*i.e.* citronellol caprate and geraniol caprate), FAMES (*i.e.* methyl oleate, methyl linoleate and methyl linolenate), triglycerides (*i.e.* triolein) as well as compounds with biological importance (*i.e.* cholesterol acetate and neoabietic acid), organic peroxides (*i.e.* cumene hydroperoxide, lauroyl and benzoyl peroxides) and drugs (*i.e.* artemisinin) has been analyzed (**Figure 2.38**). This scope was first composed of primary oxidation products (mono-hydroperoxides) which are the marker of oxidation in food and perfumes. Even in mono-hydroperoxides are then deteriorated into volatiles compounds, the scope has been extended to secondary oxidation products (hydroperoxy cyclic peroxides, di-, tri- and hexa-peroxides). Only one typical regioisomer is represented for the hydroperoxides when samples contain a mixture of isomers.



**Figure 2.38:** Selection of compounds that can be detected by ESI-MS with  $\text{Cs}^+$

All the hydroperoxides and peroxides are well ionized with  $\text{Cs}^+$  under ESI-MS analysis. **Figure 2.39** points out the DLI-ESI-MS spectra of squalene hydroperoxide, artemisinin, triolein hydroperoxide and C18:2 hydroperoxides. The other spectra can be found in the experimental part (**Fig. S2.22**).



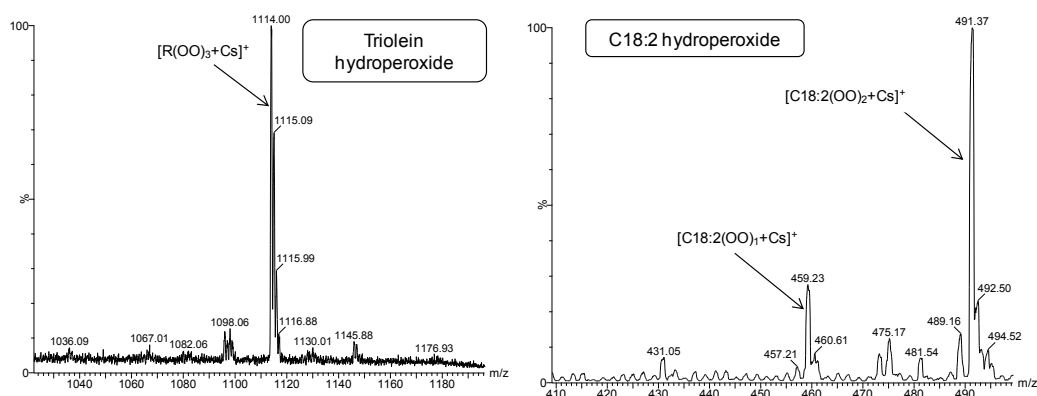


**Figure 2.39:** DLI-ESI-MS spectra in ion-positive mode (ES+) of squalene hydroperoxide (SQ(OO)<sub>1</sub>), artemisinin (R(OO)<sub>1</sub>), triolein hydroperoxide (R(OO)<sub>3</sub>) and methyl linoleate hydroperoxides (C18:2(OO)<sub>1</sub> + C18:2(OO)<sub>2</sub>) ([analytes] = 4 × 10<sup>-6</sup> M) with Cs<sup>+</sup> (10<sup>-4</sup> M) (solvent: H<sub>2</sub>O/MeOH 50/50 v:v)

As regards to the hydroperoxides and peroxides of mono-terpenes (*i.e.* α-terpinene, limonene, citronellol and linalool), the DLI-ESI-MS spectra obtained are compared to that of Cs<sup>+</sup> itself in order to eliminate interfering peaks. **Figure 2.40** shows the DLI-ESI-MS spectrum of linalool hydroperoxides and that of Cs<sup>+</sup> itself and points out the peaks related to the [R(OO)<sub>1</sub>+Cs]<sup>+</sup> adduct.

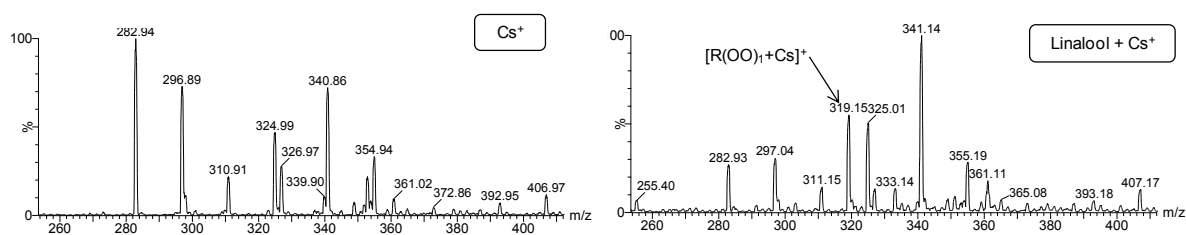


**Figure 2.40:** DLI-ESI-MS spectra in ion-positive mode (ES+) of linalool hydroperoxide ([R(OO)<sub>1</sub>]) = 4 × 10<sup>-6</sup> M) with Cs<sup>+</sup> (10<sup>-4</sup> M) compared to that of Cs<sup>+</sup> (solvent: H<sub>2</sub>O/MeOH 50/50 v:v)

To conclude, with the suppression of the peaks overlap, the large shift of the molecular mass and the strong decrease of dehydration and fragmentation, Cs<sup>+</sup> is the unique relevant ion for the selective and sensitive detection of intact unsaturated hydroperoxides.

### 3.3 Liquid chromatography - Electrospray Ionization and Coordination Ion Spray Mass Spectrometry (LC-MS and LC-MS/MS)

As LC-UV is not efficient to separate hydroperoxides and peroxides contained in complex mixtures of oxidized FAMES and terpenoids, LC-MS and LC-MS/MS were used to improve their detection and identification. Terpenes, FAMES and their respective peroxides are ionized by H<sup>+</sup>, Li<sup>+</sup>, Na<sup>+</sup>, Ag<sup>+</sup> and H<sup>+</sup> acetates. Ag<sup>+</sup> is involved in Coordination Ion Spray Mass Spectrometry (CIS-MS) whereas other ions studied are concerned by ElectroSpray Ionization (ESI-MS). For these experiments, liquid chromatography was coupled with mass spectrometry (LC-MS) in which the quadrupole 1 (Q1) has been used to select compounds by following the corresponding mass of targeted adducts according to a method called Single Ion Recording (SIR) mode (Q2 and Q3 are switch off). Parent adducts obtained were then fragmented thanks to collision with inert gas (argon) in Q2 which is called Collision-Induced Dissociation (CID) experiment. The cone voltages and collision energies have been optimized to find the best conditions and select daughters adducts in Q3. Finally, LC-MS/MS constituted by 3 quadrupoles (Q1, Q2 and Q3) was in this case used to identify compounds by

following the proper transitions from parent to daughter characteristic of the molecule studied. This is called Multiple Reaction Monitoring (MRM) mode (Fig. 2.41). The conditions of elution, type of column and mass spectrometry parameters used for the separation *via* LC-MS and LC-MS/MS are described in the experimental section.

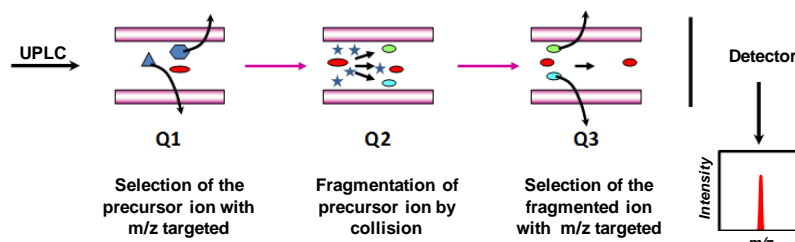


Figure 2.41: Representation of the mass spectrometry detection and the Single Ion Recording (SIR) and Multiple Reaction Monitoring (MRM) modes

### 3.3.1 Terpenoids and related hydroperoxides

The molecular formulas  $C_xH_yO_z$  of esterified terpenes synthesized (*i.e.* 3,7-dimethyloctyl decanoate, citronellol caprate and geraniol caprate) were confirmed by DLI-MS experiments.  $Na^+$ ,  $NH_4^+$  and  $H^+$  with  $AcO^-$  as counterion were used to ionize these parent molecules.

- *Direct Liquid Injection – Mass Spectrometry (DLI-MS)*

Figure 2.42 shows the mass spectrum of the 3,7-dimethyloctyl decanoate identified by  $[M+H]^+$ ,  $[M+NH_4]^+$  and  $[M+Na]^+$  adducts. Moreover, the formation of the  $[2M+Na]^+$  adduct is characteristic of the ionization with sodium.

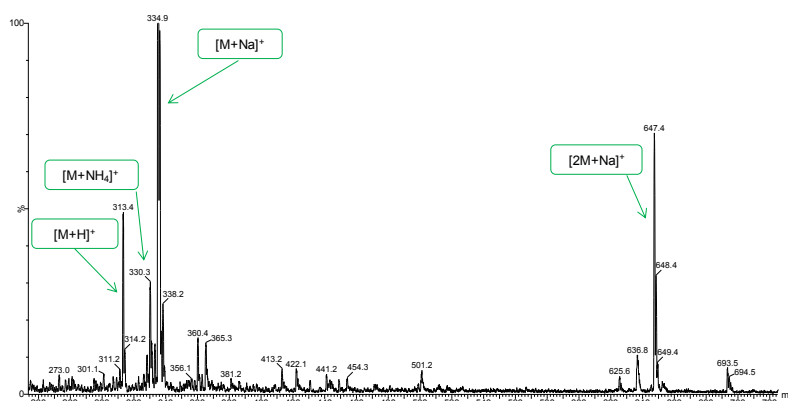
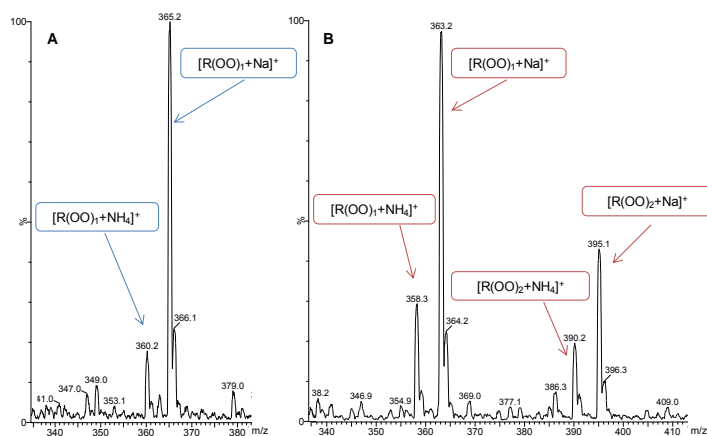


Figure 2.42: DLI-ESI-MS spectrum in ion positive mode (ES+) of 3,7-dimethyloctyl decanoate ( $6 \times 10^{-7}$  M) with  $Na^+$ ,  $H^+$  and  $NH_4^+$  acetates ( $[ion] = 10^{-3}$  M) (solvent:  $H_2O/MeOH$  50/50 v:v)

The formation of hydroperoxides synthesized by photooxidation was also confirmed by DLI-MS thanks to their ionization with the same cations (*i.e.*  $Na^+$ ,  $NH_4^+$  and  $H^+$ ). In agreement with LC-UV and NMR, DLI-MS analysis confirms that no hydroperoxide is formed during the photooxidation of 3,7-dimethyloctyl decanoate since this compound does not have any double bond. Figure 2.43 points out the formation of mono-hydroperoxide from citronellol caprate and geraniol caprate as  $[M+Na]^+$  ( $m/z = 365$  and  $363$  respectively) and  $[M+NH_4]^+$  ( $m/z = 360$  and  $358$  respectively) adducts. On the other hand, the photooxidation of geraniol caprate leads also to di-hydroperoxides characterized by  $[R(OO)_2+Na]^+$  and  $[R(OO)_2+NH_4]^+$  adducts ( $m/z = 395$  and  $390$ ) as already described by LC-UV and NMR analyses.



**Figure 2.43:** DLI-ESI-MS spectrum in ion positive mode of A) mono-hydroperoxides from citronellol caprate ( $[\text{R}(\text{OO})_1] = 3.2 \times 10^{-7} \text{ M}$ ) and B) mono- and di-hydroperoxides from geraniol caprate ( $[\text{R}(\text{OO})_1 + \text{R}(\text{OO})_2] = 3.2 \times 10^{-7} \text{ M}$ ) with  $\text{Na}^+$  and  $\text{NH}_4^+$  acetates ( $10^{-3} \text{ M}$ ) (solvent:  $\text{H}_2\text{O}/\text{MeOH}$  50/50 v:v)

Mass spectrometry investigations are extremely helpful for qualitative analysis compared to UV experiments. Indeed, ESI-MS experiments lead directly to the mass characterization of the targeted molecules. However, that is only applied when measuring a simple component. If multiple components are injected simultaneously, it becomes extremely difficult to analyze the spectra. Therefore, mass spectrometry is generally coupled with the LC separation process.

- *LC-MS in Single Ion Recording (SIR) mode*

Ultra performance liquid chromatography (UPLC) coupled with mass spectrometry (MS) has been used to separate and identify respectively terpenes and their hydroperoxides. Ions ( $\text{H}^+$  and  $\text{NH}_4^+$  with  $\text{AcO}^-$  as counterion) are incorporated in the mobile phase and the SIR mode allowed us to monitor the formation of adducts. Mono-hydroperoxides from citronellol caprate were monitored under the  $[\text{R}(\text{OO})_1+\text{Na}]^+$  ( $m/z = 365$ ) and  $[\text{R}(\text{OO})_1+\text{NH}_4]^+$  ( $m/z = 360$ ) forms whereas the terpene was obtained under the  $[\text{M}+\text{H}]^+$  form ( $m/z = 311$ ). **Figure 2.44** presents the SIR final chromatogram (A) which is the combination of those of each adduct monitored. Mono-hydroperoxide is revealed by one peak detected with  $\text{Na}^+$  (D) and  $\text{NH}_4^+$  (C) followed by the terpene adduct  $[\text{M}+\text{H}]^+$  (B).

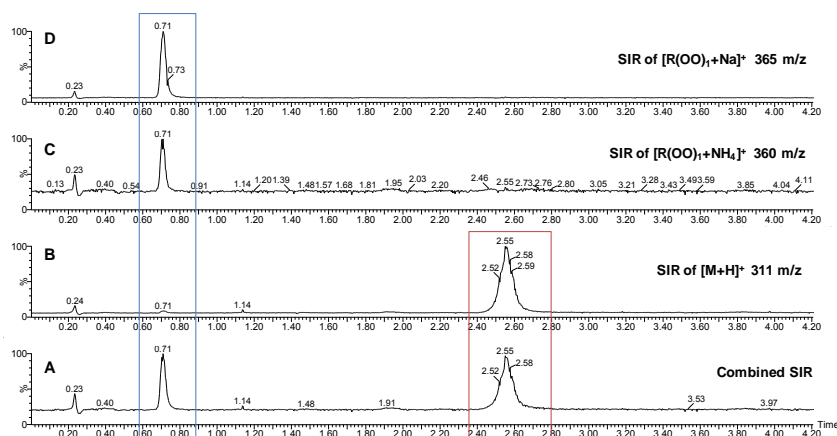


**Figure 2.44:** LC-MS chromatogram of combined SIR (A) from citronellol caprate  $[\text{M}+\text{H}]^+$  ( $m/z = 311$ ) and mono-hydroperoxide  $[\text{R}(\text{OO})_1+\text{NH}_4]^+$  ( $m/z = 360$ )  $[\text{R}(\text{OO})_1+\text{Na}]^+$  ( $m/z = 365$ ) in ion-positive mode (ES+)

Mono-hydroperoxides from geraniol caprate were monitored under the  $[\text{R}(\text{OO})_1+\text{Na}]^+$  ( $m/z = 363$ ) and  $[\text{R}(\text{OO})_1+\text{NH}_4]^+$  ( $m/z = 358$ ) forms and di-hydroperoxides were followed *via*  $[\text{R}(\text{OO})_2+\text{Na}]^+$  ( $m/z = 395$ ) and  $[\text{R}(\text{OO})_2+\text{NH}_4]^+$  ( $m/z = 390$ ) adducts. Moreover, the terpene was characterized by the  $[\text{M}+\text{H}]^+$

( $m/z = 309$ ) and  $[M+Na]^+$  ( $m/z = 331$ ) adducts. **Figure 2.45** shows the chromatogram of separated mono-, di-hydroperoxides and geraniol caprate. They are identified thanks to their respective adducts formed with  $Na^+$ ,  $NH_4^+$  and  $H^+$ . The SIR chromatogram of  $[M+Na]^+$  and  $[M+H]^+$  points out an undesired large peak related to another compound with the same MW as geraniol caprate in our sample.

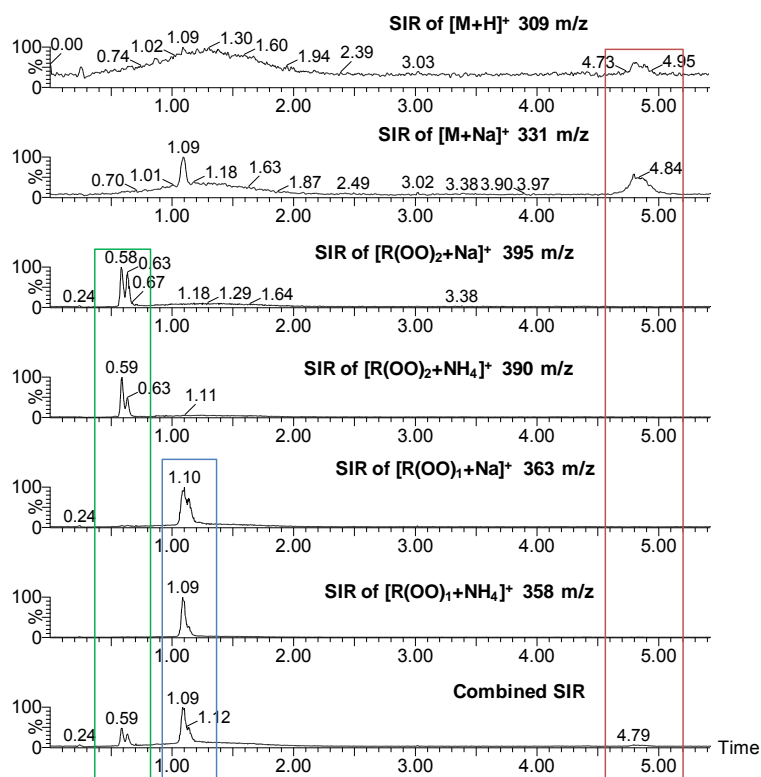


**Figure 2.45** : LC-MS chromatogram of combined SIR from geraniol caprate  $[M + H]^+$  ( $m/z = 309$ )  $[M + Na]^+$  ( $m/z = 331$ ), mono-hydroperoxide  $[ROOH + NH_4]^+$  ( $m/z = 358$ )  $[ROOH + Na]^+$  ( $m/z = 363$ ) and di-hydroperoxide  $[R(OOH)_2 + NH_4]^+$  ( $m/z = 390$ )  $[R(OOH)_2 + 395]^+$  ( $m/z = 363$ ) in ion-positive mode (ES+)

LC-MS systems combine the outstanding separation resolution of liquid chromatography with the qualitative capabilities of mass spectrometry. The mass spectra obtained for these scan measurements provides molecular mass for eluted compounds, which supplements the qualitative information based on retention times obtained using LC-UV. Nevertheless, the SIR mode has some drawbacks (i.e. undesirable peaks with the same MW as targeted molecules) and the Multiple Reaction Monitoring (MRM) mode is preferred.

- *LC-MS/MS in Multiple Reaction Monitoring (MRM) mode*

Adducts monitored at accurate  $m/z$  in the SIR mode could be also characteristic of unwanted other compounds which complicate the chromatogram. Consequently, it is more relevant to work under the MRM mode because each transition found is distinctive of a unique compound. A relevant identification is based on the retention time, two characteristic transitions from parent to daughters and the ratio of the two transitions. The Intellistart program scanned cone voltages and collision energies to find the best condition of fragmentation (**Fig. S2.3**). The daughters revealed by fragmentation were always obtained in the form of  $[M+X]^+$  adducts. Respective cone voltage and collision energy related to the fragmentation of each compound studied are developed in the experimental part. In the case of terpenes and related hydroperoxides, adducts formed with  $NH_4^+$

and  $H^+$  have been selected because  $[M+Na]^+$  adducts were not fragmented. **Table 2.11** points out the two transitions used to identify mono-hydroperoxides  $R(OO)_1$  and citronellol caprate.

Compound	Mass (a.m.u)	Cation ( $X^+$ )	$[M+X]^+$ (m/z)	Daughter adducts (m/z)
Citronellol caprate $R(OO)_1$	342	$NH_4^+$	360	95
			360	81
Citronellol caprate	310	$H^+$	311	83
			311	55

**Table 2.11:** Fragmentation of citronellol caprate and its mono-hydroperoxide under the form of  $[M+H]^+$  and  $[R(OO)_1+NH_4]^+$  in ion-positive mode (ES+)

**Figure 2.46** shows the chromatogram of well separated citronellol caprate and hydroperoxide. They are identified with their own transitions above-mentioned. The two regioisomers of ROOH are co-eluted under these conditions.

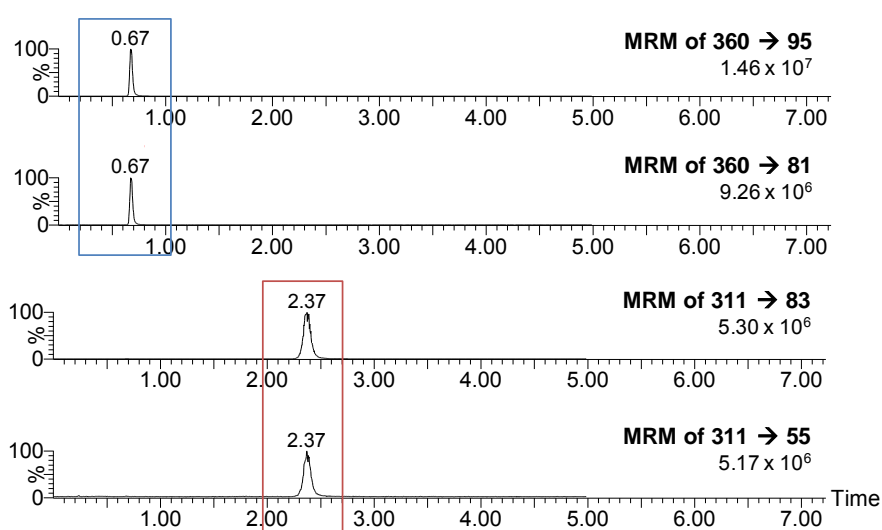


**Figure 2.46:** LC-MS/MS (MRM mode) analysis of citronellol caprate ( $1.6 \times 10^{-6}$  M) and its two hydroperoxides ( $6 \times 10^{-7}$  M) via the fragmentation of  $[R(OO)_1+NH_4]^+$  ( $360 \rightarrow 95$ ,  $360 \rightarrow 81$ ) and  $[M+H]^+$  ( $311 \rightarrow 83$ ,  $311 \rightarrow 55$ ) adducts in ion-positive mode (ES+)

**Table 2.12** points out the two transitions used to identify the all possible 9 mono- and the 18 di-hydroperoxides ( $R(OO)_1$  and  $R(OO)_2$ ) from geraniol caprate. Geraniol caprate was studied under its  $[M+H]^+$  form whereas hydroperoxides were characterized by  $[R(OO)_1+NH_4]^+$  and  $[R(OO)_2+NH_4]^+$  adducts.

Compound	Mass (a.m.u)	Cation ( $X^+$ )	$[M+X]^+$ (m/z)	Daughter adducts (m/z)
Geraniol caprate $R(OO)_2$	372	$NH_4^+$	390	95
			390	81
Geraniol caprate $R(OO)_1$	340	$NH_4^+$	358	135
			358	93
Citronellol caprate	308	$H^+$	309	227
			309	179

**Table 2.12:** Fragmentation of geraniol caprate and its mono- and di-hydroperoxides under the form of  $[M+H]^+$ ,  $[R(OO)_1+NH_4]^+$  and  $[R(OO)_2+NH_4]^+$  respectively in ion-positive mode (ES+)

Figure 2.47 shows the chromatogram of well separated geraniol caprate with  $R(OO)_1$  and  $R(OO)_2$ . They are identified thanks to their own transitions above-mentioned.

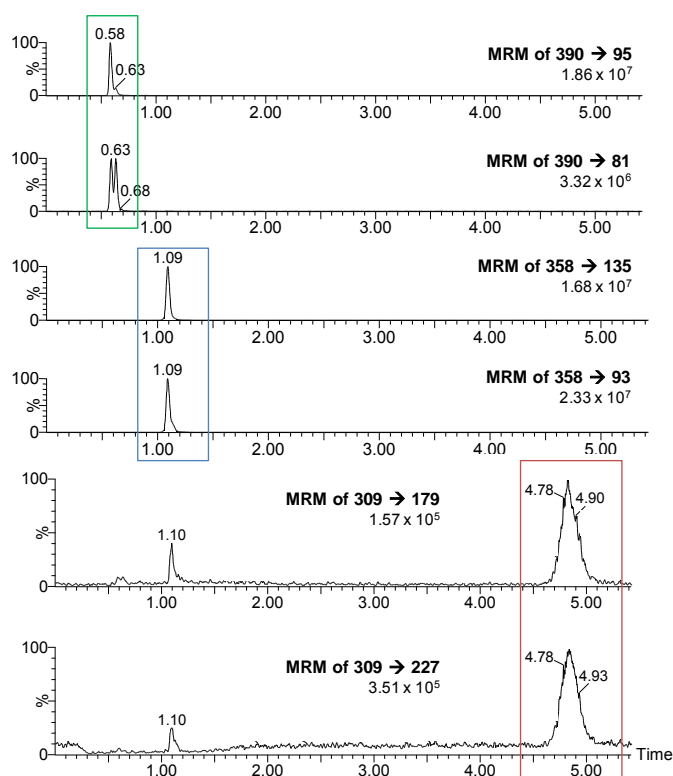


Figure 2.47: LC-MS/MS (MRM mode) analysis of geraniol caprate ( $[M] = 1.6 \times 10^{-6}$  M) and mono- with di-hydroperoxides ( $[R(OO)_1] + [R(OO)_2] = 6 \times 10^{-7}$  M) via the fragmentation of  $[R(OO)_2+NH_4]^+$  ( $390 \rightarrow 95$ ,  $390 \rightarrow 81$ ),  $[R(OO)_1+NH_4]^+$  ( $358 \rightarrow 135$ ,  $358 \rightarrow 93$ ) and  $[M+H]^+$  ( $309 \rightarrow 179$ ,  $309 \rightarrow 227$ ) adducts in ion-positive mode (ES+)

Di-hydroperoxides were identified by the  $390 \rightarrow 81$  transition as 2 close peaks whereas the  $390 \rightarrow 95$  transition is only responsible for the detection of one signal. Indeed, this second transition could be specific of some regioisomers. Then, as for citronellol caprate, regioisomers of mono-hydroperoxide are co-eluted under our experiment conditions. Geraniol caprate is finally detected with the lowest intensity.

The LC-MS (SIR mode) analyses showed that the technique lacked selectivity with interfering peaks whereas LC-MS/MS (MRM mode) lead to unambiguous identification of substrates and hydroperoxides. These two terpenoids with their hydroperoxides are used as FAMES model to develop an accurate method to separate and analyze peroxides. Therefore, the same methods have been dedicated to the study of a complex mixture of photooxidized FAMES from linseed oil.

### 3.3.2 FAMES of linseed oil and peroxides

#### ▪ Separation and analysis of FAMES from linseed oil

As for terpenes, FAMES of linseed oil obtained by transesterification of the linseed oil have been first analyzed by DLI-MS to find characteristic adducts with various ions. They are then separated and detected by coupled LC-MS (SIR mode) and LC-MS/MS (MRM mode). Table 2.13 presents the adducts studied for the identification of methyl linolenate (C18:3), methyl linoleate (C18:2) and methyl oleate (C18:1) contained in FAMES of linseed oil with  $H^+$ ,  $NH_4^+$  and  $Na^+$  ions during DLI-MS experiments.

Compound	Mass (a.m.u)	Cation (X <sup>+</sup> )	[M+X] <sup>+</sup> (m/z)
Methyl linolenate C18:3	292	H <sup>+</sup>	293
		NH <sub>4</sub> <sup>+</sup>	310
		Na <sup>+</sup>	315
-----			
Methyl linoleate C18:2	294	H <sup>+</sup>	295
Methyl oleate C18:1	296	NH <sub>4</sub> <sup>+</sup>	312
		NH <sub>4</sub> <sup>+</sup>	314

Table 2.13: Adducts formed between methyl linolenate (C18:3), methyl linoleate (C18:2) and methyl oleate (C18:1) with cations (H<sup>+</sup>, NH<sub>4</sub><sup>+</sup> and Na<sup>+</sup>) during DLI-MS experiments in ion-positive mode (ES+)

The monitoring of the combined 6 adducts above-mentioned well characterize the three analyzed FAMES leading to a full separation by LC-MS (Fig. 2.48). It is also possible to differentiate them by LC-MS/MS (MRM mode). Table 2.14 points out the transitions used to identify FAMES. C18:3 and C18:1 were characterized by [M+H]<sup>+</sup> adducts whereas C18:2 was studied under its [M+NH<sub>4</sub>]<sup>+</sup> form.

Compound	Mass (a.m.u)	Ion	[M + X] <sup>+</sup> (m/z)	Daughter adducts (m/z)
Methyl linolenate C18:3	292	H <sup>+</sup>	293	95
			293	81
			293	67
-----				
Methyl linoleate C18:2	294	NH <sub>4</sub> <sup>+</sup>	312	263
			312	245
-----				
Methyl oleate C18:1	296	H <sup>+</sup>	297	265
			297	247

Table 2.14: Fragmentation of C18:3, C18:2 and C18:1 under the form of [M+NH<sub>4</sub>]<sup>+</sup> and [M+H]<sup>+</sup> adducts in ion-positive mode (ES+)

The same spectrum as for the LC-MS analysis was obtained. Figure 2.48 reveals C18:3, C18:2 and C18:1 at retention time (t<sub>r</sub>) of 1.60, 2.09 and 2.89 min respectively.

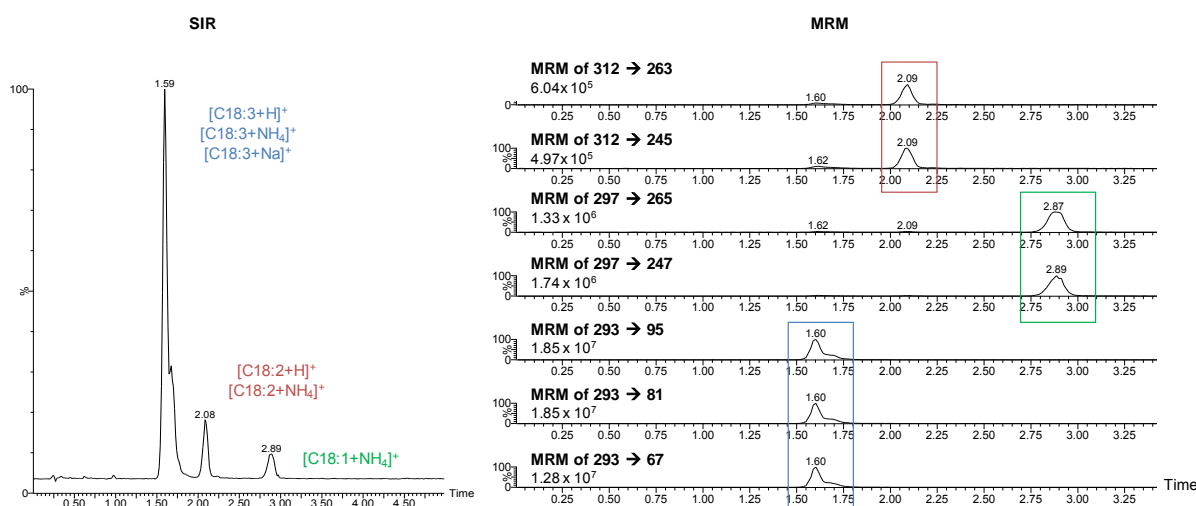


Figure 2.48: LC-MS chromatograms of combined SIR from FAMES of linseed oil ( $1.6 \times 10^{-6}$  M) constituted by C18:3 [M+H]<sup>+</sup> (293 m/z) [M+NH<sub>4</sub>]<sup>+</sup> (m/z = 310) [M+Na]<sup>+</sup> (m/z = 315), C18:2 [M+H]<sup>+</sup> (m/z = 295) [M+NH<sub>4</sub>]<sup>+</sup> (m/z = 312) and C18:1 [M+NH<sub>4</sub>]<sup>+</sup> (m/z = 314), LC-MS/MS (MRM mode) analysis of FAMES of linseed oil ( $1.6 \times 10^{-6}$  M) via the fragmentation of [C18:3+H]<sup>+</sup> (293 → 95, 293 → 81 and 293 → 67), [C18:2+NH<sub>4</sub>]<sup>+</sup> (312 → 263, 312 → 245) and [C18:1+H]<sup>+</sup> (297 → 265, 297 → 247) adducts in ion-positive mode (ES+)

Nevertheless, it is not possible to easily identify FAMES by coordination with Ag<sup>+</sup> in SIR mode. The advantage given by the two silver isotopes <sup>107</sup>Ag and <sup>109</sup>Ag for the identification of FAMES is now a drawback because, added to a difference of 2 a.m.u between each FAME (C18:1 296 a.m.u, C18:2

294 a.m.u and C18/3 292 a.m.u), there is an overlap of mass signals (**Table 2.15**). The MRM mode should be the relevant mode to differentiate the different FAMEs based on transitions from parents to daughters (a separation process is not needed).

	Mass (a.m.u)	$[M+^{107}\text{Ag}]^+$ (m/z)	$[M+^{109}\text{Ag}]^+$ (m/z)
Methyl linolenate C18:3	292	399	<b>401</b>
Methyl linoleate C18:2	294	<b>401</b>	<b>403</b>
Methyl oleate C18:1	296	<b>403</b>	406

Table 2.15: Mass signals for C18:3, C18:2 and C18:1 with  $\text{Ag}^+$  ( $[M+\text{Ag}_1]^+$  and  $[M+\text{Ag}_2]^+$ )

▪ *Separation and analysis of peroxides from the photooxidation of FAMEs of linseed oil*

LC-MS/MS in MRM mode is the most significant method to separate and identify mixture of peroxides in the light of the complex chemical structure elucidation given by LC-UV and NMR investigations. First of all, peroxide mixture has been analyzed under DLI-MS experiment. **Figure 2.49** shows that, on the form of  $[M+\text{Na}]^+$  and  $[M+\text{Li}]^+$  adducts, mono-hydroperoxides  $\text{R}(\text{OO})_1$  from C18:3, C18:2 and C18:1 are identified. Moreover, di-peroxides  $\text{R}(\text{OO})_2$  from C18:3 and C18:2 are also highlighted. Finally, tri-peroxides  $\text{R}(\text{OO})_3$  from C18:3 are also described.

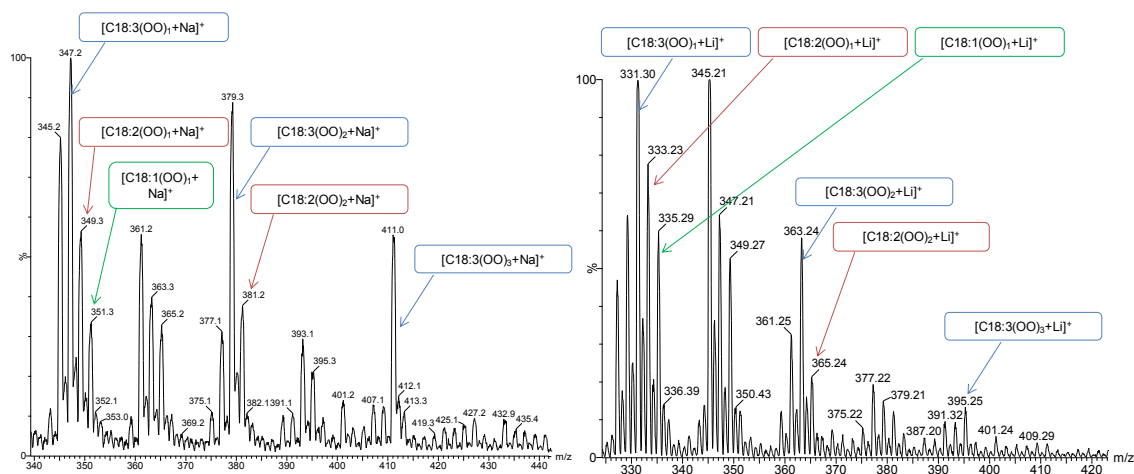


Figure 2.49: DLI-ESI-MS spectra in ion positive mode ( $\text{ES}^+$ ) of a peroxide mixture from FAMEs of linseed oil ( $2 \times 10^{-5} \text{ M}$ ) with  $\text{Na}^+$  already present in the system and  $\text{Li}^+$  ( $2 \times 10^{-3} \text{ M}$ ) (solvent:  $\text{H}_2\text{O}/\text{MeOH}$  50/50 v:v)

Some mass signals are not assigned to hydroperoxides. Indeed, whatever the cation used ( $\text{Li}^+$  or  $\text{Na}^+$ ),  $\text{R}(\text{OO})_2$  and  $\text{R}(\text{OO})_3$  adducts derived from C18:3 and C18:2 are degraded without the use of fragmentation conditions (**Table 2.16**). As the photooxidation process is a smooth method to get stable hydroperoxides, we assumed that the fragmentation of hydroperoxides comes with the elevated temperature used in the MS source.

	$\text{R}(\text{OO})_2$ (m/z)		$\text{R}(\text{OO})_3$ (m/z)
	C18:3	C18:2	C18:3
$[\text{M}+\text{Na}]^+$	379	381	411
$-\text{H}_2\text{O}_2$ (-34 a.m.u)	345	347	377
$-\text{H}_2\text{O}$ (-18 a.m.u)	361	363	393
$-\text{O}$ (-16 a.m.u)	/	365	395
$[\text{M}+\text{Li}]^+$	363	365	395
$-\text{H}_2\text{O}_2$ (-34 a.m.u)	329	331	361
$-\text{H}_2\text{O}$ (-18 a.m.u)	345	347	377
$-\text{O}$ (-16 a.m.u)	/	349	379

Table 2.16: Mass (m/z) of  $\text{R}(\text{OO})_2$  from C18:3 and C18:2 and  $\text{R}(\text{OO})_3$  from C18:3 and related compound with a loss of  $\text{H}_2\text{O}$  (-18 a.m.u),  $\text{H}_2\text{O}_2$  (-34 a.m.u) and one oxygen atom (-16 a.m.u) with  $\text{Na}^+$  and  $\text{Li}^+$  cations

This easy fragmentation of the hydroperoxide group is characterized by the formation of an allylic epoxide or enone derivative by single dehydration ( $-H_2O$ ) or a conjugated diene by elimination of hydrogen peroxide ( $-H_2O_2$ ) (Fig. 2.50).<sup>246, 247</sup> As described by Giuffrida *et al.*, the neutral loss of hydrogen peroxide is specific to the hydroperoxide function and can be used for structural identification of hydroperoxyl group in molecules.<sup>246</sup> In addition,  $R(OO)_2$  from C18:2 and  $R(OO)_3$  from C18:3 could also be described by a loss of one oxygen atom.

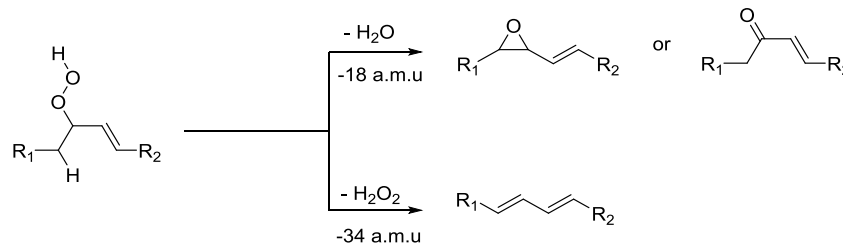


Figure 2.50: Fragmentation of hydroperoxides into epoxides ( $-H_2O$ ) and conjugated diene ( $-H_2O_2$ )<sup>246</sup>

This is in agreement with the oxidized species obtained from the singlet oxygenation of FAMES described in literature. Indeed, mono-hydroperoxides, di-hydroperoxides and hydroperoxy (bis)cyclic peroxides are still bearing thermal sensitive hydroperoxide function which is fragmented under our MS experiments (Fig. 2.51).<sup>36, 71, 119, 126, 128</sup>

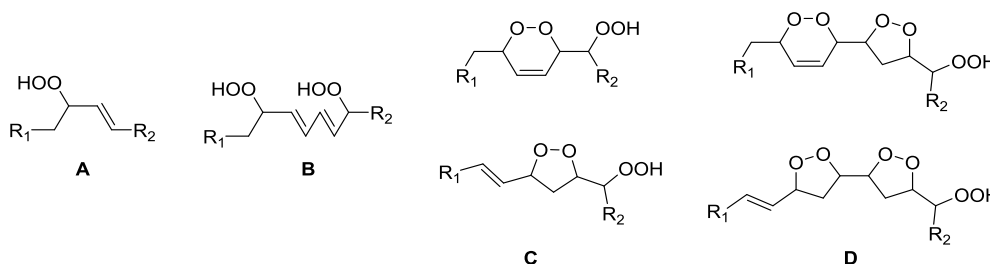


Figure 2.51: A) Mono-hydroperoxides, B) di-hydroperoxides, C) hydroperoxy cyclic peroxide and D) hydroperoxy bis-cyclic peroxides formed during the photooxidation of FAMES<sup>36, 71, 119, 126, 128</sup>

Separated photooxidized methyl oleate (C18:1), methyl linoleate (C18:2) and methyl linolenate (C18:3) are used to facilitate the fragmentation of FAMES peroxides. More specifically, this avoids the overlapping of mass peaks when  $Ag^+$  is used. The thermal decomposition of peroxides (hydroperoxides and cyclic peroxides) from methyl oleate, linoleate and linolenate *via*  $\alpha$  and  $\beta$  scissions described in the literature survey (Fig. 2.52) help us to investigate the daughters formed.<sup>36, 68, 73, 228</sup>

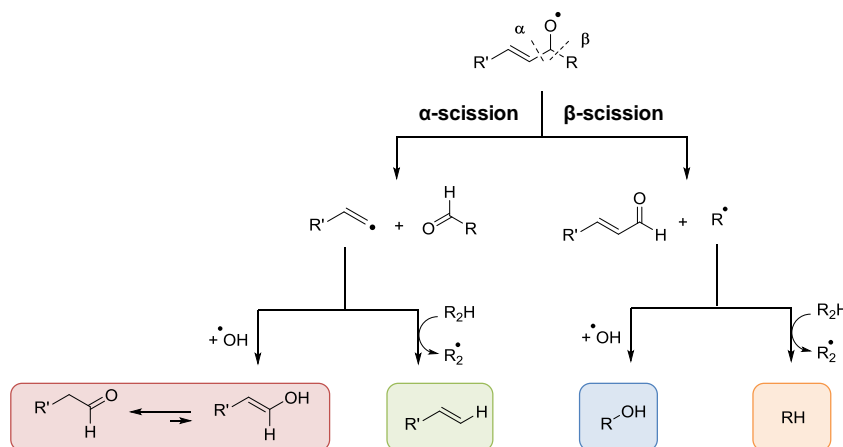


Figure 2.52:  $\alpha$ - and  $\beta$ -scissions of the alkoxy radicals of unsaturated fatty acids<sup>36</sup>



**Table 2.18** shows the  $m/z$  of daughters adducts  $[N+X]^+$  obtained during the fragmentation of mono-hydroperoxides  $C_{18}:2(OO)_1$  and di-peroxides  $C_{18}:2(OO)_2$  recovered during the photooxidation of  $C_{18}:2$ .

<b>C18:2(OO)<sub>1</sub> 326 a.m.u</b>					<b>C18:2(OO)<sub>2</sub> 358 a.m.u</b>				
Ion	Li <sup>+</sup>	Na <sup>+</sup>	<sup>107</sup> Ag <sup>+</sup>	NH <sub>4</sub> <sup>+</sup>	Ion	Li <sup>+</sup>	Na <sup>+</sup>	<sup>107</sup> Ag <sup>+</sup>	NH <sub>4</sub> <sup>+</sup>
$m/z$	7	23	107	18	$m/z$	7	23	107	18
$[M+X]^+$ ( $m/z$ )	333	349	433	344	$[M+X]^+$ ( $m/z$ )	365	381	465	376
Daughters	315	331	415	293	Daughters	205	221	305	78
$[N+X]^+$	291	221	305	81	$[N+X]^+$	277	209	293	191
( $m/z$ )	250	209	293	95	( $m/z$ )	109	235	319	139
	135	261	333	277		185	347	/	193
	107	135	107	109		307	293	/	91

**Table 2.18:** Fragmentation of  $C_{18}:2(OO)_1$  and  $C_{18}:2(OO)_2$  under the form of  $[M+Li]^+$ ,  $[M+Na]^+$ ,  $[M+^{107}Ag]^+$  and  $[M+NH_4]^+$  adducts; fragmentation into epoxide or enone ( $m/z = 315, 331$  and  $415$ , dehydration of  $C_{18}:2(OO)_1$ ,  $-H_2O$ ,  $-18$  a.m.u), methyl 9-oxononanoate ( $m/z = 209$  and  $293$ ), 2-octene ( $m/z = 135$ ), 2-octene-1-ol and methyl 10-oxo-8-decenoate ( $m/z = 221$  and  $305$ ), methyl 12-oxo-9-dodecenoate ( $m/z = 333$ ), methyl 13-oxo-9,11-tridecadienoate ( $m/z = 261$ ) and hexanal ( $m/z = 107$ )

**Figures 2.54** shows the chemical structure of daughters formed during the fragmentation of  $C_{18}:2(OO)_1$  in agreement with the mass described in **table 2.18**.

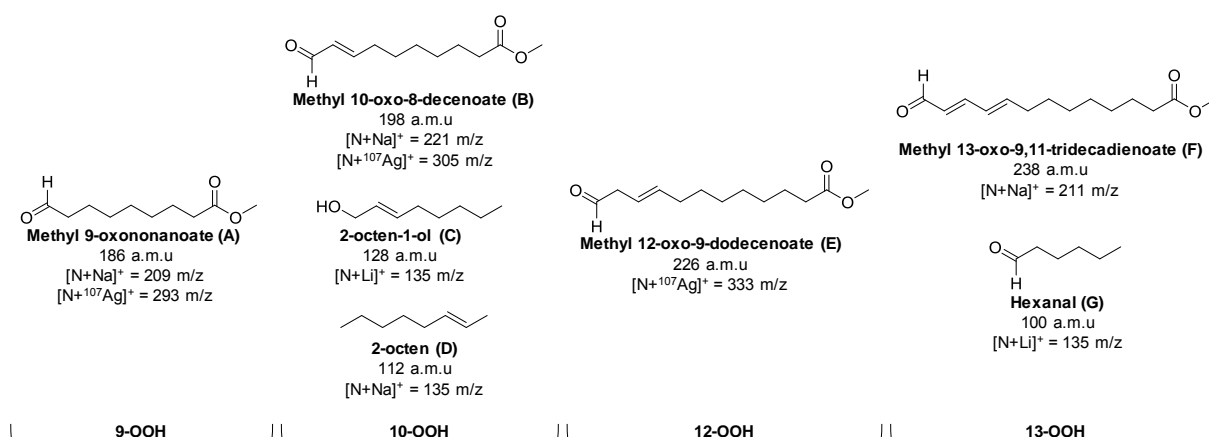


**Figure 2.54:** Chemical structure elucidation of daughters formed during the  $C_{18}:2(OO)_1$  fragmentation<sup>36, 68, 73, 228</sup>

The formation of 4 regioisomers of mono-hydroperoxides (9-OOH, 10-OOH, 12-OOH and 13-OOH) during the photooxidation of  $C_{18}:2$  is highlighted by the fragmentation of  $C_{18}:2(OO)_1$  into different daughters. As before, the dehydration of  $C_{18}:2(OO)_1$  ( $-H_2O$ ) is revealed by the  $[N+Li]^+$ ,  $[N+Na]^+$  and  $[N+^{107}Ag]^+$  daughters adducts ( $m/z = 315, 331$  and  $415$  respectively) related to the epoxide or enone formation. The 9-OOH regioisomer is pointed out by the  $[N+Na]^+$  and  $[N+^{107}Ag]^+$  daughters adducts ( $m/z = 209$  and  $293$  respectively) describing methyl 9-oxononanoate (**A**, 186 a.m.u). Then, the 10-OOH regioisomer is revealed by the  $[N+Na]^+$  and  $[N+Li]^+$  daughter adduct ( $m/z = 135$ ) related to the fragmentation into 2-octene (**D**, 112 a.m.u) and 2-octene-1-ol (**C**, 128 a.m.u). The other  $[N+Na]^+$  ( $m/z = 221$ ) and  $[N+^{107}Ag]^+$  ( $m/z = 305$ ) daughters adducts characterize the formation of 10-oxo-8-decenoate (**B**, 198 a.m.u). Moreover, the 12-OOH regioisomer is revealed by the  $[N+^{107}Ag]^+$  daughter adduct ( $m/z = 333$ ) which corresponds to methyl 12-oxo-9-dodecenoate (**E**, 226 a.m.u). Finally, the formation of the 13-OOH regioisomer during the photooxidation of  $C_{18}:2$  is attested by the  $[N+Na]^+$  ( $m/z = 261$ ) and  $[N+Li]^+$  ( $m/z = 107$ ) daughters adducts corresponding to methyl 13-oxo-9,11-tridecadienoate (**F**, 238 a.m.u) and hexanal (**G**, 100 a.m.u) respectively.

Figures 2.55 shows the chemical structure of daughters formed during the fragmentation of C18:2(OO)<sub>2</sub> (hydroperoxy cyclic peroxides) in agreement with some mass described in table 2.18.

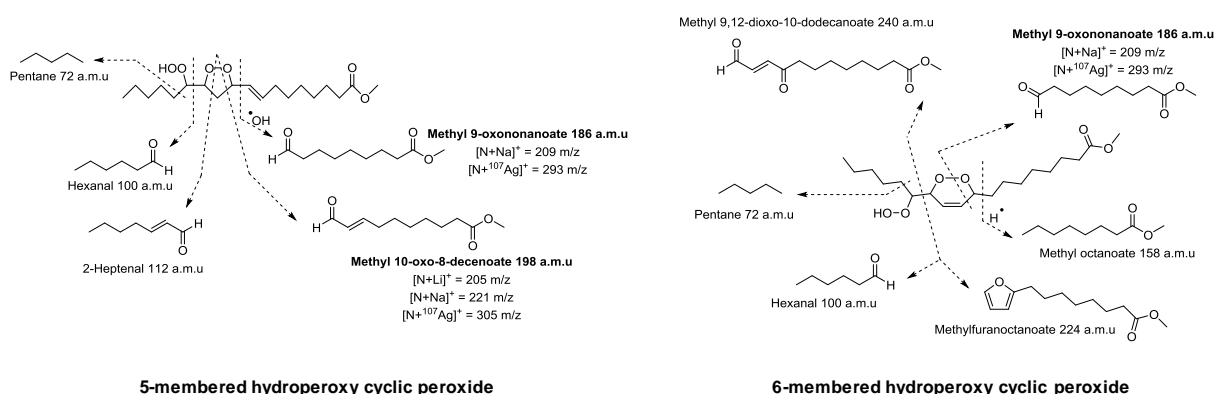


Figure 2.55: Fragmentation of 5-membered and 6-membered hydroperoxy cyclic peroxides (C18:2(OO)<sub>2</sub>)<sup>36, 125, 126</sup>

The [N+Li]<sup>+</sup>, [N+Na]<sup>+</sup> and [N+<sup>107</sup>Ag]<sup>+</sup> daughters adducts (m/z = 205, 221 and 305 respectively) are related to the formation of methyl 10-oxo-8-decenoate (198 a.m.u). Moreover, other [N+Na]<sup>+</sup> and [N+<sup>107</sup>Ag]<sup>+</sup> daughters adducts (m/z = 209 and 293 respectively) point out the fragmentation into methyl 9-oxononanoate (186 a.m.u). The fragmentation of C18:2(OO)<sub>2</sub> does not lead to the loss of H<sub>2</sub>O compared to C18:2(OO)<sub>1</sub>. This is probably because hydroperoxy cyclic peroxides are more stable than mono-hydroperoxides. These three important findings are in favor of the formation of 5-membered and 6-membered hydroperoxy cyclic peroxides.

Table 2.19 and 2.10 show the m/z of daughters adducts [N+X]<sup>+</sup> obtained during the fragmentation of mono-hydroperoxides C18:3(OO)<sub>1</sub>, di-peroxides C18:3(OO)<sub>2</sub> and tri-peroxides C18:3(OO)<sub>3</sub> recovered during the photooxidation of C18:3.

C18:3(OO) <sub>1</sub> 324 a.m.u					C18:3(OO) <sub>2</sub> 356 a.m.u				
Ion	Li <sup>+</sup>	Na <sup>+</sup>	<sup>107</sup> Ag <sup>+</sup>	NH <sub>4</sub> <sup>+</sup>	Ion	Li <sup>+</sup>	Na <sup>+</sup>	<sup>107</sup> Ag <sup>+</sup>	NH <sub>4</sub> <sup>+</sup>
m/z	7	23	107	18	m/z	7	23	107	18
[M+X] <sup>+</sup> (m/z)	331	347	431	342	[M+X] <sup>+</sup> (m/z)	363	379	463	374
Daughters [N+X] <sup>+</sup> (m/z)	245	329	413	78	Daughters [N+X] <sup>+</sup> (m/z)	205	221	305	78
	233	261	333	93		193	209	293	91
	273	301	373	291		233	275	333	90
	193	209	293	259		219	345	95	121
	205	221	107	121		93	205	/	105

Table 2.19: Fragmentation of C18:3(OO)<sub>1</sub> and C18:3(OO)<sub>2</sub> under the form of [M+Li]<sup>+</sup>, [M+Na]<sup>+</sup>, [M+<sup>107</sup>Ag]<sup>+</sup> and [M+NH<sub>4</sub>]<sup>+</sup> adducts; fragmentation into epoxide (m/z = 329 and 413, dehydration of C18:2(OO)<sub>1</sub>, -H<sub>2</sub>O, -18 a.m.u), methyl 9-oxononanoate (m/z = 193, 209 and 293), methyl 10-oxo-8-decenoate (m/z = 205, 221 and 305), methyl 12-oxo-9-dodecanoate (m/z = 233 and 333), methyl 13-oxo-9,11-tridecadienoate and methyl 9,12-butadecadienoate (m/z = 261 and 245), methyl 16-oxo-9,12,14-hexadecatrienoate and methyl 15-oxo-9,12-pentadecadienoate (m/z = 301, 273 and 373) and methyl 11-oxo-9-undecenoate (m/z = 219)

C18:3(OO) <sub>3</sub> 388 a.m.u				
Ion	Li <sup>+</sup>	Na <sup>+</sup>	Ag <sub>1</sub> <sup>+</sup>	NH <sub>4</sub> <sup>+</sup>
m/z	7	23	107	18
[M+X] <sup>+</sup> (m/z)	395	411	495	406
Daughters [N+X] <sup>+</sup> (m/z)	205	221	305	78
	193	209	293	95
	233	249	333	94
	219	281	/	97
	81	377	/	91

Table 2.20: Fragmentation of C18:3(OO)<sub>3</sub> under the form of [M+Li]<sup>+</sup>, [M+Na]<sup>+</sup>, [M+<sup>107</sup>Ag]<sup>+</sup> and [M+NH<sub>4</sub>]<sup>+</sup> adducts; fragmentation into methyl 9-oxononanoate (m/z = 193, 209 and 293), methyl 10-oxo-8-decenoate (m/z = 205, 221 and 305) and methyl 12-oxo-9-dodecenoate (m/z = 233, 249 and 333)

Figures 2.56 shows the chemical structure of daughters formed during the fragmentation of C18:3(OO)<sub>1</sub> in agreement with the mass described in table 2.19.

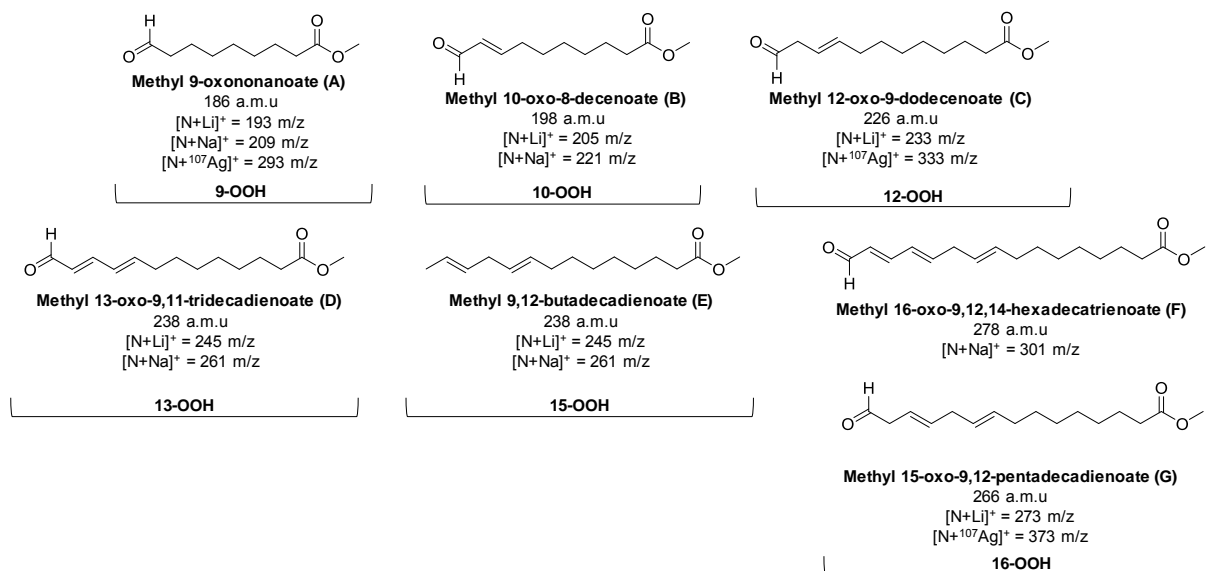


Figure 2.56: Chemical structure elucidation of daughters formed during the C18:3(OO)<sub>1</sub> fragmentation<sup>36, 68, 73, 228</sup>

The formation of 6 regioisomers of mono-hydroperoxides (9-OOH, 10-OOH, 12-OOH, 13-OOH, 15-OOH and 16-OOH) during the photooxidation of C18:3 is highlighted by the fragmentation of C18:2(OO)<sub>1</sub> into different daughters. As before, the dehydration of C18:3(OO)<sub>1</sub> (-H<sub>2</sub>O) is revealed by the [N+Na]<sup>+</sup> and [N+<sup>107</sup>Ag]<sup>+</sup> daughters adducts (m/z = 329 and 413 respectively) related to the epoxide or enone formation (306 a.m.u). The 9-OOH regioisomer is shown by the [N+Li]<sup>+</sup>, [N+Na]<sup>+</sup> and [N+<sup>107</sup>Ag]<sup>+</sup> daughter adducts (m/z = 193, 209 and 293 respectively) describing methyl 9-oxononanoate (A, 186 a.m.u). Then, the 10-OOH regioisomer is revealed by the [N+Na]<sup>+</sup> (m/z = 221) and [N+Li]<sup>+</sup> (m/z = 205) daughters adducts related to methyl 10-oxo-8-decenoate (B, 198 a.m.u). Moreover, the 12-OOH regioisomer is identified by the [N+Li]<sup>+</sup> (m/z = 233) and [N+<sup>107</sup>Ag]<sup>+</sup> (m/z = 333) daughters adducts which corresponds to methyl 12-oxo-9-dodecenoate (C, 226 a.m.u). The formation of the 13-OOH regioisomer is highlighted by the [N+Na]<sup>+</sup> (m/z = 261) and [N+Li]<sup>+</sup> (m/z = 245) daughters adducts related to methyl 13-oxo-9,11-tridecadienoate (D, 238 a.m.u). However, these two daughter adducts represent also methyl 9,12-butadecadienoate (E, 238 a.m.u) involved in

the characterization of the 15-OOH regioisomer. Finally, the 16-OOH regioisomer is pointed out by the  $[N+Li]^+$  ( $m/z = 273$ ) and  $[N+^{107}Ag]^+$  ( $m/z = 373$ ) daughter adducts corresponding to methyl 16-oxo-9,12,14-hexadecatrienoate (**F**, 278 a.m.u) and the  $[N+Na]^+$  ( $m/z = 301$ ) daughter adduct related to methyl 15-oxo-9,12-pentadecadienoate (**G**, 266 a.m.u).

Figures 2.57 shows the chemical structure of daughters formed during the fragmentation of  $C_{18:3}(OO)_2$  (di-hydroperoxides and hydroperoxy cyclic peroxides) in agreement with some mass described in table 2.19.

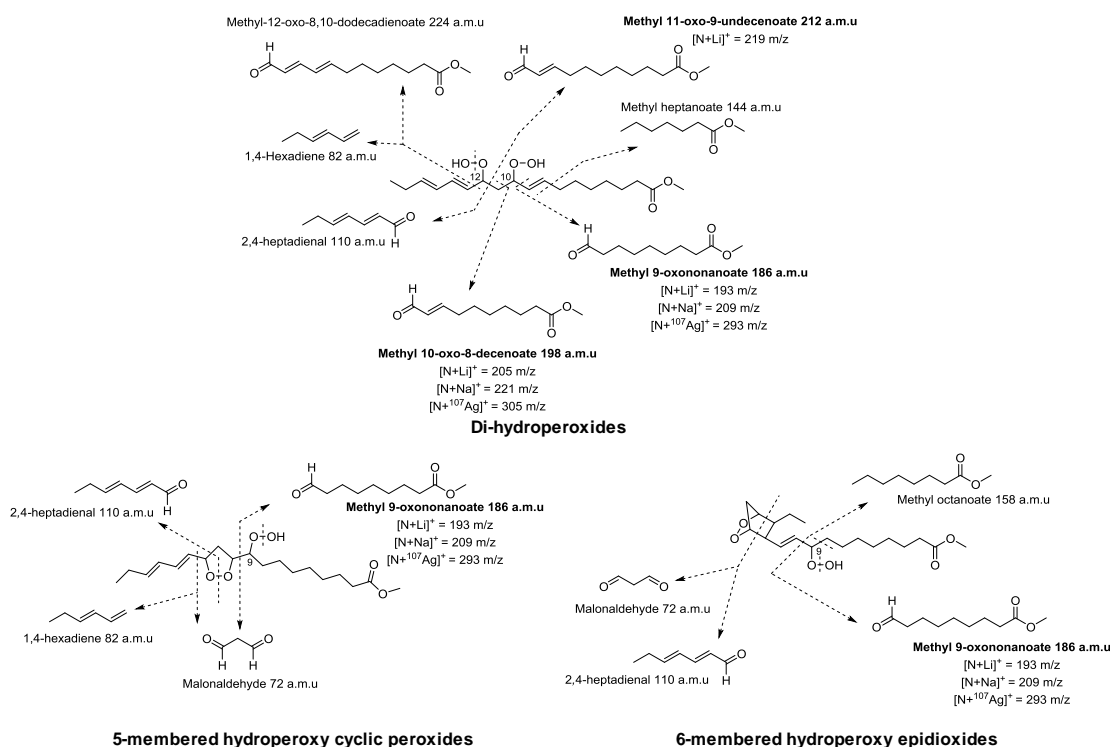


Figure 2.57: Fragmentation of di-hydroperoxides 5-membered hydroperoxy cyclic peroxides and 6-membered hydroperoxy epidioxides ( $C_{18:3}(OO)_2$ )<sup>36, 125, 126</sup>

The fragmentation of di-peroxides  $C_{18:3}(OO)_2$  does not favor the dehydration process ( $-H_2O$ ) compared to mono-hydroperoxides ( $C_{18:3}(OO)_1$ ). However, the  $[N+Li]^+$ ,  $[N+Na]^+$  and  $[N+^{107}Ag]^+$  daughters adducts ( $m/z = 205$ ,  $221$  and  $305$  respectively) are related to the fragmentation of  $C_{18:3}(OO)_2$  into methyl 10-oxo-8-decenoate (198 a.m.u). Moreover, the  $[N+Li]^+$  ( $m/z = 193$ ),  $[N+Na]^+$  ( $209 m/z$ ) and  $[N+^{107}Ag]^+$  ( $m/z = 293$ ) daughters adducts point out the formation of methyl 9-oxononanoate (186 a.m.u) characteristic of di-hydroperoxides and hydroperoxy cyclic peroxides. Finally, the  $[M+Li]^+$  ( $m/z = 219$ ) daughter adduct is related to the methyl 11-oxo-9-undecenoate (212 a.m.u) formation highlighting the fragmentation of di-hydroperoxides. Consequently, the  $C_{18:3}(OO)_2$  obtained from the singlet oxygenation of  $C_{18:3}$  are composed by a mixture of di-hydroperoxides and hydroperoxy cyclic peroxides.

Figure 2.58 shows the chemical structure of daughters formed during the fragmentation of C18:3(OO)<sub>3</sub> (hydroperoxy bis-cyclic peroxides) in agreement with some mass described in table 2.20.

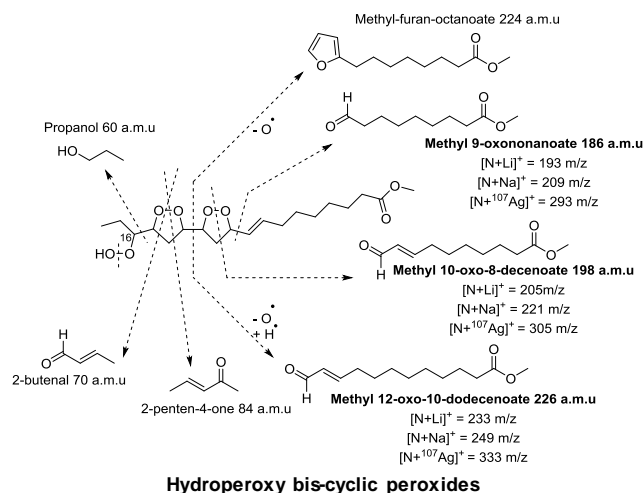


Figure 2.58: Fragmentation of hydroperoxy bis-cyclic peroxides (C18:3(OO)<sub>3</sub>)<sup>36, 125, 126</sup>

As for C18:3(OO)<sub>2</sub>, the fragmentation of tri-peroxides C18:3(OO)<sub>3</sub> does not favor the dehydration process (-H<sub>2</sub>O). However, the [N+Li]<sup>+</sup>, [N+Na]<sup>+</sup> and [N+<sup>107</sup>Ag]<sup>+</sup> daughters adducts (m/z = 205, 221 and 305 respectively) are related to the fragmentation of C18:3(OO)<sub>3</sub> into methyl 10-oxo-8-decenoate (198 a.m.u). Moreover, the [N+Li]<sup>+</sup> (m/z = 193), [N+Na]<sup>+</sup> (m/z = 209) and [N+<sup>107</sup>Ag]<sup>+</sup> (m/z = 293) daughters adducts highlight the formation of methyl 9-oxononanoate (186 a.m.u). Finally, the [N+Li]<sup>+</sup>, [N+Na]<sup>+</sup> and [N+<sup>107</sup>Ag]<sup>+</sup> daughters adducts (m/z = 233, 249 and 333 respectively) point out the thermal degradation of C18:3(OO)<sub>3</sub> into methyl 12-oxo-10-dodecenoate (226 a.m.u). Therefore, the C18:3(OO)<sub>3</sub> obtained from the singlet oxygenation of C18:3 are composed by a mixture of various hydroperoxy bis-cyclic peroxides.

The chemical structures of other daughters are not elucidated. The daughters adducts formed with NH<sub>4</sub><sup>+</sup> [N+NH<sub>4</sub>]<sup>+</sup> differ completely from that of the other adducts ([N+Li]<sup>+</sup>, [N+Na]<sup>+</sup> and [N+<sup>107</sup>Ag]<sup>+</sup>). Indeed, [N+NH<sub>4</sub>]<sup>+</sup> adducts seems to be related to volatile organic compounds (VOC) with lower mass.

Two or three transitions from parents [M+X]<sup>+</sup> to daughters [N+X]<sup>+</sup> (X = Li, Na, <sup>107</sup>Ag and NH<sub>4</sub>) highlighted previously have been used to identified peroxides (*i.e.* C18:1(OO)<sub>1</sub>, C18:2(OO)<sub>1</sub>, C18:2(OO)<sub>2</sub>, C18:3(OO)<sub>1</sub>, C18:3(OO)<sub>2</sub> and C18:3(OO)<sub>3</sub>) *via* LC-MS/MS (MRM mode). Figure 2.59 points out the LC-MS/MS chromatogram with <sup>107</sup>Ag<sup>+</sup> composed by the MRM of 2 or 3 channels related to each peroxide. Chromatograms obtained with Li<sup>+</sup>, Na<sup>+</sup> and NH<sub>4</sub><sup>+</sup> are showed in the experimental section.

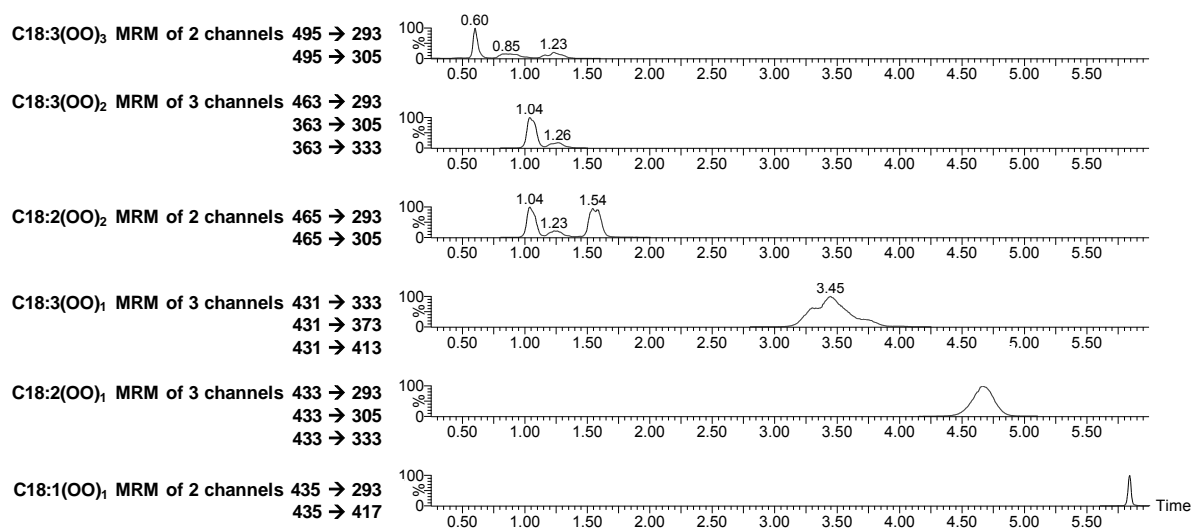


Figure 2.59: LC-MS/MS (MRM mode) chromatogram of mixture of peroxides obtained from the photooxidation of FAMES of linseed oil ( $3 \times 10^{-2}$  M) with  $^{107}\text{Ag}^+$  as cation

The C18:1(OO)<sub>1</sub> mono-hydroperoxide ( $t_r = 5.80$  min) appears as a thin peak because there is just 2 regioisomers (9- and 10-OOH) whereas other C18:2(OO)<sub>1</sub> and C18:3(OO)<sub>1</sub> peaks ( $t_r = 3.45$  and 4.65 min respectively) are larger due to more isomers. The intensities obtained for peroxides peaks are related to the transitions selected. Indeed, all of them are not specific to the same isomer which impacts chromatograms intensities profiles. Therefore, there are some differences in the chromatograms obtained with different ions. Based on proper transitions from parent  $[\text{M}+\text{X}]^+$  to daughters  $[\text{N}+\text{X}]^+$  ( $\text{X} = \text{Li}, \text{Na}, ^{107}\text{Ag}$  and  $\text{NH}_4$ ), mono-hydroperoxides C18:1(OO)<sub>1</sub>, C18:2(OO)<sub>1</sub> and C18:3(OO)<sub>1</sub>, di-peroxides C18:2(OO)<sub>2</sub>, C18:3(OO)<sub>2</sub> and tri-peroxides C18:3(OO)<sub>3</sub> are well identified as schematized by figure 2.60.

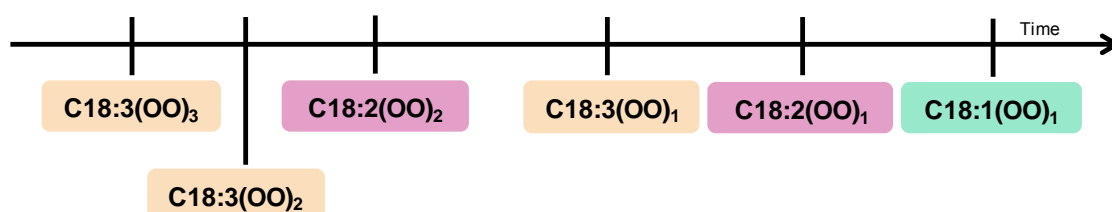


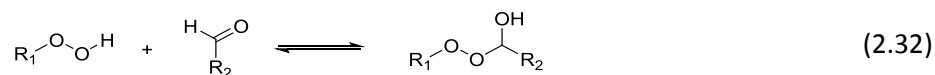
Figure 2.60: Simplification of the separated peroxide mixture from the photooxidation of FAMES of linseed oil

While the separation of this complex mixture of peroxides was not complete with liquid chromatography, LC-UV and that NMR analysis was too complex to undertake without pre-separation of all the peroxides, LC-MS/MS (MRM mode) is a rapid, sensitive and powerful way to separate and characterize complex mixture of peroxides.

### 3.4 Formation of peroxyhemiacetals during the oxidation of edible oils

Terpenes are, as for (poly)unsaturated lipid, easily autoxidized and form allergenic hydroperoxides. Firmenich company, by the way of Calandra *et al.*, developed a method for the detection of hydroperoxides by coupling LC and chemiluminescence reaction as detector.<sup>248</sup> In addition to hydroperoxides detection, they highlight in 2016 the formation of peroxyhemiacetal by reaction of terpene hydroperoxides and endogenous aldehydes. Indeed, electron rich species ROOH reversibly attack electrophilic carbonyl from aldehydes leading to peroxyhemiacetal formation (Eq.

**2.32).** The reversible formation of peroxyhemiacetals from hydroperoxides reveals its possible role as a reservoir of hydroperoxides which could extend the allergenic potential of oxidized terpenes.



As the formation of such peroxyhemiacetal of fatty acid has never been reported so far, we investigated the possible formation of this type of peroxy compounds through the reaction between hydroperoxides and endogenous aldehydes in edible oils. Guillén *et al.* identified hexanal, octanal and nonanal as the most abundant aldehydes found in edible oils (*i.e.* olive, sunflower and linseed oils).<sup>249</sup> We simplified the analysis by using a model system prepared by mixing nonanal (1 equiv.) with pure mono-hydroperoxides (C18:1(OO)<sub>1</sub>, 1 equiv.) from methyl oleate obtained by singlet oxygenation (**Fig. 2.61**). The mixture is stirred for several hours in CDCl<sub>3</sub> at room temperature and analyzed by NMR and Direct Liquid Injection Mass Spectrometry (DLI-MS). As for hydroperoxides, peroxyhemiacetals are thermally sensitive making their GC analysis impossible without pre-derivatization.

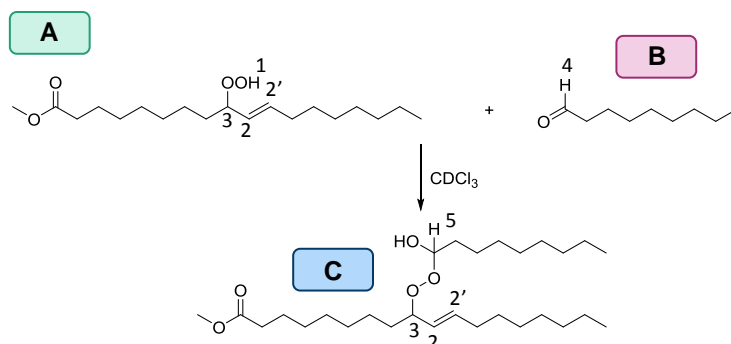


**Figure 2.61:** Formation of peroxyhemiacetal through the reaction of nonanal and C18:1(OO)<sub>1</sub>, the numbers indicate the hydrogen pointed out by <sup>1</sup>H NMR

We tried to characterize the peroxyhemiacetal by <sup>1</sup>H-NMR. **Figure 2.62** shows the <sup>1</sup>H-NMR spectrum of C18:1(OO)<sub>1</sub> (A), nonanal (B) and mixture of both compounds (C) with relevant hydrogen studied. The monitoring of the aldehydic proton (4) highlights a decrease in nonanal concentrations. Moreover, the slight apparition of hydrogen (5) describing the formation of peroxyhemiacetal is in favor of the reaction between hydroperoxide and nonanal.

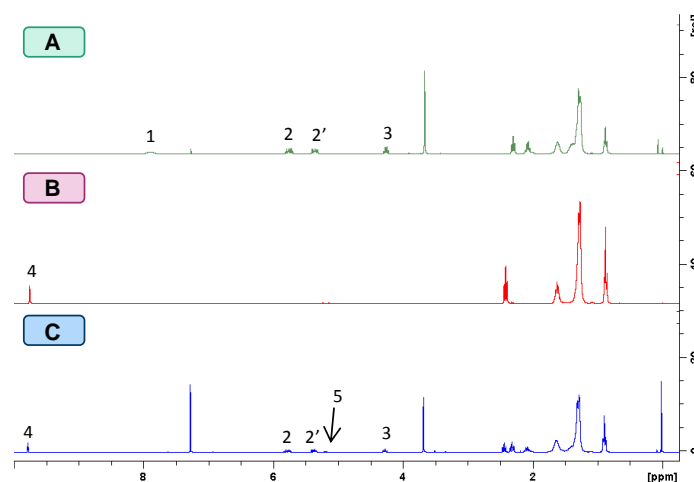


**Figure 2.62:** <sup>1</sup>H NMR spectrum of mono-hydroperoxide from C18:1 (A), nonanal (B) and mixture of both substrates (C)

The identification of peroxyhemiacetal by  $^1\text{H}$  NMR is not really clear. Therefore, the same mixture is analyzed by DLI-MS by adding  $\text{Li}^+$ ,  $\text{Na}^+$ ,  $\text{Cs}^+$  and  $\text{Ag}^+$  cations. **Table 2.21** gathers the  $m/z$  of expected adducts.

Ions	m/z	Mono-hydroperoxide (A)	Nonanal (B)	Peroxyhemiacetal (C)
		328 a.m.u	142 a.m.u	470 a.m.u
$\text{Li}^+$	7	335	149	477
$\text{Na}^+$	23	351	165	493
$\text{Cs}^+$	133	461	275	603
$\text{Ag}^+$	107/109	435/437	249/251	577/579

**Table 2.21:** M/z of expected adducts obtained by ionization of mono-hydroperoxides (A), nonanal (B) and peroxyhemiacetal (C) with  $\text{Li}^+$ ,  $\text{Na}^+$ ,  $\text{Cs}^+$  and  $\text{Ag}^+$

**Figure 2.63** shows the mass spectra obtained after ionization of the mixtures with  $\text{Li}^+$ ,  $\text{Na}^+$ ,  $\text{Cs}^+$  and  $\text{Ag}^+$  cations and highlights the expected  $[\text{C}+\text{X}]^+$  adducts for peroxyhemiacetal. Moreover, there is still presence of mono-hydroperoxide characterized by  $[\text{A}+\text{X}]^+$  adducts. Finally, nonanal is not ionized by ESI-MS analysis and  $[\text{B}+\text{X}]^+$  adducts are not identified whereas  $^1\text{H}$  NMR points out the remaining nonanal. This is probably due to its saturated structure which is weakly ionized by ESI-MS. Other mass peaks obtained are not explained apart from those related to a loss of  $\text{H}_2\text{O}$  for  $\text{C}_{18}:1(\text{OO})_1$  with  $\text{Li}^+$  (317  $m/z$ ) and probably 2  $\text{H}_2\text{O}$  for peroxyhemiacetal with  $\text{Ag}^+$  ( $m/z = 541/543$ ). Consequently, mass spectrometry analysis is also a relevant method for the detection of peroxyhemiacetal.

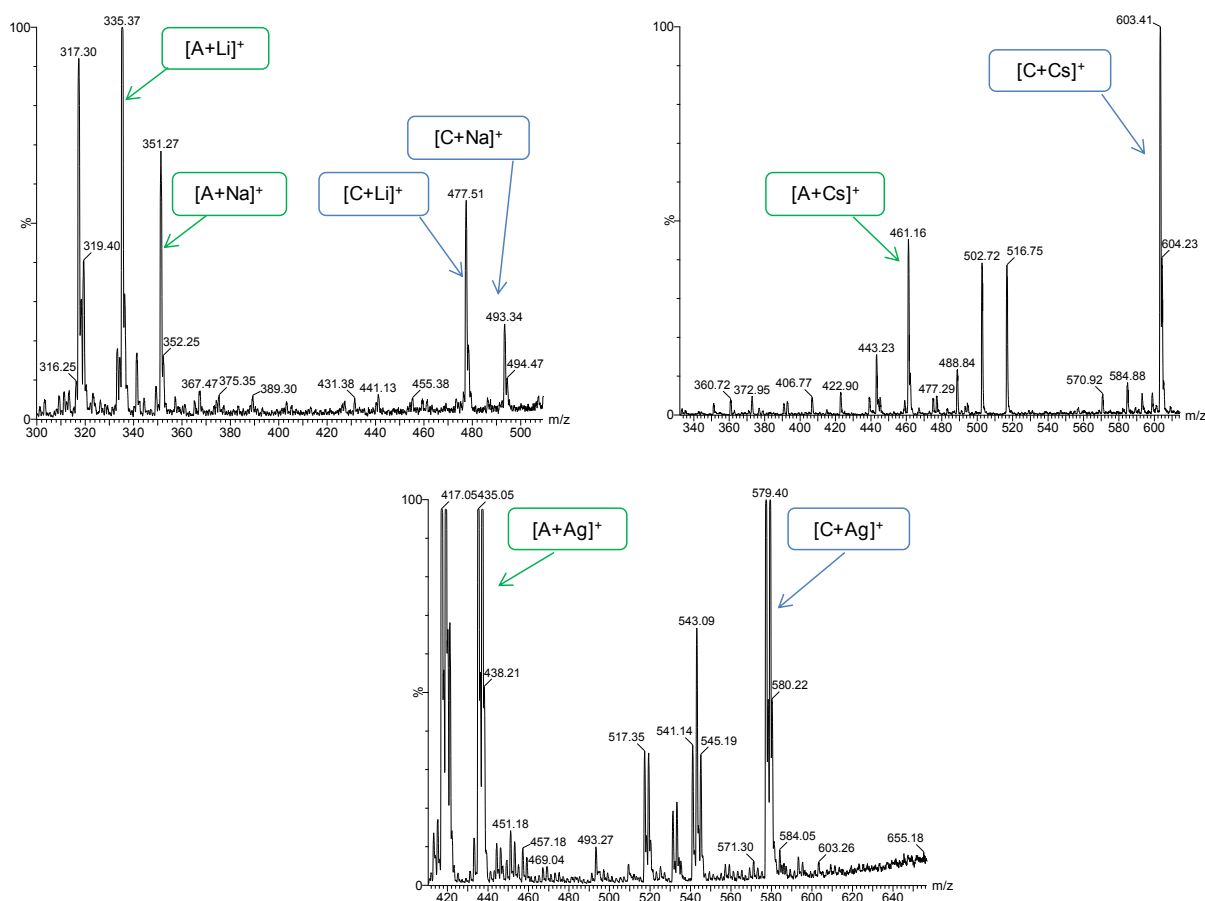


**Figure 2.63:** DLI-MS spectrums of mono-hydroperoxide and nonanal mixture ( $[\text{ROOH}] = [\text{nonanal}] = 6 \times 10^{-5} \text{ M}$ ) with  $\text{Na}^+$  already present in the mass system,  $\text{Li}^+$ ,  $\text{Cs}^+$  and  $\text{Ag}^+$  ( $10^{-3} \text{ M}$ ) in acetonitrile

### 3.5 Conclusion

The analysis of traces of hydroperoxides was a relevant challenge because of their thermal degradation. The derivatization and reduction of hydroperoxides before GC-MS analysis which is time consuming and not specific is not used anymore. UV detection coupled with LC separation is too simple analytical technique leading to a loss of information in the chemical structure elucidation. Finally, RMN analysis without appropriate standards is not an effective technique to detect and analyze complex mixtures of lipid peroxides.

Mass spectrometry analysis is the best technique to elucidate the composition of oxidized lipids. ElectroSpray ionization (ESI) with monovalent ions ( $\text{Li}^+$ ,  $\text{Na}^+$ ,  $\text{K}^+$  and  $\text{Cs}^+$ ) and Coordination IonSpray (CIS) with  $\text{Ag}^+$  show great ionization of hydroperoxides and cyclic peroxides. Nevertheless, divalent alkaline earth metal ions ( $\text{Be}^{2+}$ ,  $\text{Ca}^{2+}$  and  $\text{Ba}^{2+}$ ) are not able to ionize peroxides. With regard to its affinity for double bonds,  $\text{Ag}^+$  is not specific of peroxides and enhances also the ionization of FAMES. Moreover, alkali metal ions investigated show a gradual decline in affinity with hydroperoxides and FAMES which goes along with the down in the alkali metal group.  $\text{Cs}^+$  is the most promising ion for the selective detection of intact unsaturated hydroperoxides and peroxides. Indeed, it does not ionize non-oxidized substrates and strongly enhance the ionization of hydroperoxides, suppresses the overlap of peaks obtained with other cations, shifts the molecular mass of peroxides adducts out of the background where a lot of low molecular weights contaminate the mass spectrum and limits the fragmentation of hydroperoxides into epoxide, alcohol and aldehydes.

The detection of peroxyhemiacetals could be a new crucial investigation in food. Indeed, we showed for the first time that their formation in food is possible through the reaction of hydroperoxides and endogenous aldehydes as for fragrances.<sup>248</sup> Alkali ( $\text{Li}^+$ ,  $\text{Na}^+$  and  $\text{Cs}^+$ ) and metal ( $\text{Ag}^+$ ) cations are the most interesting ions for the detection of peroxyhemiacetals. Further examinations on peroxyhemiacetal effects in food (stability and organoleptic properties) are required since it could have a positive effect through the decrease of the hydroperoxide content and delay the oxidation process. Conversely, peroxyhemiacetal could extend undesirable effects of hydroperoxides since they could act as a reservoir for this radical initiator.

LC-MS/MS is the most promising method to separate and elucidate the chemical structures of peroxides with post-column injection of ions. The MRM mode allows the following of characteristic transitions related to the fragmentation from parent to daughters. The chemical structure of daughters is another probe of each regioisomers formed during the oxidation of oils. A specific detection into a FAME matrix discriminating hydroperoxides at the nanomole level is obtained. Moreover, the characteristic daughters obtained from the fragmentation of mono-hydroperoxides should be used with a change in chromatographic conditions to separate each regioisomer. Finally, oils are composed by triglycerides and not FAMES. All our knowledge developed for the analysis of hydroperoxides and peroxides from FAMES used as model of oxidized oil could be transposed for the investigation of real oxidized triglycerides.

## CHAPTER 2. EXPERIMENTAL PART

---

## 1. Materials and methods

### 1.1 Reagents

Solvents are of the purest grade commercially available from Sigma-Aldrich and Biosolve. Potassium acetate ( $\geq 99\%$ ), sodium acetate ( $\geq 99\%$ ), cesium acetate ( $\geq 99.99\%$ ), barium acetate ( $99\%$ ), lithium acetate ( $99.95\%$ ), calcium acetate monohydrate ( $\geq 99\%$ ), ammonium acetate ( $\geq 99\%$ ), silver acetate ( $99.99\%$ ), beryllium sulfate tetrahydrate ( $\geq 99\%$ ), methyl stearate ( $99\%$ ), methyl oleate ( $99\%$ ), methyl linoleate ( $\geq 99\%$ ), methyl linolenate ( $\geq 99\%$ ), citronellol ( $95\%$ ), geraniol ( $98\%$ ), decanoyl chloride ( $98\%$ ), rose bengal ( $95\%$ ), pyridine ( $99\%$ ), 3,7-dimethyl-1-octanol ( $\geq 98\%$ ), squalene ( $\geq 98\%$ ), triolein ( $\geq 99\%$ ), cholesterol acetate ( $> 97\%$ ), limonene ( $\geq 99\%$ ), benzoyl peroxide ( $> 97\%$ ), cumene hydroperoxide ( $80\%$ ), tert-butyl hydroperoxide ( $70\text{ wt}\%$  in water), lauroyl peroxide ( $97\%$ ) are from Sigma-Aldrich.  $\alpha$ -Terpinene ( $> 90\%$ ) and artemisinin ( $> 97\%$ ) are from TCI. Linalool ( $97\%$ ) is from Alfa Aesar. Aluminium oxide, basic, Brockmann I, for chromatography,  $50\text{-}200\ \mu\text{m}$ ,  $60\ \text{\AA}$  is from Acros Organics. Refined linseed oil is from Vandeputte Group, Belgium. FAME mix GLC-10 containing palmitic acid methyl ester (C16:0), stearic acid methyl ester (C18:0), oleic acid methyl ester (C18:1), linoleic acid methyl ester (C18:2) and linolenic acid methyl ester (C18:3) is from Supelco.

### 1.2 Xevo TQ-S device, Direct Liquid Injection (DLI) and LC-MS/MS methods



Figure S2.1: UPLC (Acquity H-Class) coupled with Xevo TQ-S (mass detector)

Ultra Performance Liquid Chromatography (UPLC) is coupled with the MS-MS triple quadrupole Xevo TQ-S. It is composed by an automatic sample kept at  $5\ ^\circ\text{C}$  (1), the column (2, Agilent, Poroshell, C8,  $2.7\ \mu\text{m}$ ,  $2.1 \times 50\ \text{mm}$  or Phenomenex, Kinetex, C18,  $2.6\ \mu\text{m}$ ,  $100 \times 2.1\ \text{mm}$ ), UV detector (3), direct liquid infusion (DLI) or post-column injection (4) and mass detector (5).

The detection conditions are as follows: capillary voltage:  $3.00\ \text{kV}$ , cone voltage:  $20\ \text{V}$ , source offset voltage:  $30\ \text{V}$  (positive ion mode), desolvation gas flow (nitrogen):  $350\ \text{L/h}$ , cone gas flow:  $150\ \text{L/h}$ , nebulizer gas flow:  $7.0\ \text{bar}$ , collision gas flow:  $0.25\ \text{mL/min}$ , solvation temperature:  $250\ ^\circ\text{C}$ , run duration:  $0.4\ \text{min}$ , scan time:  $0.2\ \text{sec}$ , infusion flow:  $5\ \mu\text{L/min}$ .

Analytical software (MassLynx, version 4.1) is used for the system control and data processing.

- *Influence of ions for the detection of FAMES and hydroperoxides (DLI-ESI-MS)*

Methyl stearate, methyl oleate, methyl linoleate, methyl linolenate and mono-hydroperoxide of methyl oleate ( $10^{-6}$  mol.L $^{-1}$ ) are mixed with appropriate ion ( $H^+$ ,  $Li^+$ ,  $Na^+$ ,  $K^+$ ,  $Rb^+$ ,  $Cs^+$ ,  $Be^{2+}$ ,  $Ca^{2+}$ ,  $Ba^{2+}$ ,  $Ag^+$  and  $NH_4^+$ ) at various concentrations ( $10^{-5}$ ,  $3 \times 10^{-5}$ ,  $10^{-4}$ ,  $3 \times 10^{-4}$ ,  $10^{-3}$  mol.L $^{-1}$ ) in  $H_2O/MeOH$  solvent (50:50 v/v). The flow for direct liquid injection (DLI) is  $5 \mu L \cdot min^{-1}$ . Continuum data is collected for 40 scans over the mass range 150-475 m/z and an average on three values is calculated (**Fig. S2.2**). The run duration goes on 8 min with a scan time of 0.2 s. For the selective detection of hydroperoxides and peroxides with  $Cs^+$  by ESI-MS, the analytes ( $4 \times 10^{-6}$  mol.L $^{-1}$ ) are mixed with  $Cs^+$  ( $10^{-4}$  mol.L $^{-1}$ ) in  $H_2O/MeOH$  solvent (50:50 v/v). The flow for direct liquid injection (DLI) is  $20 \mu L \cdot min^{-1}$ .

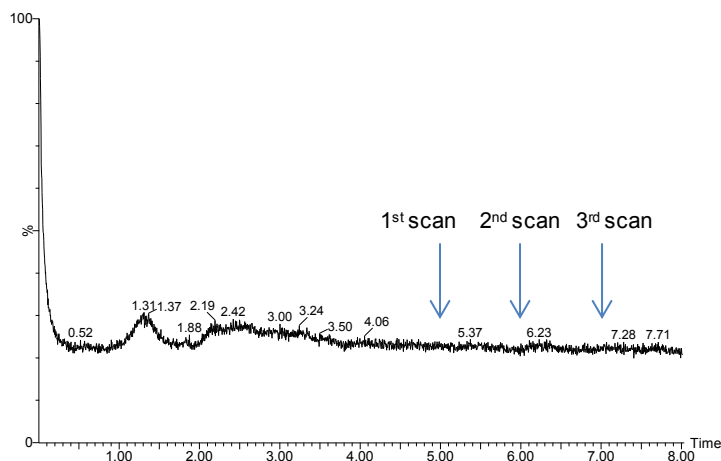


**Figure S2.2:** Continuum run duration of DLI-MS experiments

- *Liquid chromatography – ElectroSpray ionization and Coordination ionspray Mass spectrometry (LC-MS/MS)*

For Direct Liquid Injection, terpenes (3,7-dimethyloctyl decanoate, citronellol caprate or geraniol caprate), FAMES of linseed oil, methyl oleate, methyl linoleate, methyl linolenate and their respective peroxides ( $6 \times 10^{-7}$  mol.L $^{-1}$ ) are mixed with appropriate ions ( $10^{-3}$  M) and a flow rate of  $5 \mu L \cdot min^{-1}$  is used.

For LC-MS and LC-MS/MS analysis, terpenes (citronellol caprate or geraniol caprate,  $1.6 \times 10^{-6}$  mol.L $^{-1}$ ) are mixed with respective hydroperoxides ( $6 \times 10^{-7}$  mol.L $^{-1}$ ) in MeOH solvent. Sample rack is kept at  $5^\circ C$ . ACN/ $H_2O$  eluent is used at an 80/20 ratio (v:v) for citronellol caprate experiments whereas a 70/30 ratio is utilized for geraniol caprate analysis.  $NH_4^+$  and  $H^+$  ions are added to the eluent. Flow rate of  $0.5 mL \cdot min^{-1}$ , injection volume of  $5 \mu L$  and Phenomenex column (C18,  $2.6 \mu m$ ,  $100 \times 2.1$  mm) are employed for the separation process. For the SIR mode, the formation of adducts is followed *via* their respective m/z value. For the MRM mode, the transition from parent to daughter characteristic of each molecule (found with the Intellistart program) is used to monitor the separation (**Fig. S2.3**).

FAMES of linseed oil ( $1.6 \times 10^{-6}$  mol.L $^{-1}$ ) are solubilized into MeOH. ACN/ $H_2O$  eluent is used at a 65/35 ratio (v:v) and ions ( $NH_4^+$  and  $H^+$ ) are added to the eluent. Sample rack is kept at  $5^\circ C$ . Flow rate of  $0.5 mL \cdot min^{-1}$ , injection volume of  $5 \mu L$  and Poroshell column (Agilent, C8,  $2.7 \mu m$ ,  $2.1 \times 50$  mm) are employed for the separation process. For the SIR mode, the formation of adducts is followed *via* their respective m/z value. For the MRM mode, the transition from parent to daughter characteristic of each molecule is used to monitor the separation.

The peroxides mixture of FAMES of linseed oil ( $2 \times 10^{-5} \text{ mol.L}^{-1}$ ) is solubilized into MeOH. Sample rack is kept at  $5 \text{ }^\circ\text{C}$ . ACN/ $\text{H}_2\text{O}$  eluent is used at a 50/50 ratio (v:v) and ions ( $\text{Li}^+$ ,  $\text{Ag}^+$  and  $\text{NH}_4^+$ ) are added by post-column injection during all the run ( $10 \text{ mg.mL}^{-1}$ ) at a flow rate of  $10 \text{ } \mu\text{L.min}^{-1}$ . Flow rate of  $0.5 \text{ mL.min}^{-1}$ , injection volume of  $10 \text{ } \mu\text{L}$  and Poroshell column (Agilent, C8,  $2.7 \text{ } \mu\text{m}$ ,  $2.1 \times 50 \text{ mm}$ ) are employed for the separation process. For the MRM mode, the transition from parent to daughter characteristic of each molecule is used to monitor the separation.

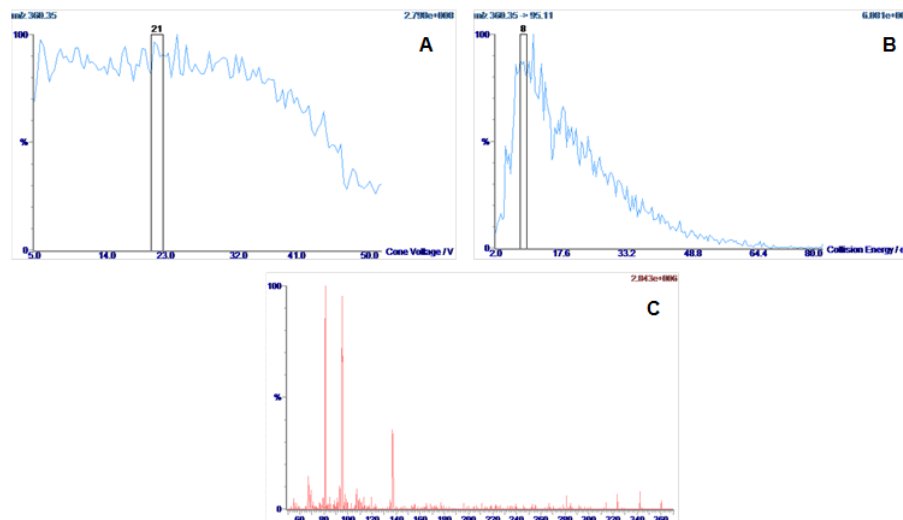
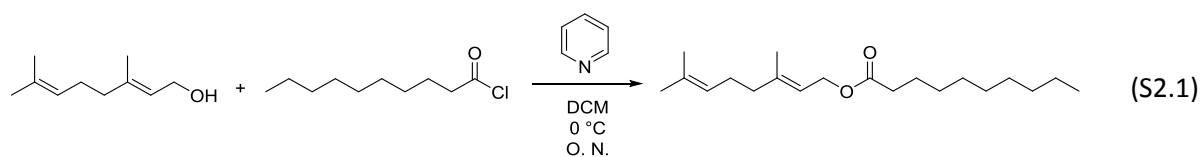


Figure S2.3: Intellistart fragmentation program: scan of cone voltage (A, 21 V, collision energy (B, 8 eV) and fragmentation spectrum (C) in the case of citronellol caprate hydroperoxide fragmentation  $[\text{R}(\text{OO})_1 + \text{NH}_4]^+$

### 1.3 Synthesis of terpenoids by esterification

Terpenes (1 equiv. 3,7-dimethyl-1-octanol, 10 g, 63.1 mmol; 1 equiv. citronellol, 10 g, 57.5 mmol or 1 equiv. geraniol, 10 g, 64.8 mmol) are dissolved into dichloromethane (DCM, 40 mL) contained in a round bottom flask. Pyridine (30 mL) is added to the mixture under stirring. The mixture is then cool down to  $0 \text{ }^\circ\text{C}$ . In another round bottom flask, decanoyl chloride (1 equiv.) is dissolved into dichloromethane (DCM, 30 mL). It is then added drop-by-drop to the solution of terpene and pyridine *via* a dropping funnel and all the compounds react during 14 hours (over night). A thin-layer chromatography (TLC) with hexane/diisopropyl ether (3/1, v/v) as eluent is used to check the progress of the reaction. All the dichloromethane used is evaporated under vacuum. The synthesized terpenoids are solubilized into petroleum ether and three successive washing with water are undertaken in order to eliminate the pyridinium salts. The two phases are separated and the organic layer is dried *via* magnesium sulfate. The petroleum ether is then evaporated under vacuum and terpenoids derivatives are collected. The esterification reaction of terpenes (3,7-dimethyl-1-octanol, citronellol and geraniol, into 3,7-dimethyloctyl decanoate, citronellol caprate and geraniol caprate is represented by the Eq. S2.1.

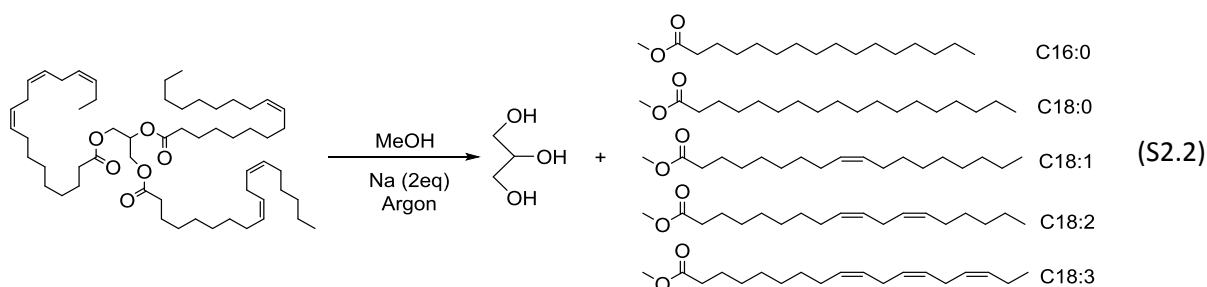


### 1.4 Purification of linseed oil

Alumina column chromatography can be used to remove antioxidants values to very low concentrations. Starting linseed oil containing antioxidants is treated for complete removal of all antioxidants present, defined as < 1 ppm. Aluminium oxide is initially conditioned by gently rinsed with in-house ultra pure water in a Buchner funnel situated above the Buchner flask. This mixture is gently manually agitated and washed three times. Rinsed alumina is placed in an oven set at 200°C for at least three hours, generally dried overnight. The dried alumina is introduced into a column above a heavy walled 500 mL filtering flask. A ratio of 2:1 oil/alumina was maintained for this effort. Two hundred grams of alumina was weighed and dispensed into the column via glass funnel. Next, portions of 400 g oil were added since the column capacity limited the full initial introduction amount. The vacuum was maintained to allow a slow but steady drip as visually witnessed into the filtering flask. All glassware was covered with aluminum foil during this separation to limit light exposure. This process offers approx 70 % recovery of starting amount. Oil was stored in an amber wide bottle and capped with nitrogen prior to freezer storage.

### 1.5 Synthesis of antioxidant-free fatty acid methyl esters (FAMES) by transesterification of purified linseed oil

The transesterification reaction of triglycerides of purified linseed oil with methanol into fatty acid methyl esters (FAMES) is represented by the Eq. S2.2.



1 L of methanol is introduced into a 2L three-necked equipped with a cooler and a bubbler. Sodium (10 g, 2 equiv.) is introduced piece by piece under argon followed by purified linseed oil (200 g, 1 equiv.). The reaction is performed overnight. FAMES are extracted with 3 x 300 mL of petroleum ether. The combined organic phases are evaporated under pressure. Isolated FAMES are stored at -20 °C.

### 1.6 Singlet oxygenation (photooxidation) of terpenoids and FAMES

The photosensitized oxidations of unsaturated substrates (0.03 M) were carried out at 5 °C in methanol with rose bengal (5 mg/mL) as sensitizer by irradiation with a sodium lamp while maintaining a continuous bubbling of O<sub>2</sub>. The experimental apparatus is illustrated by the Fig. S2.4.

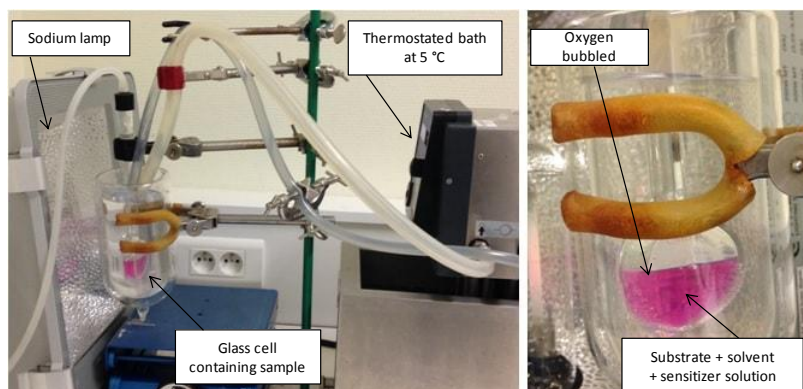
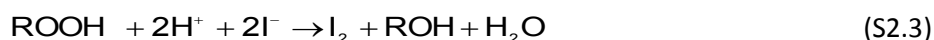


Figure S2.4: Experimental apparatus for the smooth formation of hydroperoxides by singlet oxygenation

### 1.7 Hydroperoxide titration

The formation and evaluation of the hydroperoxides obtained during the photooxidation of terpenoids and FAMES is also assessed by titration. The experimental protocol has been adapted from the French standard AFNOR NFT 60-220. The titration is based on the reaction of hydroperoxides with an excess of iodide ( $I^-$ ) ions in acidic medium (Eq. S2.3).



Then the  $I_2$  generated is titrated by a  $1.6 \text{ mmol.L}^{-1}$  pentahydrate sodium thiosulfate solution (Eq. S2.4).



When the equivalence point is reached, the amount of substance of hydroperoxides ( $n_{ROOH}$ ) is obtained with the following equation (Eq. S2.5):

$$n_{I_2} = 0.5 \times C_{Na_2S_2O_3} \times V_{eq} = n_{ROOH} \quad (S2.5)$$

Therefore, the resulting concentration of hydroperoxides  $[ROOH]_t$  is obtained with the equation S2.6.

$$[ROOH]_t = \frac{0.5 \times [Na_2S_2O_3] \times V_{eq}}{V_0} \quad (S2.6)$$

$[ROOH]_t$  and  $[Na_2S_2O_3]$  are the respective concentrations of total hydroperoxides and pentahydrate thiosulfate solutions,  $V_{eq}$  and  $V_0$  represent respectively the volume of  $Na_2S_2O_3$  added at the equivalence point and the initial volume of hydroperoxides solution added.

The reaction described by the equation S2.4 is slow and an unwanted reaction with the dioxygen is possible (Eq. S2.7).



Due to a large excess of acid or light, this reaction could be accelerated. In order to prevent from this annoyance, all the solutions must be prepared with purified water degassed thanks to argon bubbling.

The hydroperoxide solutions (0.5 mL) are put into a 50 mL Erlenmeyer flask equipped with a magnetic stirrer. Then, 6.25 mL of a chloroform/acetic acid (40:60, v/v) is added and the solution is stirred vigorously to solubilize the hydroperoxides. The saturated potassium iodide solution (0.5 mL,

14.3 g into 10 mL of H<sub>2</sub>O) is then added to the mixture which is stirred for 1 min. The Erlenmeyer flask has stopped being stirred and allowed to age 5 min in a dark place. After that, 20 mL of purified water are added to stop the reaction and the titration is performed thanks to the pentahydrate sodium thiosulfate solution (1.6 mmol.L<sup>-1</sup>). A few drops of a starch solution are added near the equivalence point and the titration is done when the blue-purple coloration vanishes totally. By the way, a systematic blank titration (without hydroperoxide) is carried out to check that all the oxygen is removed.

### 1.8 Gas chromatography – mass spectrometry analysis

A Thermofisher GC Trace equipped with an AI 3000 injector connected to Thermofisher DSQ II simple quadrupole detector is used for the GC-MS analysis of FAMES. Compound separation is achieved on a 30 m, DB5MS with 0.25 mm i.d. and 0.25 µm film thickness gas chromatographic column (J&W Scientific, Folsom, CA, USA). Carrier gas (ultra-pure helium) flow rate is 1.0 mL/min and the injector, the transfer line and the ions source are maintained at 250, 270 and 220 °C, respectively. The MS detector is used in the EI mode with an ionization voltage of 70 eV. The NIST 2008 is used to identify the chemical compounds.

For the GC analysis of FAMES linseed oil, the column is held at 130 °C for 0.5 min and then programmed at 0.3 °C.min<sup>-1</sup> to 180 °C and maintained for 5 min. Then, the column is programmed at 3 °C.min<sup>-1</sup> to 250 °C and maintained for 10 min. The compounds are injected in the Split mode with a ratio of 20. FAME mix GLC-10 is used to analyze and quantify the FAMES composition.

For the GC analysis of terpenoids synthesized (3,7-dimethyloctyl decanoate, citronellol caprate and geraniol caprate), the column is held at 60°C for 2 min and then programmed at 3°C.min<sup>-1</sup> to 250°C and maintained for 5 min.

### 1.9 Infrared analysis

Infrared spectra (IR) were recorded for the terpenoids derivative (3,7-dimethyloctyl decanoate, citronellol caprate and geraniol caprate) on a Thermo Electron Corporation apparatus type Nicolet 380 (IRTF) and wave-numbers are indicated in cm<sup>-1</sup>.

### 1.10 <sup>1</sup>H and <sup>13</sup>C NMR analysis

<sup>1</sup>H NMR spectra were recorded on a Bruker 300, calibrated relative to TMS in CDCl<sub>3</sub> solution and data are reported as follows: chemical shift in parts per million, multiplicity (bs = broad signals, s = singlet, d = doublet, t = triplet, q = quartet, m = multiplet or overlap of non-equivalent resonances), integration.

<sup>13</sup>C NMR spectra were recorded at 100 MHz in CDCl<sub>3</sub>, calibrated on CDCl<sub>3</sub> signal (77.16 ppm) and data were reported as follows: chemical shift in parts per million and CH<sub>x</sub> were X = number of hydrogen linked to the carbon, if any (deduced from ATP experiments).

### 1.11 Liquid chromatography – UV detection

The analyses were carried out in Shimadzu (LC 20 AT) high-performance liquid chromatography (HPLC) equipment with an ultraviolet detector (UV) set up at 205 nm. All chromatograms were generated by LCsolutions software. It was used a single Prevail C18 reversed-phase column (250 mm x 4.6 mm, 5  $\mu$ L). Depending of the substrates analyzed, the injection volume of 1, 10 or 20  $\mu$ L and the flow-rate of 0.5 or 1.0 mL.min<sup>-1</sup> with isocratic elution of acetonitrile (100 %) or acetonitrile/water 9:1 (v/v) were used.

### 1.12 DFT calculation of the energy of interaction

The energy of interaction between cations and targeted substrates (*i.e.* double bond, ester, hydroperoxide and unsaturated hydroperoxide) leading to the formation of adducts were investigated by Density Functional Theory (DFT). It is given by the difference between the enthalpy of formation of adduct  $[R+X]^+$  and that of substrate R and cation  $X^+$  as described by **equations S2.8** and **S2.9**.



$$E_{\text{interaction}} = H_f^0([R + X]^+) - H_f^0(R) - H_f^0(X^+) \quad (\text{S2.9})$$

All the calculations are performed using Gaussian 03 packages. The geometries of all the substrates molecules are optimized with the DFT method by using the B3LYP/6-311G (d,p) basis set. However, the geometries of all the cations and adducts are optimized with the DFT method by using the GEN basis set (charge: 1 and spin: singlet).

## 2. Results

### 2.1 NMR and IR description of terpenoids and FAMES substrates

- 3,7-dimethyloctyl decanoate

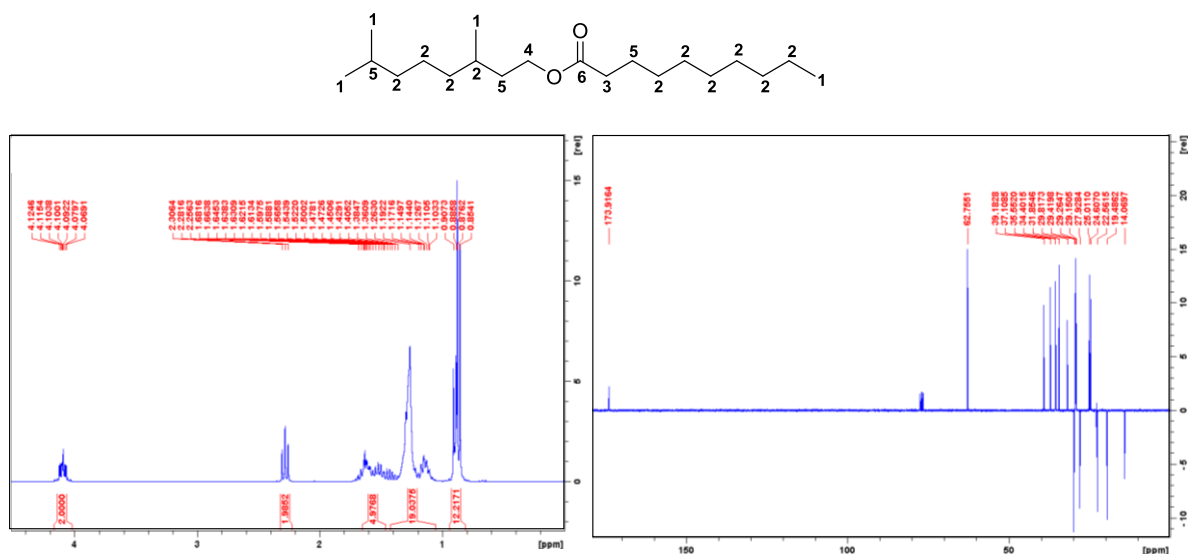


Figure S2.5: <sup>1</sup>H NMR and <sup>13</sup>C NMR spectra of 3,7-dimethyloctyl decanoate

$^1\text{H NMR } \delta$  (ppm): 0.88 (12  $\text{H}_1$ , m), 1.26 (19  $\text{H}_2$ , m), 1.57 (5  $\text{H}_5$ , m), 2.28 (2  $\text{H}_3$ , t,  $J = 7.6$  Hz), 4.09 (2  $\text{H}_4$ , m)

$^{13}\text{C NMR } \delta$  (ppm): 14.1 ( $\text{C}_1\text{H}_3$ ), 19.5 ( $\text{C}_1\text{H}_3$ ), 22.6 ( $\text{C}_1\text{H}_3$ ), 24.6 ( $\text{C}_2\text{H}_2$ ), 25.0 ( $\text{C}_2\text{H}_2$ ), 27.9 ( $\text{C}_5\text{H}$ ), 29.1 ( $\text{C}_2\text{H}_2$ ), 29.3 ( $\text{C}_2\text{H}_2$ ), 29.4 ( $\text{C}_2\text{H}_2$ ), 29.8 ( $\text{C}_2\text{H}$ ), 31.9 ( $\text{C}_5\text{H}_2$ ), 34.4 ( $\text{C}_5\text{H}_2$ ), 35.6 ( $\text{C}_2\text{H}_2$ ), 37.1 ( $\text{C}_2\text{H}_2$ ), 39.2 ( $\text{C}_2\text{H}_2$ ), 62.7 ( $\text{C}_4\text{H}_2$ ), 173.9 ( $\text{C}_6$ )

ATR-FTIR ( $\text{cm}^{-1}$ ): 2923, 1736, 1464, 1166

▪ Citronellol caprate

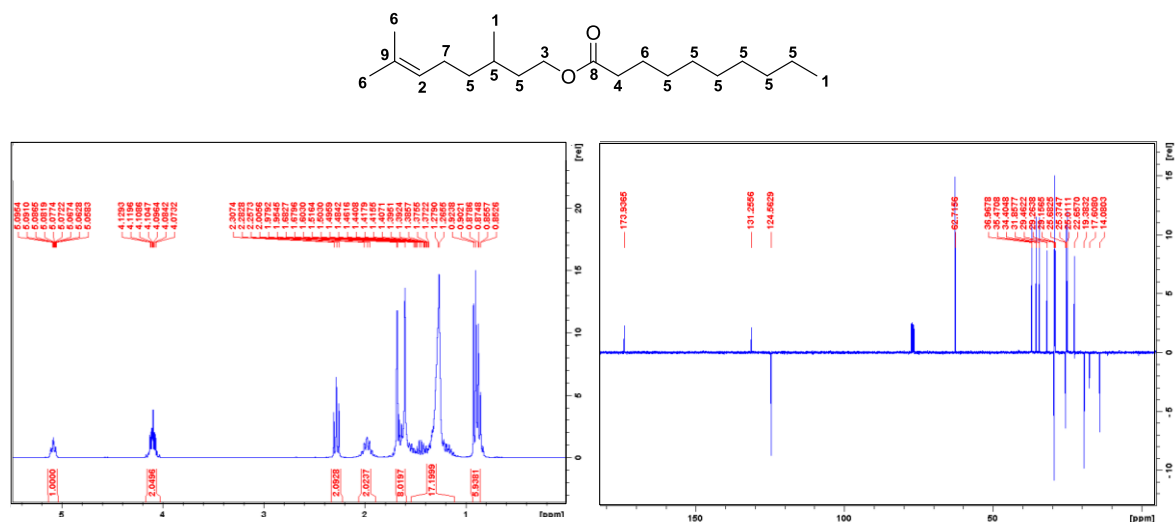


Figure S2.6:  $^1\text{H}$  and  $^{13}\text{C}$  NMR spectra of citronellol caprate

$^1\text{H NMR } \delta$  (ppm): 0.90 (6  $\text{H}_1$ , m), 1.27 (17  $\text{H}_5$ , m), 1.64 (8  $\text{H}_6$ , m), 1.97 (2  $\text{H}_7$ , m), 2.28 (2  $\text{H}_4$ , t,  $J = 7.7$  Hz), 4.09 (2  $\text{H}_3$ , m), 5.09 (1  $\text{H}_2$ , m,  $J_1 = 1.4$  Hz,  $J_2 = 7.1$  Hz)

$^{13}\text{C NMR } \delta$  (ppm): 14.1 ( $\text{CH}_3$ ), 17.6 ( $\text{CH}_3$ ), 19.4 ( $\text{CH}_3$ ), 22.7 ( $\text{CH}_2$ ), 25.0 ( $\text{CH}_2$ ), 25.4 ( $\text{CH}_2$ ), 25.7 ( $\text{CH}_3$ ), 29.2 ( $\text{CH}_2$ ), 29.5 ( $\text{CH}_2$ ), 31.9 ( $\text{CH}_2$ ), 34.4 ( $\text{CH}_2$ ), 35.5 ( $\text{CH}_2$ ), 37.0 ( $\text{CH}_2$ ), 62.7 ( $\text{CH}_2$ ), 124.6 ( $\text{C}_2\text{H}$ ), 131.3 ( $\text{C}_9$ ), 173.9 ( $\text{C}_8$ )

ATR-FTIR ( $\text{cm}^{-1}$ ): 2922, 1736, 1457, 1165

- Geraniol caprate

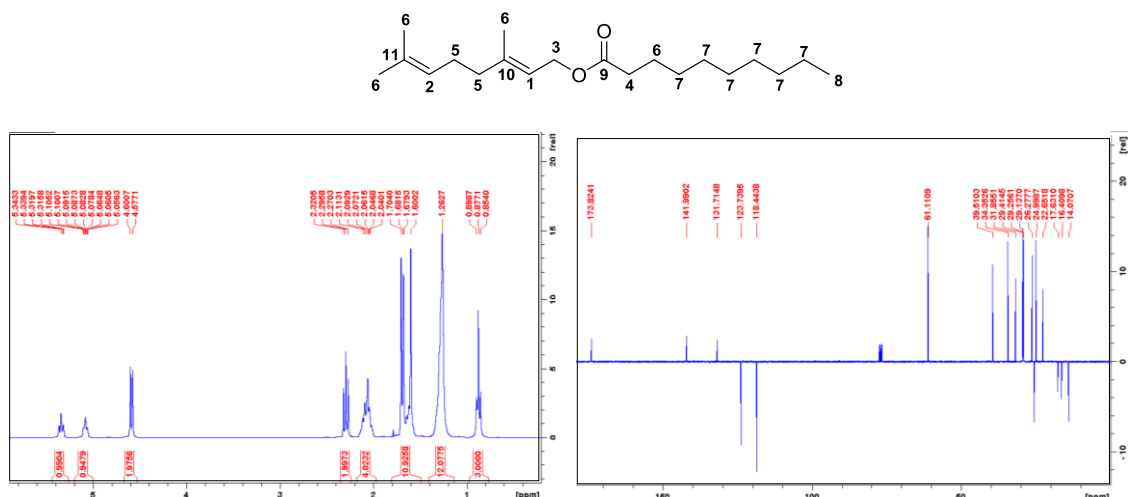


Figure S2.7:  $^1\text{H}$  and  $^{13}\text{C}$  NMR spectra of geraniol caprate

$^1\text{H}$  NMR  $\delta$  (ppm): 0.87 (3H, t,  $J = 7.0$  Hz), 1.26 (12 H<sub>7</sub>, s), 1.66 (11 H<sub>6</sub>, m), 2.06 (4 H<sub>5</sub>, m), 2.30 (2 H<sub>4</sub>, t,  $J = 7.6$  Hz), 4.60 (2 H<sub>3</sub>, d,  $J = 7.1$  Hz), 5.08 (1 H<sub>2</sub>, m), 5.34 (1 H<sub>1</sub>, td,  $J_1 = 1.1$  Hz,  $J_2 = 7.1$  Hz)

$^{13}\text{C}$  NMR  $\delta$  (ppm): 14.1 (CH<sub>3</sub>), 16.4 (CH<sub>3</sub>), 17.6 (CH<sub>3</sub>), 22.7 (CH<sub>2</sub>), 24.9 (CH<sub>2</sub>), 25.1 (CH<sub>3</sub>), 26.3 (CH<sub>2</sub>), 29.1 (CH<sub>2</sub>), 29.3 (CH<sub>2</sub>), 29.4 (CH<sub>2</sub>), 31.9 (CH<sub>2</sub>), 34.4 (CH<sub>2</sub>), 39.5 (CH<sub>2</sub>), 61.1 (CH<sub>2</sub>), 118.4 (C<sub>1</sub>H), 123.7 (C<sub>2</sub>H), 131.7 (C<sub>11</sub>), 142.0 (C<sub>10</sub>), 173.8 (C<sub>9</sub>)

ATR-FTIR (cm<sup>-1</sup>): 2922, 1731, 1454, 1161

- Methyl oleate

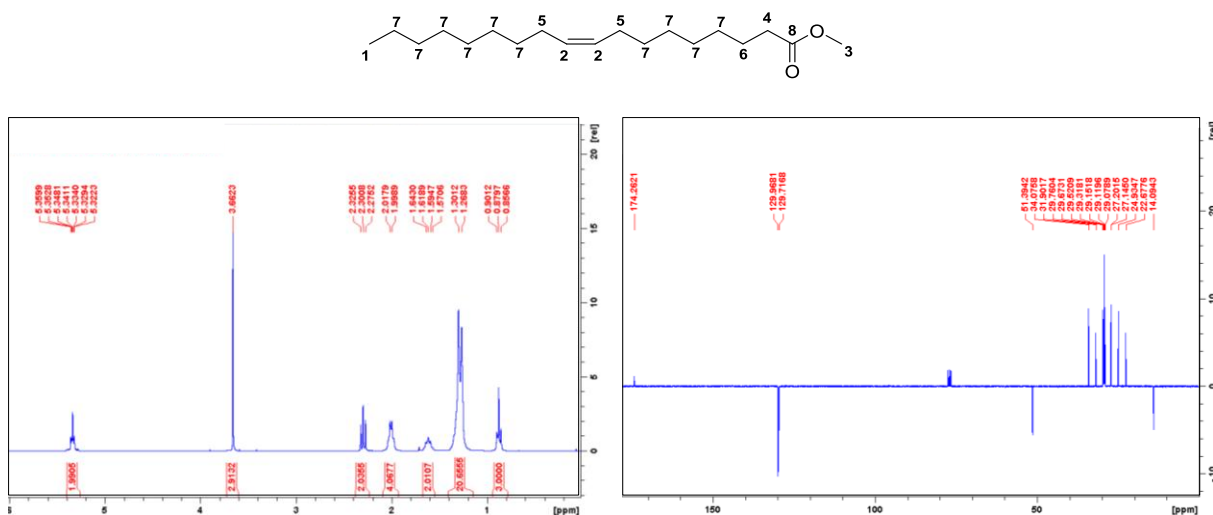


Figure S2.8:  $^1\text{H}$  and  $^{13}\text{C}$  NMR spectra of methyl oleate

$^1\text{H}$  NMR  $\delta$  (ppm): 0.88 (3 H<sub>1</sub>, t,  $J = 6.9$  Hz), 1.29 (20 H<sub>7</sub>, d), 1.60 (2 H<sub>6</sub>, q,  $J = 7.2$  Hz), 2.00 (4 H<sub>5</sub>, m), 2.30 (2 H<sub>4</sub>, t,  $J = 7.4$  Hz), 3.66 (3 H<sub>3</sub>, s), 5.34 (2 H<sub>2</sub>, m)

$^{13}\text{C}$  NMR  $\delta$  (ppm): 14.1 (CH<sub>3</sub>), 22.7 (CH<sub>2</sub>), 24.9 (CH<sub>2</sub>), 27.1 (CH<sub>2</sub>), 27.2 (CH<sub>2</sub>), 29.0 (CH<sub>2</sub>), 29.1 (CH<sub>2</sub>), 29.2 (CH<sub>2</sub>), 29.3 (2 x CH<sub>2</sub>), 29.5 (CH<sub>2</sub>), 29.7 (CH<sub>2</sub>), 29.8 (CH<sub>2</sub>), 31.9 (CH<sub>2</sub>), 34.1 (CH<sub>2</sub>), 51.4 (CH<sub>3</sub>), 129.7 (C<sub>2</sub>H), 130.0 (C<sub>2</sub>H), 174.3 (C<sub>8</sub>)

■ *Methyl linoleate*

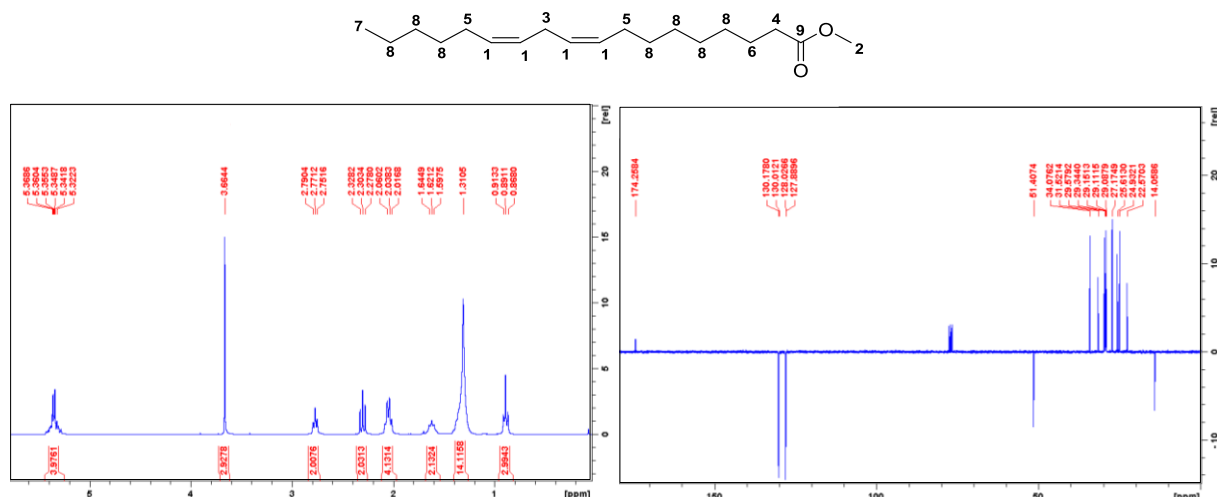


Figure S2.9:  $^1\text{H}$  and  $^{13}\text{C}$  NMR spectra of methyl linoleate

$^1\text{H}$  NMR  $\delta$  (ppm): 0.89 (3 H<sub>7</sub>, t, J = 6.9 Hz), 1.29 (20 H<sub>8</sub>, s), 1.62 (2 H<sub>6</sub>, q, J = 7.1 Hz), 2.05 (4 H<sub>5</sub>, m), 2.30 (2 H<sub>4</sub>, t, J = 7.4 Hz), 2.77 (2 H<sub>3</sub>, t, J = 5.8 Hz), 3.66 (3 H<sub>2</sub>, s), 5.35 (4 H<sub>1</sub>, m)

$^{13}\text{C}$  NMR  $\delta$  (ppm): 14.1 (CH<sub>3</sub>), 22.6 (CH<sub>2</sub>), 24.9 (CH<sub>2</sub>), 25.6 (CH<sub>2</sub>), 27.2 (2 x CH<sub>2</sub>), 29.0 (CH<sub>2</sub>), 29.1 (CH<sub>2</sub>), 29.2 (CH<sub>2</sub>), 29.3 (CH<sub>2</sub>), 29.6 (CH<sub>2</sub>), 31.5 (CH<sub>2</sub>), 34.1 (CH<sub>2</sub>), 51.4 (CH<sub>3</sub>), 127.9 (C<sub>1</sub>H), 128.0 (C<sub>1</sub>H), 130.0 (C<sub>1</sub>H), 130.2 (C<sub>1</sub>H), 174.3 (C<sub>9</sub>)

■ *Methyl linolenate*

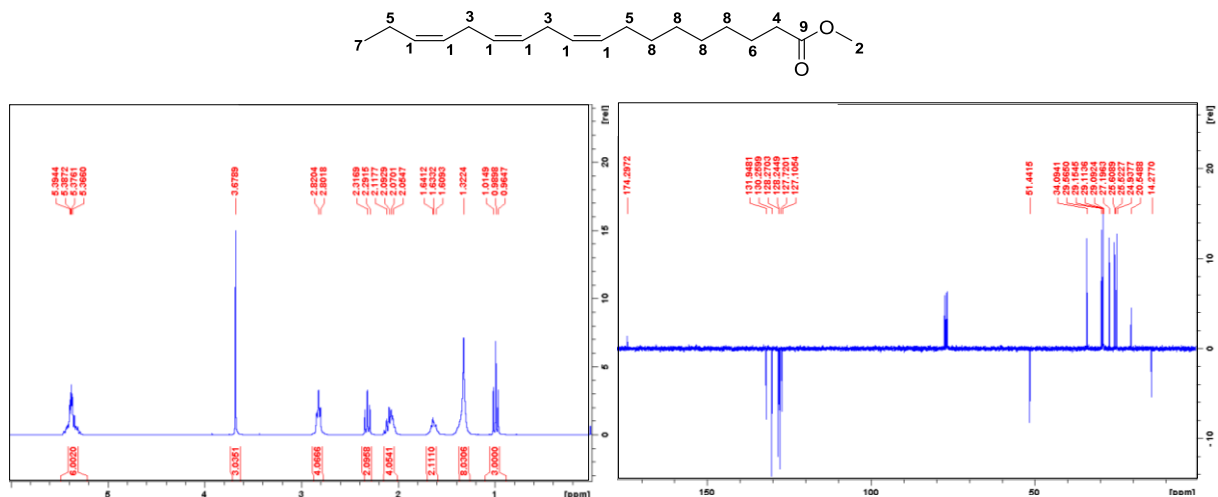


Figure S2.10:  $^1\text{H}$  and  $^{13}\text{C}$  NMR spectra of methyl linolenate

$^1\text{H}$  NMR  $\delta$  (ppm): 0.99 (3 H<sub>7</sub>, t, J = 7.5 Hz), 1.32 (8 H<sub>8</sub>, s), 1.63 (2 H<sub>6</sub>, m), 2.08 (4 H<sub>5</sub>, m), 2.32 (2 H<sub>4</sub>, t, J = 7.6 Hz), 2.82 (4 H<sub>3</sub>, t, J = 5.6 Hz), 3.68 (3 H<sub>2</sub>, s), 5.38 (6 H<sub>1</sub>, m)

$^{13}\text{C}$  NMR  $\delta$  (ppm): 14.3 (CH<sub>3</sub>), 20.5 (CH<sub>2</sub>), 24.9 (CH<sub>2</sub>), 25.5 (CH<sub>2</sub>), 25.6 (CH<sub>2</sub>), 27.2 (CH<sub>2</sub>), 29.0 (CH<sub>2</sub>), 29.1 (CH<sub>2</sub>), 29.2 (CH<sub>2</sub>), 29.6 (CH<sub>2</sub>), 34.1 (CH<sub>2</sub>), 51.4 (CH<sub>3</sub>), 127.1 (C<sub>1</sub>H), 127.7 (C<sub>1</sub>H), 128.2 (C<sub>1</sub>H), 128.3 (C<sub>1</sub>H), 130.3 (C<sub>1</sub>H), 131.9 (C<sub>1</sub>H), 174.3 (C<sub>9</sub>)

## 2.2 NMR description of terpenoids and FAMES hydroperoxides

All peroxidized compounds are mixture of isomers hydroperoxides.

### ▪ Citronellol caprate hydroperoxides

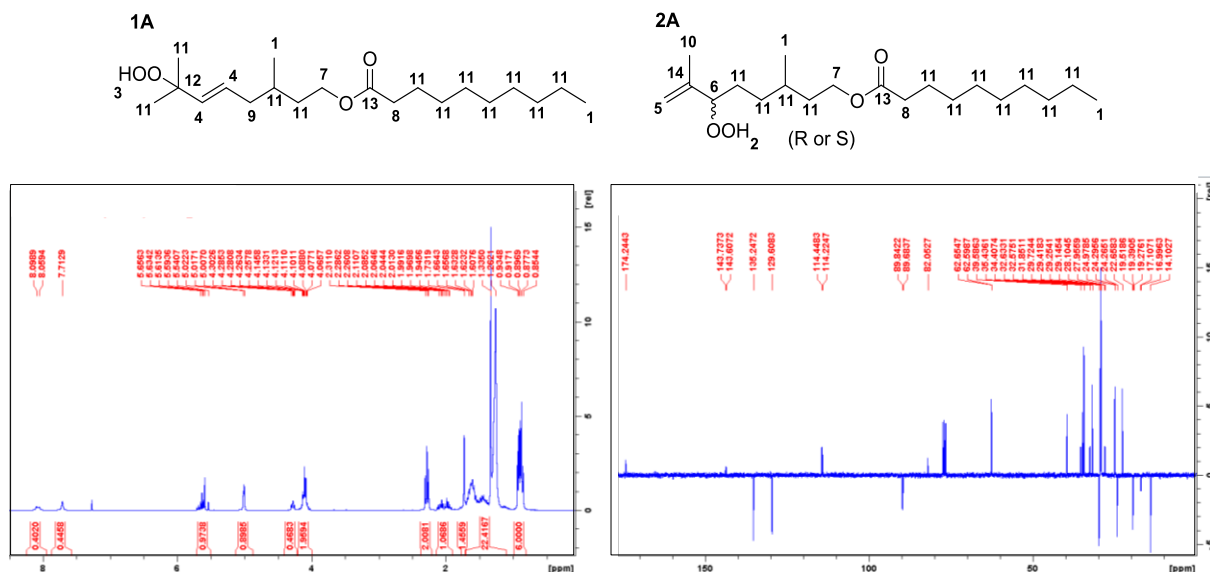


Figure S2.11:  $^1\text{H}$  and  $^{13}\text{C}$  NMR spectra of photooxidized citronellol caprate

$^1\text{H}$  NMR  $\delta$  (ppm): 0.89 (6  $\text{H}_1$ , m), 1.42 (22  $\text{H}_{11}$ , m), 1.73 (1.5  $\text{H}_{10}$ , m), 2.03 ( $\text{H}_9$ , m), 2.29 (2  $\text{H}_8$ , t,  $J = 7.6$  Hz), 4.11 (2  $\text{H}_7$ , m), 3.68 (3  $\text{H}_2$ , s), 4.28 (0.45  $\text{H}_6$ , m), 5.02 (1  $\text{H}_5$ , m), 5.62 (1  $\text{H}_4$ , m), 7.71 (0.47  $\text{H}_3$ , s), 8.08 (0.40  $\text{H}_2$ , d)

There is an isomeric ratio of 0.53(A)/0.47 (B).

$^{13}\text{C}$  NMR  $\delta$  (ppm): 14.1 ( $\text{CH}_3$ ), 17.1 ( $\text{CH}_3$ ), 19.5 ( $\text{CH}_3$ ), 22.7 ( $\text{CH}_2$ ), 24.2 ( $\text{CH}_3$ ), 25.0 ( $\text{CH}_2$ ), 27.9 ( $\text{CH}_2$ ), 28.1 ( $\text{CH}_2$ ), 29.1 ( $\text{CH}_2$ ), 29.3 ( $\text{CH}_2$ ), 29.4 ( $\text{CH}_2$ ), 29.7 (CH), 29.9 (CH), 31.9 ( $\text{CH}_2$ ), 32.6 ( $\text{CH}_2$ ), 34.4 ( $\text{CH}_2$ ), 34.9 ( $\text{CH}_2$ ), 35.4 ( $\text{CH}_2$ ), 39.6 ( $\text{CH}_2$ ), 62.6 ( $\text{CH}_2$ ), 82.1 ( $\text{C}_{12}$ ), 89.8 ( $\text{C}_6\text{H}$ ), 114.4 ( $\text{C}_5\text{H}_2$ ), 129.6 ( $\text{C}_4\text{H}$ ), 135.2 ( $\text{C}_4\text{H}$ ), 143.6 ( $\text{C}_{14}$ ), 174.2 ( $\text{C}_{13}$ )

### ▪ Geraniol caprate hydroperoxides

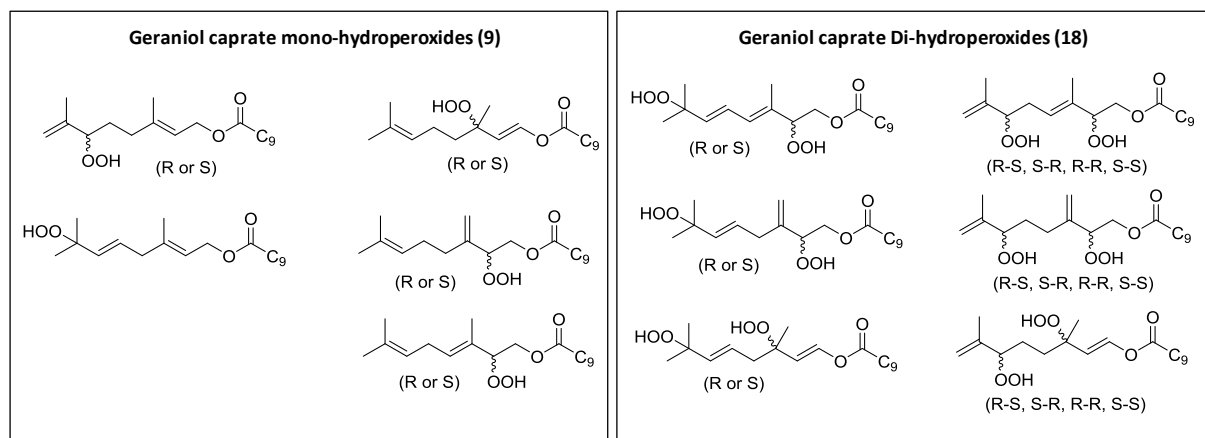
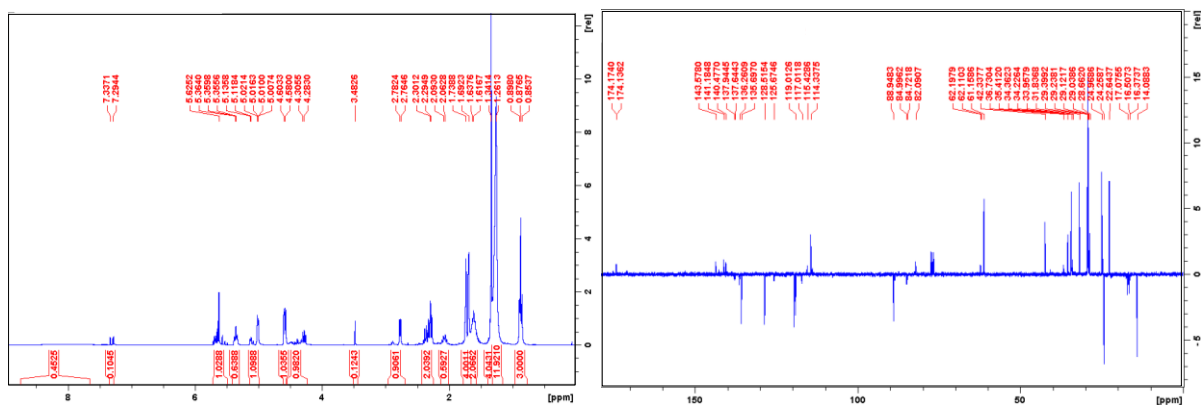


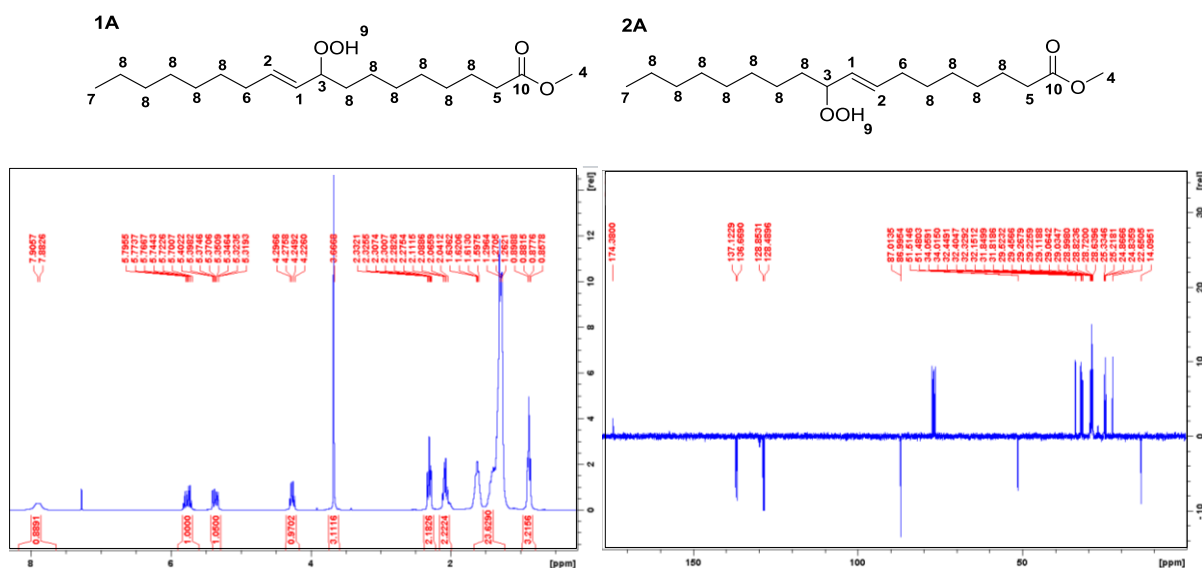
Figure S2.12: Molecular structure of all the possible *mono*- and *di*-hydroperoxides that may be obtained by singlet oxygenation of geraniol caprate

Figure S2.13:  $^1\text{H}$  and  $^{13}\text{C}$  NMR spectra of photooxidized geraniol caprate

$^1\text{H}$  NMR  $\delta$  (ppm): 0.88 (3H, t,  $J = 6.8$  Hz), 1.26 (12H, s), 1.34 (4H, s), 1.62 (2H, m), 1.72 (4H, m), 2.09 (0.6H, m), 2.31 (2H, m), 2.82 (1H, m), 3.48 (0.1H, s), 4.36 (1H, m), 4.59 (1H, d,  $J = 7.0$  Hz), 5.07 (1H, m), 5.37 (0.6H, t,  $J = 1.3$  Hz), 5.61 (1H, m), 7.33 (0.1H, s), 8.04 (0.45H, s)

$^{13}\text{C}$  NMR  $\delta$  (ppm): 14.1 ( $\text{CH}_3$ ), 16.4 ( $\text{CH}_3$ ), 16.5 ( $\text{CH}_3$ ), 17.1 ( $\text{CH}_3$ ), 22.6 ( $\text{CH}_2$ ), 24.3 ( $\text{CH}_3$ ), 25.0 ( $\text{CH}_2$ ), 29.0 ( $\text{CH}_2$ ), 28.7 ( $\text{CH}_2$ ), 29.1 ( $\text{CH}_2$ ), 29.2 ( $\text{CH}_2$ ), 29.4 ( $\text{CH}_2$ ), 31.8 ( $\text{CH}_2$ ), 34.0 ( $\text{CH}_2$ ), 34.4 ( $\text{CH}_2$ ), 35.4 ( $\text{CH}_2$ ), 36.7 ( $\text{CH}_2$ ), 42.3 ( $\text{CH}_2$ ), 61.2 ( $\text{CH}_2$ ), 62.1 ( $\text{CH}_2$ ), 82.1 (C), 84.7 (CH), 85.0 (CH), 88.9 (CH), 115.4 ( $\text{CH}_2$ ), 114.3 ( $\text{CH}_2$ ), 119.0 (CH), 117.0 (CH), 128.5 (CH), 125.7 (CH), 135.7 (CH), 136.3 (CH), 140.5 (C), 141.2 (C), 143.6 (C), 174.2 (C)

■ *Methyl oleate hydroperoxides*

Figure S2.14:  $^1\text{H}$  and  $^{13}\text{C}$  NMR spectra of photooxidized methyl oleate

$^1\text{H}$  NMR  $\delta$  (ppm): 0.88 (3  $\text{H}_7$ , m), 1.45 (22  $\text{H}_8$ , m), 2.08 (2  $\text{H}_6$ , q,  $J = 6.9$  Hz), 2.30 (2  $\text{H}_5$ , dt,  $J_1 = 2.0$ , Hz,  $J_2 = 7.4$  Hz), 3.67 (3  $\text{H}_4$ , s), 4.26 (1  $\text{H}_3$ , m), 5.38 (1  $\text{H}_2$ , m), 5.78 (1  $\text{H}_1$ , m), 7.90 (0.83  $\text{H}_9$ , s)

$^{13}\text{C}$  NMR  $\delta$  (ppm): 14.1 ( $\text{C}_7\text{H}_3$ ), 22.7 ( $\text{C}_8\text{H}_2$ ), 24.8 ( $\text{C}_8\text{H}_2$ ), 25.2 ( $\text{C}_8\text{H}_2$ ), 25.3 ( $\text{C}_8\text{H}_2$ ), 29.1 ( $\text{C}_8\text{H}_2$ ), 28.7 ( $\text{C}_8\text{H}_2$ ), 29.0 ( $\text{C}_8\text{H}_2$ ), 29.3 ( $\text{C}_8\text{H}_2$ ), 29.5 ( $\text{C}_8\text{H}_2$ ), 31.8 ( $\text{C}_8\text{H}_2$ ), 32.1 ( $\text{C}_8\text{H}_2$ ), 32.3 ( $\text{C}_8\text{H}_2$ ), 32.4 ( $\text{C}_8\text{H}_2$ ), 34.0 ( $\text{C}_8\text{H}_2$ ), 51.5 ( $\text{C}_4\text{H}_3$ ), 87.0 ( $\text{C}_3\text{H}$ ), 128.5 ( $\text{C}_2\text{H}$ ), 128.9 ( $\text{C}_2\text{H}$ ), 136.7 ( $\text{C}_1\text{H}$ ), 137.1 ( $\text{C}_1\text{H}$ ), 174.4 ( $\text{C}_{10}$ )

▪ Methyl linoleate hydroperoxides

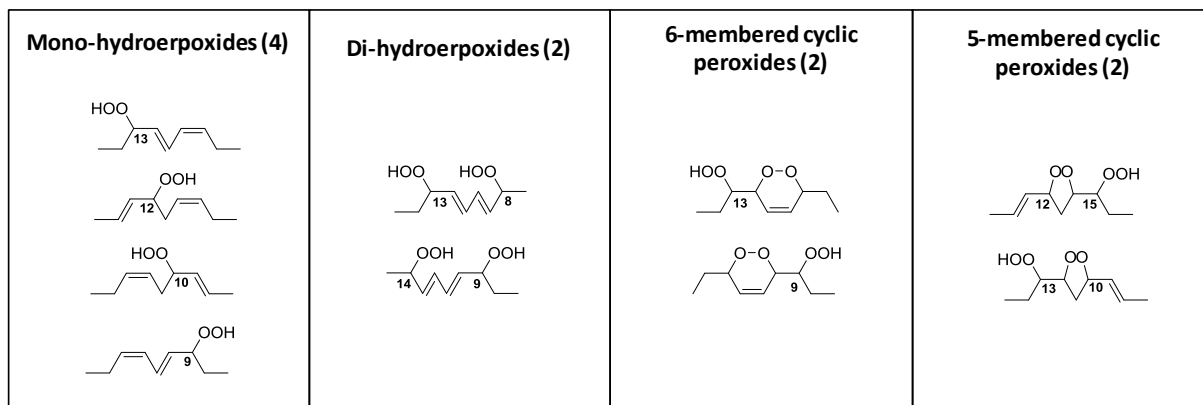


Figure S2.15: Molecular structure of all the possible *mono*-, *di*-hydroperoxides, 6- and 5-membered cyclic peroxides that may be obtained by singlet oxygenation of methyl linoleate

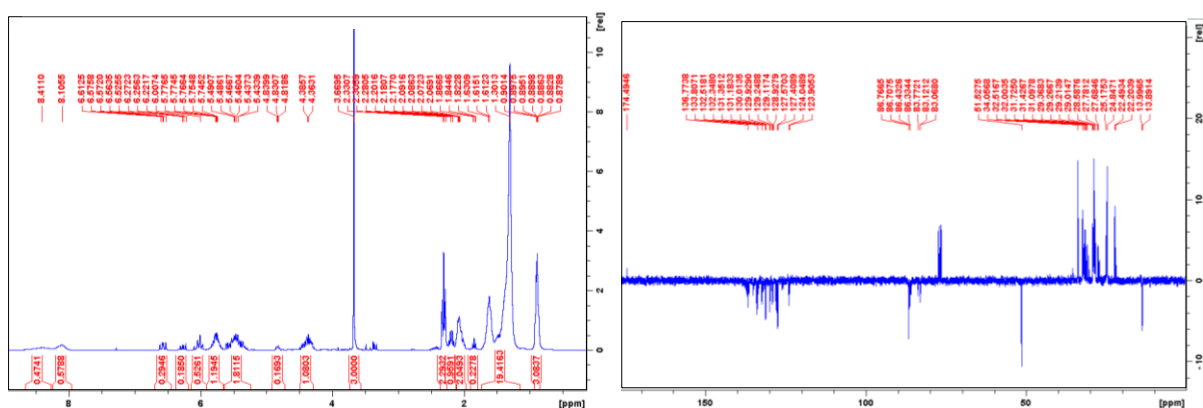


Figure S2.16:  $^1\text{H}$  and  $^{13}\text{C}$  NMR spectra of photooxidized methyl linoleate

$^1\text{H}$  NMR  $\delta$ (ppm): 0.89 (3H, m), 1.50 (19.5H, m), 1.85 (1H, t,  $J = 6.6$  Hz), 2.06 (2H, m), 2.20 (1H, m), 2.30 (2.3H, t,  $J = 7.6$  Hz), 3.66 (3H, s), 4.37 (1H, m), 4.83 (0.17H, m), 5.47 (1.8H, m), 5.78 (1.19H, m), 6.01 (0.53H, m), 6.27 (0.18H, m), 6.58 (0.30H, m), 8.11 (0.57H, s), 8.41 (0.47H, s)

$^{13}\text{C}$  NMR  $\delta$ (ppm): 14.0 (CH<sub>3</sub>), 22.2 (CH<sub>2</sub>), 24.1 (CH<sub>2</sub>), 24.8 (CH<sub>2</sub>), 25.2 (CH<sub>2</sub>), 27.7 (CH<sub>2</sub>), 27.8 (CH<sub>2</sub>), 28.6 (CH<sub>2</sub>), 29.0 (CH<sub>2</sub>), 29.3 (CH<sub>2</sub>), 29.4 (CH<sub>2</sub>), 31.1 (CH<sub>2</sub>), 31.4 (CH<sub>2</sub>), 31.7 (CH<sub>2</sub>), 32.0 (CH<sub>2</sub>), 51.5 (CH<sub>3</sub>), 83.0 (CH), 83.1 (CH), 83.8 (CH), 86.3 (CH), 86.4 (CH), 86.7 (CH), 86.8 (CH), 123.9 (CH), 124.0 (CH), 127.4 (CH), 127.6 (CH), 128.9 (CH), 129.1 (CH), 129.2 (CH), 130.0 (CH), 131.2 (CH), 131.4 (CH), 132.3 (CH), 132.5 (CH), 133.8 (CH), 136.8 (CH), 174.5 (C)



Time (h)	$V_{\text{eq moy}}$ (mL) <sup>a</sup>	$[\text{ROOH}]_{\text{moy}}$ (mmol.L <sup>-1</sup> ) <sup>a</sup>	Std. Dev. (mmol.L <sup>-1</sup> )
36	21.6	34.78	0.68
39	21.95	35.34	0.57

<sup>a</sup>Average on two values,  $[\text{Na}_2\text{S}_2\text{O}_3] = 1.6 \text{ mmol.L}^{-1}$ ,  $V_0 = 0.5 \text{ mL}$

**Table S2.1: Hydroperoxide titration of photooxidized methyl oleate**

▪ *Methyl linoleate hydroperoxides*

Time (h)	$V_{\text{eq moy}}$ (mL) <sup>a</sup>	$[\text{ROOH}]_{\text{moy}}$ (mmol.L <sup>-1</sup> ) <sup>a</sup>	Std. Dev. (mmol.L <sup>-1</sup> )
0	0.8	1.27	0.22
4	9.95	15.82	1.01
8	14.15	22.50	1.01
12	17.15	27.27	0.79
16	20.2	32.12	1.35
20	22.15	35.22	1.46
24	23.65	37.60	0.79
28	25.2	40.17	0.90
32	26.35	41.90	1.01
36	27.1	43.09	0.90
40	27.1	43.09	0.67

<sup>a</sup>Average on two values,  $[\text{Na}_2\text{S}_2\text{O}_3] = 1.6 \text{ mmol.L}^{-1}$ ,  $V_0 = 0.5 \text{ mL}$

**Table S2.2: Hydroperoxide titration of photooxidized methyl linoleate**

▪ *Methyl linolenate hydroperoxides*

Time (h)	$V_{\text{eq moy}}$ (mL) <sup>a</sup>	$[\text{ROOH}]_{\text{moy}}$ (mmol.L <sup>-1</sup> ) <sup>a</sup>	Std. Dev. (mmol.L <sup>-1</sup> )
0	1.5	2.4	0.68
4	11.2	17.92	0.91
8	18.15	29.04	0.57
12	23.15	37.04	1.02
16	28.2	45.12	0.91
20	30.45	48.72	0.79
24	32.3	51.68	0.91
28	33.35	53.36	1.02
32	34.0	54.4	1.36
36	34.4	55.04	1.36
40	34.8	55.68	1.81

<sup>a</sup>Average on two values,  $[\text{Na}_2\text{S}_2\text{O}_3] = 1.6 \text{ mmol.L}^{-1}$ ,  $V_0 = 0.5 \text{ mL}$

**Table S2.3: Hydroperoxide titration of photooxidized methyl linolenate**

## 2.4 Atomic mass of adducts formed with various cations

	Alkali metal							Non metallic	Transition metal	Alkaline earth metal		
	/	H <sup>+</sup>	Li <sup>+</sup>	Na <sup>+</sup>	K <sup>+</sup>	Rb <sup>+</sup>	Cs <sup>+</sup>	NH <sub>4</sub> <sup>+</sup>	Ag <sup>+</sup>	Be <sup>2+</sup>	Ca <sup>2+</sup>	Ba <sup>2+</sup>
	/	1	7	23	39	85	133	18	107/109	9	40	137
<b>C18:0</b>	298	299	305	321	337	383	431	316	405/407	153	169	217
<b>C18:1</b>	296	297	303	319	335	381	439	314	403/405	152	168	216
<b>C18:2</b>	294	295	301	317	333	379	437	312	401/403	151	167	215
<b>C18:3</b>	292	293	299	315	331	377	435	310	399/401	150	166	214
<b>3,7-Dimethyloctyl decanoate</b>	312	313	319	335	351	397	445	330	419/421	160	176	224
<b>Citronellol caprate</b>	310	311	317	333	349	395	443	328	417/419	159	175	223
<b>Geraniol caprate</b>	308	309	315	331	347	393	441	326	415/417	158	174	222
<b>C18:1(OO)<sub>1</sub></b>	328	329	335	351	367	413	461	346	435/437	168	184	232
<b>C18:2(OO)<sub>1</sub></b>	326	327	333	349	365	411	459	344	433/435	167	183	231
<b>C18:3(OO)<sub>1</sub></b>	324	325	331	347	363	409	457	342	431/433	166	182	230
<b>C18:2(OO)<sub>2</sub></b>	358	359	365	381	397	443	491	376	465/467	183	199	247
<b>C18:3(OO)<sub>2</sub></b>	356	357	363	379	395	441	489	374	463/465	182	198	246
<b>C18:3(OO)<sub>3</sub></b>	388	389	395	411	427	473	521	406	495/497	198	214	262
<b>Citronellol caprate R(OO)<sub>1</sub></b>	342	343	349	365	381	427	475	360	449/451	175	191	239
<b>Geraniol caprate R(OO)<sub>1</sub></b>	340	341	347	363	379	425	473	358	447/449	174	190	238
<b>Geraniol caprate R(OO)<sub>2</sub></b>	372	373	379	395	411	457	505	390	479/481	190	206	254

Table S2.4: M/z values of alkali metal (H<sup>+</sup>, Li<sup>+</sup>, Na<sup>+</sup>, K<sup>+</sup>, Rb<sup>+</sup> and Cs<sup>+</sup>), non metallic (NH<sub>4</sub><sup>+</sup>), transition metal (Ag<sup>+</sup>) and alkaline earth metal (Be<sup>2+</sup>, Ca<sup>2+</sup> and Ba<sup>2+</sup>) ions and m/z values related to the formation of adducts between ions and analytes

## 2.5 Absolute intensities of adducts formed between ions and analytes

	C18:0	C18:1	C18:2	C18:3	C18:1(OO) <sub>1</sub>	Epoxide (-18 a.m.u)
H <sup>+</sup>	4.27 × 10 <sup>6</sup>	4.89 × 10 <sup>6</sup>	6.29 × 10 <sup>6</sup>	7.12 × 10 <sup>6</sup>	1.31 × 10 <sup>6</sup>	/
Li <sup>+</sup>	1.69 × 10 <sup>6</sup>	3.29 × 10 <sup>7</sup>	5.20 × 10 <sup>7</sup>	7.14 × 10 <sup>7</sup>	4.45 × 10 <sup>7</sup>	6.59 × 10 <sup>6</sup>
Na <sup>+</sup>	2.22 × 10 <sup>6</sup>	2.28 × 10 <sup>7</sup>	2.18 × 10 <sup>7</sup>	4.11 × 10 <sup>7</sup>	3.88 × 10 <sup>7</sup>	3.16 × 10 <sup>6</sup>
K <sup>+</sup>	1.12 × 10 <sup>6</sup>	2.54 × 10 <sup>6</sup>	4.48 × 10 <sup>6</sup>	1.08 × 10 <sup>7</sup>	3.49 × 10 <sup>7</sup>	2.77 × 10 <sup>6</sup>
Rb <sup>+</sup>	1.71 × 10 <sup>6</sup>	3.83 × 10 <sup>5</sup>	1.29 × 10 <sup>6</sup>	5.31 × 10 <sup>6</sup>	1.56 × 10 <sup>7</sup>	1.74 × 10 <sup>6</sup>
Cs <sup>+</sup>	6.24 × 10 <sup>5</sup>	1.46 × 10 <sup>6</sup>	2.15 × 10 <sup>6</sup>	3.16 × 10 <sup>6</sup>	1.42 × 10 <sup>7</sup>	1.23 × 10 <sup>6</sup>
NH <sub>4</sub> <sup>+</sup>	5.84 × 10 <sup>5</sup>	1.06 × 10 <sup>6</sup>	2.92 × 10 <sup>6</sup>	5.16 × 10 <sup>6</sup>	4.09 × 10 <sup>6</sup>	1.72 × 10 <sup>6</sup>
Ag <sup>+</sup>	7.22 × 10 <sup>5</sup>	1.08 × 10 <sup>7</sup>	2.34 × 10 <sup>7</sup>	4.73 × 10 <sup>7</sup>	2.83 × 10 <sup>7</sup>	6.02 × 10 <sup>6</sup>

Table S2.5: Absolute intensity (coups) of C18:0, C18:1, C18:2, C18:3, C18:1(OO)<sub>1</sub> and epoxide from C18:1 adducts ([X] = 10<sup>-6</sup> M) formed separately with H<sup>+</sup>, Li<sup>+</sup>, Na<sup>+</sup>, K<sup>+</sup>, Rb<sup>+</sup>, Cs<sup>+</sup>, NH<sub>4</sub><sup>+</sup> and Ag<sup>+</sup> acetates during Direct Liquid Injection (DLI) ESI-MS (average on three values)

	C18:1	C18:2	C18:3
H <sup>+</sup>	2.77 × 10 <sup>6</sup>	4.09 × 10 <sup>6</sup>	7.65 × 10 <sup>6</sup>
Li <sup>+</sup>	1.13 × 10 <sup>7</sup>	2.28 × 10 <sup>7</sup>	3.69 × 10 <sup>7</sup>
Na <sup>+</sup>	7.28 × 10 <sup>6</sup>	1.60 × 10 <sup>7</sup>	3.06 × 10 <sup>7</sup>
K <sup>+</sup>	3.97 × 10 <sup>6</sup>	5.86 × 10 <sup>6</sup>	8.06 × 10 <sup>6</sup>
Cs <sup>+</sup>	1.09 × 10 <sup>6</sup>	1.48 × 10 <sup>6</sup>	2.16 × 10 <sup>6</sup>
NH <sub>4</sub> <sup>+</sup>	5.00 × 10 <sup>6</sup>	1.51 × 10 <sup>7</sup>	3.03 × 10 <sup>6</sup>

Table S2.6: Absolute intensity (coups) of an equimolar mixture of C18:1, C18:2 and C18:3 ([C18:1] = [C18:2] = [C18:3] = 10<sup>-6</sup> M) with H<sup>+</sup>, Li<sup>+</sup>, Na<sup>+</sup>, K<sup>+</sup>, Cs<sup>+</sup> and NH<sub>4</sub><sup>+</sup> ([ion] = 10<sup>-3</sup> M) during Direct Liquid Injection (DLI) ESI-MS (average on three values)

	[ion] (M)	C18:1	C18:1(OO) <sub>1</sub>		[ion] (M)	C18:1	C18:1(OO) <sub>1</sub>
H <sup>+</sup>	10 <sup>-5</sup>	1.00 × 10 <sup>6</sup>	6.79 × 10 <sup>5</sup>	Ag <sup>+</sup>	10 <sup>-5</sup>	8.52 × 10 <sup>5</sup>	2.03 × 10 <sup>6</sup>
	3 × 10 <sup>-5</sup>	9.79 × 10 <sup>5</sup>	8.17 × 10 <sup>5</sup>		3 × 10 <sup>-5</sup>	3.21 × 10 <sup>6</sup>	4.20 × 10 <sup>6</sup>
	10 <sup>-4</sup>	1.10 × 10 <sup>6</sup>	8.27 × 10 <sup>5</sup>		10 <sup>-4</sup>	9.10 × 10 <sup>6</sup>	1.37 × 10 <sup>7</sup>
	3 × 10 <sup>-4</sup>	1.53 × 10 <sup>6</sup>	9.26 × 10 <sup>5</sup>		3 × 10 <sup>-4</sup>	8.34 × 10 <sup>6</sup>	1.44 × 10 <sup>7</sup>
	10 <sup>-3</sup>	3.60 × 10 <sup>6</sup>	4.77 × 10 <sup>6</sup>		10 <sup>-3</sup>	3.59 × 10 <sup>7</sup>	5.39 × 10 <sup>7</sup>
Li <sup>+</sup>	10 <sup>-5</sup>	4.81 × 10 <sup>6</sup>	2.02 × 10 <sup>7</sup>	Na <sup>+</sup>	10 <sup>-5</sup>	2.47 × 10 <sup>6</sup>	1.85 × 10 <sup>7</sup>
	3 × 10 <sup>-5</sup>	9.08 × 10 <sup>6</sup>	2.52 × 10 <sup>7</sup>		3 × 10 <sup>-5</sup>	7.56 × 10 <sup>6</sup>	4.33 × 10 <sup>7</sup>
	10 <sup>-4</sup>	1.20 × 10 <sup>8</sup>	1.31 × 10 <sup>8</sup>		10 <sup>-4</sup>	3.55 × 10 <sup>7</sup>	1.18 × 10 <sup>8</sup>
	3 × 10 <sup>-4</sup>	3.70 × 10 <sup>6</sup>	6.80 × 10 <sup>7</sup>		3 × 10 <sup>-4</sup>	2.51 × 10 <sup>6</sup>	6.28 × 10 <sup>7</sup>
	10 <sup>-3</sup>	2.95 × 10 <sup>6</sup>	4.04 × 10 <sup>7</sup>		10 <sup>-3</sup>	3.05 × 10 <sup>6</sup>	5.25 × 10 <sup>7</sup>
K <sup>+</sup>	10 <sup>-5</sup>	1.44 × 10 <sup>6</sup>	9.58 × 10 <sup>6</sup>	Cs <sup>+</sup>	10 <sup>-5</sup>	1.50 × 10 <sup>5</sup>	7.73 × 10 <sup>6</sup>
	3 × 10 <sup>-5</sup>	5.51 × 10 <sup>6</sup>	3.92 × 10 <sup>7</sup>		3 × 10 <sup>-5</sup>	3.92 × 10 <sup>5</sup>	2.39 × 10 <sup>7</sup>
	10 <sup>-4</sup>	2.39 × 10 <sup>7</sup>	1.06 × 10 <sup>8</sup>		10 <sup>-4</sup>	4.70 × 10 <sup>5</sup>	4.04 × 10 <sup>7</sup>
	3 × 10 <sup>-4</sup>	1.51 × 10 <sup>6</sup>	4.26 × 10 <sup>7</sup>		3 × 10 <sup>-4</sup>	6.92 × 10 <sup>5</sup>	4.47 × 10 <sup>7</sup>
	10 <sup>-3</sup>	1.80 × 10 <sup>6</sup>	4.49 × 10 <sup>7</sup>		10 <sup>-3</sup>	5.52 × 10 <sup>5</sup>	3.41 × 10 <sup>7</sup>

Table S2.7: Absolute intensity (coups) of equimolar mixture between C18:1 and C18:1 (OO)<sub>1</sub> ([C18:1] = [C18:1 (OO)<sub>1</sub>] = 10<sup>-6</sup> M) adducts formed with H<sup>+</sup>, Li<sup>+</sup>, Na<sup>+</sup>, K<sup>+</sup>, Cs<sup>+</sup> and Ag<sup>+</sup> acetates at various concentrations ([ion] = 10<sup>-5</sup>, 3 × 10<sup>-5</sup>, 10<sup>-4</sup>, 3 × 10<sup>-4</sup> and 10<sup>-3</sup> M) during Direct Liquid Injection (DLI) ESI-MS (average on three values)

Ratio	[C18:1+Cs] <sup>+</sup>	[C18:1(OO) <sub>1</sub> +Cs] <sup>+</sup>
50/50	4.26 x 10 <sup>5</sup>	4.26 x 10 <sup>7</sup>
90/10	6.18 x 10 <sup>5</sup>	1.16 x 10 <sup>7</sup>
99/1	5.43 x 10 <sup>5</sup>	4.42 x 10 <sup>6</sup>
99.9/0.1	4.55 x 10 <sup>5</sup>	3.01 x 10 <sup>6</sup>

Table S2. 8: Absolute intensity of peaks observed through ionization of mixtures of C18:1 and C18:1(OO)<sub>1</sub> at various ratios (50/50: [C18:1] = [C18:1(OO)<sub>1</sub>] = 10<sup>-6</sup> M; 90/10: [C18:1] = 1.8 x 10<sup>-6</sup> M and [C18:1(OO)<sub>1</sub>] = 2 x 10<sup>-7</sup> M; 99/1: [C18:1] = 1.98 x 10<sup>-6</sup> M and [C18:1(OO)<sub>1</sub>] = 2 x 10<sup>-8</sup> M; 99.9/0.1: [C18:1] = 1.998 x 10<sup>-6</sup> M and [C18:1(OO)<sub>1</sub>] = 2 x 10<sup>-9</sup> M with Cs<sup>+</sup> acetate (10<sup>-4</sup> M) during Direct Liquid Injection (DLI) ESI-MS in ion-positive mode (ES+) (average on three values)

	Citronellol	R(OO) <sub>1</sub>	Epoxide (- 18 a.m.u)	Alcohol (- 16 a.m.u)
H <sup>+</sup>	5.21 x 10 <sup>6</sup>	2.88 x 10 <sup>6</sup>	1.19 x 10 <sup>7</sup>	8.81 x 10 <sup>6</sup>
Li <sup>+</sup>	1.28 x 10 <sup>8</sup>	1.34 x 10 <sup>8</sup>	1.34 x 10 <sup>8</sup>	1.34 x 10 <sup>8</sup>
Na <sup>+</sup>	7.63 x 10 <sup>7</sup>	1.38 x 10 <sup>8</sup>	5.70 x 10 <sup>7</sup>	9.29 x 10 <sup>7</sup>
Cs <sup>+</sup>	7.31 x 10 <sup>5</sup>	1.14 x 10 <sup>7</sup>	1.07 x 10 <sup>6</sup>	7.84 x 10 <sup>5</sup>
Ag <sup>+</sup>	1.34 x 10 <sup>8</sup>			

Table S2.9: Absolute intensity of peaks observed through ionization of an equimolar mixture of citronellol and R(OO)<sub>1</sub> pointing out the fragmentation into of epoxide (- 18 a.m.u) and alcohol (- 16 a.m.u), ([R] = [R(OO)<sub>1</sub>] = 10<sup>-6</sup> M) with each separate H<sup>+</sup>, Li<sup>+</sup>, Na<sup>+</sup>, Cs<sup>+</sup> and Ag<sup>+</sup> ions (10<sup>-4</sup> M) during Direct Liquid Injection (DLI) ESI-MS in ion-positive mode (ES+) (average on three values)

## 2.6 Fragmentation of adducts and m/z values for daughters

Compound	Mass (a.m.u)	[M+H] <sup>+</sup> (m/z)	Daughters (m/z)	Cone voltage (V)	Collision Energy (eV)	Ion Mode
Citronellol caprate	310	311	83	30	30	ES+
		311	69	30	30	ES+
		311	55	30	30	ES+
Geraniol caprate	308	309	227	30	30	ES+
		309	179	30	30	ES+
		309	81	30	30	ES+

Table S2.10: Fragmentation *via* Intellistart of citronellol caprate and geraniol caprate under the form of [M+H]<sup>+</sup>

Compound	Mass (a.m.u)	[M+X] <sup>+</sup> (m/z)	Daughters (m/z)	Cone voltage (V)	Collision Energy (eV)	Ion Mode
Citronellol caprate	342	360	137	21	12	ES+
		360	95	21	8	ES+
		360	81	21	22	ES+
ROOH	342	449	431	31	12	ES+
		449	259	31	18	ES+
		449	219	31	16	ES+

Table S2.11: Fragmentation *via* Intellistart of R(OO)<sub>1</sub> from citronellol caprate under the form of [R(OO)<sub>1</sub>+NH<sub>4</sub>]<sup>+</sup> and [R(OO)<sub>1</sub>+<sup>107</sup>Ag]<sup>+</sup>

Compound	Mass (a.m.u)	[M+X] <sup>+</sup> (m/z)	Daughters (m/z)	Cone voltage (V)	Collision Energy (eV)	Ion Mode
Geraniol caprate ROOH	340	358	135	15	6	ES+
		358	107	15	26	ES+
		358	93	15	12	ES+
	340	358	81	15	12	ES+
		447	257	23	16	ES+
		447	217	23	14	ES+
Geraniol caprate R(OOH) <sub>2</sub>	372	447	107	23	34	ES+
		390	155	13	8	ES+
		390	109	13	8	ES+
	372	390	95	13	12	ES+
		390	81	13	12	ES+
		390	67	13	28	ES+
372	479	247	31	14	ES+	
	479	107	31	32	ES+	
	479	95	31	32	ES+	

Table S2.12: Fragmentation *via* Intellistart of R(OO)<sub>1</sub> and R(OO)<sub>2</sub> from geraniol caprate under the form of [M+NH<sub>4</sub>]<sup>+</sup> and [M+<sup>107</sup>Ag]<sup>+</sup>

Compound	Mass (a.m.u)	[M+H] <sup>+</sup> (m/z)	Daughters (m/z)	Cone voltage (V)	Collision Energy (eV)	Ion Mode
Geraniol caprate	308	309	227	36	22	ES+
		309	179	36	16	ES+
		309	81	36	14	ES+

Table S2.13: Fragmentation *via* Intellistart of geraniol caprate under the form of [M+H]<sup>+</sup>

Compound	Mass (a.m.u)	[M+X] <sup>+</sup> (m/z)	Daughters (m/z)	Cone voltage (V)	Collision Energy (eV)	Ion Mode
C18:3	292	293	95	27	18	ES+
		293	81	27	26	ES+
		293	67	27	28	ES+
C18:2	294	312	263	12	15	ES+
		312	245	12	15	ES+
C18:1	296	297	265	9	10	ES+
		297	247	9	10	ES+

Table S2.14: Fragmentation *via* Intellistart of C18:3, C18:2 and C18:1 under the form of [M+NH<sub>4</sub>]<sup>+</sup> and [M+H]<sup>+</sup>

Compound	Mass (a.m.u)	[M+Na] <sup>+</sup> (m/z)	Daughters (m/z)	Cone voltage (V)	Collision Energy (eV)	Ion Mode
C18:3(OO) <sub>1</sub>	324	347	221	44	12	ES+
		347	261	44	10	ES+
		347	329	44	6	ES+
		347	301	44	12	ES+
		347	209	44	8	ES+

Compound	Mass (a.m.u)	[M+Na] <sup>+</sup> (m/z)	Daughters (m/z)	Cone voltage (V)	Collision Energy (eV)	Ion Mode
C18:3(OO) <sub>2</sub>	356	379	221	66	12	ES+
		379	209	66	10	ES+
		379	275	66	10	ES+
		379	345	66	10	ES+
		379	261	66	10	ES+
C18:3(OO) <sub>3</sub>	388	411	221	52	16	ES+
		411	209	52	10	ES+
		411	281	52	10	ES+
		411	249	52	10	ES+
		411	377	52	10	ES+
C18:2(OO) <sub>1</sub>	326	349	221	32	10	ES+
		349	261	32	12	ES+
		349	331	32	4	ES+
		349	209	32	6	ES+
		349	135	32	12	ES+
C18:2(OO) <sub>2</sub>	358	381	221	72	10	ES+
		381	347	72	10	ES+
		381	235	72	10	ES+
		381	209	72	10	ES+
C18:1(OO) <sub>1</sub>	328	351	221	34	10	ES+
		351	209	34	8	ES+
		351	177	34	12	ES+
		351	333	34	10	ES+
		351	181	34	10	ES+

Table S2.15: Fragmentation *via* Intellistart of C18:3(OO)<sub>1</sub>, C18:3(OO)<sub>2</sub>, C18:3(OO)<sub>3</sub>, C18:2(OO)<sub>1</sub>, C18:2(OO)<sub>2</sub> and C18:1(OO)<sub>1</sub> under the form of [M+Na]<sup>+</sup>

Compound	Mass (a.m.u)	[M+Li] <sup>+</sup> (m/z)	Daughters (m/z)	Cone voltage (V)	Collision Energy (eV)	Ion Mode
C18:3(OO) <sub>1</sub>	324	331	233	34	16	ES+
		331	273	34	14	ES+
		331	193	34	16	ES+
		331	205	34	12	ES+
		331	245	34	6	ES+
C18:3(OO) <sub>2</sub>	356	363	205	26	12	ES+
		363	193	26	14	ES+
		363	233	26	12	ES+
		363	93	26	22	ES+
		363	219	26	12	ES+
C18:3(OO) <sub>3</sub>	388	395	205	24	12	ES+
		395	193	24	14	ES+
		395	219	24	14	ES+
		395	233	24	12	ES+
		395	81	24	26	ES+
C18:2(OO) <sub>1</sub>	326	333	291	20	6	ES+
		333	250	20	18	ES+
		333	107	20	32	ES+
		333	135	20	16	ES+
		333	315	20	6	ES+

Compound	Mass (a.m.u)	[M+Li] <sup>+</sup> (m/z)	Daughters (m/z)	Cone voltage (V)	Collision Energy (eV)	Ion Mode
C18:2(OO) <sub>2</sub>	358	365	205	10	18	ES+
		365	277	10	12	ES+
		365	107	10	30	ES+
		365	185	10	22	ES+
		365	307	10	20	ES+
C18:1(OO) <sub>1</sub>	328	335	193	2	10	ES+
		335	317	2	10	ES+
		335	205	2	14	ES+
		335	179	2	16	ES+
		335	161	2	10	ES+

Table S2.16: Fragmentation *via* Intellistart of C18:3(OO)<sub>1</sub>, C18:3(OO)<sub>2</sub>, C18:3(OO)<sub>3</sub>, C18:2(OO)<sub>1</sub>, C18:2(OO)<sub>2</sub> and C18:1(OO)<sub>1</sub> under the form of under the form of [M+Li]<sup>+</sup>

Compound	Mass (a.m.u)	[M+ <sup>107</sup> Ag] <sup>+</sup> (m/z)	Daughters (m/z)	Cone voltage (V)	Collision Energy (eV)	Ion Mode
C18:3(OO) <sub>1</sub>	324	431	107	18	46	ES+
		431	413	18	10	ES+
		431	373	18	10	ES+
		431	333	18	10	ES+
C18:3(OO) <sub>2</sub>	356	463	107	32	32	ES+
		463	293	32	12	ES+
		463	305	32	12	ES+
		463	333	32	12	ES+
		463	95	32	28	ES+
C18:3(OO) <sub>3</sub>	388	495	107	38	36	ES+
		495	293	38	14	ES+
		495	333	38	12	ES+
		495	305	38	16	ES+
C18:2(OO) <sub>1</sub>	326	433	107	8	34	ES+
		433	333	8	12	ES+
		433	293	8	16	ES+
		433	415	8	12	ES+
		433	305	8	14	ES+
C18:2(OO) <sub>2</sub>	358	465	107	14	32	ES+
		465	293	14	12	ES+
		465	305	14	12	ES+
		465	319	14	12	ES+
C18:1(OO) <sub>1</sub>	328	435	293	4	10	ES+
		435	107	4	32	ES+
		435	417	4	12	ES+
		435	279	4	16	ES+
		435	78	4	30	ES+

Table S2.17: Fragmentation *via* Intellistart of C18:3(OO)<sub>1</sub>, C18:3(OO)<sub>2</sub>, C18:3(OO)<sub>3</sub>, C18:2(OO)<sub>1</sub>, C18:2(OO)<sub>2</sub> and C18:1(OO)<sub>1</sub> under the form of [M+<sup>107</sup>Ag]<sup>+</sup>

Compound	Mass (a.m.u)	[M+NH <sub>4</sub> ] <sup>+</sup> (m/z)	Daughters (m/z)	Cone voltage (V)	Collision Energy (eV)	Ion Mode
C18:3(OO) <sub>1</sub>	324	342	78	12	20	ES+
		342	93	12	22	ES+
		342	291	12	8	ES+
		342	259	12	6	ES+
		342	121	12	8	ES+
C18:3(OO) <sub>2</sub>	356	374	78	2	18	ES+
		374	91	2	30	ES+
		374	90	2	14	ES+
		374	121	2	16	ES+
		374	105	2	30	ES+
C18:3(OO) <sub>3</sub>	388	406	78	14	20	ES+
		406	95	14	16	ES+
		406	94	14	10	ES+
		406	97	14	16	ES+
		406	91	14	34	ES+
C18:2(OO) <sub>1</sub>	326	344	293	14	6	ES+
		344	81	14	20	ES+
		344	95	14	22	ES+
		344	277	14	4	ES+
		344	109	14	14	ES+
C18:2(OO) <sub>2</sub>	358	376	78	14	18	ES+
		376	139	14	6	ES+
		376	191	14	8	ES+
		376	91	14	22	ES+
		376	193	14	6	ES+
C18:1(OO) <sub>1</sub>	328	346	295	12	6	ES+
		346	263	12	10	ES+
		346	311	12	2	ES+
		346	81	12	22	ES+
		346	95	12	24	ES+

Table S2.18: Fragmentation *via* Intellistart of C18:3(OO)<sub>1</sub>, C18:3(OO)<sub>2</sub>, C18:3(OO)<sub>3</sub>, C18:2(OO)<sub>1</sub>, C18:2(OO)<sub>2</sub> and C18:1(OO)<sub>1</sub> under the form of [M+NH<sub>4</sub>]<sup>+</sup>

## 2.7 LC-MS/MS chromatograms for the separation of photooxidized FAMES of linseed oil with $\text{Na}^+$ , $\text{NH}_4^+$ and $\text{Li}^+$

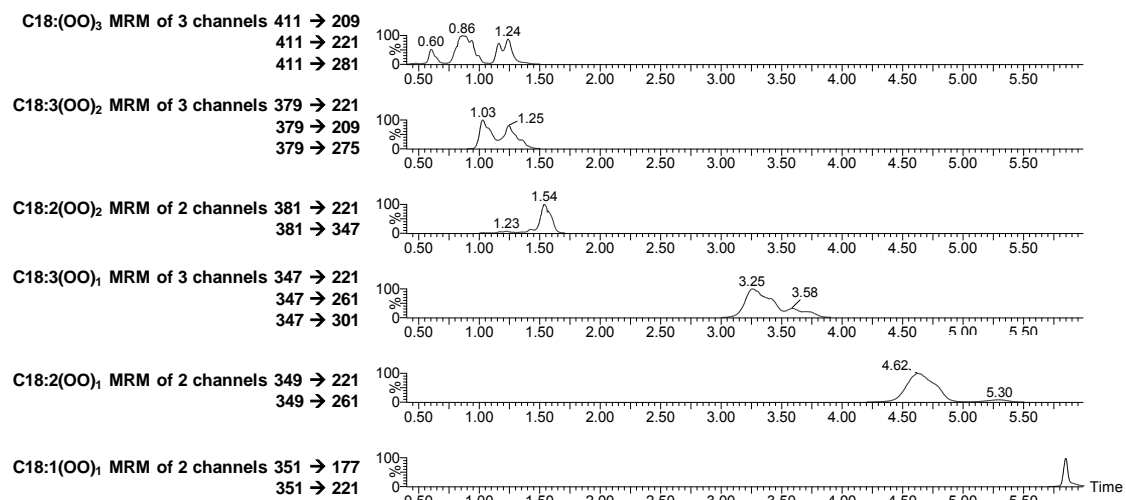


Figure S2.19: LC-MS/MS (MRM mode) of FAMES of linseed oil peroxides mixture with  $\text{Na}^+$

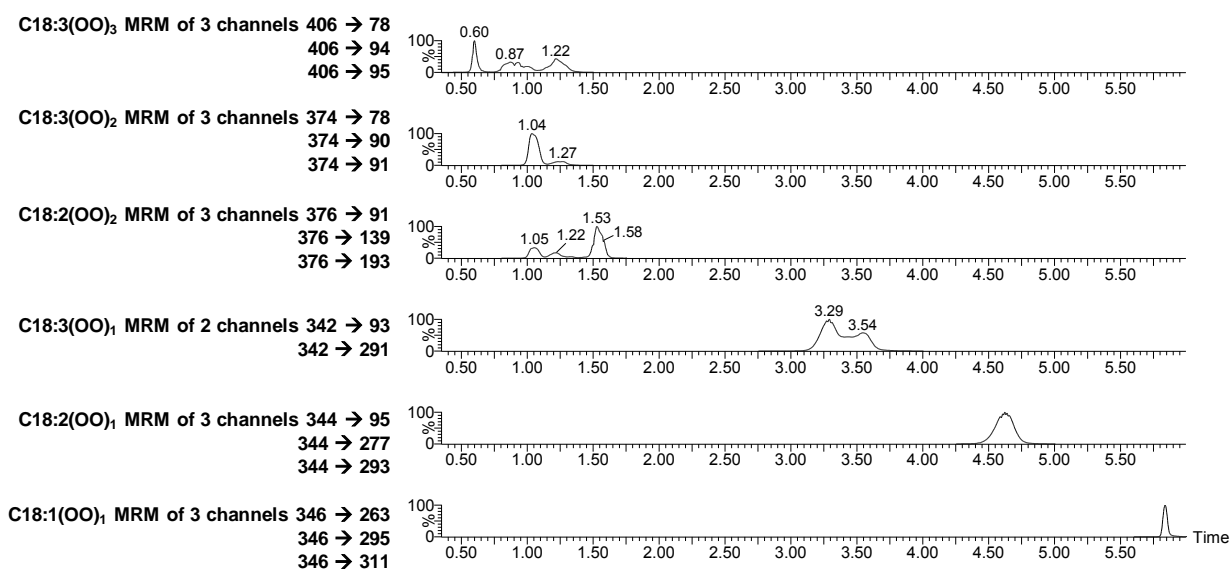


Figure S2.20: LC-MS/MS (MRM mode) of FAMES of linseed oil peroxides mixture with  $\text{NH}_4^+$

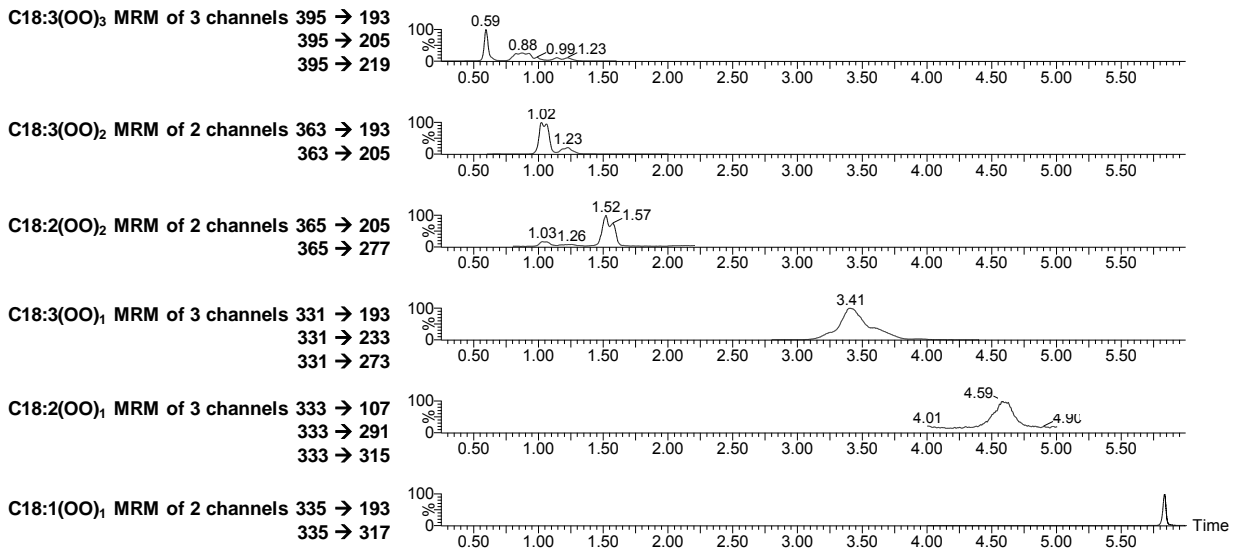
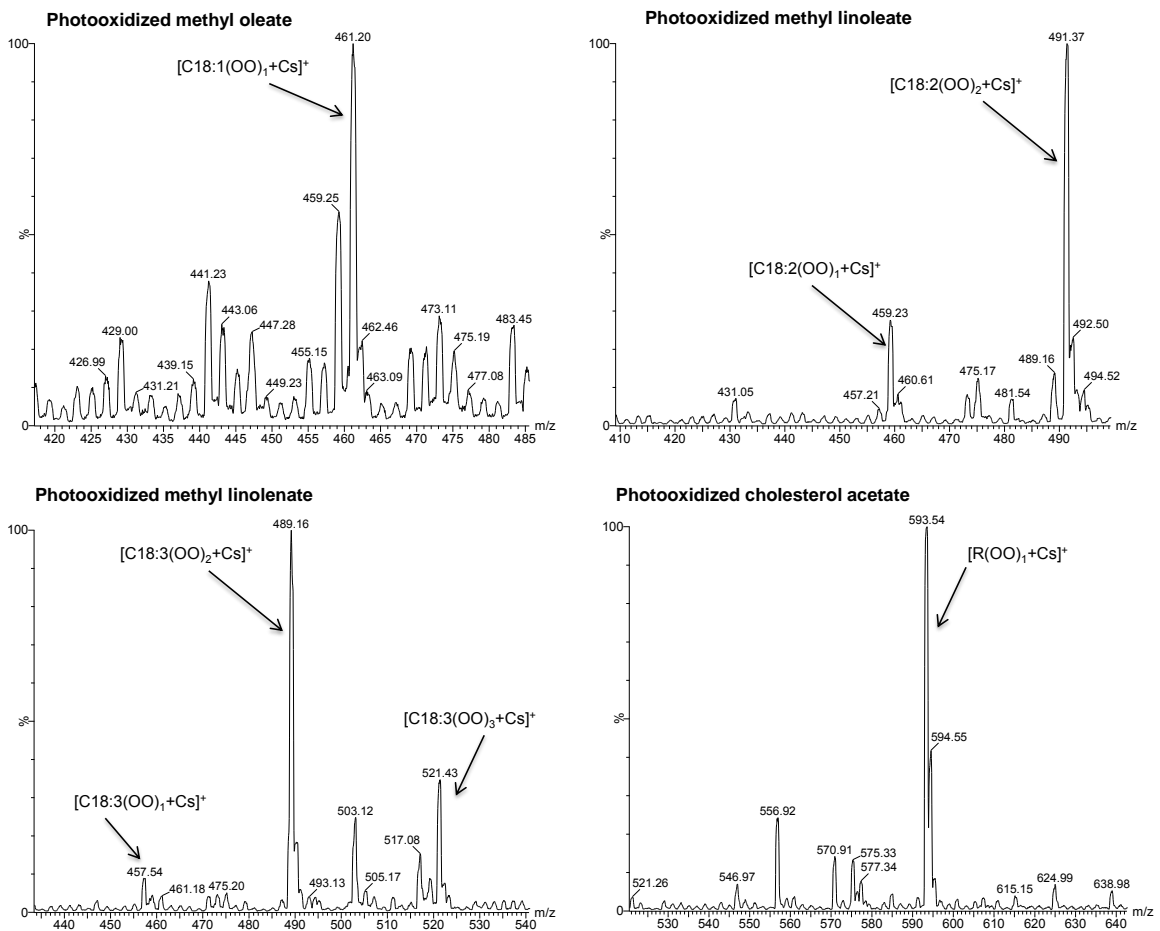
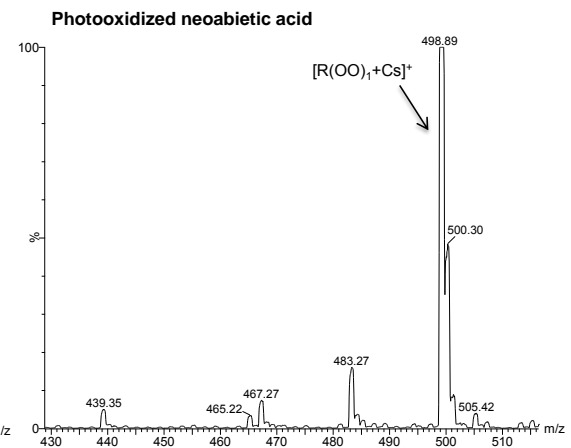
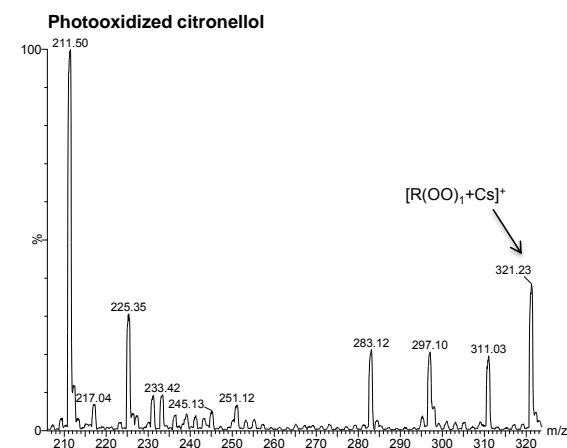
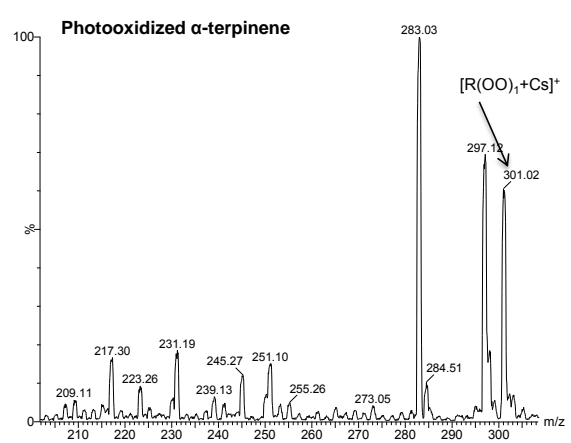
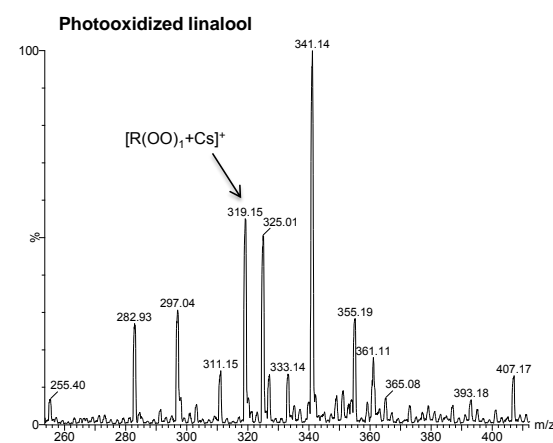
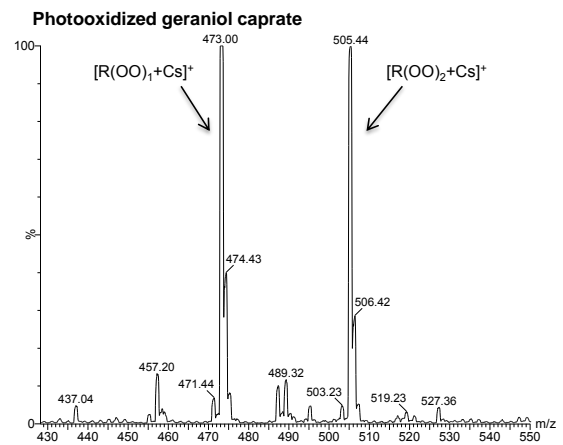
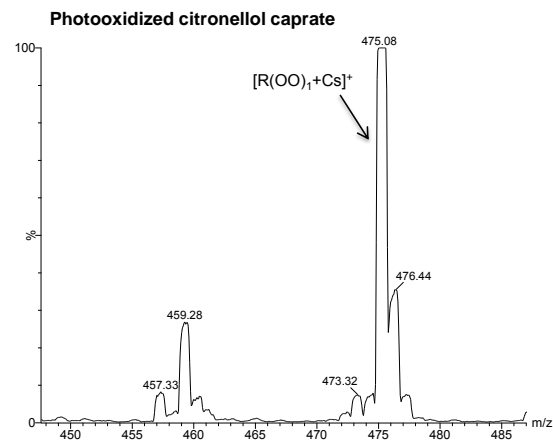
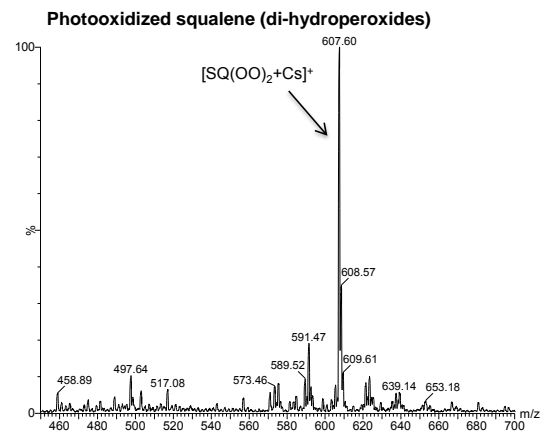
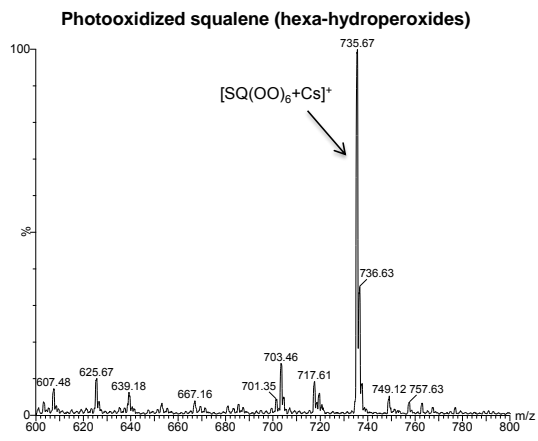


Figure S2.21: LC-MS/MS (MRM mode) of FAMES of linseed oil peroxides mixture with Li<sup>+</sup>

## 2.8 DLI-ESI-MS spectra of ionized hydroperoxides and peroxides with Cs<sup>+</sup>





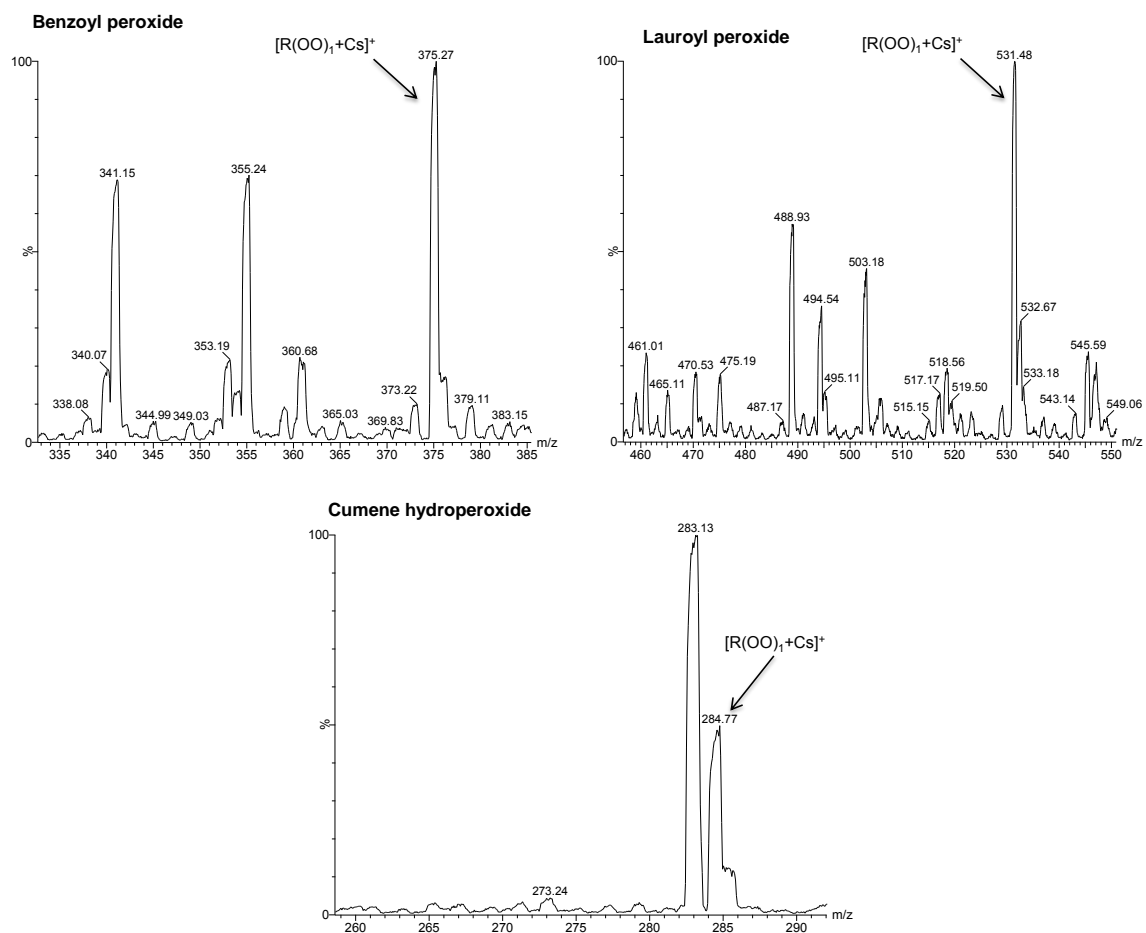


Figure S2.22: DLI-ESI-MS spectra in ion-positive mode (ES<sup>+</sup>) of , benzoyl peroxide, lauroyl peroxide, cumene hydroperoxide and photooxidized methyl oleate, methyl linoelate, methyl linolenate, cholesterol acetate, squalene, citronellol caprate, geraniol caprate, linalool,  $\alpha$ -terpinene, citronellol, neoabietic acid ([analyte] =  $4 \times 10^{-6}$  M) with Cs<sup>+</sup> ( $10^{-4}$  M) (solvent: H<sub>2</sub>O/MeOH 50/50 v:v)



# CHAPTER 3. PRESERVATION OF OMEGA-3 OILS BY NATURAL PHENOLIC ANTIOXIDANTS: THERMODYNAMIC, KINETIC AND OXIDATIVE INVESTIGATIONS

---

## 1. Introduction

As regards to the oxidation of (poly)unsaturated fatty acids and more precisely of edible oils rich in omega-3, food industrialists have to protect food in order to extend the lifetime of products and maintain their organoleptic properties. Indeed, as demonstrated in **chapter 1**, unsaturated fatty acids are easily oxidized leading to many oxidation products. These oxidation compounds are made up of mono-hydroperoxides as primary oxidation products and secondary oxidation products including dihydroperoxides, cyclic peroxides, volatile organic compounds...

To protect oils, industrialists incorporate into formulations additives named antioxidants. **Figure 3.1** shows that antioxidants are particularly studied in order to protect unsaturated fatty acids against oxidation in the field of food (more than 50%).<sup>250</sup> Antioxidants are also studied in pharmacology and biochemistry for the protection of fatty acids present in cell membranes for the prevention of atherosclerosis.<sup>251</sup> Antioxidants are also incorporated into polymers to protect them against degradation during their processing. Finally, more and more natural antioxidants are added to skin care products for their anti-pollution power.<sup>252</sup>

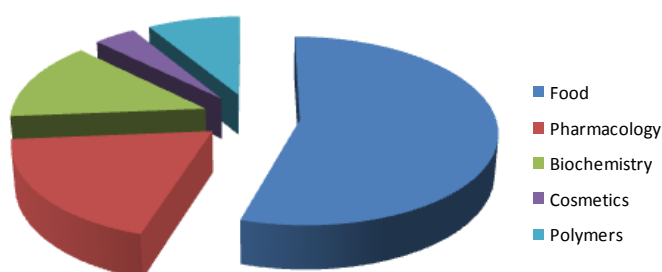


**Figure 3.1:** Main study areas of the use of antioxidants during the inhibition of the oxidation of unsaturated fatty acids with the Scifinder® database – keywords: “antioxidants”, “oxidation” and “unsaturated fatty acids”

Since 1980, there is an increasingly number of references, patents and articles as regards to the study of antioxidants for the inhibition of fatty acids oxidation (**Fig. 3.2**). Indeed, industrials and academic researchers are studying their antioxidant properties to delay the oxidative process. Thanks to a growing distrust of consumers who push the search for natural alternatives with equal or greater efficiency than synthetic antioxidants, there is an increase of published references for natural antioxidants since 2000.

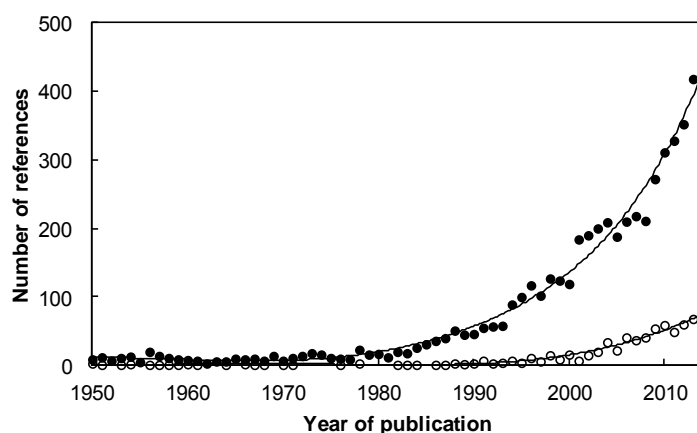


**Figure 3.2:** Number of references (articles and patents) vs their year of publication using “fatty acids” and “oxidation” coupled with “antioxidant” (black dots) or “natural antioxidants” (white dots) via the Scifinder® database

Nevertheless, theoretical methods and experimental investigations are rarely combined and always made on few antioxidants. Therefore, based on literature, it is difficult to compare the effects of a large scope of antioxidants during the protection of our targeted substrate and highlight the required conditions on the chemical structure of phenols to enhance the inhibition of oxidation. It is in the context of protection of edible oil rich in omega-3 that thermodynamic, kinetic and oxidative properties of natural polyphenols are studied in comparison to synthetic antioxidants.

## 2. Literature survey on the measuring of the antioxidant power

This literature survey is focused on different tests dedicated to the evaluation of the antioxidant power of phenols. The tests highlighting the chain breaking antioxidants which play their role in the inhibition of oxidation by hydrogen transfers are just taking into account. Since, when the oxidation process is engaged, they are the unique solution to delay and stop it.

Results obtained for the action of antioxidants on the inhibition of oxidation are dependent on the experimental conditions and the substrates involved during the studies.<sup>253-256</sup> In most cases, the oxidation is initiated by an increase of temperature, heat or pressure and by addition of metals, enzymes and free radicals as catalyst of oxidation.<sup>257-259</sup> Thereby, it is essential to select tests which are comparative to the real situation of oxidation and always bring face to face different tests to compare results. Generally, good correlations are observed between parameters obtained with various methods.<sup>253</sup>

The most common experimental methods for the evaluation of chain-breaking antioxidant power are based on direct or indirect evaluations of **1)** the consumption of substrates or oxygen, **2)** the formation of oxidized products and **3)** the formation or consumption of free radical species.

### 2.1 Measurement of substrate consumption or formation of oxidation products

#### 2.1.1 Inhibited Oxygen Uptake method (IOU)

The first referenced method works on the evaluation of oxygen consumption during the oxidation of substrates in presence of antioxidant.<sup>260, 261</sup> The rate of oxygen consumption ( $\Delta O_2$ ) is defined by **equation 3.1** where [RH] is the concentration of substrate,  $k_p$  and  $k_{inh}$  are respectively the kinetic rate constants of the propagation and inhibition stages and  $\tau$  is the induction time when antioxidant inhibits the oxidation.<sup>262</sup> The kinetic rate constant of inhibition ( $k_{inh}$ ) is then calculated thanks to the other parameters obtained experimentally.

$$\Delta [O_2] = - \frac{k_p [RH]}{k_{inh}} \ln \left( 1 - \frac{t}{\tau} \right) \quad (3.1)$$

The most popular substrates oxidized in presence of antioxidant are cumene and styrene whose kinetic rates of propagation are known at 30 °C<sup>263-265</sup>, 0.32 and 41.0 M<sup>-1</sup>.s<sup>-1</sup> respectively. As an example, **figure 3.3** shows the autoxidation of styrene without antioxidant (**a**) or with 2,6-*di-tert-butyl-4-methoxyphenol* (**b**) and  $\alpha$ -tocopherol (**c**) as phenolic antioxidants. This test is based on the measurement of oxygen during the autoxidation of styrene. Without antioxidant, there is a fast oxidation of styrene (fast consumption of O<sub>2</sub>). Moreover,  $\alpha$ -tocopherol inhibits the autoxidation process for a long time (low consumption of O<sub>2</sub>) whereas 2,6-*di-tert-butyl-4-methoxyphenol* just slow down the autoxidation process.

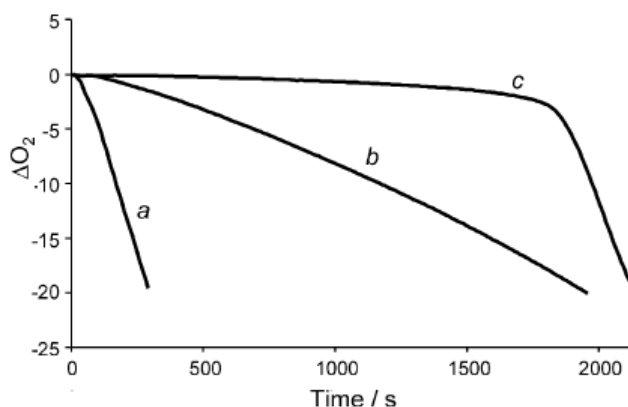


Figure 3.3: Oxygen consumption during the autoxidation of styrene (4.2M) in chlorobenzene initiated by the 2,2'-azobis (2,4-dimethylvaleronitrile) (DMVN): a) without antioxidant, b) with  $5 \times 10^{-6}$  M of 2,6-di-*tert*-butyl-4-methoxyphenol and, c) with  $5 \times 10^{-6}$  M of  $\alpha$ -tocopherol<sup>262</sup>

Nevertheless, the experimental conditions are too drastic compared to the reality of oxidation with a high pressure of oxygen and elevated concentration of antioxidants. Moreover, the induction period is not always well defined and the monitoring of oxygen consumption is not precise when the rate of oxidation is low.<sup>260, 266</sup>

### 2.1.2 Quantification of oxidized products by UV spectrometry

Several authors studied the autoxidation of unsaturated fatty acids such as linoleic acid by using an initiator (AIBN or copper) and following the advancement of the autoxidation by UV spectrometry at a single wavelength (234 nm).<sup>267, 268</sup> Indeed, conjugated diene hydroperoxides formed during the autoxidation of linoleic acid have a maximum of absorption at this wavelength (Fig. 3.4).<sup>260, 267</sup>

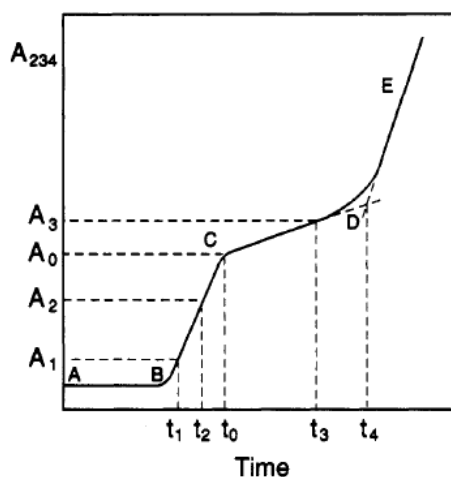


Figure 3.4: Monitoring of the formation of conjugated diene peroxides with UV spectrometry at  $\lambda = 234$  nm<sup>260, 267</sup>

As shown by figure 3.4, the autoxidation of linoleic acid is divided into different steps: **1)** during the phase AB, there is no oxidation under normal conditions, **2)** at point B, addition of the oxidation initiator AAPH (2,2'-azobis(2-amidinopropane) dihydrochloride) triggers the autoxidation process, **3)** during the phase BC, there is an accumulation of oxidized products, **4)** at point C, the addition of  $\alpha$ -tocopherol as antioxidant inhibits autoxidation and slows down the formation of hydroperoxides, **5)** at point D, all the antioxidant is consumed and **6)** during the phase DE, the autoxidation reaction takes place with the same kinetic as the phase BC. The antioxidant power is deduced via the phase CD named the induction period.<sup>260, 267</sup>

This experiment technique has some advantages. The concentration of substrate used is ten times lower than that used for the Inhibited Oxygen Uptake (IOU) method. Moreover, the UV spectrometry analysis could be made in homogenous and heterogeneous environment (organic solvent or micelle). Nevertheless, in the field of food, a lot of organic compounds absorb at 234 nm and disturb the analysis.<sup>260</sup>

### 2.1.3 Headspace of hexanal and oxidized products in biological systems

The following of the hexanal formation during the oxidation of biological systems such as low-density lipoproteins (LDL) mixed with initiator of radicals (Cu(II))<sup>269</sup> and antioxidant is another way to analyze the antioxidant power.<sup>270</sup> Indeed, hexanal is one of the major products formed during the oxidation of unsaturated fatty acids.<sup>271</sup> The formation of this oxidized species is followed and quantified with headspace gas chromatography.<sup>272</sup>

The main inconvenient of this analytical method is that hexanal is not an impartial factor. Indeed, it is a secondary oxidation product from the decomposition of hydroperoxides but other oxidation products are also obtained. Moreover, the relatively high boiling point of hexanal (131 °C) and its low vapor pressure at room temperature lead to its large concentration in solution favoring errors on the real concentration of hexanal measured by headspace.<sup>260</sup> Consequently, the headspace analytical technique is not an accurate method to determine the antioxidant power.

### 2.1.4 Measuring of hydroperoxides during the oxidation of lipids

As shown previously, hydroperoxides play an important role in the oxidative system. Their quantification allows determining the level of oxidized of damaged oils. The measurement of hydroperoxide by iodometric titration is the oldest method use to follow the degradation of fatty acids as already discussed.<sup>205</sup> Nevertheless, it is a non-sensitive and non-selective method. Indeed, there are side reactions as the addition of iodine onto double bonds of unsaturated fatty acids and oxidation of iodine by dissolved oxygen. Consequently, others methods for the determination of peroxides species have been developed but iodometric titration is always the standard procedure.<sup>273</sup>

## 2.2 Experimental methods for the detection of free radicals

### 2.2.1 Electron Paramagnetic Resonance spectroscopy (EPR)

Electron Paramagnetic Resonance (EPR) or Electron Spin Resonance (ESR) spectroscopy is the only one analytical method dedicated to the specific analysis of free radicals.<sup>274-276</sup> Nevertheless, this method could not detect free radicals obtained during the oxidation process because their lifetime is too short. Numerous methods have been set up to overcome this problem of detection such as pulse radiolysis, UV photolysis and spin-trap addition.<sup>277-279</sup>

EPR spectroscopy was used by Pedulli *et al.* in order to study the antioxidant power of phenolic antioxidants.<sup>262</sup> It determines the required energy to break the phenolic bond by homolytic cleavage. The hydrogen atom formed (H<sup>•</sup>) is then transferred to the oxidized oil to stop the oxidation. This parameter is called Bond Dissociation Enthalpy (BDE).<sup>280</sup> It is the most specific experimental technique to determine this thermodynamic parameter.

The experimentation starts with the measure of the equilibrium constant  $K_1$  under photolysis for the hydrogen transfer between two phenols and their respective radicals (**Eq. 3.2**). Then, the relative

concentration of phenolic radicals are obtained with EPR spectroscopy and **equation 3.3** reveals the BDE of studied phenol (ArOH) using the perfectly known BDE of the reference 2,4,6-*tri-tert*-butylphenol (Ar'OH).<sup>281</sup>



$$\text{BDE}(\text{ArO}-\text{H}) = \text{BDE}(\text{Ar}'\text{O}-\text{H}) - RT \ln(K_1) \quad (3.3)$$

The main inconvenient of EPR spectroscopy is that the equipment is expensive and the procedure are sometimes difficult to set up.<sup>253</sup>

### 2.2.2 2,2-Diphenyl-1-picrylhydrazil radical (DPPH<sup>•</sup>) scavenging test

The DPPH<sup>•</sup> test<sup>253, 260, 282, 283</sup> is commonly used to evaluate the antioxidant power of phenolic compounds. It is a stable radical with a maximum of absorption around 515-520 nm (violet). When antioxidants are mixed with this radical, there is a transfer of hydrogen from the antioxidant to DPPH<sup>•</sup> radical. The DPPH<sup>•</sup> radical catches the hydrogen and becomes yellow (**Fig. 3.5**).

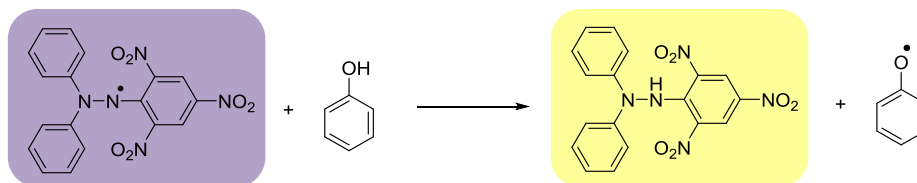


**Figure 3.5: Hydrogen atom transfer from phenol to DPPH<sup>•</sup> radical**

Consequently, it is easy to follow the hydrogen transfer by UV-visible spectrometry. This test points out the kinetic rates of hydrogen transfer and the number of hydrogen transfer called the stoichiometric number. Generally, few kinetic results are described in literature but authors are discussing about the EC<sub>50</sub> parameter which is the amount of antioxidant required to inhibit 50 % of the initial DPPH<sup>•</sup> concentration. This test is very well-liked by researchers because of its easy application, the quickness of the analysis and the inexpensive cost of substrates and device. Nevertheless, results obtained are dependent on solvent and steric hindrance of compounds.<sup>284, 285</sup>

## 2.3 Selected tests to determine the antioxidant power of phenols

We focused on various theoretical and experimental tests to evaluate the antioxidant power of phenols as regards to the oxidation of edible oils rich in omega-3:

- 1) a thermodynamic point of view with the molecular modeling of phenolic antioxidants and its respective phenolic radicals to determine Bond Dissociation Enthalpies (BDE) and Ionization Potentials (IP) of phenols,
- 2) a kinetic approach with the DPPH<sup>•</sup> test which mimics the behavior of antioxidants in oxidized process highlighting kinetic rates of hydrogen transfer and number of radicals trapped by molecule of phenols (stoichiometric number),
- 3) a global way to measure the consumption of oxygen (RapidOxy<sup>®</sup>) and the formation of volatile compounds (Rancimat) during the autoxidation of polyunsaturated fatty acids and their derivatives such as Fatty Acid Methyl Esters (FAMES).

These tests seem to be the most suitable and relevant analytic methods to study the antioxidant power of phenolic antioxidants during the preservation of edible oils rich in omega-3. All of the materials, protocols, methods and results are developed in the experimental part.

### 3. Thermodynamic properties of phenolic antioxidants

Free radicals play an important role in the degradation of organoleptic properties of food as regards to oxidation process. Moreover, they are involved in the oxidation of other compounds such as fragrances and biological molecules.<sup>286, 287</sup> In order to reduce the damages of these free radicals, scientists are studying the effectiveness of non-toxic antioxidants.<sup>288</sup> Different factors influence the antioxidant power of phenols:<sup>289</sup>

- 1) A low value of BDE for the phenolic bond favors the transfer of phenolic hydrogen to free radicals  $R^{\bullet}$ ,  $RO^{\bullet}$  and  $ROO^{\bullet}$ .<sup>290-295</sup>
- 2) A high value of Ionization Potential (IP) disadvantages the transfer of electron from phenols to oxygen leading to a reduction of the pro-oxidant potential of the antioxidant.<sup>289, 290, 296-299</sup>
- 3) The formation of stable radicals after the transfer of the phenolic hydrogen reduces the toxic effect of phenolic radicals into the body.<sup>297, 300</sup> Indeed, the impact of phenolic radicals after their ingestion is more and more taking into account by experts from academia and industries.
- 4) A high solubility of the phenol into the protected substrates improves the antioxidant power.<sup>301, 302</sup>

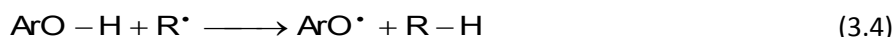
Phenols have to meet all these requirements to have an effective antioxidant power. More precisely, authors showed that the most important parameters which must be taken into account for the development of a new antioxidant are BDE and IP.<sup>289, 290, 295, 298, 299, 303-312</sup> In most cases, these two parameters are determined by Density Functional Theory (DFT) calculations.<sup>289, 290, 295, 298, 299, 303-312</sup>

First of all, we determine the impact on BDE of the position and the type of substituents commonly found on phenolic ring in order to identify general tendencies. Then, BDEs and IPs are calculated for a large range of phenolic antioxidants. A DFT method described in the experimental section *via* the Gaussian 03 – Revision E.01 package is used. Moreover, our theoretical results are compared with those found in literature whether they were experimentally or theoretically obtained. The solvent effect is also studied because it could influence the preferred conformation of phenol by intermolecular hydrogen bonding which modifies BDE and reaction mechanism of phenols.<sup>313, 314</sup> Therefore, we are also focused on the  $pK_a$  value of phenols since it could influence BDEs and IPs.

#### 3.1 Definition of BDE, IP and $pK_a$ parameters

Generally speaking, phenolic antioxidants (ArO-H) inhibit peroxy radicals ( $ROO^{\bullet}$ ) formation via hydrogen transfer according to three kinds of mechanisms controlled by thermodynamic parameters (*i.e.* BDE, IP and  $pK_a$ ).

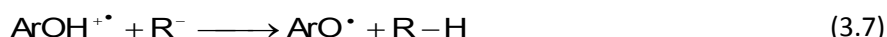
The first system is a radical mechanism called HAT (Hydrogen Atom Transfer) or concerted proton/electron transfer (CPET) in which phenols transfer hydrogen atom. It is governed by the enthalpy of dissociation of the O-H bond<sup>290, 304, 315</sup> defined by **equations 3.4 and 3.5**.



$$\text{BDE} (\text{ArO} - \text{H}) = \text{H}_f^{\circ} (\text{ArO}^{\bullet}) + \text{H}_f^{\circ} (\text{H}^{\bullet}) - \text{H}_f^{\circ} (\text{ArO} - \text{H}) \quad (3.5)$$

$\text{R}^{\bullet}$  is the inhibited radical and  $\text{R}-\text{H}$  corresponds to the substrate formed.  $\text{H}_f^{\circ}(\text{ArO}-\text{H})$ ,  $\text{H}_f^{\circ}(\text{ArO}^{\bullet})$  and  $\text{H}_f^{\circ}(\text{H}^{\bullet})$  are the enthalpy of formation of phenol, phenoxy radical and radical hydrogen atom respectively. In non-polar solvent, phenolic antioxidants act following this radical mechanism. The lower of BDE of phenol is, the better the antioxidant activity should be. Indeed, the kinetic rate of hydrogen transfer is related to the activation energy  $E_a$ , which is itself linked to the BDE.<sup>316</sup>

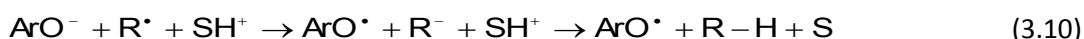
Then, the HAT mechanism is bringing into opposition with the SET-PT mechanism (Sequential Electron Transfer – Proton Transfer). In this case, phenols transfer firstly an electron and then a proton<sup>290, 304, 315</sup> following **equations 3.6 and 3.7**.



$$\text{IP} (\text{ArO} - \text{H}) = \text{H}_f^{\circ} (\text{ArO} - \text{H}^{+\bullet}) - \text{H}_f^{\circ} (\text{ArO} - \text{H}) \quad (3.8)$$

$\text{R}^{\bullet}$  is the inhibited radical and  $\text{R}-\text{H}$  corresponds to the substrate formed.  $\text{H}_f^{\circ}(\text{ArO}-\text{H})$  and  $\text{H}_f^{\circ}(\text{ArO}-\text{H}^{+\bullet})$  are the enthalpy of formation of phenol and cation respectively. Authors are focused on the interpretation of the hydrogen transfer mechanism and opposed HAT and SET mechanisms. Based on the reaction of  $\alpha$ -tocopherol with peroxy radicals, Nagaoka *et al.* argued in favor of the SET mechanism<sup>317</sup> whereas Burton and co-workers assumed the one step HAT system.<sup>318</sup> Nevertheless, the ionization potential (IP), as expressed by **equation 3.8**, is useful to discuss about the stability of the phenol in the presence of oxygen.<sup>296</sup>

Finally, a third system has been suggested some years ago. It is called SPLET mechanism (Sequential Proton Loss Electron Transfer).<sup>285, 319, 320</sup> In a polar media (S), phenols are dissociated into phenolate and then transfer one electron to the radical which finally receive a labile proton (**Eqs. 3.9 and 3.10**).



This mechanism depends on the acidity of phenols and polarity of solvents.  $\text{pK}_a$  of phenols is therefore an important parameter. It could be also calculated by DFT method<sup>321</sup> as for BDE and IP, but we just used literature values.

HAT mechanism could compete with SPLET system for the same phenol according to the chemical structure of phenols and polarity of solvents. The predominance of these mechanisms will be more developed thereafter with DPPH<sup>•</sup> test. The calculation of BDEs and IPs allows discussing about the influence of substituents found on phenolic ring and building a scale of reactivity of phenolic antioxidants.

### 3.2 Determination of the antioxidant power with BDE calculation

As above-mentioned, the most common experimental technique to determine BDEs is EPR spectroscopy.<sup>262, 281, 322</sup> Nevertheless, there are simple alternatives as semi empirical calculations (AM1, AM2...) and more complex calculations using DFT. This technique allows comparing with reliability compounds from the same family.<sup>290</sup> A number of theoretical investigations with various basis set<sup>299, 307, 323-325</sup> have been reported to determine BDEs of phenols.

Theoretical molecular modeling is favored for the determination of BDEs. The hybrid functional B3LYP (Becke, three parameter, Lee-Yang-Parr) was selected to get accurate results within a short time. It is a functional hybrid because it gathers technique based on Hartree-Fock and DFT approximations. The basis set selected is 6-311 G++(2d,2p) using the 2d,2p orbitals of atoms.<sup>290, 296, 310, 315</sup>

Enthalpies of formation of phenol and phenoxy radical have been calculated separately. The geometry of phenols was quickly optimized by Molecular Mechanics (MM) method based on Universal Force Field (UFF) computation using general rules focused on atoms, their hybridizations and connectivities. This allows to accelerate the second optimization made with DFT-B3LYP/6-311G (d,p) method which take into account all the electrons of the molecule. This final geometries were used as inputs to the final energy B3LYP/6-311G ++ (2d,2p) calculation. Then, zero-point energy (ZPE) has been taken into account to correct BDEs values thanks to the frequency calculation *via* B3LYP/6-311G (d,p) method. For species having several conformers, all of them were investigated. The conformer with the lowest electronic energy is retained. The absence of imaginary frequency implies that the geometric configuration of the molecule is at a minimum potential with the lowest energy. The geometry of phenoxy radicals were optimized from that of phenol by snatching the phenolic hydrogen. Then, the same procedure as for phenols was used. The entire method is called B3LYP/6-311++G(2d,2p)//B3LYP/6-311G(d,p).

#### 3.2.1 Substituent effects on BDEs

We first discuss about the group contribution on BDEs which depends on the nature of substituent and its position on the phenolic ring. The absolute BDE of phenol and  $\Delta$ BDEs of phenolic antioxidants compared to value of phenol (82.2 kcal.mol<sup>-1</sup>) are listed in **table 3.1**. The comparison of calculated BDEs with literature points out some discrepancies. For example, in the case of phenol, DFT calculation gives a BDE of 82.2 kcal.mol<sup>-1</sup> while the most reliable gas-phase BDE reported in the literature by Mulder *et al.* is 86.7 kcal.mol<sup>-1</sup><sup>326</sup>. However, it is known that a systematic underestimation of about 5 kcal.mol<sup>-1</sup> can arise from DFT calculation. Hence, it is better to consider  $\Delta$ BDE values compared to BDE of phenol as reported in **tables 3.1** and **3.2**.

	N°	Substituent	Position	Electronic effect		H-bonding		BDE (kcal.mol <sup>-1</sup> )		ΔBDE (kcal.mol <sup>-1</sup> )	
				ArOH	ArO <sup>•</sup>	ArOH	ArO <sup>•</sup>	Calc.	Literature		
	1	- H	-					82.2	-	-	
Alkyl groups (-R)	2	-CH <sub>3</sub>	<i>o</i>	--	++			80.2	-2.0	-2.1 <sup>299</sup> , -1.9 <sup>327</sup> , -2.0 <sup>311</sup> , -2.1 <sup>309</sup>	
	3	-CH <sub>3</sub>	<i>m</i>	-	+			82.2	0	-0.5 <sup>299</sup> , -0.4 <sup>327</sup> , -0.4 <sup>290</sup> , -0.5 <sup>292</sup>	
	4	-CH <sub>3</sub>	<i>p</i>	--	++			80.1	-2.1	-2.1 <sup>298, 299</sup> , -2.1 <sup>327</sup> , -2.0 <sup>328</sup> , -2.5 <sup>290</sup>	
	5	-CH <sub>2</sub> CH <sub>3</sub>	<i>o</i>	--	++			80.1	-2.1	nd	
	6	-CH <sub>2</sub> CH <sub>3</sub>	<i>m</i>	-	+			81.4	-0.8	nd	
	7	-CH <sub>2</sub> CH <sub>3</sub>	<i>p</i>	--	++			80.0	-2.2	nd	
	8	-C(CH <sub>3</sub> ) <sub>3</sub>	<i>o</i>	---	+++			79.3	-2.9	-3.2 <sup>290</sup> , -3.3 <sup>290</sup>	
	9	-C(CH <sub>3</sub> ) <sub>3</sub>	<i>m</i>	-	+			82.0	-0.2	-0.9 <sup>299</sup> , -0.6 <sup>290</sup>	
	10	-C(CH <sub>3</sub> ) <sub>3</sub>	<i>p</i>	--	++			80.5	-1.7	-1.9 <sup>299</sup> , -2.0 <sup>290</sup> , -1.7 <sup>309</sup> , -1.9 <sup>329</sup>	
	Alkene groups (-R)	11	-CH <sub>2</sub> -CH=CH <sub>2</sub>	<i>o</i>	--	++			80.2	-2.0	-2.4 <sup>311</sup> , -1.6 <sup>330</sup>
12		-CH=CH-CH <sub>3</sub>	<i>o</i>	--	+++			79.2	-3.0	nd	
13		-CH=CH-CH <sub>3</sub>	<i>m</i>	+	-			83.5	+1.3	nd	
14		-CH=CH-CH <sub>3</sub>	<i>p</i>	---	+++			77.3	-4.9	nd	
Methoxy groups (-OR)	15	-OCH <sub>3</sub>	<i>o</i>	--	++	++		80.4	-1.8	-1.4 <sup>290</sup> , -0.9 <sup>322</sup> , -2.3 <sup>284</sup>	
	16	-OCH <sub>3</sub>	<i>m</i>	+	-			83.1	+0.9	-1.2 <sup>299</sup> , -0.5 <sup>327</sup> , -1.2 <sup>290</sup> , -0.7 <sup>309</sup>	
	17	-OCH <sub>3</sub>	<i>p</i>	--	++			77.6	-4.6	-5.7 <sup>298, 299</sup> , -5.9 <sup>327</sup> , -4.4 <sup>292</sup> , -4.1 <sup>329</sup>	
Hydroxyl groups (-OH)	18	-OH	<i>o</i>	--	++	++	++	73.4	-8.8	-9.1 <sup>290</sup> , -7.2 <sup>305</sup> , -8.9 <sup>307</sup> , -6.8 <sup>322</sup>	
	19	-OH	<i>m</i>	-	+			81.2	-1.0	-0.2 <sup>299</sup> , -0.3 <sup>327</sup> , -0.3 <sup>290</sup>	
	20	-OH	<i>p</i>	--	++			77.2	-5.0	-5.0 <sup>328</sup> , -5.8 <sup>290</sup> , -5.8 <sup>327</sup>	
	21	-CO <sub>2</sub> H	<i>o</i>	++	--	+++		95.2	+13.0	+7.7 <sup>290</sup> , +11.4 <sup>311</sup>	
Carboxyl groups (-CO <sub>2</sub> R)	22	-CO <sub>2</sub> H	<i>m</i>	+	-			84.5	+2.3	+2.7 <sup>290</sup>	
	23	-CO <sub>2</sub> H	<i>p</i>	+	--			84.7	+2.5	+2.8 <sup>290</sup> , +2.5 <sup>330</sup>	
	24	-CO <sub>2</sub> CH <sub>3</sub>	<i>o</i>	++	--	+++		94.9	+12.7	+12.2 <sup>311</sup>	
	25	-CO <sub>2</sub> CH <sub>3</sub>	<i>m</i>	+	-			84.1	+1.9	nd	
	26	-CO <sub>2</sub> CH <sub>3</sub>	<i>p</i>	+	-			84.1	+1.9	+1.7 <sup>309</sup>	

nd: not determined

Table 3.1: Contributions to BDEs of the ArO-H bond of phenols bearing different *ortho* (*o*), *meta* (*m*) or *para* (*p*) substituents calculated with B3LYP/6-311++G(2d,2p)//B3LYP/6-311G(d,p) DFT method in vacuum. ΔBDE are calculated from the BDE of phenol (82.2 kcal.mol<sup>-1</sup>). Electronic effects which destabilize (-) and stabilize (+) ArOH and ArO<sup>•</sup> are indicated, H-bonding which stabilize (+) ArOH and ArO<sup>•</sup> are illustrated

Values on the group contribution of BDEs obtained are consistent with published theoretical values as reported in **table 3.1** except for methoxy substituent (**entry 16**) which is overestimated but allows anyway discussing its effect. Moreover, **figure 3.6** shows that our values of BDE calculated in vacuum are also consistent with those obtained experimentally *via* EPR spectroscopy by Pedulli *et al.*<sup>262</sup>

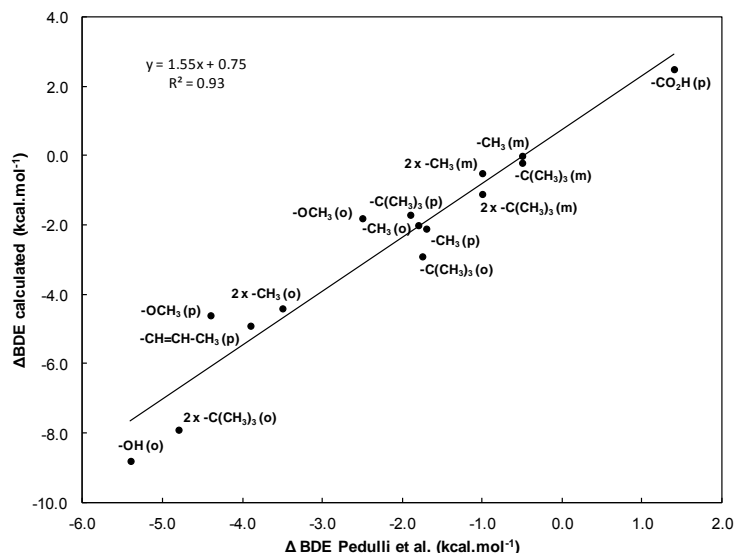


**Figure 3.6:** Correlation between  $\Delta$ BDE calculated in vacuum by B3LYP/6-311++G(2d,2p)/B3LYP/6-311G(d,p) method and those obtained experimentally with EPR spectroscopy by Pedulli *et al.*<sup>262</sup>

**Table 3.1** summarizes the effect of substituents that we classified into four groups: alkyl (-R), methoxy (-OR), hydroxyl (-OH) and carboxyl (-CO<sub>2</sub>R) groups. The effect of electron-donating and electron-withdrawing substituents has been studied in numerous experimental and theoretical works from early 90's.<sup>262, 290</sup>

Generally speaking, lower BDEs are obtained for electron-donating groups (EDG) by destabilizing the phenol and/or stabilizing the phenoxyl radical by electronic effects and intramolecular hydrogen bondings has already described by Lucarini *et al.*<sup>262</sup> Indeed, passing from phenol to phenoxyl radical permits to change the electronic behavior from donor (hydroxyl group) to strongly acceptor (radical oxygen atom) which comes along with a decrease of the energy state of phenoxyl radical (**Fig. 3.7**). Because of the O-H BDE is given by the difference between the energy of phenoxyl radical (plus that of the hydrogen atom) and that of the starting phenol, there is a decrease of BDE with electron donating groups.

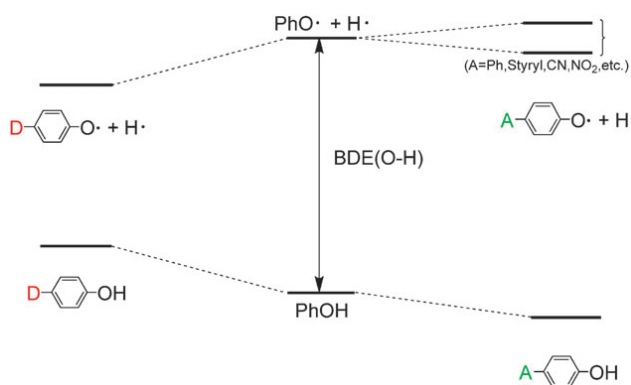


**Figure 3.7:** Representation of the enthalpies of phenol (Ph-OH) and phenoxyl radical (PhO<sup>•</sup>) to get the Bond dissociation Enthalpy BDE(O-H). Differentiation of electron-donating groups (D) and electron-withdrawing groups (A)<sup>281</sup>

As expected, alkyl substituents decrease BDEs *via* electronic effects (**Table 3.1**). *Ortho*-methyl (**entry 2**), *para*-*tert*-butyl (**entry 10**), *ortho*-ethyl (**entry 5**) and *ortho*-propenyl (**entry 12**) substituents decrease BDE values of -2.0, -1.7, -2.1 and -3.0 kcal.mol<sup>-1</sup> respectively. *Ortho*-*tert*butyl group (**entry 8**) implies a steric hindrance and leads to a decrease of the O-H bond strength. This steric repulsion vanishes when the phenoxyl radical is formed and BDE decreases of -2.9 kcal.mol<sup>-1</sup> as supported by EPR experiments.<sup>280</sup>

*Ortho*-substitution by an OH group leads to a stronger decrease of BDE compared to an OCH<sub>3</sub> group (**entry 18 vs entry 15**) (-8.8 and -1.8 kcal.mol<sup>-1</sup> respectively). As reported by Wright and co-workers, this results from the disappearance of the intramolecular hydrogen bonding for the phenoxyl radical in the case of OCH<sub>3</sub> (situation B) while with the OH group, the radical stabilization becomes more important (situation A), leading to a strongly decrease of BDE (**Fig. 3.8**)<sup>290</sup>.

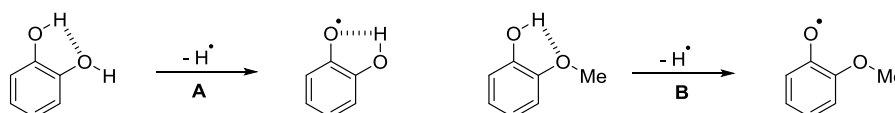


**Figure 3.8:** Substitution by *ortho*-hydroxyl (A) or *ortho*-methoxy (B) group, disappearance of the intramolecular hydrogen bonding in the case of *ortho*-methoxy group (B)

Compared to the *o*-allyl group (**entry 11**), *o*-propenyl substituent (**entry 12**) allows further electron delocalization which increases the stability of phenoxyl radical and leads to a stronger BDE decrease from -3.0 and -2.0 kcal.mol<sup>-1</sup> respectively. Moreover, a substitution by a conjugated double bond in *para*-position (**entry 14**) favors the delocalization of unpaired electron, a strong stabilization of the phenoxyl radical and a better decrease of BDE (-4.9 kcal.mol<sup>-1</sup>) compared to *ortho*- (-3.0 kcal.mol<sup>-1</sup>, **entry 12**) and *meta*- (+1.3 kcal.mol<sup>-1</sup>, **entry 13**) positions as shown by EPR spectroscopy.<sup>280</sup> However, *meta*- alkyl, alkoxy and hydroxyl groups have low or no impact compared to *ortho*- and *para*-substitutions.<sup>262, 303, 327</sup>

On the contrary, higher BDEs are obtained for electron-withdrawing groups (EWG). These groups induce a stabilization of the starting phenol which decreases its energy level. Nevertheless, the effect on the phenoxyl radical is more difficult to interpret because it is depending on the possible delocalization of the unpaired electron. In most cases, the impact of withdrawing groups on the energy level of phenoxyl radical is very weak (**Fig. 3.7**). As an example, a -COOH group in *ortho*-position favors intramolecular hydrogen bonding which increases the stabilization of phenols.<sup>290, 311</sup> Nevertheless, it disappears when the phenoxyl radical is formed. Therefore, both effects are unfavorable for an easy transfer of the hydrogen involving a strong increase of +13.0 kcal.mol<sup>-1</sup> (**entry 21, Fig. 3.9**).

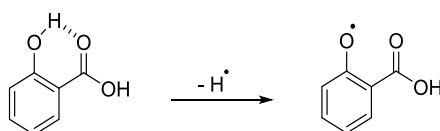


**Figure 3.9:** Stabilization of the phenol by intramolecular hydrogen bonding and destabilization of the phenolic radical with the *ortho*-carboxyl group

Using ReqEPR, Pedulli and co-workers have demonstrated the additive effect of some alkyl substituents and supported the results with some additivity rules.<sup>262</sup> With theoretical calculation using B3LYP/6-311++G(2d,2p)//B3LYP/6-311G(d,p) DFT method, additive effects are also found for methyl and *tert*-butyl substituents (Table 3.2).

Entry	Ring position substituents			BDE (kcal.mol <sup>-1</sup> )	ΔBDE (kcal.mol <sup>-1</sup> )	
	<i>Ortho</i> -	<i>Meta</i> -	<i>Para</i> -		Calc.	Literature
27	2 x -CH <sub>3</sub>			77.8	-4.4	-3.8 <sup>262</sup> , -3.5 <sup>281</sup>
28		2 x -CH <sub>3</sub>		81.7	-0.5	-1.7 <sup>262</sup>
29	2 x -CH <sub>3</sub>		-CH <sub>3</sub>	75.8	-6.4	-5.6 <sup>262</sup> , -5.2 <sup>281</sup>
30	-CH <sub>3</sub>	-CH <sub>3</sub>		79.6	-2.6	nd
31	-CH <sub>3</sub>		-CH <sub>3</sub>	78.2	-4.0	nd
32		-CH <sub>3</sub>	-CH <sub>3</sub>	80.0	-2.2	nd
33	2 x -CH <sub>3</sub>	2 x -CH <sub>3</sub>	-CH <sub>3</sub>	74.5	-7.7	nd
34	2 x -C(CH <sub>3</sub> ) <sub>3</sub>			74.3	-7.9	-5.5 <sup>262</sup> , -4.8 <sup>281</sup>
35		2 x -C(CH <sub>3</sub> ) <sub>3</sub>		81.1	-1.1	-1.7 <sup>262</sup> , -1.0 <sup>281</sup>

nd: not determined

Table 3.2: Contributions to BDEs of phenols bearing different *ortho* (*o*), *meta* (*m*) or *para* (*p*) alkyl substituents. ΔBDE are calculated with BDE of phenol (82.2 kcal.mol<sup>-1</sup>)

*Ortho*-methyl substituents exhibit additive effects with ΔBDE of -2.0 and -4.4 kcal.mol<sup>-1</sup> respectively (comparing entry 2, Table 3.1 and entry 27, Table 3.2). A second *ortho-tert*butyl substituent increases the steric repulsion on the phenolic hydrogen inducing a higher O-H bond strength. The effect disappears when the phenoxyl radical is formed. Consequently, the difference between energy levels of phenol and phenoxyl radical is smaller than that with only one *ortho-tert*butyl group. Thereby, there is more than an additive effect: two *ortho-tert*-butyl groups decrease the BDE of -7.9 kcal.mol<sup>-1</sup> (entry 34, Table 3.2) while one *ortho-tert*butyl group just decreases the BDE of -2.9 kcal.mol<sup>-1</sup> (entry 8, Table 3.1).

To conclude (Fig. 3.10), a substitution by electron-donating (EDG, alkyl, methoxy, and hydroxyl) group decreases BDEs whereas electron-withdrawing group (EWG, carboxyl) increases BDEs. Moreover, the *meta*- position has low or no impact on BDEs compared to *ortho*- and *para*- positions. In the light of the correlation between our calculated BDEs with theoretical and experimental results obtained by authors, we confirm that our DFT method of calculation is consistent.

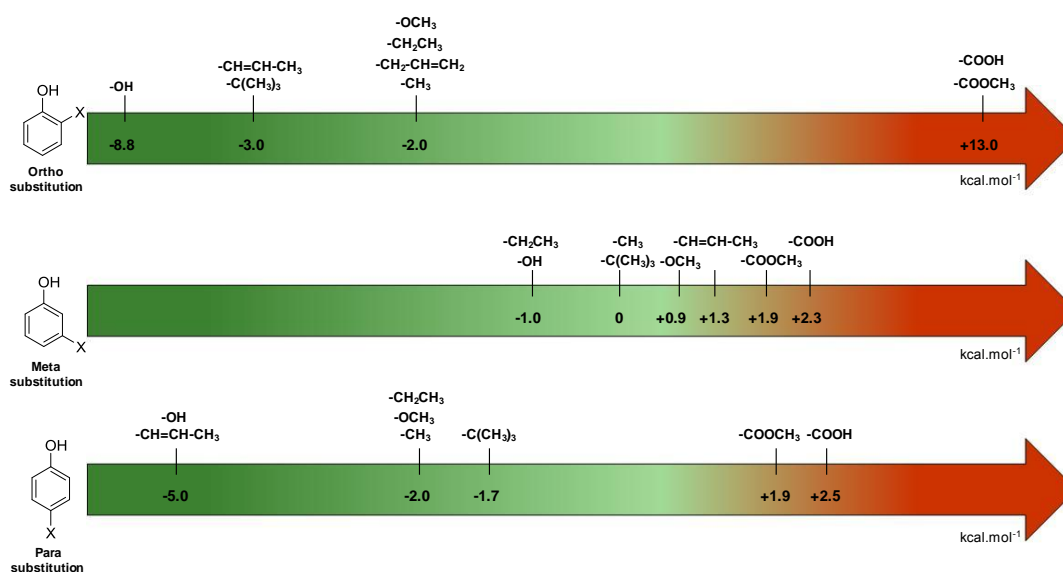


Figure 3.10: Impact on the calculated BDEs with B3LYP/6-311++G(2d,2p)//B3LYP/6-311G(d,p) DFT method in vacuum of the substituents studied as a function of their position on the phenolic ring

### 3.2.2 Determination of BDEs for phenolic antioxidants: scale of reactivity

Extensive researches have been done on the isolation, purification and identification of various antioxidants present in fruits, vegetable, tea and food. All the (poly)phenols studied in this work are presented in **table 3.3** gathering their respective name and number associated. They are ranged by classes of antioxidants and from the lowest BDE to the highest BDE. They have various numbers of OH groups and their respective chemical structures divide them into different families of antioxidants. The antioxidant power of 10 synthetic antioxidants, 4 tocopherols, 8 hydroxybenzoic and 8 hydroxycinnamic acids derivatives, 24 flavonoids, 3 catechins, 2 stilbenes, eugenol and isoeugenol, 3 phenols found in olive oil, 1 lignan, 3 coumarins, carnosol and carnosic acid are studied by DFT calculation. BDEs of all the O-H sites for each molecule have been calculated and results are described in experimental part. The lowest BDE is presented in following tables. We have chosen as references three phenolic antioxidants widely used in industry. These phenols are  $\alpha$ -tocopherol **11**, BHT **7** and BHA **5** which have a BDE of 69.1, 72.4 and 72.3 kcal.mol<sup>-1</sup> respectively.

N°	Name	N°	Name	N°	Name
<b>Synthetic phenols</b>		<b>Flavonols</b>		<b>Catechins</b>	
1	5-Tert-butylpyrogallol	31	Gossypetin	55	Epigallocatechin gallate
2	Pyrogallol	32	Myricetin	56	Gallocatechin
3	Hydroxyquinol	33	Azaleatin	57	Catechin
4	Propyl gallate	34	Quercetin		
5	BHA	35	Fisetin	<b>Stilbenes</b>	
6	4-Tert-butylcatechol	36	Laricitrin	58	Piceatannol
7	BHT	37	Syringetin	59	Resveratrol
8	TBHQ	38	Rhamnazin		
9	<i>o</i> -Tert-butyl- <i>p</i> -cresol	39	Kaempferide	<b>Aromatic phenols</b>	
10	Phloroglucinol	40	Isorhamnetin	60	Isoeugenol
		41	Morin	61	Eugenol
		42	Kaempferol		
		43	Galagin	<b>Phenols from olive oil</b>	
<b>Tocopherols</b>				62	Hydroxytyrosol
11	$\alpha$ -Tocopherol			63	Catechol
12	$\beta$ -Tocopherol			64	Tyrosol
13	$\gamma$ -Tocopherol				
14	$\delta$ -Tocopherol	44	Luteolin		
		45	Apigenin	<b>Lignans</b>	
<b>Hydroxybenzoic acids</b>				65	Sesamol
15	Gallic acid	<b>Flavanonols</b>			
16	Protocatechuic acid	46	Taxifolin	<b>Coumarins</b>	
17	Syringic acid	47	Aromadredrin	66	Methylesculetin
18	Ellagic acid			67	Aesculetin
19	Gentisic acid			68	Nordalbergin
20	Vanillic acid	48	Eriodictyol		
21	PHBA	49	Homoeriodictyol	<b>Carnosic acid derivatives</b>	
22	Salicylic acid	50	Hesperetin	69	Carnosol
		51	Naringenin	70	Carnosic acid
<b>Hydroxycinnamic acids</b>					
23	Rosmarinic acid	<b>Isoflavones</b>			
24	Caffeic acid	52	Glycitein		
25	Chlorogenic acid	53	Genistein		
26	Sinapic acid	54	Daidzein		
27	Ferulic acid				
28	<i>o</i> -Coumaric acid				
29	<i>p</i> -Coumaric acid				
30	<i>m</i> -Coumaric acid				

Table 3.3: Names and associated numbers of polyphenols studied

- *Synthetic phenolic antioxidants*

**Figure 3.11** and **table 3.4** show the general chemical structure and BDEs of synthetic antioxidants. In most cases, these phenols are alkylated to increase their solubility in oils and fats. Because of toxicity, some efficient antioxidants for polymers are no longer tolerated when they are intended to be ingested. In recent years, the toxicity of BHT **7** and BHA **5** have extensively been studied and they are now very controversial.<sup>53</sup> Consequently, their ban in the near future is expected. One of the current alternatives is the natural (poly)phenols.



**Figure 3.11:** Chemical structure of synthetic antioxidants

N°	R <sub>2</sub>	R <sub>3</sub>	R <sub>4</sub>	R <sub>5</sub>	R <sub>6</sub>	BDE (kcal.mol <sup>-1</sup> )
<b>1</b>	OH	H	C(CH <sub>3</sub> ) <sub>3</sub>	H	OH	66.6 (nd)
<b>2</b>	OH	H	H	H	OH	68.0 (77.7 <sup>331</sup> )
<b>3</b>	H	H	OH	H	OH	69.1 (70.4 <sup>332</sup> )
<b>4</b>	OH	H	C(O)OC <sub>3</sub> H <sub>7</sub>	H	OH	69.6 (77.1 <sup>324</sup> )
<b>5</b>	C(CH <sub>3</sub> ) <sub>3</sub>	H	OCH <sub>3</sub>	H	H	72.3 (80.7 <sup>324</sup> )
<b>6</b>	H	H	C(CH <sub>3</sub> ) <sub>3</sub>	H	OH	72.3 (81.1 <sup>333</sup> )
<b>7</b>	C(CH <sub>3</sub> ) <sub>3</sub>	H	CH <sub>3</sub>	H	C(CH <sub>3</sub> ) <sub>3</sub>	72.4 (79.9 <sup>334</sup> )
<b>8</b>	H	H	OH	H	C(CH <sub>3</sub> ) <sub>3</sub>	74.3 (76.9 <sup>335</sup> )
<b>9</b>	H	H	CH <sub>3</sub>	H	C(CH <sub>3</sub> ) <sub>3</sub>	77.4 (78.1 <sup>336</sup> )
<b>10</b>	H	OH	H	OH	H	83.0 (87.7 <sup>331</sup> )

**Table 3.4:** BDEs of synthetic antioxidants

We point out that 5-*tert*-butylpyrogallol **1** and pyrogallol **2** have the lowest BDEs of synthetic antioxidants (respectively 66.6 and 68.0 kcal.mol<sup>-1</sup>). The rules highlighted on the substituent effects are respected. Indeed, a substitution of the phenolic ring by two *ortho*-hydroxyl groups improves the stability of the central hydroxyl group and also that of the phenolic radical. Hydroxyquinol **3** has a combined structure of catechol and hydroquinone reaching a low BDE of 69.1 kcal.mol<sup>-1</sup>. Then, other phenols such as BHA **5**, BHT **7** and TBHQ **8** with a substitution by alkyl (methyl, *tert*butyl) and/or hydroxyl/methoxy groups follow with respective BDEs of 72.3, 72.4 and 74.3 kcal.mol<sup>-1</sup>. Finally, phloroglucinol **10** has the highest BDE (83.0 kcal.mol<sup>-1</sup>) of all the synthetic antioxidants studied.

- *Tocopherols*

**Figure 3.12** and **table 3.5** gather BDEs of  $\alpha$ -,  $\beta$ -,  $\gamma$ - and  $\delta$ -tocopherols. Tocopherols are monophenolic compounds derived from chromanol which are very soluble in oils making  $\alpha$ -tocopherol **11** the most important antioxidant in edible fats and oils.<sup>164</sup> These phenols are frequently found in vegetable oils especially soybean, sunflower and palm oils. The four derivatives of tocopherol are distinguishable by the number and the position of the methyl substituents which impact the BDEs.

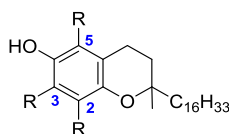


**Figure 3.12:** Chemical structure of tocopherols

N°	R <sub>2</sub>	R <sub>3</sub>	R <sub>5</sub>	BDE (kcal.mol <sup>-1</sup> )
<b>11</b>	CH <sub>3</sub>	CH <sub>3</sub>	CH <sub>3</sub>	69.1 (71.7 <sup>304</sup> )
<b>12</b>	CH <sub>3</sub>	H	CH <sub>3</sub>	73.4 (77.7 <sup>290</sup> )
<b>13</b>	CH <sub>3</sub>	CH <sub>3</sub>	H	73.5 (78.2 <sup>290</sup> )
<b>14</b>	CH <sub>3</sub>	H	H	75.4 (79.8 <sup>290</sup> )

Table 3.5: BDEs of tocopherols

$\alpha$ -Tocopherol **11** exhibits a lower BDE than  $\beta$ -,  $\gamma$ - and  $\delta$ -tocopherols. This low BDE (69.1 kcal.mol<sup>-1</sup>) results from different factors:<sup>334</sup> **1**) the alkoxy group in *p*-position, **2**) the four alkyl substituents on the phenolic ring, **3**) the molecular rigidity imposed by the pyran structure. Consequently,  $\alpha$ -tocopherol **11** is expected to be the most powerful tocopherol.

▪ *Derivatives of hydroxybenzoic and hydroxycinnamic acids*

Phenolic acids are another important class of antioxidants ubiquitous in plant food (*i.e.* fruit, vegetable, coffee).<sup>337</sup> There are simple phenolic acids including derivatives of hydroxybenzoic (**Fig. 3.13, Table 3.6**) and hydroxycinnamic (**Fig. 3.15, Table 3.7**) acids.

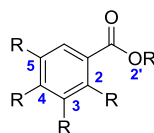
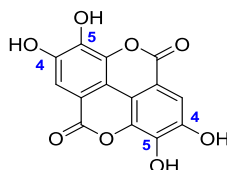


Figure 3.13: Chemical structure of hydroxybenzoic acid derivatives

N°	R <sub>2</sub>	R <sub>3</sub>	R <sub>4</sub>	R <sub>5</sub>	R <sub>2</sub> '	BDE (kcal.mol <sup>-1</sup> )
<b>15</b>	H	OH	OH	OH	H	70.2 (72.2 <sup>323</sup> )
<b>16</b>	H	OH	OH	H	H	75.5 (79.6 <sup>331</sup> )
<b>17</b>	H	OCH <sub>3</sub>	OH	OCH <sub>3</sub>	H	78.1 (82.7 <sup>338</sup> )
<b>18</b>	H	OH	OH	OC(O)-	-C <sub>6</sub> H(OH) <sub>2</sub>	78.4 (77.1 <sup>339</sup> )
<b>19</b>	OH	H	H	OH	H	79.5 (80.0 <sup>339</sup> )
<b>21</b>	H	OCH <sub>3</sub>	OH	H	H	83.1 (87.0 <sup>338</sup> )
<b>22</b>	H	H	OH	H	H	84.7 (89.2 <sup>331</sup> )
<b>21</b>	OH	H	H	H	H	95.2 (93.0 <sup>331</sup> )

Table 3.6: BDEs of hydroxybenzoic acid derivatives

**Table 3.6** shows that the hydroxybenzoic acid derivative with the lowest BDE is gallic acid **15** (70.2 kcal.mol<sup>-1</sup>). As for 5-tertbutylpyrogallol **1** and propyl gallate **4**, the low BDE is obtained thanks to the two *ortho*-hydroxyl groups on the phenolic ring. Except for gallic acid **15**, derivatives of hydroxybenzoic acids have highest BDEs (BDE > 75 kcal.mol<sup>-1</sup>). Indeed, they just have one *ortho*-hydroxyl or *ortho*-methoxy group. A substitution by two *ortho*-hydroxyl groups (gallic acid, **15**) allows a much stronger decrease of BDE than a substitution by two *ortho*-methoxy groups (syringic acid, **17**), which have BDEs of 70.2 and 78.1 kcal.mol<sup>-1</sup> respectively. Ellagic acid **18** (**Fig. 3.14**), which is a particular combination of two molecules of gallic acid, has a relatively high BDE (78.4 kcal.mol<sup>-1</sup>).

Figure 3.14: Chemical structure of ellagic acid (**18**)

Moreover, as discussed in the substituent effect part, the *ortho*-carboxyl group (salicylic acid, **22**) drastically increases the BDE value and, thereby, decreases the antioxidant power.

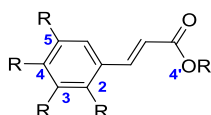


Figure 3.15: Chemical structure of hydroxycinnamic acid derivatives

N°	R <sub>2</sub>	R <sub>3</sub>	R <sub>4</sub>	R <sub>5</sub>	R <sub>4'</sub>	BDE (kcal.mol <sup>-1</sup> )
<b>23</b>	H	OH	OH	H	C <sub>9</sub> O <sub>4</sub> H <sub>10</sub>	69.2 (75.3 <sup>338</sup> )
<b>24</b>	H	OH	OH	H	H	72.1 (73.6 <sup>323</sup> )
<b>25</b>	H	OH	OH	H	C <sub>6</sub> H <sub>2</sub> (OH) <sub>3</sub> CO <sub>2</sub> H	73.4 (78.7 <sup>340</sup> )
<b>26</b>	H	OCH <sub>3</sub>	OH	OCH <sub>3</sub>	H	75.4 (81.2 <sup>284</sup> )
<b>27</b>	H	OCH <sub>3</sub>	OH	H	H	79.7 (84.5 <sup>331</sup> )
<b>28</b>	OH	H	H	H	H	80.1 (84.4 <sup>331</sup> )
<b>29</b>	H	H	OH	H	H	80.5 (84.9 <sup>331</sup> )
<b>30</b>	H	OH	H	H	H	84.4 (88.1 <sup>341</sup> )

Table 3.7: BDEs of hydroxycinnamic acid derivatives

Furthermore, the hydroxycinnamic acid with the lowest BDE is rosmarinic acid **23** (Fig. 3.16, 69.2 kcal.mol<sup>-1</sup>). The phenolic site (4) involved for the lowest BDE corresponds to better delocalization of the unpaired electron thanks to the conjugated double bond.

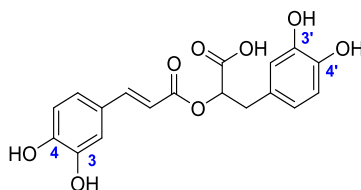


Figure 3.16: Chemical structure of rosmarinic acid (**23**)

It is then followed by caffeic acid **24** (72.1 kcal.mol<sup>-1</sup>), chlorogenic acid **25** (73.4 kcal.mol<sup>-1</sup>) and sinapic acid **26** (75.4 kcal.mol<sup>-1</sup>) acids. Thanks to a better delocalization of the unpaired electron for the phenolic radical, hydroxycinnamic acids have lower BDE than hydroxybenzoic acids. As an example, caffeic acid **24** (72.1 kcal.mol<sup>-1</sup>) could have a better antioxidant power compared to protocatechuic acid **16** (75.5 kcal.mol<sup>-1</sup>) (Fig. 3.17).

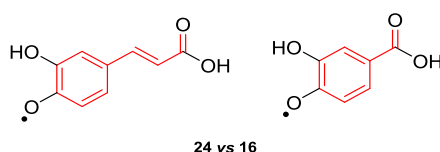


Figure 3.17: Comparison between caffeic acid **24** and protocatechuic acid **16**

#### ▪ Flavonoids

The class of flavonoids gathers more than 4000 different polyphenols found in leaves, stems, roots, fruits or seeds.<sup>342</sup> Their general chemical structure contains three rings A, B and C (Fig. 3.18).

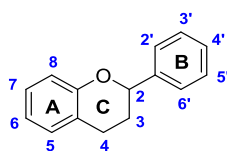


Figure 3.18: Chemical structure of flavonoids

The presence of carbonyls, double bonds and hydroxyl group on the pyranyl ring C divides the flavonoids into different subclasses called flavonols, flavones, flavanone, flavonones, isoflavone and flavanols. Substitution of A and B rings distinguishes the different phenolic antioxidant of each subclasses. The antioxidant activity of flavonoids by the way of preventive and chain-breaking mechanisms depends on various factors:<sup>342</sup> **1)** the metal-chelating potential that is strongly dependent on the arrangement of hydroxyl and carbonyl groups around the molecule, **2)** the presence of electron-donating substituents and **3)** their ability to delocalize the unpaired electron leading to the formation of stable phenoxyl radical. Moreover, it has been shown that the phenolic ring B is the most active cycle.<sup>343</sup>

Flavonols (*i.e.* gossypetin **31**, myricetin **32**, quercetin **34** and morin **41**) have the 3-hydroxyflavone backbone which includes double bond and hydroxyl group on the pyranyl ring C (**Fig. 3.19, Table 3.8**).

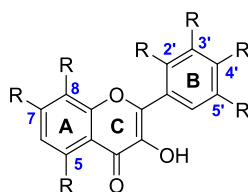


Figure 3.19: Chemical structures of flavonols

N°	R <sub>2'</sub>	R <sub>3'</sub>	R <sub>4'</sub>	R' <sub>5</sub>	R <sub>5</sub>	R <sub>7</sub>	R <sub>8</sub>	BDE (kcal.mol <sup>-1</sup> )
<b>31</b>	H	OH	OH	H	OH	OH	OH	66.6 (65.5 <sup>325</sup> )
<b>32</b>	H	OH	OH	OH	OH	OH	H	67.4 (71.1 <sup>344</sup> )
<b>33</b>	H	OH	OH	H	OCH <sub>3</sub>	OH	H	71.1 (66.1 <sup>325</sup> )
<b>34</b>	H	OH	OH	H	OH	OH	H	71.8 (72.3 <sup>323</sup> )
<b>35</b>	H	H	OH	OH	H	OH	H	72.3 (70.3 <sup>344</sup> )
<b>36</b>	H	OCH <sub>3</sub>	OH	OH	OH	OH	H	72.5 (66.9 <sup>325</sup> )
<b>37</b>	H	OCH <sub>3</sub>	OH	OCH <sub>3</sub>	OH	OH	H	75.7 (63.8 <sup>325</sup> )
<b>38</b>	H	OCH <sub>3</sub>	OH	H	OH	OCH <sub>3</sub>	H	79.6 (65.2 <sup>325</sup> )
<b>39</b>	H	H	OCH <sub>3</sub>	H	OH	OH	H	79.8 (73.8 <sup>325</sup> )
<b>40</b>	H	OCH <sub>3</sub>	OH	H	OH	OH	H	79.8 (72.9 <sup>325</sup> )
<b>41</b>	OH	H	OH	H	OH	OH	H	79.8 (76.9 <sup>344</sup> )
<b>42</b>	H	H	OH	H	OH	OH	H	80.1 (80.9 <sup>323</sup> )
<b>43</b>	H	H	H	H	OH	OH	H	81.2 (76.0 <sup>344</sup> )

Table 3.8: BDEs of flavonols

The flavonol with the lowest BDE is gossypetin **31** (66.6 kcal.mol<sup>-1</sup>). As regards to its low BDE, it should be the most powerful flavonoid but it is difficult to test it because of its high price (600 € / 50 mg in 2016 from extrasynthese). The phenolic site involved is situated on the ring A as also demonstrated by Pérez-González *et al.*<sup>325</sup> Except gossypetin **31**, the O-H group (R<sub>4'</sub> position) on the B ring is always the most reactive site. However, flavonoids without this hydroxyl group (R<sub>4'</sub> position) are exceptions to this rule. As examples, kaempferide (**39**) and galangin (**43**) have their most hydroxyl reactive site on the ring C (C<sub>3</sub> position). Gossypetin **31** is followed by myricetin **32** (67.4 kcal.mol<sup>-1</sup>) and quercetin **34** (71.8 kcal.mol<sup>-1</sup>). Because of a *tri*-hydroxyl structure, myricetin **33** is one of the most reactive flavonol.

Flavones such as luteolin **44** and apigenin **45** are mainly found in cereals and herbs. They have the same chemical structure as flavonols without the hydroxyl group on the pyranil ring C (**Fig. 3.20**, **Table 3.9**).

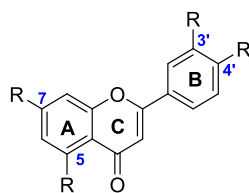


Figure 3.20: Chemical structure of flavones

N°	R <sub>3'</sub>	R <sub>4'</sub>	R <sub>5</sub>	R <sub>7</sub>	BDE (kcal.mol <sup>-1</sup> )
<b>44</b>	OH	OH	OH	OH	73.1 (74.5 <sup>323</sup> )
<b>45</b>	H	OH	OH	OH	82.1 (82.9 <sup>323</sup> )

Table 3.9: BDEs of flavones

Flavones exhibit higher BDEs than flavonols. Indeed, luteolin **44** (73.1 kcal.mol<sup>-1</sup>) and apigenin **45** (82.1 kcal.mol<sup>-1</sup>) have higher BDE than quercetin **34** (71.8 kcal.mol<sup>-1</sup>) and kaempferol **42** (80.1 kcal.mol<sup>-1</sup>) respectively (**Fig. 3.21**). This is due to the absence of OH group in the C ring. BDEs of O-H group for flavones in site R<sub>4'</sub> are about 2 kcal.mol<sup>-1</sup> higher than for flavonols. Therefore, with equivalent substituents, flavones should be less reactive than flavonols through the HAT mechanism.

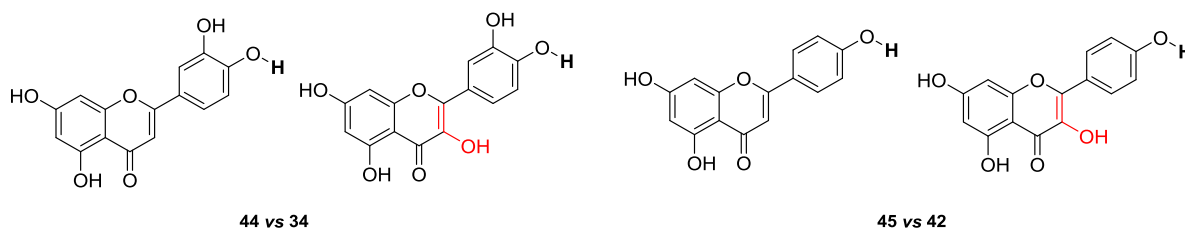


Figure 3.21: Comparison between flavones (**44** and **45**) with flavonols (**34** and **42**)

2,3-Dihydroflavonols (*i.e.* taxifolin **46** and aromadedrin **47**) and flavanones (*i.e.* eriodictyol **48**, homoeriodictyol **49**, hesperetin **50** and naringenin **51**) are other classes of flavonoids. (**Fig. 3.22**, **Table 3.10**) are studied. They have the same chemical structure as flavonols but without the double bond on the pyranil ring C. Taxifolin **46** (73.2 kcal.mol<sup>-1</sup>) has a lower BDE than aromadedrin **47** (82.3 kcal.mol<sup>-1</sup>). Flavanones do not have double bond and hydroxyl group on the pyranil site C. The flavanone with the lowest BDE is eriodictyol **48** (73.6 kcal.mol<sup>-1</sup>).

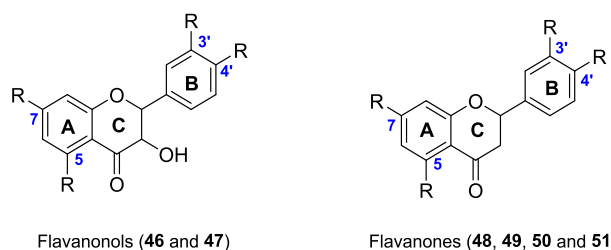


Figure 3.22: Chemical structure of 2,3-dihydroxyflavonols (**46** and **47**) and flavanones (**48**, **49**, **50** and **51**)

N°	R <sub>3'</sub>	R <sub>4'</sub>	R <sub>5</sub>	R <sub>7</sub>	BDE (kcal.mol <sup>-1</sup> )
<b>2,3-Dihydroxyflavonols</b>					
<b>46</b>	OH	OH	OH	OH	73.2 (74.7 <sup>323</sup> )
<b>47</b>	H	OH	OH	OH	82.3 (75.7 <sup>325</sup> )
<b>Flavanones</b>					
<b>48</b>	OH	OH	OH	OH	73.6 (73.6 <sup>344</sup> )
<b>49</b>	OCH <sub>3</sub>	OH	OH	OH	80.8 (75.1 <sup>325</sup> )
<b>50</b>	OH	OCH <sub>3</sub>	OH	OH	82.2 (77.4 <sup>344</sup> )
<b>51</b>	H	OH	OH	OH	82.4 (81.4 <sup>344</sup> )

Table 3.10: BDEs of 2,3-dihydroxyflavonols (46, 47) and flavanones (48, 49, 50, 51)

As for flavones, the lowest BDE corresponds to the OH on the site R<sub>4'</sub>. In addition, the presence of a second OH group at the B ring decreases BDE from 82.3 (**47**) to 73.2 (**46**) kcal.mol<sup>-1</sup>. 2,3-Dihydroxyflavonols have higher BDEs than flavonols by comparing taxifolin **46** (73.2 kcal.mol<sup>-1</sup>) with quercetin **34** (71.8 kcal.mol<sup>-1</sup>) and kaempferol **42** (80.1 kcal.mol<sup>-1</sup>) with aromadedrin **47** (82.3 kcal.mol<sup>-1</sup>) (Fig. 3.23). BDEs of O-H group for 2,3-dihydroxyflavonols in site R<sub>4'</sub> are about 2 kcal.mol<sup>-1</sup> higher than for flavonols.

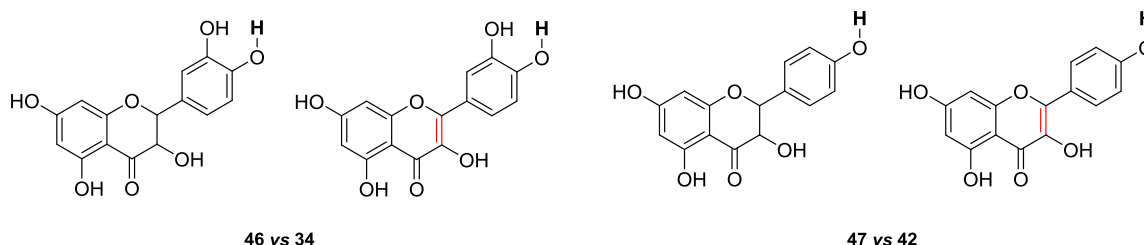


Figure 3.23: Comparison between 2,3-dihydroxyflavonols (46 and 47) and flavonols (34 and 42)

Flavanones have higher BDEs than flavonols by comparing eriodictyol **48** (73.6 kcal.mol<sup>-1</sup>) and quercetin **34** (71.8 kcal.mol<sup>-1</sup>) (Fig. 3.24). BDEs of the O-H group in site R<sub>4'</sub> is also about 2 kcal.mol<sup>-1</sup> higher than for flavonols. That is a logical finding since the conjugation is broken due to the single bond. Therefore, the major effects are due to the neighboring groups.

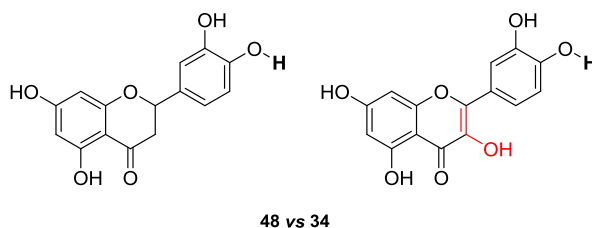


Figure 3.24: Comparison between flavanones (48) and flavonols (34)

Isoflavones (*i.e.* glycetin **52**, genistein **53** and daidzein **54**) are also studied (Fig. 3.25, Table 3.11). They are similar with flavones except that the B ring is bound to the C<sub>3</sub> position instead of the C<sub>2</sub>. The three isoflavones studied have almost the same BDE (81.0 kcal.mol<sup>-1</sup>). The OH group involved is located on the carbon C<sub>4'</sub>.

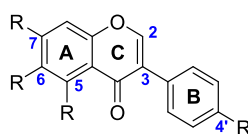


Figure 3.25: Chemical structure of isoflavones

N°	R <sub>4'</sub>	R <sub>5</sub>	R <sub>6</sub>	R <sub>7</sub>	BDE (kcal.mol <sup>-1</sup> )
52	OH	H	OCH <sub>3</sub>	OH	80.1 (78.0 <sup>344</sup> )
53	OH	OH	H	OH	81.0 (78.0 <sup>344</sup> )
54	OH	H	H	OH	81.9 (78.3 <sup>344</sup> )

Table 3.11: BDEs of isoflavones

BDEs of isoflavones studied are close to that of apigenin **45** (82.1 kcal.mol<sup>-1</sup>) suggesting that the location of the ring B does not alter the hydrogen transfer. Therefore, the antioxidant power of flavones and isoflavone should be similar when they have the same number of hydroxyl groups on the ring B.

Finally, the last class of flavonoid studied is catechins also called flavanols (Fig. 3.26, Table 3.12) which are abundant in tea (*i.e.* epigallocatechin gallate **55**, gallic catechin **56** and catechin **57**).

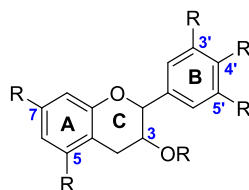


Figure 3.26: Chemical structure of catechins

N°	R <sub>3'</sub>	R <sub>4'</sub>	R <sub>5'</sub>	R <sub>3</sub>	R <sub>5</sub>	R <sub>7</sub>	BDE (kcal.mol <sup>-1</sup> )
55	OH	OH	OH	C(O)C <sub>6</sub> H <sub>2</sub> (OH) <sub>3</sub>	OH	OH	66.5 (69.0 <sup>344</sup> )
56	OH	OH	OH	H	OH	OH	68.5 (63.7 <sup>325</sup> )
57	OH	OH	H	H	OH	OH	74.4 (74.2 <sup>323</sup> )

Table 3.12: BDEs of catechins

Table 3.12 points out that the two catechins with the lowest BDE have a *tri*-hydroxyl structure, namely epigallocatechin gallate **55** (66.5 kcal.mol<sup>-1</sup>) and gallic catechin **56** (68.6 kcal.mol<sup>-1</sup>).

The detailed study of the flavonoid family highlights the crucial importance of the *tri*-hydroxyl structure to decrease BDEs. As a consequence, flavonols (*i.e.* myricetin **32**) and catechins (*i.e.* epigallocatechin gallate **55** and gallic catechin **56**) seem to be the most promising antioxidants if we refer to their low BDEs.

- *Tri*-hydroxy antioxidants

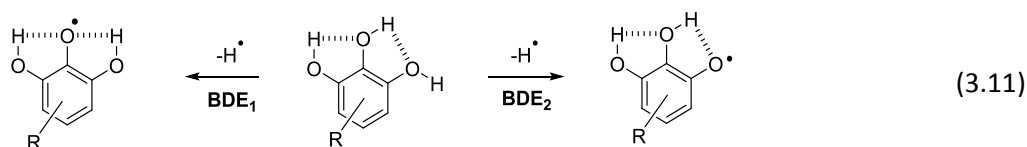
The position of the 3 OH groups on the phenyl ring is an important parameter (Fig. 3.27). Table 3.13 gathers the *tri*-hydroxyl compounds studied previously. A substitution of the phenolic ring by two *ortho*-hydroxyl substituents permits to drastically decrease the value of BDE. It is the case for epigallocatechin gallate **55** (66.5 kcal.mol<sup>-1</sup>), 5-*tert*-butylpyrogallol **1** (66.6 kcal.mol<sup>-1</sup>), myricetin **32** (67.4 kcal.mol<sup>-1</sup>), pyrogallol **2** (68.0 kcal.mol<sup>-1</sup>), gallic catechin **56** (68.5 kcal.mol<sup>-1</sup>), propyl gallate **4** (69.6 kcal.mol<sup>-1</sup>) and gallic acid **15** (70.2 kcal.mol<sup>-1</sup>). In contrast, a phenol with two *meta*-hydroxyl groups (*i.e.* phloroglucinol **10**) does not lead to a decrease of BDE. Indeed, the *meta* position is very unfavorable.

Figure 3.27: Chemical structure of *tri*-hydroxy antioxidants

N°	R <sub>2</sub>	R <sub>3</sub>	R <sub>4</sub>	R <sub>5</sub>	R <sub>6</sub>	BDE (kcal.mol <sup>-1</sup> )
55	OH		C <sub>15</sub> H <sub>13</sub> O <sub>8</sub>		OH	66.5 (69.0 <sup>344</sup> )
1	OH		C(CH <sub>3</sub> ) <sub>3</sub>		OH	66.6 (nd)
32	OH		C <sub>9</sub> H <sub>5</sub> O <sub>5</sub>		OH	67.4 (71.1 <sup>344</sup> )
2	OH				OH	68.0 (77.7 <sup>331</sup> )
56	OH		C <sub>9</sub> H <sub>13</sub> O <sub>9</sub>		OH	68.5 (63.7 <sup>325</sup> )
3			OH		OH	69.1 (70.4 <sup>332</sup> )
4	OH		C(O)OC <sub>3</sub> H <sub>7</sub>		OH	69.6 (77.1 <sup>324</sup> )
15	OH		CO <sub>2</sub> H		OH	70.2 (72.2 <sup>323</sup> )
10		OH		OH		83.0 (87.7 <sup>331</sup> )

Table 3.13: BDEs of *tri*-hydroxyl antioxidants

Wright and co-workers have reported that the central phenoxyl radical stabilized by two hydrogen bonds is the more stable conformer compared to the phenol stabilized by only one intramolecular hydrogen bond (Eq. 3.11)<sup>290</sup>.



As the phenol parent is the same in both cases, BDE is lower when the phenoxyl radical is formed at the central hydroxyl group than on the side hydroxyl group (Table 3.14).

Number	Phenoxyl radical structure 1	BDE <sub>1</sub> <sup>a</sup>	Phenoxyl radical structure 2	BDE <sub>2</sub> <sup>a</sup>
1		66.6		74.1
32		67.4		76.3
4		69.6		75.7
15		70.2		76.3

Table 3.14: BDEs for 5-*tert*-butylpyrogallol (1), myricetin (32), propyl gallate (4) and gallic acid (15) taking into account the formation of hydroxyl radical at the central or on the side hydroxyl group, <sup>a</sup>BDE in kcal.mol<sup>-1</sup>

- Stilbenes

The two stilbenes studied (*i.e.* piceatannol **58** and resveratrol **59**) are natural polyphenols present in many plants such as grapes (Figure 3.28, Table 3.15).

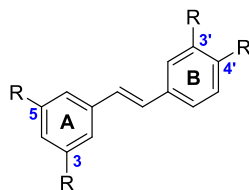


Figure 3.28: Chemical structure of stilbenes

N°	R <sub>3'</sub>	R <sub>4'</sub>	R <sub>3</sub>	R <sub>5</sub>	BDE (kcal.mol <sup>-1</sup> )
<b>58</b>	OH	OH	OH	OH	68.7 (62.9 <sup>325</sup> )
<b>59</b>	H	OH	OH	OH	76.7 (70.3 <sup>325</sup> )

Table 3.15: BDEs of stilbenes

Piceatannol **58** differs from resveratrol **59** with an OH group in site R<sub>3'</sub>, which decreases the BDE (68.7 kcal.mol<sup>-1</sup>). Given its low BDE, its antioxidant power should be excellent through a hydrogen transfer mechanism. The higher reactivity of the ring B is due to the catechol structure (OH in *ortho* position) while in ring A, the hydroxyl groups are in *meta* positions. Two-catechol moieties as presented by figure 3.29 have a better influence of BDE (67.7 kcal.mol<sup>-1</sup>) and points out this not-natural and not-commercial antioxidant as the more reactive stilbene.

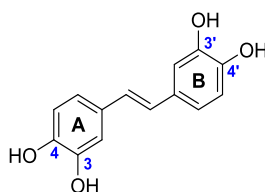


Figure 3.29: Chemical structure of the stilbene with the lowest BDE

- Eugenol and isoeugenol

Eugenol **61** is a phenol found in clove essence oil whereas isoeugenol **60** is present in ylang-ylang essential oil. Their chemical structure is presented by figure 3.30 and respective BDEs are gathered in table 3.16. Thanks to a better delocalization of the unpaired electron for the phenolic radical, isoeugenol **60** has a lower BDE than eugenol **61** of around 4 kcal.mol<sup>-1</sup>.

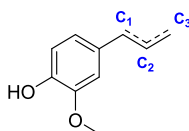


Figure 3.30: Chemical structure of isoeugenol (60) and eugenol (61)

N°	C <sub>1</sub> -C <sub>2</sub>	C <sub>2</sub> -C <sub>3</sub>	BDE (kcal.mol <sup>-1</sup> )
<b>60</b>	-CH=CH-	-CH-CH <sub>3</sub>	76.6 (83.8 <sup>334</sup> )
<b>61</b>	-CH <sub>2</sub> -CH-	-CH=CH <sub>2</sub>	80.2 (86.8 <sup>334</sup> )

Table 3.16: BDEs of isoeugenol 60 and eugenol 61

- Antioxidants in olive oil

Hydroxytyrosol **62**, catechol **63** and tyrosol **64** (Figure 3.31) are antioxidant found in olive oil.<sup>345</sup> Their BDEs are investigated (Table 3.17) and hydroxytyrosol **62** is the phenol with the lowest BDE (72.1 kcal.mol<sup>-1</sup>) followed by catechol **63** (73.4 kcal.mol<sup>-1</sup>) and tyrosol **64** (81.0 kcal.mol<sup>-1</sup>). It highlights another time the crucial role of the catechol moiety. Indeed, tyrosol **65** (81.0 kcal.mol<sup>-1</sup>), without *ortho*-hydroxyl substituent, has a high BDE.

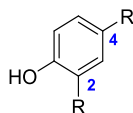


Figure 3.31: Chemical structure of antioxidants found in olive oil

N°	R <sub>2</sub>	R <sub>4</sub>	BDE (kcal.mol <sup>-1</sup> )
<b>62</b>	OH	CH <sub>2</sub> CH <sub>2</sub> OH	72.1 (73.5 <sup>323</sup> )
<b>63</b>	OH	H	73.4 (76.4 <sup>331</sup> )
<b>64</b>	H	CH <sub>2</sub> CH <sub>2</sub> OH	81.0 (87.8 <sup>324</sup> )

Table 3.17: BDEs of antioxidants found in olive oil

- Lignans

Sesamol **65** (Figure 3.32, Table 3.18) is a lignan found in sesame oil. It is a potent antioxidant and anti-inflammatory agent in various oxidative systems.<sup>346</sup> Lignans are phenylpropanoids derived from phenylalanine and include also sesamin, sesamol, sesaminol and sesamolol.<sup>164</sup> The BDE investigation is focused on sesamol **65** (75.1 kcal.mol<sup>-1</sup>).

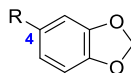


Figure 3.32: Chemical structure of lignans

N°	R <sub>4</sub>	BDE (kcal.mol <sup>-1</sup> )
<b>65</b>	OH	75.1 (80.6 <sup>284</sup> )

Table 3.18: BDEs of lignans

- Coumarins

The main coumarin called aesculetin **67** is found in tonka bean. Methyl and phenyl substituents can be grafted at the C<sub>4</sub> position but they have no impact on BDEs. Respective BDEs are gathered in table 3.19 and chemical structure is shown by figure 3.33.

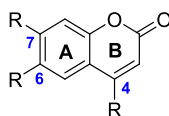


Figure 3.33: Chemical structure of coumarins

N°	R <sub>4</sub>	R <sub>6</sub>	R <sub>7</sub>	BDE (kcal.mol <sup>-1</sup> )
<b>66</b>	CH <sub>3</sub>	OH	OH	72.0 (72.1 <sup>347</sup> )
<b>67</b>	H	OH	OH	72.5 (73.1 <sup>347</sup> )
<b>68</b>	C <sub>6</sub> H <sub>5</sub>	OH	OH	72.6 (nd)

Table 3.19: BDEs of coumarins

- Carnosic acid and carnosol

Carnosol **69** and carnosic acid **70** are the two major components with rosmarinic acid **23** (already described,  $69.2 \text{ kcal}\cdot\text{mol}^{-1}$ ) of rosemary extract (*Rosmarinus officinalis* L.) and are authorized in food in the form of extract.<sup>348</sup> The chemical structure (Fig. 3.34) and BDEs (Table 3.20) are pointed out and indicates that both of them have the same BDE ( $70.8$  and  $70.7 \text{ kcal}\cdot\text{mol}^{-1}$ ).

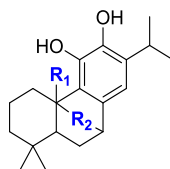


Figure 3.34: Chemical structure of carnosol (**69**) and carnosic acid (**70**)

N°	R <sub>1</sub>	R <sub>2</sub>	BDE (kcal.mol <sup>-1</sup> )
<b>69</b>	/	-C(O)O-	70.7 (nd)
<b>70</b>	-CO <sub>2</sub> H	/	70.8 (nd)

Table 3.20: BDEs of carnosol (**69**) and carnosic acid (**70**)

In order to know which substituent has a major impact on BDE, the chemical structure of carnosic acid (**H**) is decomposed into smaller molecules (Fig. 3.35).

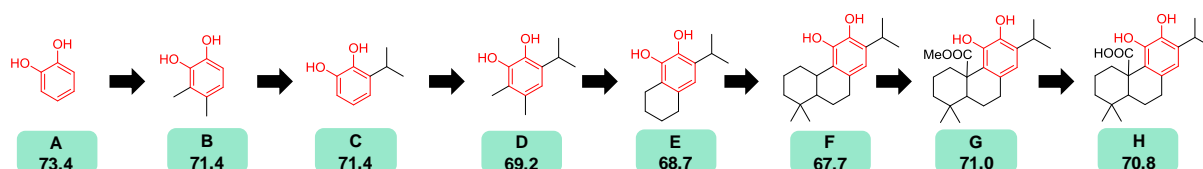


Figure 3.35: Substructure of carnosic acid (**H**) and their related BDEs calculated with B3LYP/6-311++G(2d,2p)//B3LYP/6-311G(d,p) DFT method in vacuum

The lowest BDE is attributed to the chemical structure **F**. It is constituted by all the alkyl substituents (isopropyl, methyl, cyclohexane) and *ortho*-hydroxyl group which are electron-donating groups allowing a decrease of BDE. On the contrary, the addition of methyl ester (**G**) and carboxylic (**H**) groups increase BDEs because of their electron withdrawing impact.

- Scale of reactivity

BDEs of phenols are strongly influenced by the number, nature and position of the substituents linked to the phenol ring as many times reported in the literature.<sup>280, 281, 299, 323-325, 336, 349-351</sup> Nevertheless, as the results are dependent on the method of calculation used, it is not possible to compare literature values found in various publications which are not based on the same process of calculation. As an example, the BDE of apigenin **45** was found to be  $75.6 \text{ kcal}\cdot\text{mol}^{-1}$  by Perez-Gonzalez *et al.*<sup>325</sup> and  $82.2 \text{ kcal}\cdot\text{mol}^{-1}$  by Leopoldini *et al.*<sup>323</sup> Moreover, BDE of 5-*tert*-butylpyrogallol **1**, carnosol **69** and carnosic acid **70** were not investigated by authors. Therefore, we use the B3LYP/6-311++G(2d,2p)/B3LYP/6-311G(d,p) method for the 70 phenols investigated. However, figure 3.36 shows that our theoretical results are consistent with those obtained by Leopoldini *et al.*<sup>323</sup> ( $R^2 = 0.98$ ), Li *et al.*<sup>324</sup> ( $R^2 = 0.96$ ) and Pérez-Gonzalez *et al.*<sup>325</sup> ( $R^2 = 0.97$ ) pointing out our method as a relevant way to get BDEs. Nevertheless, BDEs of some phenols (**31**, **37**, **38**, **41**, **42**, **43** and **50**) revealed by Pérez-Gonzalez *et al.* are not correlated with our results whereas the main values follow the tendency.<sup>325</sup>

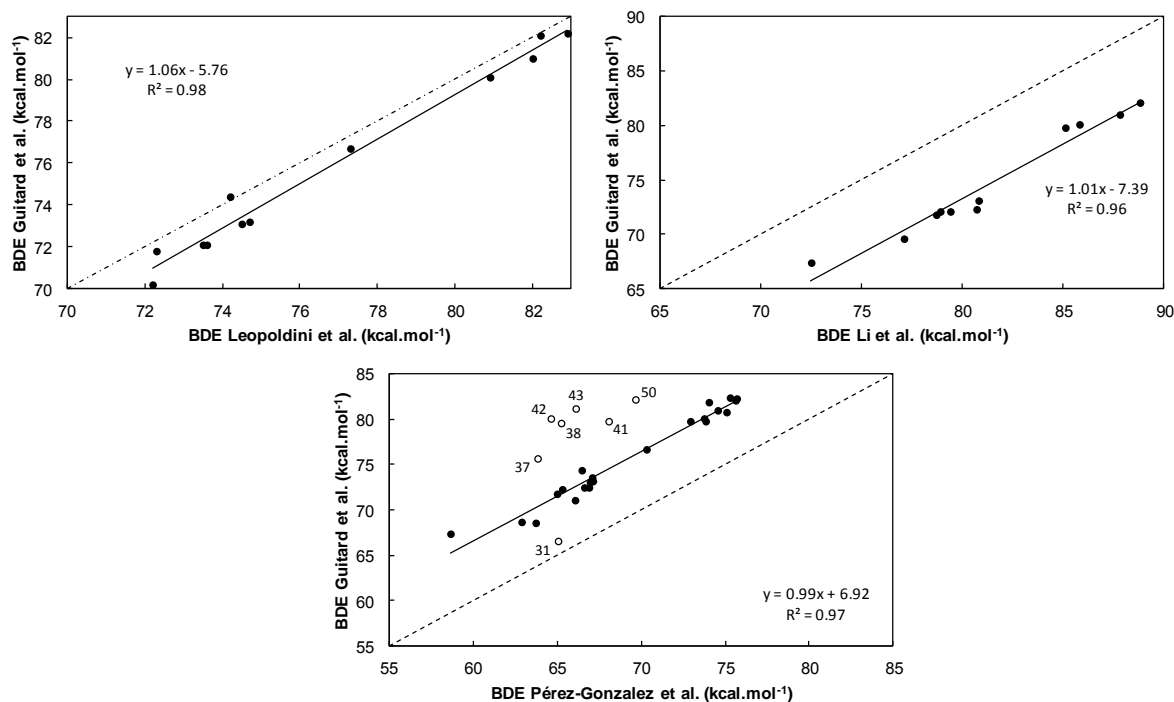


Figure 3.36: Correlations of our calculated BDEs (Guitard *et al.*) with those of Leopoldini *et al.*<sup>323</sup>, Li *et al.*<sup>324</sup> and Pérez-Gonzalez *et al.*<sup>325</sup>

Based on the BDEs of the studied phenols, a scale of predictive reactivity has been established from the lowest to the highest BDEs (**Figure 3.37**). It reveals four classes of antioxidants: **1)** antioxidants with very low BDE from 65 to 70 kcal.mol<sup>-1</sup>, **2)** antioxidants with low BDE from 70 to 75 kcal.mol<sup>-1</sup>, **3)** antioxidants with medium BDE from 75 to 80 kcal.mol<sup>-1</sup> and **4)** antioxidants with high BDE from 80 to 95 kcal.mol<sup>-1</sup>. The antioxidants with the lowest BDEs are expected to have the best antioxidant power. The phenolic sites involved for the lowest BDE are indicated in bold.

Very low BDEs have been obtained for 5-*tert*-butylpyrogallol **1**, myricetin **32**, propyl gallate **4**, gallic acid **15** and epigallocatechin gallate **55** which are pyrogallol derivatives. This class contains also  $\alpha$ -tocopherol **11** with a BDE of 69.1 kcal.mol<sup>-1</sup>. Rosmarinic acid **23**,arnosic acid **70** andarnosol **69** also exhibit a very low BDE. Indeed, they bear a catechol-type ring moiety, conjugated double bonds and alkyl substituents on the phenol rings which strongly contribute to lower the BDE.

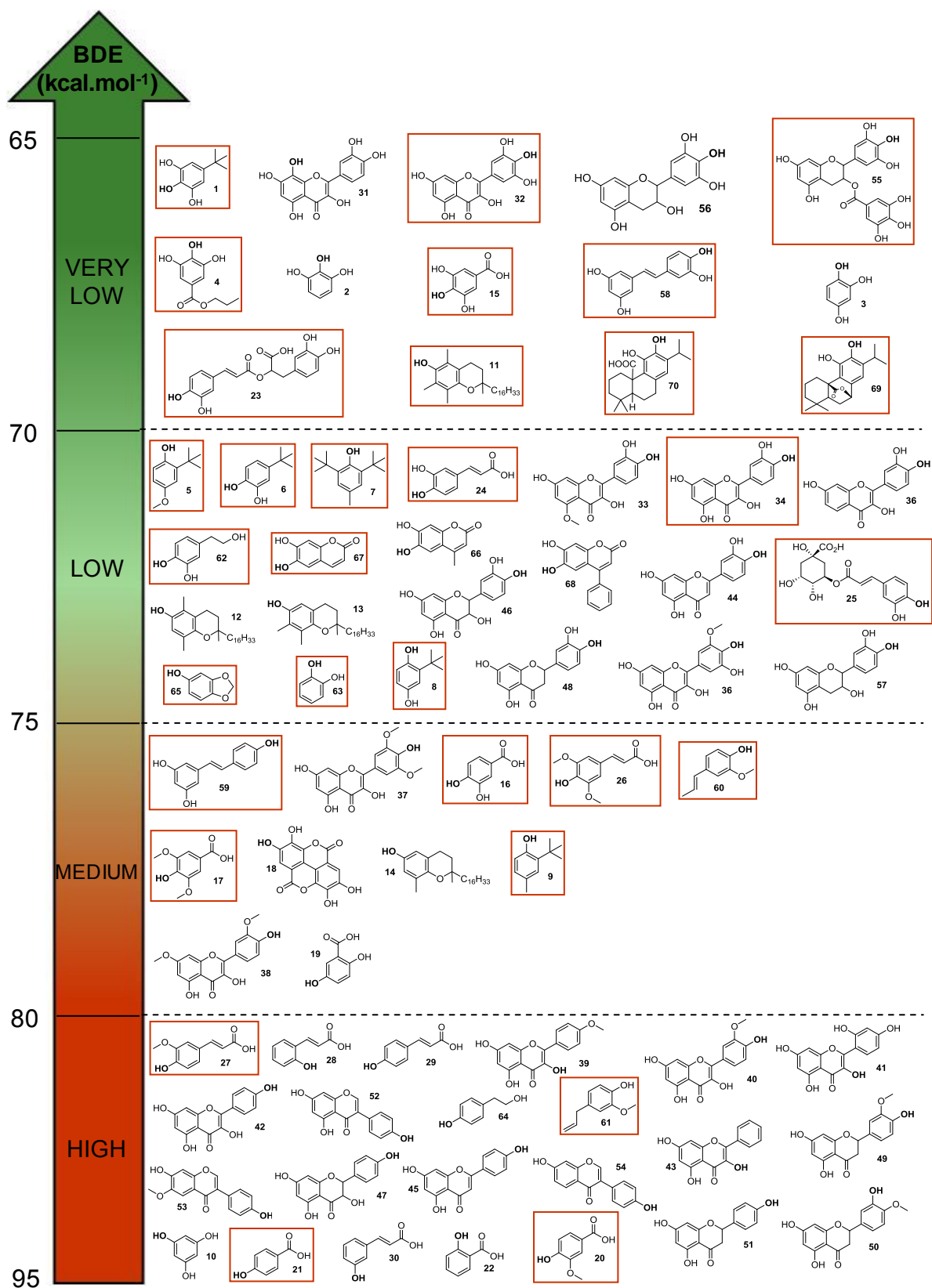


Figure 3.37: Scale of reactivity of 70 phenolic antioxidants as a function of their calculated BDE in vacuum, framed molecules correspond to selected antioxidants further studied experimentally

Then, catechol **63** itself and catechol-based derivatives with flavonol structure (*i.e.* quercetin **34**), alkyl substituent (*i.e.* 4-*tert*-butyl-catechol **6**, hydroxytyrosol **62**) and conjugated double bonds (*i.e.* caffeic acid **24** and chlorogenic acid **25**) have low BDEs. Moreover, monophenols with OCH<sub>3</sub> groups (BHA **5**), *ortho*- and *para*- alkyl substituents (BHT **7**) and substituted hydroquinone (TBHQ **8**) belong to this second class of antioxidants. Finally, there is also monophenol with dioxolane moiety (*i.e.* sesamol **65**).

The category of antioxidants with medium BDE includes catechol-based derivative with electron-withdrawing group EWG (*i.e.* protocatechuic acid **16**) and monophenols with OCH<sub>3</sub> groups (*i.e.* syringic acid **17**, isoeugenol **60**), conjugated double bond (*i.e.* resveratrol **59**) and alkyl substituents (*i.e.* *o*-*tert*-butyl-*p*-cresol **9**).

Finally, vanillic acid **20**, PHBA **21**, ferulic acid **27**, eugenol **61** and tyrosol **64** have high BDEs and are expected to be poorly reactive considering the HAT mechanism. Moreover, the simplest structure of hydroxycinnamic acid derivatives (*o*-, *p*- and *m*- coumaric acids **28**, **29** and **30**) and phloroglucinol **10** (phenol with two OH groups in *meta* position) have the highest BDEs. Vanillic acid **20**, PHBA **21** and salicylic acid **22** have a higher BDE than phenol itself (82.2 kcal.mol<sup>-1</sup>) due to the effect of electron-withdrawing group (EWG).

We conclude that a powerful antioxidant must have pyrogallol (*i.e.* gallic acid **15**, myricetin **32**, epigallocatechin gallate **55** and galocatechin **56**) or catechol moieties (*i.e.* rosmarinic acid **23**, carnosic acid **70** and carnosol **69**) conjugated with *para*-electron-donating substituents. They are the best natural alternative to  $\alpha$ -tocopherol **11** and synthetic phenolic antioxidants. Phenols above-mentioned and framed in red at **figure 3.37** are selected to represent various classes of antioxidants and evaluate their antioxidant power with experimental methods.

### 3.2.3 Solvent effects on BDEs

As antioxidants may be used in matrixes of different polarities *i.e.* hydrophobic (neat oil), hydrophilic (aqueous solutions) or mixed (emulsions), it is important to know how the polarity of the matrix influences the antioxidant power of phenols. Therefore, BDEs of phenolic antioxidants are calculated in four solvents with variable polarity: toluene, ethyl acetate, ethanol and water. The DFT method models a solvation sphere around the studied compound which depends on a lot of parameters characteristic of each solvent. They are ranged as a function of their dielectric constant ( $\epsilon$ ) and BDEs are indicated in **table 3.21**.

N°	Name	$\epsilon$	BDE (kcal.mol <sup>-1</sup> )				
			Vacuum /	Toluene 2.4	Ethyl acetate 6.0	Ethanol 24.3	Water 78.5
<b>1</b>	<b>5-Tert-butyl-pyrogallol</b>		66.6	66.9	69.5	71.4	71.8
<b>4</b>	<b>Propyl gallate</b>		72.3	72.6	75.0	75.8	76.1
<b>5</b>	<b>BHA</b>		72.3	73.0	74.0	72.5	72.8
<b>6</b>	<b>4-Tert-butylcatechol</b>		72.3	72.6	75.0	75.8	76.1
<b>7</b>	<b>BHT</b>		72.4	72.4	72.3	73.9	74.9
<b>8</b>	<b>TBHQ</b>		74.3	74.9	75.2	75.2	75.5
<b>9</b>	<b><i>o</i>-Tert-butyl-<i>p</i>-cresol</b>		77.4	78.1	76.5	77.4	77.7
<b>15</b>	<b>Gallic acid</b>		70.2	69.8	73.6	75.8	76.2
<b>16</b>	<b>Protocatechuic acid</b>		75.5	75.0	79.2	80.2	80.5
<b>17</b>	<b>Syringic acid</b>		78.1	78.8	79.2	79.3	79.6

N°	Name	ε	BDE (kcal.mol <sup>-1</sup> )				
			Vacuum /	Toluene 2.4	Ethyl acetate 6.0	Ethanol 24.3	Water 78.5
20	Vanillic acid		83.1	83.9	78.6	82.2	82.2
24	Caffeic acid		72.1	72.4	75.3	76.4	76.5
26	Sinapic acid		75.4	74.8	81.2	76.3	76.6
27	Ferulic acid		79.7	80.2	78.9	78.5	78.4
60	Isoeugenol		76.6	75.7	75.3	74.1	74.4
61	Eugenol		80.2	79.6	78.7	77.9	77.8
63	Catechol		73.4	73.5	76.2	76.9	77.3
62	Hydroxytyrosol		72.1	71.6	75.2	75.6	75.9
67	Aesculetin		72.5	73.4	77.0	78.3	78.8

Table 3.21: BDEs of various phenols calculated with B3LYP/6-311++G(2d,2p)//B3LYP/6-311G(d,p) DFT method in vacuum, toluene, ethyl acetate, ethanol and water

Figure 3.38A shows that BDEs calculated in vacuum and toluene are correlated ( $R^2 = 0.95$ ), which specify that a hydrocarbon solvent does not alter the intramolecular hydrogen bonding involved in phenol and phenoxyl radical. On the other hand, values obtained in ethanol and water are also very well correlated ( $R^2 = 1.00$ ) as illustrated in figure 3.38B. This is somewhat surprising since those solvents have very different dielectric constant. It is probable that the DFT calculation, by creating a solvation sphere, does not make the difference between ethanol and water.

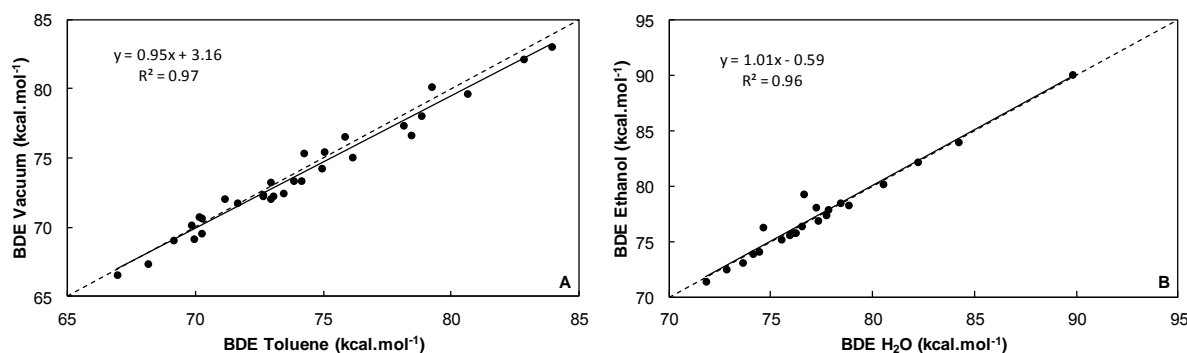


Figure 3.38: Correlation of BDEs of phenols calculated with DFT method A) in vacuum with toluene and B) in ethanol with water

As expected, the correlation between BDEs calculated in vacuum and water (Fig. 3.39) is poor except for phenols substituted by *ortho*-alkyl groups (■5, 7, 8, 9,  $R^2 = 0.96$ ). Actually, the intramolecular hydrogen bonding occurring in a non-polar environment is disrupted in water in favor of intermolecular H-bonding.

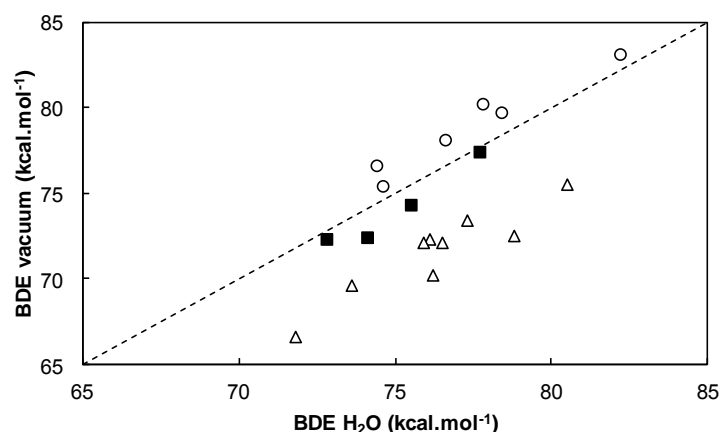


Figure 3.39: Correlation of BDEs for phenols (■ *ortho*-alkylphenols 5, 7, 8, 9, ○ *ortho*-methoxyphenols 17, 20, 26, 27, 60, 61 and △ *ortho*-hydroxyphenols 1, 4, 6, 15, 16, 24, 62,

On one hand, BDEs in polar solvent ( $H_2O$ ) for *ortho*-methoxyphenols (○, 17, 20, 26, 27, 60 and 61) are lower than in vacuum. Therefore, intramolecular interactions in water are involved in the increase of hydrogen availability. Figure 3.40 points out a model where water could be linked with the phenolic hydrogen and also with the *ortho*-methoxy substituent. This implies a decrease of the intramolecular hydrogen bonding and the phenolic hydrogen is more available leading to a decrease of BDEs.

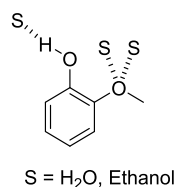


Figure 3.40: Supposed conformer for the *ortho*-methoxyphenols in water<sup>311</sup>

On the other hand, BDEs for *ortho*-hydroxyphenols (△, 1, 4, 6, 15, 16, 24, 62, 63 and 67) are higher in water than in vacuum. This is the result of a stronger stabilization of the parent molecule making the hydrogen abstraction more difficult (Fig. 3.41). Indeed, the energy required to break the OH bond is higher in water than in vacuum and BDEs increases. This phenomena was already been reported by Bakalbassis *et al.* by DFT calculation of BDE for catechol in water, benzene and vacuum.<sup>307</sup>

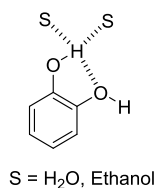


Figure 3.41: Supposed conformer for the *ortho*-hydroxyphenols in water<sup>311</sup>

Figure 3.42 shows the correlation between BDEs calculated in Hydrogen Bond Acceptor (HBA) solvent (ethyl acetate) and in apolar matrix (vacuum). BDEs of *ortho*-alkyl (■, 5, 7, 8 and 9) and *ortho*-methoxy (○, 17, 20, 26, 27, 60 and 61) phenols seem to be not influenced by the polarity of ethyl acetate. Among the alkyl monophenols, BDEs of *ortho*-*di*-substituted (BHT, 7) and *ortho*-*para*-*di*-substituted (*o*-*tert*-butyl-*p*-cresol 9) phenols are not be changed. Therefore, the steric hindrance of phenolic function decreases interactions with solvent. Nevertheless, BDEs of *ortho*-hydroxyphenols

( $\Delta$ , **1**, **4**, **6**, **15**, **16**, **24**, **62**, **63** and **67**) are higher in ethyl acetate. The solvent is linked to the phenolic hydrogen which drastically stabilizes the phenol and increase BDEs.

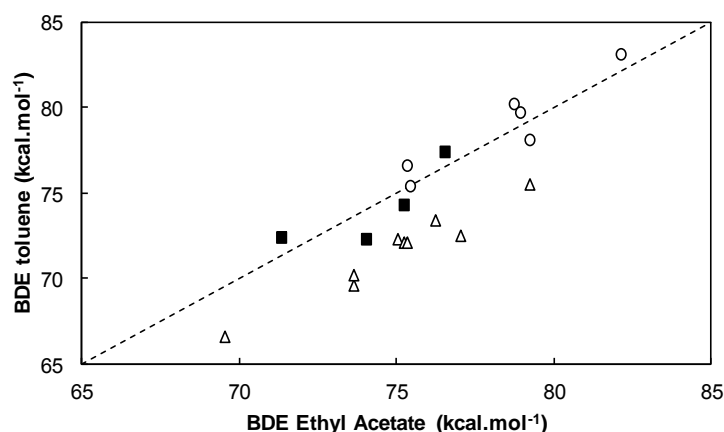


Figure 3.42: Correlation of BDEs for phenols (■ *ortho*-alkylphenols **5**, **7**, **8**, **9**, ○ *ortho*-methoxyphenols **17**, **20**, **26**, **27**, **60**, **61** and  $\Delta$  *ortho*-hydroxyphenols **1**, **4**, **6**, **15**, **16**, **24**, **62**, **63**, **67**) calculated with DFT method in vacuum and ethyl acetate

However, Korth *et al.* obtained opposing effects and showed that BDE of guaiacol (*ortho*-methoxyphenol) calculated in ethyl acetate is higher than in benzene.<sup>311, 352</sup> This increase is related to the interaction with the solvent (ethyl acetate) which is in favor of the conformer D (Fig. 3.43). Experimentally, they pointed out that guaiacol is mostly obtained as its D form (85 %) and also as its C form (14%). The hydrogen is drastically stabilized and becomes very few available to a transfer of hydrogen which is related to an increase of the BDE.

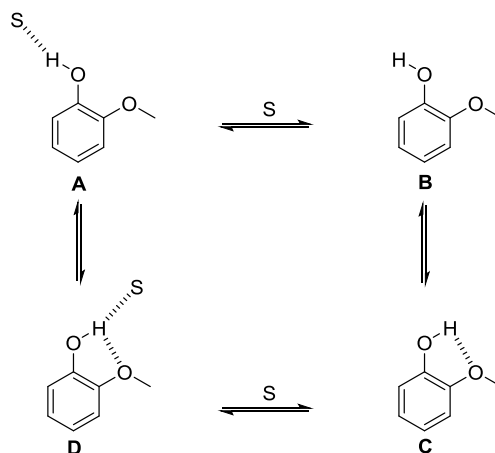


Figure 3.43: Supposed conformer for guaiacol (*ortho*-methoxyphenol) in ethyl acetate<sup>311, 352</sup>

Gaussian software models a solvation sphere around the studied compound but intermolecular hydrogen bondings are not taking into account and need to be forced by adding molecules of solvent. With the solvation sphere, phenol itself gets a BDE of 84.0 kcal.mol<sup>-1</sup> in ethanol whereas, with the modeling of one molecule of solvent, BDE rises to 85.3 kcal.mol<sup>-1</sup>. The addition of more molecules of solvent could be more representative to reality. Nevertheless, the study of polyphenols possessing numerous intermolecular hydrogen bonding sites is time-consuming.

Moreover, the structural configuration of phenols has a crucial impact on the stabilization with solvents. Indeed, various conformers of phenols are obtained when they are solubilized and each of them impacts BDEs. Nevertheless, GAUSSIAN software works only with 1 geometry of phenols. Therefore, it is primordial to know the different forms of phenols with their relative predominance. COSMOconf could be a great way to get all the possible conformers in vacuum. Then, COSMO-RS

puts all these conformers in the solvent of study, taking into account the intramolecular hydrogen bondings leading to the percentage of occurrence for each conformer. As an example, Gaussian gives one conformer whereas COSMOconf reveals 4 different possible conformers in vacuum for gallic acid (Fig. 3.44).

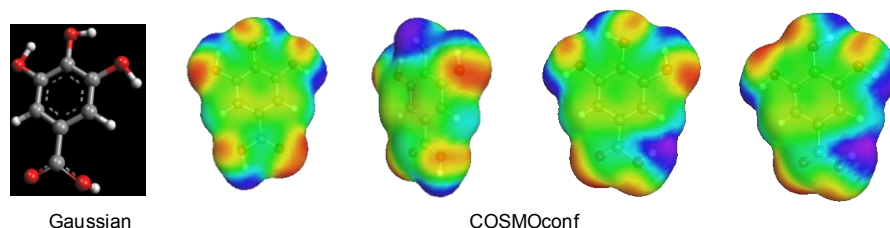


Figure 3.44: Comparison of conformers obtained by Gaussian (1) and COSMOconf (4) software

Consequently, the combination of COSMOconf, COSMO-RS and GAUSSIAN software could be a great alternative to calculate accurate BDEs of polyphenols in various solvents. Nevertheless, this part was not investigated during this thesis because of time but it could be part of another project.

### 3.2.4 Ionization Potential (IP) and stability of phenols

As described previously, the ionization potential (IP) is not relevant to discuss about the efficiency of phenols as antioxidants because the SET-PT mechanism was eliminated by experimental data.<sup>290</sup> However, IP is a good descriptor to predict the stability of phenols against oxygen. Indeed, the lower the IP is, the more the phenol could react with oxygen to the detriment of its antioxidant power. Consequently, a highly effective antioxidant should have a low BDE and conversely a high IP. As an example, Witjman et al. calculated a BDE of 74.8 kcal.mol<sup>-1</sup> and an IP of 159.3 kcal.mol<sup>-1</sup> for  $\alpha$ -tocopherol.<sup>346</sup> Ionization potentials of various natural and synthetic phenols have been calculated by the B3LYP/6-311++G(2d,2p)//B3LYP/6-311G(d,p) DFT method in various solvents (Table 3.22) following equations 3.9 and 3.11 already described.



$$\text{IP}(\text{ArO} - \text{H}) = H_f^{\circ}(\text{ArO} - \text{H}^{\bullet+}) - H_f^{\circ}(\text{ArO} - \text{H}) \quad (3.11)$$

N°	Name	$\epsilon$	IP (kcal.mol <sup>-1</sup> )			
			Vacuum /	Toluene 2.4	Ethanol 24.3	Water 78.5
1	5-tert-butyl-pyrogallol	178.7	178.4	134.2	132.3	
4	Propyl gallate	189.6	188.1	153.3	151.2	
5	BHA	168.5	167.9	138.5	137.7	
6	4-tert-butylcatechol	182.4	182.5	133.4	133.4	
7	BHT	173.4	171.9	137.8	136.2	
8	TBHQ	176.3	176.9	129.6	128.7	
9	o-tert-butyl-p-cresol	185.9	185.2	135.7	135.7	
11	$\alpha$ -tocopherol	160.3	162.4	nd	nd	
15	Gallic acid	194.4	195.8	143.8	141.6	
16	Protocatechuic acid	195.1	196.7	144.1	142.0	
17	Syringic acid	188.2	187.5	145.6	145.6	
20	Vanillic acid	190.0	189.4	145.0	143.9	
23	Rosmarinic acid	174.4	173.4	137.4	135.1	
24	Caffeic acid	183.0	183.3	136.5	134.7	
26	Sinapic acid	177.6	176.6	135.8	135.5	

N°	Name	$\epsilon$	IP (kcal.mol <sup>-1</sup> )			
			Vacuum	Toluene	Ethanol	Water
			/	2.4	24.3	78.5
27	Ferulic acid		179.1	179.9	137.0	134.5
32	Myricetin		182.6	183.9	130.6	129.2
34	Quercetin		181.8	183.6	131.1	129.4
60	Isoeugenol		166.6	165.4	127.4	125.9
61	Eugenol		176.9	180.8	136.6	133.8
62	Hydroxytyrosol		182.6	183.7	134.8	133.1
63	Catechol		188.1	188.8	137.4	134.6
67	Aesculetin		184.6	184.0	139.5	136.6
69	Carnosol		180.9	180.2	nd	nd
70	Carnosic acid		181.4	183.6	nd	nd

Table 3.22: IPs calculated with B3LYP/6-311++G(2d,2p)//B3LYP/6-311G(d,p) DFT method in vacuum, toluene, ethanol and water of various phenols

As BDEs and IPs of phenolic antioxidants represent important features, it is particularly useful to correlate these two thermodynamic parameters. Klein and co-workers have already published the correlation between these two crucial parameters making the difference between *para* and *meta* substitutions.<sup>299</sup> Moreover, they obtained two different linear dependence for anilines and phenols.<sup>298</sup>

As for correlations of BDEs in vacuum and toluene and in ethanol and water, there are great correlations of IPs with 0.98 and 0.99 correlation coefficients respectively (Fig. 3.45). Therefore, a hydrocarbon solvent does not alter the intermolecular interactions involved in the phenol as for BDEs. Moreover, values obtained in ethanol and water are also very well correlated which is surprising because the two solvents have not the same dielectric constant.

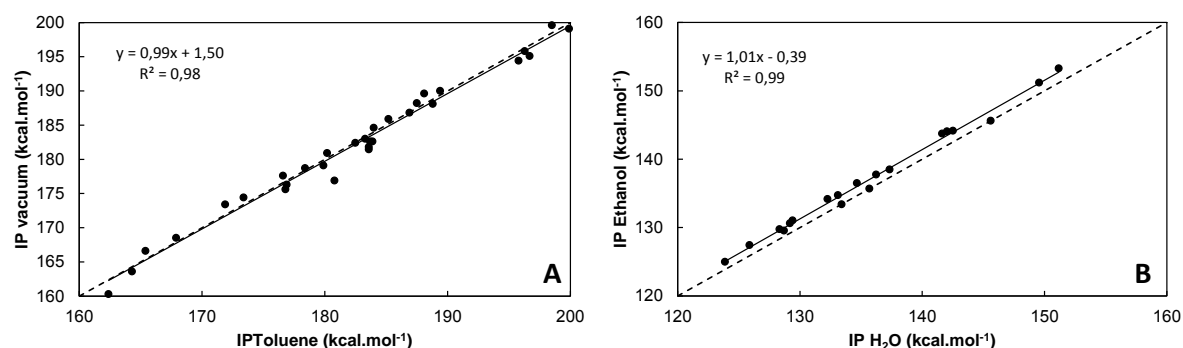
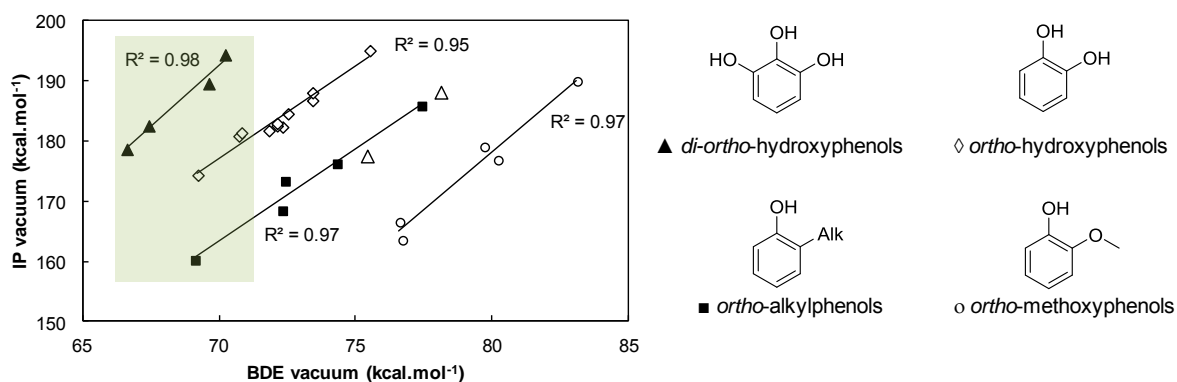


Figure 3.45: Correlations of IPs of phenols calculated with DFT method A) in vacuum with toluene and B) in ethanol with water

Most interestingly, our calculations highlight also some linear correlations between BDEs and IPs determined in vacuum for various families of phenols (Fig. 3.46). As expected, in all four series the drop in the IP values accompanies a drop in BDEs. This is unfavorable for the antioxidant effectiveness. Optimal substituent should simultaneously cause the decrease in BDE and the increase in IP which express a reasonable air-stability. Zhang *et al.* attributed also the same correlation of BDEs and IPs for catechol compounds.<sup>289</sup>



**Figure 3.46:** Correlations of IPs and BDEs of phenols ( $\blacktriangle$  *di-ortho-hydroxyphenols*,  $\diamond$  *ortho-hydroxyphenols*,  $\blacksquare$  *ortho-alkylphenols*,  $\circ$  *ortho-methoxyphenols*, and  $\triangle$  *di-ortho-methoxyphenols*) calculated with DFT method in vacuum, green zone points out the most promising phenols

*Di-ortho-hydroxyl* ( $\blacktriangle$ , **1**, **4**, **15** and **32**) and *ortho-hydroxyl* ( $\diamond$ , **6**, **16**, **23**, **24**, **34**, **62**, **63** and **67**) substituents lead to a strong decrease of BDEs with a simultaneous low decrease of IPs which is favorable for good antioxidant properties. Most precisely, rosmarinic acid **23**, carnosol **69** and carnosic acid **70** are the most promising catechol derivatives.  $\alpha$ -Tocopherol **11** is the *ortho-alkyl* substituent ( $\blacksquare$ , **5**, **7**, **8**, **9** and **11**) with really suitable thermodynamic parameters which lead to excellent antioxidant properties. However, BHT **8** and BHA **6** have highest BDEs. *Ortho-methoxy* derivatives ( $\circ$ , **20**, **27**, **60** and **61**) have medium antioxidant power with higher BDEs and lower IPs. They are more sensitive to oxidation than alkyl, catechol and pyrogallol compounds. That is important to note that *di-ortho-methoxy* substituents ( $\triangle$ , **17** and **26**) have better impact on the antioxidant power of phenols than mono-*ortho-methoxy* groups ( $\circ$ ) because of lowest BDE and highest IP values.

In each series of substituted phenols, we have already shown that electron-donating groups (EDG, alkyl, methoxy and hydroxyl) decrease BDEs whereas electron-withdrawing groups (EWG, carboxyl) have opposite effect. We described here the same effect on IPs. Considering pyrogallol structures ( $\blacktriangle$ ), we point out that 5-*tert*-butylpyrogallol **1** ( $178.7 \text{ kcal.mol}^{-1}$ ) has lower IP than propyl gallate ( $189.6 \text{ kcal.mol}^{-1}$ ) thanks to the *tert*butyl substituent. For catechol derivatives, 4-*tert*-butylcatechol **6** ( $182.4 \text{ kcal.mol}^{-1}$ ) has lower IP than catechol **63** ( $188.1 \text{ kcal.mol}^{-1}$ ) thanks to the *tert*butyl substituent. Nevertheless, protocatechuic acid **16** ( $195.1 \text{ kcal.mol}^{-1}$ ) has the highest IP because of the carboxyl group. Consequently, the stronger is the electron-donating power of substituents, the more sensitive to oxygen the phenol should be.

IP values are also calculated in ethanol to discuss about the variation of stability. **Figure 3.47** shows the correlation of IPs obtained in vacuum and ethanol. We highlight that phenols are less stable in polar solvent which is related to lower IPs. This tendency was already been described by Leopoldini *et al.*<sup>304</sup>

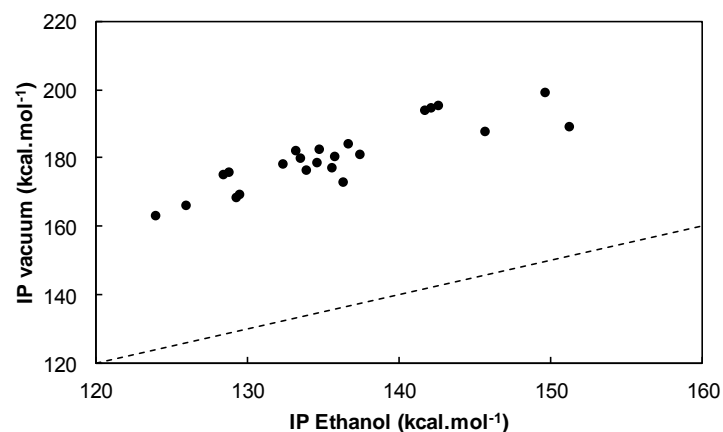


Figure 3.47: Correlation of IPs of phenols calculated with a DFT method in vacuum and ethanol

Phenols studied are relatively stable to oxygen with the lowest IP of  $160.3 \text{ kcal.mol}^{-1}$  for  $\alpha$ -tocopherol **11**. These theoretical calculations show that several natural phenols exhibit suitable BDEs and IPs required to act as powerful phenolic antioxidants and are thus promising candidates to replace synthetic phenols. In particular, the compounds located within the green zone (Fig. 3.46) *i.e.* pyrogallol (gallic acid **15** and myricetin **32**), catechol (rosmarinic acid **23**, carnosol **69** and carnosic acid **70**) derivatives and  $\alpha$ -tocopherol **11** have relatively low BDEs and high IPs. Moreover, phenols are less stable in polar solvents where they could react more rapidly with oxygen resulting in a decrease of their antioxidant power.

### 3.2.5 $pK_a$ and acidity of phenols

Phenols act as antioxidants through the inhibition of lipid radicals by hydrogen atom transfer (HAT) in apolar solvent. In polar matrixes, phenols may react following another mechanism related to the equilibrium between phenols and phenolate forms. For this Sequential Proton Loss Electron Transfer (SPLET) mechanism, the  $pK_a$  of the phenol is a key parameter. In order to discuss about the competition between these two mechanisms, it is necessary to know the effect of various substituents on the  $pK_a$ . Experimental  $pK_a$  from the Physprop database are extracted from the work of Svobodova *et al.* who correlated these values to predicted ones obtained from different computational strategies and models.<sup>353</sup> Some results published by Perrin<sup>354</sup> and Jover *et al.*<sup>355</sup> complete our study. Table 3.23 gathers  $pK_a$  values and  $\Delta pK_a$  calculated from the value of phenol itself in  $H_2O$  ( $pK_a = 9.99$ )<sup>353-355</sup> with respective  $\Delta BDE$  calculated previously with our DFT method.

As expected, all the alkyl substituents increase the  $pK_a$  since their electro-donating effect strengthens the O-H bond. The higher the  $pK_a$  of the phenolic hydrogen is, the weaker the dissociation of the phenol is. Therefore, phenolic compounds with *tert*-butyl and methyl substituents (*i.e.* BHA **5**, BHT **7**, *o-tert*-butyl-*p*-cresol **9** and  $\alpha$ -tocopherol **11**) are weakly dissociated and react according to the HAT mechanism. Moreover, the *para*-methoxy group of BHA **7** (Table 3.23, entry **18**) also increases the  $\Delta pK_a$  and accentuates the stability of the phenol.

	N°	Substitution			pKa	$\Delta pK_a$	$\Delta BDE$ (kcal.mol <sup>-1</sup> )
		<i>Ortho</i> -	<i>Meta</i> -	<i>Para</i> -			
Alkyl groups	1	-CH <sub>3</sub>			10.30 <sup>353</sup>	+0.31	-2.0
	2		-CH <sub>3</sub>		10.10 <sup>353</sup>	+0.11	0.0
	3			-CH <sub>3</sub>	10.30 <sup>353</sup>	+0.31	-2.1
	4	2 x -CH <sub>3</sub>			10.60 <sup>353</sup>	+0.61	-4.4
	5		2 x -CH <sub>3</sub>		10.20 <sup>353</sup>	+0.21	-0.5
	6	2 x -CH <sub>3</sub>		-CH <sub>3</sub>	10.90 <sup>353</sup>	+0.91	-6.4
	7	-CH <sub>3</sub>	-CH <sub>3</sub>		10.40 <sup>353</sup>	+0.41	-2.6
	8	-CH <sub>3</sub>		-CH <sub>3</sub>	10.60 <sup>353</sup>	+0.61	-4.0
	9		-CH <sub>3</sub>	-CH <sub>3</sub>	10.40 <sup>353</sup>	+0.41	-2.2
	10	-C(CH <sub>3</sub> ) <sub>3</sub>			10.62 <sup>354</sup>	+0.63	-2.9
	11		-C(CH <sub>3</sub> ) <sub>3</sub>		10.12 <sup>354</sup>	+0.13	-0.2
	12			-C(CH <sub>3</sub> ) <sub>3</sub>	10.23 <sup>354</sup>	+0.24	-1.7
	13	2 x -C(CH <sub>3</sub> ) <sub>3</sub>			12.16 <sup>355</sup>	+2.17	-7.9
	14		2 x -C(CH <sub>3</sub> ) <sub>3</sub>		10.29 <sup>355</sup>	+0.30	-1.1
	15			-CH=CH-CH <sub>3</sub>	9.58 <sup>353</sup>	-0.41	-4.9
Methoxy groups	16	-OCH <sub>3</sub>			9.98 <sup>353</sup>	-0.01	-1.8
	17		-OCH <sub>3</sub>		9.65 <sup>353</sup>	-0.34	+0.9
	18			-OCH <sub>3</sub>	10.10 <sup>353</sup>	+0.11	-4.6
Hydroxyl groups	19	-OH			9.50 <sup>354</sup>	-0.49	-8.8
	20		-OH		9.32 <sup>354</sup>	-0.67	-1.0
	21			-OH	11.40 <sup>354</sup>	+0.14	-5.0
Carboxyl groups	22		-CO <sub>2</sub> H		9.92 <sup>354</sup>	-0.07	+2.3
	23			-CO <sub>2</sub> H	9.46 <sup>354</sup>	-0.53	+2.5

Table 3.23: Variation of pK<sub>a</sub> values<sup>353-355</sup> as a function of the nature and position of the substituents,  $\Delta pK_a = pK_a - pK_a(\text{phenol})$  and  $\Delta BDEs$  are calculated with the B3LYP/6-311++G(2d,2p)//B3LYP/6-311G(d,p) DFT method

Figure 3.48 points out the correlations between  $\Delta BDE$  and  $\Delta pK_a$  for methyl and *tert*-butyl substituents.

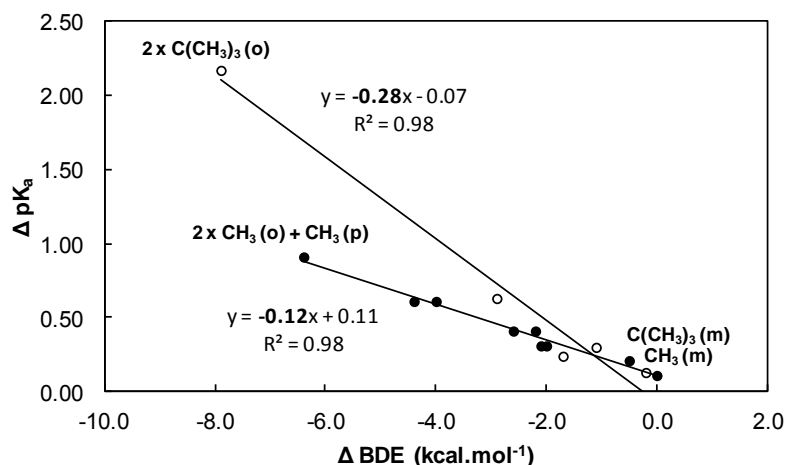


Figure 3.48: Correlations between  $\Delta BDE$  and  $\Delta pK_a$  for methyl (●) and *tert*-butyl (○) phenols

*Meta*-alkyl substituents are not stabilizing phenols (weak  $\Delta BDE$  and  $\Delta pK_a$ ) whereas *ortho*- and *para*-alkyl groups lead to stronger  $\Delta pK_a$  and lower  $\Delta BDE$  highlighting a weak dissociation of phenols into phenolate but preferentially a transfer of hydrogen by radical mechanism. The higher slope of  $\Delta pK_a = f(\Delta BDE)$  for *tert*-butyl groups (-0.28) is due to the stronger electro-donating effect of this group compared to methyl substituents (-0.12).

Conversely, phenols may be dissociated ( $\Delta pK_a < 0$ ) when negative charge of the phenolate is delocalized on its entire chemical structure (*i.e.* *ortho*-OH, *para*-propenyl and *para*-COOH). Consequently, catechol derivatives and isoeugenol should be sensitive to pH and react by the SPLET mechanism. Moreover, the acidity of phenols is strengthened with low  $pK_a$  and high BDE leading to their stronger dissociation into phenolate (**Fig. 3.49**). Consequently, *ortho*-methoxyphenols (OCH<sub>3</sub>) and phenols with carboxylic functions (COOH) are sensitive to pH and react by the SPLET mechanism in polar solvents. Hydroxyl and methoxy groups in *para* position have the same intermediate effect as for *ortho*-hydroxyl and *para*-propenyl functions favoring both HAT and SPLET mechanisms.

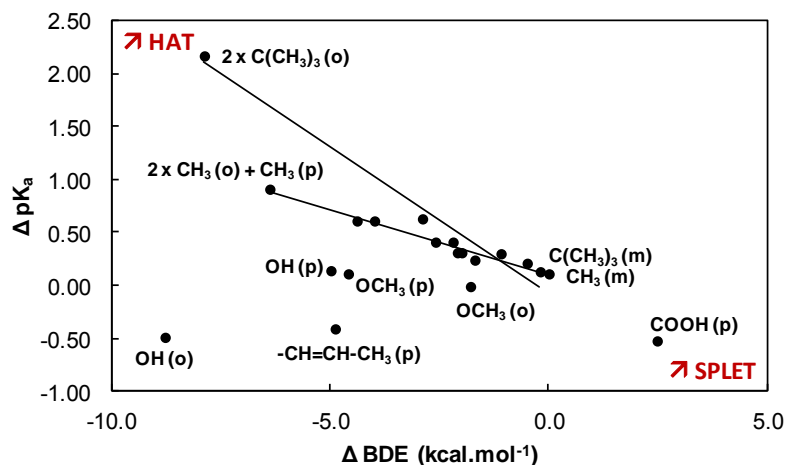


Figure 3.49: BDE changes as a function of  $pK_a$  variations for various substituents born by the phenolic ring

### 3.3 Conclusion

The nature and the position of the substituents bound to the phenolic ring have a major impact on BDEs. This thermodynamic parameter drives the antioxidant efficiency of phenols according to a radical mechanism (HAT) in apolar solvents. A substitution by an electron-donating group (EDG, alkyl, methoxy, and hydroxyl) decreases BDEs whereas an electron withdrawing group (EWG, carboxyl) increases BDEs. Indeed, the lower of BDE of phenol is, the better the antioxidant activity should be. A powerful antioxidant must have a chemical structure including pyrogallol (myricetin **32**, gallic acid **15**) or catechol moiety (rosmarinic acid **23**, carnosol **69** and carnosic acid **70**) conjugated with *para*-electron-donating substituents. They are the best natural alternative to  $\alpha$ -tocopherol **11** and synthetic phenols. Moreover, as regards to the solvent effect on BDEs, *ortho*-methoxyphenols seem to be the best antioxidants in polar protic solvents whereas in hydrogen bond acceptor solvents (*i.e.* ethyl acetate), catechol and pyrogallol derivatives remain the most effective antioxidants with the lowest BDEs.

As regards to the ionization potential (IP) calculation, we highlighted that lower IPs favor the reactivity of phenols with oxygen to the detriment of its antioxidant power. Consequently, an optimal antioxidant should have simultaneous a low BDE and a high IP. Unfortunately, the drop in the IP values accompanies drop in BDEs since electron-donating groups decrease both BDEs and IPs whereas electron-withdrawing groups have opposite effects. The best compromise is obtained with natural phenols having three types of sub-structures, *i.e.* pyrogallol (gallic acid **15** and myricetin **32**), catechol (rosmarinic acid **23**, carnosol **69** and carnosic acid **70**) and polyalkylphenols with alcoxyl function ( $\alpha$ -tocopherol **11**). It is noteworthy that phenols are less stable in polar solvents in which they react more rapidly with oxygen with a concomitant decrease of their antioxidant power.

Substituents also modify the  $pK_a$  values of phenols. This thermodynamic parameter is responsible of an alternative pathway of reaction called SPLET mechanism favored in polar solvents. *Ortho*-methoxy and carboxyl substituents have a strong impact on the decrease of  $pK_a$  of the phenolic hydrogen. This increase in acidity improves the reactivity of these phenols in polar solvents. Conversely, alkyl groups increase the  $pK_a$  leading to a negligible dissociation of antioxidants which favor their reaction by radical mechanism in polar matrixes. Hydroxyl functions have intermediate effects favoring both HAT and SPLET mechanisms.

Finally, the consideration of all the physic-chemical parameters influencing the antioxidant power allows us to point out a number of phenols with promising antioxidant properties (**Fig. 3.37**). These theoretical predictions have been tested in the following paragraph by kinetic studies carried out with the DPPH<sup>\*</sup> test to confirm the tendencies and the efficiency of promising phenols. Furthermore, the quantification of the number of hydrogen atoms released per molecule of antioxidant is used to deepen our knowledge on the mechanism of action of phenols. Finally, global methods able to monitor either the consumption of oxygen (RapidOxy<sup>®</sup>) or the formation of acidic volatile compounds (Rancimat) during the autoxidation of omega-3 Fatty Acid Methyl Esters (FAMES) were used to detect the most effective phenolic antioxidants under actual conditions.

## 4. Experimental determinations of the efficiency of phenolic antioxidants

Oxidation affects the flavor, color and odor of foods. Edible oils and more particularly omega-3 oils are particularly sensitive to oxygen and are therefore subject to oxidative degradation. Therefore, the main goal of food manufacturers is to market products with a long lifetime. During the storage period, oils have to keep their organoleptic properties; therefore, preventing oils from autoxidation and rancidity is essential. In this way, food formulators currently add inexpensive and effective synthetic antioxidants such as BHT and BHA. Nevertheless, there is ongoing controversy about the safety of these two phenolic antioxidants. Nowadays, a major trend appeared with the incorporation of natural phenolic antioxidants into edible oils. In this part, we studied the different reaction mechanisms of phenols in various solvents and evaluated their antioxidant efficiency by three experimental methods: **1**) the DPPH<sup>\*</sup> test and the monitoring of **2**) oxygen consumption or formation of acidic volatile compounds during the autoxidation of omega-3 oils. We selected for this study 24 natural phenolic antioxidants in comparison to 8 synthetic ones which have been highlighted in the previous theoretical section.

### 4.1 Selection of phenolic antioxidant studied

To have a broad overview of the different classes of phenolic antioxidants, 32 phenols have been investigated (**Fig. 3.50**).  $\alpha$ -Tocopherol **11**, chosen as the reference, is a very effective natural antioxidant widely used in food as well as ascorbyl palmitate **71**. On the other hand, the ubiquitous synthetic antioxidants 5-*tert*-butyl-pyrogallol **1**, propyl gallate (PG) **4**, BHA **5**, 4-*tert*-butyl-catechol **6**, BHT **7**, TBHQ **8** and *o*-*tert*-butyl-*p*-cresol **9** and have also been studied for comparison. Gallic acid **15**, protocatechuic acid **16**, syringic acid **17**, vanillic acid **20** and *p*-hydroxybenzoic acid (PHBA) **21** were selected because they are derivatives of hydroxybenzoic acid. In the same way, rosmarinic acid **23**, caffeic acid **24**, chlorogenic acid **25**, sinapic acid **26** and ferulic acid **27** were retained because they derive from hydroxycinnamic acid. Isoeugenol **60** and eugenol **61** are considered as classical monophenols, with both fragrant and antioxidant properties, and were included to investigate the

effect of the double bond position. Hydroxytyrosol **62** and catechol **63** are polyphenols found in olive oil.<sup>345</sup> The other antioxidants represent different classes of phenolic compounds: myricetin **32**, quercetin **34**, and epigallocatechin gallate **55** for the flavonoids<sup>356</sup>, piceatannol **58** and resveratrol **59**, sesamol **65** and aesculetin **67** are categorized as stilbenes, lignans and coumarins respectively. Finally, carnosol **69** and carnosic acid **70** are the major components of rosemary extract (*Rosmarinus officinalis* L.) with rosmarinic acid **23** and are authorized in food in the form of extract.<sup>348</sup>

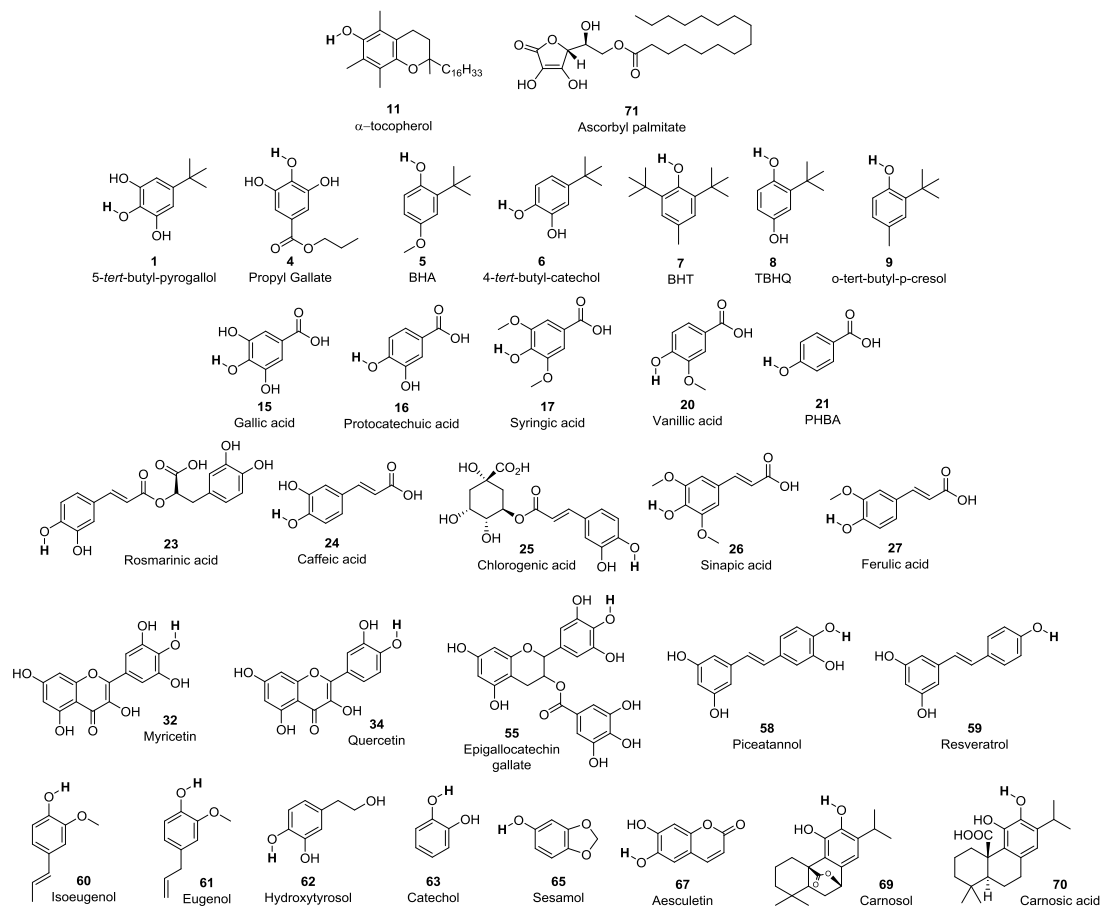


Figure 3.50: Chemical structures of phenolic antioxidants studied, hydrogen atoms with the lowest BDE are indicated in bold

## 4.2 DPPH<sup>•</sup> or 2,2-diphenyl-1-picrylhydrazil radical test

### 4.2.1 Principles

The DPPH<sup>•</sup> test<sup>253, 260, 282, 283, 357</sup> was firstly used in 1995 and, since it becomes one of the most popular methods to evaluate the antioxidant power of phenolic compounds (Fig. 3.51).

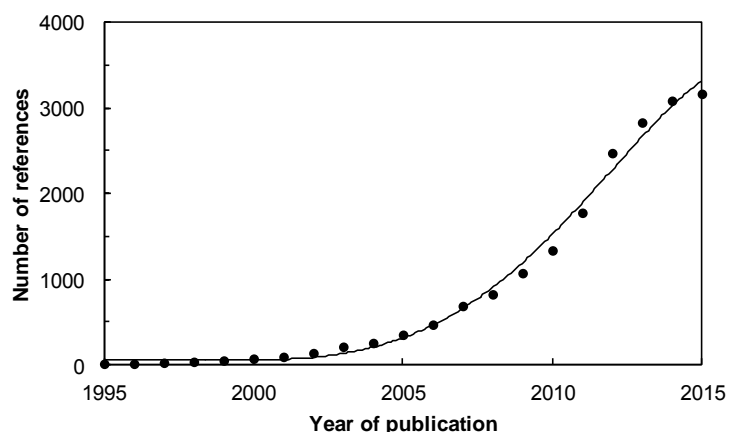


Figure 3.51: Number of references vs their year of publication using “antioxidant” and “DPPH” via the Scifinder® database

It is a stable radical with a maximum of absorption around 515-520 nm (violet). When antioxidants such as  $\alpha$ -tocopherol **11** are mixed with this stable radical, there is a transfer of hydrogen from the antioxidant to the DPPH<sup>•</sup> radical. The DPPH<sup>•</sup> radical traps hydrogen atoms and becomes yellow (Fig. 3.52).

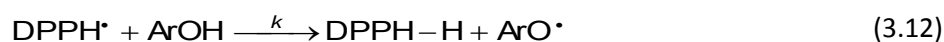


Figure 3.52: Reaction of hydrogen transfer from phenols ( $\alpha$ -tocopherol **11**) to the DPPH<sup>•</sup> radical

Consequently, it is easy to follow the transfer of hydrogen by UV-visible spectrometry. The parameters highlighted by this test are the kinetic rates and the number of hydrogen (stoichiometric number) transfer from phenols to the stable radical. These experimental analyses reveal the scale of reactivity of phenols and discuss about the Kinetic Solvent Effects (KSE).<sup>285, 358, 359</sup>

#### 4.2.1.1 Kinetic rate of hydrogen transfer

Two different procedures have been employed depending on the reactivity of the phenols under studied. The kinetics of the reaction between DPPH<sup>•</sup> and a phenol ArOH may be described according to equations 3.12 and 3.13.



$$\frac{d[\text{DPPH}^{\bullet}]}{dt} = -k[\text{DPPH}^{\bullet}][\text{ArOH}] \quad (3.13)$$

- Poorly reactive phenols

Phenols with low reactivity (*i.e.* BHT **7**, *o*-*tert*-butyl-*p*-cresol **9**, protocatechuic acid **16** and vanillic acid **20**, and eugenol **61**) are introduced in excess at different concentrations in order to accelerate the reaction. Under these conditions,  $[ArOH] \approx [ArOH]_0$  and **equation 3.13** simplifies into **equation 3.14** where  $k_{app} = k \times [ArOH]_0$  is the apparent rate constant of the pseudo first-order kinetics (FOK) defined by **equation 3.15**.

$$\frac{d[DPPH^*]}{dt} = -k_{app} [DPPH^*] \quad (3.14)$$

$$[DPPH^*] = [DPPH^*]_0 \exp(-k_{app} t) = [DPPH^*]_0 (-k [ArOH]_0 t) \quad (3.15)$$

At 515 nm, DPPH<sup>\*</sup> and DPPH<sub>2</sub> exhibit a strong ( $\epsilon$ ) and a weak ( $\epsilon'$ ) molar absorption coefficient respectively which allows to monitor the disappearance of DPPH<sup>\*</sup>. **Equations 3.16 to 3.19** are used to express the evolution of  $[DPPH^*]$  vs the absorbances  $A$ ,  $A_0$  and  $A_f$ .

$$A_0 = \epsilon [DPPH^*]_0 \quad (3.16)$$

$$A_f = \epsilon' [DPPH_2]_f = \epsilon' [DPPH^*]_0 \quad (3.17)$$

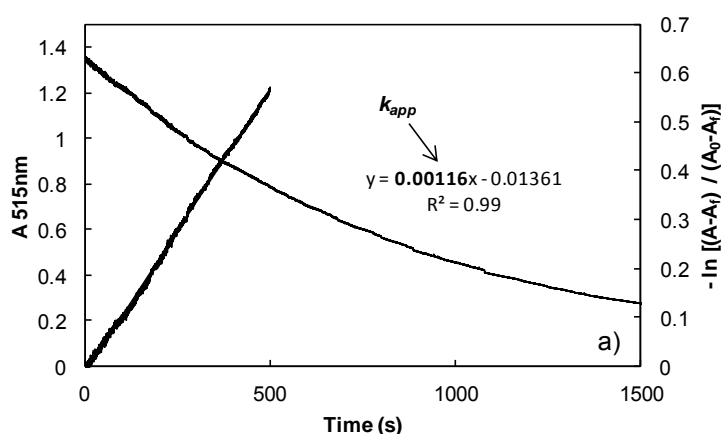
$$A = \epsilon [DPPH^*] + \epsilon' [DPPH^*] \quad (3.18)$$

$$[DPPH^*] = [DPPH^*]_0 \frac{(A - A_f)}{(A_0 - A_f)} \quad (3.19)$$

By replacing  $[DPPH^*]$  and  $[DPPH^*]_0$  in the above **equation 3.15**, **equation 3.20** is obtained providing the apparent rate constants  $k_{app}$  as the slope of the linearized curve obtained by plotting  $\ln(A - A_f) / (A_0 - A_f)$  vs time.

$$\ln \frac{(A - A_f)}{(A_0 - A_f)} = -k_{app} [ArOH]_0 t \quad (3.20)$$

Finally, the plot of the apparent kinetic rate  $k_{app}$  vs the initial concentration of antioxidant  $[ArOH]_0$  gives the kinetic rate of hydrogen transfer  $k$  for poorly reactive phenols following the (FOK) reaction. **Figure 3.53** shows an example of FOK kinetics with BHT **7** in toluene.



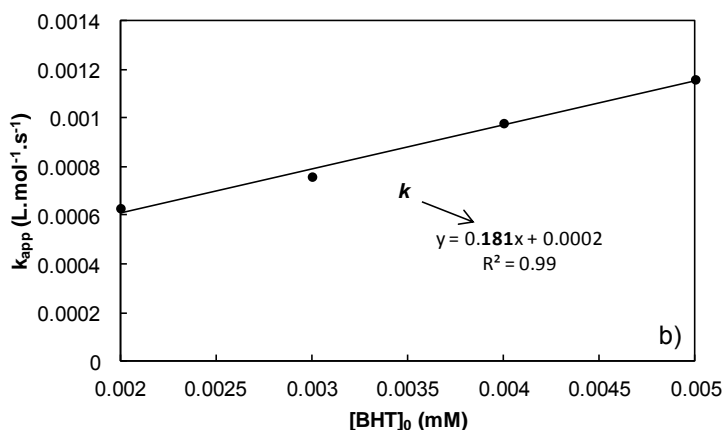


Figure 3.53: a) Evolution of the absorbance at 515 nm of a solution of DPPH<sup>•</sup> in the presence of an excess of BHT 7 in toluene at 20 °C, linearization of the logarithm of the absorbance using the final FOK equation 3.20 and b) Regression constants of apparent kinetic rates ( $k_{app}$ ) vs the initial concentrations of BHT 7

- *Very/moderately reactive phenols*

On the other hand, for more reactive phenols, ArOH and DPPH<sup>•</sup> are mixed in stoichiometric amounts. Under these conditions, [DPPH<sup>•</sup>] = [ArOH] and the general kinetics of the reaction between DPPH<sup>•</sup> and a phenol ArOH above-mentioned (equation 3.13) is changed into equations 3.21 and 3.22 describing the second order kinetics (SOK).

$$\frac{d[\text{DPPH}^{\bullet}]}{dt} = -k [\text{DPPH}^{\bullet}]^2 \quad (3.21)$$

$$\frac{1}{[\text{DPPH}^{\bullet}]} - \frac{1}{[\text{DPPH}^{\bullet}]_0} = -k t \quad (3.22)$$

Equation 3.22 can be expressed as a function of the absorbances A, A<sub>0</sub> and A<sub>f</sub> giving equation 3.22 providing the rate constants k as the slope of the linearized curve obtained by plotting [1/(A - A<sub>f</sub>) - 1/A<sub>0</sub>] vs time.

$$\frac{1}{(A - A_f)} - \frac{1}{A_0} = \frac{k}{(\epsilon - \epsilon')} t \quad (3.23)$$

Figure 3.54 shows an example of SOK kinetics with α-tocopherol 11 in toluene. The rate constant of the reaction is determined during the first 15 seconds of the reaction when only the reaction of phenolic hydrogen with DPPH<sup>•</sup> occurs and other dismutation or second any hydrogen transfer can be neglected.

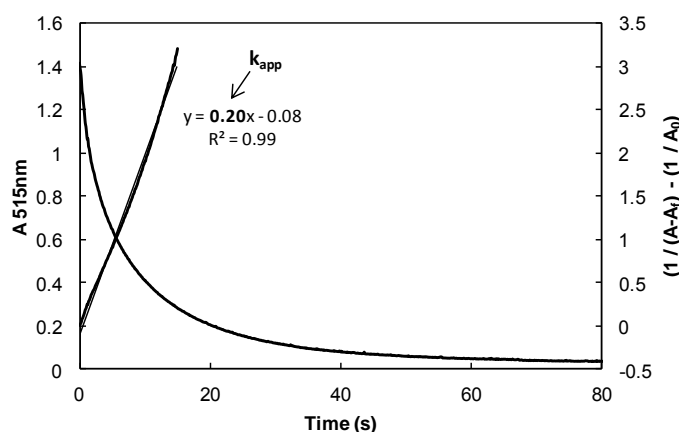


Figure 3.54: Evolution of the absorbance of DPPH<sup>•</sup> radical at 515 nm ( $1.25 \times 10^{-4} \text{ mol.L}^{-1}$ ) in the presence of α-tocopherol 11 ( $1.25 \times 10^{-4} \text{ mol.L}^{-1}$ ) in toluene at 20 °C. Linearization curve according to SOK equation 3.23

To confirm that pseudo First Order Kinetics (FOK) and Second Order Kinetics (SOK) give same results for the same phenolic antioxidants, two phenols with poor reactivities, namely vanillic acid **20** and eugenol **61** are studied under both kinetic conditions leading to similar values of the rate constants  $k$ . However, the end products obtained are not phenolic radicals ( $\text{ArO}^\bullet$ ) but *o*-quinone compounds or solvent adducts, an alternative theoretical treatment could be used as described by Dangles *et al.*<sup>357</sup>

#### 4.2.1.2 Stoichiometry of the hydrogen transfer reaction

Phenolic antioxidants are also characterized by the maximum number of  $\text{H}^\bullet$  radicals trapped per antioxidant molecule, named the stoichiometric number  $\sigma_{\text{exp}}$ . When phenols are mixed in limited amount with an excess of  $\text{DPPH}^\bullet$ , the reaction reach a stationary state and the absorbance get to a fixed value.<sup>360</sup> Indeed, the study of different molar ratios  $n_{\text{phenol}}/n_{\text{DPPH}^\bullet}$  (with fixed  $n_{\text{DPPH}^\bullet}$  and variable  $n_{\text{phenol}}$  values) with the percentage of  $\text{DPPH}^\bullet$  remaining in solution allows determining the molar ratio required to consume 50% of the initial  $\text{DPPH}^\bullet$  (Fig. 3.55). This experimental value is called  $\text{EC}_{50}$ . The antioxidant efficiency of phenols is particularly high when its  $\text{EC}_{50}$  value is low.  $\text{EC}_{50}$  value allows determining the stoichiometric number as defined by the equation 3.24.

$$\sigma_{\text{exp}} = \frac{1}{2 \times \text{EC}_{50}} \quad (3.24)$$

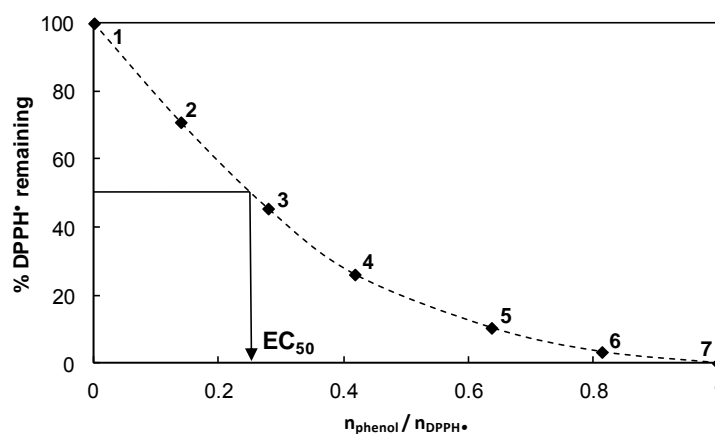


Figure 3.55: Evolution of the % of  $\text{DPPH}^\bullet$  remaining in toluene at the stationary state vs various molar ratios  $n_{\text{phenol}}/n_{\text{DPPH}^\bullet}$  (0 (1), 0.14 (2), 0.28 (3), 0.42 (4), 0.64 (5), 0.81 (6) and 1.0 (7)) for  $\alpha$ -tocopherol **11** and determination of its  $\text{EC}_{50}$  value

This method requires the set up of various assays for the same antioxidant in order to test different molar ratios and point out the evolution of the curve. Consequently, an easier way to calculate the stoichiometric number  $\sigma_{\text{exp}}$  is based on the monitoring of the absorbance of  $\text{DPPH}^\bullet$  (in excess) for only one initial concentration of phenol (limited concentration). This identifies one molar ratio  $n_{\text{phenol}}/n_{\text{DPPH}^\bullet}$  indicated previously and leads to  $\sigma_{\text{exp}}$  values calculated according to equation 3.25.<sup>357</sup>

$$\sigma_{\text{exp}} = \frac{[\text{DPPH}^\bullet]_0 - [\text{DPPH}^\bullet]_f}{[\text{ArOH}]_0} = \frac{A_0 - A_f}{(\epsilon - \epsilon')[\text{ArOH}]_0} \quad (3.25)$$

This alternative method is used here to determinate the stoichiometric number  $\sigma_{\text{exp}}$  for selected phenols in order to rationalize their effectiveness. Three concentrations of antioxidants are tested for some compounds (*i.e.* tocopherol **11**, figure 3.56) to show the link between the two methods. Indeed, the different molar ratios tested here (0.14, 0.28 and 0.42) are required for the determination of the  $\text{EC}_{50}$  value (Fig. 3.55).

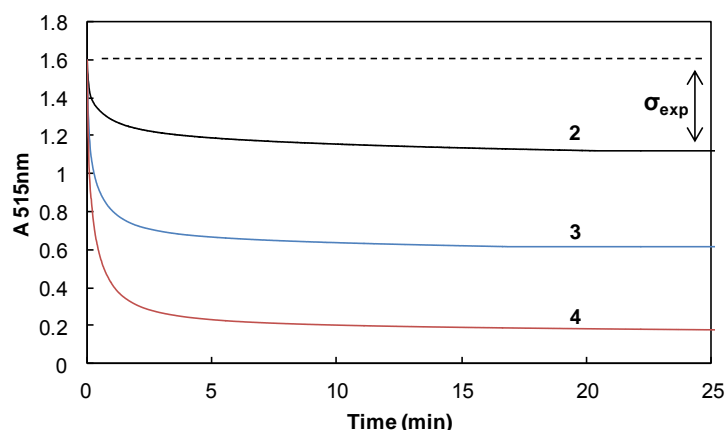


Figure 3.56: Evolution of the absorbance of DPPH<sup>•</sup> radical at 515 nm ( $1.5 \times 10^{-4}$  M) in the presence of  $\alpha$ -tocopherol **11** at different concentrations in toluene at 20 °C. [ $\alpha$ -tocopherol] =  $2.07 \times 10^{-5}$  M,  $n_{\text{phenol}}/n_{\text{DPPH}^\bullet}$  = 0.14 (black curve, 2), [ $\alpha$ -tocopherol] =  $4.14 \times 10^{-5}$  M,  $n_{\text{phenol}}/n_{\text{DPPH}^\bullet}$  = 0.28 (blue curve, 3) and [ $\alpha$ -tocopherol] =  $6.21 \times 10^{-5}$  M,  $n_{\text{phenol}}/n_{\text{DPPH}^\bullet}$  = 0.42 (red curve, 4)

#### 4.2.2 Kinetic rate constants of hydrogen transfer in apolar aprotic solvent: scale of reactivity of phenolic antioxidants

The potential antioxidant properties revealed by thermodynamic parameters (*i.e.* BDEs and IPs) are tested with the determination of the kinetic rates of hydrogen transfer. A scale of reactivity of phenols in toluene is built since it is an oxidation-inert solvent which does not interfere in the hydrogen transfer. Nevertheless, this apolar solvent does not solubilize all the phenols under study. **Table 3.24** gathers the values of  $k$  measured in toluene, BDEs calculated in vacuum and  $\Delta$ BDEs obtained with our value of phenol itself ( $82.2 \text{ kcal}\cdot\text{mol}^{-1}$ ).

The antioxidant activity of phenols should be evaluated with kinetic rates of hydrogen transfer to peroxy radical  $\text{ROO}^\bullet$  or with BDEs. Foti *et al.* have already shown the correlation between these two parameters in alkane or aromatic hydrocarbons.<sup>284</sup> The mechanism involved in apolar aprotic solvents is called Hydrogen Atom Transfer (HAT) which competes with Sequential Proton Loss Electron Transfer (SPLET) mechanism for polar solvents. Logarithms of kinetic rates obtained for  $\alpha$ -tocopherol (**11**), sinapic acid (**26**), ferulic acid (**27**), catechol (**63**) and sesamol (**65**) are consistent with the logarithm of values published by Foti *et al.*<sup>284</sup>

Phenols	BDE ( $\text{kcal}\cdot\text{mol}^{-1}$ )	$\Delta$ BDE <sup>c</sup> ( $\text{kcal}\cdot\text{mol}^{-1}$ )		$k$ ( $\text{M}^{-1}\cdot\text{s}^{-1}$ )	
		Calc.	Literature	SOK <sup>a</sup>	FOK <sup>b</sup>
<b>1</b>	66.6	-15.6	nd	9480	
<b>4</b>	69.6	-12.6	-11.2 <sup>290</sup> , -11.8 <sup>324</sup>	1240	
<b>5</b>	72.3	-9.9	-8.9 <sup>290</sup> , -8.2 <sup>324</sup>	184	
<b>6</b>	72.3	-9.9	-7.7 <sup>340</sup>	776	
<b>7</b>	72.4	-9.8	-7.3 <sup>262</sup>		0.18
<b>8</b>	74.3	-7.9	nd	600	
<b>9</b>	77.4	-4.8	nd		0.36
<b>11</b>	69.1	-13.1	-11.3 <sup>290</sup> , -11.2 <sup>304, 323</sup> , -12.1 <sup>361</sup>	2690	
<b>17</b>	78.1	-4.1	-3.3 <sup>316, 338</sup>	10.6	
<b>20</b>	83.1	+0.9	+1.2 <sup>338</sup>	1.4	1.0
<b>26</b>	75.4	-6.8	-5.8 <sup>316</sup> , -7.1 <sup>284</sup>	165	
<b>27</b>	79.7	-2.5	-2.0 <sup>331</sup> , -3.1 <sup>284</sup>	8.4	

Phenols	BDE (kcal.mol <sup>-1</sup> )	$\Delta$ BDE <sup>c</sup> (kcal.mol <sup>-1</sup> )		$k$ (M <sup>-1</sup> .s <sup>-1</sup> )	
		Calc.	Literature	SOK <sup>a</sup>	FOK <sup>b</sup>
<b>60</b>	76.6	-5.6	nd	37.8	
<b>61</b>	80.2	-2.0	-3.7 <sup>262</sup>	3.9	2.7
<b>62</b>	72.1	-10.1	-9.40 <sup>304</sup> , -10.5 <sup>324</sup>	1070	
<b>63</b>	73.4	-8.8	-6.9 <sup>292, 323</sup> , -8.9 <sup>307</sup> , -10.1 <sup>331</sup>	400	
<b>65</b>	75.1	-7.1	-7.2 <sup>284</sup>	250	
<b>69</b>	70.7	-11.5	nd	1680	
<b>70</b>	70.8	-11.4	nd	640	

<sup>a</sup> SOK: Second Order Kinetics ([DPPH<sup>\*</sup>]<sub>0</sub> = [ArOH]<sub>0</sub>), <sup>b</sup> FOK: pseudo-First Order Kinetics ([ArOH]<sub>0</sub> >> [DPPH<sup>\*</sup>]<sub>0</sub>),

<sup>c</sup>  $\Delta$ BDE = BDE - BDE<sub>phenol</sub>, nd: not determined

**Table 3.24:** BDEs of ArO-H computed in vacuum and  $\Delta$ BDE are calculated compared to the BDE of phenol (82.2 kcal.mol<sup>-1</sup>), Rate constants  $k$  of hydrogen transfer from ArOH to DPPH<sup>\*</sup> in toluene at 20°C

**Figure 3.57** points out that logarithms of the rate constants for the reaction of hydrogen transfer from phenol to DPPH<sup>\*</sup> are well correlated to BDEs of phenols ( $R^2 = 0.96$ ) confirming that the radical HAT mechanism occurs in toluene. Nevertheless, there are some exceptions. Indeed, due to steric hindrance of *ortho*- and *di-ortho-tert*butyl groups for BHA **5**, BHT **7** and *o-tert*-butyl-*p*-cresol **9**, kinetic transfer constants  $k$  slow down drastically. Indeed, kinetic rate constants  $k$  are very low and do not follow the trend curve as explained by Marteau *et al.*<sup>334, 336</sup> Moreover, *tri*-hydroxyphenols (**1**, **4**) react faster than *di*-hydroxyphenols (**6**, **62**, **63**, **69** and **70**) which themselves react faster than monophenols (**17**, **20**, **26**, **27**, **60**, **61** and **65**) except for  $\alpha$ -tocopherol **11**.

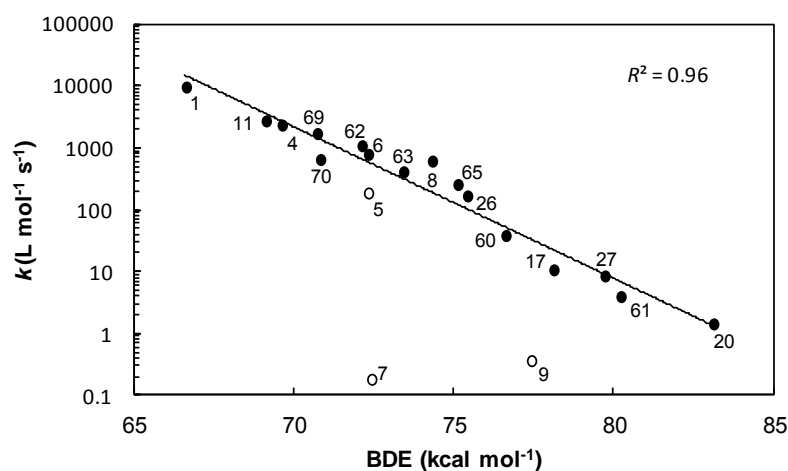


**Figure 3.57:** Logarithm of the rate constants ( $\log k$ ) for the reaction of phenolic antioxidants with DPPH<sup>\*</sup> (○ hindered phenols and ● other phenols) in toluene vs *their* BDEs calculated with the DFT method in vacuum

More precisely, 5-*tert*-butyl-pyrogallol **1** and propyl gallate **4** are the most reactive synthetic phenols in toluene. With regards to natural phenolic antioxidants,  $\alpha$ -tocopherol **11** exhibits the highest kinetic rates (2670 M<sup>-1</sup>.s<sup>-1</sup>) followed by carnosol **69** (1680 M<sup>-1</sup>.s<sup>-1</sup>), hydroxytyrosol **62** (1070 M<sup>-1</sup>.s<sup>-1</sup>) and carnosic acid **70** (640 M<sup>-1</sup>.s<sup>-1</sup>). It is noteworthy that rosmarinic acid **23** and myricetin **32** are not soluble in toluene but, as regards to their very low BDEs, they should be very reactive in apolar matrixes as demonstrated by Tikhonov *et al.* for myricetin.<sup>362</sup>  $\log k$  decreases with the BDEs as also demonstrated by Foti *et al.* in heptane<sup>284</sup> and Marteau *et al.* in *m*-xylene<sup>334</sup>. Foti *et al.* have also proven that kinetic rate constants obtained with DPPH<sup>\*</sup> are correlated with the reaction of phenols with peroxy radicals ROO<sup>\*</sup>. Therefore, this test mimics the behavior of phenolic antioxidants during the preservation of oils oxidation *via* hydrogen transfer thanks to a radical mechanism.<sup>363</sup> Although the conditions and method used to determine the kinetic rates constants are different for authors,

our results obtained with the DPPH<sup>•</sup> test are consistent with the literature and confirm our scale of reactivity. Finally, it is also important to note that the scale of reactivity in apolar aprotic solvents differs from that in hydrogen bond acceptor (HBA) and polar solvents. For example, caffeic acid **24** becomes more efficient than  $\alpha$ -tocopherol **11** in water<sup>364</sup> while the antioxidant capacity of rosmarinic acid **23** is higher than that of  $\alpha$ -tocopherol **11** in methanol.<sup>365, 366</sup> In order to study the kinetic effects of solvents, the DPPH<sup>•</sup> test is set up in various matrixes.

#### 4.2.3 Kinetic Solvent Effects (KSEs) on the reactivity of phenolic antioxidants

Phenols are used as antioxidants in various matrixes such as water, ethanol and oil for detergents, fragrances and food respectively. Therefore, the impact of solvent polarities on the antioxidant efficiency of phenols is evaluated. Moreover, cetiol A is tested to have closer conditions to oils in order to find the best solvent to model oils. The ability of solvents to accept hydrogen bonds is studied with the Abraham's parameter ( $\beta$ ). It is ranged from 0 to 1 where 1 characterizes a very good hydrogen bond acceptor (HBA) solvent. **Table 3.25** gathers the kinetic rate constants obtained in toluene, ethyl acetate, cetiol A and ethanol with their calculated logarithm. Their Abraham's parameters are notified in brackets.

Phenols	$k^a$	Log $k$	$k^a$	Log $k$	$k^a$	Log $k$	$k$	Log $k$
	Toluene ( $\beta^b = 0.14$ )		EtOAc ( $\beta^b = 0.47$ )		Cetiol A		Ethanol ( $\beta^b = 0.44$ )	
<b>1</b>	9480	3.98	190	2.28	709	2.85	2119	3.33
<b>4</b>	1240	3.36	44	1.64	61	1.78	1453	3.16
<b>5</b>	184	2.26	7.4	0.87	nd	/	30	1.48
<b>6</b>	776	2.89	18	1.26	59	1.77	318	2.50
<b>7</b>	0.18	-0.74	0.08	-1.10	nd	/	0.04	-1.40
<b>8</b>	600	2.78	40	1.60	103	2.01	111	2.05
<b>9</b>	0.36	-0.44	0.09	-1.05	nd	/	0.08	-1.10
<b>11</b>	2690	3.43	210	2.32	432	2.64	400	2.60
<b>15</b>	ns	/	7.8	0.89	nd	/	75	1.88
<b>16</b>	ns	/	0.79	-0.10	nd	/	51	1.71
<b>17</b>	10.6	1.02	0.08	-1.10	nd	/	27	1.43
<b>20</b>	1.4	0.15	0.01	-2.0	nd	/	nd	/
<b>23</b>	ns	/	31	1.49	nd	/	157	2.20
<b>24</b>	ns	/	10	1.00	nd	/	303	2.48
<b>25</b>	ns	/	8.6	0.93	nd	/	23	1.35
<b>26</b>	165	2.22	23	1.36	nd	/	402	2.60
<b>27</b>	8.4	0.92	1.03	0.01	nd	/	17	1.22
<b>32</b>	ns	/	67	1.83	nd	/	439	2.64
<b>34</b>	ns	/	18	1.26	nd	/	78	1.89
<b>55</b>	ns	/	187	2.27	nd	/	2048	3.31
<b>59</b>	ns	/	1.4	0.16	nd	/	64	1.81
<b>60</b>	37.8	1.58	5.4	0.73	nd	/	146	2.16
<b>61</b>	3.9	0.59	0.47	-0.33	nd	/	9.0	0.95
<b>62</b>	1070	3.03	13	1.11	nd	/	241	2.38
<b>63</b>	400	2.61	3.7	0.57	nd	/	133	2.12
<b>65</b>	250	2.40	5.5	0.74	nd	/	130	2.11
<b>67</b>	ns	/	14	1.15	nd	/	2486	3.40
<b>69</b>	1680	3.23	47	1.67	nd	/	5326	3.73
<b>70</b>	640	2.81	103	2.01	230	2.63	3690	3.57
<b>71</b>	1101	3.04	68	1.83	197	2.29	14629	4.17

ns: not soluble, nd: not determined, <sup>a</sup>mol.L<sup>-1</sup>.s<sup>-1</sup>, <sup>b</sup>Abraham's parameter<sup>367, 368</sup>

**Table 3.25:**  $k$  of hydrogen transfer from ArOH to DPPH<sup>•</sup> in toluene, ethyl acetate, cetiol A and ethanol at 20°C

In apolar aprotic solvents (*i.e.* alkanes, aromatics as toluene), there is not intermolecular hydrogen bonding between phenols and solvent. Indeed, *via* a radical mechanisms (HAT), there is a transfer of hydrogen from phenols to DPPH<sup>•</sup> with the kinetic rate constant  $k_{HAT}$ .

The largest kinetic solvent effects (KSEs) observed for hydrogen atom abstractions is mainly a consequence of hydrogen bonding to solvents with hydrogen bond acceptor (HBA) capability (ketones, ethers, esters as ethyl acetate and cetiol A). The kinetic solvent effect (KSE) impact the HAT mechanism. An intermolecular hydrogen-bonded ArOH is essentially unreactive to DPPH<sup>•</sup> due to the steric protection of the hydroxyl group by solvent. Only the non hydrogen-bonded phenols are reactive. Consequently, the concentration of non hydrogen-bonded reactive ArOH depends on the total concentration of phenol  $[ArOH]_0$  and the equilibrium constant  $K_{ArOH/S}^S$ .<sup>285, 320</sup>

**Figure 3.58** points out the comparative kinetic rate constants obtained in toluene ( $\beta = 0.14$ ) and ethyl acetate ( $\beta = 0.47$ ).

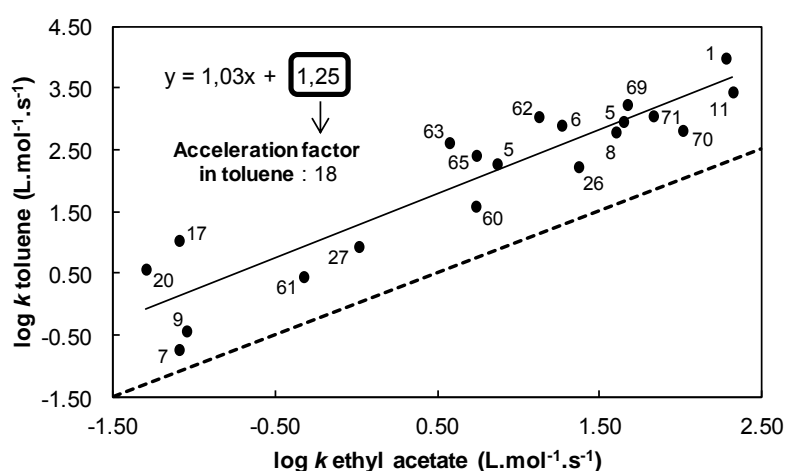


**Figure 3.58:** Correlation between logarithms of kinetic rate constants obtained for phenols with DPPH<sup>•</sup> in toluene ( $\beta = 0.14$ ) and ethyl acetate ( $\beta = 0.47$ )

As expected, all the phenolic antioxidants studied are more reactive in toluene than in ethyl acetate because of the HBA properties. On average, kinetic rate constants in toluene are increase about 18 times. As for toluene, 5-*tert*-butylpyrogallol **1** and propyl gallate **4** are the most reactive synthetic phenols ( $190$  and  $44 \text{ M}^{-1}.\text{s}^{-1}$  respectively). As regards to natural phenolic antioxidant,  $\alpha$ -tocopherol **11** exhibits the higher kinetic rate constant ( $210 \text{ M}^{-1}.\text{s}^{-1}$ ) followed by epigallocatechin gallate **55** ( $187 \text{ M}^{-1}.\text{s}^{-1}$ ), carnosic acid **70** ( $103 \text{ M}^{-1}.\text{s}^{-1}$ ) and myricetin **31** ( $67 \text{ M}^{-1}.\text{s}^{-1}$ ).

Cetiol A also called hexyl laurate is then used as another HBA solvent to mimic the reality of oils. **Figure 3.59** compares the kinetic rate constants obtained in ethyl acetate and cetiol A for some phenols (**1**, **4**, **6**, **8**, **11**, **70** and **71**). On average, kinetic rates in cetiol A are just increase about 2 times compared to ethyl acetate. Therefore, ethyl acetate is a good model to investigate the mechanisms implied in ester oils.

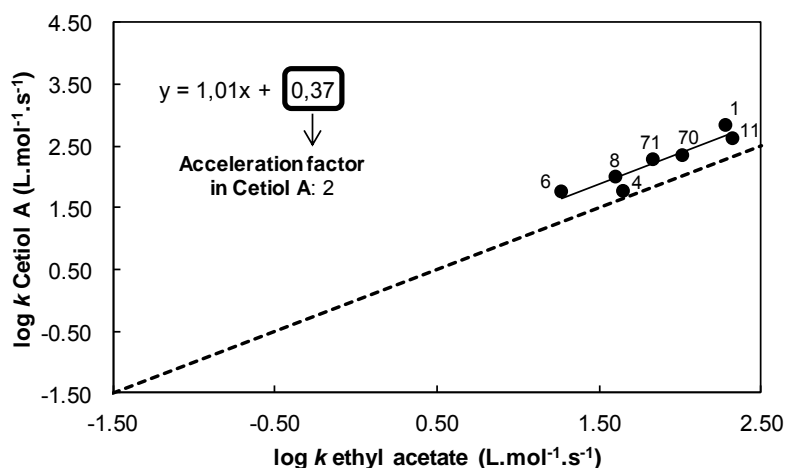


Figure 3.59: Correlation between logarithms of kinetic rate constants obtained for phenols with DPPH<sup>•</sup> in cetiol A and ethyl acetate ( $\beta = 0.47$ )

Finally, ethanol is studied as another HBA solvent ( $\beta = 0.44$ ). Figure 3.60 points out the comparison of kinetic rate constants obtained in toluene and ethanol. HAT and SPLET mechanisms are in competition in polar protic solvents and the reactivity of phenols depends on their chemical structures.

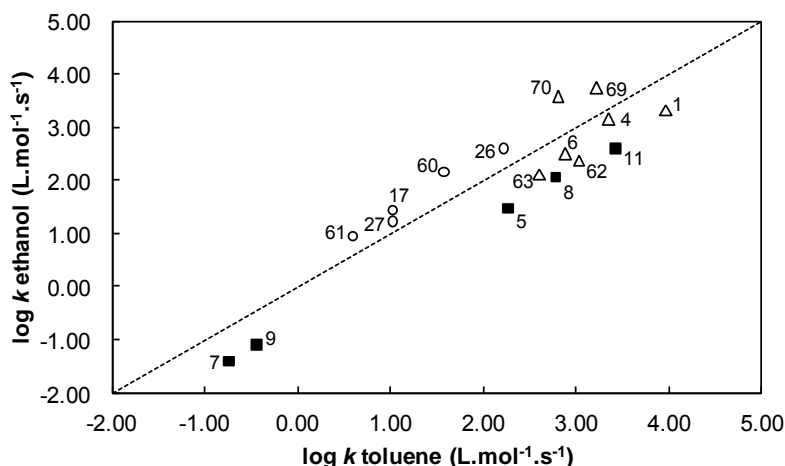
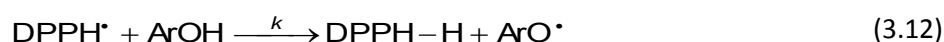


Figure 3.60: Correlation between logarithms of kinetic rate constant obtained for phenols with DPPH<sup>•</sup> in ethanol and toluene ( $\Delta$  *ortho*-hydroxyphenols 1, 4, 6, 62, 63, 69 and 70,  $\blacksquare$  *ortho*-alkylphenols 5, 7, 8, 9 and 11,  $\circ$  *ortho*-methoxyphenols 26, 27 60 and 61)

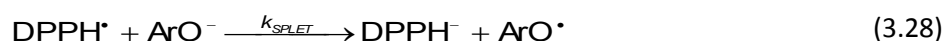
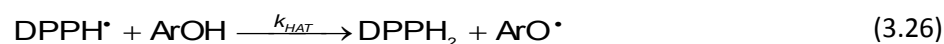
*Ortho*-alkylphenols ( $\blacksquare$  5, 7, 8, 9 and 11) are more reactive in toluene than in ethanol favoring the HAT mechanism. The study of BDE and pKa for alkylphenols showing their higher potential reactivity in apolar solvents is confirmed. Conversely, *ortho*-methoxyphenols ( $\circ$  26, 27, 60 and 61) are more reactive in ethanol than in toluene as highlighted before with the BDE/pKa combination. Indeed, in polar protic solvents, they react preferentially by SPLET mechanism instead of radical HAT process. The main *ortho*-hydroxyphenols ( $\Delta$ , 1, 4, 6, 62 and 63) are more efficient in toluene. However, carnosol 69 and carnosic acid 70 are the two catechol structures more efficient in ethanol. This supports the fact that *ortho*-OH groups favor both HAT and SPLET mechanisms as developed in the theoretical part.

The general kinetic of the reaction between DPPH<sup>•</sup> and a phenol ArOH already shown are described according to **equations 3.11** and **3.12**.



$$\frac{d[\text{DPPH}^{\bullet}]}{dt} = -k[\text{DPPH}^{\bullet}][\text{ArOH}] \quad (3.13)$$

This study highlights the contribution of two predominant systems for the reaction of phenols into polar solvents, *i.e.* the HAT and SPLET mechanisms. The HAT mechanism is defined by **equation 3.26** whereas **equations 3.27** and **3.28** characterize the SPLET mechanism.



Consequently, the combination of these two mechanism changes the **equation 3.13** into **equation 3.29**.

$$-\frac{d[\text{DPPH}^{\bullet}]}{dt} = k_{\text{HAT}}[\text{DPPH}^{\bullet}][\text{ArOH}] + k_{\text{SPLET}}[\text{DPPH}^{\bullet}][\text{ArO}^{-}] \quad (3.29)$$

The concentration of phenolate ions in water is expressed with the dissociation constant  $K_a$  ( $K_a = [\text{ArO}^{-}][\text{H}^{+}]/[\text{ArOH}]$ ) and the concentration of non-dissociated phenols [ArOH] in solvent leading to **equation 3.30**.

$$-\frac{d[\text{DPPH}^{\bullet}]}{dt} = k_{\text{HAT}}[\text{DPPH}^{\bullet}][\text{ArOH}] + k_{\text{SPLET}}[\text{DPPH}^{\bullet}] \frac{K_a[\text{ArOH}]}{[\text{H}^{+}]} \quad (3.30)$$

Finally, with the hypothesis of  $[\text{ArOH}] = [\text{ArOH}]_0$ , the global kinetic rate constant is defined according to **equation 3.31**.

$$k = k_{\text{HAT}} + k_{\text{SPLET}} \frac{K_a}{[\text{H}^{+}]} \quad (3.31)$$

Consequently, the lower is the pKa of phenols, the higher is the global kinetic rate constants in polar solvents. For *ortho*-methoxyphenols, global kinetic rate constant  $k$  depends only on the second part of the equation if the SPLET mechanism takes place. Indeed, Litwinienko *et al.* shown that a few amount of phenolate is enough to increase  $k$  because  $k_{\text{SPLET}}$  is very high.<sup>358</sup> Conversely, *ortho*-alkylphenols reacts following the HAT mechanism and only the first part of the equation characterizes the global kinetic rate constant.

**Figure 3.61** shows the correlation of pKa and BDEs of phenols. *Ortho*-alkylphenols (■, BHA **5**, BHT **7**, TBHQ **8**, *o*-*tert*-butyl-*p*-cresol **9** and  $\alpha$ -tocopherol **11**) have low acidity with pKa of 10.57, 12.20, 10.80, 11.64 and 11.92 respectively. Indeed, there is no dissociation of these phenols and the HAT mechanism is favored in polar protic solvents. Conversely, *ortho*-methoxyphenols (○, sinapic acid **26**, ferulic acid **27**, isoeugenol **60** and eugenol **61**) have simultaneous low pKa (9.21, 9.39, 9.88 and 10.29 respectively) and high BDEs. Due to their relatively strong acidity, they are significantly dissociated in polar solvent where kinetic rate constant  $k_{\text{SPLET}}$  prevails. Finally, *ortho*-hydroxyphenols (Δ, 5-*tert*-butylpyrogallol **1**, propyl gallate **4**, 4-*tert*-butyl-catechol **7**, hydroxytyrosol **62** and catechol **63**) have low pKa as for *ortho*-methoxyphenols (○). Nevertheless, they have very low BDEs which favor the HAT mechanism in polar solvents.

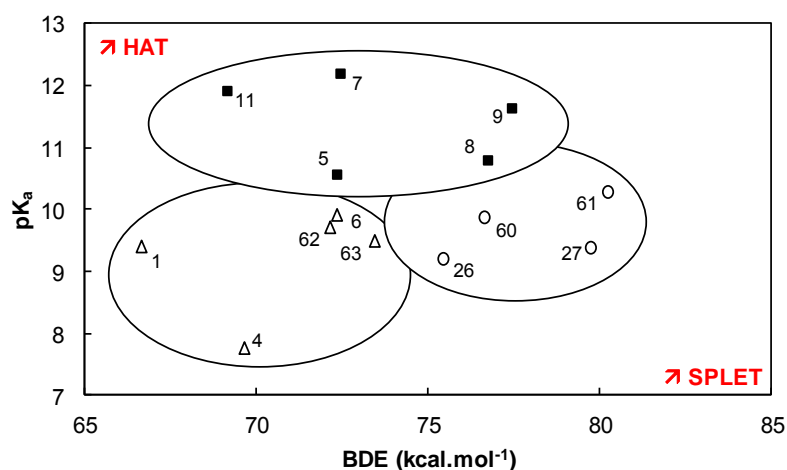


Figure 3.61: Correlation between pKa values obtained from literature for *ortho*-methoxyphenols (○), *ortho*-alkylphenols (■), *ortho*-hydroxyphenols (Δ) and calculated BDEs

Figure 3.62 resumes the three kinds of solvents studied (*i.e.* apolar aprotic, HBA and polar protic solvents) and the HAT or SPLET mechanisms involved during the hydrogen transfer from phenols to DPPH<sup>•</sup>.<sup>369</sup> In HBA solvents such as oils, the reactivity of phenols decrease compared to apolar solvents because of the stabilization of the phenolic hydrogen.  $\alpha$ -Tocopherol **11**, epigallocatechin gallate **55**, carnosic acid **70** and myricetin **32** are the most efficient natural phenolic antioxidants with the higher kinetic rate constants. Conversely, in alcohol solutions, the most acidic antioxidants are the *ortho*-methoxyphenols which are somewhat dissociated into phenolate which react faster by electro transfer.

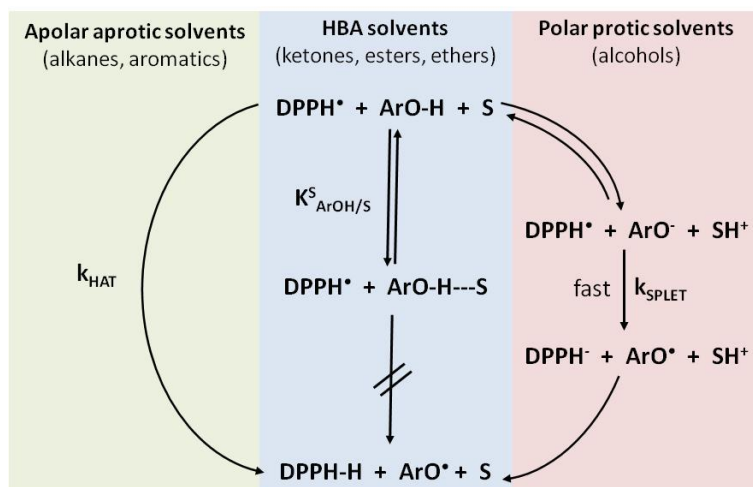


Figure 3.62: HAT and SPLET mechanisms involved during the hydrogen transfer from phenols to DPPH<sup>•</sup> radical into apolar aprotic, HBA and polar protic solvents<sup>369</sup>

#### 4.2.4 Stoichiometric number $\sigma_{\text{exp}}$ of phenolic antioxidants

Phenolic antioxidants are also characterized by the maximum number of radicals trapped by one antioxidant molecule, named the stoichiometric number  $\sigma_{\text{exp}}$ . Table 3.26 summarizes  $\sigma_{\text{exp}}$  obtained in the same three solvents as for the kinetic rate constants determination (*i.e.* toluene, ethyl acetate and ethanol).

The stoichiometric number depends on the nature of the substituents at the *ortho* and *para* positions of the phenolic ring. Moreover, the determination of the number of hydrogen transfer

provides information on the oxidation products, but usually, several competitive pathways are simultaneously involved making the interpretation not straightforward. The mechanism of interaction between DPPH<sup>•</sup> and phenols takes place in two steps: **1)** abstraction of the phenolic hydrogen and **2)** transfer of a second hydrogen or formation of reactive or not-reactive dimers from the phenoxyl radical ArO<sup>•</sup>.

Phenols	N°	Solvents		
		Toluene	Ethyl acetate	Ethanol
<b>5-Tert-butyl-pyrogallol</b>	<b>1</b>	2.1	2.0	3.0
<b>Propyl gallate</b>	<b>4</b>	3.9	3.3	4.2
<b>BHA</b>	<b>5</b>	2.0	2.1	2.6
<b>4-Tert-butyl-catechol</b>	<b>6</b>	2.5	2.5	2.9
<b>BHT</b>	<b>7</b>	2.0	2.0	1.0
<b>TBHQ</b>	<b>8</b>	2.0	2.0	2.3
<b><i>o</i>-Tert-butyl-<i>p</i>-cresol</b>	<b>9</b>	2.5	1.5	3.0
<b><math>\alpha</math>-Tocopherol</b>	<b>11</b>	2.0	2.0	2.1
<b>Gallic acid</b>	<b>15</b>	ns	5.0	6.4
<b>Protocatechuic acid</b>	<b>16</b>	ns	1.8	2.1
<b>Syringic acid</b>	<b>17</b>	1.1	0.7	2.2
<b>Rosmarinic acid</b>	<b>23</b>	ns	4.1	4.3
<b>Caffeic acid</b>	<b>24</b>	ns	2.0	2.3
<b>Chlorogenic acid</b>	<b>25</b>	ns	1.9	2.3
<b>Sinapic acid</b>	<b>26</b>	1.4	1.0	2.3
<b>Ferulic acid</b>	<b>27</b>	1.8	1.4	1.9
<b>Myricetin</b>	<b>32</b>	ns	3.4	4.2
<b>Quercetin</b>	<b>34</b>	ns	1.9	4.2
<b>Epigallocatechin gallate</b>	<b>55</b>	ns	5.4	nd
<b>Piceatannol</b>	<b>58</b>	ns	2.0	nd
<b>Resveratrol</b>	<b>59</b>	ns	0.9	2.1
<b>Isoeugenol</b>	<b>60</b>	0.9	1.0	2.1
<b>Eugenol</b>	<b>61</b>	2.1	0.9	3.0
<b>Hydroxytyrosol</b>	<b>62</b>	2.0	1.9	2.0
<b>Catechol</b>	<b>63</b>	1.9	2.1	2.4
<b>Sesamol</b>	<b>65</b>	2.1	2.4	2.3
<b>Aesculetin</b>	<b>67</b>	ns	2.1	4.5
<b>Carnosol</b>	<b>69</b>	1.9	2.0	2.1
<b>Carnosic acid</b>	<b>70</b>	2.0	2.1	2.1
<b>Ascorbyl palmitate</b>	<b>71</b>	2.0	2.0	2.5

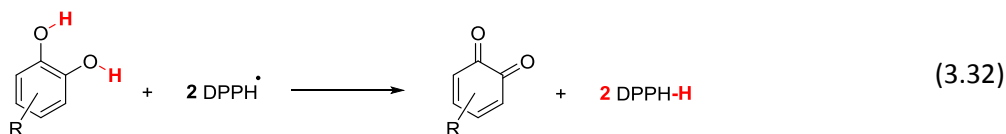
ns: not soluble, nd: not determined

**Table 3.26: Stoichiometric numbers  $\sigma_{\text{exp}}$  obtained for phenols with the DPPH<sup>•</sup> test in toluene, ethyl acetate and ethanol**

In some cases,  $\sigma_{\text{exp}}$  in ethyl acetate are lower than in toluene. As seen for the kinetic solvent effects (KSE) of ethyl acetate, HBA solvents decrease drastically the availability of the phenolic hydrogen and  $[\text{ArOH}]_0$  reacting by the HAT mechanism decrease. Indeed, the oxidized forms are the same in both solvents but they are less active in ethyl acetate. Ion-negative and ion-positive ESI mass spectrometry already used for the analysis of the composition of extracts in phenolic antioxidants<sup>370</sup>,<sup>371</sup> are used to develop supposed mechanism for the reaction of phenols with radical species.

#### 4.2.4.1 Catechol, hydroquinone and pyrogallol derivatives

Phenolic antioxidants with catechol structure are known to transfer 2 hydrogens to DPPH<sup>•</sup>. Indeed, the phenolic hydrogen from the *ortho*-OH substituent releases its second hydrogen and the *ortho*-quinone compound is formed (Eq. 3.32).



The global stoichiometric numbers of 2.0 obtained in ethyl acetate or toluene are in agreement with the reported oxidized forms of catechol derivatives 5-*tert*-butyl-pyrogallol **1**,<sup>372</sup> protocatechuic acid **16**,<sup>373</sup> caffeic acid **24**,<sup>374</sup> chlorogenic acid **25**,<sup>375</sup> catechol **63**,<sup>376</sup> hydroxytyrosol **62**,<sup>377</sup> quercetin **34**,<sup>378</sup> carnosol **69**<sup>379</sup> and carnosic acid **70**.<sup>380</sup> Ion-positive ESI-MS analysis of the oxidized form of carnosic acid **70A** supports our mechanism with the finding of the  $[\text{M}+\text{H}]^+$  peak at  $m/z = 331$  and the disappearance of the phenol peak  $[\text{M}+\text{H}]^+$  at  $m/z = 333$ . The more intense peaks correspond to the  $[\text{DPPH}^{\bullet}+\text{H}]^+$  and  $[\text{DPPH-H}+\text{H}]^+$  forms (Fig. 3.63).

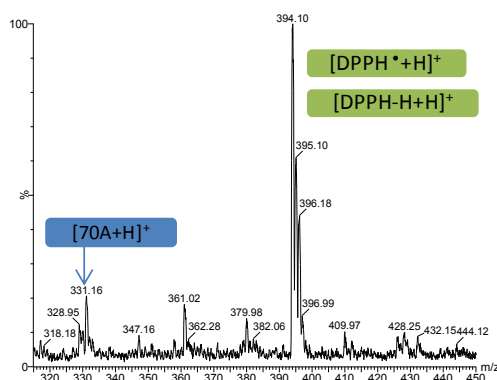
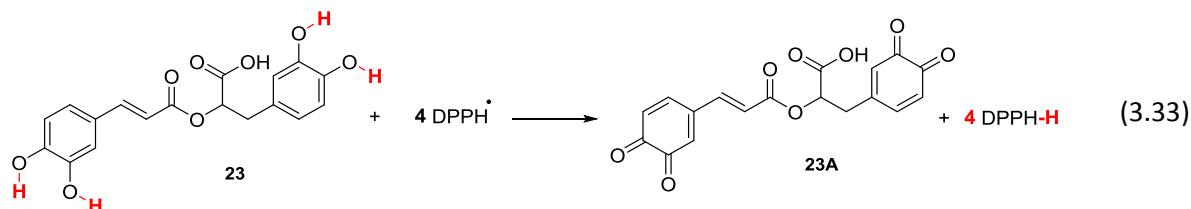


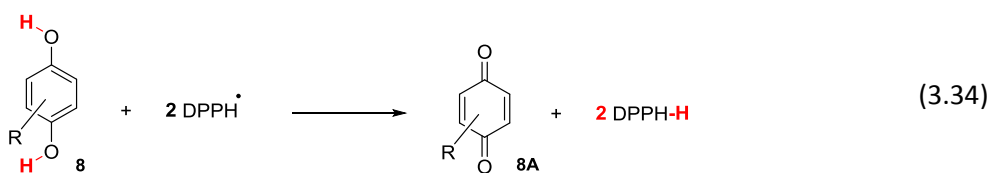
Figure 3.63: Ion-positive ESI MS analysis of the oxidation of carnosic acid **70** by DPPH<sup>•</sup> radical,  $[\text{carnosic acid}] = 3 \times 10^{-6} \text{ M}$ ,  $[\text{DPPH}^{\bullet}] = 10^{-5} \text{ M}$ ,  $[\text{H}^+] = 10^{-3} \text{ M}$  in MeOH/H<sub>2</sub>O

As for the other catechol derivatives, aesculetin **67** forms the *ortho*-quinone compounds in ethyl acetate. Nevertheless, it reaches an impressive stoichiometric number of 4.5 in ethanol. With a free *ortho*-position, aesculetin could dimerize as illustrated by Castaldi *et al.*<sup>381</sup> and then react with ethanol to form new reactive intermediates able to trap more than 2 radicals per molecule.

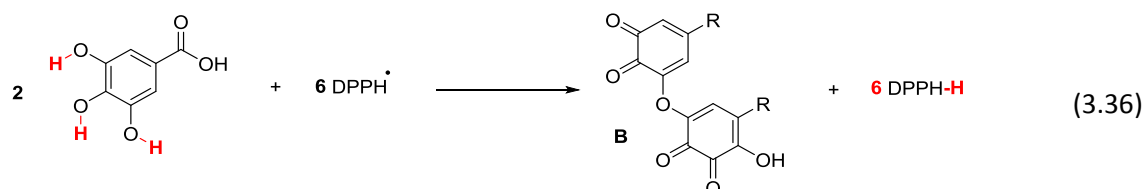
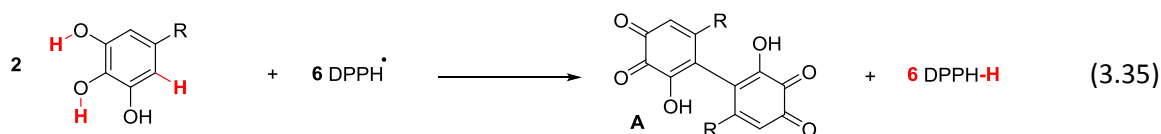
With 2 active catechol moieties (BDEs of 69.2, 72.4, 75.2 and 75.9 kcal.mol<sup>-1</sup>), rosmarinic acid **23** traps 4 radicals per molecule and forms 2 *ortho*-quinone substructures **23A** in the same molecule<sup>382</sup> which is correlated with the stoichiometric number of 4.1 (Eq. 3.33).



Antioxidants with hydroquinone structure such as TBHQ **8** give a stoichiometric number of 2.0 thanks to the formation of the *p*-quinone compound **8A** (Eq. 3.34).<sup>383</sup>



Surprisingly, propyl gallate **4**, 4-*tert*-butylcatechol **6**, gallic acid **15**, myricetin **32** and epigallocatechin gallate **55** trap respectively 3.9, 2.5, 5.0, 3.4 and 5.4 radicals per molecule in ethyl acetate. Given the number of phenolic hydrogens in their chemical structure, it is assumed that they form active dimers (Eqs. 3.35 and 3.36).<sup>384-386</sup>



Ion-negative ESI-MS analysis of the oxidized form of gallic acid in ethyl acetate reinforces our proposed mechanism of oxidation. With an identical mass of 334 u.m.a, **figure 3.64** shows the formation of C-C and C-O dimers under the form of  $[\text{M}-2\text{H}]^{2-}$  compounds at  $m/z = 332$ . This corresponds of a loss of two carboxylic hydrogens leading to the *di*-phenolate forms. Nevertheless, these dimers are just responsible of the abstraction of 3 hydrogens from gallic acid **15**. Therefore, other hydrogens could be transferred or degradation products could be obtained.

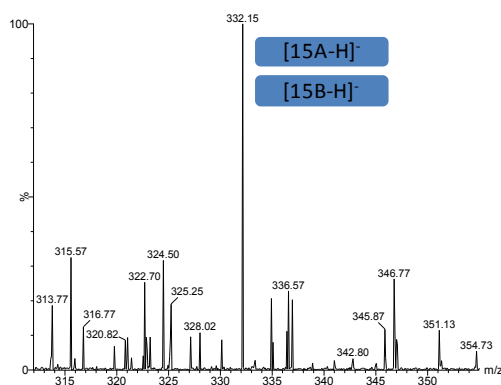
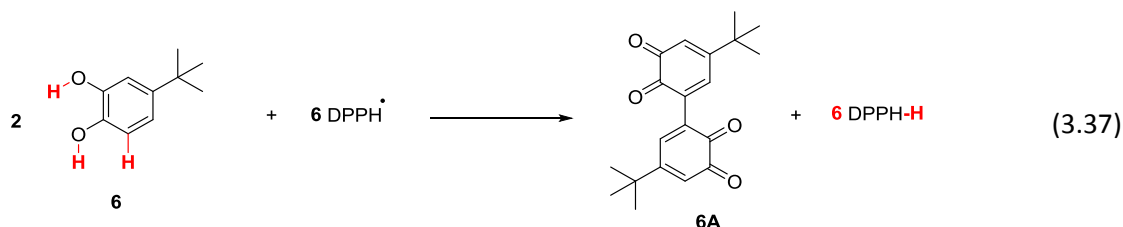
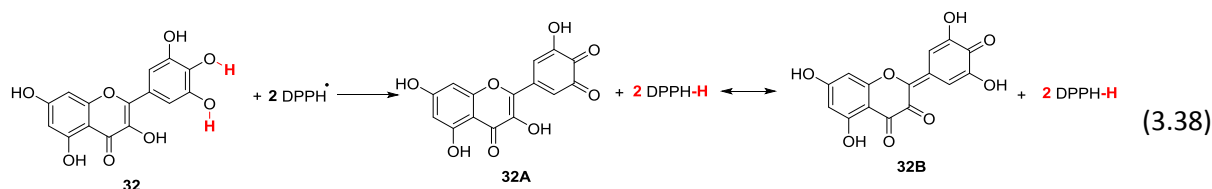


**Figure 3.64:** Ion-negative ESI MS analysis of the oxidation of gallic acid **15** by  $\text{DPPH}^{\cdot}$  radical,  $[\text{gallic acid}] = 3 \times 10^{-6} \text{ M}$ ,  $[\text{DPPH}^{\cdot}] = 10^{-5} \text{ M}$ ,  $[\text{NH}_4^+] = 10^{-3} \text{ M}$  in  $\text{MeOH}/\text{H}_2\text{O}$

With two pyrogallol moieties, epigallocatechin gallate **55** follows the same mechanism of *ortho* C-C and C-O dimers formations which is consistent with a stoichiometric number of 5.4. 4-*Tert*-butylcatechol **6**, with a catechol structure, has a stoichiometric number higher than 2.0 ( $\sigma_{\text{exp}} = 2.9$  in ethanol and 2.5 in ethyl acetate). With a free *ortho*-position, there is a C-C coupling<sup>387</sup> which results on the abstraction of 3 hydrogens and formation of dimer **6A** (Eq. 3.37).



Myricetin **32** reacts with  $\text{DPPH}^{\bullet}$  radical and transfers 2 hydrogens giving an *ortho*-quinone **32A** in equilibrium with the extended *para*-quinone **32B** (Eq. 3.38).<sup>357, 388</sup> It is the same mechanisms for quercetin which has a stoichiometric number of 1.9 in ethyl acetate.



Myricetin **32** obtained a stoichiometric number of 3.4 in ethyl acetate. In comparison with a blank analysis (Fig. 3.65, 1), ion-negative ESI mass spectrometry (Fig. 3.65, 2) shows the  $[\text{M-H}]^{-}$  peak ( $m/z = 315$ ) for the *ortho*-quinone (**32A**) and extended *para*-quinone (**32B**) compounds. Moreover, there are peaks related to the loss of 3 hydrogens ( $[\text{M-H}]^{-}$  at  $m/z = 314$ ) and 4 hydrogens ( $[\text{M-H}]^{-}$  at  $m/z = 313$ ).

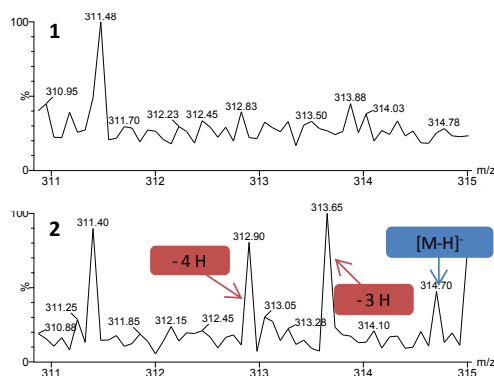


Figure 3.65: Ion-negative ESI MS analysis of a blank (1) and the oxidation of myricetin **32** (2) by  $\text{DPPH}^{\bullet}$  radical, [myricetin] =  $3 \times 10^{-6}$  M,  $[\text{DPPH}^{\bullet}] = 10^{-5}$  M,  $[\text{NH}_4^+] = 10^{-3}$  M in  $\text{MeOH}/\text{H}_2\text{O}$

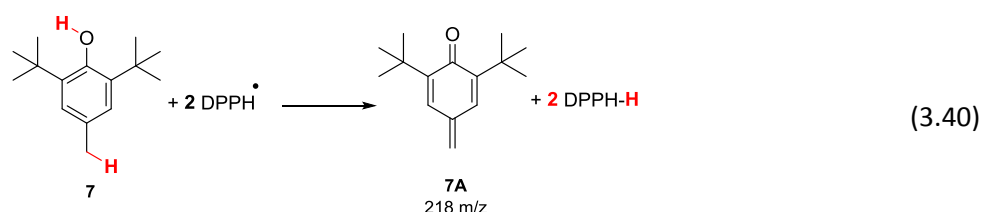
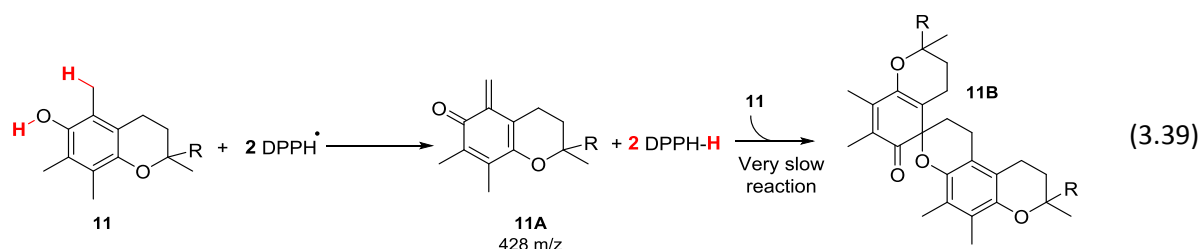
#### 4.2.4.2 Monophenols

Monophenols, which are supposed to transfer only one hydrogen per molecule, are in fact able to trap more than one radical. The free *ortho*-position on the phenolic site is a decisive factor.

##### ▪ Phenolic antioxidants without free *ortho*-position

$\alpha$ -Tocopherol **11** (Eq. 3.39) and BHT **7** (Eq. 3.40) are the only phenolic antioxidants studied without free *ortho*-position. They are known to transfer firstly the phenolic hydrogen and then a second hydrogen from the *o*- or *p*- methyl group leading to the *o*- or *p*- quinone-methide derivative, consistent with a stoichiometric number  $\sigma_{\text{exp}}$  of 2. In ethyl acetate, these *p*- and *o*- quinone-methide derivatives **11A** and **7A** are electrophilic compounds capable of reacting with the starting phenols **11** and **7** to form dimers.<sup>389-392</sup> As quinone-methides derived from  $\alpha$ -tocopherol **11A** react very slowly

with starting phenols **11**, dimerization does not take place under our experimental conditions and compound **11B** is not obtained.<sup>336</sup>



*Ortho*-quinone methide derivatives **11A** and **7A** are identified by ion-negative ( $[M-H]^-$  at  $m/z = 427$ ) and ion-positive ( $[M+H]^+$  at  $m/z = 219$ ) ESI-MS analyses respectively (Fig. 3.66). Consequently, the suggested mechanism of hydrogen transfer from  $\alpha$ -tocopherol **11** and BHT **7** is confirmed.

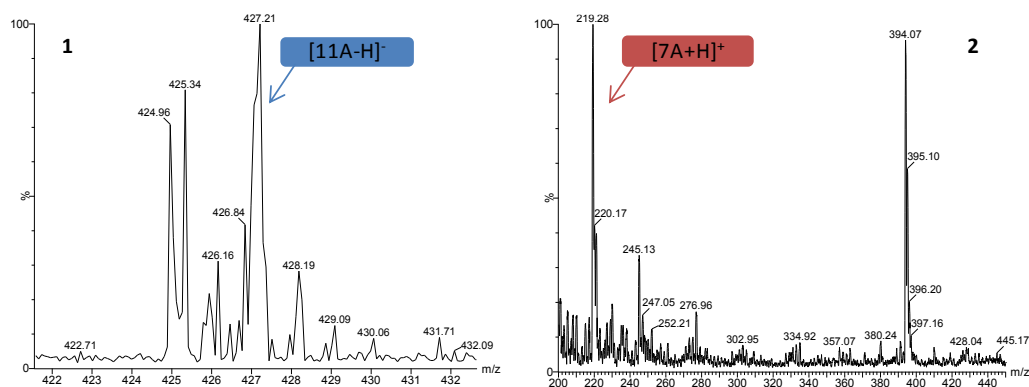
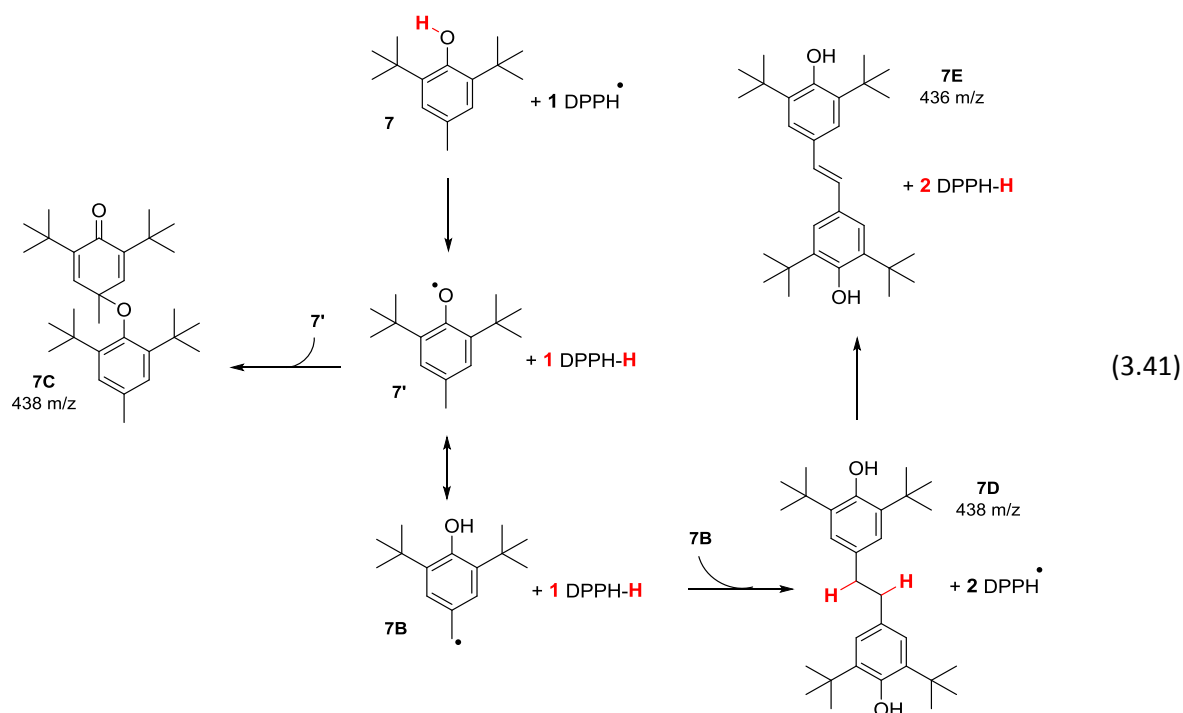


Figure 3.66: 1) Ion-negative ESI-MS analysis of the oxidation of  $\alpha$ -tocopherol **11** by  $DPPH^\bullet$  [ $\alpha$ -tocopherol] =  $3 \times 10^{-6}$  M, [ $DPPH^\bullet$ ] =  $10^{-5}$  M, [ $NH_4^+$ ] =  $10^{-3}$  M in MeOH/ $H_2O$  and 2) Ion-positive ESI-MS analysis of the oxidation of BHT **7** by  $DPPH^\bullet$  radical [BHT] =  $3 \times 10^{-6}$  M, [ $DPPH^\bullet$ ] =  $10^{-5}$  M, [ $H^+$ ] =  $10^{-3}$  M in MeOH/ $H_2O$

It is well established that dimerization occurs in the case of BHT **7** according to Bondet *et al.* (Eq. 3.41).<sup>360</sup>



Indeed, the combination of two molecules of **7B** leads to the formation of **7D** via C-C linkage and a loss of H<sub>2</sub> in order to have an entire delocalization of the electrons (**7E**).<sup>393</sup> In another way, the reaction of **7B** with **7'** leads to the dimer **7C** via C-O linkage. These different dimers are detected by ion-negative ESI-MS analyses under the form of [M-H]<sup>-</sup> adducts (Fig. 3.67).

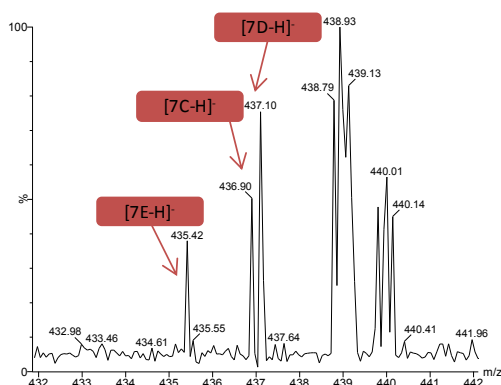
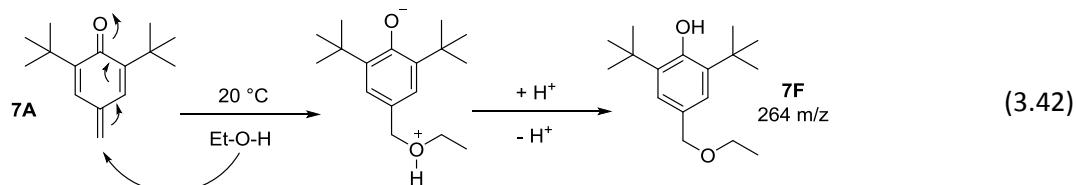


Figure 3.67: Ion-negative ESI-MS analysis the oxidation of BHT **7** by DPPH<sup>•</sup> radical in ethyl acetate, [BHT] = 3 × 10<sup>-6</sup> M, [DPPH<sup>•</sup>] = 10<sup>-5</sup> M, [NH<sub>4</sub><sup>+</sup>] = 10<sup>-3</sup> M in MeOH/H<sub>2</sub>O

Surprisingly, BHT **7** traps only one hydrogen per molecule of antioxidant in ethanol ( $\sigma_{\text{exp}} = 1.0$ ). The para-quinone methide **7A** formed in ethyl acetate is no longer detected. Instead, there is a new oxidation product ([7F-H]<sup>-</sup> at m/z = 263) resulting from the 1,6-nucleophilic reaction<sup>392</sup> of alcohol on the quinone methide **7A** (Eq. 3.42, Fig. 3.68).



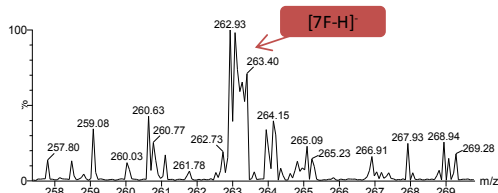
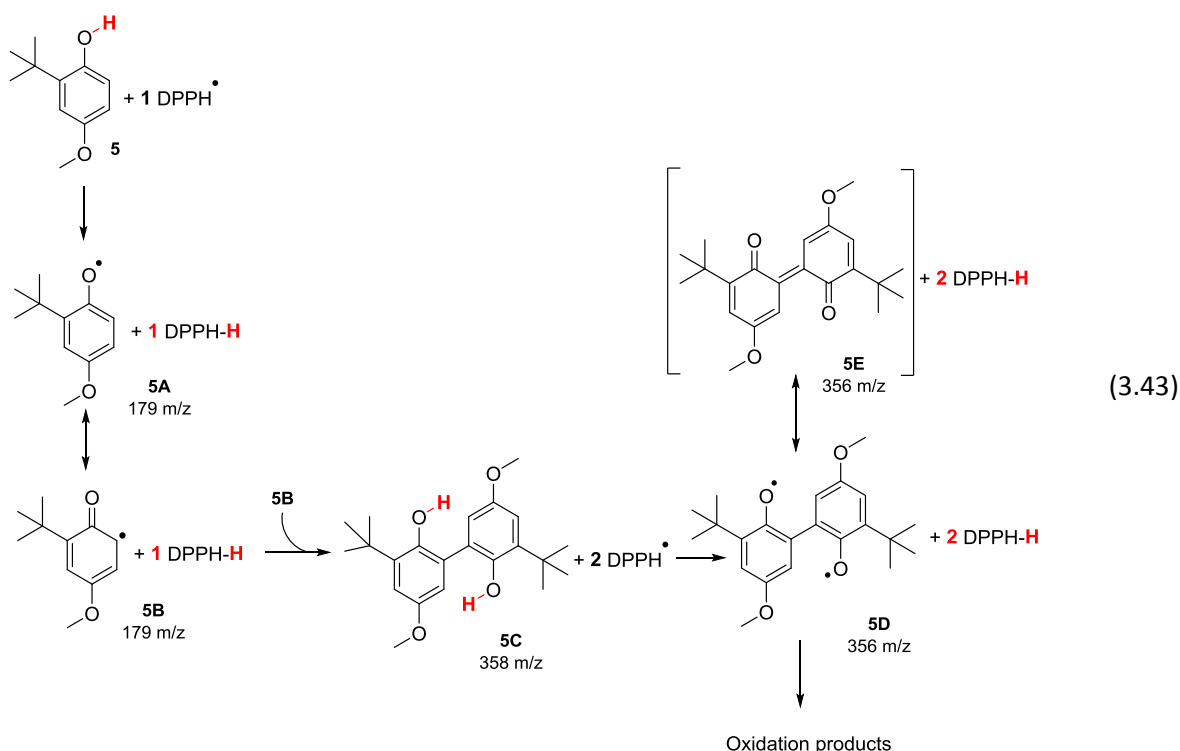


Figure 3.68: Ion-negative ESI MS analysis of the oxidation of BHT 8 by  $\text{DPPH}^\bullet$  radical in ethanol,  $[\text{BHT}] = 3 \times 10^{-6} \text{ M}$ ,  $[\text{DPPH}^\bullet] = 10^{-5} \text{ M}$ ,  $[\text{NH}_4^+] = 10^{-3} \text{ M}$  in  $\text{MeOH}/\text{H}_2\text{O}$

▪ *Phenolic antioxidants with free ortho-position*

BHA 5, which has free *ortho*-position, preferentially dimerizes at the *ortho-ortho* position, giving the diphenol 5C.<sup>394-396</sup> Then, this dimer may transfer two hydrogen atoms consistent with a stoichiometric number of 2 (Eq. 3.43).



Radical species 5A and 5B formed through the abstraction of one hydrogen atom are detected by ESI-MS analysis (Fig. 3.69, 1,  $[\text{M}+\text{H}]^+$  at  $m/z = 180$ ) and the diphenol 5C is also observed (Fig. 3.69, 2,  $[\text{M}-\text{H}]^-$  at  $m/z = 357$ ). Nevertheless, the loss of 2 hydrogen atoms leading to dimer 5E is not revealed with this analytical technique. Either because compounds 5D and 5E are not ionized or there is a degradation of the dimer 5C after the transfer of 2  $\text{H}^\bullet$ .

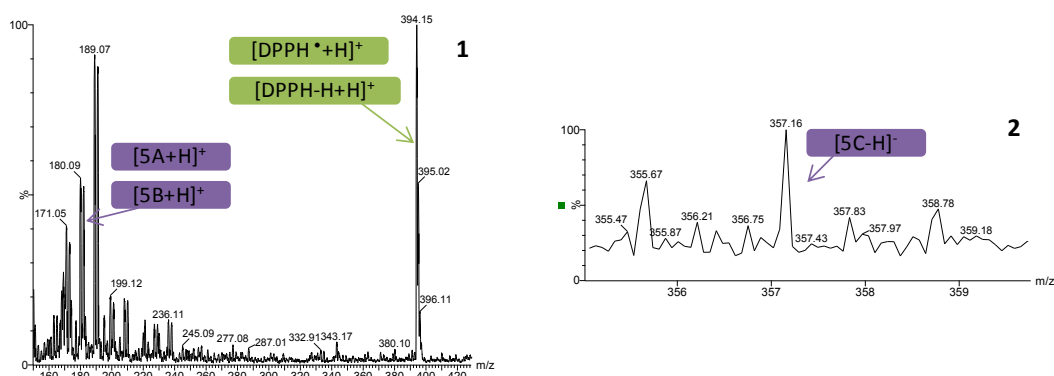


Figure 3.69: 1) Ion-positive ESI-MS analysis of the oxidation of BHA 5 by DPPH<sup>•</sup> [BHA] =  $3 \times 10^{-6}$  M, [DPPH<sup>•</sup>] =  $10^{-5}$  M, [H<sup>+</sup>] =  $10^{-3}$  M in MeOH/H<sub>2</sub>O and 2) Ion-negative ESI-MS analysis of the oxidation of BHA 5 by DPPH<sup>•</sup> [BHA] =  $3 \times 10^{-6}$  M, [DPPH<sup>•</sup>] =  $10^{-5}$  M, [NH<sub>4</sub><sup>+</sup>] =  $10^{-3}$  M in MeOH/H<sub>2</sub>O

Ferulic acid **27**, with a free *ortho* position, dimerizes at the *ortho-ortho* position giving diphenol **27A** ([M-H]<sup>-</sup> at m/z = 385) with strong antioxidant activity<sup>397</sup> since it can further transfer 2 H<sup>•</sup> with the formation of **27B** ([M-H]<sup>-</sup> at m/z = 383) (Fig. 3.70). Finally, it is in equilibrium with **27C** where the entire delocalization of electrons is possible (Eq. 3.44). Whereas it was not the case for BHA **5**, the loss of 2 H<sup>•</sup> leading to **27C** is detected in both solvents.

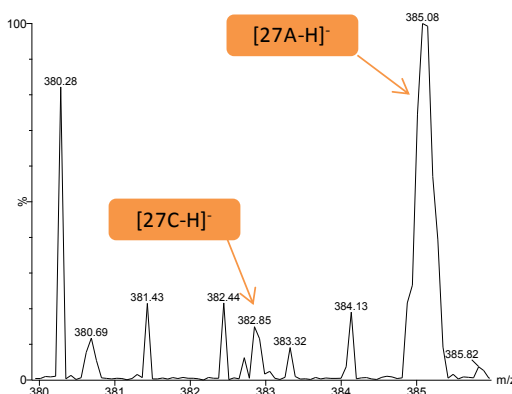
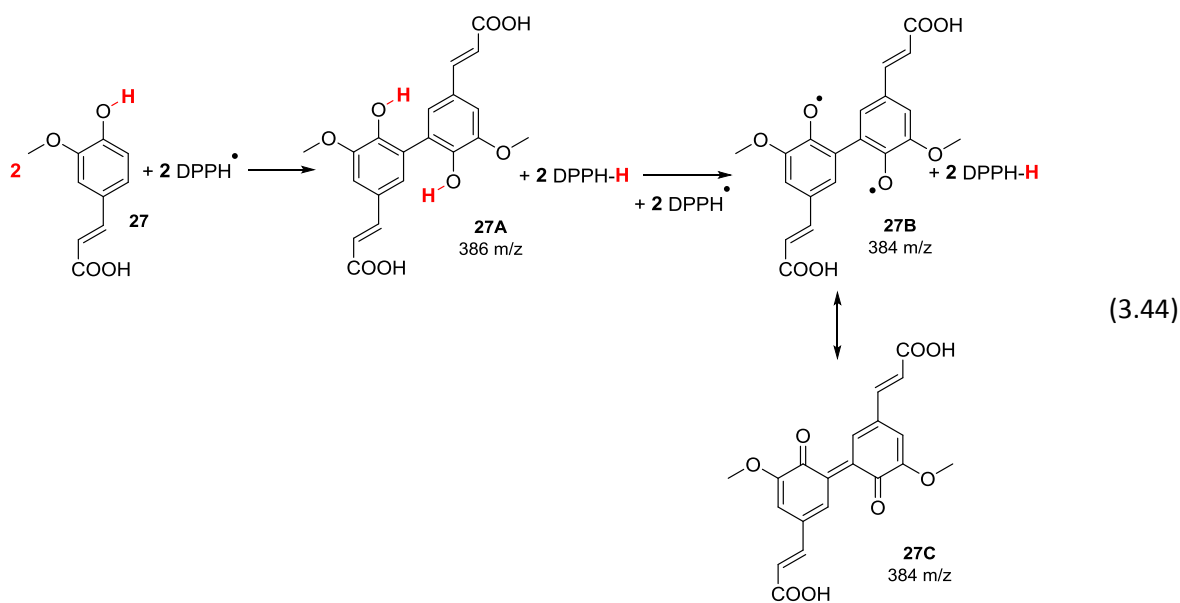
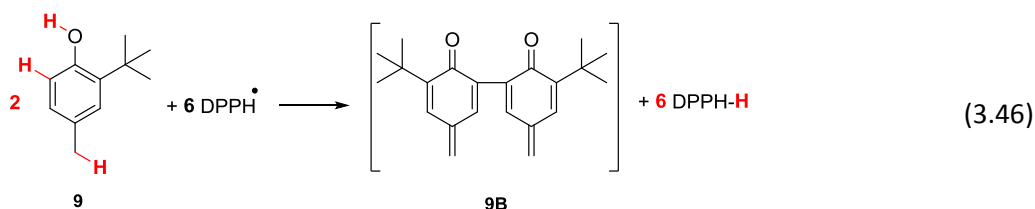
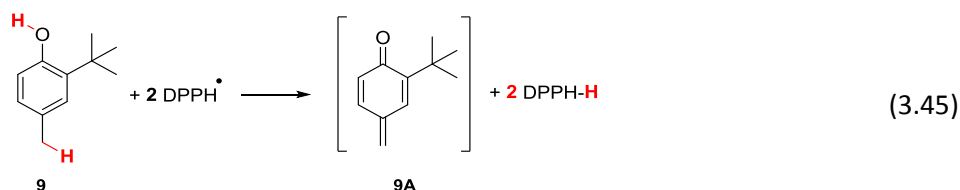


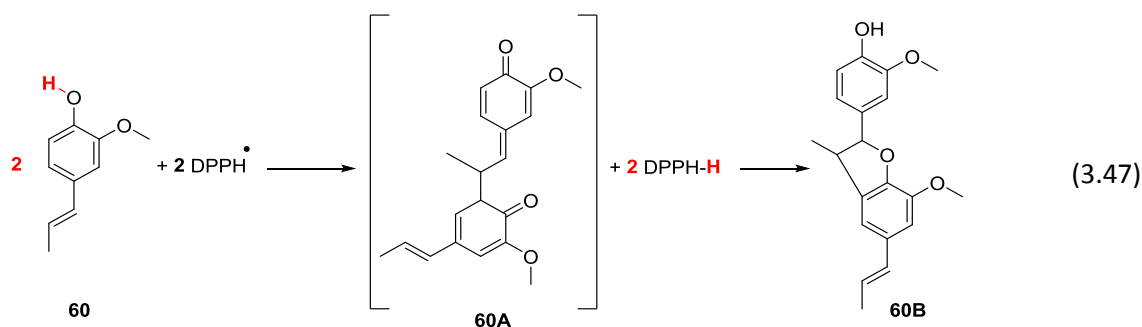
Figure 3.70: Ion-negative ESI-MS analysis of the oxidation of ferulic acid **27** by DPPH<sup>•</sup> in ethanol, [ferulic acid] =  $3 \times 10^{-6}$  M, [DPPH<sup>•</sup>] =  $10^{-5}$  M, [NH<sub>4</sub><sup>+</sup>] =  $10^{-3}$  M in MeOH/H<sub>2</sub>O

This is a perfect illustration of the effect of HBA solvents. Indeed, in ethyl acetate,  $\sigma_{\text{exp}} = 1.4$  whereas in toluene and ethanol  $\sigma_{\text{exp}} \approx 2.0$ . Intramolecular hydrogen bonding between ethyl acetate and antioxidants drastically decreases the concentration of phenols available to react *via* HAT mechanism. Therefore, diphenol are obtained in lower concentration in ethyl acetate than in toluene and ethanol.

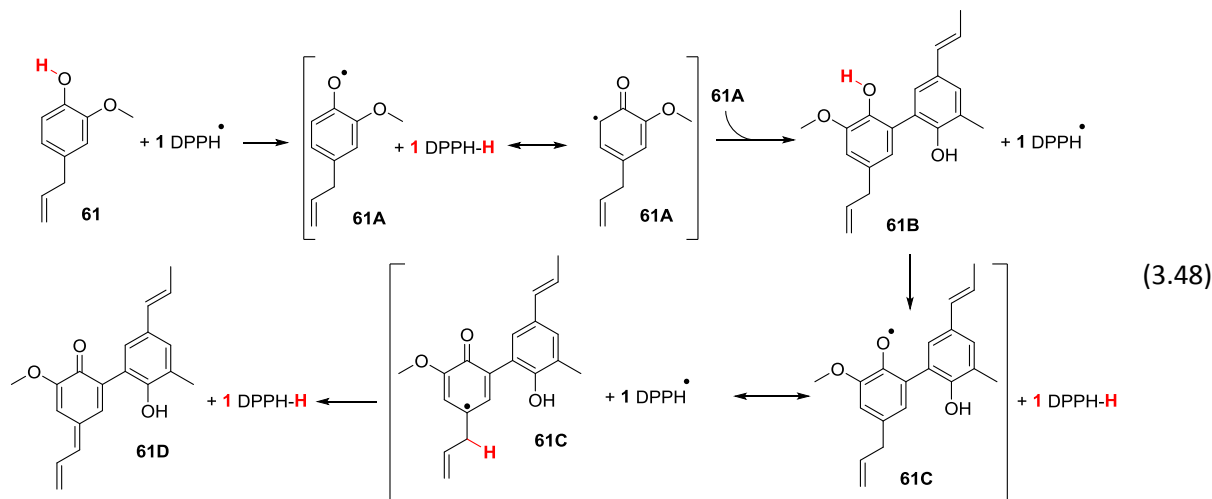
*o*-Tert-butyl-*p*-cresol **9** traps 2.5 radicals per molecule in toluene *via* 2 competitive pathways. The first one is based on the BHT mechanism with the formation of *p*-quinone methide **9A** (Eq. 3.45,  $\sigma_{\text{exp}} = 2.0$ ). The second one results from the *ortho*-dimerization leading to C-C dimer **9B** (Eq. 3.46,  $\sigma_{\text{exp}} = 3.0$ ).<sup>398</sup>



The radical-scavenging capacity of isoeugenol **60** in toluene and ethyl acetate is totally different from that of the other phenols, since it only traps one radical per molecule ( $\sigma_{\text{exp}} = 1.0$ ). Indeed, its phenoxyl radical dimerizes giving dehydrodiisoeugenol **60B** (Eq. 3.47), the antioxidant activity of which, evaluated by the DPPH $\cdot$  test, was reported to be very weak and practically negligible compared to that of isoeugenol **60**.<sup>399</sup> The formation of a non-reactive dimer implies the stoichiometric number of 1. Conversely, isoeugenol **60** traps two radicals per molecule in ethanol ( $\sigma_{\text{exp}} = 2.0$ ). This implies that the dimer formed becomes reactive in polar protic solvent increasing the antioxidant activity of isoeugenol **60**. As for isoeugenol, resveratrol **59** reaches a stoichiometric number of 0.9 in ethyl acetate whereas it gives 2.1 in ethanol. As described by Shingai *et al.*<sup>400</sup>, the dimers formed are not active in ethyl acetate because of kinetic solvent effects (KSEs) but become reactive in ethanol.

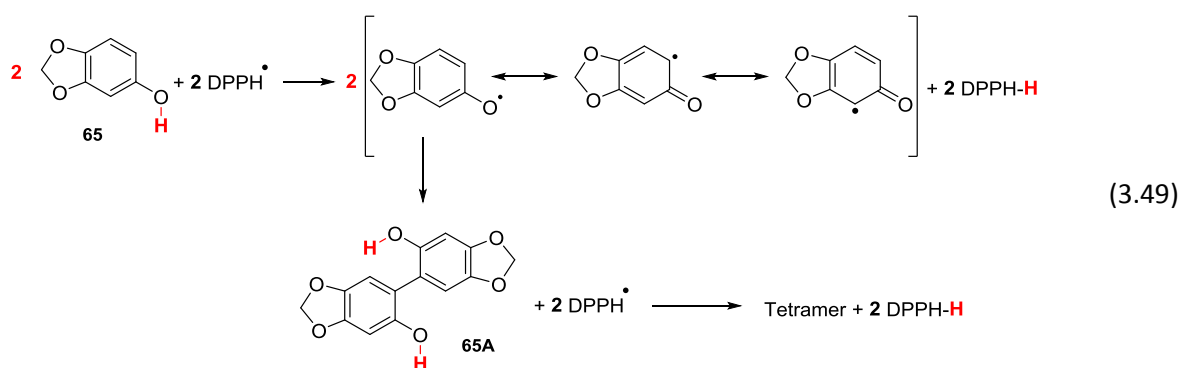


Eugenol **61**, with a similar chemical structure as isoeugenol **60**, has a higher stoichiometric number in toluene ( $\sigma_{\text{exp}} = 2.1$ ). This is consistent with values found in literature. Based on the reactive intermediates detected by GC and LC-MS, Bortolomeazzi *et al.* suggested the following mechanism of action (Eq. 3.48).<sup>399</sup> There is abstraction of the phenolic hydrogen and, at the free *ortho*-position, the phenoxyl radical **61A** dimerizes and forms the diphenol **61B**. This dimer has a higher activity than the parent phenol and transfer 2 other  $\text{H}^\bullet$  leading to **61D** which is consistent with our value of stoichiometric number ( $\sigma_{\text{exp}} = 2.1$ ).



Because of the kinetic solvent effect (KSE), this dimer becomes non-reactive in ethyl acetate and the stoichiometric number decreases ( $\sigma_{\text{exp}} = 0.9$ ). *Via* the fast SPLET mechanism involved in ethanol, eugenol **61** traps 3 radicals per molecule ( $\sigma_{\text{exp}} = 3.0$ ). Bortolomeazzi *et al.* showed that there are reactions between reactive intermediates and solvent of study (methanol).<sup>399</sup> Therefore, in our case, it could induce the formation of new products which become actives and transfer more than 2  $\text{H}^\bullet$ .

Sesamol **65** releases its first phenolic hydrogen and the oxidized compound **65A** is formed *via* dimerization.<sup>401</sup> It could then transfer 2 supplementary  $\text{H}^\bullet$  in agreement with a stoichiometric number of 2.1 (Eq. 3.49).



Antioxidants with the highest stoichiometric number are phenols that exhibit a catechol or a pyrogallol moiety as well as a free *ortho*-position such as gallic acid **15**, myricetin **32** and epigallocatechin gallate **55**. These structural requirements lead to diphenols as reactive intermediates which trap more than 2 radicals per molecule. Kinetic solvent effects (KSEs) decrease the activity of dimers formed and stoichiometric numbers in polar protic solvents are higher than in

HBA solvents. The oxidation of phenolic antioxidants via DPPH<sup>•</sup> test combined with the ion-negative and ion-positive ESI-MS analyses is a powerful method to identify phenolic compounds with effective antioxidant properties and rationalize the antioxidant mechanisms.

#### 4.2.5 Conclusion

The comparison of the kinetic rate constants of hydrogen transfer from phenols to DPPH<sup>•</sup> shows that the chemical structures of phenols dramatically impact their reactivity. Moreover, this influences also the number of radical trapped by each molecule of antioxidant. The structural features required to provide excellent antioxidant properties are found to be: **1)** pyrogallol or catechol moieties, **2)** conjugation with *para*-electron-donating groups (EDG) and **3)** free ortho-position. Indeed, these key parameters lead to *i)* low BDEs, *ii)* relatively high IPs and *iii)* the formation of reactive dimers which increase the number of trapped radicals. Based on these considerations, gallic acid **15**, myricetin **32** and epigallocatechin gallate **55** as pyrogallol derivatives, rosmarinic acid **23**, carnosol **69** and carnosic acid **70** as catechol derivatives appears to be the most promising natural phenolic alternatives to  $\alpha$ -tocopherol **11** and synthetic phenols.

In order to confirm these predictions based on thermodynamic and DPPH<sup>•</sup> studies, phenols studied previously are tested in more realistic conditions to protect omega-3 oils during their oxidation by O<sub>2</sub> in RapidOxy<sup>®</sup> and Rancimat tests.

### 4.3 Antioxidant activity of phenolic compounds against the oxidation of omega-3 oils

Autoxidation of oils and more precisely edible oils rich in omega-3 by oxygen (<sup>3</sup>O<sub>2</sub>) has been studied for a long time as developed in the **chapter 1**.<sup>36</sup> The oxidation mechanism of poly(unsaturated) fatty acids and FAMES derivatives leads to the formation of hydroperoxides, cyclic peroxides, ketones... related to the loss of organoleptic properties for food. Phenolic antioxidants are, most of the time, incorporated into edible oils to avoid their oxidative degradation. The labile hydrogen (ArO-H) reacts with radicals and converts them into more stable non radical products.<sup>402</sup> As reported by Choe *et al.*, antioxidants with reduction potential ( $E^\circ \leq 500$  mV) lower than that of an alkoxy (RO<sup>•</sup>), peroxy (ROO<sup>•</sup>) and alkyl (R<sup>•</sup>) radicals of polyunsaturated fatty acids (respectively 1600, 1000 and 600 mV) can transfer the hydrogen to the radical.<sup>35</sup> These reduction potentials were obtained from flash photolysis and pulse radiolysis. This clearly shows that antioxidants react with lipid peroxy radicals before they react with other lipid molecules to produce further free radicals.

For the study, FAMES of linseed oil were synthesized by transesterification. They were composed of 5.3% of methyl palmitate (C16:0), 5.3% of methyl stearate (C18:0), 33.1% of methyl oleate (C18:1), 11.2% of methyl linoleate (C18:2) and 45.1% of methyl linolenate (C18:3,  $\omega$ -3) as determined by GC/MS analyses. Besides the BDE calculations and the DPPH<sup>•</sup> test, the autoxidation of omega-3 oils in the presence of the different phenols has been kinetically investigated by measuring the oxygen consumption using the RapidOxy<sup>®</sup> apparatus which provides information on induction periods (IP) and oxidation rates ( $R_{ox}$ ). Moreover, the formation of volatile organic acid compounds (*i.e.* formic acid) was investigated by monitoring the conductivity of water during the oxidation of omega-3 oils with antioxidants thanks to a stay in the US laboratory of Cargill located in Minnesota.

### 4.3.1 RapidOxy® analyses

#### 4.3.1.1 Principles and results

Figure 3.71 presents the RapidOxy® apparatus which is particularly suitable to follow the inhibition of oil autoxidation.<sup>39</sup> For more information, see the experimental part.

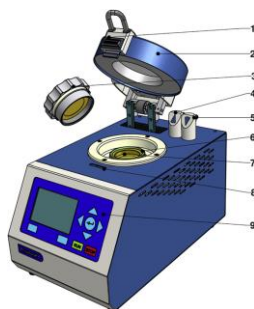


Figure 3.71: RapidOxy® apparatus for measurement of oxygen consumption during the autoxidation process

Figure 3.72 points out that the curves corresponding to the oxygen consumption vs time exhibit three stages.

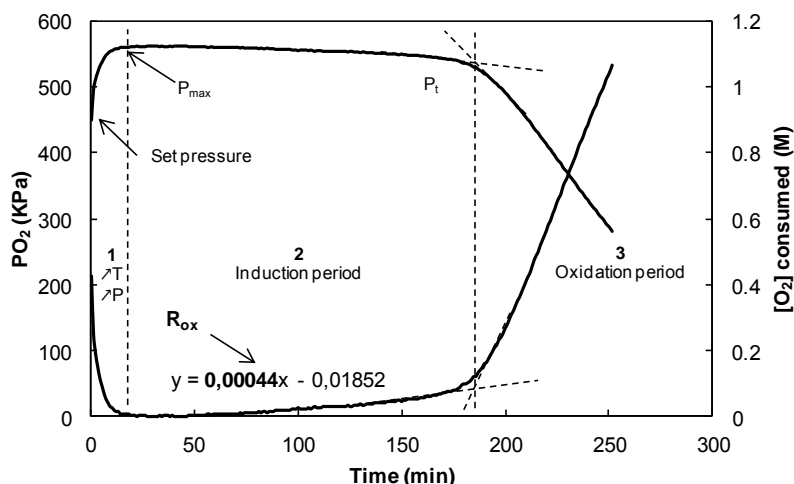


Figure 3.72: Evolution of the oxygen pressure (left axis) and oxygen concentration (right axis) during the oxidation of FAMES of linseed oil with  $[BHT] = 5 \times 10^{-4} \text{ mol.L}^{-1}$  at  $90 \text{ }^\circ\text{C}$

After the set pressure (450 kPa) is reached, the cell is heated to  $90 \text{ }^\circ\text{C}$  and the pressure increases (1). Then, the maximum pressure stabilizes and then slowly decreases during the induction period in which the phenolic antioxidant is effective and the oxidation of FAMES is prevented (2). Finally, the phenol is completely consumed and the oxidation of the oil takes place (3). Moreover, the oxygen consumed vs time, *i.e.*  $-d[O_2]/dt$ , can be used as an indicator of the oxidability<sup>39</sup>.

Experiments were stopped when the pressure of oxygen had decreased down to half of the starting value after heating ( $P_f = P_{\max}/2$ ). The evolution of the pressure was then converted to a concentration of oxygen consumed in the liquid phase  $\Delta[O_2]_t$  defined by Eq. 3.50 where  $V_{\text{tot}}$  and  $V_{\text{liq}}$  are the volumes of the cell and the FAMES respectively,  $P_{\max}$  is the maximum pressure obtained a few minutes after heating the cell and  $P_t$  is the pressure measured at a given time.

$$\Delta[O_2]_t = \frac{(P_{\max} - P_t)}{RT} \times \frac{(V_{\text{tot}} - V_{\text{liq}})}{V_{\text{liq}}} \quad (3.50)$$

Oxidation rate  $R_{ox}$  is defined as the rate when oxygen is consumed in the presence of phenolic antioxidants. It corresponds to the slope of the trend curve of  $[O_2]$  consumed during the induction period. **Table 3.27** gathers these two different parameters for all the phenols studied and BDEs and stoichiometric numbers already discussed are also indicated.

Phenols	N°	Induction Period IP (min)	Oxidation rate $R_{ox}$ (mM.min <sup>-1</sup> )	BDE vacuum (kcal.mol <sup>-1</sup> )	$\sigma_{exp}$ (Ethyl acetate)	$k$ (M <sup>-1</sup> .s <sup>-1</sup> )
5-Tert-butyl-pyrogallol	1	234	0.06	66.6	2.0	190
Propyl gallate	4	162	0.26	69.6	3.3	44
BHA	5	167	0.35	72.3	2.1	7.4
4-Tert-butyl-catechol	6	220	0.37	72.3	2.5	18
BHT	7	131	0.44	72.4	2.0	0.08
TBHQ	8	45	0.53	74.3	2.0	40
o-tert-butyl-p-cresol	9	56	0.77	77.4	1.5	0.09
$\alpha$ -tocopherol	11	177	0.17	69.1	2.0	210
Gallic acid	15	178	0.32	70.2	5.0	7.8
Protocatechuic acid	16	50	0.62	75.5	1.8	0.79
Syringic acid	17	37	0.76	78.1	0.7	0.08
Vanillic acid	20	5	1.03	83.1	0	0.01
PHBA	21	6	1.20	84.7	0	0.01
Rosmarinic acid	23	262	0.27	69.2	4.1	31
Caffeic acid	24	148	0.36	72.1	2.0	10
Chlorogenic acid	25	138	0.48	73.4	1.9	8.6
Sinapic acid	26	54	0.57	75.4	1.0	23
Ferulic acid	27	28	0.82	79.7	1.4	1.03
Myricetin	32	262	0.11	67.4	3.4	67
Quercetin	34	135	0.34	71.8	1.9	18
Epigallocatechin gallate	55	476	0.08	66.5	5.4	187
Piceatannol	58	313	0.20	68.7	2.0	314
Resveratrol	59	67	0.68	76.7	0.9	1.4
Isoeugenol	60	49	0.72	76.6	1.0	5.4
Eugenol	61	27	0.93	80.2	0.9	0.47
Hydroxytyrosol	62	172	0.30	72.1	1.9	13
Catechol	63	147	0.46	73.4	2.1	3.7
Sesamol	65	161	0.55	75.1	2.4	5.5
Aesculetin	67	112	0.50	72.5	2.1	14
Carnosol	69	166	0.35	70.7	2.0	47
Carnosic acid	70	230	0.29	70.8	2.1	103
Ascorbyl palmitate	71	5	1.20	/	2.0	68

Table 3.27: Induction periods (IP) and oxidation rates ( $R_{ox}$ ) for phenols obtained during the autoxidation of linseed oil FAMES via the RapidOxy® test, BDEs calculated in vacuum with stoichiometric numbers ( $\sigma_{exp}$ ) and kinetic rate constants ( $k$ ) obtained with the DPPH® test in ethyl acetate are indicated

#### 4.3.1.2 Discussion

- Induction periods (IP) and oxidation rates ( $R_{ox}$ )

**Figure 3.73** shows the correlation between oxidation rate ( $R_{ox}$ ) and induction period (IP). The longer is the induction period, the more effective the phenolic antioxidant is against the autoxidation of FAMES. Moreover, phenols are powerful antioxidants when the oxidation rate  $R_{ox}$  is weak which mean that they inhibit peroxy radicals and reduce the consumption of oxygen (5-tert-butyl-pyrogallol **1**, 0.06 mM.min<sup>-1</sup>). Conversely, in the case of inefficient phenols,  $R_{ox}$  is higher and closer to

that obtained without added antioxidants. Indeed, there is not inhibition of radicals and the consumption of oxygen is not reduced (vanillic acid **20**,  $1.03 \text{ mM}\cdot\text{min}^{-1}$ ).

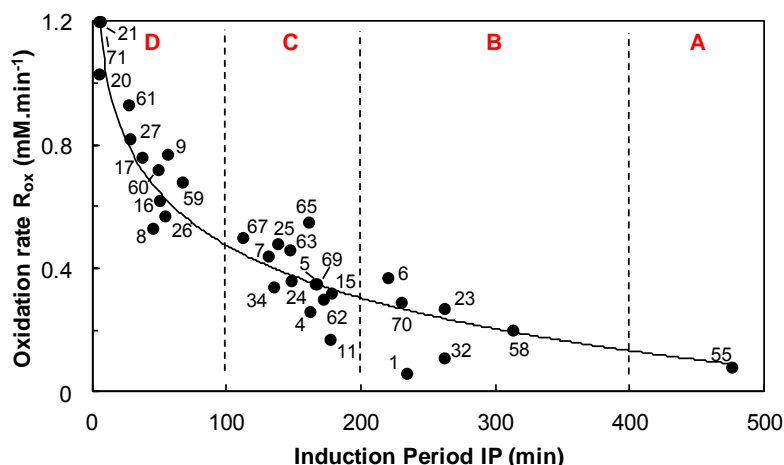


Figure 3.73: Oxidation rate ( $R_{ox}$ ) vs Induction Period (IP) for the preservation of FAMES of linseed oil against oxidation

Four categories of phenolic antioxidants can be distinguished. First of all, epigallocatechin gallate **55** is by far the most reactive phenol categorized as extremely effective antioxidant (A) with a combination of the highest induction period ( $\approx 500 \text{ min}$ ) and the lowest oxidation rate ( $0.08 \text{ mM}\cdot\text{min}^{-1}$ ). Then phenols of category B (**1**, **6**, **23**, **32**, **58** and **70**) are considered as highly effective antioxidants and are ranging between induction periods from 200 to 400 min with low oxidation rates (from 0.06 to  $0.37 \text{ mM}\cdot\text{min}^{-1}$ ). Furthermore, moderately effective phenols of category C (**4**, **5**, **7**, **11**, **15**, **24**, **25**, **34**, **62**, **63**, **65**, **67** and **69**) have an IP between 200 and 100 min and medium  $R_{ox}$  (from 0.17 to  $0.55 \text{ mM}\cdot\text{min}^{-1}$ ). Finally, phenols **8**, **9**, **16**, **17**, **20**, **21**, **26**, **27**, **59**, **60** and **61** of category D have an induction period lower than 100 min and the highest  $R_{ox}$  (from 0.53 to  $1.20 \text{ mM}\cdot\text{min}^{-1}$ ). They are considered as poorly effective antioxidants.

- BDEs, stoichiometric numbers ( $\sigma_{exp}$ ) and kinetic rate constants ( $k$ ): prediction of the efficiency of phenolic antioxidants

Figure 3.74 shows that the most efficient antioxidants are those with the lowest BDEs but no clear correlation between induction periods and BDEs could be obtained ( $R^2 = 0.68$ ). There seems to be an exponential tendency. Indeed, for examples, epigallocatechin gallate **55**, piceatannol **58**, rosmarinic acid **23** are largely out to the trend curve. Epigallocatechin gallate **55** with the lowest BDE ( $66.5 \text{ kcal}\cdot\text{mol}^{-1}$ ) is the most effective phenolic antioxidants for the protection of FAMES of linseed oil oxidation. Conversely, PHBA **21** has the highest BDE ( $84.7 \text{ kcal}\cdot\text{mol}^{-1}$ ) and does not allow the protection of FAMES against oxidation.

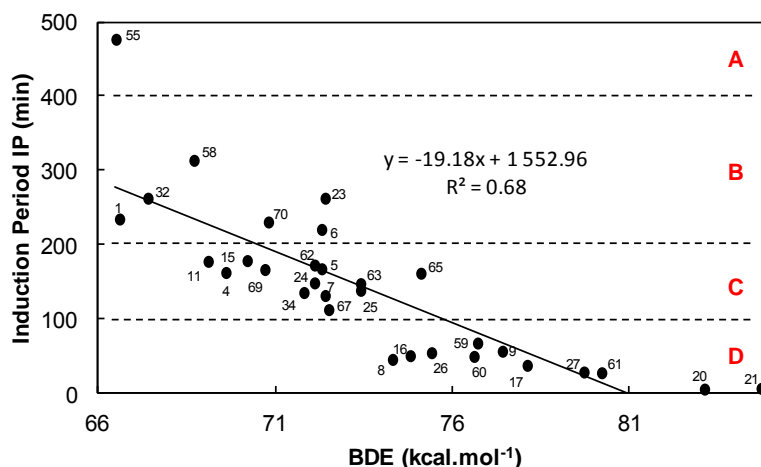


Figure 3.74: Induction periods (IP) vs BDEs calculated with the DFT method

Thereby, different parameters seem to have an influence on the antioxidant power of phenols. The number of radicals trapped by molecule of antioxidant is an important factor for the inhibition of oxidation and influences the induction period as illustrated by figure 3.75.

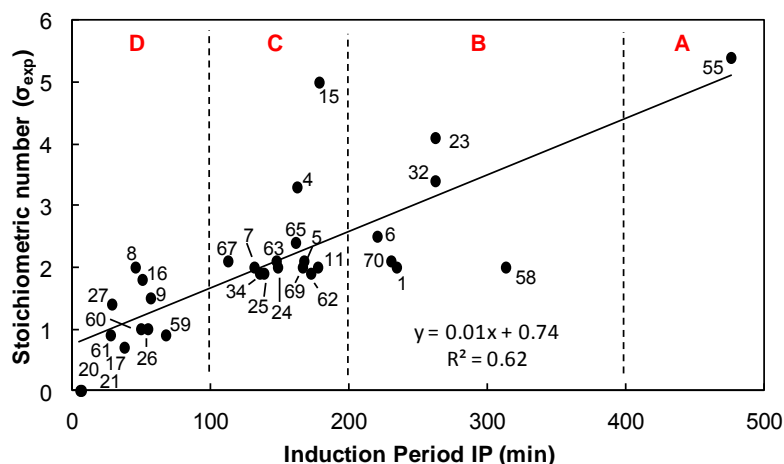
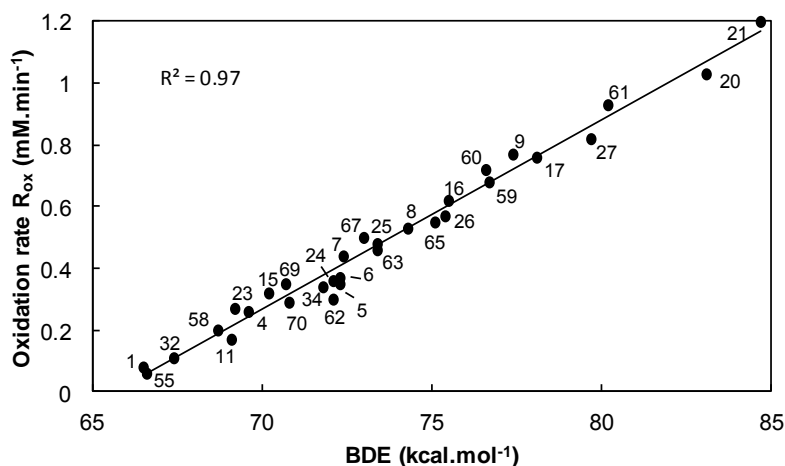


Figure 3.75: Stoichiometric number ( $\sigma_{\text{exp}}$ ) determined with the DPPH<sup>•</sup> test vs induction period (IP) obtained with the RapidOxy<sup>®</sup> experiments

The trend displayed is clear: highly effective antioxidants are polyphenols characterized by high stoichiometric numbers. As an example, epigallocatechin gallate **55** traps more than 5 radicals per molecule of antioxidant and delays the oxidation process of about 500 minutes. Conversely, poorly effective antioxidants are those with low stoichiometric numbers as for syringic acid **17**, isoeugenol **60** and sinapic acid **26**. They transfer too few hydrogen atoms to be efficient on the delayed action of the oxidation process. Basically, moderately effective antioxidants (**4**, **5**, **7**, **11**, **15**, **24**, **25**, **34**, **62**, **63**, **65**, **67** and **69**) trap 2 radicals per molecule. Nevertheless, there are some exceptions and the correlation is poor ( $R^2 = 0.62$ ). Indeed, gallic acid **15** and propyl gallate **4** have higher stoichiometric numbers compared to moderately effective antioxidants ( $\sigma_{\text{exp}} > 2.0$ ). Moreover, phenols with equal stoichiometric numbers as moderately effective antioxidants ( $\sigma_{\text{exp}} = 2$ ) are characterized as poorly effective phenols as attested by their low induction periods (*i.e.* TBHQ **8** and protocatechuic acid **16**). Finally, piceatannol **58** which is considered as highly effective antioxidant traps only 2 radicals per molecule of phenol.

Accordingly, the number of radicals trapped by one molecule of phenol ( $\sigma_{\text{exp}}$ ) is a crucial parameter for the protection of FAMES against oxidation but the exceptions above-mentioned point out other essential factors as the BDE. Indeed, there is a very good correlation between oxidation rates ( $R_{\text{ox}}$ ) and BDEs ( $R^2 = 0.97$ , **Fig. 3.76**). We have previously described a correlation between BDEs and kinetic rates (DPPH $^{\bullet}$  test) involving a transfer of hydrogen according to the radical HAT mechanism. Thereby, we assume that the mechanism involved during the inhibition of oxidation by phenolic antioxidants is also a radical mechanism. Contrary to the observation made with the DPPH $^{\bullet}$  test, hindered phenols (*i.e.* BHA **5**, BHT **7** and *o*-*tert*-butyl-*p*-cresol **9**) are close to the correlation straight line. Their reactions with peroxy radicals ROO $^{\bullet}$ , which are less hindered than DPPH $^{\bullet}$ , are not inhibited and they play their antioxidant role.



**Figure 3.76:** Oxidation rates ( $R_{\text{ox}}$ ) vs BDEs calculated with the DFT method

Thereby, a multivariable linear regression is undertaken in which the induction periods (IP) could be linked to 3 independent variables previously studied: BDEs, stoichiometric numbers ( $\sigma_{\text{exp}}$ ) and kinetic rate constants ( $k$ ). Theoretical induction periods could be expressed as these 3 parameters following the **equation 3.51**.

$$\text{IP} = 454.5 + 41.5 \sigma_{\text{exp}} + 0.51k - 5.71\text{BDE} \quad (3.51)$$

**Table 3.28** shows that the coefficients of the regression are in agreement with the effects identified for each factor. Indeed, high stoichiometric numbers ( $\sigma_{\text{exp}}$ ) and strong kinetic rate constants ( $k$ ) are related to an increase of induction periods. Moreover, phenols with high BDEs drastically decrease IP.

Factor	Coefficient	Induction period ( $\text{IP}_{\text{exp}}$ )
$\sigma_{\text{exp}} \nearrow$	+41.5	$\nearrow \nearrow$
$k \nearrow$	+0.51	$\nearrow$
BDE $\nearrow$	-5.71	$\searrow \searrow \searrow$

**Table 3.28:** Influence of the 3 variables ( $\sigma_{\text{exp}}$ ,  $k$  and BDE) on experimental induction periods ( $\text{IP}_{\text{exp}}$ )

**Figure 3.77** points out the correlation of experimental induction periods obtained by the RapidOxy $^{\text{®}}$  test with theoretical ones given by the **equation 3.53**. The linear correlation ( $R^2 = 0.83$ ) highlights that theoretical induction periods could be calculated knowing the BDEs, kinetic rate constants and stoichiometric numbers of phenols. Therefore, the efficiency of phenolic antioxidants

for the preservation of FAMES of linseed oil against oxidation is predicted by the use of thermodynamic, kinetic and stoichiometric parameters.

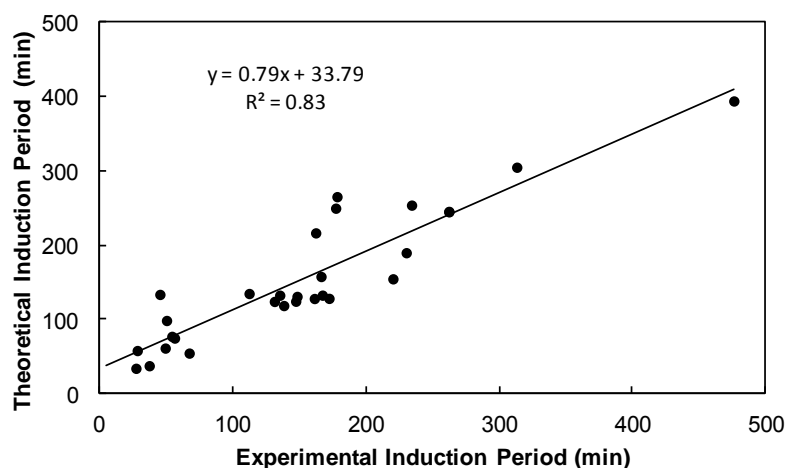


Figure 3.77: Theoretical induction periods given by the equation 3.53 vs experimental induction periods obtained with the RapidOxy® test

- 4 classes of phenolic antioxidants

Consequently, the antioxidant power of phenols is determined by a combination of parameters: their BDE, the number of radicals trapped by one molecule of phenols and their kinetic rate constants. Based on these characteristics, the 4 classes of antioxidants pointed out by the RapidOxy® experiments can be extended as follows:

First of all, epigallocatechin gallate **55** is the most effective antioxidant due to its pyrogallol and galloyl moieties which drastically decreases the BDE ( $66.5 \text{ kcal.mol}^{-1}$ ) and increases the number of radicals trapped by molecule ( $\sigma_{\text{exp}} = 5.4$ ). Moreover, it is one of the most reactive phenol with DPPH\* in ethyl acetate ( $k = 187 \text{ M}^{-1}.\text{s}^{-1}$ ).

Then, phenols of category B (**1**, **6**, **23**, **32**, **58** and **70**) are highly effective antioxidants. Pyrogallol structures (*i.e* 5-*tert*-butyl-pyrogallol **1** and myricetin **32**) and catechol moieties (*i.e* 4-*tert*-butyl-pyrogallol **6**, rosmarinic acid **23**, piceatannol **58** and carnosic acid **70**) possessing *ortho*-, *para*- or *conjugated* electron-donating groups (EDG) has low BDEs and stoichiometric number ( $\sigma_{\text{exp}}$ ) higher than 2.0 or significant kinetic rates constants ( $k$ ).

Furthermore, phenols of category C (**5**, **6**, **8**, **12**, **16**, **24**, **26**, **35**, **63**, **64**, **66**, **67** and **70**) are considered as moderately effective antioxidants. Monophenols such as BHA **5**, BHT **7**,  $\alpha$ -tocopherol **11** and sesamol **65** are able to transfer two hydrogens ( $\sigma_{\text{exp}} = 2$ ). All the catechol derivatives categorized as moderately effective antioxidants are just capable to transfer two hydrogens. Consequently, there is formation of *ortho*-quinone methide derivatives.<sup>351</sup> Gallic acid **15** and propyl gallate **4**, identified as exception by their higher stoichiometric number (5 and 3.3 respectively), do not transfer their hydrogen enough quickly and the oxidation takes place at a rate of 0.32 and 0.26  $\text{mM}.\text{min}^{-1}$  respectively. Therefore, even if these antioxidants could transfer more than 2 hydrogens, they are not highly efficient for the protection of omega-3 oils. Moreover, kinetic rate constants ( $k$ ) obtained in ethyl acetate are lower than those of phenols of class A and B. It is noteworthy that carnosol **69** is less efficient than carnosic acid **70** while they have close chemical structure and equal stoichiometric number ( $\sigma_{\text{exp}} = 2.0$ ) as obtained during the DPPH\* test. This is probably because

carnosic acid **70** could transfer more than 2 hydrogens during the protection of oils compared to its reactivity with the DPPH<sup>•</sup> radical ( $\sigma_{\text{LOO}\cdot} > \sigma_{\text{DPPH}\cdot}$ ) as showed by Zhang *et al.*<sup>403</sup> (Fig. 3.78).

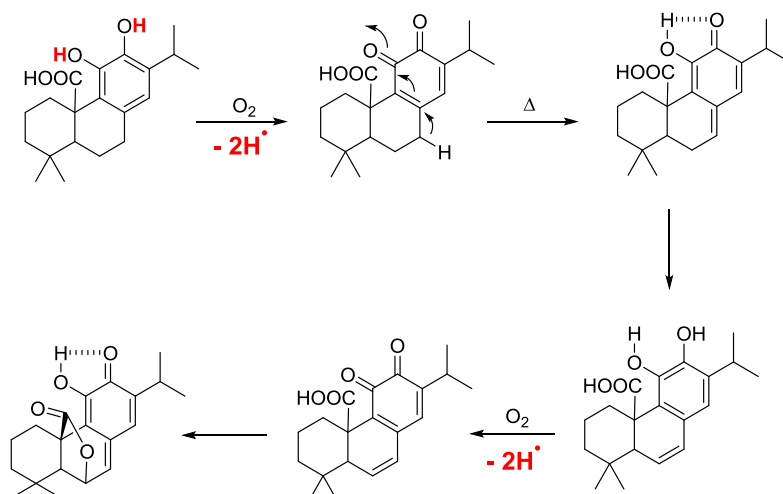
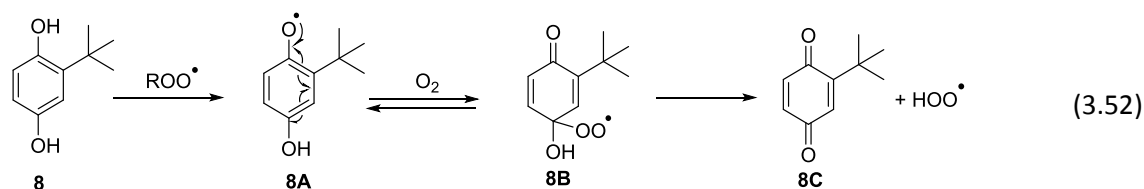


Figure 3.78: The cascade effect of carnosic acid **70** during its degradation pathway

Finally, phenols **8**, **9**, **10**, **16**, **17**, **20**, **21**, **26**, **27**, **59**, **60** and **61** belongs to category D and are considered as poorly effective antioxidants. Even if TBHQ **8** and protocatechuic acid **16** are catechol or hydroquinone derivatives with a stoichiometric number of 2 ( $\sigma_{\text{exp}} = 2$ ), they are poorly reactive. Indeed, **16** reacts very slowly with the DPPH<sup>•</sup> radical and **8** could be subjected to thermal decomposition, volatilization or absorption by the food leading to a decrease of its antioxidant power.<sup>405</sup> The radical formed could also react with oxygen as described by Valgimigli *et al.* and decrease its antioxidant power.<sup>406</sup> Indeed, after the transfer of one H<sup>•</sup> to peroxy radical ROO<sup>•</sup>, the semiquinonic radical **8A** could react with oxygen and formed the hydroperoxy radical **8B**. This radical could then initiate a new oxidation process by releasing a hydroperoxy radical leading to the formation of *para*-quinone **8C** (Eq. 3.52). In this case, the stoichiometric number of the reaction is closed to zero ( $\sigma = 0.3$ ) and hydroquinone derivatives act as pro-oxidant.



Surprisingly, ascorbyl palmitate **71** has no antioxidant power whereas it is considered as powerful antioxidant by authors.<sup>407</sup> It could be degraded under our oxidation conditions. All the other antioxidants gathered in this category D are monophenols with low kinetic rate constants and stoichiometric numbers ( $\sigma_{\text{exp}} < 2$ ). They are not capable to form dimers and are not competitive with the other monophenols of the class B (BHA **5**, BHT **7** and  $\alpha$ -tocopherol **11**,  $\sigma_{\text{exp}} = 2$ ).

- *Effect of the antioxidant concentration and the kind of oil studied*

The antioxidant power of phenols depends on the concentration of antioxidants. Therefore, the impact of their concentration on the induction period obtained during the preservation of FAMES of linseed oil was investigated (Fig. 3.79).

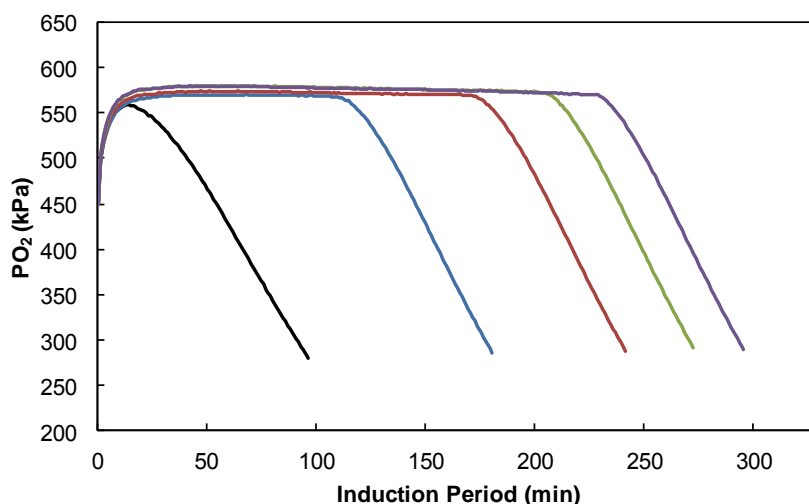


Figure 3.79: Following of the oxygen pressure decrease during the oxidation of FAMES linseed oil ( $P = 450$  kPa and  $T = 90$  °C) in the presence of 0 mM (black curve), 0.25 mM (bleu curve), 0.5 mM (red curve), 0.75 mM (red curve) and 1.0 mM (violet curve) of  $\alpha$ -tocopherol **11**

Oxidation rates ( $R_{ox}$ ) are considered as independent of the initial concentration of phenols. The induction period is the only changing parameter. **Figure 3.80** shows the impact of the concentration of antioxidants ( $\bullet$  rosmarinic acid **23**,  $\circ$  myricetin **32**,  $\square$  gallic acid **15** and  $\blacksquare$   $\alpha$ -tocopherol **11**) on the inhibition of FAMES linseed oil oxidation (induction period). Curves fit a second order polynomial law and linear tendencies are not obtained. BHA **5**, BHT **7** and caffeic acid **24** are also studied and show the same tendency as gallic acid **15** ( $\square$ ). For more results, see the experimental part.

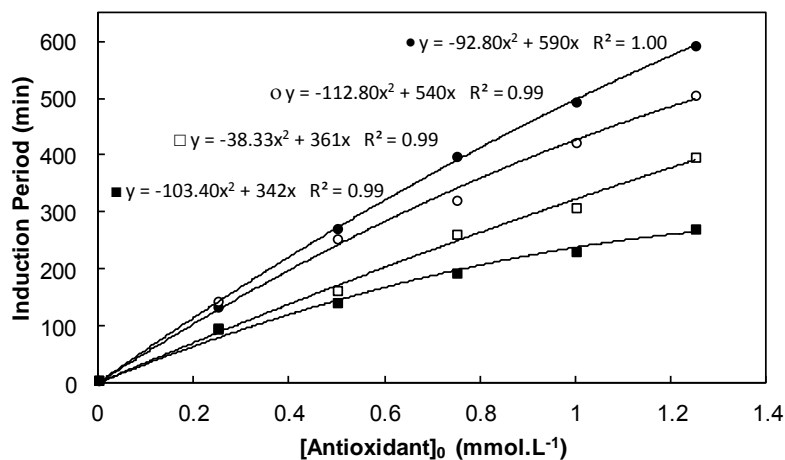


Figure 3.80: Induction periods for phenols obtained vs their concentrations ( $\bullet$  rosmarinic acid **23**,  $\circ$  myricetin **32**,  $\square$  gallic acid **15** and  $\blacksquare$   $\alpha$ -tocopherol **11**)

At high concentration (1.25 mM), rosmarinic acid **23** is the most effective antioxidant with an induction period of  $\approx 600$  min. The scale of reactivity of phenols introduced at high concentration is the following: rosmarinic acid **23** > myricetin **32** >> gallic acid **15**  $\approx$  caffeic acid **24**  $\approx$  BHA **5**  $\approx$  BHT **7** >  $\alpha$ -tocopherol **11**.  $\alpha$ -Tocopherol **11** ( $\blacksquare$ ) is much more reactive at low concentration. Indeed, 0.25 mM of  $\alpha$ -tocopherol **11** inhibits the FAMES linseed oil oxidation during  $\approx 100$  min whereas a concentration five times higher preserves FAMES just during  $\approx 270$  min. Moreover, at high concentrations,  $\alpha$ -tocopherol **11** becomes the least effective antioxidant. It could be explained by its pro-oxidant capacities when it is incorporated at high concentration as demonstrated by Jerzykiewicz *et al.*<sup>408</sup> and Kim *et al.*<sup>409</sup> This unfavorable effect is due to the oxidized forms of  $\alpha$ -tocopherol (*i.e.*  $\alpha$ -tocopherol peroxy radical **11A**,  $\alpha$ -tocopherol oxy radical **11B**,  $\alpha$ -tocopherolquinone oxy radical **11C**, **Fig. 3.81**) obtained during the oxidation of oils after the transfer of its phenolic hydrogen. These

oxidized forms of  $\alpha$ -tocopherol **11** with polar hydroxyl and non-polar hydrocarbons are less soluble in oil and move to the surface. They decrease the surface tension between air and oil and favor the move of oxygen from air to oil accelerating the oxidation process. Moreover, its pro-oxidant effect could also be due to the  $\alpha$ -tocopheryl radical which reacts reversibly with unperoxidized lipids and lipid hydroperoxides by chain-transfer generating alkyl and peroxy radicals respectively.

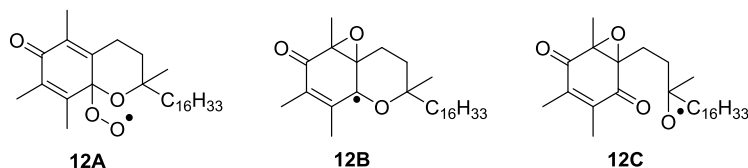


Figure 3.81: Oxidized forms of  $\alpha$ -tocopherol **11** obtained from the oxidation of oils after the transfer of the phenolic hydrogen ( $\alpha$ -tocopherol peroxy radical **11A**,  $\alpha$ -tocopherol oxy radical **11B** and  $\alpha$ -tocopherolquinone oxy radical **11C**)<sup>409</sup>

FAMES of linseed oil are used as omega-3 food model to study the antioxidant effectiveness of phenols. Nevertheless, oils are composed of triglycerides and not FAMES. Consequently, the effects of phenolic antioxidants (*i.e.* TBHQ **8**,  $\alpha$ -tocopherol **11**, gallic acid **15**, rosmarinic acid **23**, myricetin **32**, epigallocatechin gallate **55** and carnosic acid **70**) are also studied for the preservation of linseed oil (triglycerides). Figure 3.82 points out the comparative effects of phenols for the protection of triglycerides and FAMES of linseed oil. The good correlations obtained ( $R^2 = 0.99$ ) for induction periods and oxidation rates highlights that phenolic antioxidants have the same efficiency for the protection of FAMES and triglycerides of linseed oil.

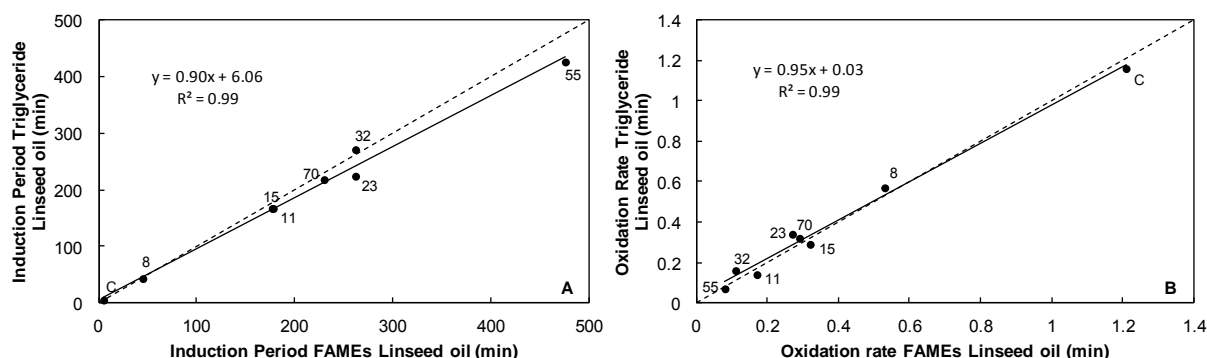


Figure 3.82: Comparative effects of phenolic antioxidant (**8**, **11**, **15**, **23**, **32**, **55** and **70**) for the protection of triglycerides and FAMES of linseed oil according to A) induction periods and B) oxidation rates (C = control = without antioxidant)

The composition of oil impacts the phenolic antioxidant efficiency. Fish oil is composed by eicosapentaenoic (EPA, 20:5) and docosahexaenoic (DHA, 22:6) acids which contain more bis-allylic hydrogens than  $\alpha$ -linolenic acid (ALA, C18:3) found in linseed oil. Therefore, fish oil is highly subjected to oxidation compared to linseed oil and phenolic antioxidants should haven't the same efficiency for both substrates. Figure 3.83 shows the comparative effects of phenols (*i.e.* TBHQ **8**,  $\alpha$ -tocopherol **11**, gallic acid **15**, rosmarinic acid **23**, myricetin **32**, epigallocatechin gallate **55** and carnosic acid **70**) for the protection of fish and linseed oil. The scale of reactivity of antioxidants is similar for both oxidized substrates. As expected, longer induction periods and lower oxidation rates are obtained for the oxidation of linseed oil because of the higher oxidability of fish oil.

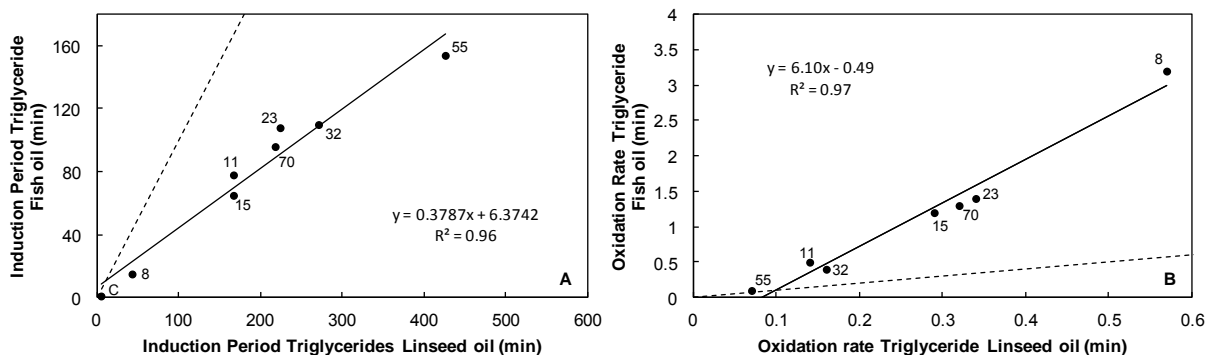


Figure 3.83: Comparative effects of phenolic antioxidant (8, 11, 15, 23, 32, 55 and 70) for the protection of triglycerides fish oil and linseed oil according to A) induction periods and B) oxidation rates (C = control = without antioxidant)

### 4.3.2 Rancimat experiments

The experiments made on the Rancimat device were conducted during a stay in the US laboratory of Cargill, Minneapolis.

#### 4.3.2.1 Principles and results

The Rancimat device (Fig. 3.84A) is used to determine the inhibition of oil autoxidation.<sup>410, 411</sup> A stream of purified air (9 L/h) is passed through a sample of oil which is held in a water bath (90 °C). The temperature of 90 °C was selected to be comparative with RapidOxy® experiments. The effluent air from oils or fat samples is then bubbled through to a vessel containing deionized water. The conductivity of water is continually monitored during this process. The effluent air contains volatile organic acids, swept from the oxidizing oil, that cause an increase in the conductivity of water as the oxidation proceeds. Formic acid is the predominant organic acid formed. The scheme of the Rancimat process is specified by the figure 3.84B.

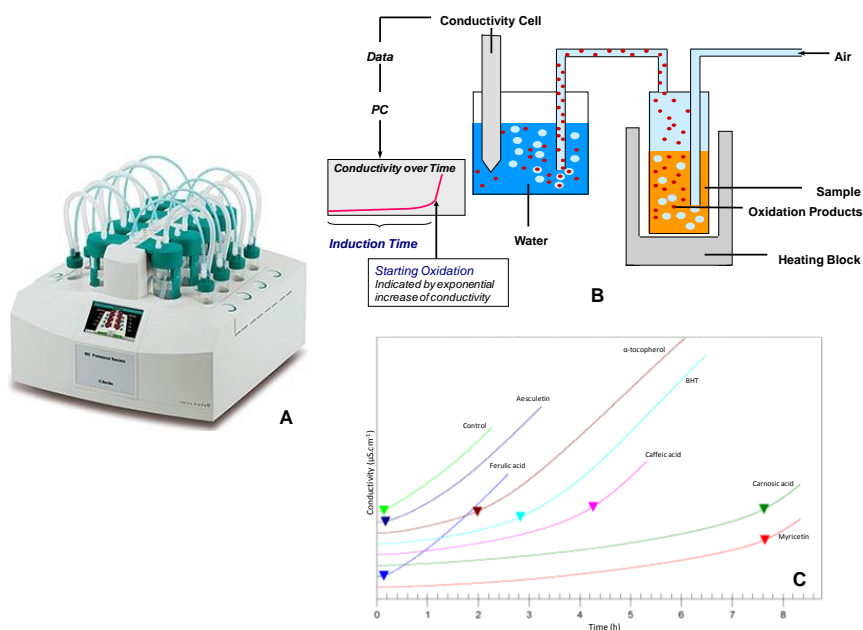


Figure 3.84: A) Biodiesel Rancimat apparatus, B) scheme of the Rancimat process and C) monitoring of the water conductivity during Rancimat experiments, oxidation of fish oil in the presence of aesculetin 67, ferulic acid 27, α-tocopherol 11, BHT 7, caffeic acid 24, carnosic acid 70 and myricetin 32 at 500 ppm, T = 90 °C, the end of the induction period is illustrated by ▼

The conductivity of water may be monitored and the induction point is defined as the point of maximum change in the rate of oxidation. This test highlights the induction period (or oxidation stability index OSI) where phenolic antioxidants are efficient. **Figure 3.84C** shows the experimental graph obtained for the oxidation of fish oil (Arista oil) in the presence of antioxidants.

**Table 3.29** gathers the induction periods (IP) obtained from phenols incorporated in FAMES linseed oil and fish oil. All the antioxidants tested increase the stability of FAMES linseed oil and fish oil as regards to the higher induction periods compared to those without phenols (control).

Phenols	N°	Induction Periods (IP)	
		FAMES linseed oil (h)	Fish oil (h)
Control	/	0.21	0.15
BHT	7	6.79	2.93
TBHQ	8	28.86	16.41
$\alpha$ -Tocopherol	11	3.84	2.04
Rosmarinic acid	23	9.07	3.00
Caffeic acid	24	9.41	4.09
Ferulic acid	27	0.34	0.14
Myricetin	32	10.60	6.83
Resveratrol	59	1.66	0.14
Hydroxytyrosol	62	11.23	8.51
Aesculetin	67	3.60	0.20
Carnosic acid	70	10.71	7.32

Table 3.29: Induction periods (h) obtained for phenols during the oxidation of FAMES linseed oil and fish oil

#### 4.3.2.2 Discussion

**Figure 3.85** points out the comparison between the efficiency of phenolic antioxidants (7, 8, 11, 23, 24, 27, 32, 59, 62, 67 and 70) for the preservation of fish oil and linseed oil against oxidation.

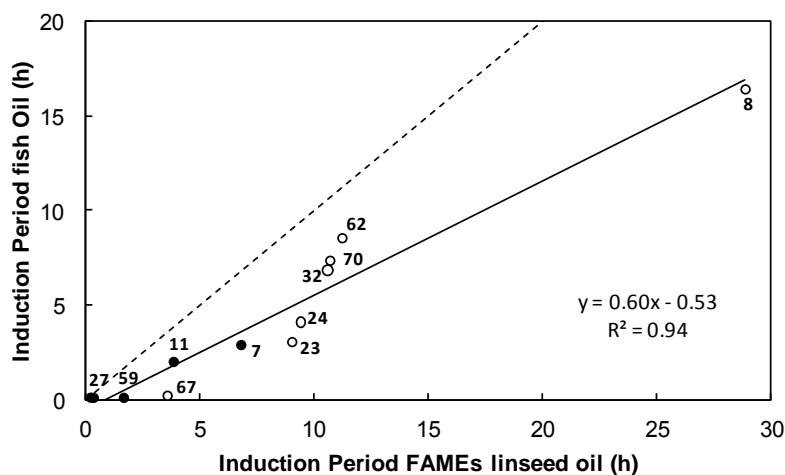


Figure 3.85: Correlation between induction periods obtained during the oxidation of fish oil and FAMES linseed oil with the use of *di*- and *tri*-hydroxyphenols (○ 8, 23, 24, 32, 62, 67 and 70) and *monophenols* (● 7, 11, 27 and 59)

As explained before, the induction periods obtained during the oxidation of fish oil are lower than those for FAMES of linseed oil. Phenols with low impact on the oxidation of FAMES linseed oil (*i.e.* ferulic acid 27, resveratrol 59 and aesculetin 67) are definitely not efficient for the protection of fish oil. Therefore, there is a direct relationship between the oil composition and its oxidation stability. The higher is the number of bis-allylic hydrogens on PUFAs, the lower is its oxidation stability as already described by Tavares *et al.*<sup>412</sup> The correlation obtained between both parameters ( $R^2 = 0.94$ )

shows that the efficiency of phenolic antioxidants depends on the fatty acid composition of oils whereas the scale of reactivity of phenols is identical in both oils.

The more powerful antioxidants studied on Rancimat analyses are *di*- and *tri*-hydroxyphenols (*o*, TBHQ **8**, rosmarinic acid **23**, caffeic acid **24**, myricetin **32**, hydroxytyrosol **62** and carnolic acid **70**). As highlighted by Liang *et al.*, the antioxidant abilities of phenolic antioxidants depend on the number of hydroxyl groups on the phenolic core at the *ortho*- and *para*-positions.<sup>413</sup> There is an exception with aesculetin **67** which is not really efficient although it is a catechol compound. This is related to its poor solubility in oils. Finally, monophenols (•, BHT **7**,  $\alpha$ -tocopherol **11**, ferulic acid **27** and resveratrol **59**) are the less effective antioxidants.

Surprisingly, among the antioxidants employed in this study, TBHQ **8** results in the strongest increase in IP whereas  $\alpha$ -tocopherol **11** is poorly reactive. Hossain *et al.* showed a good performance of TBHQ **8** in fish oil biodiesel compared to the antioxidant effect of BHT **7**.<sup>414</sup> Moreover, Pinto *et al.* pointed out that TBHQ is highly efficient for the protection of ethyl peanut oil biodiesel compared to green tea extract and  $\alpha$ -tocopherol.<sup>415</sup> As mentioned by Pinto *et al.*,  $\alpha$ -tocopherol does not enough protect oils because of its pro-oxidant effect or its degradation under the condition of study. Tavares *et al.* also identified TBHQ **8** as the best alternative to BHT **7** thanks to its antioxidant mechanism.<sup>412</sup> Indeed, quinone and hydroquinone formed by dismutation of the semiquinonic radical act as powerful antioxidants by preventing the formation of volatile products. Jain and Sharma supported this finding by the way that TBHQ **8** inhibits both primary and secondary oxidation process.<sup>416</sup>

**Figure 3.86** shows the comparison between induction periods obtained with the RapidOxy<sup>®</sup> and Rancimat tests for the protection of FAMES of linseed oil against oxidation. As expected, induction periods resulting on the RapidOxy<sup>®</sup> test are lower than those obtained with the Rancimat test as already described by Botella *et al.* during the oxidation of biodiesel.<sup>417</sup> The RapidOxy<sup>®</sup> is based on the oxygen consumption during oxidation process with the formation of non-volatile compounds (*i.e.* hydroperoxides, peroxides and ketones). Conversely, the Rancimat follows the formation of volatile compounds after the degradation of peroxides and the cleavage of C-C bonds. Therefore, RapidOxy<sup>®</sup> is related to the first stage of oxidation whereas Rancimat highlights a later stage of oxidation and could explain the differences observed.

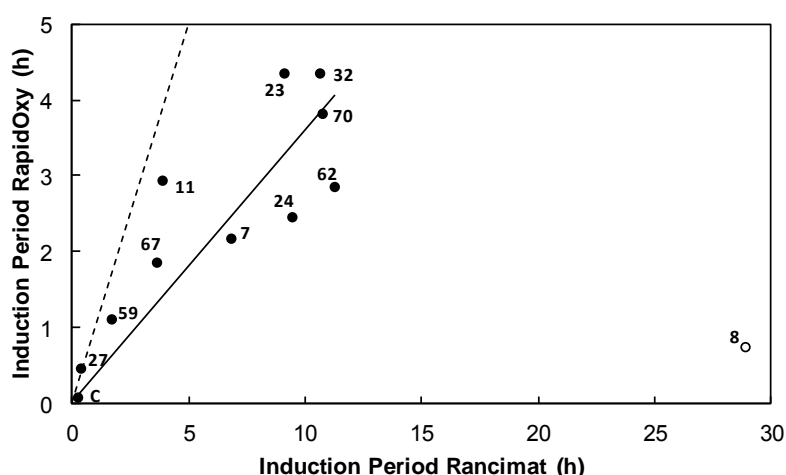


**Figure 3.86:** Comparison between induction periods obtained during RapidOxy<sup>®</sup> and Rancimat experiments for the protection of FAMES linseed oil against oxidation by phenolic antioxidants (7, 8, 11, 23, 24, 27, 32, 59, 62, 67 and 70)

The tendency given by the comparison of these two types of induction periods is clear but with a weak correlation in contrast with the results of Botella *et al.*<sup>417</sup> Indeed, they correlate results for the oxidation of biodiesel without antioxidants or by adding two antioxidants (*i.e.* 4-allyl-2,6-dimethoxyphenol and catechol) in samples at various concentrations. This weak correlation could be due to the concentration of phenols introduced into oils. Indeed, the concentration of phenols for RapidOxy® analyses (0.5 mM) is 250 times higher than that for Rancimat tests (0.002 mM). Given that Rancimat analyzes later stage of oxidation, it would be time consuming to use the same concentration as for RapidOxy®. Conversely, as RapidOxy® is accomplished under drastic conditions ( $P_{O_2} = 450$  kPa and  $T = 90$  °C), it is not possible to differentiate phenols using Rancimat concentrations. The scale of reactivity of phenols is about the same in both methods except for TBHQ **8** as above-mentioned.

### 4.3.3 Conclusion

RapidOxy® and Rancimat analyses are two relevant methods to analyze the oxidation of oils. Despite RapidOxy® analyses the first stage of oxidation with the consumption of oxygen and Rancimat is based on the formation of volatiles compounds in later stage of oxidation, phenolic antioxidants are ranged in the same scale of reactivity except for TBHQ **8**. Moreover, FAMES are shown to be great omega-3 food models and the higher is the number of bis-allylic hydrogens on fatty acids, the lower is the stability of oils against oxidation. It is also highlighted that the antioxidant abilities of phenolic antioxidants depend on the number of hydroxyl groups on the phenolic core at the *ortho*- and *para*-positions.

Furthermore, the efficiency of phenolic antioxidants for the preservation of FAMES of linseed oil against oxidation is predicted using thermodynamic (BDEs) kinetic ( $k$ ) and stoichiometric ( $\sigma_{exp}$ ) parameters. Oxidative studies show that natural phenols as rosmarinic acid **23**, myricetin **32**, epigallocatechin gallate **55** and carnosic acid **70** are more effective than  $\alpha$ -tocopherol **11** for the preservation of omega-3 oils against oxidation.

## 5. Conclusions

The objectives of this second chapter were to understand the mechanism of protection of omega-3 oils by phenolic antioxidants and find the best alternative to  $\alpha$ -tocopherol and synthetic phenols. Thermodynamic investigations (BDE, IP, pKa), kinetic studies ( $k$ ), stoichiometric calculations ( $\sigma_{exp}$ ) and oxidative (RapidOxy®, Rancimat) tests were undertaken, each of them leading to proper information. With the study of a large range of phenols, a kinetic approach *via* the DPPH· test combined with thermodynamic data in which BDE, IP and pKa were phenols are considered highlight two different mechanism of action depending on the chemical structures of phenols and polarity of matrices. Substitutions of the phenolic core by electron-donating groups (EDG, alkyl, methoxy, and hydroxyl) decrease BDEs whereas electron-withdrawing groups (EWG, carboxyl) increase BDEs. The radical HAT mechanism implies the hydrogen transfer from phenols to peroxy radicals ROO· and predominates in food. Moreover, kinetic rate constants related to the transfer of hydrogens are correlated to BDEs. Indeed, the lowest BDEs lead to the best antioxidant properties. In alcohol solutions, the dissociation of phenols into phenolate is responsible on the SPLET mechanism. It is favored for acidic (low pKa) *ortho*-methoxyphenols in polar solvents whereas other phenols with higher pKa and lower BDEs are less sensitive to this mechanism.

The study of the preservation of omega-3 oils by the measurement of the oxygen consumption in the first stage of oxidation (RapidOxy®) and the formation of volatile compounds in the later stage of oxidation (Rancimat) highlights the same order of reactivity for phenols. The antioxidant abilities of phenolic antioxidants reacting *via* radical HAT mechanism depend on the number of hydroxyl groups on the phenolic core and on the number of radicals ( $\sigma_{\text{exp}}$ ) trapped by molecule of phenol. The conditions of oxidation used in both tests are not close to the reality of oxidation of oils. Consequently, it would be interesting to study the efficiency of phenols during the oxidation of omega-3 oils under normal conditions, *i.e.* with air at 20 °C, and compare results with those obtained during stronger conditions. Moreover, the MS analysis could be an interesting way to quantify the oxidized species formed and compare their predominance in function of the antioxidant used. Therefore, it could be a way to orientate the oxidation process of oils leading to the less harmful species.

The study of 24 natural phenolic antioxidants in comparison to 8 synthetic ones leads to a scale of reactivity (**Fig. 3.87**) based on BDE calculation, kinetic rate constants and stoichiometric numbers (DPPH<sup>•</sup> test) with the inhibition capacities of phenols during the oxidation of omega-3 oil. The efficiency of phenolic antioxidants (induction periods IP) is predicted using thermodynamic (BDEs), kinetic ( $k$ ) and stoichiometric ( $\sigma_{\text{exp}}$ ) parameters according to **equation 3.51**.

$$IP = 454.5 + 41.5 \sigma_{\text{exp}} + 0.51k - 5.71BDE \quad (3.51)$$

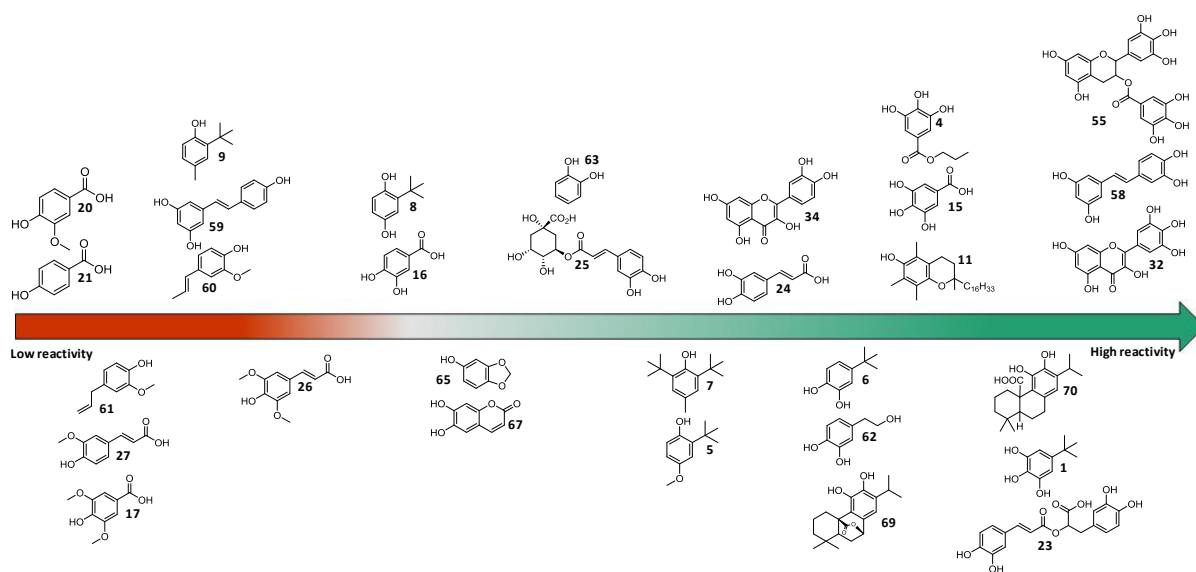


**Figure 3.87: General scale of reactivity of phenolic antioxidant based on BDE calculations, kinetic rates constants ( $k$ ) and stoichiometric numbers (DPPH<sup>•</sup> test) with the inhibition capacities of phenols during the oxidation of omega-3 oils**

*Tri*-hydroxyphenols are more reactive than *di*-hydroxyphenols which are more powerful than monophenols. Natural phenols, *i.e.* rosmarinic acid **23**, myricetin **32**, epigallocatechin gallate **55**, piceatannol **58** and carnosic acid **70** are the best natural alternatives to  $\alpha$ -tocopherol **11** and synthetic antioxidants for the protection of edible oil rich in omega-3 from oxidation and sustain their physiological benefits.

Based on these findings, requirements for the chemical structures of efficient antioxidants (high induction periods IP and low oxidation rates  $R_{\text{ox}}$ ) for the protection of omega-3 oils against oxidation are: **1)** catechol or pyrogallol structure, **2)** conjugated with *para*-electron-donating group (EDG) and **3)** free *ortho* position. This has an impressive impact on important parameters driving the efficiency of phenolic antioxidants. Indeed, effective phenolic antioxidants obtained *i)* very low BDEs, *ii)* high

ionization potentials (IPs), *iii*) high kinetic rate constant of hydrogen transfer ( $k$ ) and *iv*) high number of radicals trapped by molecule of phenols ( $\sigma_{\text{exp}}$ ) with the formation of active dimers.

In this chapter, the mechanisms of action of only one phenolic antioxidant for the protection of edible oil rich in omega-3 are investigated. Nevertheless, antioxidants could interact with other phenols leading to synergistic effects. Scientists are increasingly working on the understanding of synergies between phenolic antioxidants. Synergies effects are the key parameter to improve the efficiency of antioxidants. This reduces the toxicity of some antioxidants by avoiding the formation of their radicals or oxidized products, which could be harmful for the consumers. Therefore, the **chapter 4** is dedicated to highlight and understand synergistic effects between phenolic antioxidants for food applications.

## CHAPTER 3. EXPERIMENTAL PART

---

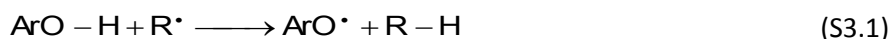
## 1. Materials

Solvents are of the purest grade commercially available from Sigma-Aldrich. The 2,2-diphenyl-1-picrylhydrazyl (DPPH<sup>•</sup>) radical is purchased from Sigma-Aldrich and kept at a temperature lower than 5 °C. Catechol **63** (≥ 99 %), 4-hydroxybenzoic acid **21** (PHBA, ≥ 99 %), rosmarinic acid **23** (96 %), quercetin **34** (≥ 98 %), 2-tert-butyl-4-methylphenol **9** (99 %), salicylic acid **22** (> 99 %), tert-butylhydroquinone **8** (TBHQ, 97 %), 4-hydroxy-3-methoxybenzoic acid **20** (vanillic acid, 97 %), sesamol **65** (98 %), propyl gallate **4** (PG, ≥ 98 %), isoeugenol **60** (98 %), 3-tert-butyl-4-hydroxyanisole **5** (BHA, 98 %), 3,4-dihydroxybenzoic acid **16** (protocatechuic acid, 97 %), 2,6-di-tertbutyl-4-methylphenol **7** (BHT, ≥ 99 %), 3,4-dihydroxycinnamic acid **24** (caffeic acid, 97 %), ferulic acid **27** (99 %), α-tocopherol **11** (≥ 96 %) and sodium (in kerosene, pieces, > 99.8 %) are from Sigma-Aldrich. 3,5-dimethoxy-4-hydroxycinnamic acid **26** (sinapic acid, 98 %), 5-tert-butylpyrogallol **1** (97 %), syringic acid **17** (≥ 98 %), eugenol **61** (99 %), 6,7-dihydroxycoumarin **67** (aesculetin, ≥ 98 %), epigallocatechin gallate **55** (98 %) and L-ascorbyl palmitate **71** (99 %) are from Alfa Aesar. 3,4-dihydroxyphenyl ethanol **62** (hydroxytyrosol), myricetin **32** (≥ 98 %), chlorogenic acid **25** (≥ 95 %) and carnosic acid **70** (≥ 95 %) are from Cayman Chemical Company. Gallic acid **15** (≥ 95 %) is from ACROS and 4-tert-butylpyrogallol **6** (≥ 98 %) is from Merck. Resveratrol **59** (≥ 98 %) is from TCI and carnosol **69** is from Chromadex. Aluminium oxide, basic, Brockmann I, for chromatography, 50-200 μm, 60 Å is from Acros Organics. Refined linseed oil is from Vandeputte Group, Belgium. FAME mix GLC-10 containing palmitic acid methyl ester (C16:0), stearic acid methyl ester (C18:0), oleic acid methyl ester (C18:1), linoleic acid methyl ester (C18:2) and linolenic acid methyl ester (C18:3) is from Supelco.

## 2. Protocols and methods

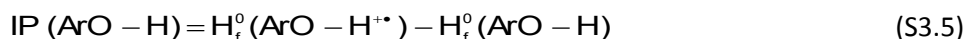
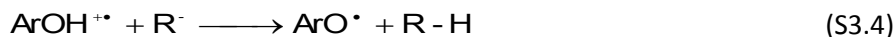
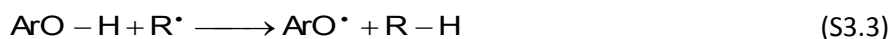
### 2.1 Calculation of the Bond Dissociation Enthalpies BDEs (O-H) and Ionization Potential IP

The so-called BDE of the O-H bonds in a phenol, which corresponds in fact to the bond dissociation enthalpy, is given by the difference between enthalpy of the phenoxyl radical (plus that of the hydrogen atom) and that of the starting phenol as described by **equations S3.1** and **S3.2**. All the calculations are performed using Gaussian 03 packages. The geometries of all the parent molecules are firstly optimized using the PM3 method and then the DFT one by using the B3LYP/6-311G (d,p) basis set. The first method is used to speed up the convergence of the optimization by the second one. The zero-point energy (ZPE) is considered to correct the BDE values. Geometries from this method are used as inputs to the final energy B3LYP/6-311G ++ (2d,2p) calculation. For species having several conformers, all of them are investigated. The conformer with the lowest electronic energy is retained. For radicals, the optimization also used the PM3 step plus the final UB3LYP/6-311 G (d,p) method. The zero-point energy (ZPE) is also considered to correct the BDE values. Geometries are then used as inputs to the final UB3LYP/6-311 G ++ (2d,2p) calculation. Calculations are performed in toluene, ethyl acetate and ethanol. The method is described as B3LYP/6-311++G(2d,2p)//B3LYP/6-311G(d,p).



$$\text{BDE}(\text{ArO} - \text{H}) = H_f^{\circ}(\text{ArO}^{\bullet}) + H_f^{\circ}(\text{H}^{\bullet}) - H_f^{\circ}(\text{ArO} - \text{H}) \quad (\text{S3.2})$$

Calculations of ionization potential IP followed the same B3LYP/6-311++G(2d,2p)//B3LYP/6-311G(d,p) method as described by **equations S3.3** to **S3.5**.



## 2.2 Determination of the rate constants for hydrogen transfer from phenols to DPPH<sup>•</sup> radical

Solutions of DPPH<sup>•</sup> are prepared in each solvent used at a concentration of ca.  $5 \cdot 10^{-3}$  M by sonicating the mixture until all DPPH<sup>•</sup> crystals are dissolved. The solutions are then maintained under argon at 20 °C. For phenols **7**, **9**, **16**, **21** and **61**, solutions are prepared in solvents of study at a concentration varying from  $6 \times 10^{-2}$  to  $2 \times 10^{-1}$  mol.L<sup>-1</sup>. Typically, 200-500 μL of the phenol solutions are added to 500 μL of DPPH<sup>•</sup> solution in a 50 mL glass reactor equipped with a UV fibre (from Varian equipped with a dip-probe; Varian, les Ulis, France) containing 20 mL of deoxygenated solvent maintained at 20 °C as represented Equipment for UV-visible analysis and curve presenting the visualization of the lag time are presented in **figure S3.1**.

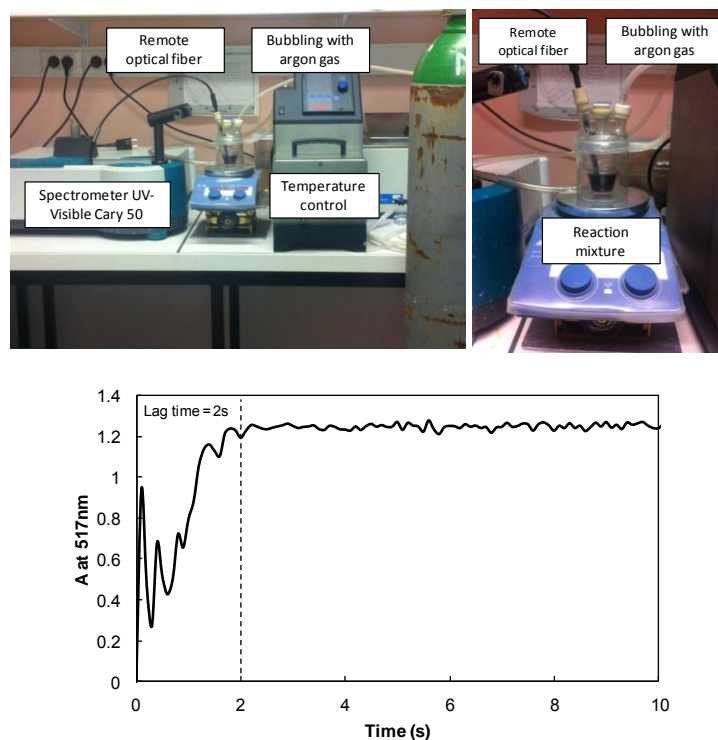


**Figure S3.1:** Equipment for UV-visible analysis and evolution of the absorbance of DPPH<sup>•</sup> radical at 515 nm (0.12 mM) without phenols in toluene at 20 °C, visualization of the lag time

The hydrogen transfer reaction from phenol to the DPPH<sup>•</sup> radical is accompanied by a change in the UV-visible spectrum and is monitored at 515 nm with a Varian spectrophotometer (Cary 50, 10 pts.s<sup>-1</sup>). The loss of DPPH<sup>•</sup> absorbance in the presence of an excess of phenol follows pseudo-first-order kinetics (FOK) as described by the **equation S3.6**.

$$\text{Ln} \frac{(A - A_f)}{(A_0 - A_f)} = -k [\text{ArOH}]_0 t \quad (\text{S3.6})$$

The rate constants were determined for at least four different phenol concentrations plotting  $k_{\text{DPPH}}$  versus  $[\text{phenol}]_0$ . **Figure S3.2** gives an example for BHT **7**.

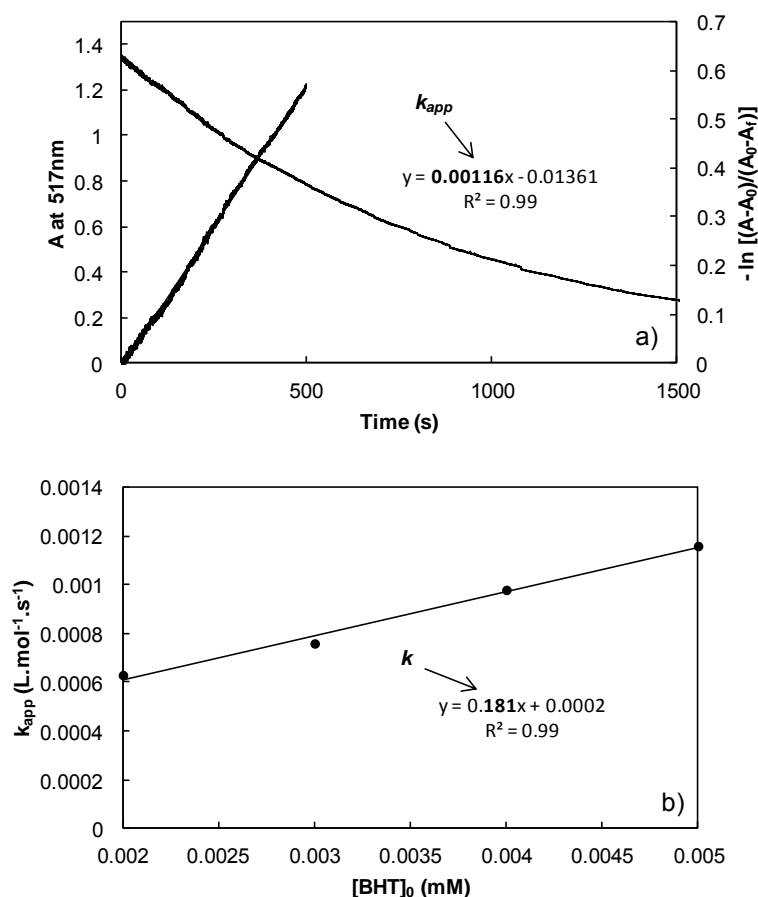


Figure S3.2: a) change in the absorbance at 515 nm of a solution of DPPH\* in the presence of an excess of BHT 7 in toluene, linearization of the logarithm of the absorbance using the final SOK equation as a function of time (Eq. S3.6) and b) Regression constants of apparent kinetic rates as a function of initial concentrations of BHT 7

For other phenols, the reaction with DPPH\* radical is very fast and the rate constants were determined by using stoichiometric conditions at 515 nm considering a second-order kinetics (SOK) ( $[DPPH^*]/[tocopherol] = 1/1$ ) as expressed by **equation S3.7**.

$$\frac{1}{(A - A_f)} - \frac{1}{(A_0)} = \frac{k}{(\epsilon - \epsilon')} t \quad (S3.7)$$

For these phenols, solutions were prepared in solvent of study at a concentration of ca.  $5 \cdot 10^{-3}$  M by sonicating until all crystals were dissolved. **Figure S3.3** gives an example for  $\alpha$ -tocopherol **11**.

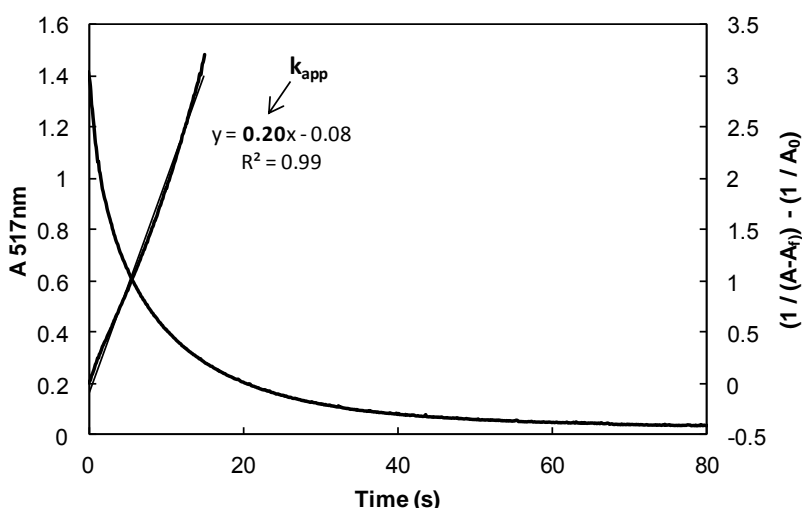


Figure S3.3: Evolution of the absorbance of DPPH<sup>•</sup> radical at 515 nm ( $1.25 \times 10^{-4} \text{ mol.L}^{-1}$ ) in the presence of  $\alpha$ -tocopherol 11 ( $1.25 \times 10^{-4} \text{ mol.L}^{-1}$ ) in toluene at 20 °C. Linearization curve according to the final SOK equation (Eq. S3.7)

Depending on the solvent,  $\epsilon$  and  $\epsilon'$  values for DPPH<sup>•</sup> radical are summarized in **table S3.1**.

	$\lambda = 515 \text{ nm}$		$\lambda = 600 \text{ nm}$	
	$\epsilon \text{ (L.mol}^{-1}.\text{cm}^{-1})$	$\epsilon' \text{ (L.mol}^{-1}.\text{cm}^{-1})$	$\epsilon \text{ (L.mol}^{-1}.\text{cm}^{-1})$	$\epsilon' \text{ (L.mol}^{-1}.\text{cm}^{-1})$
<b>Toluene</b>	11766	24	4250	6
<b>Ethyl Acetate</b>	11085	22	4993	13
<b>Cetiol A</b>	11432	29	4973	11
<b>Ethanol</b>	9260	19	4237	8

Table S3.1: Values of  $\epsilon$  and  $\epsilon'$  for DPPH<sup>•</sup> radical in toluene, ethyl acetate, cetiol A and ethanol

### 2.3 Determination of the stoichiometric number for the reaction of phenolic antioxidants with the DPPH<sup>•</sup> radical

Solutions of DPPH<sup>•</sup> are prepared in the solvent of study at a concentration of ca.  $1.5 \times 10^{-4} \text{ M}$  by sonicating the mixture until all DPPH<sup>•</sup> crystals were dissolved. The solutions are then maintained under argon at 20 °C. For phenols, solutions are prepared in the same solvent at a concentration of  $2.07 \times 10^{-3} \text{ M}$  by sonicating until all crystals are dissolved. Typically, 20  $\mu\text{L}$  of the phenol solutions are added to 2.0 mL of a DPPH<sup>•</sup> solution in a UV cell stirred and maintained at 20 °C. The absorbance change is monitored at 515 nm by using the UV-Visible Cary 60 every seconds or minutes. Final  $A_f$  and initial  $A_0$  absorbances are used to determine the stoichiometric number  $\sigma_{\text{exp}}$  according to **equation S3.8**.

$$\sigma_{\text{exp}} = \frac{[\text{DPPH}^{\bullet}]_0 - [\text{DPPH}^{\bullet}]_f}{[\text{ArOH}]_0} = \frac{A_0 - A_f}{(\epsilon - \epsilon')[\text{ArOH}]_0} \quad (\text{S3.8})$$

Final absorbances are collected when constant values are reached during at least thirty minutes. In order to estimate the effect of the concentration on the  $\sigma_{\text{exp}}$ , some phenols are used in various concentrations. Solutions of DPPH<sup>•</sup> were prepared in toluene at a concentration of ca.  $10^{-4} \text{ M}$  by sonicating the mixture until all DPPH<sup>•</sup> crystals were dissolved. The solutions were then maintained under argon at 20 °C. For phenols, solutions were also prepared in toluene at a concentration of ca.  $2 \times 10^{-3} - 5 \times 10^{-3} \text{ M}$  by sonicating until all crystals were dissolved. Typically, 10 to 30  $\mu\text{L}$  of the phenol

solutions were added to 2.8 mL of a DPPH<sup>•</sup> solution in a UV cell stirred and maintained at 20 °C. The absorbance change was monitored at 515 nm by using the UV-Visible Cary 60 every seconds or minutes. Final  $A_f$  and initial  $A_0$  absorbances were used to determine the stoichiometric number  $\sigma$  according to **equation S3.8**. Final absorbances were collected when constant values were reached during at least thirty minutes. **Figure S3.4** shows the example of various concentration of  $\alpha$ -tocopherol **11** in toluene.

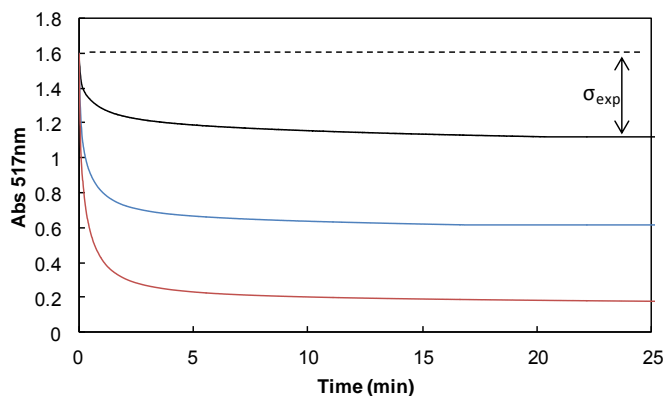


**Figure S3.4:** Evolution of the absorbance of DPPH<sup>•</sup> radical at 515 nm ( $1.5 \times 10^{-4}$  M) in the presence of  $\alpha$ -tocopherol **11** at different concentrations in toluene at 20 °C. [ $\alpha$ -tocopherol] =  $2.07 \times 10^{-5}$  M (black curve),  $4.14 \times 10^{-5}$  M (blue curve) and  $6.21 \times 10^{-5}$  M (red curve)

## 2.4 Ion-negative and ion-positive Electrospray ionization (ESI) mass spectrometry (MS) analysis

The oxidized phenolic compounds obtained from the DPPH<sup>•</sup> test are detected by a Xevo TQ-S triple quadrupole-mass spectrometer (Waters). In the positive ion mode, solutions of phenols with DPPH<sup>•</sup> ( $[\text{phenol}]_0 = 5 \times 10^{-5}$  M,  $[\text{DPPH}^{\bullet}]_0 = 1.5 \times 10^{-4}$  M) are directly mixed with formic acid ( $[\text{HCOOH}] = 10^{-3}$  M) to reach the following concentrations:  $[\text{phenol}]_0 = 3 \times 10^{-6}$  M and  $[\text{DPPH}^{\bullet}]_0 = 10^{-5}$  M. In the negative ion mode, solutions of phenols with DPPH<sup>•</sup> ( $[\text{phenol}]_0 = 5 \times 10^{-5}$  M,  $[\text{DPPH}^{\bullet}]_0 = 1.5 \times 10^{-4}$  M) are directly mixed with ammonium acetate ( $[\text{CH}_3\text{COONH}_4] = 10^{-3}$  M) to reach the same concentrations as for the positive ion mode.

The detection conditions are as follows: capillary voltage: 3.00 kV, cone voltage: 20 V, source offset voltage: 30V (60V for negative ion mode), desolvation gas flow (nitrogen): 350 L/h, cone gas flow: 150 L/h, nebulizer gas flow: 7.0 bar, collision gas flow: 0.25 mL/min, solvation temperature: 250 °C, run duration: 0.4 min, scan time: 0.2 sec, infusion flow: 5  $\mu\text{L}/\text{min}$ .

Analytical software (MassLynx, version 4.1) is used for the system control and data processing.

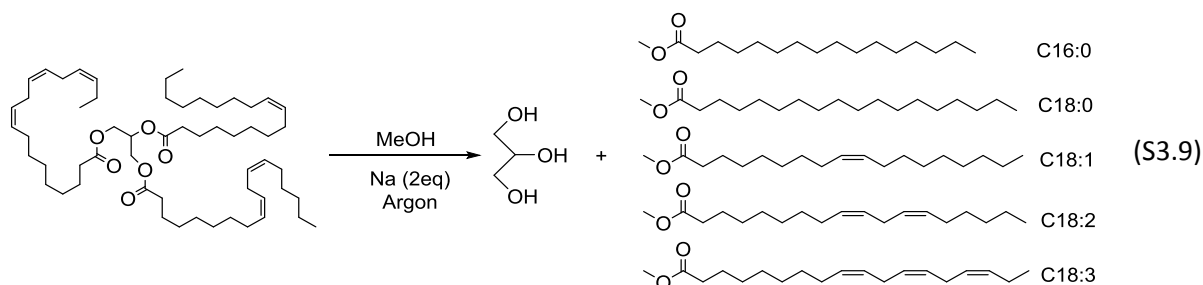
## 2.5 Purification of linseed oil

Alumina column chromatography can be used to remove antioxidants to very low concentrations. Starting linseed oil containing antioxidants is treated for complete removal of all antioxidants present, defined as < 1 ppm. Aluminium oxide is initially conditioned by gently rinsed with in-house ultra pure water in a Buchner funnel situated above the Buchner flask. This mixture is gently manually agitated and washed three times. Rinsed alumina is placed in an oven set at 200°C for at least three hours, generally dried overnight. The dried alumina is introduced into a column above a heavy walled 500 mL filtering flask. A ratio of 2:1 oil: alumina was maintained for this effort. Two

hundred grams of alumina was weighed and dispensed into the column via glass funnel. Next, portions of 400 g oil were added since the column capacity limited the full initial introduction amount. The vacuum was maintained to allow a slow but steady drip as visually witnessed into the filtering flask. All glassware was covered with aluminum foil during this separation to limit light exposure. This process offers approx 70% recovery of starting amount. Oil was stored in an amber wide bottle and capped with nitrogen prior to freezer storage.

## 2.6 Synthesis of antioxidant-free fatty acid methyl esters (FAMES) by transesterification of purified linseed oil

The transesterification reaction of triglycerides of purified linseed oil with methanol into fatty acid methyl esters (FAMES) is represented by the **equation S3.9**.



1 L of methanol is introduced into a 2L three-necked equipped with a cooler and a bubbler. Sodium (10 g, 2 equiv.) is introduced piece by piece under argon followed by purified linseed oil (200 g, 1 equiv.). The reaction is performed overnight. FAMES are extracted with 3 x 300 mL of petroleum ether. The combined organic phases are evaporated under pressure. Isolated FAMES are stored at -20 °C.

## 2.7 Gas chromatography – mass spectrometry analysis

A Thermofisher GC Trace equipped with an AI 3000 injector connected to Thermofisher DSQ II simple quadrupole detector is used for the GC-MS analysis of FAMES. Compound separation is achieved on a 30 m, DB5MS with 0.25 mm i.d. and 0.25  $\mu\text{m}$  film thickness gas chromatographic column (J&W Scientific, Folsom, CA, USA). Carrier gas (ultra-pure helium) flow rate is 1.0 mL/min and the injector, the transfer line and the ions source are maintained at 250, 270 and 220 °C, respectively. The MS detector is used in the EI mode with an ionization voltage of 70 eV. The column is held at 130 °C for 0.5 min and then programmed at 0.3 °C.min<sup>-1</sup> to 180 °C and maintained for 5 min. Then, the column is programmed at 3 °C.min<sup>-1</sup> to 250 °C and maintained for 10 min. The compounds are injected in the Split mode with a ratio of 20. FAME mix GLC-10 is used to analyze and quantify the FAMES composition

The same equipment is used for the analysis of antioxidant oxidation. The changes are made in the column programming. The column is held at 60 °C for 2min and then programmed at 3 °C.min<sup>-1</sup> to 250 °C and maintained for 5 min.

## 2.8 <sup>1</sup>H and <sup>13</sup>C NMR analysis

<sup>1</sup>H NMR spectra were recorded on a Bruker 300, calibrated relative to TMS in CDCl<sub>3</sub> solution and data are reported as follows: chemical shift in parts per million, multiplicity (bs = broad signals,

s = singlet, d = doublet, t = triplet, q = quartet, m = multiplet or overlap of non-equivalent resonances), integration.  $^{13}\text{C}$  NMR spectra were recorded at 100 MHz in  $\text{CDCl}_3$ , calibrated on  $\text{CDCl}_3$  signal (77.16 ppm).

## 2.9 Autoxidation of FAMES of linseed oil by the RapidOxy®: Effect of the phenolic antioxidants

2 mL FAMES of linseed oil are introduced into the RapidOxy® cell (25mL) at room temperature. Phenol solutions are prepared in ethyl acetate, solvent inert to oxidation, at  $10^{-2} \text{ mol.L}^{-1}$  and 100  $\mu\text{L}$  are introduced in 2 mL FAMES linseed oil to get a  $5 \times 10^{-4} \text{ mol.L}^{-1}$  solution. The cell is then closed and heated at  $90^\circ\text{C}$  under a pure oxygen pressure of 450 kPa leading to the FAMES linseed oil oxidation. The pressure is monitored up to 50 % of the maxima pressure is reached. The RapidOxy® apparatus (Figure S3.5) is equipped with an inox cell (7, dim 20x40x26 cm) corresponding to a total volume of 25 mL in which the sample is introduced at ambient temperature.

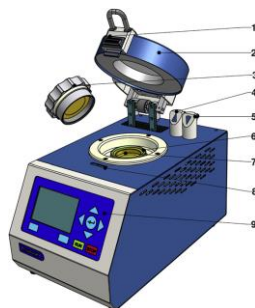


Figure S3.5: RapidOxy® apparatus for measurement of oxygen consumption during the autoxidation process

The cell is then closed by a screw cap (3) and a safety hood (2), which is locked by a latch (1 and 8). The gas is removed of the cell by the extraction gas connection (4) and replaced by only pure dioxygen, which is injected through the gas alimentation (5) at the pressure on the interface screen (9) (450 kPa). The cell is then heated up to the temperature set ( $90^\circ\text{C}$ ) and the pressure is monitored every minute by the pressure sensor (6). The experiment is ended when the pressure reached 50% of the maximum pressure. The pressure decrease is converted into a concentration of oxygen per volumes of the FAMES solution (Eq. S3.10) as represented by the figure S3.6.

$$\Delta[\text{O}_2]_t = \frac{(P_{\max} - P_t)}{RT} \times \frac{(V_{\text{tot}} - V_{\text{liq}})}{V_{\text{liq}}} \quad (\text{S3.10})$$

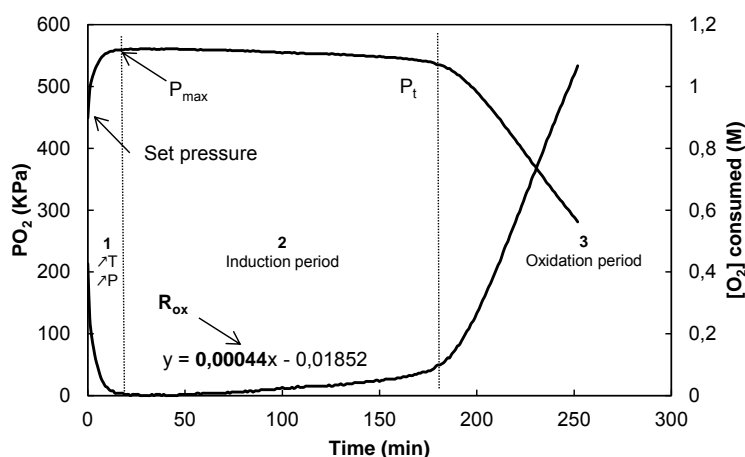


Figure S3.6: Monitoring of the oxygen pressure (primary axis) and the concentration of oxygen consumed (secondary axis) during the oxidation of FAMES of linseed oil in the presence of  $[\text{BHT}] = 5 \times 10^{-4} \text{ M}$  at  $90^\circ\text{C}$

## 2.10 Autoxidation of FAMES of linseed oil with the Rancimat® and effect of the phenolic antioxidants

The Rancimat device (**Fig. S3.7**) is used to determine the inhibition of oil autoxidation. A stream of purified air (9 L/h) is passed through a sample of oil which is held in a water bath (90 °C). The temperature of 90 °C was selected to be comparative with RapidOxy® experiments. The effluent air from oils or fat samples is then bubbled through to a vessel containing deionized water. The conductivity of water is continually monitored during this process. The effluent air contains volatile organic acids, swept from the oxidizing oil, that cause an increase in the conductivity of water as the oxidation proceeds. Formic acid is the predominant organic acid formed. The conductivity of water may be monitored and the induction point is defined as the point of maximum change in the rate of oxidation. This test highlights the induction period (or oxidation stability index OSI) where phenolic antioxidants are efficient.

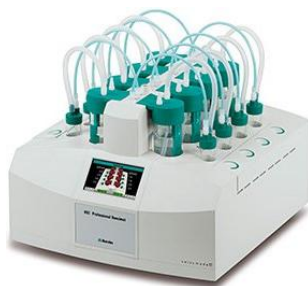
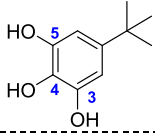
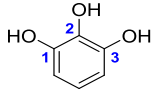
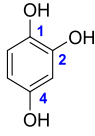
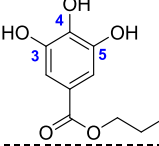
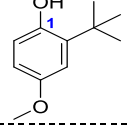
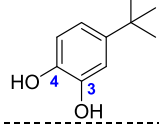
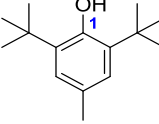
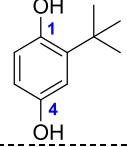
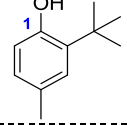
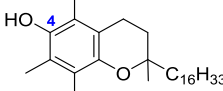
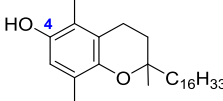
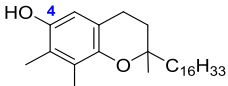
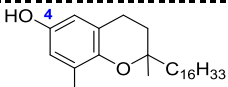
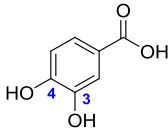
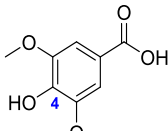
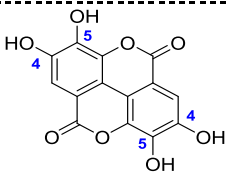
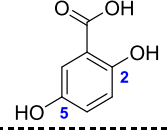
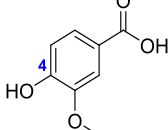
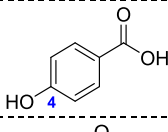
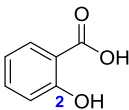
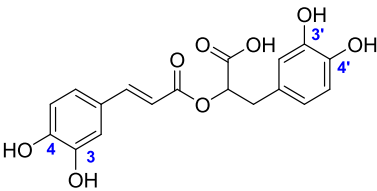
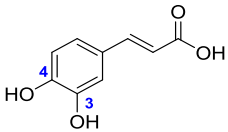


Figure S3.7: Biodiesel Rancimat apparatus,

### 3. Results

#### 3.1 Bond dissociation enthalpies BDE (O-H)

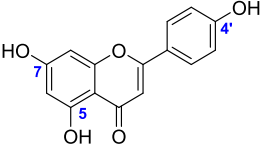
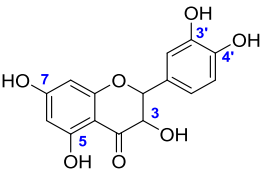
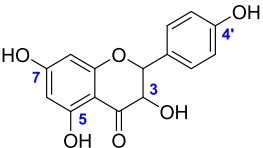
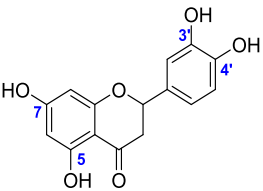
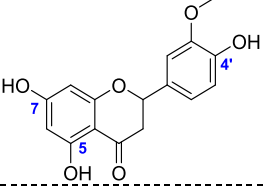
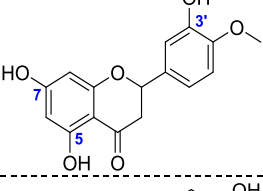
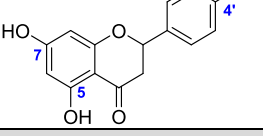
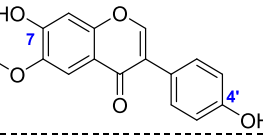
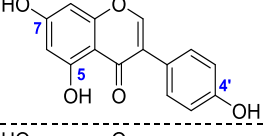
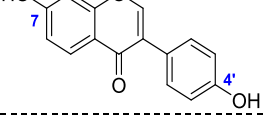
Number	Name	Structure	Site	BDE O-H (kcal.mol <sup>-1</sup> )
<b>Synthetic antioxidants</b>				
1	5-Tert-butyl-pyrogallol		4 3,5	66.6 74.1
2	Pyrogallol		2 1,3	68.0 74.4
3	Hydroxyquinol		1 2 4	69.1 72.1 75.9
4	Propyl gallate		4 3,5	69.6 75.7
5	BHA		1	72.3
6	4-Tert-butyl-catechol		4 3	72.3 73.2
7	BHT		1	72.4
8	TBHQ		1 4	74.3 76.7
9	<i>o</i> -Tert-butyl- <i>p</i> -cresol		1	77.4
10	Phloroglucinol		1,3,5	83.0
<b>Tocopherols</b>				
11	$\alpha$ -Tocopherol		4	69.1
12	$\beta$ -Tocopherol		4	73.4

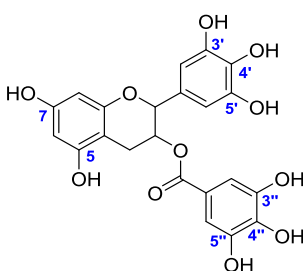
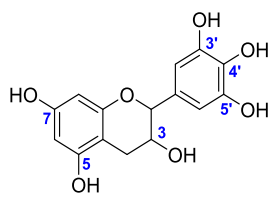
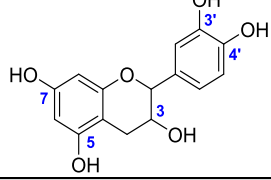
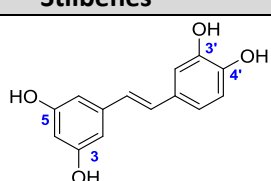
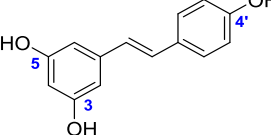
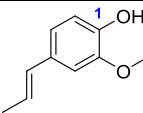
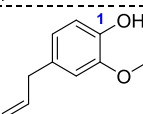
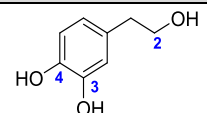
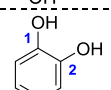
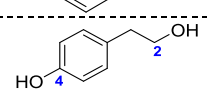
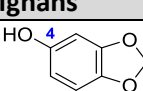
Number	Name	Structure	Site	BDE O-H (kcal.mol <sup>-1</sup> )
13	γ-Tocopherol		4	73.5
14	δ-Tocopherol		4	75.4
<b>Derivatives of hydroxybenzoic acids</b>				
15	Gallic acid		4 3,5	70.2 76.3
16	Protocatechuic acid		4 3	75.5 75.6
17	Syringic acid		4	78.1
18	Ellagic acid		4 5	78.4 78.9
19	Gentisic acid		5 2	79.5 84.6
20	Vanillic acid		4	83.1
21	PHBA		4	84.7
22	Salicylic acid		1	95.2
<b>Hydroxycinnamic acid derivatives</b>				
23	Rosmarinic acid		4 3 4' 3'	69.2 75.2 72.4 75.9
24	Caffeic acid		4 3	72.1 74.6

Number	Name	Structure	Site	BDE O-H (kcal.mol <sup>-1</sup> )
25	Chlorogenic acid		4	73.4
			3	75.9
26	Sinapic acid		4	75.4
27	Ferulic acid		4	79.7
28	<i>o</i> -Coumaric acid		2	80.1
29	<i>p</i> -Coumaric acid		4	80.5
30	<i>m</i> -Coumaric acid		3	84.4
<b>Flavonols</b>				
31	Gossypetin		3'	75.1
			4'	72.4
			3	79.8
			5	88.2
			7	71.7
			8	66.6
32	Myricetin		3'	76.1
			4'	67.4
			5'	76.3
			3	79.6
			5	93.8
			7	85.8
33	Azaleatin		3'	73.9
			4'	71.1
			3	81.9
34	Quercetin		7	84.6
			3'	74.3
			4'	71.8
			3	80.4
35	Fisetin		5	95.0
			7	84.9
			3'	75.3
			4'	72.3
35	Fisetin		3	80.9
			7	83.9

Number	Name	Structure	Site	BDE O-H (kcal.mol <sup>-1</sup> )
36	Laricitrin		4'	<b>72.5</b>
			5'	79.4
			3	80.6
			5	94.9
37	Syringetin		4'	<b>75.7</b>
			3	79.0
			5	93.7
			7	85.4
38	Rhamnazin		4'	<b>79.6</b>
			3	80.8
39	Kaempferide		5	93.9
			7	85.4
40	Isorhamnetin		4'	<b>79.8</b>
			3	80.2
			5	94.0
			7	85.1
41	Morin		2'	82.9
			4'	82.2
			3	<b>79.8</b>
			5	94.6
42	Kaempferol		4'	<b>80.1</b>
			3	80.5
			5	94.8
			7	85.2
43	Galangin		3	<b>81.2</b>
			5	94.0
44	Luteolin		7	86.2
			3'	74.9
			4'	<b>73.1</b>
44	Luteolin		5	113.2
			7	86.6

**Flavones**

Number	Name	Structure	Site	BDE O-H (kcal.mol <sup>-1</sup> )
45	Apigenin		4'	<b>82.1</b>
			5	98.4
			7	86.5
<b>3,4-Dihydroxyflavonols</b>				
46	Taxifolin		4'	<b>73.2</b>
			3'	73.5
			3	103.4
			5	94.8
47	Aromadedrin		7	87.3
			4'	<b>82.3</b>
			3	97.8
			5	95.7
<b>Flavones</b>				
48	Eriodictyol		4'	<b>73.8</b>
			3'	<b>73.6</b>
			5	103.8
49	Homoeriodictyol		7	87.6
			4'	<b>80.8</b>
			5	96.8
50	Hesperetin		7	87.8
			3'	<b>82.2</b>
			5	103.6
51	Naringenin		7	87.7
			4'	<b>82.4</b>
			5	96.7
<b>Isoflavones</b>				
52	Glycitein		4'	<b>80.1</b>
			7	84.1
53	Genistein		4'	<b>81.0</b>
			5	112.5
54	Daidzein		7	87.3
			4'	<b>81.9</b>
			7	84.8

Number	Name	Structure	Site	BDE O-H (kcal.mol <sup>-1</sup> )
<b>Catechins</b>				
55	Epigallocatechin gallate		3'	73.5
			4'	<b>66.5</b>
			5'	73.1
			3''	75.8
			4''	68.6
			5''	75.4
			5	79.6
7	83.4			
-----				
56	Galocatechin		3'	75.8
			4'	<b>68.6</b>
			5'	75.2
			3	100.8
			5	79.2
7	82.0			
-----				
57	Catechin		3'	82.5
			4'	<b>74.4</b>
			3	102.4
			5	79.1
7	82.9			
<b>Stilbenes</b>				
58	Piceatannol		4'	<b>68.7</b>
			5'	71.2
			3	82.1
			5	82.9
-----				
59	Resveratrol		4'	<b>76.7</b>
			3	82.7
			5	82.0
<b>Isoeugenol and eugenol</b>				
60	Isoeugenol		1	<b>76.6</b>
-----				
61	Eugenol		1	<b>80.2</b>
<b>Antioxidants in olive oil</b>				
62	Hydroxytyrosol		4	<b>72.1</b>
			3	72.8
			2	97.4
-----				
63	Catechol		1,2	<b>73.4</b>
-----				
64	Tyrosol		4	<b>81.0</b>
			2	97.5
<b>Lignans</b>				
65	Sesamol		4	<b>75.1</b>

Number	Name	Structure	Site	BDE O-H (kcal.mol <sup>-1</sup> )
<b>Coumarins</b>				
66	Methylesculetin		6	72.0
			7	73.4
67	Aesculetin		6	72.5
			7	73.0
68	Nordalbergin		6	72.6
			7	73.2
<b>Carnosol and carnosic acid</b>				
69	Carnosol		6	70.7
			5	71.6
70	Carnosic acid		6	70.8
			5	71.4

Table S3.2: BDE values of the ArO-H bond of phenols calculated with the B3LYP/6-311++G(2d,2p)//B3LYP/6-311G(d,p) DFT method in vacuum

### 3.2 Kinetics rate constants of hydrogen transfer from phenolic antioxidants to the DPPH<sup>•</sup> radical in toluene

Phenol	Methods	10 <sup>4</sup> x [DPPH <sup>•</sup> ] (M)	10 <sup>3</sup> x [ArOH] <sub>0</sub> (M)	10 <sup>3</sup> x k <sub>app</sub> <sup>a</sup>	10 <sup>3</sup> x Std. Dev.	k (M <sup>-1</sup> .s <sup>-1</sup> ) <sup>a</sup>
1	SOK	1.25	0.125	805.8	3.4	9480
4	SOK	1.25	0.125	195.5	2.0	2300
5	SOK	1.25	0.125	15.7	1.1	184
6	SOK	1.25	0.125	65.9	1.5	776
			2.0	0.63		
			3.0	0.76		
			4.0	0.98	/	0.18
7	FOK	1.25	5.0	1.16		
			0.125	51.3	0.2	603
			0.9	0.38		
			1.35	0.58		
9	FOK	1.25	1.80	0.70	/	0.36
			2.25	0.88		
			0.125	228.6	2.4	2686
11	SOK	1.25	0.125	0.90	0.03	11
17	SOK	1.25	0.125	0.12	0.01	1.41
20	SOK	1.25	0.125	0.12	0.01	1.41
			2.0	2.03		
			3.0	3.04		
			4.0	3.92	/	0.98
			5.0	5.01		

Phenol	Methods	$10^4 \times [\text{DPPH}^\bullet] \text{ (M)}$	$10^3 \times [\text{ArOH}]_0 \text{ (M)}$	$10^3 \times k_{\text{app}}^a$	$10^3 \times \text{Std. Dev.}$	$k \text{ (M}^{-1}\cdot\text{s}^{-1})^a$
<b>26<sup>b</sup></b>	SOK	1.25	0.125	14.1	1.9	165
<b>27</b>	SOK	1.25	0.125	0.71	0.06	8.40
<b>60</b>	SOK	1.25	0.125	3.21	0.17	38
			0.9	2.58		
<b>61</b>	FOK	1.25	1.35	3.88	/	2.73
			1.8	5.23		
			2.25	6.23		
<b>61</b>	SOK	1.25	0.125	0.33	0.01	3.90
<b>62</b>	SOK	1.25	0.125	90.8	2.2	1068
<b>63</b>	SOK	1.25	0.125	34.4	0.3	405
<b>65</b>	SOK	1.25	0.125	21.5	0.1	252
<b>69</b>	SOK	1.25	0.125	142.7	8.9	1679
<b>70</b>	SOK	1.25	0.125	54.3	0.3	639
<b>71</b>	FOK	1.25	0.125	93.6	1.5	1101

<sup>a</sup> Average of three values, <sup>b</sup>  $\lambda = 600 \text{ nm}$

Table S3.3: Kinetics rate constants of hydrogen transfer from phenolic antioxidants to the DPPH<sup>•</sup> radical in toluene,  $\lambda = 515 \text{ nm}$

### 3.3 Kinetics rate constants of hydrogen transfer from phenolic antioxidants to the DPPH<sup>•</sup> radical in ethyl acetate

Phenol	Methods	$10^4 \times [\text{DPPH}^\bullet] \text{ (M)}$	$10^3 \times [\text{ArOH}]_0 \text{ (M)}$	$10^3 \times k_{\text{app}}^a$	$10^3 \times \text{Std. Dev.}$	$k \text{ (M}^{-1}\cdot\text{s}^{-1})^a$
<b>1</b>	SOK	1.25	0.125	17.1	0.1	190
<b>4</b>	SOK	1.25	0.125	4.0	0.9	44
<b>5</b>	SOK	1.25	0.125	0.66	0.07	7.4
<b>6</b>	SOK	1.25	0.125	1.66	0.03	18
			2.0	0.13		
<b>7</b>	FOK	1.25	3.0	0.22	/	0.08
			4.0	0.29		
			5.0	0.38		
<b>8</b>	SOK	1.25	0.125	3.59	0.24	40
			0.9	0.08		
<b>9</b>	FOK	1.25	1.35	0.11	/	0.09
			1.80	0.15		
			2.25	0.19		
<b>11</b>	SOK	1.25	0.125	19.0	0.2	210
<b>15</b>	SOK	1.25	0.125	0.70	0.09	7.80
			0.60	0.31		
<b>16</b>	SOK	1.25	0.90	0.44	/	0.79
			1.20	0.68		
			1.50	0.90		
<b>17</b>	SOK	1.25	0.125	0.007	0	0.08
<b>20</b>	FOK	1.25	0.125	0.0009	0	0.01
<b>23</b>	SOK	1.25	0.125	2.84	0.07	31
<b>24</b>	SOK	1.25	0.125	0.94	0.04	10
<b>25</b>	SOK	1.25	0.125	0.77	0.04	8.6
<b>26</b>	SOK	1.25	0.125	4.69	0.02	23
<b>27</b>	SOK	1.25	0.125	0.09	0.01	1.03

Phenol	Methods	$10^4 \times [\text{DPPH}^\bullet] \text{ (M)}$	$10^3 \times [\text{ArOH}]_0 \text{ (M)}$	$10^3 \times k_{\text{app}}^a$	$10^3 \times \text{Std. Dev.}$	$k \text{ (M}^{-1}\cdot\text{s}^{-1})^a$
<b>32<sup>b</sup></b>	SOK	1.25	0.125	13.4	0.3	67
<b>34<sup>b</sup></b>	SOK	1.25	0.125	3.64	0.05	18
<b>55</b>	SOK	1.25	0.125	16.9	0.8	187
<b>58</b>	SOK	1.25	0.125	28.3	0.5	314
<b>59</b>	SOK	1.25	0.125	0.29	0.03	1.43
<b>60</b>	SOK	1.25	0.125	0.49	0.02	5.43
			0.9	0.90		
<b>61</b>	FOK	1.25	1.35	1.35	/	0.47
			1.8	1.80		
			2.25	2.25		
<b>62</b>	SOK	1.25	0.125	1.20	0.04	13
<b>63</b>	SOK	1.25	0.125	0.34	0.03	3.73
<b>65</b>	SOK	1.25	0.125	0.49	0.02	5.47
<b>67</b>	SOK	1.25	0.125	1.29	0.02	14
<b>69</b>	SOK	1.25	0.125	4.22	0.02	47
<b>70</b>	SOK	1.25	0.125	9.28	0.02	103

<sup>a</sup> Average of three values, <sup>b</sup>  $\lambda = 600 \text{ nm}$

Table S3.4: Kinetics rate constants of hydrogen transfer from phenolic antioxidants to the DPPH<sup>•</sup> radical in ethyl acetate,  $\lambda = 515 \text{ nm}$

### 3.4 Kinetics rate constants of hydrogen transfer from phenolic antioxidants to the DPPH<sup>•</sup> radical in ethanol

Phenol	Methods	$10^4 \times [\text{DPPH}^\bullet] \text{ (M)}$	$10^3 \times [\text{ArOH}]_0 \text{ (M)}$	$10^3 \times k_{\text{app}}^a$	$10^3 \times \text{Std. Dev.}$	$k \text{ (M}^{-1}\cdot\text{s}^{-1})^a$
<b>1</b>	SOK	1.25	0.125	228.8	6.8	2119
<b>4</b>	SOK	1.25	0.125	156.9	2.0	1453
<b>5</b>	SOK	1.25	0.125	3.22	0.28	30
<b>6</b>	SOK	1.25	0.125	34.4	0.4	318
			2.2	0.10		
			3.3	0.14		
<b>7</b>	FOK	1.25	4.4	0.20	/	0.04
			5.5	0.24		
			0.125	12.0		
0.90	0.07					
<b>8</b>	SOK	1.25	1.35	0.10	/	0.08
			1.80	0.14		
			2.25	0.17		
<b>9</b>	FOK	1.25	0.125	43.1	1.4	400
<b>11</b>	SOK	1.25	0.125	8.05	0.25	75
<b>15</b>	SOK	1.25	0.125	5.54	0.04	51
<b>16</b>	SOK	1.25	0.125	2.91	0.35	27
<b>17</b>	SOK	1.25	0.125	32.7	2.0	303
<b>24</b>	SOK	1.25	0.125	2.42	0.08	23
<b>25</b>	SOK	1.25	0.125	94.9	1.3	402
<b>26<sup>b</sup></b>	SOK	1.25	0.125	1.79	0.01	17
<b>27</b>	SOK	1.25	0.125	103.6	2.2	439
<b>32<sup>b</sup></b>	SOK	1.25	0.125	18.4	0.9	78
<b>34<sup>b</sup></b>	SOK	1.25	0.125	221.2	7.3	2048
<b>55</b>	SOK	1.25	0.125	6.92	0.80	64.0
<b>59</b>	SOK	1.25	0.125	15.8	0.5	146
<b>60</b>	SOK	1.25	0.125			

Phenol	Methods	$10^4 \times [\text{DPPH}^\bullet] \text{ (M)}$	$10^3 \times [\text{ArOH}]_0 \text{ (M)}$	$10^3 \times k_{\text{app}}^a$	$10^3 \times \text{Std. Dev.}$	$k \text{ (M}^{-1}\cdot\text{s}^{-1}\text{)}^a$
61	FOK	1.25	0.9	6.51	/	9.0
			1.35	11.5		
			1.8	15.2		
			2.25	18.8		
63	SOK	1.25	0.125	14.3	0.9	133
62	SOK	1.25	0.125	26.0	2.6	241
65	SOK	1.25	0.125	14.2	0.6	130
67	SOK	1.25	0.125	268.5	21.5	2486
23	SOK	1.25	0.125	16.9	0.8	157
69	SOK	1.25	0.125	574.2	13.4	5327
70	SOK	1.25	0.125	398.5	4.6	3690
71	FOK	1.25	0.125	1580	152	14629

<sup>a</sup> Average of three values, <sup>b</sup>  $\lambda = 600 \text{ nm}$

Table S3.5: Kinetics rate constants of hydrogen transfer from phenolic antioxidants to the DPPH<sup>•</sup> radical in ethanol,  $\lambda = 515 \text{ nm}$

### 3.5 Kinetics rate constants of hydrogen transfer from phenolic antioxidants to the DPPH<sup>•</sup> radical in Cetiol A at 20 °C

Phenol	Methods	$10^4 \times [\text{DPPH}^\bullet] \text{ (M)}$	$10^4 \times [\text{ArOH}]_0 \text{ (M)}$	$10^3 \times k_{\text{app}}^a$	$10^3 \times \text{Std. Dev.}$	$k \text{ (M}^{-1}\cdot\text{s}^{-1}\text{)}^a$
1	SOK	1.25	1.25	62.0	0.1	709
4	SOK	1.25	1.25	5.34	0.2	61
6	SOK	1.25	1.25	5.16	0.11	59
8	SOK	1.25	1.25	17.7	0.2	203
11	SOK	1.25	1.25	37.5	0.1	432
70	FOK	1.25	1.25	20.1	0.1	230
71	SOK	1.25	1.25	17.2	0.06	197

<sup>a</sup> Average of three values

Table S3.6: Kinetics rate constants of hydrogen transfer from phenolic antioxidants to the DPPH<sup>•</sup> radical in Cetiol A,  $\lambda = 515 \text{ nm}$

### 3.6 Determination of the stoichiometric numbers $\sigma_{\text{exp}}$ in toluene, effect of the concentration of antioxidants

Phenol <sup>a</sup>	$10^5 \times [\text{ArOH}]_0 \text{ (M)}$	$A_0$	$A_f$	$\sigma_{\text{exp}}$	$\sigma_{\text{average}}$
1	2.14	1.14	0.63	2.0	2.1
	2.86	1.14	0.44	2.1	
	3.57	1.14	0.28	2.1	
5	1.43	1.25	0.93	1.9	2.0
	2.85	1.23	0.55	2.0	
	4.28	1.40	0.44	1.9	
7	1.42	1.34	1.00	2.0	2.0
	2.84	1.25	0.55	2.1	
	4.25	1.24	0.27	1.9	
8	1.43	1.45	1.12	2.0	2.0
	2.86	1.48	0.78	2.0	
	4.29	1.45	0.43	2.0	

Phenol <sup>a</sup>	$10^5 \times [\text{ArOH}]_0 \text{ (M)}$	$A_0$	$A_f$	$\sigma_{\text{exp}}$	$\sigma_{\text{average}}$
9	1.43	1.57	1.13	2.6	2.6
	2.86	1.45	0.59	2.6	
	4.29	1.47	0.22	2.5	
11	1.39	1.38	1.06	2.0	2.0
	2.79	1.38	0.75	1.9	
	4.18	1.37	0.35	2.1	
60	1.43	1.48	1.30	1.1	1.0
	2.86	1.52	1.18	1.0	
	4.29	1.47	0.95	1.0	
61	1.43	1.49	1.15	2.0	2.0
	2.86	1.38	0.71	2.0	
	4.29	1.46	0.45	2.0	
63	1.43	1.58	1.25	2.0	2.0
	2.86	1.53	0.86	2.0	
	4.29	1.50	0.52	1.9	
70	2.14	1.24	0.70	2.1	2.1
	2.86	1.24	0.51	2.2	
	3.57	1.24	0.34	2.1	
71	2.14	1.21	0.71	2.0	2.0
	2.86	1.21	0.55	2.0	
	3.57	1.21	0.39	2.0	

<sup>a</sup>  $[\text{DPPH}^*] = 1.0 \times 10^{-4} \text{ M}$ ,  $\lambda = 515 \text{ nm}$ ,  $T = 20 \text{ }^\circ\text{C}$

Table S3.7: Determination of the stoichiometric numbers  $\sigma_{\text{exp}}$  in toluene, effect of the concentration of antioxidants

### 3.7 Determination of the stoichiometric numbers $\sigma_{\text{exp}}$ in toluene

Phenol <sup>a</sup>	$A_0$	$A_f$	$\sigma_{\text{exp}}$	Phenol <sup>a</sup>	$A_0$	$A_f$	$\sigma_{\text{exp}}$
<b>1</b>	1.60	1.09	2.1	<b>26</b>	1.60	1.10	1.4
<b>4</b>	1.60	0.64	3.9	<b>27</b>	1.60	1.15	1.8
<b>5</b>	1.60	1.12	2.0	<b>60</b>	1.60	1.38	0.9
<b>6</b>	1.60	0.98	2.5	<b>61</b>	1.60	1.08	2.1
<b>7</b>	1.60	1.10	2.0	<b>62</b>	1.60	1.12	2.0
<b>8</b>	1.60	1.12	2.0	<b>63</b>	1.60	1.13	1.9
<b>9</b>	1.60	1.00	2.5	<b>65</b>	1.60	1.10	2.1
<b>11</b>	1.60	1.12	2.0	<b>69</b>	1.60	1.14	1.9
<b>17</b>	1.60	1.33	1.1	<b>70</b>	1.60	1.12	2.0
<b>20</b>	1.60	1.43	0.7	<b>71</b>	1.60	1.11	2.0

<sup>a</sup>  $[\text{DPPH}^*] = 1.5 \times 10^{-4} \text{ M}$ ,  $[\text{ArOH}]_0 = 2.07 \times 10^{-5} \text{ M}$ ,  $\lambda = 515 \text{ nm}$ ,  $T = 20 \text{ }^\circ\text{C}$

Table S3.8: Determination of the stoichiometric numbers  $\sigma_{\text{exp}}$  in toluene

### 3.8 Determination of the stoichiometric numbers $\sigma_{\text{exp}}$ in ethyl acetate

Phenol <sup>a</sup>	A <sub>0</sub>	A <sub>f</sub>	$\sigma_{\text{exp}}$	Phenol <sup>a</sup>	A <sub>0</sub>	A <sub>f</sub>	$\sigma_{\text{exp}}$
1	1.62	1.16	2.0	26	1.60	1.38	1.0
4	1.60	0.85	3.3	27	1.60	1.29	1.4
5	1.60	1.11	2.1	32	1.61	0.83	3.4
6	1.60	1.03	2.5	34	1.60	1.17	1.9
7	1.60	1.16	2.0	55	1.60	0.35	5.4
8	1.61	1.16	2.0	58	1.60	0.61	2.0
9	1.60	1.25	1.5	59	1.60	1.40	0.9
11	1.61	1.15	2.0	60	1.60	1.38	1.0
15	1.60	0.46	5.0	61	1.60	1.40	0.9
16	1.60	1.18	1.8	62	1.62	1.18	1.9
17	1.60	1.43	0.7	63	1.60	1.11	2.1
20	1.60	1.60	0	65	1.60	1.05	2.4
21	1.60	1.60	0	67	1.61	1.11	2.1
23	1.60	0.65	4.1	69	1.61	1.14	2.0
24	1.63	1.17	2.0	70	1.60	1.13	2.1
25	1.61	1.17	1.9	71	1.62	1.16	2.0

<sup>a</sup> [DPPH<sup>•</sup>] = 1.5 × 10<sup>-4</sup> M, [ArOH]<sub>0</sub> = 2.07 × 10<sup>-5</sup>, λ = 515 nm, T = 20 °C,

nd: not determined

Table S3.9: Determination of the stoichiometric numbers  $\sigma_{\text{exp}}$  in ethyl acetate

### 3.9 Determination of the stoichiometric numbers $\sigma$ of the hydrogen transfer from phenols to the DPPH<sup>•</sup> radical in ethanol

Phenol <sup>a</sup>	A <sub>0</sub>	A <sub>f</sub>	$\sigma_{\text{exp}}$	Phenol <sup>a</sup>	A <sub>0</sub>	A <sub>f</sub>	$\sigma_{\text{exp}}$
1	1.60	1.03	3.0	25	1.60	1.15	2.3
4	1.61	0.80	4.2	26	1.60	1.15	2.3
5	1.61	1.12	2.6	27	1.60	1.23	1.9
6	1.60	1.06	2.9	32	1.60	0.80	4.2
7	1.60	1.41	1.0	34	1.60	0.80	4.2
8	1.60	1.15	2.3	59	1.61	1.20	2.1
9	1.60	0.86	3.0	60	1.60	1.19	2.1
11	1.60	1.19	2.1	61	1.60	1.03	3.0
15	1.60	0.37	6.4	62	1.60	1.22	2.0
16	1.60	1.20	2.1	63	1.60	1.13	2.4
17	1.60	1.17	2.2	65	1.60	1.16	2.3
20	1.60	1.60	0	67	1.60	0.73	4.5
21	1.60	1.60	0	69	1.60	1.19	2.1
23	1.60	0.77	4.3	70	1.60	1.19	2.1
24	1.60	1.16	2.3	71	1.60	1.12	2.5

<sup>a</sup> [DPPH<sup>•</sup>] = 1.5 × 10<sup>-4</sup> M, [ArOH]<sub>0</sub> = 2.07 × 10<sup>-5</sup>, λ = 515 nm, T = 20 °C, nd: not determined

Table S3.10: Determination of the stoichiometric numbers  $\sigma_{\text{exp}}$  in ethanol

### 3.10 Induction periods (IP) and oxidation rates ( $R_{ox}$ ) for the inhibition of FAMES of linseed oil oxidation by phenolic antioxidants during the RapidOxy® test

Phenol	Induction Period IP (min) <sup>a</sup>	Std. Dev.	Oxidation rate $R_{ox}$ (mM.min <sup>-1</sup> ) <sup>a</sup>	Std. Dev.
Control	5	1	1.21	0.04
1	234	5	0.06	0.03
4	162	11	0.26	0.02
5	167	2	0.35	0.05
6	220	10	0.37	0.02
7	131	1	0.44	0.07
8	45	2	0.53	0.06
9	56	2	0.77	0.02
11	177	2	0.17	0.01
15	178	6	0.32	0.04
16	50	4	0.62	0.03
17	37	6	0.76	0.11
20	5	1	1.03	0.04
21	6	1	1.20	0.05
24	148	5	0.36	0.02
25	138	2	0.48	0.02
26	54	6	0.57	0.05
27	28	2	0.82	0.02
32	262	9	0.11	0.02
34	135	8	0.34	0.01
55	476	37	0.08	0.03
58	313	10	0.29	0.04
59	67	2	0.68	0.04
60	49	1	0.72	0.02
61	27	2	0.93	0.05
62	172	3	0.30	0.02
63	147	3	0.46	0.01
65	161	2	0.55	0.01
67	112	8	0.50	0.03
23	262	14	0.27	0.01
69	166	6	0.35	0.01
70	230	8	0.29	0.02
71	5	1	1.20	0.05

<sup>a</sup> Average of three values, [Phenol]<sub>0</sub> = 0.5 mM, 2 mL of FAMES linseed oil,  
P = 450 kPa, T = 90°C

**Table S3.11: Induction periods (IP) and oxidation rates ( $R_{ox}$ ) for the inhibition of FAMES of linseed oil oxidation by phenolic antioxidants during the RapidOxy® test**

### 3.11 Effect of the concentration of phenolic antioxidants on the Induction periods (IP) during the inhibition of FAMES of linseed oil

Phenol	[ArOH] <sub>0</sub> (mM)	Induction Period IP (min) <sup>a</sup>	Std. Dev. (min)	Phenol	[ArOH] <sub>0</sub> (mM)	Induction Period IP (min) <sup>a</sup>	Std. Dev. (min)
/	/	5	1	/	/	5	1
<b>5</b>	0.25	105	5	<b>24</b>	0.25	93	3
	0.50	184	7		0.50	169	4
	0.75	244	8		0.75	237	7
	1.00	287	6		1.00	288	9
	1.25	349	6		1.25	350	6
<b>7</b>	0.25	72	3	<b>32</b>	0.25	144	5
	0.50	140	6		0.50	254	14
	0.75	208	6		0.75	321	10
	1.00	256	5		1.00	423	11
	1.25	323	13		1.25	506	6
<b>11</b>	0.25	97	10	<b>23</b>	0.25	134	5
	0.50	142	8		0.50	272	4
	0.75	194	13		0.75	398	8
	1.00	231	5		1.00	494	10
	1.25	271	9		1.25	593	11
<b>15</b>	0.25	95	5	<b>70</b>	0.25	128	9
	0.50	163	10		0.50	186	9
	0.75	262	8		0.75	255	5
	1.00	308	13		1.00	336	6
	1.25	397	6		1.25	386	14

<sup>a</sup> Average of three values, FAMES linseed oil, T = 90 °C, P = 450 kPa

**Table S3.12:** Effect of the concentration of phenolic antioxidants on the Induction periods (IP) during the inhibition of FAMES of linseed oil

### 3.12 Induction periods (IP) for the inhibition of FAMES of linseed oil and fish oil against oxidation by phenolic antioxidants during the Rancimat test

Phenol	FAMES Linseed oil		Fish oil	
	Induction Period IP (h) <sup>a</sup>	Std. Dev.	Induction Period IP (h) <sup>a</sup>	Std. Dev.
Control	0.21	0.01	0.15	0.01
7	6.79	0.48	2.93	0.08
8	28.86	2.63	16.41	0.58
11	3.84	0.11	2.04	0.07
23	9.07	0.54	3.00	0.18
24	9.41	0.75	4.09	0.28
27	0.34	0.06	0.14	0.01
32	10.60	1.20	6.83	0.94
59	1.66	0.21	0.15	0.02
62	11.23	0.25	8.51	0.27
67	3.60	0.50	0.20	0.04
70	10.71	0.38	7.32	0.51

<sup>a</sup>Average of three values, [Phenol]<sub>0</sub> = 500 ppm, 5 g of FAMES linseed oil or Arista fish oil, T = 90°C, F<sub>purified air</sub> = 9 L/h

**Table S3.13: Induction periods (IP) for the inhibition of FAMES of linseed oil and Arista fish oil oxidation by phenolic antioxidants during the Rancimat test**

# CHAPTER 4. SYNERGY BETWEEN PHENOLIC ANTIOXIDANTS FOR FOOD APPLICATIONS

---

## 1. Introduction

Interest in omega-3, and especially in  $\alpha$ -Linolenic (ALA), eicosapentaenoic (EPA) and docosahexaenoic (DHA) polyunsaturated fatty acids, is increasing due to their nutritional benefits. Nevertheless, their high number of bis-allylic hydrogens is responsible for food degradation and loss of their organoleptic properties. Consequently, the addition of antioxidants is essential for the preservation of food products to extend their lifetime. Moreover, as the range of commercial antioxidants is restricted and subject to strict regulations, one alternative is to take advantage of synergies that can take place between allowed antioxidants. As shown in **figure 4.1**, the number of references (*i.e.* articles, reviews, patents...) referring to the combination of “antioxidant” and “synergy” keywords found with the Scifinder<sup>®</sup> database is increasing since 1990.

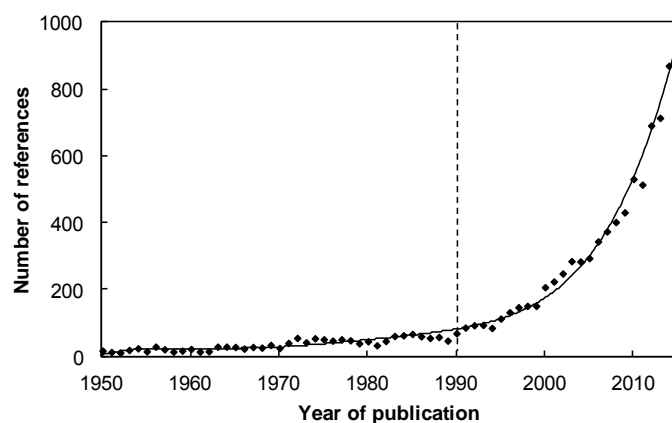


**Figure 4.1:** Exponential increase of the number of references (articles and patents) found by coupling the keywords “antioxidant” and “synergy” via the Scifinder<sup>®</sup> database

This analysis also highlights three main domains of applications: food (53 %), biochemistry (40%) and polymers (9 %). **Figure 4.2** provides an overview of the ten main journals dealing with antioxidants.

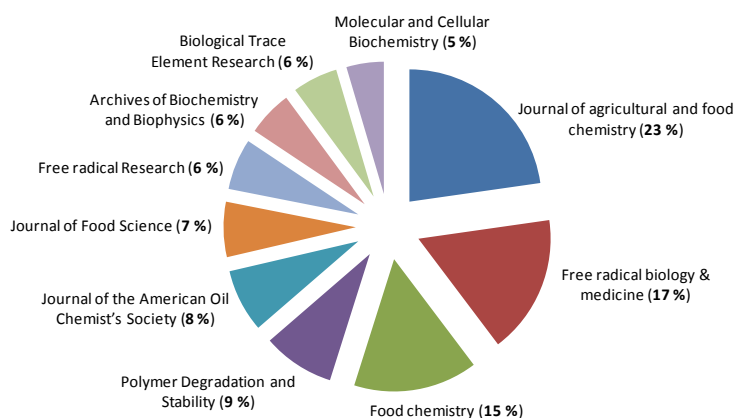


**Figure 4.2:** Ten main scientific journals highlighting the keywords “antioxidant” coupled with “synergy” via the Scifinder database

$\alpha$ -Tocopherol is by far the most widely used natural phenolic antioxidant (**Fig. 4.3**). It acts by inhibiting the propagation step of the free-radical autoxidation mechanism of food by reacting with free radicals. However, it is not the most efficient phenolic antioxidant and it presents a pro-oxidant activity at high concentration. Therefore, it is primordial to study synergies between  $\alpha$ -tocopherol and co-antioxidants to decrease its concentration. Other combinations of phenolic antioxidants are also investigated.

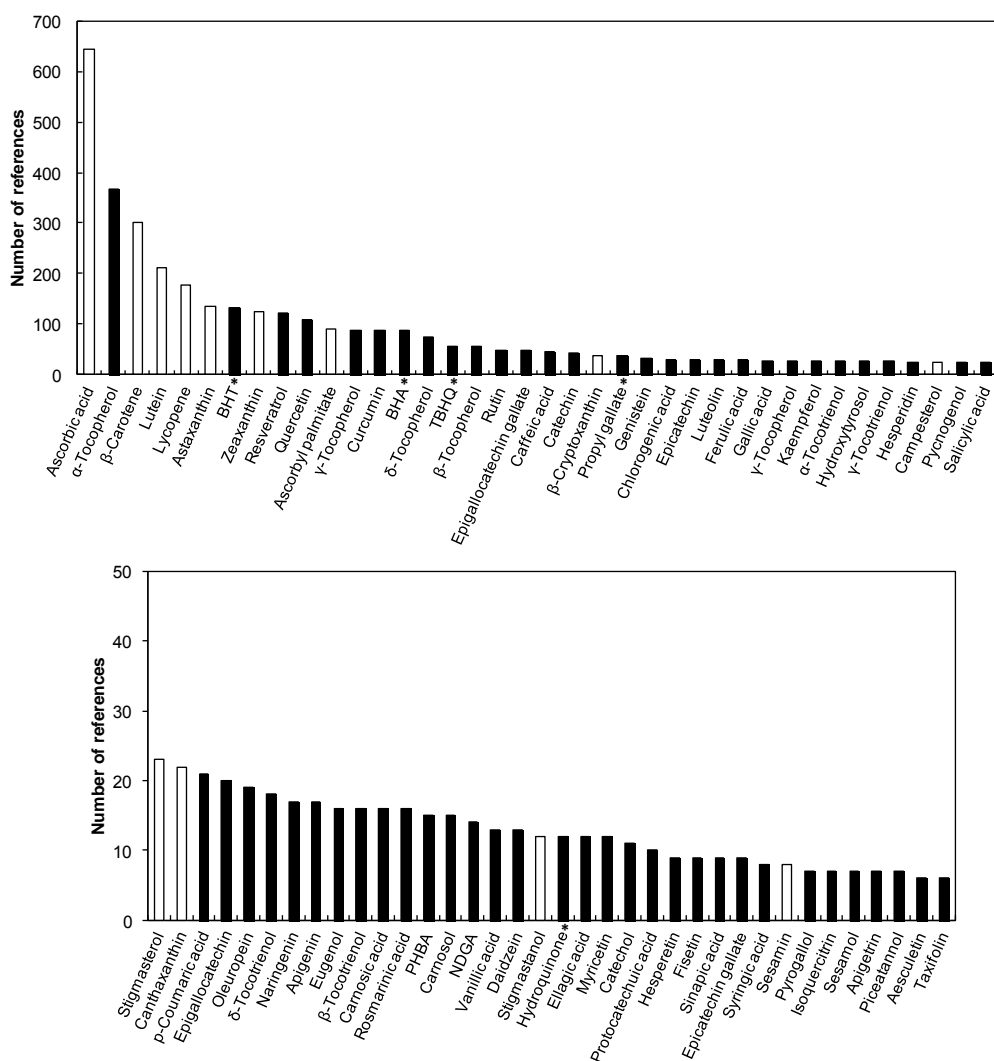


Figure 4.3: Number of references found for “antioxidant” via the Scifinder® database (■ phenolic antioxidants, □ others antioxidants, \*synthetic phenols)

## 2. Literature survey

Most interesting articles found in literature dealing with synergies between  $\alpha$ -tocopherol and co-antioxidants are gathered in **table 4.1** where the targets and techniques used to follow the oxidation are indicated. Synergism exists when two or more antioxidants exhibit a higher effectiveness compared to the effect predicted from the sum of their individual effect. In most cases, regeneration of  $\alpha$ -tocopherol by co-phenolic antioxidants or ascorbic acid is described. As  $\alpha$ -tocopherol is found in our cells composed by PUFAs, the understanding of synergistic effects may have an interest for human health.<sup>418-420</sup> Moreover, a combination of two antioxidants characterized by different preventing actions also leads to synergism. Indeed, a combination of metal chelators (*i.e.* flavonoids, EDTA, strong acids) with free radical scavengers is a good example of this type of synergy mainly due to the “sparing action” of free radical scavengers by chelators.<sup>164</sup>

Nevertheless, while the mode of action of antioxidants can be understood through kinetic and thermodynamic studies, the mechanisms involved during synergies between antioxidants remain unclear. General mechanisms and key parameters highlighted by authors are developed in this literature survey.

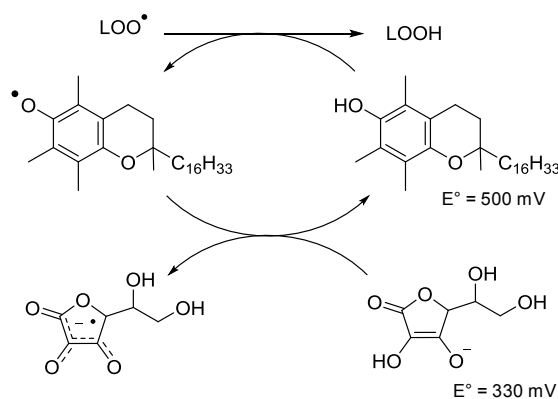
Co-antioxidant	Substrate/matrix		Monomers	DPPH <sup>•</sup> test	ESR	Techniques to monitor the oxidation			Concentration of antioxidant	Refs.
	Food models	Biological systems				O <sub>2</sub> consumption	ROOH titration	Formation of oxidized species		
<b>Ascorbic acid</b> and derivatives	Methyl linoleate, lard and SDS micelles	Liposomes, membranes, LDL and human platelets	Styrene	x	x	x		x	x	333, 421-433
<b>Flavonoids</b>	Linoleic acid, emulsions and sunflower oil	LDL and rat liver microsomes		x	x	x	x	x	x	433-442
<b>Synthetic phenols</b>	Linoleic acid		Styrene	x		x		x		333, 443-445
Derivatives of <b>Hydroxybenzoic acid</b>	Linoleic acid	Rat liver microsomes		x	x	x		x	x	433, 435, 442
Derivative of <b>Hydroxycinnamic acid</b>	Linoleic acid and fish muscle	LDL			x			x	x	430, 446, 447
<b>Catechol</b> derivatives			Styrene	x	x	x				333, 433
<b>Carotenoids</b>	Palm olein	Microsomal membranes and liposomes		x	x			x		448-451
<b>Resveratrol</b> and analogues	Linoleic acid	Micelles					x			452
<b>Phospholipids</b>	Linoleic acid, safflower oil, FAMES mixture and sardine oil					x	x	x		420, 453-459
<b>Amino, organic acids and EDTA</b>	methyl linoleate, linoleic acid, emulsions					x	x	x		444, 460, 461

Table 4.1: Synergies between  $\alpha$ -tocopherol and co-antioxidant reported in the literature, depending on the field of analysis, the techniques used to monitor the oxidation and the references of articles (Scifinder<sup>®</sup> database, keywords “antioxidant” and “synergy”)

## 2.1 Regeneration of the primary antioxidant by the co-antioxidant(s)

### ▪ Ascorbic acid and reduction potentials ( $E^{\circ}$ )

The most studied combination of two antioxidants is  $\alpha$ -tocopherol (vitamin E) and ascorbic acid (vitamin C). As described in **table 4.1**, several authors have investigated the impact of this mixture on the antioxidant activity in food<sup>425</sup>, biological systems<sup>429</sup> and during the autoxidation of styrene.<sup>333</sup> From these studies, it can be concluded that regeneration of the most effective free radical scavenger antioxidant (primary) by the less effective free radical scavenger antioxidant (co-antioxidant) occurs when one of them has a higher reduction potential than the other.<sup>164</sup> The free radical scavenger with the highest reduction potential ( $E^{\circ}$ ) acts as primary antioxidant and the other one, with a lowest reduction potential, regenerate the primary antioxidant. With respective reduction potentials of 500 and 330 mV,<sup>164</sup>  $\alpha$ -tocopherol acts as antioxidant by giving  $H^{\bullet}$  to peroxy ( $LOO^{\bullet}$ ) radicals leading to the formation of the  $\alpha$ -tocopheroxyl radical whereas ascorbic acid gives hydrogen to regenerate  $\alpha$ -tocopherol (**Fig. 4.4**). Golumbic and Mattill have first reported the increased antioxidant activity of  $\alpha$ -tocopherol by addition of ascorbic acid during the oxidation of lipids.<sup>424</sup> While  $\alpha$ -tocopherol is no more efficient after 20 hours of oxidation, 0.1 % of ascorbic acid extended the protective effects of around 300 hours. Consequently, ascorbic acid has no direct reation with  $LOO^{\bullet}$  but regenerates  $\alpha$ -tocopherol.



**Figure 4.4: General mechanism of synergy by the regeneration of  $\alpha$ -tocopherol ( $E^{\circ} = 500 \text{ mV}$ ) by ascorbic acid ( $E^{\circ} = 330 \text{ mV}$ ) in biological lipid/water model**

Ascorbic acid regenerates other phenols than  $\alpha$ -tocopherol. Boots *et al.* identified the regeneration of quercetin<sup>462</sup> and other flavonoids<sup>434</sup> (*i.e.* catechins, epicatechin, kaempferol and isorhamnetin) during oxidation processes.

### ▪ Synthetic phenols: kinetic rate constants of synergism and heterodimers formation

As synthetic phenolic antioxidants are widely used to protect oils, synergistic behaviors are also studied for their mixture with  $\alpha$ -tocopherol. As described by Kurechi *et al.* *via* DPPH $^{\bullet}$  test, the rapid hydrogen donating capabilities from the co-antioxidant to the primary antioxidant is responsible for the regeneration of  $\alpha$ -tocopherol by BHT.<sup>445</sup> Marteau *et al.* deeply investigated the dramatic solvent effect on this synergy *via* DPPH $^{\bullet}$  test.<sup>463</sup> They have shown that BHT regenerates  $\alpha$ -tocopherol from tocopheroxyl radical in apolar aprotic solvents by transferring two hydrogen atoms (**Fig. 4.5**).

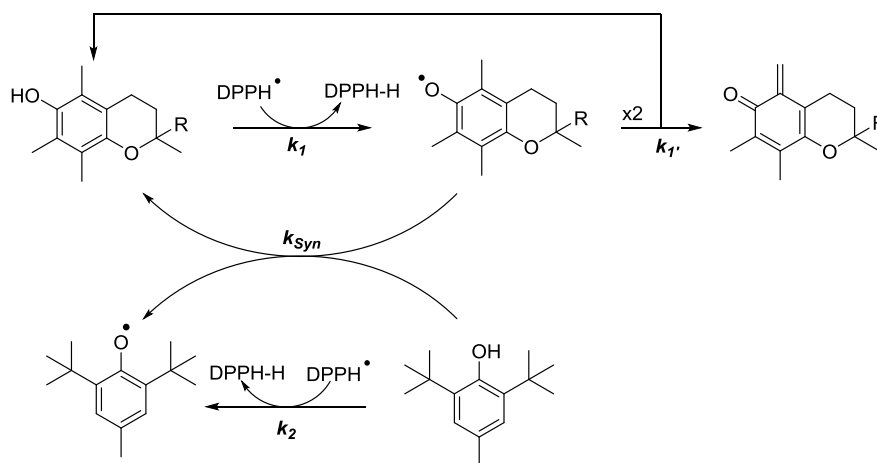


Figure 4.5: Regeneration of  $\alpha$ -tocopherol by BHT in apolar aprotic solvents<sup>463</sup>

The kinetic rate constant of synergy ( $k_{Syn}$ ) between co-antioxidant ( $CoAH_2$ ) and  $\alpha$ -tocopherol is sufficiently high to be competitive with the dismutation reaction ( $k_{Dism}$ ) of the tocopheroxyl radical ( $AH^\bullet$ ) (Eqs. 4.1 and 4.2). Nevertheless, the regeneration is suppressed in polar protic solvents due to a fast electron transfer from the tocopheroxyl radical to  $DPPH^\bullet$ .

$$k_{Syn} [AH^\bullet][CoAH_2] \geq k_{Dism} [AH^\bullet][AH^\bullet] \quad (4.1)$$

$$[CoAH_2] \geq \frac{k_{Dism}}{k_{Syn}} [AH^\bullet] \quad (4.2)$$

Besides  $\alpha$ -tocopherol, several other synergies have been reported between synthetic phenols. TBHQ mixed with BHA, propyl gallate (PG) or pyrogallol (PY) for example have shown synergistic effects as described by Guzman *et al.* during the oxidation of biodiesel.<sup>464</sup> The percent synergism (%SYN) was calculated on the basis of the induction periods observed according to **equation 4.3** where  $IP_{mix}$ ,  $IP_0$ ,  $IP_1$  and  $IP_2$  are the induction periods of the sample with mixture of phenols, the control sample and the sample with the individual antioxidants.<sup>464</sup>

$$\%SYN = \frac{(IP_{mix} - IP_0) - [(IP_1 - IP_0) + (IP_2 - IP_0)]}{(IP_1 - IP_0) + (IP_2 - IP_0)} \quad (4.3)$$

They pointed out that synergistic effects (%SYN) depend on the FAMES composition of biodiesel described in **table 4.2**. Indeed, the same equimolar mixture of TBHQ/PY showed synergistic (%SYN = 34) and antagonist (%SYN = -4) effects during the protection of distilled soybean oil (DSBO) and poultry fat (DPF) respectively.

Fatty acids	C14:0	C16:0	C16:1	C18:0	C18:1	C18:2	C18:3
DSBO	0	12.4	0	4.1	22.1	54.2	7.2
DPF	1.6	25.9	4.1	6.1	36.0	25.0	1.4

Table 4.2 : Fatty acid compositions of distilled soybean oil (DSBO) and poultry fat (DPF)<sup>464</sup>

As for the combination of  $\alpha$ -tocopherol and BHT, the mechanism of regeneration of the most effective antioxidant (PY) by the other one (TBHQ) was responsible for synergistic effect. Moreover, the formation of active heterodimers was also suggested to be part of synergism (Fig. 4.6).<sup>465</sup>

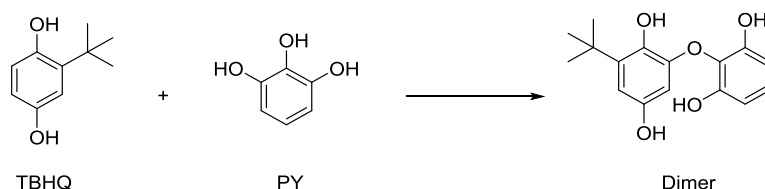


Figure 4.6: Suggested mechanism for the synergistic behavior of TBHQ and PY with the formation of dimer<sup>466</sup>

- *Flavonoids as co-antioxidants: their own antioxidant power leads the regeneration efficiency*

Synergistic effects can be also obtained between  $\alpha$ -tocopherol and flavonoids (Table 4.1).<sup>433-442</sup> The authors have studied mixtures of  $\alpha$ -tocopherol with various flavonols (*i.e.* quercetin, kaempferol and myricetin) and catechins (*i.e.* epicatechin EC, epigallocatechin EGC, epicatechin gallate ECG and epigallocatechin gallate EGCG) during the oxidation of food<sup>437</sup> and biological<sup>442</sup> systems. Based on extended induction periods and lower oxidation rates, Marinova *et al.* highlighted the regeneration of myricetin by  $\alpha$ -tocopherol (Table 4.3).<sup>439</sup>

Antioxidant	Concentration x 10 <sup>4</sup> (mol.L <sup>-1</sup> )	Induction period (h)	Oxidation rate x 10 <sup>7</sup> (M.s <sup>-1</sup> )
$\alpha$ -tocopherol	3	5.5	5.05
Myricetin	3.2	8.9	3.27
Equimolar mixture	6.2	20.5	1.98

Table 4.3: Kinetic parameters characterizing inhibited oxidation of sunflower oil at 100 °C by  $\alpha$ -tocopherol, myricetin and equimolar mixture<sup>439</sup>

Jia *et al.* reported synergistic behaviors with polyphenols from green tea during the peroxidation of linoleic acid.<sup>435</sup> Their relative co-antioxidant efficiency followed their own antioxidant power giving the decreasing activity sequence with  $\alpha$ -tocopherol: EGCG >> ECG ~ EGC > EC. It was thus assumed that the regeneration of  $\alpha$ -tocopherol should be the predominant reaction in the presence of green tea polyphenols (Fig. 4.7).<sup>435</sup>

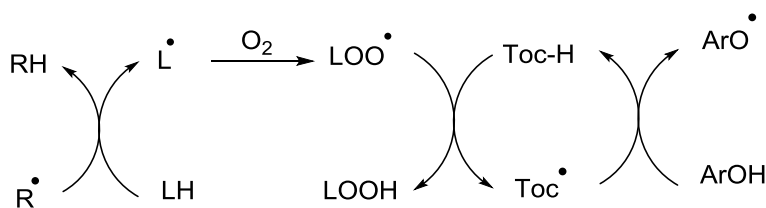


Figure 4.7: Synergistic mechanism between  $\alpha$ -tocopherol (Toc-H) and tea polyphenols (ArOH) for the inhibition of linoleic acid oxidation in alcohol/water solution, R<sup>•</sup> = initiating radical, LOO<sup>•</sup> = propagating radical<sup>435</sup>

- *Hydroxybenzoic and hydroxycinnamic acids: comparison between monophenols and catechols with BDE dependence*

Authors suggested a regeneration of  $\alpha$ -tocopherol by hydroxybenzoic and hydroxycinnamic acid derivatives. As demonstrated by Pazos *et al.* *via* ESR spectroscopy, gallic and protocatechuic acids can transfer hydrogens to the  $\alpha$ -tocopheroxyl radical and regenerate  $\alpha$ -tocopherol.<sup>433</sup> Moreover, Laranjinha *et al.* showed that caffeic acid, which a catechol moiety, delays the  $\alpha$ -tocopherol consumption and restore it during the oxidation of low density lipoprotein (LDL) particles with ferrylmyoglobin.<sup>430</sup> Nevertheless, these authors pointed out that mono-hydroxyl compounds (*i.e.* *p*-

hydroxybenzoic, vanillic and syringic acids) did not reduce the concentration of  $\alpha$ -tocopheroxyl radical.<sup>433</sup> Moreover, *p*-coumaric acid accelerates the rate of  $\alpha$ -tocopherol consumption.<sup>430</sup>

The inability of mono-hydroxyphenolic acids to regenerate  $\alpha$ -tocopherol is due to their much higher BDEs compared to that of  $\alpha$ -tocopherol. Indeed, Kadoma *et al.* highlight that a co-antioxidant may be very effective in the regeneration of  $\alpha$ -tocopherol when its BDE is similar to that of the primary antioxidant ( $\alpha$ -toco) (Eq. 4.4).<sup>467</sup>

$$\text{BDE}_{\alpha\text{-toco}} \approx \text{BDE}_{\text{CoAH}_2} \quad (4.4)$$

- *Complex mixtures of phenols with more than 2 co-antioxidants: effect of the concentration of antioxidants*

More complex mixtures of antioxidants have also found to be particularly efficient in homogeneous and biphasic systems compared to the additive effects of each compounds. Indeed, a combination of lycopene ( $15.63 \mu\text{mol.L}^{-1}$ ),  $\alpha$ -tocopherol ( $5.0 \mu\text{mol.L}^{-1}$ ), ascorbic acid ( $0.16 \mu\text{mol.L}^{-1}$ ) and  $\beta$ -carotene ( $10.83 \mu\text{mol.L}^{-1}$ ) showed highest synergistic effect through the DPPH $\cdot$  test.<sup>450</sup> The change in the concentrations used in mixture could modify the interactions between antioxidants leading to the loss of synergy. Therefore, the concentration of phenols used in mixture is an important parameter.

Dai *et al.* identified synergism by the combination of green tea polyphenols with  $\alpha$ -tocopherol and ascorbic acid.<sup>468</sup> The monitoring of the formation of linoleic acid hydroperoxides in SDS micelles revealed a synergism due to the regeneration of  $\alpha$ -tocopherol (TOH) by green tea polyphenols (GOH) which are in turn regenerated by vitamin C (VC) (Fig. 4.8).<sup>468</sup> The oxidation potentials of TOH, EGCG and VC reported by Dai and co-workers (0.26, 0.23 and 0.04 V respectively) support the mechanism of regeneration.<sup>468</sup>

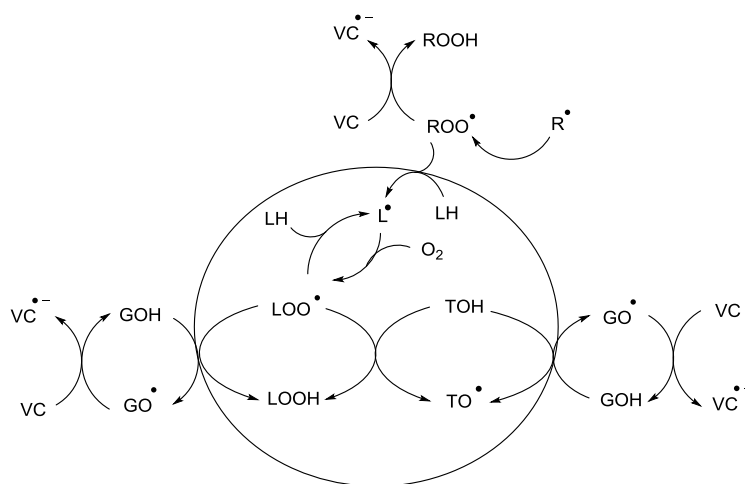


Figure 4.8: Synergistic antioxidant mechanism of green tea polyphenols (GOH), vitamin C (VC) and  $\alpha$ -tocopherol (TOH) in SDS (sodium dodecyl sulfate) micelles<sup>468</sup>

- *Interaction between phenols by  $\pi$ - $\pi$  stacking*

The regeneration of the most effective antioxidant by the less effective one is a mechanism of action suggested. The great regenerations of rosmarinic and caffeic acids by quercetin could be also due to the formation of stable intermolecular complexes between flavonol and cinnamic acids (Fig. 4.9).<sup>447</sup> These complexes are probably obtained by  $\pi$ - $\pi$  stacking between the aromatic ring of

phenolic acid and the B-ring of flavonol and the complex is stabilized by hydrogen bonding. Conversely, the antagonist effect obtained between rosmarinic acid and catechin could be explained by a low structural analogy leading to the absence of interaction. Other phenomena could also explain the results. Among them, there are the polarity of molecules, the reaction rates of antioxidants with lipids, the influence of the environment and the concentration of phenols. Indeed, the concentration of antioxidants are probably too low to consider  $\pi$ - $\pi$  stacking.

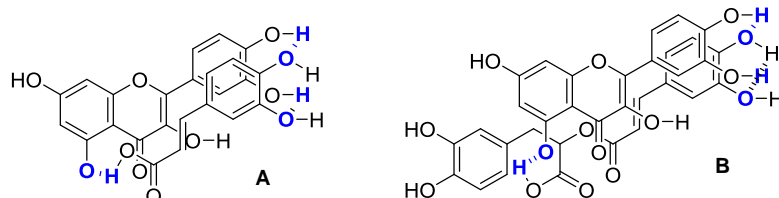


Figure 4.9: Possible interactions in quercetin/caffeic acid (A) and quercetin/rosmarinic acid (B) complexes:  $\pi$ - $\pi$  stacking between aromatic rings and intermolecular hydrogen bondings<sup>447</sup>

## 2.2 Kinetic approaches

Besides a large number of publications dealing with synergies, Amorati *et al.* have proposed a more precise mechanism of regeneration based on three examples of synergy observed during the inhibition of styrene oxidation: **1)**  $\alpha$ -tocopherol/ascorbic acid, **2)**  $\alpha$ -tocopherol/1,9-dimethylphenothiazine (MPTZ) and **3)**  $\alpha$ -tocopherol/*tert*-butyl-catechol (Fig. 4.10).<sup>333</sup> Their theory is based on kinetic rates of hydrogen transfer in each step of interaction between the antioxidants, the concentrations of compounds and the thermodynamic data (*i.e.* BDEs of the antioxidants).

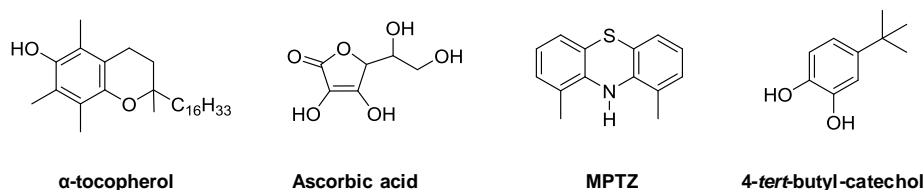
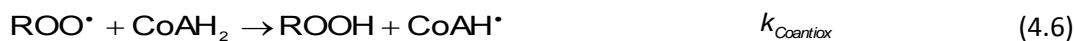


Figure 4.10: Chemical structures of antioxidants studied in mixture by Amorati *et al.*<sup>333</sup>

As largely discussed above, the synergistic effect between two phenols is mainly due to the regeneration of the most effective phenol by the other one. The primary antioxidant ( $AH_2$ ) is defined as the most efficient during the inhibition of oxidation which react faster with peroxy radicals ( $LOO^\bullet$ ). The other phenol is called co-antioxidant ( $CoAH_2$ ) which gives hydrogen atoms to the primary phenoxyl radical ( $AH^\bullet$ ) leading to its regeneration and formation of oxidized co-antioxidant ( $CoAH^\bullet$ ).

The initiation step required for the oxidation of styrene or other substrate (RH) leads to the formation of primary peroxy radicals ( $ROO^\bullet$ ). The inhibition of oxidation by two phenols which have first no interaction is described by equations 4.5 to 4.8. Equations 4.7 and 4.8 result on the combination of phenoxyl and peroxy radicals leading to the formation of non-radical products or to the transfer of a second hydrogen atom.



When synergism appears between two phenols, a supplementary step has to be considered. In most cases, the regeneration of the primary antioxidant by co-antioxidant is in equilibrium with the reverse reaction (Eq. 4.9). The combination of  $\alpha$ -tocopherol and ascorbic acid is a particular mixture because the hydrogen transfer from the co-antioxidant (ascorbic acid) to the primary antioxidant ( $\alpha$ -tocopherol) is irreversible ( $k_{Syn} \gg k_{-Syn}$ ) and the equilibrium is not applied anymore.



The induction period ( $\tau$ ) highlights the protective effect against oxidation with mixture of phenols. It is defined by the induction period given by the primary antioxidant ( $\tau_0$ ) added to that for the interaction antioxidant/co-antioxidant (Eq. 4.10).<sup>444</sup>

$$\tau = \tau_0 + \tau_0 \alpha \frac{[CoAH_2]}{[AH_2]} \quad (4.10)$$

$[CoAH_2]$  and  $[AH_2]$  are the respective concentrations of co-antioxidant and antioxidant,  $\alpha$  parameter, ranged from 0 (no synergy) to 1 (optimal synergy), defines the regeneration coefficient and  $\tau_0$  is the induction period given by the primary antioxidant. An optimal synergy shows that all the co-antioxidant regenerates the primary antioxidant which depends on the chemical structure of phenols. The ability of co-antioxidant to regenerate the primary antioxidant is explained with the kinetic rate constants of reaction between phenoxyl radicals ( $AH^{\bullet}$  and  $CoAH^{\bullet}$ ) and peroxy radicals ( $ROO^{\bullet}$ ), respectively  $k'_{Antiox}$  (Eq. 4.7) and  $k'_{Coantiox}$  (Eq. 4.8), and with the equilibrium constant  $K_r$  between the antioxidant, the co-antioxidant and their respective radicals ( $AH^{\bullet}$  and  $CoAH^{\bullet}$ ) (Eq. 4.11).

$$\alpha = K_r \times \frac{k'_{Coantiox}}{k'_{Antiox}} = \frac{[AH_2][CoAH^{\bullet}]}{[AH^{\bullet}][CoAH_2]} \times \frac{k'_{Coantiox}}{k'_{Antiox}} \quad (4.11)$$

When synergism is obtained, the reaction of regeneration (Eq. 4.9) competes with the reaction between the phenoxyl radicals from the antioxidant ( $AH^{\bullet}$ ) and the peroxy radicals ( $ROO^{\bullet}$ ) (Eq. 4.7). That means that the rate of hydrogen transfer from the co-antioxidant ( $CoAH_2$ ) to the phenoxyl radical ( $AH^{\bullet}$ ) ( $k_{Syn}[CoAH_2][AH^{\bullet}]$ , Eq. 4.9) is higher or at least equal to that of the reaction of  $AH^{\bullet}$  with peroxy radicals  $ROO^{\bullet}$  ( $k'_{Antiox}[AH^{\bullet}][ROO^{\bullet}]$ , Eq. 4.7) leading to **equation 4.12**.

$$k'_{Antiox} [AH^{\bullet}][ROO^{\bullet}] \leq k_{Syn} [AH^{\bullet}][CoAH_2] \quad (4.12)$$

Therefore, the increase of the kinetic rate constant between  $AH^{\bullet}$  and  $ROO^{\bullet}$  ( $k'_{Antiox}$ ) does not favor the regeneration (Eqs. 4.7 vs 4.9). Based on the equilibrium constant  $K_r$ , the consumption of the co-phenolic radical shifts the equilibrium in favor of the regeneration process. Generally speaking, high equilibrium constant ( $K_r$ ) favors the regeneration of the primary antioxidant by co-antioxidant and the regeneration coefficient ( $\alpha$ ) is close to 1.

In the case of irreversible regeneration ( $k_{Syn} \gg k_{-Syn}$ ) or when co-phenoxyl radicals ( $CoAH^{\bullet}$ ) are consumed faster by  $ROO^{\bullet}$  (Eq. 4.8) than by the regeneration process (Eq. 4.9) ( $k'_{Coantiox}[ROO^{\bullet}] \gg k_{-Syn}[AH_2]$ ), the required condition for the regeneration process (Eq. 4.9) is still available. It can also be illustrated by **equation 4.13** which implies that synergistic effects are favored with high concentration of co-antioxidant ( $CoAH_2$ ) and low concentration of peroxy radical ( $ROO^{\bullet}$ ). This last condition is indirectly related to a high concentration of antioxidant ( $AH_2$ ) because it is the main phenol to inhibit the peroxy radical formation.

$$[CoAH_2] \geq \frac{k'_{Antiox}}{k_{Syn}} [ROO^{\bullet}] \quad (4.13)$$

Amorati *et al.* reported in 2003 an interesting correlation between the equilibrium constant ( $K_r$ ) and the BDE of phenols (Eq. 4.14).<sup>444</sup>

$$-RT \ln K_r \approx \Delta BDE = BDE_{\text{CoAH}_2} - BDE_{\text{Antiox}} \quad (4.14)$$

$\Delta BDE$  is a positive value because antioxidant is more reactive than co-antioxidant characterized by a lowest BDE in apolar solvent ( $BDE_{\text{CoAH}_2} > BDE_{\text{Antiox}}$ ). Consequently, a low  $\Delta BDE$  leads to highest equilibrium constant ( $K_r$ ) and significant synergistic effects.

### 2.3 Conclusion

The synergy between two or more antioxidants is based on the regeneration of the most effective free radical scavenger antioxidant (primary) by the less effective one (co-antioxidant). The compound with the higher reduction potential acts as the primary antioxidant. The regeneration of the primary antioxidant depends on many factors: **1)** the hydrogen donating ability of co-antioxidants, **2)** the BDE of the co-antioxidant have to be lower or at least similar to that of the antioxidant, **3)** the concentration of antioxidants and **4)** a high structural analogy between the two antioxidants ( $\pi$ - $\pi$  stacking and intermolecular hydrogen bonding).

Kinetic approaches have allowed a better understanding of the regeneration of primary antioxidants by co-antioxidants. The reaction of regeneration could compete with the reaction between the phenoxyl radicals from the antioxidant ( $AH^*$ ) and the peroxy radicals ( $ROO^*$ ). Moreover, added to a combination of high concentration of co-antioxidant with low concentration of peroxy radicals, the  $\Delta BDE$ s between antioxidants must be low to improve the process of regeneration.

Nevertheless, the studies dealing with the regeneration of  $\alpha$ -tocopherol involved only few co-phenolic antioxidants. Indeed, reactive co-antioxidants highlighted in the literature are not in relation to each other. Consequently, we focused on synergies between  $\alpha$ -tocopherol and various co-antioxidants but also on other natural phenol combinations for food applications. Based on mechanistic and kinetic approaches of literature, we will propose detailed mechanisms of regeneration. Indeed, the reactions of dismutation or dimerization of phenoxyl radicals are rarely considered in the literature while such pathways explain the formation of dimers.

## 3. Synergy between $\alpha$ -tocopherol and co-antioxidants as well as other phenolic mixtures for the preservation of omega-3 oils

$\alpha$ -Tocopherol was the phenolic antioxidant selected as a reference. Indeed, even if it has all the required conditions for its use in food (*i.e.* good solubility in various matrixes, low toxicity and natural origin) this is not the most efficient phenolic antioxidant for the protection of omega-3 oils against oxidation and sometimes, it can also lead to a pro-oxidant effect.

Consequently, it is a relevant challenge to incorporate a mixture of antioxidants including  $\alpha$ -tocopherol to extend its antioxidant activity. The objective is to understand how it is possible to maintain and improve the antioxidant property of  $\alpha$ -tocopherol by the incorporation of co-antioxidants. In another way, other combinations of natural phenols have also been briefly studied. The co-antioxidants studied (Fig. 4.11) are those described previously in terms of their own thermodynamic, kinetic and oxidative parameters. A part of the investigation of synergism involving  $\alpha$ -tocopherol as primary antioxidant had been already discussed during the PhD of Clémentine

Marteau<sup>369</sup> for the preservation of perfumes and more precisely terpenes/terpenoids. The scope of co-antioxidants is here extended for a food application.

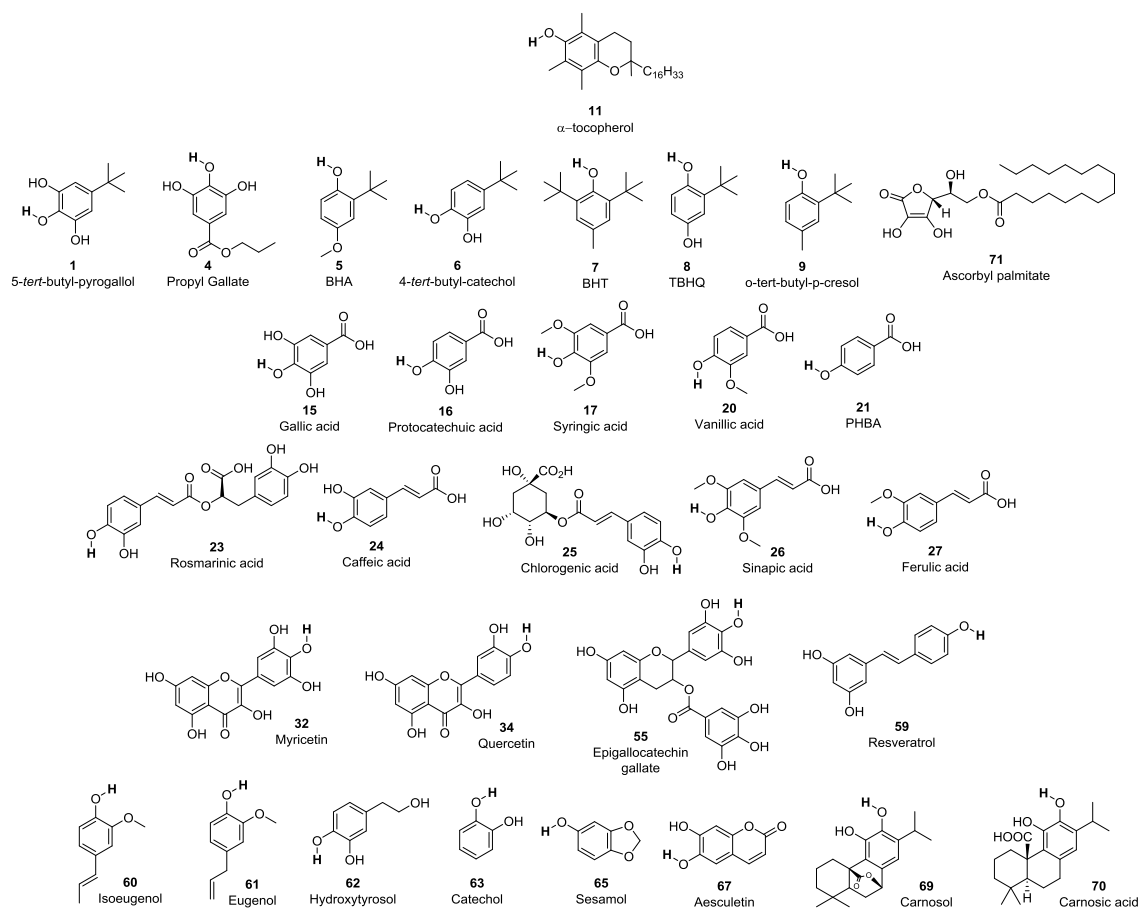


Figure 4.11: Chemical structures of co-antioxidants studied with  $\alpha$ -tocopherol 11, hydrogen atoms with the lowest BDE are indicated in bold

### 3.1 Methods and approaches to study synergies between antioxidants

Mixtures of  $\alpha$ -tocopherol and co-antioxidants with different chemical structures and thermodynamic parameters have been studied *via* the DPPH<sup>\*</sup> test. Moreover, the impact of matrices on the antioxidant efficiency of mixtures was inspected. The efficiency of co-antioxidant in the regeneration of  $\alpha$ -tocopherol during the inhibition of omega-3 oils oxidation is finally investigated. The main goal of this study was to identify the required conditions in terms of initial reaction rate, concentration, BDE... *etc.* in order to observe possible synergisms and suggest reaction mechanism consistent with that of Amorati *et al.*<sup>333, 444</sup>

As presented in the chapter 3 (see paragraph 4.2.1), the DPPH<sup>\*</sup> test is a simple and fast method useful to understand mechanisms responsible for synergism. The two parameters used are the initial reaction rate for mixture of phenols ( $V_{i\text{ Mix}}$ ) and the number of hydrogen transfer from the phenols to the stable radical called the stoichiometric number ( $\sigma_{\text{Mix}}$ ). These two crucial parameters were determined first in toluene (apolar aprotic solvent) to avoid solvent interactions. In this kind of solvent, the mechanism implied during the hydrogen transfer is called Hydrogen Atom Transfer (HAT). Furthermore, Hydrogen Bond Acceptor (HBA) solvents (*i.e.* ethyl acetate) and polar protic solvents (*i.e.* ethanol) were used to study the kinetic Solvent Effects (KSEs) on the reactivity of mixture of phenols.

### 3.1.1 Initial reaction rates of mixtures ( $V_{i\text{ Mix}}$ )

Initial reaction rates ( $V_{i\text{ Mix}}$ ) are determined by mixing an equimolar mixture of  $\alpha$ -tocopherol ( $\alpha$ -toco, 62.5  $\mu\text{M}$ ) and co-antioxidant ( $\text{CoAH}_2$ , 62.5  $\mu\text{M}$ ) with  $\text{DPPH}^*$  as described by the **equation 4.15**. **Figure 4.12** gives an example of the equimolar mixture of  $\alpha$ -tocopherol **11** and 4-*tert*-butyl-catechol **6** in toluene and the calculation of the initial reaction rate ( $V_{i\text{ Mix}}$ ). The slope of the tangent of the curve obtained during the first second of reaction highlights a difference of absorbance (A) vs time (s). Thanks to the Beer-Lambert law ( $A = \epsilon \cdot l \cdot C$ ), it is converted into the initial reaction rate  $V_i$  ( $\mu\text{mol} \cdot \text{L}^{-1} \cdot \text{s}^{-1}$ )

$$V_i = k_{\alpha\text{-toco}} [\alpha\text{-Toco}] [\text{DPPH}^*] + k_{\text{Co-Antiox}} [\text{Co-Antiox}] [\text{DPPH}^*] \quad (4.15)$$

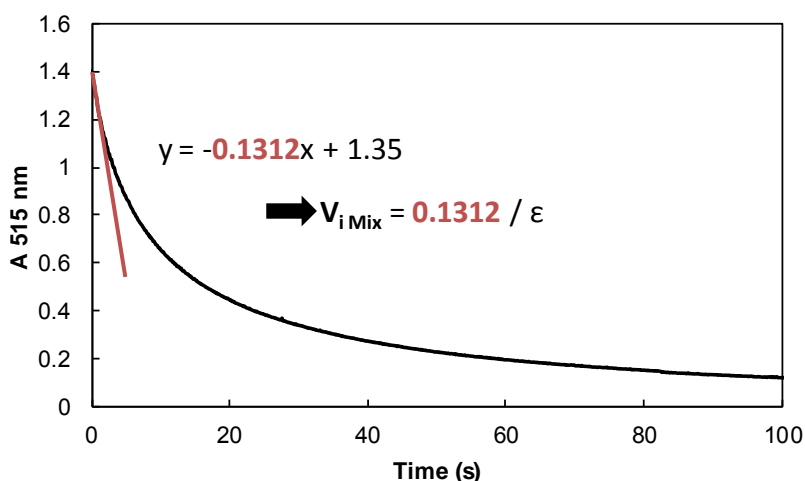


**Figure 4.12:** Evolution of the absorbance of  $\text{DPPH}^*$  radical at 515 nm ( $1.25 \times 10^{-4} \text{ mol} \cdot \text{L}^{-1}$ ) with an equimolar mixture of  $\alpha$ -tocopherol **11** and 4-*tert*-butyl-catechol **6**,  $[\text{antioxidant}] = [\text{co-antioxidant}] = 6.25 \times 10^{-5} \text{ mol} \cdot \text{L}^{-1}$  in toluene at 20 °C, calculation of the initial reaction rate of mixture ( $V_{i\text{ Mix}}$ )

In order to determine synergistic effect between equimolar mixtures of  $\alpha$ -tocopherol (62.5  $\mu\text{M}$ ) and co-antioxidants (62.5  $\mu\text{M}$ ), the experimental initial reaction rates of mixture ( $V_{i\text{ Mix}}$ ) were compared to the theoretical sum of their individual effect ( $V_{i\text{ Add}}$ ). It is showed first that the initial reaction rate of  $\alpha$ -tocopherol at 62.5  $\mu\text{M}$  ( $V_{i\alpha\text{-toco}}$ ) is divided by two compared to its reactivity at 125  $\mu\text{M}$  ( $2V_{i\alpha\text{-toco}}$ ) in the three solvents used (toluene, ethyl acetate and ethanol) (**Table 4.4**). This pointed out a reactivity characterized by a first order kinetic law.

Solvent	Initial reaction rate of $\alpha$ -tocopherol $V_{i\alpha\text{-toco}}$ ( $\mu\text{mol} \cdot \text{s}^{-1}$ )	
	$[\alpha\text{-toco}] = 125 \mu\text{M}$	$[\alpha\text{-toco}] = 62.5 \mu\text{M}$
Toluene	16.4	8.2
Ethyl acetate	1.92	0.96
Ethanol	5.6	2.8

**Table 4.4:** Influence of the concentration  $\alpha$ -tocopherol and the solvent on its initial reaction rates ( $V_{i\alpha\text{-toco}}$ )

Because all the co-antioxidants were previously studied at a concentration of 125  $\mu\text{M}$  ( $2V_{i\text{ Co-Antiox}}$ , 3<sup>rd</sup> chapter), we suggested first that they all react following a first order kinetic law as  $\alpha$ -tocopherol. Therefore, the initial reaction rates of co-antioxidants at 62.5  $\mu\text{M}$  ( $V_{i\text{ Co-Antiox}}$ ) are divided by two compared to their reactivity at 125  $\mu\text{M}$  ( $2V_{i\text{ Co-Antiox}}$ ). Consequently, the theoretical additivity of individual effect ( $V_{i\text{ Add}}$ ) between  $\alpha$ -tocopherol (62.5  $\mu\text{M}$ ) and co-antioxidants (62.5  $\mu\text{M}$ ) is described by the **equation 4.16**.

$$V_{i\text{ Add}} = V_{i\alpha\text{-Toco}} + V_{i\text{ Co-Antiox}} \quad (4.16)$$

Synergism would be obtained if experimental initial reaction rates of mixtures ( $V_{i\text{ Mix}}$ ) are higher than theoretical addivities ( $V_{i\text{ Add}}$ ) (Eq. 4.17). Conversely, antagonism would be characterized by lower  $V_{i\text{ Mix}}$  compared to  $V_{i\text{ Add}}$  (Eq. 4.18).

$$V_{i\text{ Mix}} > V_{i\text{ Add}} \quad (4.17)$$

$$V_{i\text{ Mix}} < V_{i\text{ Add}} \quad (4.18)$$

Finally, the main initial reaction rates of co-antioxidants at 65  $\mu\text{M}$  ( $V_{i\text{ Co-Antiox}}$ ) are lower than that of  $\alpha$ -tocopherol (65  $\mu\text{M}$ ,  $V_{i\text{ } \alpha\text{-toco}}$ ). Therefore, if the co-antioxidant added leads to higher initial reaction rates of mixture ( $V_{i\text{ Mix}}$ ) compared to the use of  $\alpha$ -tocopherol itself as co-antioxidant, super synergistic effects could be observed (Eq. 4.19).

$$V_i (\alpha - \text{Toco} + \text{Co} - \text{Antiox}) > V_i (\alpha - \text{Toco} + \alpha - \text{Toco}) \quad (4.19)$$

### 3.1.2 Stoichiometric numbers ( $\sigma_{\text{Mix}}$ )

The absorbance of the DPPH $^{\bullet}$  radical was followed at 515 nm with a limiting amount of an equimolar combination of two phenols ( $4.14 \times 10^{-5}$  M) in the three solvents of studies (*i.e.* toluene, ethyl acetate and ethanol). The determination of the variation of absorbance vs the initial concentration of mixture of phenols leads to  $\sigma_{\text{Mix}}$  values (Eq. 4.20, Tables S4.2, S4.3 and S4.4).

$$\sigma_{\text{Mix}} = \frac{[\text{DPPH}^{\bullet}]_0 - [\text{DPPH}^{\bullet}]_f}{[\text{ArOH}]_0} = \frac{A_0 - A_f}{(\epsilon - \epsilon')[\alpha - \text{toco} + \text{CoAH}_2]_0} \quad (4.20)$$

If the stoichiometric number of the mixture ( $\sigma_{\text{Mix}}$ ) is higher than the average of the individual effect of both phenol ( $(\sigma_{\alpha\text{-toco}} + \sigma_{\text{CoAH}_2})/2$ ), there is an increase of the number of radicals trapped by molecules of phenols suggested as synergistic effect (Eq. 4.21). Nevertheless, if  $\sigma_{\text{Mix}}$  is lower or at least equal to the average of the individual effect of both phenols, there is just additivity of their respective effects. Final absorbances are collected when constant values are reached during at least thirty minutes. Figure 4.13 shows the equimolar mixture of  $\alpha$ -tocopherol **11** and BHT **7** in toluene which results are discussed later.

$$\sigma_{\text{Mix}} > \frac{\sigma_{\alpha\text{-toco}} + \sigma_{\text{CoAH}_2}}{2} \quad (4.21)$$

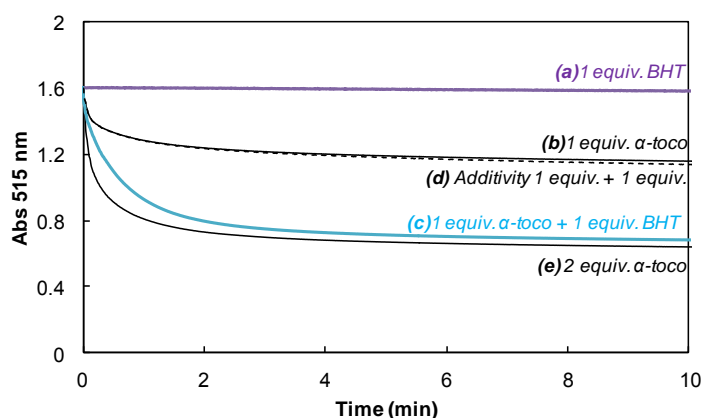


Figure 4.13: Evolution of the absorbance of DPPH $^{\bullet}$  radical at 515 nm ( $1.5 \times 10^{-4}$  M) with (a) 1 equiv. of BHT **7** ( $2.07 \times 10^{-5}$  M), (b) 1 equiv. of  $\alpha$ -tocopherol **11** ( $2.07 \times 10^{-5}$  M), (c) equimolar mixture of both antioxidants [ $\alpha$ -tocopherol] + [BHT] =  $4.14 \times 10^{-5}$  M (d) additivity profile (dotted line) and (e) 2 equiv. of  $\alpha$ -tocopherol **11** ( $4.14 \times 10^{-5}$  M) in toluene at 20  $^{\circ}\text{C}$ <sup>369</sup>

### 3.2 Synergistic behaviors in apolar aprotic solvents

Table 4.5 presents the initial reaction rate obtained for the combinations of  $\alpha$ -tocopherol (62.5  $\mu\text{M}$ ) and co-antioxidant (62.5  $\mu\text{M}$ ) ( $V_{i \text{ Mix}}$ ) with the respective initial reaction rate for each co-antioxidant (62.5  $\mu\text{M}$ ,  $V_{i \text{ Co-Antiox}}$ ) and the theoretical additivity of individual effects ( $V_{i \text{ Add}}$ ). Co-antioxidants are ranked from the lowest to the highest BDEs.

Co-Antioxidants	N°	BDE	Initial reaction rate $V_i$ ( $\mu\text{mol.L}^{-1}.\text{s}^{-1}$ )			Synergy?
			Experimental $V_{i \text{ Mix}}$	Hypotheses $V_{i \text{ Co-Antiox}}$	$V_{i \text{ Add}}$	
5-Tert-butyl-pyrogallol	1	66.6	36.7	15.9	29.1	+++
$\alpha$ -Tocopherol	11	69.1	16.4	8.2	16.4	/
Propyl gallate	4	69.6	18.2	3.0	11.2	+++
Carnosol	69	70.7	13.6	2.7	10.9	++
Carnosic acid	70	70.8	17.1	3.1	11.3	+++
Hydroxytyrosol	62	72.1	14.4	2.6	10.8	++
BHA	5	72.3	11.2	0.7	8.9	++
4-Tert-butylcatechol	6	72.3	12.8	1.8	9.9	++
BHT	7	72.4	11.4	0.0005	8.2	++
Ascorbyl palmitate	71	73.3	27.5	3.3	11.5	+++
Catechol	63	73.4	11.4	1.6	9.8	++
TBHQ	8	74.3	19.4	2.2	10.4	+++
Sesamol	65	75.1	11.2	0.6	8.8	+
Sinapic acid	26	75.4	10.9	0.5	8.7	+
Isoeugenol	60	76.6	8.5	0.2	8.4	-
<i>o</i> -Tert-butyl- <i>p</i> -cresol	9	77.4	8.1	0.001	8.2	-
Syringic acid	17	78.1	8.3	0.02	8.2	-
Ferulic acid	27	79.7	8.1	0.02	8.2	-
Eugenol	61	80.2	8.0	0.02	8.2	-
Vanillic acid	20	83.1	8.0	0.0002	8.2	-

Table 4.5: Initial reaction rate  $V_i$  for equimolar mixtures of  $\alpha$ -tocopherol (62.5  $\mu\text{M}$ ) and co-antioxidant (62.5  $\mu\text{M}$ ) ( $V_{i \text{ Mix}}$ ) in toluene compared to the initial reaction rate of co-antioxidant (62.5  $\mu\text{M}$ ,  $V_{i \text{ Co-Antiox}}$ ) and the theoretical additivity of effects ( $V_{i \text{ Add}}$ ), + and - point out synergism and additivity respectively, BDEs ( $\text{kcal.mol}^{-1}$ ) are calculated with our DFT method

Figure 4.14 shows the correlation between experimental initial reaction rates of phenol mixtures ( $V_{i \text{ Mix}}$ , [ $\alpha$ -tocopherol] = [co-antioxidant] = 62.5  $\mu\text{M}$ ) and that of co-antioxidants ( $V_{i \text{ Co-Antiox}}$ , [Co-Antiox] = 62.5  $\mu\text{M}$ ).

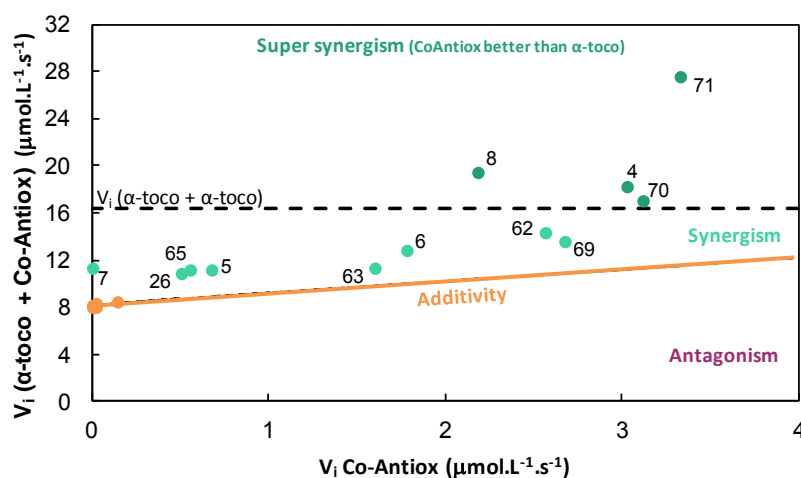
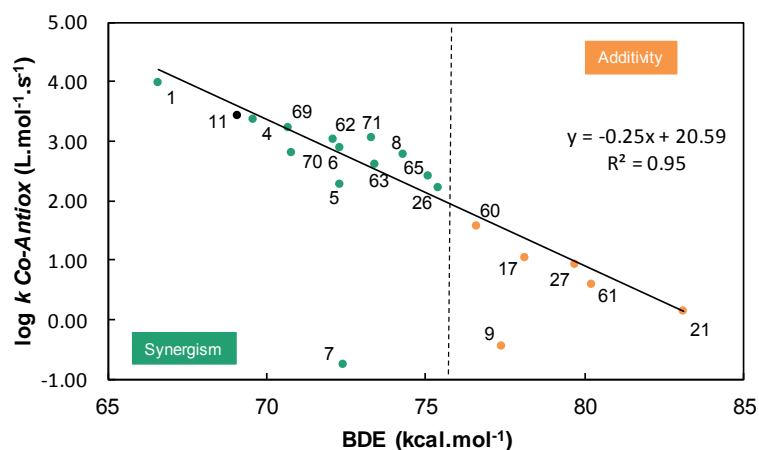


Figure 4.14: Experimental initial reaction rates of phenol mixtures ( $V_{i \text{ Mix}}$ ,  $\alpha$ -tocopherol + co-antioxidant) vs initial reaction rates of co-antioxidants ( $V_{i \text{ Co-Antiox}}$ ) in toluene

Pyrogallol (propyl gallate **4**), hydroquinone (TBHQ **8**) derivatives, one catechol compound (carnosic acid **70**) and ascorbyl palmitate **71** provide super synergistic effects. All the other catechol derivatives (*i.e.* 4-*tert*-butylcatechol **6**, catechol **63**, hydroxytyrosol **62** and carnosol **69**) and some monophenols (*i.e.* BHA **5**, BHT **7**, sinapic acid **26** and sesamol **65**) show synergism with  $\alpha$ -tocopherol **11**. Finally, other monophenols (*i.e.* *o*-*tert*-butyl-*p*-cresol **9**, syringic acid **17**, vanillic acid **20**, ferulic acid **27**, isoeugenol **60** and eugenol **61**) are not capable to regenerate  $\alpha$ -tocopherol **11** and  $V_{i\text{ Mix}}$  are close to that of additivity. Finally, antagonist effects were not observed with the DPPH<sup>•</sup> test.

In apolar aprotic solvents (*i.e.* toluene), the radical HAT mechanism leads the reaction between phenols and DPPH<sup>•</sup> radical and BDEs determine their reactivity.<sup>262</sup> **Figure 4.15** illustrates kinetic rate constants ( $\log k_{\text{Co-Antiox}}$ ) vs thermodynamic parameters (BDE) of co-antioxidants. Moreover, their capacity to act as co-antioxidants to regenerate  $\alpha$ -tocopherol **11** is schematized in green (•, synergism and super synergism). Conversely, co-antioxidants which are not able to regenerate  $\alpha$ -tocopherol **11** are in orange (•, additivity).



**Figure 4.15:** Kinetic rate constants of hydrogen transfer ( $\log k_{\text{Co-Antiox}}$ ) obtained in toluene vs  $\text{BDE}_{\text{CoAH}_2}$  calculated in vacuum by the DFT B3LYP/6-311++G(2d,2p)//B3LYP/6-311G(d,p) method, green (•) and orange (•) dots illustrate respectively co-antioxidants capable to regenerate  $\alpha$ -tocopherol **11** (synergism and super synergism) or not (additivity) respectively

BDEs determine the reactivity of phenols and their capacity to regenerate  $\alpha$ -tocopherol **11**. Indeed, co-antioxidants with BDEs lower than  $76 \text{ kcal.mol}^{-1}$  regenerate  $\alpha$ -tocopherol **11** whatever their kinetic rate constants. Conversely, co-antioxidants with BDEs higher than  $76 \text{ kcal.mol}^{-1}$  are not able to regenerate  $\alpha$ -tocopherol **11**. More precisely, a  $\Delta\text{BDE}$  variation of  $7.0 \text{ kcal.mol}^{-1}$  compared to that of  $\alpha$ -tocopherol is a key thermodynamic factor for co-antioxidants capable to regenerate  $\alpha$ -tocopherol (Eq. 4.22).

$$\Delta\text{BDE} \leq 7 \text{ kcal.mol}^{-1} \quad (4.22)$$

### 3.2.1 Reaction of $\alpha$ -tocopherol

First of all, it is crucial to study the reaction of  $\alpha$ -tocopherol **11** with DPPH<sup>•</sup> because it is our key compound for the understanding of synergism. The stationary state of the final absorbance leads to the determination of the number of radical trapped by molecule of phenol ( $\sigma_{\text{exp}} = 2$ ). Kinetic rate constant of  $\alpha$ -tocopherol **11** with galvinoxyl radical ( $\text{BDE} = 78.9 \text{ kcal.mol}^{-1}$ ) was described by Lucarini and Pedulli in 1994.<sup>469</sup> There is equilibrium between these two compounds during the reaction.

Moreover, the BDE of galvinoxyl radical is closed to that of the DPPH<sup>•</sup> radical as determined by Foti *et al.* (BDE = 78.9 kcal.mol<sup>-1</sup>).<sup>470</sup> An irreversible reaction between  $\alpha$ -tocopherol **11** and DPPH<sup>•</sup> is considered to simplify the discussion. Based on the works of these authors, the reaction scheme for the reaction of  $\alpha$ -tocopherol **11** with a large excess of DPPH<sup>•</sup> is suggested (Fig. 4.16).

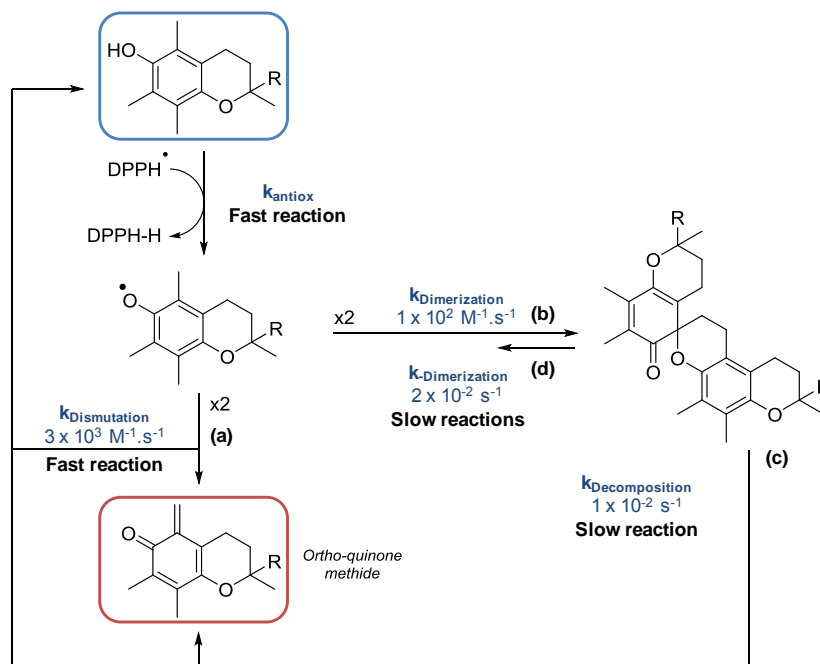


Figure 4.16: Reaction between  $\alpha$ -tocopherol **11** and a large excess of DPPH<sup>•</sup><sup>469</sup>

The tocopheroxyl radical is quickly formed by the reaction of  $\alpha$ -tocopherol **11** and DPPH<sup>•</sup> ( $k = 2686 \text{ M}^{-1} \cdot \text{s}^{-1}$ ). This radical then preferentially follows a dismutation step (a,  $k_{\text{Dism}} = 3 \times 10^3 \text{ M}^{-1} \cdot \text{s}^{-1}$ )<sup>469</sup> forming *ortho*-quinone methide compound and regenerating  $\alpha$ -tocopherol. Bowry and Ingold described in 1995 that the kinetic step controlling the dismutation of the tocopheroxyl radical is the hydrogen transfer from *ortho*-methyl group to phenoxyl group (Fig. 4.17).<sup>391</sup>

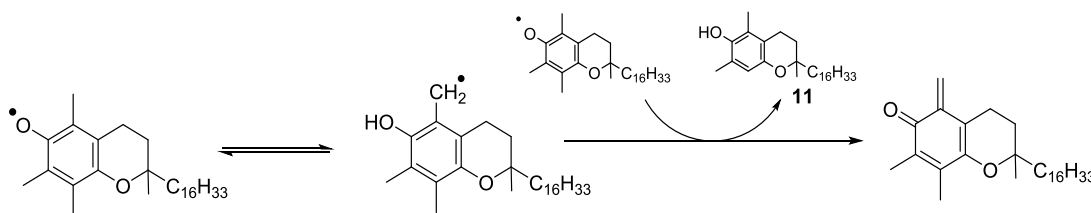


Figure 4.17: Dismutation reaction of the tocopheroxyl radical<sup>391</sup>

The dimerization of the tocopheroxyl radical (b,  $k_{\text{Dimer}} = 1 \times 10^2 \text{ M}^{-1} \cdot \text{s}^{-1}$ ) is slower than the reaction of dismutation (a). Moreover, the decomposition of the dimer is the less favorable reaction (c,  $k_{\text{Decomp}} = 1 \times 10^{-2} \text{ s}^{-1}$ ). It is assumed that the molecular decomposition of the dimer is not favorable and it is preferentially decomposed into 2 tocopheroxyl radicals (d,  $k_{\text{Dimer}} = 2 \times 10^{-2} \text{ s}^{-1}$ ).

The experiments carried out with an excess of DPPH<sup>•</sup> leads to a two step reaction mechanism (Fig. 4.18). The first step is due to a rapid transfer of the phenolic hydrogen from  $\alpha$ -tocopherol (AH<sub>2</sub>). The second step corresponds to the dismutation of two molecules of tocopheroxyl radical (AH<sup>•</sup>) giving the *ortho*-quinone methide (A) and regenerating  $\alpha$ -tocopherol (AH<sub>2</sub>) which can then react with DPPH<sup>•</sup>.

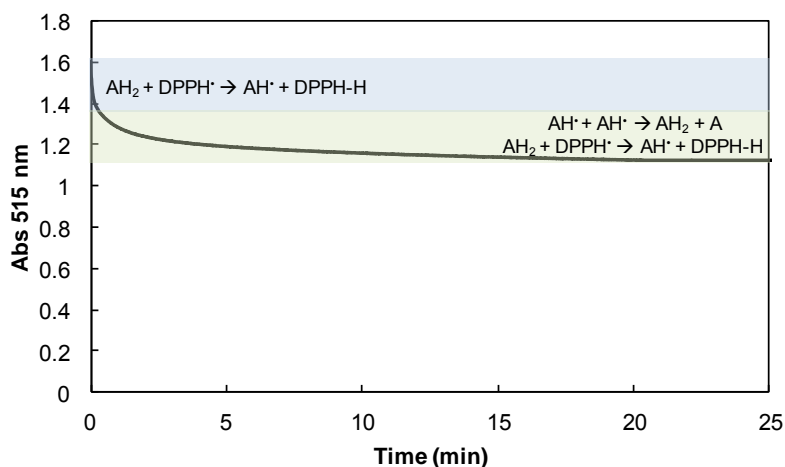


Figure 4.18: Evolution of the DPPH<sup>\*</sup> absorbance at 515 nm ( $1.5 \times 10^{-4}$  M) in toluene with  $\alpha$ -tocopherol **11** ( $2.07 \times 10^{-5}$  M)

### 3.2.2 Synergism with reactive monophenols and catechol derivatives

All the catechol derivatives (*i.e.* 4-*tert*-butylcatechol **6**, hydroxytyrosol **62**, catechol **63** and carnosol **69**) and reactive monophenols (*i.e.* BHA **5**, BHT **7**, sinapic acid **26** and sesamol **65**) regenerate  $\alpha$ -tocopherol **11**. All these compounds have a BDE close to that of  $\alpha$ -tocopherol with a  $\Delta$ BDE lower than  $7.0 \text{ kcal}\cdot\text{mol}^{-1}$ . Catechol compounds and monophenols do not react by the same pathway and their respective reaction mechanism is detailed below.

#### 3.2.2.1 Monophenols as co-antioxidants

- *Butylated Hydroxytoluene (BHT)*

Lucarini and Pedulli have reported the reactivity of BHT with galvinoxyl radical.<sup>469</sup> Based on their kinetic approaches, the reactivity of BHT **7** ( $2.07 \times 10^{-5}$  M) with DPPH<sup>\*</sup> ( $1.5 \times 10^{-4}$  M) in the presence or absence of  $\alpha$ -tocopherol **11** ( $2.07 \times 10^{-5}$  M) has been investigated (Fig. 4.19). BHT **7** reacts very slowly with DPPH<sup>\*</sup> and the decrease of the absorbance is very low (< 1 %) because of the steric hindrance of the phenolic hydrogen. However,  $\alpha$ -tocopherol **11** introduced at the same concentration leads to a quick decrease of the absorbance (from 1.6 to 1.12) at 515 nm.

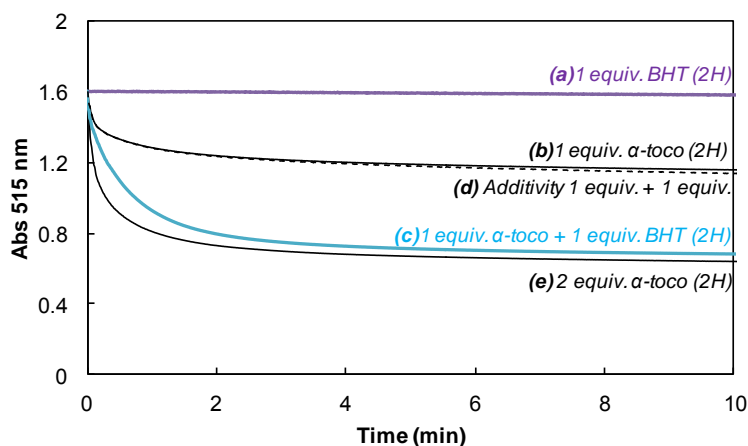


Figure 4.19: Absorbance at 515 nm of DPPH<sup>\*</sup> ( $1.5 \times 10^{-4}$  M) with (a) 1 equiv. BHT **7** ( $2.07 \times 10^{-5}$  M), (b) 1 equiv.  $\alpha$ -tocopherol **11** ( $2.07 \times 10^{-5}$  M), (c) experimental 1 equiv.  $\alpha$ -tocopherol **11** with 1 equiv. BHT **7** ( $2.07 \times 10^{-5} + 2.07 \times 10^{-5} = 4.14 \times 10^{-5}$  M), (d, dotted line) theoretical additivity of 1 equiv.  $\alpha$ -tocopherol **11** with 1 equiv. BHT **7** ( $2.07 \times 10^{-5} + 2.07 \times 10^{-5} = 4.14 \times 10^{-5}$  M) and (e) 2 equiv.  $\alpha$ -tocopherol **11** ( $4.14 \times 10^{-5}$  M)<sup>463</sup>

The phenoxyl radical formed by abstraction of the phenolic hydrogen from BHT **7** can react according to 5 different reaction pathways related to a number of DPPH<sup>•</sup> radicals inhibited ( $\sigma_{\text{exp}}$  equal to 1, 2 or 3 (Fig. 4.20).<sup>360, 469</sup>

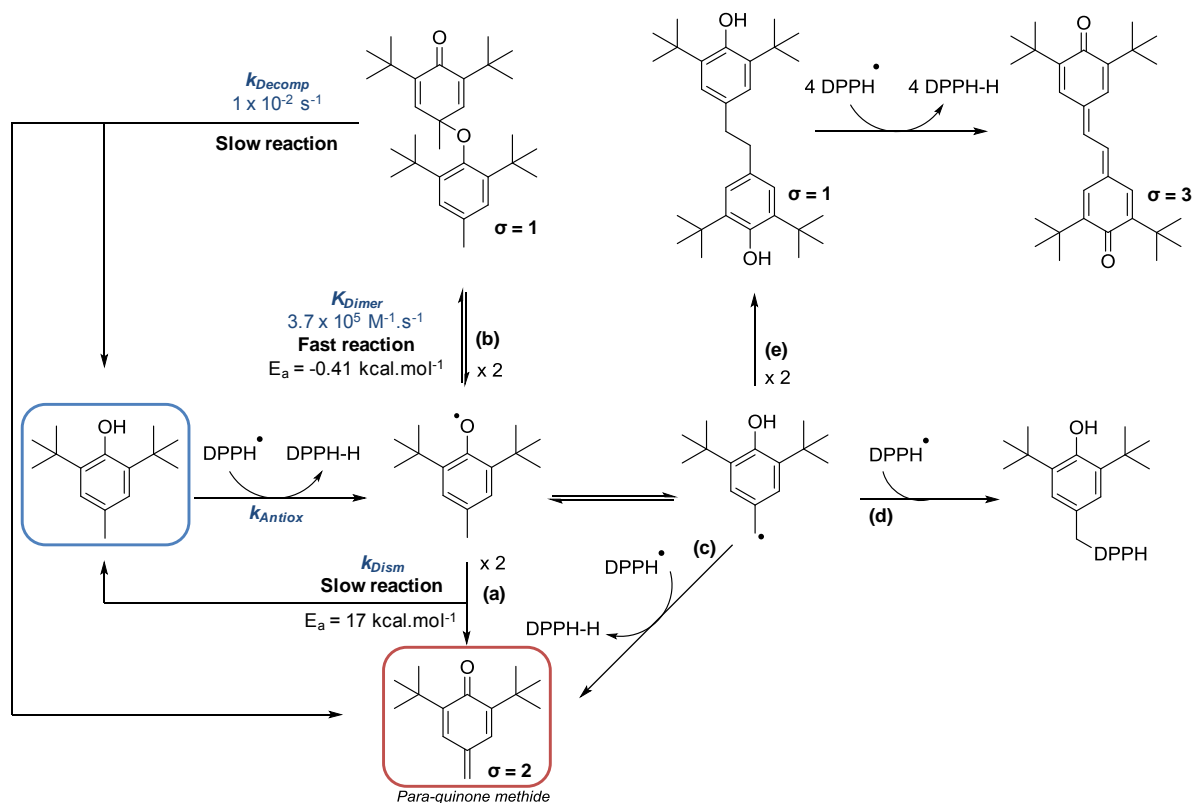
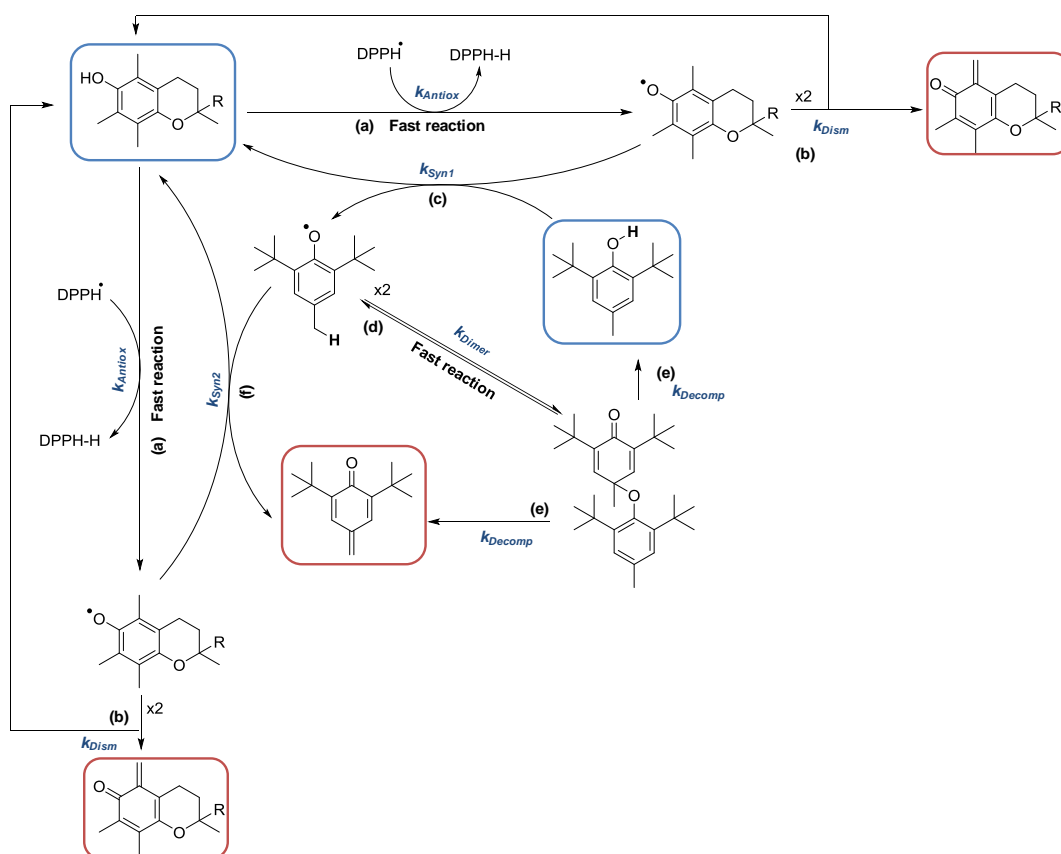


Figure 4.20: Possible reaction pathways of BHT **7** with a large excess of DPPH<sup>•</sup><sup>360, 469</sup>

The experimental stoichiometric number of BHT ( $\sigma_{\text{exp}} = 2.0$ ) related to the inhibition of 2 molecules of DPPH<sup>•</sup> per molecule of phenol excludes pathway **e**. The identification of the oxidized compounds by ion-negative ESI-MS analysis reveals that *para*-quinone methide (**a**,  $\sigma_{\text{exp}} = 2$ ) and C-O dimer (**b**,  $\sigma_{\text{exp}} = 1$ ) are the major components obtained. This dimer could then be decomposed into BHT and *para*-quinone methide. Moreover, Lucarini *et al.* suggested that a recombination of the galvinoxyl radical with the phenoxyl radical of BHT is not favorable. This reinforces our hypothesis on the unfavorable reaction between DPPH<sup>•</sup> and the phenoxyl radical of BHT (**d**) because of the steric hindrance.<sup>469</sup> The last possible pathway is a second transfer of hydrogen from the phenoxyl radical of BHT to DPPH<sup>•</sup> leading to *para*-quinone methide (**c**). The BDE calculation related to the abstraction of the second hydrogen located on the methyl group is very low ( $\text{BDE}_2 = 57.4 \text{ kcal.mol}^{-1}$ ). The pathway **c** is so a thermodynamic possible reaction especially because it is a non-hindered hydrogen. Moreover, except for Parnell and Russell<sup>471</sup>, Lucarini *et al.*<sup>469</sup> and Weiner *et al.*<sup>472</sup> have suggested that the dimerization step (**b**) is more favorable than the dismutation (**a**) as regards to their respective activation energies ( $-0.41$  and  $17 \text{ kcal.mol}^{-1}$ ). Furthermore, they have estimated the equilibrium constant related to the formation of the BHT dimers at  $3.7 \times 10^5 \text{ M}^{-1}$  whereas it is about  $4.8 \times 10^{-3} \text{ M}^{-1}$  for  $\alpha$ -tocopherol, which confirms the fast formation of the dimer.<sup>469</sup>

The equimolar mixture of  $\alpha$ -tocopherol **11** and BHT **7** leads to a fast decrease of the absorbance (from 1.6 to 0.61) at 515 nm in 10 minutes which is equivalent to the reactivity of 2 equiv.  $\alpha$ -tocopherol (Fig. 4.19). Consequently, BHT **7** acts as co-antioxidant and one molecule of BHT is capable to regenerate one molecule of  $\alpha$ -tocopherol **11**. The antioxidant efficiency of this mixture is

much more important than the simple additivity of separate effect. **Figure 4.21** suggests the reaction mechanism implicated for the regeneration of  $\alpha$ -tocopherol **11** by BHT **7**.



**Figure 4.21:** Possible reaction pathways of equimolar mixtures of  $\alpha$ -tocopherol **11** and BHT **7** with a large excess of  $\text{DPPH}^\bullet$

First of all,  $\alpha$ -tocopherol **11** quickly transfers its phenolic hydrogen to the  $\text{DPPH}^\bullet$  (**a**,  $k_{\text{Antiox}}$ ) giving the tocopheroxyl radical. A synergistic effect is obtained if the reaction of regeneration (**c**,  $k_{\text{Syn1}}$ ) competes with the dismutation pathway (**b**,  $k_{\text{Dism}}$ ) of tocopheroxyl radical into  $\alpha$ -tocopherol **11** and *ortho*-quinone methide (**Eq. 4.23**).

$$k_{\text{Dism}} [\alpha\text{-toco}^\bullet] \leq k_{\text{Syn1}} [\text{BHT}] \quad (4.23)$$

$\alpha$ -Tocopherol **11** regenerated reacts again with  $\text{DPPH}^\bullet$  (**a**) whereas the phenoxyl radical of BHT **7** can follow two different pathways. As demonstrated by Lucarini *et al.*<sup>469</sup> and Weiner *et al.*<sup>472</sup>, the BHT phenoxyl radical prefers to dimerize (**d**,  $k_{\text{Dimer}}$ ). This dimer is then decomposed into BHT **7** (**e**,  $k_{\text{Decomp}}$ ) which undergoes a regeneration cycle and formation of *para*-quinone methide. Another way of reaction could be suggested with the abstraction of the second hydrogen of the methyl group (**f**,  $k_{\text{Syn2}}$ ). This thermodynamic favorable reaction ( $\text{BDE}_2 = 57.4 \text{ kcal.mol}^{-1}$ ) is not mentioned by authors because of the fast dimerization reaction. The transfer of this second hydrogen could compete with the reaction of dimerization and with the reaction of dismutation of the tocopheroxyl radical ( $\alpha$ -toco $^\bullet$ ) leading to a second cycle for the regeneration of  $\alpha$ -tocopherol (**Eq. 4.24**). Consequently, there is a high regeneration of  $\alpha$ -tocopherol **11** and the initial reaction rate of mixture ( $V_{i \text{ Mix}} = 11.4 \mu\text{mol.L}^{-1}.\text{s}^{-1}$ ) is much higher than the additivity rules ( $V_{i \text{ Add}} = 8.20 \mu\text{mol.L}^{-1}.\text{s}^{-1}$ ).

$$k_{\text{Dism}} [\alpha\text{-toco}^\bullet] \leq k_{\text{Syn2}} [\text{BHT}^\bullet] \quad (4.24)$$

This interesting synergy between  $\alpha$ -tocopherol **11** and BHT **7** was not observed by Amorati *et al.* during the oxidation of styrene whereas in our case, the regeneration process is unambiguous.<sup>444</sup> This difference highlights that synergism depends on radicals and reactions involved. The monitoring

of the oxygen consumption during the preservation of FAMES of linseed oil against oxidation will confirm or contradict our conclusions found with the DPPH<sup>•</sup> test (see paragraph 3.3.2).

These two kinetic rate constants of regeneration ( $k_{Syn1}$  and  $k_{Syn2}$ ) are gathered into a global kinetic rate constant ( $k_{Syn}$ ) and the required conditions to observe synergies with general co-antioxidants ( $CoAH_2$ ) are pointed out by the **equation 4.25**. Since in all our experiments initial concentrations of  $\alpha$ -tocopherol, co-antioxidants and DPPH<sup>•</sup> are identical and kinetic rate constant of tocopheroxyl radical dismutation ( $k_{Dism}$ ) don't change, co-antioxidants able to regenerate  $\alpha$ -tocopherol **11** must respect the condition given by the **equation 4.26**. In this way, the kinetic rate constant of regeneration ( $k_{Syn}$ ) is competitive with the reaction of dismutation ( $k_{Dism}$ ).

$$[CoAH_2] \geq \frac{k_{Dism}}{k_{Syn}} [AH^{\bullet}] \quad (4.25)$$

$$k_{Syn} \geq \frac{[AH^{\bullet}]}{[CoAH_2]} k_{Dism} \quad (4.26)$$

- *BHA, sinapic acid and sesamol*

BHA **5**, sinapic acid **26** and sesamol **65** are also monophenols capable to regenerate  $\alpha$ -tocopherol **11** (**Figs. 4.14 and 4.15**). Amorati *et al.* have been interested on the reactivity of 1,9-dimethylphenothiazine (MPTZ) with  $\alpha$ -tocopherol **11** during the autoxidation of styrene (**Fig. 4.22**).<sup>333</sup>

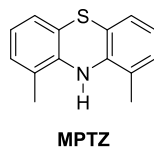
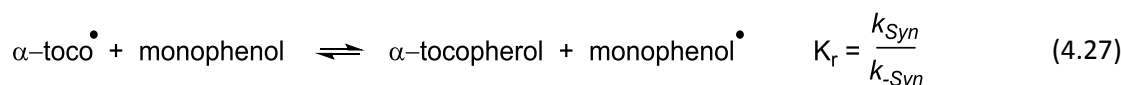


**Figure 4.22: Chemical structure of 1,9-dimethylphenothiazine (MPTZ)**<sup>333</sup>

They pointed out that the regeneration step is always in equilibrium with the reverse reaction (**Eq. 4.27**). Therefore, the kinetic rate constant of synergy ( $k_{Syn}$ ) has to be higher than that of the reverse reaction ( $k_{-Syn}$ ).



Consequently, it is suggested that the hydrogen transfer to the tocopheroxyl radical ( $\alpha\text{-toco}^{\bullet}$ ) is faster than the reverse reaction. The required condition for synergism developed for BHT **7** is also respected (**Eq. 4.28**).

$$k_{Syn} \geq \frac{[\alpha\text{-toco}^{\bullet}]}{[BHA]} k_{Dism} \quad (4.28)$$

Moreover, the regeneration with the phenolic hydrogen of BHA **5** (**c**,  $k_{Syn1}$ ) could be faster than with DPPH<sup>•</sup> (**d**,  $k_{CoAH2}$ ). The formation of an active dimer (**e**,  $k_{Dim}$ ) also competes with the dismutation of the tocopheroxyl radical. The mechanism of regeneration is suggested by **figure 4.23**.

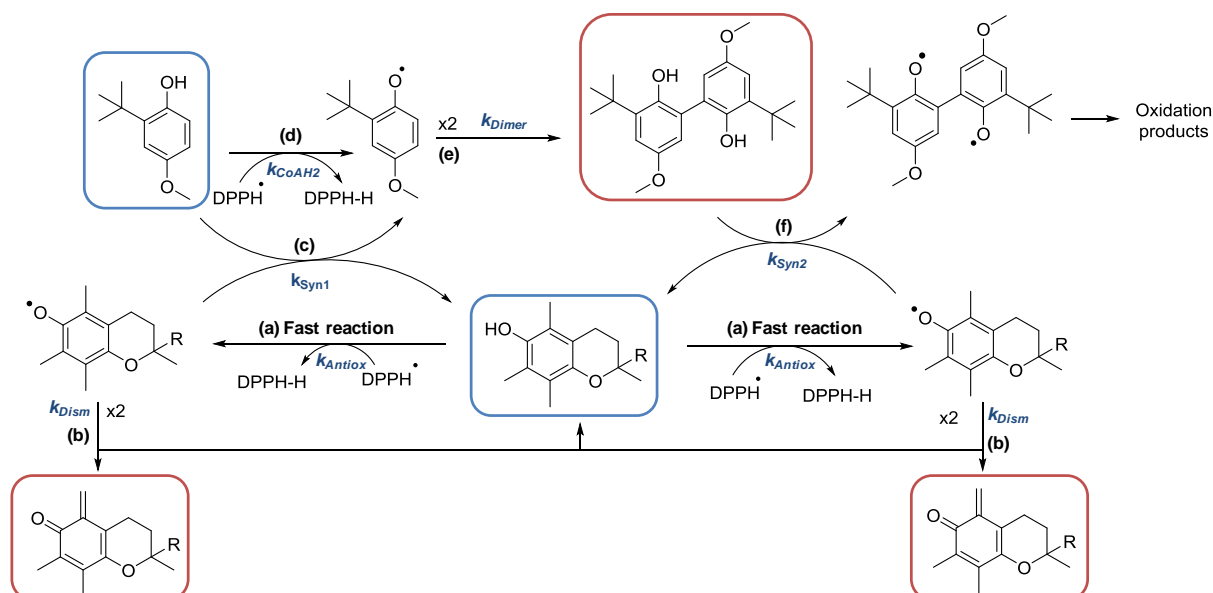
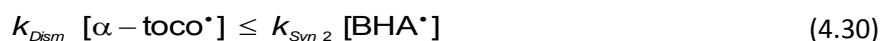
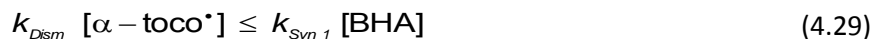


Figure 4.23: Reaction of equimolar mixture of  $\alpha$ -tocopherol **11** and BHA **5** with a large excess of DPPH $^{\bullet}$  radicals

The kinetics of regeneration (**c**,  $k_{Syn1}$ ) is higher than the dismutation of  $\alpha$ -toco $^{\bullet}$  and the regeneration process occurs with the phenolic hydrogen of BHA **5** (Eq. 4.29). BHA could trap 2 molecules of DPPH $^{\bullet}$  radical ( $\sigma_{exp} = 2.0$ ) although it is a monophenol. This is due to the formation of active dimer (**e**,  $k_{Dimer}$ ) which transfers its two phenolic hydrogens (**f**,  $k_{Syn2}$ ) and becomes also competitive with the dismutation of the tocopheroxy radical (**b**,  $k_{Dism}$ ) (Eq. 4.30). Consequently, there is a high regeneration of  $\alpha$ -tocopherol **11** and the initial reaction rate of mixture ( $V_{i\ Mix} = 11.2\ \mu\text{mol}\cdot\text{L}^{-1}\cdot\text{s}^{-1}$ ) is much higher than the additivity rules ( $V_{i\ Add} = 8.88\ \mu\text{mol}\cdot\text{L}^{-1}\cdot\text{s}^{-1}$ ).



### 3.2.2.2 Catechol derivatives as co-antioxidants

All the catechol derivatives (*i.e.* 4-*tert*-butylcatechol **6**, hydroxytyrosol **62**, catechol **63** and carnosol **69**) are able to regenerate  $\alpha$ -tocopherol **11**. The reactions of catechol derivatives (**6**, **62**, **63** and **69**,  $2.07 \times 10^{-5}\ \text{M}$ ) with DPPH $^{\bullet}$  ( $1.5 \times 10^{-4}\ \text{M}$ ) in the presence or absence of  $\alpha$ -tocopherol **11** ( $2.07 \times 10^{-5}\ \text{M}$ ) were investigated. Figure 4.24 points out the reaction of catechol **63** with and without  $\alpha$ -tocopherol **11**.

Catechol **63** reacts slower than  $\alpha$ -tocopherol **11** with the DPPH $^{\bullet}$  radical but both antioxidants are able to trap 2 molecules of DPPH $^{\bullet}$  per molecule of phenol. The mixture of phenols leads also to a stoichiometric number of 2.0. Therefore, the number of hydrogen transfer for phenolic mixtures is always an average of the individual effects. The synergism highlighted comes from the faster decrease of the absorbance at 515 nm in 2 minutes resulting in a fast regeneration of  $\alpha$ -tocopherol **11**.

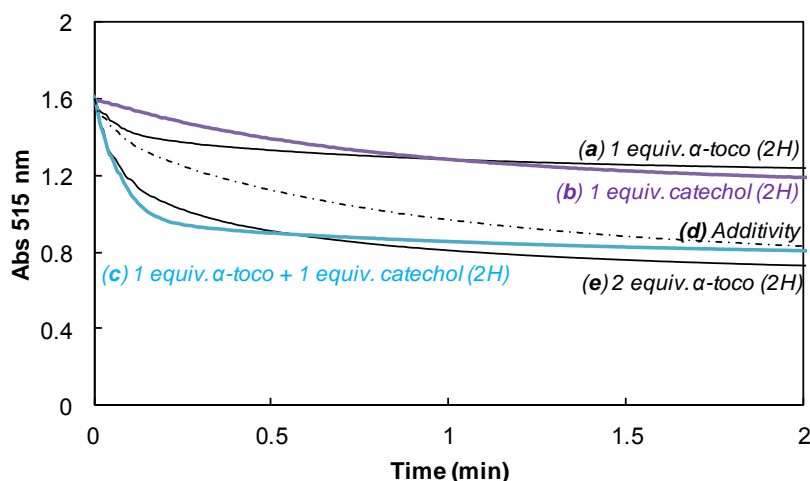


Figure 4.24: Absorbance at 515 nm of DPPH<sup>•</sup> ( $1.5 \times 10^{-4}$  M) with (a) 1 equiv.  $\alpha$ -tocopherol **11** ( $2.07 \times 10^{-5}$  M), (b) 1 equiv. catechol **63** ( $2.07 \times 10^{-5}$  M), (c) experimental 1 equiv.  $\alpha$ -tocopherol **11** with 1 equiv. catechol **63** ( $2.07 \times 10^{-5} + 2.07 \times 10^{-5} = 4.14 \times 10^{-5}$  M), (d, dotted line) theoretical additivity of 1 equiv.  $\alpha$ -tocopherol **11** with 1 equiv. catechol **63** ( $2.07 \times 10^{-5} + 2.07 \times 10^{-5} = 4.14 \times 10^{-5}$  M) and (e) 2 equiv.  $\alpha$ -tocopherol **11** ( $4.14 \times 10^{-5}$  M)

Mixtures of  $\alpha$ -tocopherol **11** and catechol derivatives (**6**, **62**, **63** and **69**) provide another example of regeneration of  $\alpha$ -tocopherol **11** through a different mechanism. Amorati *et al.* have been also interested on the reactivity of 4-*tert*-butylcatechol **6** with  $\alpha$ -tocopherol **11** during the autoxidation of styrene.<sup>333</sup> Based on their kinetic approaches and our BDEs, a mechanism of regeneration involving catechol derivatives as co-antioxidant is described (Fig. 4.26).

The complete recycling of  $\alpha$ -tocopherol **11** by catechol derivatives could be explained in terms of two step mechanism as demonstrated by Amorati *et al.*<sup>333</sup> In the first step, the hydrogen transfer takes place between catechol derivatives and tocopheroxyl radical ( $\alpha$ -toco<sup>•</sup>) forming semiquinone radical (**d**,  $k_{Syn1} = 2.8 \times 10^3 \text{ M}^{-1} \cdot \text{s}^{-1}$ ). Nevertheless, the reverse reaction (**d**) is characterized by a higher kinetic rate constant ( $k_{-Syn} = 3.5 \times 10^5 \text{ M}^{-1} \cdot \text{s}^{-1}$ ). Moreover, the co-antioxidant is more reactive with the DPPH<sup>•</sup> radical (**c**,  $k_{CoAH2} = 5.6 \times 10^5 \text{ M}^{-1} \cdot \text{s}^{-1}$ ). These kinetic parameters are not in favor of the regeneration process of  $\alpha$ -tocopherol **11** with the transfer of the first phenolic hydrogen.

In the second step, the resulting semiquinone radical reacts with  $\alpha$ -toco<sup>•</sup> to regenerate  $\alpha$ -tocopherol **11** providing the *ortho*-quinone derivatives (**f**,  $k_{Syn2}$ ). It is a thermodynamic irreversible process because it is easier to transfer the second hydrogen from the semiquinone radical ( $\text{BDE}_2$ ) than the first phenolic hydrogen ( $\text{BDE}_1$ ) from catechol derivatives (Fig. 4.25, Table 4.6).

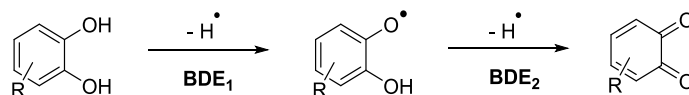


Figure 4.25: Representation of the abstraction of the first ( $\text{BDE}_1$ ) and second ( $\text{BDE}_2$ ) phenolic hydrogens for catechol derivatives (**6**, **62**, **63**, **69** and **70**)

Co-antioxidants	N°	$\text{BDE}_1$	$\text{BDE}_2$
		(kcal.mol <sup>-1</sup> )	
4- <i>Tert</i> -butylcatechol	<b>6</b>	72.3	71.9
Hydroxytyrosol	<b>62</b>	72.1	71.0
Catechol	<b>63</b>	73.4	71.4
Carnosol	<b>69</b>	70.7	69.5
Carnosic acid	<b>70</b>	70.8	68.6

Table 4.6:  $\text{BDE}_1$  and  $\text{BDE}_2$  calculated in vacuum by the DFT B3LYP/6-311++G(2d,2p)//B3LYP/6-311G(d,p) method

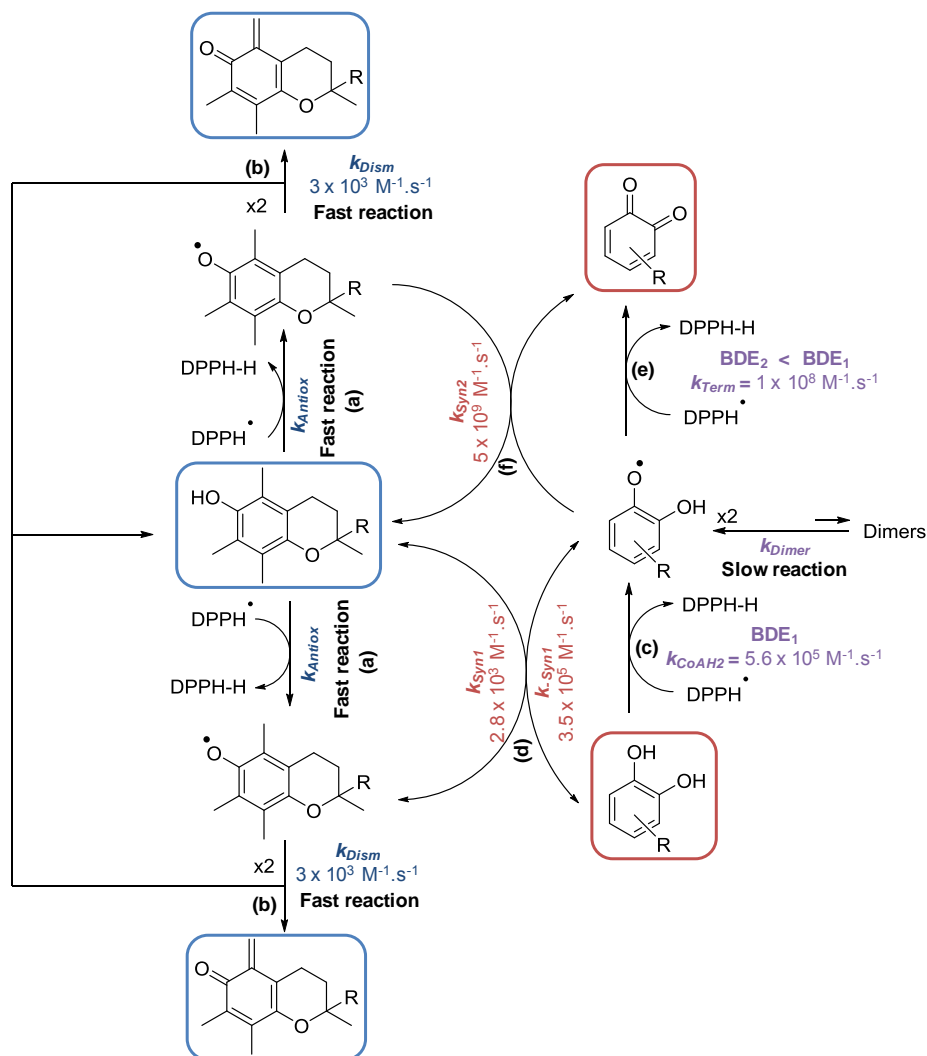


Figure 4.26: Proposed mechanism for the reaction of equimolar mixture of  $\alpha$ -tocopherol **11** and catechol derivatives (**6**, **62**, **63**, **69** and **70**) with a large excess of  $\text{DPPH}^{\bullet}$ <sup>333</sup>

This irreversible regeneration has also been proved by the kinetic study made by Amorati *et al.*<sup>333</sup> The kinetic of regeneration ( $k_{\text{Syn}2} = 5 \times 10^9 \text{ M}^{-1} \cdot \text{s}^{-1}$ ) is higher than that of the termination reaction between semiquinone and  $\text{DPPH}^{\bullet}$  radicals ( $k_{\text{Term}} = 1 \times 10^8 \text{ M}^{-1} \cdot \text{s}^{-1}$ ). We concluded that the reaction of regeneration of  $\alpha$ -tocopherol **11** by the semiquinone radical (**f**) is so fast that it overwhelms the hydrogen transfer from catechol to  $\alpha$ -toco $^{\bullet}$  (**d**). The hydrogen transfer from the semiquinone radical represents the driving force of the regeneration process and allows the recycling of  $\alpha$ -tocopherol **11** practically irreversible under typical autoxidation conditions.

Since the regeneration of  $\alpha$ -tocopherol **11** is likely to be essentially irreversible with any catechol derivatives, the regeneration factor only depends on the  $k_{\text{Syn}}/k_{\text{CoAH}2}$  ratio. Indeed, if the regeneration of  $\alpha$ -tocopherol **11** by a substituted catechol is not complete, this should only depend on the low  $k_{\text{Syn}}$  value for the hydrogen transfer from catechol to tocopheroxyl radical.

### 3.2.3 Super synergism with ascorbic and carnosic acids, hydroquinone and pyrogallol derivatives

DPPH<sup>•</sup> experiments highlight four super synergies when  $\alpha$ -tocopherol **11** is mixed with TBHQ **8**, ascorbyl palmitate **71**, carnosic acid **70** and propyl gallate **4**. As for catechol and reactive monophenols which regenerate  $\alpha$ -tocopherol **11**, there is an increase of initial reaction rates for mixtures whereas the number of radicals trapped by molecule of phenols is always an average of the individual effects.

- *Carnosic acid as a co-antioxidant*

As discussed before, carnosic acid **70** is the only catechol derivative leading to super synergism with  $\alpha$ -tocopherol. It is probably due to the irreversible involvement of the first ( $k_{Syn1}$ ) and second ( $k_{Syn2}$ ) phenolic hydrogens in the regeneration process whereas all the other catechol compounds regenerate  $\alpha$ -tocopherol preferentially with just their second phenolic hydrogen ( $k_{Syn2}$ ).

- *Hydroquinone as a co-antioxidant*

TBHQ **8** and more broadly hydroquinone-based compounds are characterized by a high reactivity of the semiquinone radical which quickly transfers a second hydrogen.<sup>406</sup> This result obtained by Valgimigli *et al.* was confirmed by our BDE calculations (**Fig. 4.27**). Indeed, the transfer of the second phenolic hydrogen is easier ( $BDE_2 = 57.1 \text{ kcal.mol}^{-1}$ ) than for the first one ( $BDE_1 = 74.3 \text{ kcal.mol}^{-1}$ ). The super synergism could be due to the lower  $BDE_2$  for hydroquinone compared to catechol derivatives.

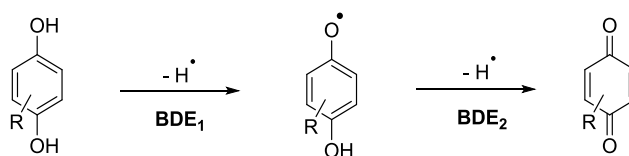


Figure 4.27: Representation of the abstraction of the first ( $BDE_1$ ) and second ( $BDE_2$ ) phenolic hydrogen for hydroquinone derivatives

Foti and Daquino have studied the hydrogen transfer reaction from ubiquinol-0 (Q), which is a hydroquinone derivative (**Fig. 4.28**), to DPPH<sup>•</sup>.<sup>470</sup>

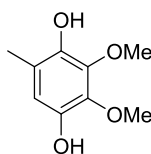
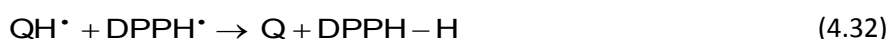


Figure 4.28: Chemical structure of ubiquinol-0<sup>470</sup>

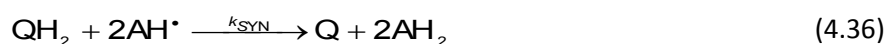
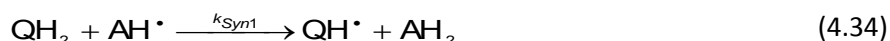
After the transfer of one phenolic hydrogen, 90 % of the semiquinone radical (QH<sup>•</sup>) reacts by dismutation (**Eq. 4.31**) and 10 % reacts with DPPH<sup>•</sup> (**Eq. 4.32**).<sup>470</sup> Moreover, the kinetic rate constant of dismutation reaction has been estimated by Schultz *et al.*<sup>473</sup> at  $2.2 \times 10^8 \text{ M}^{-1}.\text{s}^{-1}$  in acetonitrile solution whereas the reaction of QH<sup>•</sup> with DPPH<sup>•</sup> is just about  $1.5 \times 10^5 \text{ M}^{-1}.\text{s}^{-1}$ .



Ingold and Bowry have also suggested that the disappearance of the tocopheroxyl radical ( $\text{AH}^\bullet$ ) could be accelerated with hydroquinone compounds ( $\text{QH}_2$ ) because the reaction of regeneration is very fast, even if there is a low concentration of hydroquinone (Eq. 4.33).<sup>391</sup>



With the combination of these observations, the kinetic rate-limiting step of the regeneration process is the transfer of the first phenolic hydrogen from hydroquinone compounds ( $\text{QH}_2$ ) to the tocopheroxyl radical ( $\text{AH}^\bullet$ ) ( $k_{\text{Syn1}}$ , Eq. 4.34). Then, the regeneration of  $\alpha$ -tocopherol from its tocopheroxyl radical ( $\text{AH}^\bullet$ ) by the co-phenolic radical ( $\text{QH}^\bullet$ ) is faster than the first step ( $k_{\text{Syn2}} \gg k_{\text{Syn1}}$ , Eq. 4.35). Consequently, the mechanism of action between  $\alpha$ -tocopherol and hydroquinone derivatives is summarized by the equation 4.36 ( $k_{\text{SYN}}$ ). The radical formed by co-antioxidants ( $\text{QH}^\bullet$ ) is extremely reactive and improves the antioxidant efficiency of the mixture by regenerating  $\alpha$ -tocopherol **11**.



▪ *Ascorbic acid derivatives as co-antioxidants*

As described before, there is an irreversible regeneration from ascorbic acid derivatives ( $\text{CoAH}_2$ ) to tocopheroxyl radical.<sup>333</sup> DPPH $^\bullet$  test highlights a drastic kinetic improvement of the reaction of equimolar mixture of phenols ( $V_{i \text{ Mix}} = 27.5 \mu\text{mol.L}^{-1}.\text{s}^{-1}$ ) compared to the use of  $\alpha$ -tocopherol as co-antioxidant ( $V_{i \alpha\text{-toco}+\alpha\text{-toco}} = 16.4 \mu\text{mol.L}^{-1}.\text{s}^{-1}$ ). These results are in agreement with those found by Amorati *et al.*<sup>333</sup> by EPR experiments ( $k_{\text{Mix}} = 1.55 \times 10^6 \text{ M}^{-1}.\text{s}^{-1}$ ,  $k_{\alpha\text{-toco}} = 5.6 \times 10^5 \text{ M}^{-1}.\text{s}^{-1}$  and  $k_{\text{Vitamin C}} = 7.5 \times 10^4 \text{ M}^{-1}.\text{s}^{-1}$ ) during the autoxidation of styrene.<sup>333</sup>

The transfer of the second hydrogen is favored as shown by the BDEs comparison related to the transfer of the first ( $\text{BDE}_1 = 73.3 \text{ kcal.mol}^{-1}$ ) and second ( $\text{BDE}_2 = 61.1 \text{ kcal.mol}^{-1}$ )  $\text{H}^\bullet$  which is related to the formation of the dehydroascorbic acid derivatives (Fig. 4.29).<sup>474</sup>

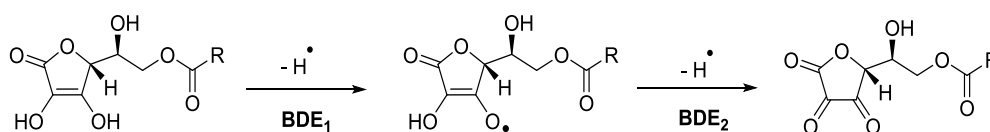


Figure 4.29:  $\text{BDE}_1$  and  $\text{BDE}_2$  calculated in vacuum by the DFT B3LYP/6-311++G(2d,2p)//B3LYP/6-311G(d,p) method for ascorbyl palmitate **71**

Both of the hydrogens released are involved in the regeneration of  $\alpha$ -tocopherol **11**. Indeed, we assumed that DPPH $^\bullet$  first reacts with  $\alpha$ -tocopherol **11** leading to the tocopheroxyl radical which immediately reacts with ascorbyl palmitate **71** to regenerate  $\alpha$ -tocopherol **12** and forms dehydroascorbic acid derivatives (Fig. 4.30).

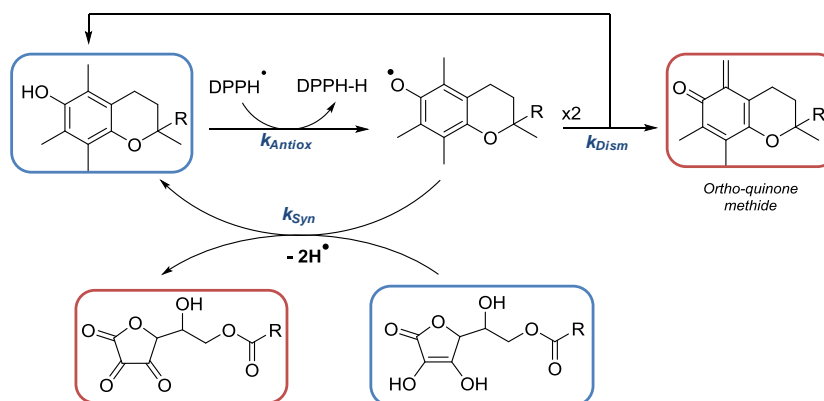


Figure 4.30: Suggested regeneration mechanism of  $\alpha$ -tocopherol **11** by ascorbyl palmitate **71**

▪ *Pyrogallol derivatives as co-antioxidants*

Propyl gallate **4** and 5-*tert*-butylpyrogallol **1** are the two pyrogallol derivatives studied in apolar aprotic solvent because of the insolubility of gallic acid **15**, myricetin **32** and epigallocatechin gallate **55**. DPPH $\cdot$  test highlights a drastic kinetic improvement for the reaction of the equimolar mixture with propyl gallate **4** ( $V_{i\text{ Mix}} = 18.2 \mu\text{mol}\cdot\text{L}^{-1}\cdot\text{s}^{-1}$ ) compared to the use of  $\alpha$ -tocopherol as co-antioxidant ( $V_{i\text{ } \alpha\text{-toco}+\alpha\text{-toco}} = 16.4 \mu\text{mol}\cdot\text{L}^{-1}\cdot\text{s}^{-1}$ ). As described before, Amorati *et al.* showed a correlation between equilibrium constant  $K_r$  and BDEs of phenols (Eq. 4.37).<sup>444</sup>

$$-RT \ln K_r \approx \Delta\text{BDE} = \text{BDE}_{\text{CoAH}_2} - \text{BDE}_{\text{Antiox}} \quad (4.37)$$

$\Delta\text{BDE}$  is always a positive value because the antioxidant is more reactive than the co-antioxidant ( $\text{BDE}_{\text{CoAH}_2} > \text{BDE}_{\text{Antiox}}$ ). Moreover, low  $\Delta\text{BDE}$ s are related to high equilibrium constant ( $K_r$ ) and synergism becomes more significant. Consequently, the very low difference of BDE ( $\Delta\text{BDE} = 0.5 \text{ kcal}\cdot\text{mol}^{-1}$ ) between  $\alpha$ -tocopherol **11** and propyl gallate **4** (with respective BDEs of 69.1 and 69.6  $\text{kcal}\cdot\text{mol}^{-1}$ ) is responsible of the super synergistic effect found with the DPPH $\cdot$  test. Nevertheless, BDE was not decreasing for the abstraction of the second and third hydrogen compared to catechol derivatives (Fig. 4.31, Table 4.7).

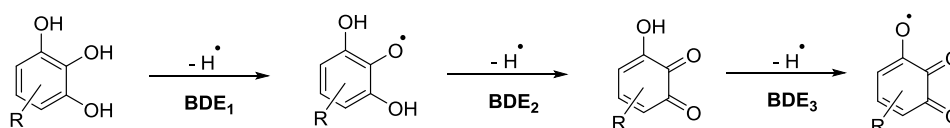


Figure 4.31: Representation of the abstraction of the first ( $\text{BDE}_1$ ), second ( $\text{BDE}_2$ ) and third ( $\text{BDE}_3$ ) phenolic hydrogen for pyrogallol derivatives (**1** and **4**)

Co-antioxidants	N $^\circ$	$\sigma_{\text{exp}}$	$\text{BDE}_1$	$\text{BDE}_2$	$\text{BDE}_3$
			(kcal.mol $^{-1}$ )		
5- <i>Tert</i> -butylpyrogallol	<b>1</b>	2.1	66.6	70.9	81.3
Propyl gallate	<b>4</b>	3.9	69.6	73.5	81.9

Table 4.7:  $\text{BDE}_1$ ,  $\text{BDE}_2$  and  $\text{BDE}_3$  for pyrogallol derivatives (**1**, **4**) calculated in vacuum by the DFT B3LYP/6-311++G(2d,2p)//B3LYP/6-311G(d,p) method

Propyl gallate **4** acts as a co-antioxidant for the regeneration of  $\alpha$ -tocopherol **11** *via* the transfer of the first phenolic hydrogen. As for catechol compounds, the regeneration factor depends on the  $k_{\text{Syn}}/k_{\text{CoAH}_2}$  ratio. Indeed, the kinetic of regeneration ( $k_{\text{Syn}}$ ) is really high compared to the reaction of the co-antioxidant with the DPPH $\cdot$  radical ( $k_{\text{Syn}} \gg k_{\text{CoAH}_2}$ ). Moreover, even if  $\text{BDE}_2$  is higher than  $\text{BDE}_1$ , the second phenolic hydrogen could also participate to the regeneration process leading to *ortho*-

quinone derivatives. Nevertheless, the abstraction of the third phenolic hydrogen is not thermodynamically favorable ( $BDE_3 \gg BDE_2$ ) and does not participate to the regeneration cycle. The active dimers formed in the case of propyl gallate **4** ( $\sigma_{exp} = 3.9$ ) are also involved during the regeneration process.

A super synergy is also obtained with 5-*tert*-butylpyrogallol **1**. It is not represented on **figure 4.14** because its initial reaction rate ( $V_{i\ Co-Antiox} = 15.9\ \mu\text{mol}\cdot\text{L}^{-1}\cdot\text{s}^{-1}$ ) is higher than that of  $\alpha$ -tocopherol **11** ( $V_{i\ \alpha-toco} = 8.2\ \mu\text{mol}\cdot\text{L}^{-1}\cdot\text{s}^{-1}$ ). Anyway, the reactivity of the equimolar mixture ( $V_{i\ Mix} = 36.7\ \mu\text{mol}\cdot\text{L}^{-1}\cdot\text{s}^{-1}$ ) is really high compared to that of additivity ( $V_{i\ Add} = 24.1\ \mu\text{mol}\cdot\text{L}^{-1}\cdot\text{s}^{-1}$ ) highlighting a super synergy. We assumed that 5-*tert*-butyl-pyrogallol **1** ( $BDE = 66.6\ \text{kcal}\cdot\text{mol}^{-1}$ ) act as a primary antioxidant and  $\alpha$ -tocopherol **11** ( $BDE = 69.1\ \text{kcal}\cdot\text{mol}^{-1}$ ) plays the role of co-antioxidant.

### 3.2.4 Additivity with poorly reactive monophenols

Poorly reactive monophenols (*i.e.* *o-tert*-butyl-*p*-cresol **9**, syringic acid **17**, vanillic acid **20**, ferulic acid **27**, isoeugenol **60** and eugenol **61**) are not able to regenerate  $\alpha$ -tocopherol **11**. Indeed, initial reaction rates of mixtures ( $V_{i\ Mix}$ ) are close to that of additivity ( $V_{i\ Add}$ ). Even if these monophenols can transfer more than one hydrogen, there is not regeneration of  $\alpha$ -tocopherol **11**.

Based on the Amorati *et al.* equation (**Eq. 4.37**)<sup>444</sup>, we assumed that a high difference between BDEs of antioxidant and co-antioxidants don't favor synergism. Therefore, when  $\Delta BDE$  is higher than  $7\ \text{kcal}\cdot\text{mol}^{-1}$  (**Eq. 4.38**), there is no regeneration.

$$\Delta BDE \geq 7\ \text{kcal}\cdot\text{mol}^{-1} \quad (4.38)$$

The following kinetic approach has been suggested to understand the additivity of the effects. First of all,  $\alpha$ -tocopherol **11** quickly transfers its phenolic hydrogen to the DPPH<sup>•</sup> leading to the tocopheroxyl radical. The additive effect is obtained if the reaction of regeneration ( $k_{Syn}$ ) does not compete with the dismutation reaction of tocopheroxyl radicals ( $k_{Dism}$ ,  $\alpha$ -toco<sup>•</sup>) (**Eq. 4.39**). The required condition to observe synergism is reversed with poorly reactive monophenols (**Eq. 4.40**).

$$k_{Dism} [\alpha\text{-toco}^{\bullet}] \geq k_{Syn} [\text{CoAH}_2] \quad (4.39)$$

$$k_{Syn} \leq \frac{[\text{AH}^{\bullet}]}{[\text{CoAH}_2]} k_{Dism} \quad (4.40)$$

## 3.3 Kinetic Solvent Effects (KSEs) on synergism

As discussed in the **chapter 3**, polar solvents have an impact on the reactivity of phenols. Therefore, the same equimolar mixture of  $\alpha$ -tocopherol and co-antioxidants have also been studied in Hydrogen Bond Acceptor (HBA, *i.e.* ethyl acetate) and polar protic (*i.e.* ethanol) solvents.

### 3.3.1 Hydrogen Bond Acceptor (HBA) solvents

**Table 4.8** presents the initial reaction rate obtained for the combinations of  $\alpha$ -tocopherol (62.5  $\mu\text{M}$ ) and co-antioxidant (62.5  $\mu\text{M}$ ) ( $V_{i\ Mix}$ ) with the respective initial reaction rate for each co-antioxidant (62.5  $\mu\text{M}$ ,  $V_{i\ Co-Antiox}$ ) and the theoretical additivity of individual effects ( $V_{i\ Add}$ ). Co-antioxidants are ranked from the lowest to the highest BDEs.



Pyrogallol compounds (*i.e.* 5-*tert*-butylcatechol **1** and myricetin **32**), one catechol derivative (*i.e.* carnosic acid **70**) and ascorbyl palmitate **71** show super synergism with  $\alpha$ -tocopherol **11**. Other pyrogallol compounds (*i.e.* propyl gallate **4** and gallic acid **15**), catechol derivatives (*i.e.* 4-*tert*-butylcatechol **6**, rosmarinic acid **23**, caffeic acid **24**, chlorogenic acid **25**, quercetin **34**, hydroxytyrosol **62**, catechol **63** and carnosol **69**), hydroquinone (*i.e.* TBHQ **8**) and two monophenols (*i.e.* BHA **5** and BHT **7**) regenerate  $\alpha$ -tocopherol **11** leading to synergism (Fig. 4.32). Finally, other less reactive monophenols (*i.e.* *o*-*tert*-butyl-*p*-cresol **9**, syringic acid **17**, vanillic acid **20**, sinapic acid **26**, ferulic acid **27**, resveratrol **59**, isoeugenol **60**, eugenol **61** and sesamol **65**) and one catechol compound (*i.e.* protocatechuic acid **16**) are not capable to regenerate  $\alpha$ -tocopherol **11** (Fig. 4.32). The initial reaction rates of mixtures ( $V_{i\text{ Mix}}$ ) are close to that of additivity ( $V_{i\text{ Add}}$ ). However, antagonism effect was not identified.

Kinetic solvent effects (KSEs) have been studied during the reaction of various radicals with phenols<sup>285, 320</sup> but not for couple of phenols. Figure 4.33 illustrates kinetic rate constants ( $\log k_{\text{Co-Antiox}}$ ) vs thermodynamic parameters (BDE) of co-antioxidants. Moreover, their capacity to act as co-antioxidants in order to regenerate  $\alpha$ -tocopherol **11** is schematized in green ( $\bullet$ , synergism and super synergism). Conversely, co-antioxidants which are not able to regenerate  $\alpha$ -tocopherol **11** are in orange ( $\bullet$ , additivity).

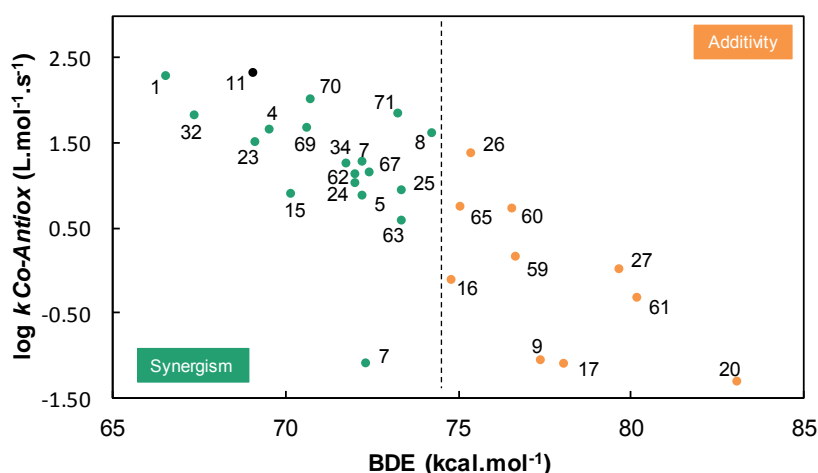


Figure 4.33: Kinetic rate constants of hydrogen transfer ( $\log k_{\text{Co-Antiox}}$ ) obtained in ethyl acetate vs  $\text{BDE}_{\text{CoAH}_2}$  calculated in vacuum by the DFT B3LYP/6-311++G(2d,2p)//B3LYP/6-311G(d,p) method, green ( $\bullet$ ) and orange ( $\bullet$ ) dots illustrate respectively co-antioxidants capable to regenerate  $\alpha$ -tocopherol **11** (synergism and super synergism) or not (additivity) respectively

In order to compare the effect of all the co-antioxidants, BDEs calculated in vacuum are chosen. As in toluene, BDEs determine the reactivity of phenols and their capacity to regenerate  $\alpha$ -tocopherol **11**. Indeed, co-antioxidants with BDEs lower than  $74.5 \text{ kcal.mol}^{-1}$  regenerate  $\alpha$ -tocopherol **11** whatever their kinetic rate constants. Conversely, co-antioxidants with BDEs higher than  $74.5 \text{ kcal.mol}^{-1}$  are not able to regenerate  $\alpha$ -tocopherol **11**. More precisely, a  $\Delta\text{BDE}$  variation of  $5.4 \text{ kcal.mol}^{-1}$  compared to that of  $\alpha$ -tocopherol is a key thermodynamic factor for co-antioxidants capable to regenerate  $\alpha$ -tocopherol in HBA solvents (Eq. 4.41).

$$\Delta\text{BDE} \leq 5.4 \text{ kcal.mol}^{-1} \quad (4.41)$$

The mechanism implicated for the different mixtures of phenols are the same as in apolar aprotic solvent (*i.e.* toluene). The number of radicals trapped by molecule of phenols is always an average of the individual effects. Nevertheless, compared to toluene, the BDE limitation found shifts and co-antioxidants involved in super synergism, synergism and additivity effects are different.

- *Super synergism and synergism*

DPPH<sup>•</sup> experiments highlight four super synergisms when  $\alpha$ -tocopherol **11** is mixed with 5-*tert*-butylpyrogallol **1**, myricetin **32**, carnosic acid **70** and ascorbyl palmitate **71**. For example, the initial reaction rate of 5-*tert*-butylpyrogallol **1** ( $V_{i\text{ Co-Antiox}} = 0.72 \mu\text{mol.L}^{-1}.\text{s}^{-1}$ ) is quite similar to that of  $\alpha$ -tocopherol **11** ( $V_{i\text{ } \alpha\text{-toco}} = 0.96 \mu\text{mol.L}^{-1}.\text{s}^{-1}$ ). However, the reactivity of the equimolar mixture ( $V_{i\text{ Mix}} = 2.33 \mu\text{mol.L}^{-1}.\text{s}^{-1}$ ) is much higher than the additive effects ( $V_{i\text{ Add}} = 1.68 \mu\text{mol.L}^{-1}.\text{s}^{-1}$ ) highlighting a super synergism. It is the same case for myricetin **32**. They are the two pyrogallol structures leading to super synergistic effects. Indeed, the lower initial reaction rates of propyl gallate **4** and gallic acid **15** ( $V_{i\text{ Co-Antiox}} = 0.46$  and  $0.36 \mu\text{mol.L}^{-1}.\text{s}^{-1}$ ) lead to less drastic effect compared to 5-*tert*-butylpyrogallol **1** and myricetin **32**.

On one hand, carnosic acid **70** combined with of  $\alpha$ -tocopherol **11**, leads to super synergistic effects. The kinetic rate of regeneration ( $k_{\text{Syn}}$ ) is enough high and become very competitive with the reaction of dismutation ( $k_{\text{Dism}}$ ) (Eq. 4.42). On the other hand,  $k_{\text{Syn}}$  of other catechols derivatives (*i.e.* 4-*tert*-butylcatechol **6**, rosmarinic acid **23**, caffeic acid **24**, chlorogenic acid **25**, quercetin **34**, hydroxytyrosol **62**, catechol **63**, aesculetin **67**, and carnosol **69**) are less competitive with  $k_{\text{Dism}}$  and lead only to synergism (Eq. 4.43).

$$k_{\text{Syn}} \gg \frac{[\text{AH}^{\bullet}]}{[\text{CoAH}_2]} k_{\text{Dism}} \quad (4.42)$$

$$k_{\text{Syn}} > \frac{[\text{AH}^{\bullet}]}{[\text{CoAH}_2]} k_{\text{Dism}} \quad (4.43)$$

As for toluene, there is a drastic kinetic improvement for the reaction of ascorbyl palmitate **71** and  $\alpha$ -tocopherol **11** ( $V_{i\text{ Mix}} = 2.56 \mu\text{mol.L}^{-1}.\text{s}^{-1}$ ) compared to the use of  $\alpha$ -tocopherol as co-antioxidant ( $V_{i\text{ } \alpha\text{-toco}+\alpha\text{-toco}} = 1.92 \mu\text{mol.L}^{-1}.\text{s}^{-1}$ ). Super synergistic effect obtained with TBHQ **8** in toluene disappears in favor of synergism in ethyl acetate. The transfer of the second phenolic hydrogen, which is the key parameter, could be more difficult in ethyl acetate because of intermolecular hydrogen bonding which decrease its availability. Therefore, the regeneration of  $\alpha$ -tocopherol **11** by TBHQ **8** decreases in HBA solvents. BHA **5** and BHT **7** are the only two monophenols able to regenerate  $\alpha$ -tocopherol **11** by the same mechanism as in toluene.

- *Additive effects*

Finally, less reactive monophenols (*i.e.* *o*-*tert*-butyl-*p*-cresol **9**, syringic acid **17**, vanillic acid **20**, sinapic acid **26**, ferulic acid **27**, resveratrol **59**, isoeugenol **60**, eugenol **61** and sesamol **65**) was not capable to regenerate  $\alpha$ -tocopherol **11** in HBA solvent (*i.e.* ethyl acetate). Indeed, the initial reaction rates of mixtures are closed to that of additivity. Moreover, protocatechuic acid **17** is the only catechol derivative not favorable to synergism. Even if it is a catechol compound, its poor initial reaction rate in ethyl acetate ( $V_{i\text{ Co-Antiox}} = 0.02 \mu\text{mol.L}^{-1}.\text{s}^{-1}$ ) does not favor the regeneration of  $\alpha$ -tocopherol **11**. Therefore, the kinetic rate constants for hydrogen transfer from all these poorly reactive phenols to  $\alpha$ -toco<sup>•</sup> ( $k_{\text{Syn}}$ ) are really low compared to the dismutation reaction (Eq. 4.44).

$$k_{\text{Syn}} < \frac{[\text{AH}^{\bullet}]}{[\text{CoAH}_2]} k_{\text{Dism}} \quad (4.44)$$

### 3.3.2 Preservation of omega-3 oils against oxidation by mixture of phenols

As ethyl acetate was found previously to well model oils, synergistic profile was investigated with the RapidOxy® apparatus during the preservation of omega-3 oils against oxidation. Synergistic effect (%Syn) of mixtures of phenols ( $[\alpha\text{-tocopherol}] = [\text{co-antioxidant}] = 0.25 \text{ mM}$ ) was calculated with **equations 4.45** and **4.46**, where  $IP_{\text{mix}}$  and  $IP_{\text{add}}$  correspond to the induction periods of mixtures and the average of their individual effects respectively. A positive value (%Syn > 0) defines synergistic effect while %Syn < 0 corresponds to antagonism between the two antioxidants. Moreover, high synergistic effect points out great regeneration of the primary antioxidant.

$$\%Syn = 100 \times \frac{IP_{\text{mix}} - IP_{\text{add}}}{IP_{\text{add}}} \quad (4.45)$$

$$IP_{\text{add}} = \frac{IP_{\text{Antiox1}} + IP_{\text{Antiox2}}}{2} \quad (4.46)$$

A concentration of primary antioxidant ( $[\alpha\text{-tocopherol}] = 0.5 \text{ mM}$ ) added to various concentration of co-antioxidant ( $[\text{CoAH}_2]$  from 0 to 1.0 mM) were used to calculate the coefficient of regeneration ( $\alpha$ ). Ratios (R) of  $[\text{co-antioxidant}]/[\text{antioxidant}]$  of 0.2, 0.5, 1 and 2 have been studied. The plot of the induction periods related to each ratio leads to straight lines defined by **equation 4.47** and characterized by the coefficient of regeneration ( $\alpha$ ) and the induction period of  $\alpha$ -tocopherol at 0.5 mM ( $\tau_0$ ) as the slope of the tendency curve. The regeneration coefficient is ranged from 0 (no synergy) to 1 (optimal synergy) and optimal synergy highlights that all the co-antioxidant can regenerate the primary antioxidant.

$$\tau = \tau_0 + \tau_0 \alpha \frac{[\text{Co} - \text{AH}_2]}{[\alpha - \text{tocopherol}]} \quad (4.47)$$

**Figure 4.34** gives an example of  $\alpha$ -tocopherol **11**/BHT **7** mixture which results are developed later

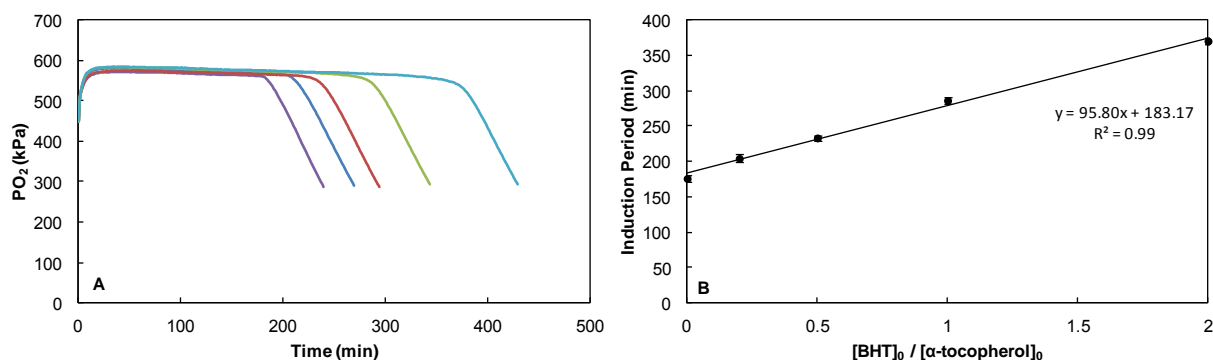


**Figure 4.34:** A) Monitoring of the oxygen pressure during the inhibition of FAMES linseed oil oxidation with  $[\alpha\text{-tocopherol}] = 0.5 \text{ mM}$  and  $[\text{BHT}] = 0 \text{ mM}$  ( $R = 0$ , violet curve),  $[\text{BHT}] = 0.1\text{mM}$  ( $R = 0.2$ , blue curve),  $[\text{BHT}] = 0.25\text{mM}$  ( $R = 0.5$ , red curve),  $[\text{BHT}] = 0.5\text{mM}$  ( $R = 1$ , green curve) and  $[\text{BHT}] = 1 \text{ mM}$  ( $R = 2$ , turquoise curve), B) Evolution of the induction period vs  $[\text{BHT}]_0/[\alpha\text{-tocopherol}]_0$  ratios

- *$\alpha$ -Tocopherol as primary antioxidant*

**Table 4.9** gathers synergistic effects (%Syn) and regeneration coefficients ( $\alpha$ ) for all the co-antioxidants tested with  $\alpha$ -tocopherol **11** for the protection of FAMES linseed oil against oxidation. Results are compared with those given by the DPPH\* test. Co-antioxidants are ranked from the lowest to the highest BDEs.

Co-antioxidant	N°	BDE	%Syn	$\alpha$ (%)	Synergy?	
					RapidOxy®	DPPH* EtOAc
Myricetin	32	67.4	55	100	+++	+++
Rosmarinic acid	23	69.2	10	83	++	++
Propyl gallate	4	69.6	47	90	+++	++
Gallic acid	15	70.2	57	100	+++	++
Carnosol	69	70.7	4	35	+	++
Carnosic acid	70	70.8	25	100	++	+++
Quercetin	34	71.8	12	32	++	++
Hydroxytyrosol	62	72.1	7	84	+	++
Caffeic acid	24	72.1	17	30	++	++
BHA	5	72.3	2	55	+	+
4-Tert-butylcatechol	6	72.3	11	92	++	++
BHT	7	72.4	12	51	++	+
Aesculetin	67	72.5	9	nd	+	++
Ascorbyl palmitate	71	73.3	9	2	+	+++
Chlorogenic acid	25	73.4	3	nd	+	++
Catechol	63	73.4	5	40	+	++
TBHQ	8	74.3	51	76	+++	++
Protocatechuic acid	16	74.8	-3	nd	-	-
Sesamol	65	75.1	-1	nd	-	-
Sinapic acid	26	75.4	-17	nd	x	-
Isoeugenol	60	76.6	-9	nd	x	-
Resveratrol	59	76.7	-8	nd	x	-
<i>o</i> -Tert-butyl- <i>p</i> -cresol	9	77.4	-9	nd	x	-
Syringic acid	17	78.1	-18	nd	x	-
Ferulic acid	27	79.7	-8	nd	x	-
Eugenol	61	80.2	-6	nd	x	-
Vanillic acid	20	83.1	-5	nd	x	-

nd: not determined

**Table 4.9: Synergistic effect (%Syn) and coefficient of regeneration ( $\alpha$ ) obtained for co-antioxidants tested with  $\alpha$ -tocopherol **11**, BDEs (kcal.mol<sup>-1</sup>) are calculated with the DFT method, synergism (+), additivity (-) and antagonism (x) obtained with the RapidOxy® apparatus or DPPH\* test are indicated**

The radical HAT mechanism is the driving force for the protection of oils thanks to the radical cleavage of the phenolic functions. BDEs, stoichiometric numbers ( $\sigma_{\text{exp}}$ ) and kinetic rate constants of hydrogen transfer ( $k$ ) determine the reactivity of phenols. **Figure 4.35** points out the previous induction periods ( $IP_{\text{Co-Antiox}}$ ) obtained for each antioxidant studied vs their respective thermodynamic parameters (BDEs). Their capacity to act as co-antioxidants to regenerate  $\alpha$ -tocopherol **11** is schematized in green (•, %Syn > 0) and phenols which are not able to regenerate  $\alpha$ -tocopherol **11** are in orange and red (• %Syn  $\approx$  0 and • %Syn < 0).

As shown previously by the DPPH\* test, BDEs determine the reactivity of co-antioxidants and their capacity to regenerate  $\alpha$ -tocopherol **11**. Surprisingly, the same BDE limitation is found with the RapidOxy® test. Co-antioxidants with BDEs lower than 74.5 kcal.mol<sup>-1</sup> regenerate  $\alpha$ -tocopherol **11** whereas co-antioxidants with higher BDEs are not able to regenerate it. Therefore, the required condition to get synergistic effects is described by **equation 4.48**.

$$\Delta\text{BDE} \leq 5.4 \text{ kcal.mol}^{-1} \quad (4.48)$$

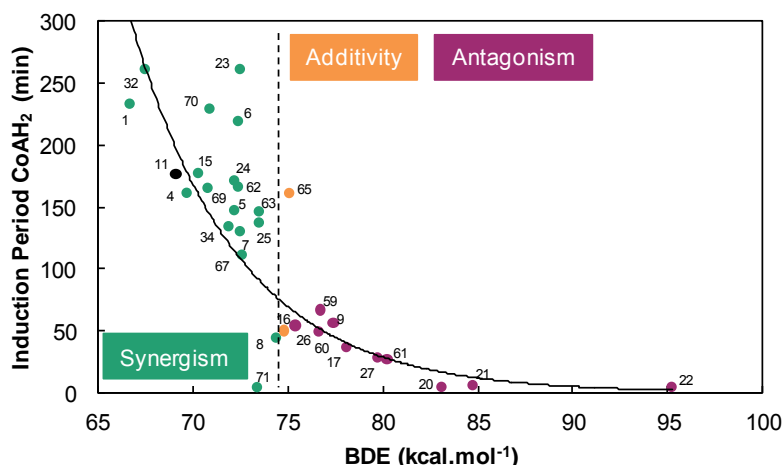


Figure 4.35: Induction periods of co-antioxidants ( $IP_{1\text{equiv. CoAH}_2}$ ) vs their respective BDE calculated in vacuum by the DFT method, green (•), orange (•) and red (•) dots illustrate phenols capable to regenerate  $\alpha$ -tocopherol **11** (synergism) or not (additivity and antagonism) respectively

The best synergistic effect (%Syn) and regeneration coefficient ( $\alpha$ ) are obtained for co-antioxidants with the closest BDEs to that of  $\alpha$ -tocopherol **11**. Indeed, propyl gallate **4**, gallic acid **15** and myricetin **32** (with respective BDEs of 69.6, 70.2 and 67.4 kcal.mol<sup>-1</sup>) allow a nearly complete regeneration ( $\alpha > 90\%$ ) of  $\alpha$ -tocopherol **11** (BDE = 69.1 kcal.mol<sup>-1</sup>). Moreover, these pyrogallol derivatives have also the highest synergistic effects (%Syn > 50%). Conversely, BHA **5**, caffeic acid **24** and quercetin **34**, characterized by higher BDEs (72.3, 72.1, 71.8 kcal.mol<sup>-1</sup> respectively), are involved in a medium regeneration of  $\alpha$ -tocopherol **11** related to intermediate synergistic effect (%Syn < 20%) (Fig. 4.36).

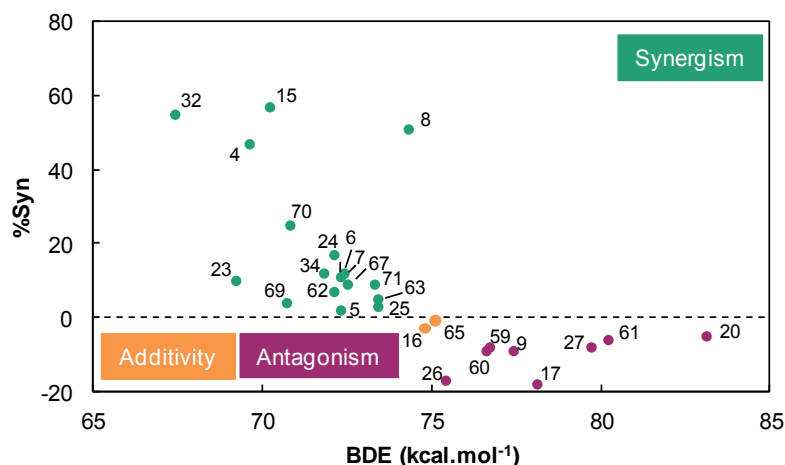


Figure 4.36: Synergistic effect (%Syn) obtained for equimolar mixture of  $\alpha$ -tocopherol **11** and co-antioxidants vs BDE of co-antioxidants calculated in vacuum by the DFT method, green (•), orange (•) and red (•) dots illustrate phenols capable to regenerate  $\alpha$ -tocopherol **11** (synergism) or not (additivity and antagonism) respectively

In most cases, pyrogallol derivatives (**4**, **15** and **32**) are more efficient in the regeneration of  $\alpha$ -tocopherol **11** than catechol compounds (**6**, **23**, **24**, **25**, **34**, **62**, **63**, **67**, **69** and **70**) which are themselves more active than monophenols (**5** and **7**). Hydroquinone derivative TBHQ **8** has a better impact than the main catechol derivatives to enhance the lifetime of  $\alpha$ -tocopherol **11** (%Syn = 51% and  $\alpha = 76\%$ ) due to an easiest transfer of the second hydrogen ( $BDE_2 < BDE_1$ ).

Surprisingly, ascorbyl palmitate **71** is weakly active on the regeneration of  $\alpha$ -tocopherol **11** (%Syn = 9 %) whereas it has shown super synergism *via* DPPH<sup>\*</sup> test. Even if ascorbyl palmitate **71** itself has no antioxidant activity during the preservation of FAMES linseed oil, it could regenerate a low concentration of  $\alpha$ -tocopherol **11**. This is probably due to the drastic conditions of oxidation which does not favor the hydrogen transfer from this co-antioxidant to  $\alpha$ -tocopherol **11**.

There is an impressive difference between the effect of carnosic acid **70** and carnosol **69**. Even if they have the same BDE, carnosic acid **70** entirely regenerates  $\alpha$ -tocopherol **11** ( $\alpha$  = 100 %) whereas carnosol **69** just enhances the shelf life of this primary antioxidant ( $\alpha$  = 35 %). This is probably because carnosic acid **70** could transfer more than 2 hydrogens during the protection of oils compared to its reactivity with the DPPH<sup>\*</sup> radical ( $\sigma_{\text{LOO}\cdot} > \sigma_{\text{DPPH}\cdot}$ ) as discussed in the 3<sup>rd</sup> chapter.

BHA **5** and BHT **7** are the only two monophenols capable to regenerate  $\alpha$ -tocopherol **11** with respective regeneration coefficients ( $\alpha$ ) of 55 and 51 %. Nevertheless, all the other monophenols studied have no synergistic effect with  $\alpha$ -tocopherol **11**. With respective %Syn of -1 and -3 %, sesamol **65** and protocatechuic acid **16** show additive effects with  $\alpha$ -tocopherol **11** whereas sinapic **26** (%Syn = -17 %) and syringic **17** (%Syn = -18 %) acids are clearly distinguished by antagonist effects.

FAMES of linseed oil are used as omega-3 food model to study the effectiveness of co-antioxidants to enhance the activity of  $\alpha$ -tocopherol **11**. Nevertheless, food is composed by triglycerides and not FAMES. Consequently, the effects of co-phenolic antioxidants (*i.e.* TBHQ **8**, gallic acid **15**, rosmarinic acid **23**, myricetin **32**, and carnosic acid **70**) were also studied for the preservation of linseed and fish oils (triglycerides).

**Figure 4.37A** points out the comparative effects of equimolar mixture of phenols ( $\alpha$ -tocopherol + co-antioxidants) for the protection of triglycerides and FAMES linseed oil.

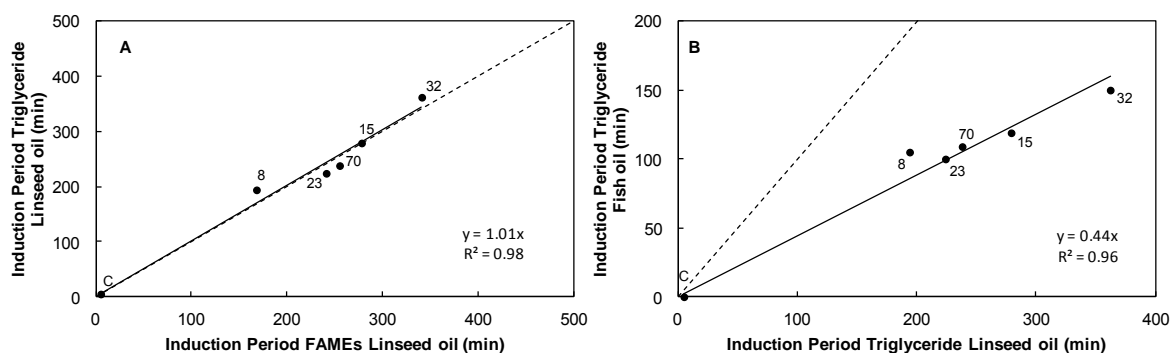


**Figure 4.37:** Comparison of the effect of equimolar mixture of  $\alpha$ -tocopherol **11** and TBHQ **8**, rosmarinic acid **23**, carnosic acid **70**, gallic acid **15** and myricetin **32** during the preservation of FAMES linseed oil, linseed oil and fish oil against oxidation

The correlations obtained ( $R^2 = 0.98$ ) highlights that phenolic mixtures have the same efficiency for the protection of FAMES and oils. Therefore, FAMES well model the oils. Moreover, induction periods obtained for the protection of fish and linseed oil (triglyceride) are well correlated ( $R^2 = 0.96$ , **Fig. 4.37B**). Even if fish oil is highly subjected to oxidation compared to linseed oil, the effects of co-antioxidants on the regeneration of  $\alpha$ -tocopherol **11** are relatively the same. They differ from the higher induction periods obtained during the oxidation of linseed oil than fish oil.

▪ *Other combinations of phenols*

Investigations on the synergistic effect (%Syn) when  $\alpha$ -tocopherol **11** is used as primary antioxidant shows that the best synergistic effects are obtained for co-antioxidants with the closest BDEs to that of  $\alpha$ -tocopherol **11**. It is interesting to study other combinations of natural phenols with different  $\Delta$ BDE compared to the primary antioxidant involved. The primary antioxidant is always characterized as the phenol with the lowest BDE. **Table 4.10** gathers induction periods (IP, in green) and synergistic effect (%Syn, in red) obtained for equimolar mixture of natural phenols. The induction periods (IP) and BDEs of co-antioxidant themselves are indicated and they are ranked from the lowest to the highest BDE.

		AH <sub>2</sub>	Myr 32	RosA 23	CarA 70	Quer 34	HyTy 62	CafA 24
		BDE	67.4	69.2	70.8	71.8	72.1	72.1
AH <sub>2</sub>	BDE	IP (min)	262	262	230	135	172	148
Myr 32	67.4	262		344	255	237	317	235
RosA 23	69.2	262	31 %		327	212	284	222
CarA 70	70.8	230	4 %	33 %		238	273	213
Quer 34	71.8	135	19 %	7 %	30 %		207	159
HyTy 62	72.1	172	46 %	31 %	36 %	34 %		210
CafA 24	72.1	148	14 %	8 %	13 %	12 %	31 %	

**Table 4.10:** Induction Periods (IP, min, in green) and Synergistic effects (%Syn, in red) for equimolar mixture of natural phenols in comparison with their respective BDEs (kcal.mol<sup>-1</sup>) and IP (min). Slight synergy (0 < %Syn < 15), medium synergy (15 ≤ %Syn < 30) and high synergy (30 ≤ %Syn). Myr = myricetin 32, RosA = rosmarinic acid 23, CarA = carnosic acid 70, Quer = Quercetin 34, HyTy = Hydroxytyrosol 62 and CafA = caffeic acid 24

As expected, the best synergistic effects (%Syn > 30 %) are obtained for the combinations of two natural phenolic antioxidants with the lowest  $\Delta$ BDE. Indeed, couples of phenols composed by Myr **32**/RosA **23**, RosA **23**/CarA **70**, CarA **70**/Quer **34**, Quer **34**/HyTy **62** and HyTy **62**/CafA **24** are the thermodynamic optimal mixture with low  $\Delta$ BDEs of 1.8, 1.6, 1.0, 0.3 and 0 kcal.mol<sup>-1</sup> respectively. Caffeic acid (CafA **24**), well regenerates hydroxytyrosol (HyTy **62**) because of their close BDEs ( $\Delta$ BDE = 0 kcal.mol<sup>-1</sup>). Nevertheless, it can weakly regenerate others phenols (%Syn = 14, 8, 13 and 12 %) which respective couples are described by highest  $\Delta$ BDE.

Hydroxytyrosol (HyTy **62**) and caffeic acid (CafA **24**), characterized by the same BDE (72.1 kcal.mol<sup>-1</sup>), do not have the same effect on the regeneration of quercetin (Quer **34**). Indeed, their respective synergistic effects are 34 and 12 %. Therefore, the thermodynamic parameter (BDE) is not the only condition which controls the regeneration. A structural analogy between two antioxidants added to intermolecular hydrogen bondings could explain the best regeneration obtained as described by Peyrat-Maillard *et al.*<sup>447</sup> Surprisingly, hydroxytyrosol (HyTy **62**) allows a great regeneration of all the other phenols studied (%Syn > 30 %) probably due to its simple and small chemical structure which could interact easily with other phenols. The best synergism (%Syn = 46 %) is obtained for the combination of hydroxytyrosol (HyTy **62**) and myricetin (Myr **32**).

### 3.3.3 Influence of polar protic medium

As the reactivity of phenolic antioxidants has been previously studied in ethanol, the transfer of hydrogen from equimolar mixtures of  $\alpha$ -tocopherol **11** and co-antioxidants to DPPH<sup>\*</sup> has also been investigated in this polar protic solvent which favors the SPLET mechanism.<sup>285, 319, 320</sup> Therefore, it is interesting to know if polar protic solvents modify synergistic effects found in the other matrices.

**Table 4.11** presents the initial reaction rate obtained for the combinations of  $\alpha$ -tocopherol (62.5  $\mu\text{M}$ ) and co-antioxidant (62.5  $\mu\text{M}$ ) ( $V_{i\text{ Mix}}$ ) with the respective initial reaction rate for each co-antioxidant (62.5  $\mu\text{M}$ ,  $V_{i\text{ Co-Antiox}}$ ) and the theoretical additivity of individual effects ( $V_{i\text{ Add}}$ ). Co-antioxidants are ranked from the lowest to the highest BDEs.

Co-Antioxidants	N°	BDE	Initial reaction rate $V_i$ ( $\mu\text{mol}\cdot\text{L}^{-1}\cdot\text{s}^{-1}$ )			Synergy?
			Experimental	Hypotheses		
			$V_{i\text{ Mix}}$	$V_{i\text{ Co-Antiox}}$	$V_{i\text{ Add}}$	
<b>5-Tert-butyl-pyrogallol</b>	<b>1</b>	66.6	9.2	6.6	9.4	-
<b>Myricetin</b>	<b>32</b>	67.4	4.4	1.8	4.5	-
<b><math>\alpha</math>-tocopherol</b>	<b>11</b>	69.1	5.6	2.8	5.6	/
<b>Rosmarinic acid</b>	<b>23</b>	69.2	3.2	0.7	3.4	-
<b>Propyl gallate</b>	<b>4</b>	69.6	7.4	4.8	7.6	-
<b>Gallic acid</b>	<b>15</b>	70.2	3.9	1.0	3.8	-
<b>Carnosol</b>	<b>69</b>	70.7	27.7	24.7	27.5	-
<b>Carnosic acid</b>	<b>70</b>	70.8	10.9	7.6	10.4	-
<b>Quercetin</b>	<b>34</b>	71.8	3.7	0.6	3.5	-
<b>Hydroxytyrosol</b>	<b>62</b>	72.1	3.9	1.0	3.8	-
<b>Caffeic acid</b>	<b>24</b>	72.1	4.2	1.4	4.2	-
<b>BHA</b>	<b>5</b>	72.3	2.9	0.2	3.0	-
<b>4-Tert-butylcatechol</b>	<b>6</b>	72.3	4.7	2.0	4.8	-
<b>BHT</b>	<b>7</b>	72.4	2.6	0.007	2.8	-
<b>Aesculetin</b>	<b>67</b>	72.5	6.4	3.4	6.2	-
<b>Ascorbyl palmitate</b>	<b>71</b>	73.3	22.3	19.4	22.2	-
<b>Chlorogenic acid</b>	<b>25</b>	73.4	3.1	0.2	3.0	-
<b>Catechol</b>	<b>63</b>	73.4	3.7	1.1	3.8	-
<b>TBHQ</b>	<b>8</b>	74.3	3.4	0.5	3.3	-
<b>Protocatechuic acid</b>	<b>16</b>	74.8	4.3	1.5	4.3	-
<b>Sesamol</b>	<b>65</b>	75.1	3.5	0.8	3.6	-
<b>Sinapic acid</b>	<b>26</b>	75.4	3.7	0.7	3.5	-
<b>Isoeugenol</b>	<b>60</b>	76.6	3.5	0.8	3.6	-
<b>Resveratrol</b>	<b>59</b>	76.7	3.3	0.3	3.1	-
<b><i>o</i>-Tert-butyl-<i>p</i>-cresol</b>	<b>9</b>	77.4	3.0	0.002	2.8	-
<b>Syringic acid</b>	<b>17</b>	78.1	3.2	0.3	3.1	-
<b>Ferulic acid</b>	<b>27</b>	79.7	3.1	0.1	2.9	-
<b>Eugenol</b>	<b>61</b>	80.2	3.1	0.3	3.1	-

**Table 4.11:** Initial reaction rate  $V_i$  for equimolar mixtures of  $\alpha$ -tocopherol (62.5  $\mu\text{M}$ ) and co-antioxidant (62.5  $\mu\text{M}$ ) ( $V_{i\text{ Mix}}$ ) in ethanol compared to the initial reaction rate of co-antioxidant (62.5  $\mu\text{M}$ ,  $V_{i\text{ Co-Antiox}}$ ) and the theoretical additive effects ( $V_{i\text{ Add}}$ ). - points out additive effects, BDEs ( $\text{kcal}\cdot\text{mol}^{-1}$ ) are calculated with our DFT method

**Figure 4.38** shows the correlation between experimental initial reaction rates of phenol mixtures ( $V_{i\text{ Mix}}$ ,  $[\alpha\text{-tocopherol}] = [\text{co-antioxidant}] = 62.5\ \mu\text{M}$ ) and that of co-antioxidants ( $V_{i\text{ Co-Antiox}}$ ,  $[\text{Co-Antiox}] = 62.5\ \mu\text{M}$ ).

Surprisingly, all the synergistic effects previously found disappeared in polar protic solvent (*i.e.* ethanol). Indeed,  $V_{i\text{ Mix}}$  are located on the additivity line. In the light of various chemical structures of all the co-antioxidants studied, we assumed that the loss of synergy could be due to a change in the reactivity of  $\alpha$ -tocopherol **11** and not because of co-antioxidants.

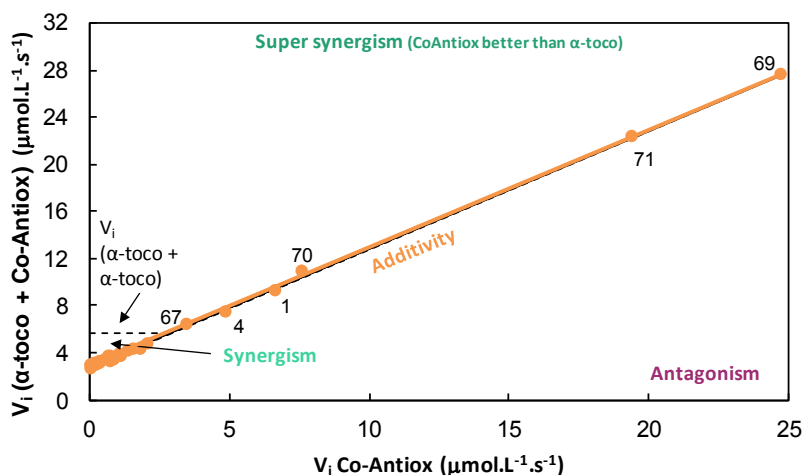


Figure 4.38: Kinetic rate constants of hydrogen transfer for mixtures of phenols ( $k_{\text{Mixer}}$ , 0.5 equiv.  $\alpha$ -tocopherol + 0.5 equiv. co-antioxidant) vs those of 1 equiv. co-antioxidants in ethanol

The best example of the loss of synergy is shown by equimolar mixture of  $\alpha$ -tocopherol **11** and BHT **7** as described by Marteau *et al.*<sup>369, 463</sup> The reactivity of BHT **7** ( $2.07 \times 10^{-5}$  M) with DPPH $^{\bullet}$  ( $1.5 \times 10^{-4}$  M) with and without  $\alpha$ -tocopherol **11** ( $2.07 \times 10^{-5}$  M) has been investigated (Fig. 4.39D). In ethanol, BHT **7** is not able to regenerate  $\alpha$ -tocopherol **11** and the reactivity of the mixture (c) is similar to that of  $\alpha$ -tocopherol alone (a). Moreover, the combination of catechol (*i.e.* hydroxytyrosol **62**, Fig. 4.39A), *ortho*-methoxy phenols (*i.e.* ferulic acid **25**, Fig. 4.39B) and pyrogallol (*i.e.* myricetin **32**, Fig. 4.39C) derivatives with  $\alpha$ -tocopherol **11** leads to additive effects.

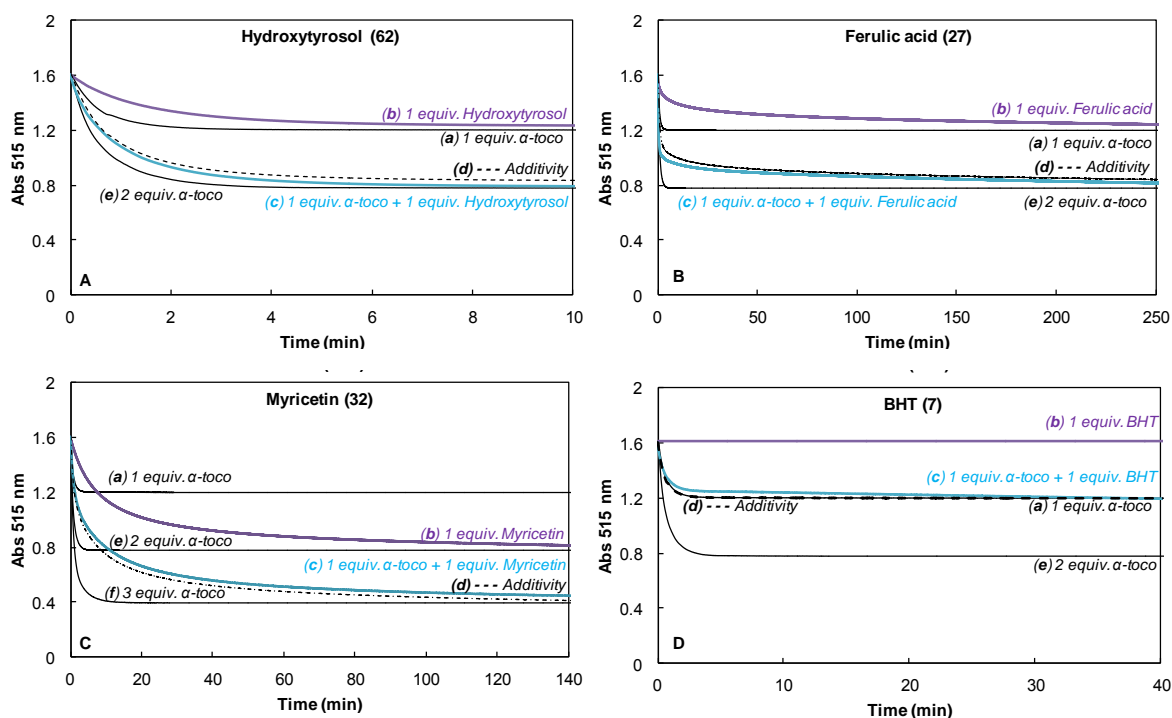


Figure 4.39: Absorbance at 515 nm of DPPH $^{\bullet}$  ( $1.5 \times 10^{-4}$  M) with  $\alpha$ -tocopherol **11** and 4 different co-antioxidants in ethanol: (A) hydroxytyrosol **62**, (B) ferulic acid **27**, (C) myricetin **32** and (D) BHT **7**, (a) 1 equiv.  $\alpha$ -tocopherol **11** ( $2.07 \times 10^{-5}$  M), (b) 1 equiv. Co-AH $_2$  ( $2.07 \times 10^{-5}$  M), (c) experimental 1 equiv.  $\alpha$ -tocopherol **11** with 1 equiv. Co-AH $_2$  ( $2.07 \times 10^{-5} + 2.07 \times 10^{-5} = 4.14 \times 10^{-5}$  M), (d) dotted line) theoretical additivity of 1 equiv.  $\alpha$ -tocopherol **11** with 1 equiv. Co-AH $_2$  ( $2.07 \times 10^{-5} + 2.07 \times 10^{-5} = 4.14 \times 10^{-5}$  M), (e) 2 equiv.  $\alpha$ -tocopherol **11** ( $4.14 \times 10^{-5}$  M) and (f) 3 equiv.  $\alpha$ -tocopherol **11** ( $6.21 \times 10^{-5}$  M)

As there is no synergy with all the co-antioxidants, we suggested that polar solvents act on  $\alpha$ -tocopherol **11** and not on co-antioxidants. Some authors investigated the reaction of  $\alpha$ -tocopherol **11** with co-antioxidants and the loss of synergy could be explained by different interactions as detailed below.

Lucarini *et al.* determined the equilibrium constant between  $\alpha$ -tocopherol **11** and hindered 2,6-di-*tert*-butyl-4-methoxyphenol with their respective phenoxyl radicals in polar and apolar solvents (Fig. 4.40).<sup>328</sup>

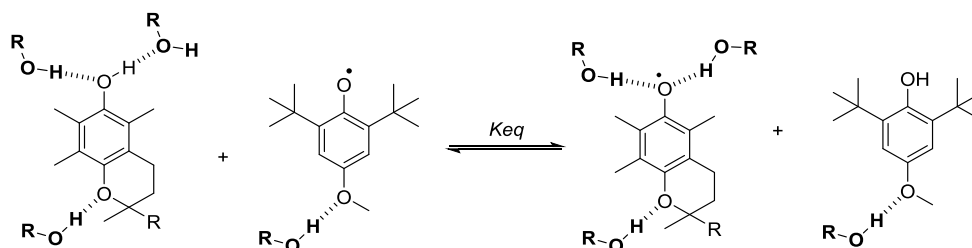


Figure 4.40: Equilibrium between  $\alpha$ -tocopherol **11** and 2,6-di-*tert*-butyl-4-methoxy-phenol with their radicals in benzene ( $K_{eq} = 1.18$ ) and benzene with 30 % of 1,1,1,3,3,3-hexafluoropropan-2-ol ( $K_{eq} = 16.72$ )<sup>328</sup>

In the case of high polar solvent donor of hydrogens, the equilibrium could be shifted towards the tocopheroxyl radical ( $K_{eq} = 1.18$  in benzene and 16.72 in benzene with 30 % of 1,1,1,3,3,3-hexafluoropropan-2-ol).<sup>328</sup> The loss of interaction between the tocopheroxyl radical and co-antioxidant (2,6-di-*tert*-butyl-4-methoxyphenol) is due to the stabilization of  $\alpha$ -toco $\cdot$  by hydrogen bonding with solvent whereas the steric hindrance of the co-antioxidant prevents any stabilization of its phenolic hydrogen.<sup>328</sup> The higher initial reaction rate from  $\alpha$ -tocopherol **11** to DPPH $\cdot$  in toluene ( $V_{i\text{ Toluene}} = 8.2 \mu\text{mol}\cdot\text{L}^{-1}\cdot\text{s}^{-1}$ ) compared to that in ethanol ( $V_{i\text{ Ethanol}} = 2.8 \mu\text{mol}\cdot\text{L}^{-1}\cdot\text{s}^{-1}$ ) is in favor of the drastic stabilization of the phenolic function by hydrogen bonding with ethanol leading to the loss of synergistic effects.

Moreover, some authors suggested another reaction pathway involving the fast transfer of one electron from tocopheroxyl radical ( $\alpha$ -toco $\cdot$ ) to peroxy radicals (ROO $\cdot$ ) leading to the phenoxonium cation.<sup>420, 475-477</sup> This cation is extremely stable in solution with a lifetime of about several hours.<sup>476, 478</sup> The positive charge of the tocopheroxylium ion is principally delocalized into the *para*-position.<sup>477, 479</sup> This alternative mechanism does not allow the hydrogen transfer from co-antioxidants to  $\alpha$ -toco $\cdot$  in alcohol solutions because of the change of  $\alpha$ -toco $\cdot$  into the highly stable tocopheroxylium ion. The action mechanism previously established in toluene or ethyl acetate for mixture of  $\alpha$ -tocopherol **11** and BHT **7** is changed in ethanol. The red part points out the new pathway and the dotted line specifies the disappearance of dismutation and synergy steps (Fig. 4.41). The formation of tocopheroxylium ion is responsible on the disappearance of  $\alpha$ -toco $\cdot$  which could not interact with co-antioxidants to make synergism. Therefore, co-antioxidants react with DPPH $\cdot$  and follow their own reactivity pathway.

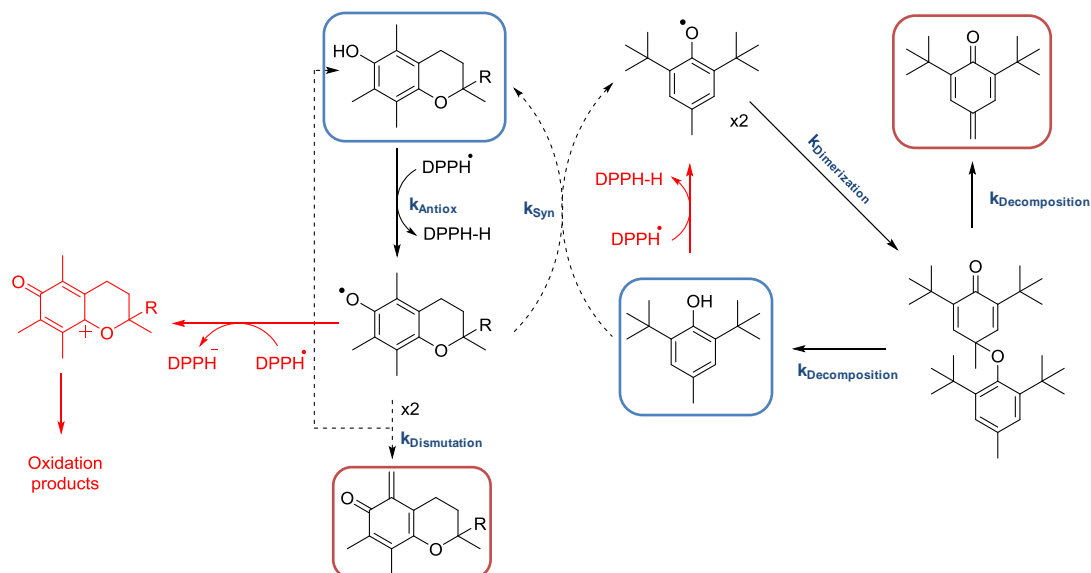


Figure 4.41: Modifications of the reaction mechanism for the combination of  $\alpha$ -tocopherol **11** and BHT **7** in polar solvents (new pathways are in red and disappearance of synergy and dismutation step are schematized by the dotted lines)<sup>369, 463</sup>

## 4. Conclusion

This chapter was dedicated to synergies between phenols and attempts to further understanding the mechanisms.  $\alpha$ -Tocopherol **11** was chosen as the primary antioxidant of reference and was mixed with co-antioxidants of various chemical structures and BDEs. The screening of co-phenolic antioxidants in various solvents highlighted the complexity of the mechanisms involved and the corresponding initial reaction rates. Based on kinetic rate constants found in literature, we discussed in details the mechanisms of action involved during the reaction of two phenolic antioxidants with  $\text{DPPH}^\bullet$  radical.

First of all, in apolar and HBA solvents, HAT radical mechanism leads the hydrogen transfer from mixture of phenols to  $\text{DPPH}^\bullet$  radical. Only co-antioxidants with low BDEs regenerate  $\alpha$ -tocopherol. Thermodynamic conditions were highlighted: reactive co-antioxidants should be in the  $\Delta\text{BDE}$  limits with  $\alpha$ -tocopherol **11** which are estimated at  $-7 \text{ kcal}\cdot\text{mol}^{-1}$  in apolar and  $-5.4 \text{ kcal}\cdot\text{mol}^{-1}$  in HBA solvents. In the presence of co-antioxidant, regeneration process competes with dismutation reaction of tocopheroxyl radicals. The phenol concentration is also a key factor as it improves the synergistic properties of co-antioxidant. These crucial conditions are also dependent on the  $k_{\text{Syn}}/k_{\text{CoAH}_2}$  ratio.

Super synergistic effects could be found with hydroquinone derivatives (TBHQ **8**) because of the formation of very reactive semiquinone radicals. Moreover, ascorbic acid derivatives show irreversible regeneration of  $\alpha$ -tocopherol **11**. BHA **5** and BHT **7** are the only monophenols capable to regenerate  $\alpha$ -tocopherol **11** in HBA solvents *via* the formation of active dimers. More precisely, there is a drastic improvement of the antioxidant properties of BHT **7** with  $\alpha$ -tocopherol **11**. Finally, reactive catechol derivatives can regenerate  $\alpha$ -tocopherol **11** thanks to the irreversible transfer of the second phenolic hydrogen ( $\text{BDE}_2 < \text{BDE}_1$ ) leading to *ortho*-quinone compounds.

The investigation of synergistic profile made by RapidOxy<sup>®</sup> during the preservation of FAMES of linseed oil against oxidation highlights that HBA solvent (*i.e.* ethyl acetate) good models oils. Indeed, the same BDE limitation is found compared to the  $\text{DPPH}^\bullet$  test. Moreover, another favorable

condition is developed: the co-antioxidants with the closest BDE to that of  $\alpha$ -tocopherol **11** lead to the best synergistic effects and the coefficient of regeneration are increased. Pyrogallol compounds allow a nearly complete regeneration of  $\alpha$ -tocopherol **11** ( $\alpha > 90\%$ ) followed by catechol derivatives and monophenols. The same required conditions are obtained with mixture of other natural phenols to improve the synergistic effects.

The polarity of solvent has a huge impact on synergistic behaviors. Indeed, there is a complete loss of synergy between  $\alpha$ -tocopherol **11** and co-antioxidants in polar protic matrix (*i.e.* ethanol) in favor of additive effects. This is due to a different reactivity of tocopheroxyl radical that does not accept anymore the hydrogen transfer from co-antioxidants. This radical reacts preferentially *via* an electron transfer as indicated by Suarna *et al.*<sup>475, 480</sup> leading to the tocopheroxylum ion which is too stable to be included in the regeneration cycle.



# CHAPTER 4. EXPERIMENTAL PART

---

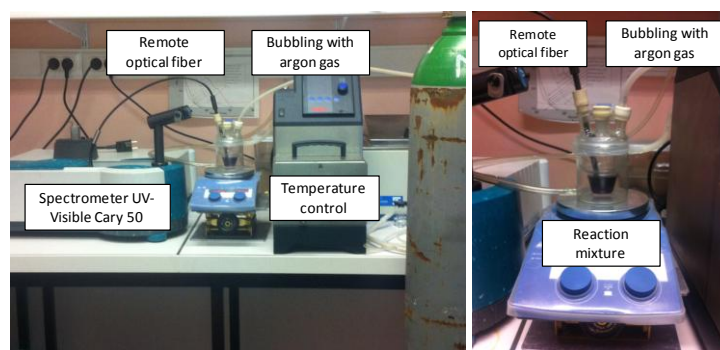
## 1. Materials

Solvents are of the purest grade commercially available from Sigma-Aldrich. The 2,2-diphenyl-1-picrylhydrazyl (DPPH<sup>•</sup>) radical is purchased from Sigma-Aldrich and kept at a temperature lower than 5 °C. Catechol **63** (≥ 99 %), 4-hydroxybenzoic acid **21** (PHBA, ≥ 99 %), rosmarinic acid **23** (96 %), quercetin **34** (≥ 98 %), 2-tert-butyl-4-methylphenol **9** (99 %), salicylic acid **22** (> 99 %), tert-butylhydroquinone **8** (TBHQ, 97 %), 4-hydroxy-3-methoxybenzoic acid **20** (vanillic acid, 97 %), sesamol **65** (98 %), propyl gallate **4** (PG, ≥ 98 %), isoeugenol **60** (98 %), 3-tert-butyl-4-hydroxyanisole **5** (BHA, 98 %), 3,4-dihydroxybenzoic acid **16** (protocatechuic acid, 97 %), 2,6-di-tertbutyl-4-methylphenol **7** (BHT, ≥ 99 %), 3,4-dihydroxycinnamic acid **24** (caffeic acid, 97 %), ferulic acid **27** (99 %), α-tocopherol **11** (≥ 96 %) and sodium (in kerosene, pieces, > 99.8 %) are from Sigma-Aldrich. 3,5-dimethoxy-4-hydroxycinnamic acid **26** (sinapic acid, 98 %), 5-tert-butylpyrogallol **1** (97 %), syringic acid **17** (≥ 98 %), eugenol **61** (99 %), 6,7-dihydroxycoumarin **67** (aesculetin, ≥ 98 %), epigallocatechin gallate **55** (98 %) and L-ascorbyl palmitate **71** (99 %) are from Alfa Aesar. 3,4-dihydroxyphenyl ethanol **62** (hydroxytyrosol), myricetin **32** (≥ 98 %), chlorogenic acid **25** (≥ 95 %) and carnosic acid **70** (≥ 95 %) are from Cayman Chemical Company. Gallic acid **15** (≥ 95 %) is from ACROS and 4-tert-butylpyrogallol **6** (≥ 98 %) is from Merck. Resveratrol **59** (≥ 98 %) is from TCI and carnosol **69** is from Chromadex. Aluminium oxide, basic, Brockmann I, for chromatography, 50-200 μm, 60 Å is from Acros Organics. Refined linseed oil is from Vandeputte Group, Belgium. FAME mix GLC-10 containing palmitic acid methyl ester (C16:0), stearic acid methyl ester (C18:0), oleic acid methyl ester (C18:1), linoleic acid methyl ester (C18:2) and linolenic acid methyl ester (C18:3) is from Supelco.

## 2. Protocols and methods

### 2.1 Determination of the kinetic rate constants for hydrogen transfer from phenols mixtures to DPPH<sup>•</sup> radical

Solutions of DPPH<sup>•</sup> are prepared in each solvent used at a concentration of ca.  $5 \times 10^{-3}$  M by sonicating the mixture until all DPPH<sup>•</sup> crystals are dissolved. The solutions are then maintained under argon at 20 °C. Solutions of phenol mixtures are prepared in solvents of study at a concentration of [antioxidant] = [co-antioxidant] =  $5 \times 10^{-3}$  M. Typically, 250 + 250 μL of each phenol constitute the phenol mixtures. 500 μL of the phenol mixtures are added to 500 μL of DPPH<sup>•</sup> solution in a 50 mL glass reactor equipped with a UV fibre (from Varian equipped with a dip-probe; Varian, les Ulis, France) containing 20 mL of deoxygenated solvent maintained at 20 °C. Equipment for UV-visible analysis and curve presenting the visualization of the lag time are presented in **figure S4.1**.



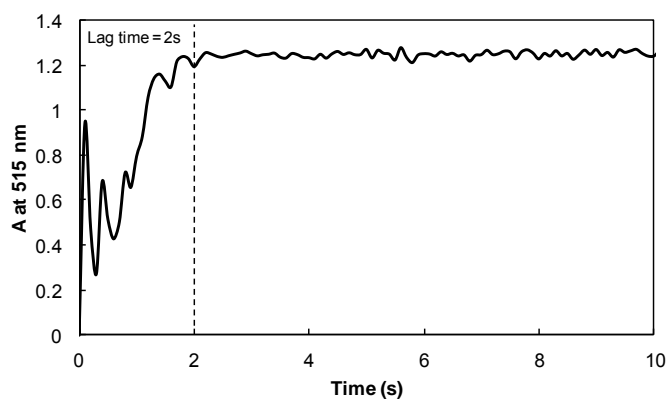


Figure S4.1: Equipment for UV-visible analysis and evolution of the absorbance of DPPH<sup>•</sup> radical at 515 nm (0.12 mM) without phenols in toluene at 20 °C, visualization of the lag time

Figure S4.2 gives an example for an equimolar mixture of  $\alpha$ -tocopherol **11** and 4-*tert*-butyl-catechol **6** in toluene.

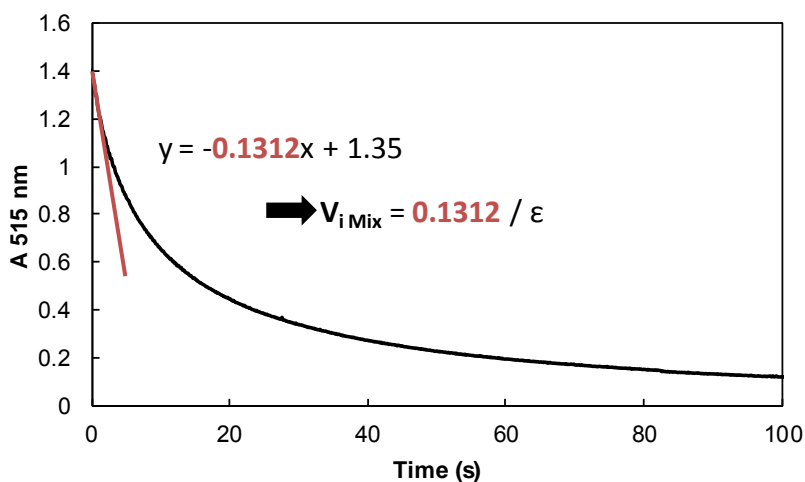


Figure S4.2: Evolution of the absorbance of DPPH<sup>•</sup> radical at 515 nm ( $1.25 \times 10^{-4} \text{ mol.L}^{-1}$ ) with an equimolar mixture of  $\alpha$ -tocopherol **11** and 4-*tert*-butyl-catechol **6**, [antioxidant] = [co-antioxidant] =  $6.25 \times 10^{-5} \text{ mol.L}^{-1}$  in toluene at 20 °C, calculation of the initial reaction rate of mixture ( $V_{i,Mix}$ )

Depending on the solvent,  $\epsilon$  and  $\epsilon'$  values for DPPH<sup>•</sup> radical are summarized in the **table S4.1**.

	$\lambda = 515 \text{ nm}$		$\lambda = 600 \text{ nm}$	
	$\epsilon \text{ (L.mol}^{-1}.\text{cm}^{-1})$	$\epsilon' \text{ (L.mol}^{-1}.\text{cm}^{-1})$	$\epsilon \text{ (L.mol}^{-1}.\text{cm}^{-1})$	$\epsilon' \text{ (L.mol}^{-1}.\text{cm}^{-1})$
<b>Toluene</b>	11766	24	4250	6
<b>Ethyl Acetate</b>	11085	22	4993	13
<b>Cetiol A</b>	11432	29	4973	11
<b>Ethanol</b>	9260	19	4237	8

Table S4.1: Values of  $\epsilon$  and  $\epsilon'$  for DPPH<sup>•</sup> radical in toluene, ethyl acetate, cetiol A and ethanol

## 2.2 Determination of the stoichiometric number for the reaction of phenol mixtures with the DPPH<sup>•</sup> radical

Solutions of DPPH<sup>•</sup> are prepared in the solvent used at a concentration of ca.  $1.5 \times 10^{-4}$  M by sonicating the mixture until all DPPH<sup>•</sup> crystals were dissolved. The solutions are then maintained under argon at 20 °C. Solutions of phenol mixtures are prepared in solvents of study at a concentration of [antioxidant] = [co-antioxidant] =  $2.07 \times 10^{-5}$  M. Typically, 20 + 20  $\mu$ L of each phenol constitute the phenol mixtures and are added to 2.0 mL of a DPPH<sup>•</sup> solution in a UV cell stirred and maintained at 20 °C. The absorbance change is monitored at 515 nm by using the UV-Visible Cary 60 every seconds or minutes. Final  $A_f$  and initial  $A_0$  absorbances are used to determine the stoichiometric number  $\sigma_{\text{Mix}}$  according to **equation S4.1**.

$$\sigma_{\text{Mix}} = \frac{[\text{DPPH}^{\bullet}]_0 - [\text{DPPH}^{\bullet}]_f}{[\text{ArOH}]_0} = \frac{A_0 - A_f}{(\epsilon - \epsilon')[\alpha\text{-toco} + \text{CoAH}_2]_0} \quad (\text{S4.1})$$

Final absorbances are collected when constant values are reached during at least thirty minutes. **Figure S4.3** shows the example of an equimolar mixture of  $\alpha$ -tocopherol **11** and BHT **7** in toluene.

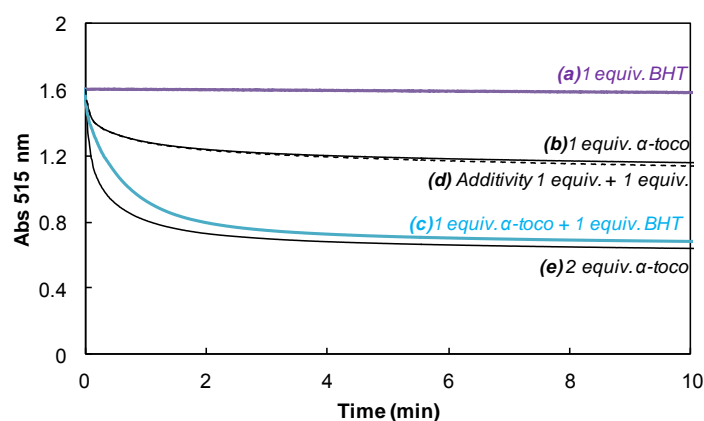


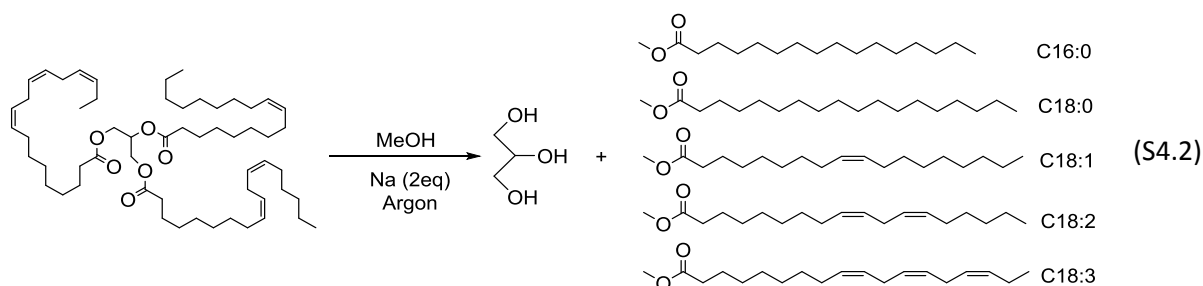
**Figure S4.3:** Evolution of the absorbance of DPPH<sup>•</sup> radical at 515 nm ( $1.5 \times 10^{-4}$  M) with (a) 1 equiv. of BHT **7** ( $2.07 \times 10^{-5}$  M), (b) 1 equiv. of  $\alpha$ -tocopherol **11** ( $2.07 \times 10^{-5}$  M), (c) equimolar mixture of both antioxidants [ $\alpha$ -tocopherol] + [BHT] =  $4.14 \times 10^{-5}$  M (d) additivity profile (dotted line) and (e) 2 equiv. of  $\alpha$ -tocopherol **11** ( $4.14 \times 10^{-5}$  M) in toluene at 20 °C

## 2.3 Purification of linseed oil

Alumina column chromatography can be used to remove antioxidants to very low concentrations. Starting linseed oil containing antioxidants is treated for complete removal of all antioxidants present, defined as < 1 ppm. Aluminium oxide is initially conditioned by gently rinsed with in-house ultra pure water in a Buchner funnel situated above the Buchner flask. This mixture is gently manually agitated and washed three times. Rinsed alumina is placed in an oven set at 200°C for at least three hours, generally dried overnight. The dried alumina is introduced into a column above a heavy walled 500 mL filtering flask. A ratio of 2:1 oil: alumina was maintained for this effort. Two hundred grams of alumina was weighed and dispensed into the column via glass funnel. Next, portions of 400 g oil were added since the column capacity limited the full initial introduction amount. The vacuum was maintained to allow a slow but steady drip as visually witnessed into the filtering flask. All glassware was covered with aluminum foil during this separation to limit light exposure. This process offers approx 70% recovery of starting amount. Oil was stored in an amber wide bottle and capped with nitrogen prior to freezer storage.

## 2.4 Synthesis of antioxidant-free fatty acid methyl esters (FAMES) by transesterification of purified linseed oil

The transesterification reaction of triglycerides of purified linseed oil with methanol into fatty acid methyl esters (FAMES) is represented by **equation S4.2**.



1 L of methanol is introduced into a 2L three-necked equipped with a cooler and a bubbler. Sodium (10 g, 2 equiv.) is introduced piece by piece under argon followed by purified linseed oil (200 g, 1 equiv.). The reaction is performed overnight. FAMES are extracted with 3 x 300 mL of petroleum ether. The combined organic phases are evaporated under pressure. Isolated FAMES are stored at -20 °C.

## 2.5 Gas chromatography – mass spectrometry analysis

A Thermofisher GC Trace equipped with an AI 3000 injector connected to Thermofisher DSQ II simple quadrupole detector is used for the GC-MS analysis of FAMES. Compound separation is achieved on a 30 m, DB5MS with 0.25 mm i.d. and 0.25 μm film thickness gas chromatographic column (J&W Scientific, Folsom, CA, USA). Carrier gas (ultra-pure helium) flow rate is 1.0 mL/min and the injector, the transfer line and the ions source are maintained at 250, 270 and 220 °C, respectively. The MS detector is used in the EI mode with an ionization voltage of 70 eV. The column is held at 130 °C for 0.5 min and then programmed at 0.3 °C.min<sup>-1</sup> to 180 °C and maintained for 5 min. Then, the column is programmed at 3 °C.min<sup>-1</sup> to 250 °C and maintained for 10 min. The compounds are injected in the Split mode with a ratio of 20. FAME mix GLC-10 is used to analyze and quantify the FAMES composition.

## 2.6 Autoxidation of FAMES of linseed oil by the RapidOxy®: Effect of the phenolic mixtures and calculation of the coefficient of regeneration

2 mL FAMES of linseed oil are introduced into the RapidOxy cell (25mL) at room temperature. Phenol solutions are prepared in ethyl acetate, solvent inert to oxidation, at 10<sup>-2</sup> mol.L<sup>-1</sup>. In order to estimate the effect of the phenolic mixture, 50 + 50 μL of each phenol constitute the phenol mixtures. 100 μL of the equimolar phenol mixture are introduced in 2 mL FAMES linseed oil to get a 5 x 10<sup>-4</sup> mol.L<sup>-1</sup> solution. The synergistic effect (%Syn) of the equimolar mixture is investigated using the **equations S4.3** and **S4.4**.

$$\%Syn = 100 \times \frac{IP_{mix} - IP_{add}}{IP_{add}} \quad (S4.3)$$

$$IP_{add} = \frac{IP_{\alpha\text{-tocopherol}} + IP_{CoAH2}}{2} \quad (S4.4)$$

The RapidOxy<sup>®</sup> apparatus (**Fig. S4.4**) is equipped with an inox cell (7, dim 20x40x26 cm) corresponding to a total volume of 25 mL in which the sample is introduced at ambient temperature. The cell is then closed by a screw cap (3) and a safety hood (2), which is locked by a latch (1 and 8). The gas is removed of the cell by the extraction gas connection (4) and replaced by only pure dioxygen, which is injected through the gas alimentation (5) at the pressure on the interface screen (9) (450 kPa). The cell is then heated up to the temperature set (90 °C) and the pressure is monitored every minute by the pressure sensor (6). The experiment is ended when the pressure reached 50% of the maximum pressure. The pressure decrease is converted into a concentration of oxygen per volumes of the FAMES solution.

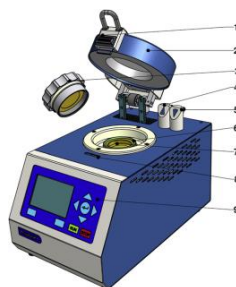


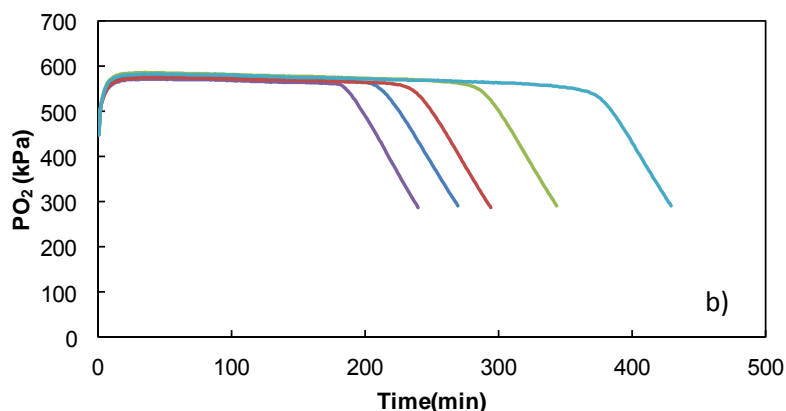
**Figure S4.4:** RapidOxy<sup>®</sup> apparatus for measurement of oxygen consumption during the autoxidation process

As regards to the calculation of the coefficient of regeneration, the volume of co-antioxidant varying from 20 to 200  $\mu\text{L}$  is added to 100  $\mu\text{L}$  of the solution of  $\alpha$ -tocopherol. Indeed, ratios (R) of [co-antioxidant]/[antioxidant] of 0.2, 0.5, 1 and 2 are studied.

$$\tau = \tau_0 + \tau_0 \alpha \frac{[\text{Co-antioxidant}]}{[\alpha\text{-tocopherol}]} \quad (\text{S4.5})$$

The equation of the tendency curve given by **equation S4.5** gives the coefficient of regeneration ( $\alpha$ ) thanks to the induction period of  $\alpha$ -tocopherol at  $5 \times 10^{-4} \text{ mol.L}^{-1}$ .

**Figure S4.5** shows the mixture of  $\alpha$ -tocopherol **11** and BHT **7**.



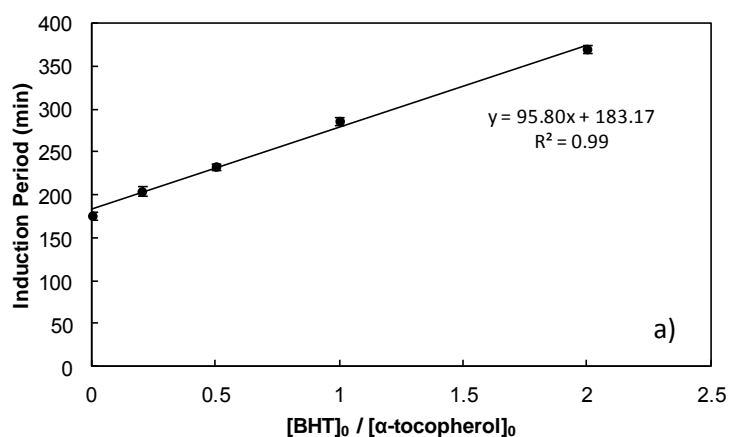


Figure S4.5: a) Monitoring of the oxygen pressure during the oxidation of FAMES of linseed oil with  $[\alpha\text{-tocopherol}] = 0.5$  mM and  $[\text{BHT}] = 0$  mM ( $R = 0$ , violet curve) 0.1 mM ( $R = 0.2$ , blue curve), 0.25 mM ( $R = 0.5$ , red curve), 0.5 mM ( $R = 1$ , green curve) and 1 mM ( $R = 2$ , turquoise curve) and b) Evolution of the induction period as a function of the ratios  $[\text{BHT}]_0 / [\alpha\text{-tocopherol}]_0$

### 3. Results

#### 3.1 Determination of the stoichiometric numbers $\sigma_{\text{exp}}$ of the hydrogen transfer from equimolar mixture of $\alpha$ -tocopherol + co-antioxidants to the $\text{DPPH}^\bullet$ radical in toluene

Co-AH <sub>2</sub> <sup>a</sup>	A <sub>0</sub>	A <sub>f</sub>	$\sigma_{\text{exp}}$	Co-AH <sub>2</sub> <sup>a</sup>	A <sub>0</sub>	A <sub>f</sub>	$\sigma_{\text{exp}}$
/	1.60	1.12	2.0	26	1.60	0.63	2.0
1	1.60	0.63	2.0	27	1.60	0.68	1.9
4	1.60	0.22	2.8	60	1.60	0.85	1.5
5	1.60	0.64	2.0	61	1.60	0.67	1.9
6	1.60	0.52	2.2	62	1.60	0.63	2.0
7	1.60	0.61	2.0	63	1.60	0.65	2.0
8	1.60	0.62	2.0	65	1.60	0.62	1.9
9	1.60	0.31	2.6	70	1.60	0.60	2.1
17	1.60	0.85	1.5	69	1.60	0.66	1.9
20	1.60	0.80	1.6	71	1.60	0.62	2.0

<sup>a</sup>  $[\alpha\text{-tocopherol}]_0 + [\text{Co-antioxidant}]_0 = 2.07 \times 10^{-5} + 2.07 \times 10^{-5} = 4.14 \times 10^{-5}$  M

Operating conditions:  $T = 20$  °C,  $\lambda = 515$  nm,  $[\text{DPPH}^\bullet] = 1.5 \times 10^{-4}$  M

Table S4.2: Determination of the stoichiometric numbers  $\sigma_{\text{exp}}$  in toluene for an equimolar mixture of  $\alpha$ -tocopherol + co-antioxidant

#### 3.2 Determination of the stoichiometric numbers $\sigma_{\text{exp}}$ of the hydrogen transfer from equimolar mixture of $\alpha$ -tocopherol + co-antioxidants to the $\text{DPPH}^\bullet$ radical in ethyl acetate

Co-AH <sub>2</sub> <sup>a</sup>	A <sub>0</sub>	A <sub>f</sub>	$\sigma_{\text{exp}}$	Co-AH <sub>2</sub> <sup>a</sup>	A <sub>0</sub>	A <sub>f</sub>	$\sigma_{\text{exp}}$
/	1.61	1.15	2.0	26	1.60	1.11	1.1
1	1.60	0.73	1.9	27	1.60	0.86	1.6
4	1.60	0.28	2.9	32	1.61	0.60	2.2
5	1.60	0.73	1.9	34	1.60	0.76	1.8
6	1.60	0.66	2.1	55	1.60	0.08	3.4

Co-AH <sub>2</sub> <sup>a</sup>	A <sub>0</sub>	A <sub>f</sub>	σ <sub>exp</sub>	Co-AH <sub>2</sub> <sup>a</sup>	A <sub>0</sub>	A <sub>f</sub>	σ <sub>exp</sub>
7	1.60	0.70	2.0	59	1.60	0.87	1.6
8	1.61	0.70	2.0	60	1.60	1.15	1.0
9	1.60	1.07	1.2	61	1.60	0.95	1.4
15	1.60	0.11	3.3	62	1.61	0.68	2.0
16	1.60	0.66	2.0	63	1.60	0.69	2.0
17	1.60	1.14	1.0	65	1.60	0.51	2.4
20	1.60	1.14	1.0	67	1.60	0.70	2.0
21	1.60	1.10	1.1	69	1.61	0.70	1.9
23	1.60	0.29	2.9	70	1.63	0.68	2.1
24	1.60	0.68	2.0	71	1.60	0.70	2.0
25	1.61	0.75	1.9				

<sup>a</sup> [α-tocopherol]<sub>0</sub> + [Co-antioxidant]<sub>0</sub> = 2.07 × 10<sup>-5</sup> + 2.07 × 10<sup>-5</sup> = 4.14 × 10<sup>-5</sup> M

Operating conditions: T = 20 °C, λ = 515 nm, [DPPH<sup>•</sup>] = 1.5 × 10<sup>-4</sup> M

**Table S4.3: Determination of the stoichiometric numbers σ<sub>exp</sub> in ethyl acetate for an equimolar mixture of α-tocopherol + co-antioxidant**

### 3.3 Determination of the stoichiometric numbers σ<sub>exp</sub> of the hydrogen transfer from equimolar mixture of α-tocopherol + co-antioxidants to the DPPH<sup>•</sup> radical in ethanol

Co-AH <sub>2</sub> <sup>a</sup>	A <sub>0</sub>	A <sub>f</sub>	σ <sub>exp</sub>	Co-AH <sub>2</sub> <sup>a</sup>	A <sub>0</sub>	A <sub>f</sub>	σ <sub>exp</sub>
/	1.60	1.19	2.1	25	1.60	0.78	2.1
1	1.60	0.63	2.5	26	1.60	0.78	2.1
4	1.60	0.39	3.1	27	1.60	0.80	2.1
5	1.60	0.75	2.2	32	1.60	0.44	3.0
6	1.60	0.68	2.4	34	1.60	0.35	3.2
7	1.61	1.17	1.1	59	1.60	0.64	2.1
8	1.60	0.78	2.1	60	1.60	0.89	1.9
9	1.60	0.93	1.7	61	1.60	0.85	2.0
15	1.60	0.18	3.7	62	1.60	0.78	2.1
16	1.60	0.76	2.2	63	1.60	0.70	2.3
17	1.60	0.83	2.0	65	1.60	0.73	2.3
20	1.60	1.15	1.2	67	1.60	0.48	3.0
21	1.60	1.18	1.1	69	1.60	0.86	1.9
23	1.60	0.44	3.0	70	1.60	0.78	2.1
24	1.60	0.75	2.2	71	1.60	0.72	2.3

<sup>a</sup> [α-tocopherol]<sub>0</sub> + [Co-antioxidant]<sub>0</sub> = 2.07 × 10<sup>-5</sup> + 2.07 × 10<sup>-5</sup> = 4.14 × 10<sup>-5</sup> M

Operating conditions: T = 20 °C, λ = 515 nm, [DPPH<sup>•</sup>] = 1.5 × 10<sup>-4</sup> M

**Table S4.4: Determination of the stoichiometric numbers σ<sub>exp</sub> in ethanol for an equimolar mixture of α-tocopherol + co-antioxidant**

### 3.4 Induction periods (IP) for the preservation of FAMES of linseed oil against oxidation by an equimolar mixture of $\alpha$ -tocopherol + Co-antioxidant during the RapidOxy® test

Co-AH <sub>2</sub>	Induction Period IP <sup>a</sup> (min)	Std. Dev. (min)	Induction Period Additivity (min) <sup>b</sup>	Synergistic effect (%) <sup>c</sup>
Control	5	1	/	/
4	250	1	170	47
5	176	2	172	2
6	220	4	199	11
7	172	2	154	12
8	168	12	111	51
9	106	2	117	-9
15	278	3	178	57
16	111	3	114	-3
17	88	3	107	-18
20	86	3	91	-5
21	88	2	92	-5
23	241	5	220	10
24	190	2	163	17
25	162	3	158	3
26	96	2	116	-17
27	95	5	103	-8
32	341	3	220	55
34	175	1	156	12
55	495	13	327	52
59	112	3	122	-8
60	103	2	113	-9
61	96	4	102	-6
62	186	5	175	7
63	170	3	162	5
65	168	7	169	-1
67	157	1	145	9
69	178	2	172	4
70	255	5	204	25
71	100	1	91	9

<sup>a</sup>Average of three values, <sup>b</sup>IP<sub>add</sub> = (IP <sub>$\alpha$ -tocopherol</sub> + IP<sub>COAH<sub>2</sub></sub>) / 2, <sup>c</sup>%Syn = 100 x ((IP<sub>mix</sub> - IP<sub>add</sub>) / 2)

[ $\alpha$ -tocopherol]<sub>0</sub> + [CoAH<sub>2</sub>]<sub>0</sub> = 0.25 mM + 0.25 mM = 0.5 mM, 2 mL of FAMES of linseed oil

P = 450 kPa, T = 90°C

**Table S4.5: Induction periods (IP) obtained during the RapidOxy® test for the inhibition of FAMES linseed oil oxidation by equimolar mixture of  $\alpha$ -tocopherol + co-antioxidant**

### 3.5 Induction periods (IP) for the preservation of FAMES of linseed oil against oxidation by different ratios of $\alpha$ -tocopherol + Co-antioxidants during the RapidOxy® test

Phenols	$[\alpha\text{-tocopherol}]_0$ (mM)	$[\text{Co-antioxidant}]_0$ (mM)	Ratio <sup>a</sup>	Induction Period <sup>b</sup> (min)	Std. dev. (min)
/	0.50	/	0	176	4
		0.10	0.2	227	7
4	0.50	0.25	0.5	290	10
		0.50	1.0	389	11
		1.00	2.0	527	7
		0.10	0.2	196	5
5	0.50	0.25	0.5	226	13
		0.50	1.0	269	8
		0.10	2.0	372	8
		0.10	0.2	216	6
6	0.50	0.25	0.5	269	5
		0.50	1.0	352	7
		1.00	2.0	512	9
		0.10	0.2	204	6
7	0.50	0.25	0.5	233	4
		0.50	1.0	286	5
		1.00	2.0	370	5
		0.10	0.2	213	13
8	0.50	0.25	0.5	273	9
		0.50	1.0	347	10
		1.00	2.0	464	4
		0.10	0.2	183	3
9	0.50	0.20	0.4	189	3
		0.30	0.6	195	3
		0.40	0.8	198	3
		0.10	0.2	225	5
15	0.50	0.25	0.5	307	10
		0.50	1.0	397	6
		1.00	2.0	572	13
		0.10	0.2	181	2
17	0.50	0.20	0.4	185	4
		0.30	0.6	189	7
		0.40	0.8	197	3
		0.10	0.2	176	2
21	0.50	0.20	0.4	177	3
		0.30	0.6	177	5
		0.40	0.8	177	5
		0.10	0.2	188	8
23	0.50	0.25	0.5	230	6
		0.50	1.0	303	7
		1.00	2.0	444	11
		0.10	0.2	190	5
24	0.50	0.25	0.5	210	4
		0.50	1.0	238	7
		1.00	2.0	283	9

Phenols	[ $\alpha$ -tocopherol] <sub>0</sub> (mM)	[Co-antioxidant] <sub>0</sub> (mM)	Ratio <sup>a</sup>	Induction Period <sup>b</sup> (min)	Std. dev. (min)
<b>25</b>	0.50	0.10	0.2	192	4
		0.20	0.4	217	7
		0.30	0.6	226	3
		0.40	0.8	247	4
<b>26</b>	0.50	0.10	0.2	182	2
		0.20	0.4	190	4
		0.30	0.6	196	3
		0.40	0.8	200	3
<b>27</b>	0.50	0.10	0.2	180	6
		0.20	0.4	183	6
		0.30	0.6	185	3
		0.40	0.8	188	4
<b>32</b>	0.50	0.10	0.2	257	10
		0.25	0.5	371	9
		0.50	1	519	16
<b>34</b>	0.50	0.10	0.2	183	6
		0.25	0.5	200	7
		0.50	1.0	226	6
		1.00	2.0	285	6
<b>55</b>	0.50	0.10	0.2	351	12
		0.20	0.4	479	8
		0.30	0.6	586	10
		0.40	0.8	684	9
<b>59</b>	0.50	0.10	0.2	179	3
		0.20	0.4	186	2
		0.30	0.6	191	5
		0.40	0.8	198	3
<b>60</b>	0.50	0.10	0.2	179	4
		0.20	0.4	184	3
		0.30	0.6	187	3
		0.40	0.8	188	4
<b>61</b>	0.50	0.10	0.2	178	3
		0.20	0.4	179	3
		0.30	0.6	182	3
		0.40	0.8	182	6
<b>62</b>	0.50	0.10	0.2	207	5
		0.25	0.5	259	5
		0.50	1.0	329	8
		1.00	2.0	476	11
<b>63</b>	0.50	0.10	0.2	183	10
		0.25	0.5	207	6
		0.50	1.0	242	14
		0.10	2.0	312	8
<b>65</b>	0.50	0.10	0.2	199	5
		0.25	0.5	213	7
		0.50	1.0	253	14
		0.10	2.0	314	14

Phenols	[ $\alpha$ -tocopherol] <sub>0</sub> (mM)	[Co-antioxidant] <sub>0</sub> (mM)	Ratio <sup>a</sup>	Induction Period <sup>b</sup> (min)	Std. dev. (min)
67	0.50	0.10	0.2	187	4
		0.20	0.4	206	4
		0.30	0.8	215	4
		0.40	0.8	224	3
69	0.50	0.10	0.20	188	5
		0.25	0.5	206	5
		0.50	1.0	237	6
70	0.50	0.10	0.2	234	8
		0.25	0.5	306	5
		0.50	1.0	391	11
71	0.50	0.10	0.2	176	1
		0.25	0.5	178	3
		0.50	1.0	180	2
		0.10	2.0	183	3

<sup>a</sup>Ratio = [Co-antioxidant]<sub>0</sub> / [ $\alpha$ -tocopherol]<sub>0</sub>, <sup>b</sup>Average of three values, 2 mL of FAMES of linseed oil

P = 450 kPa, T = 90 °C

**Table S4.6:** Induction periods (IP) obtained during the RapidOxy<sup>®</sup> test for the inhibition of FAMES of linseed oil oxidation by different concentration ratios of  $\alpha$ -tocopherol + co-antioxidant

### 3.6 Induction periods (IP) for the preservation of FAMES of linseed oil, triglyceride of linseed oil and triglyceride of fish oil against oxidation during the RapidOxy<sup>®</sup> test

Co-AH <sub>2</sub>	FAMES linseed oil		Triglyceride Linseed oil		Triglyceride Fish oil	
	IP <sup>a</sup> (min)	Std. Dev. (min)	IP <sup>a</sup> (min)	Std. Dev. (min)	IP <sup>a</sup> (min)	Std. Dev. (min)
Control	5	1	5	/	0	/
8	168	12	194	4	105	2
15	278	3	279	6	119	4
23	241	5	224	6	100	4
32	341	3	362	8	150	9
70	255	5	238	10	109	3

<sup>a</sup>Average of three values, [ $\alpha$ -tocopherol]<sub>0</sub> + [CoAH<sub>2</sub>]<sub>0</sub> = 0.25 mM + 0.25 mM = 0.5 mM

2 mL of FAMES of linseed oil, P = 450 kPa, T = 90 °C

**Table S4.7:** Induction periods (IP) obtained during the RapidOxy<sup>®</sup> test for the inhibition of FAMES of linseed oil, triglyceride of linseed oil and triglyceride of fish oil oxidation by equimolar mixture of  $\alpha$ -tocopherol + co-antioxidant

### 3.7 Induction periods (IP) for the inhibition of FAMES of linseed oil against oxidation by equimolar mixture of $\alpha$ -tocopherol + co-antioxidants during the RapidOxy<sup>®</sup> test

Phenols	Induction Period IP (min) <sup>a</sup>	Std. Dev. (min)	Induction Period Additivity (min) <sup>b</sup>	Synergistic effect (%) <sup>c</sup>
24 + 70	213	6	189	13 %
24 + 62	210	6	160	31 %
62 + 70	273	9	201	36 %
32 + 24	235	13	205	14 %
32 + 70	255	9	246	4 %

Phenols	Induction Period IP (min) <sup>a</sup>	Std. Dev. (min)	Induction Period Additivity (min) <sup>b</sup>	Synergistic effect (%) <sup>c</sup>
<b>32 + 62</b>	317	23	217	46 %
<b>32 + 23</b>	344	9	262	31 %
<b>34 + 24</b>	159	4	142	12 %
<b>34 + 70</b>	238	10	183	30 %
<b>34 + 62</b>	207	3	154	34 %
<b>32 + 34</b>	237	11	199	19 %
<b>34 + 23</b>	212	3	199	7 %
<b>23 + 24</b>	222	12	205	8 %
<b>23 + 70</b>	327	9	246	33 %
<b>23 + 62</b>	284	7	217	31 %

<sup>a</sup>Average of three values, <sup>b</sup> $IP_{add} = (IP_{phenol} + IP_{COAH_2}) / 2$ , <sup>c</sup> $\%Syn = 100 \times ((IP_{mix} - IP_{add}) / 2)$

$[phenol]_0 + [CoAH_2]_0 = 0.25 \text{ mM} + 0.25 \text{ mM} = 0.5 \text{ mM}$ , 2 mL of FAMEs of linseed oil, P = 450 kPa, T = 90°C

**Table S4.8: Induction periods (IP) obtained during the RapidOxy® test for the inhibition of FAMEs of linseed oil oxidation by equimolar mixture of various natural phenolic antioxidants (Myr = myricetin 32, RosA = rosmarinic acid 23, CarA = carnosic acid 70, Quer = Quercetin 34, HyTy = Hydroxytyrosol 62 and CafA = caffeic acid 24)**



# GENERAL CONCLUSIONS AND PROSPECTS

---

Omega-3 fatty acids capture the attention of scientists and studies have been multiplied in recent decades, highlighting their virtues and indispensable role to the body. The intake of omega-3 fatty acids leads to a significant decrease of heart attack and cardiovascular death.<sup>14</sup> Moreover, these essential nutrients reduce mortality, the risk of some cancers and mental illness such as depression, bipolar disorder, stress or Alzheimer's disease (**Fig. C.1**).<sup>21</sup> Eicosapentaenoic acid (20:5, EPA), docosahexaenoic acid (22:6, DHA) and alpha-linolenic acid (18:3, ALA) are essential omega-3 primarily found in some fish and vegetable oils. Nevertheless, given their chemical structures rich in double bonds and bis-allylic hydrogens, they are particularly sensitive to oxygen and are therefore subject to oxidative degradation leading to a deterioration of their organoleptic and nutraceutical properties.

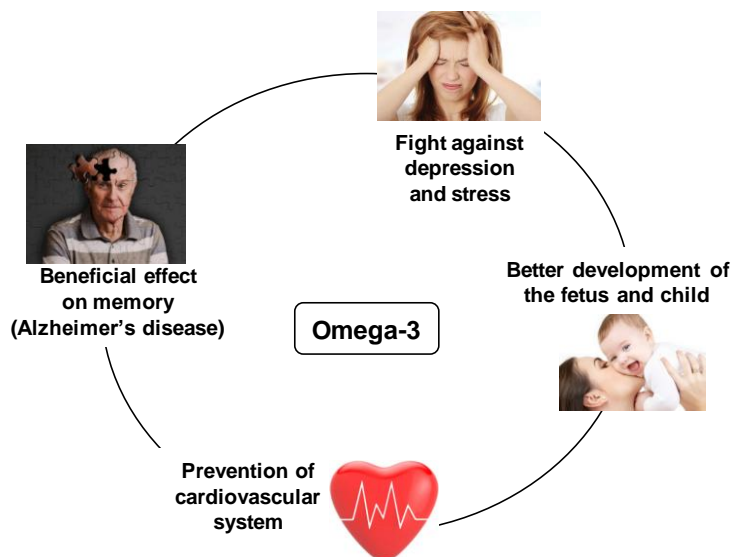


Figure C.1: Main virtues of omega-3 fatty acids<sup>24-27</sup>

- *Analytical challenge: selective analysis of traces of thermo-sensitive lipid hydroperoxides*

As regards to the complex mechanisms involved in the degradation of polyunsaturated fatty acids, it is of the utmost importance to have a method able to detect primary oxidation products generated during the first steps of the oxidation process. Nevertheless, direct detection of hydroperoxides by GC is tricky because of their thermal sensitivity and low concentration in oils. While there is a large number of analytical techniques for peroxidized species after pre-derivatization<sup>43</sup>, there are few methods for detecting hydroperoxides themselves.<sup>44, 236</sup> Consequently, it is still a major challenge to develop an analytical method for this type of compounds present as traces in oxidized oils.

A series of hydroperoxides and cyclic peroxides have been prepared at low temperature (5 °C) through the singlet oxygenation with  $^1\text{O}_2$  of terpenes, terpenoids and FAMEs. Compared to autoxidation with triplet oxygen ( $^3\text{O}_2$ ) which requires a higher temperature ( $\approx 60$  °C), this soft photochemical method allows obtaining hydroperoxides free of secondary products (**Fig. C.2**).

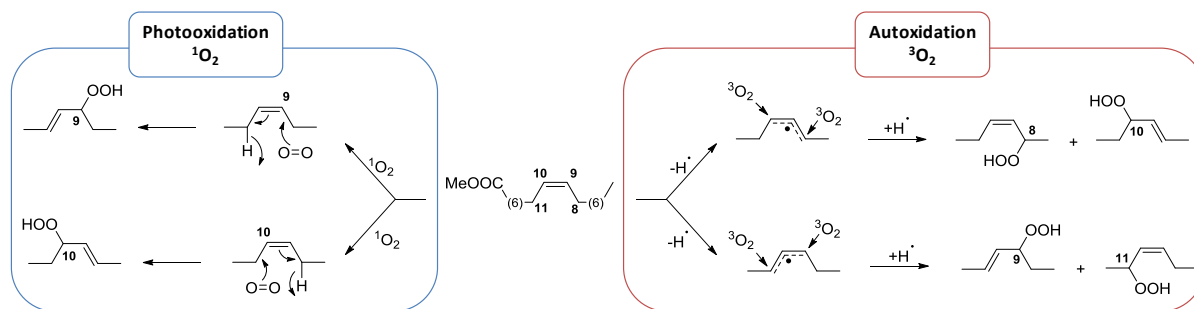


Figure C.2: Autoxidation and photooxidation mechanisms of oleic acid and formation of different hydroperoxides isomers<sup>36</sup>

The reactivity of tri-substituted olefins (*i.e.* terpenoids such as geraniol caprate and citronellol caprate) towards  $^1\text{O}_2$  is found, as expected, to be higher than that of di-substituted olefins (*i.e.* FAMES such as methyl oleate, linoleate and linolenate). The LC-UV analytical method is not able to distinguish the different regioisomers of hydroperoxides and peroxides. Moreover, this technique does not lead to a chemical structure elucidation of detected molecules. NMR is the most relevant method to perform the structural analysis of molecular compounds. Nevertheless, as is poorly sensitive, it cannot characterize traces of oxidized compounds into a complex oxidized mixture.

Mass spectrometry was found to be the most suitable technique to elucidate the composition of poorly stable hydroperoxides and peroxides mixtures. ElectroSpray ionization (ESI) with monovalent ions ( $\text{H}^+$ ,  $\text{Li}^+$ ,  $\text{Na}^+$ ,  $\text{K}^+$  and  $\text{Cs}^+$ ) and Coordination IonSpray (CIS) with  $\text{Ag}^+$  show very different ionization rate for the starting substrates and their corresponding hydroperoxides (Fig. C.3).

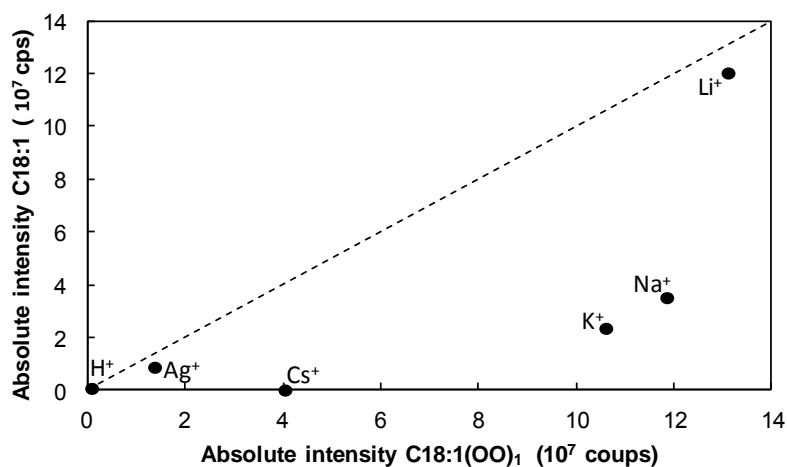


Figure C.3: Absolute intensity of the peaks observed through ionization of an equimolar mixture of  $\text{C18:1(OO)}_1$  and  $\text{C18:1}$  ( $[\text{C18:1(OO)}_1] = [\text{C18:1}] = 10^{-6} \text{ M}$ ) in the presence of  $\text{H}^+$ ,  $\text{Ag}^+$ ,  $\text{Li}^+$ ,  $\text{Na}^+$ ,  $\text{K}^+$  and  $\text{Cs}^+$  acetates ( $[\text{ion}] = 10^{-4} \text{ mol.L}^{-1}$ ) during Direct Liquid Injection (DLI) ESI-MS in ion-positive mode (ES+) (solvent:  $\text{H}_2\text{O/MeOH}$  50/50 v:v)

Alkali metal ions show a gradual decline in affinity with hydroperoxides and FAMES which increasing size of the alkali cation. Commonly used cations (*i.e.*  $\text{H}^+$ ,  $\text{Li}^+$ ,  $\text{Na}^+$ ,  $\text{K}^+$  and  $\text{Ag}^+$ ) are not the most effective ions for the selective ionization of hydroperoxides. Indeed,  $\text{H}^+$  is not efficient to induce the ionization of  $\text{C18:1}$  and  $\text{C18:1(OO)}_1$  whereas  $\text{Li}^+$  and  $\text{Ag}^+$  enhance the ionization of both compounds.  $\text{Na}^+$  and  $\text{K}^+$  have more affinity with  $\text{C18:1(OO)}_1$  but they still ionize  $\text{C18:1}$ . In addition, these ions have other drawbacks. Due to their light mass, they give adducts with low  $m/z$  (*i.e.* terpenes  $\text{MW} \approx 160 \text{ g.mol}^{-1}$ ) and related MS peaks are in the background where a lot of low molecular weight compounds contaminate the mass spectrum. Moreover, due to their high coordination affinity with ROOH, there is a decomposition of adducts into cation coordinated hydroperoxide fragments (*i.e.* epoxide, alcohol and aldehyde) leading to a decrease of the mass signal of intact ROOH.

Cesium cation ( $\text{Cs}^+$ ) is shown to be the most effective monovalent ion for the selective ionization of hydroperoxides. Indeed, it does not ionize non-oxidized substrates whereas it binds to allylic hydroperoxides. Moreover,  $\text{Cs}^+$  cumulates several advantages: (i) it avoids the overlap of peaks obtained with the two isotopes of  $\text{Ag}^+$ , (ii) it shifts the molecular mass of peroxides adducts out of the background and, (iii) it significantly limits the fragmentation of hydroperoxides into epoxide, alcohol and aldehydes. With this ESI-MS technique involving  $\text{Cs}^+$  as cation, a specific detection into a FAME matrix discriminating hydroperoxides at the nanomole level is possible. LC-MS/MS is the most selective and sensitive method to separate and elucidate the chemical structures of complex peroxides mixtures with post-column injection of ions by following the characteristic transitions related to the fragmentation from parent to daughters.

We expanded the scope of the ESI-MS method with  $\text{Cs}^+$  to a large range of hydroperoxides including derivatives of terpenoids, FAMES, triglycerides, compounds with biological importance and various common organic peroxides (Fig. C.4).

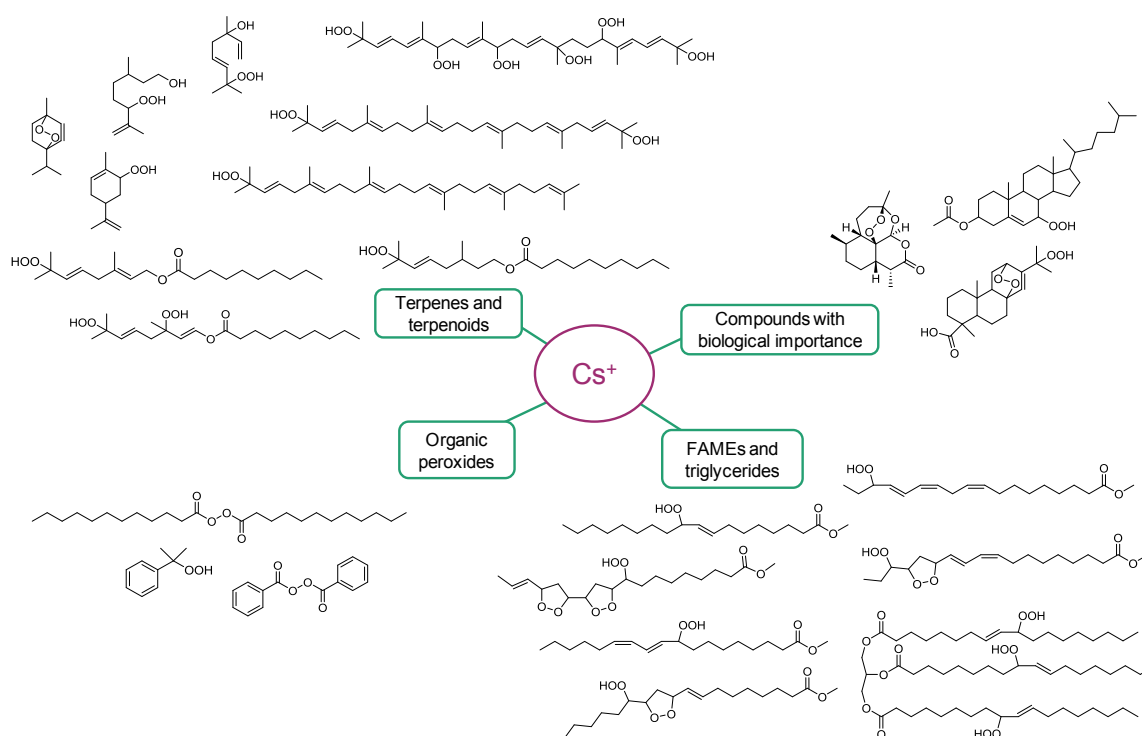
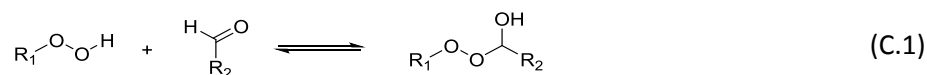


Figure C.4: Selection of compounds that can be detected by ESI-MS with  $\text{Cs}^+$

Finally, the detection of fatty peroxyhemiacetals could be a new crucial analysis of food. Indeed, we showed, for the first time, that they can be formed through the reaction of fatty hydroperoxides and endogenous aldehydes as revealed very recently for fragrances (Eq. C.1).<sup>248</sup>



Further examination of the influence of peroxyhemiacetal in food (stability, organoleptic properties and physiological effects) is required since it could have a positive effect through the decrease of the hydroperoxide content and the delay of the oxidation process. Conversely, peroxyhemiacetal could extend undesirable effects of hydroperoxides since they could act as a reservoir for this radical initiator.

- *Antioxidant challenge: structure-activity relationships and protection of omega-3 oils*

In order to prevent oxidative degradation, antioxidants are commonly introduced into oils. Synthetic phenolic antioxidants such as butylated hydroxytoluene (BHT) and butylated hydroxyanisole (BHA) are widely used but, due to an increased safety concern from the consumer side, there is a strong push to replace them by natural alternatives. In this context, we focused on natural phenolic antioxidants for the protection of omega-3 oils. Nevertheless, theoretical methods or experimental investigations are rarely combined and always made on a limited number of antioxidants. Therefore, based on literature, it is difficult to compare the effects of a large range of natural phenolic antioxidants on the protection of the same substrate and highlight the required conditions to optimize the inhibition of oxidation. Consequently, CARGILL funded this PhD thesis in order to develop structure-activity relationships and highlight the best natural antioxidants for the protection of edible oils rich in omega-3. Thermodynamic investigations through molecular modeling (BDE, IP), kinetic studies ( $k$ ) and stoichiometric calculations ( $\sigma_{\text{exp}}$ ) *via* the DPPH<sup>•</sup> test and measurement of oxygen uptake during the oxidation of oil with O<sub>2</sub> (RapidOxy<sup>®</sup>, Rancimat) were undertaken.

On one hand, the theoretical approach of molecular modeling was used to determine the Bond Dissociation Enthalpies of ArO-H bonds (BDE) with quantum computation (DFT) in different environments. The aim was to classify all the studied phenols according to their BDEs and build a thermodynamic database necessary for mechanistic interpretations. The BDE computation brings some quantitative information on the impact of the nature of substituents and their positions on the phenolic ring. We highlighted that electron-donating substituents, EDG (alkyl, methoxy, and hydroxyl) decreases BDEs whereas electron-withdrawing group, EWG (carboxylic acid, ester and aldehyde) increases BDEs. Moreover, the *meta*- position has a much smaller impact on BDEs compared to *ortho*- and *para*- positions. Finally, based on the BDEs of 70 phenols, a scale of predictive reactivity towards mobile phenolic hydrogens has been established by ranking the compounds from the lowest to the highest BDEs and dividing them into four groups (**Figure C.5**). The group of phenols with the lowest BDEs is expected to contain the most effective antioxidants.

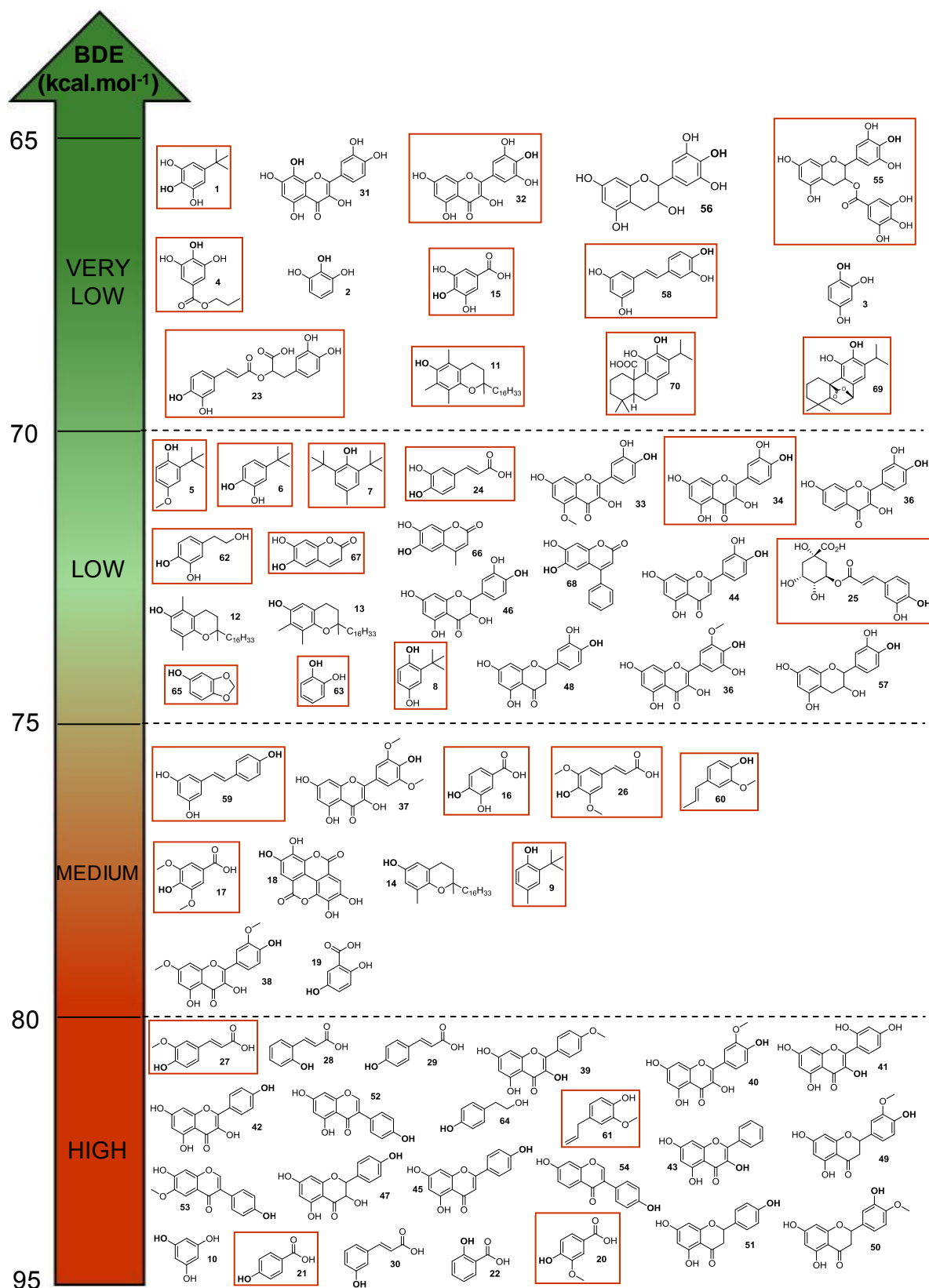


Figure C.5: Scale of reactivity of 70 phenolic antioxidants as a function of their calculated BDE in vacuum, framed molecules correspond to selected antioxidants further studied experimentally

On the other hand, scientists pointed out that a high value of ionization potential (IP) disadvantages the electron transfer from phenols to oxygen leading to the decrease of their pro-oxidant potential.<sup>298, 299</sup> Therefore, ionization potentials of phenolic antioxidants were calculated by

molecular modeling and we pointed out the impressive linear correlations between BDEs and IPs for various families of phenols (Fig. C.6). In all four series, the drop in the IPs accompanies a drop in BDEs. This is unfavorable for the antioxidant effectiveness but IPs are sufficiently high to allow a reasonable air-stability and reduce the pro-oxidant potential of antioxidants. Consequently, the most promising phenols are in the framed zone which combines relatively low BDEs and high IPs.

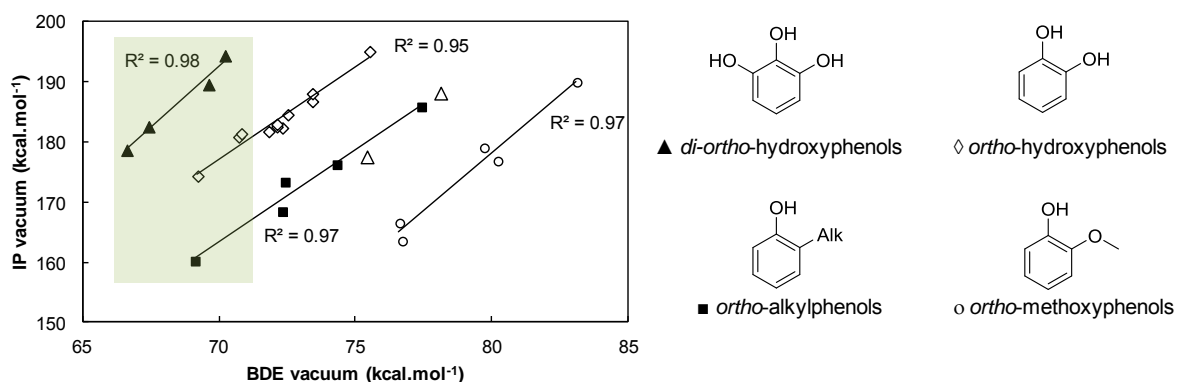


Figure C.6: Correlations between IPs and BDEs of phenols

Furthermore, to investigate the kinetics and the stoichiometric numbers of the hydrogen transfer  $H^\bullet$  from antioxidants to peroxy radicals  $ROO^\bullet$ , we mimicked this key reaction by using a stable radical called DPPH $^\bullet$ . It is generally accepted that the reaction of DPPH $^\bullet$  with phenols has good predictive power with respect to their antioxidant properties. The radical HAT mechanism implies the hydrogen transfer from phenols to peroxy radicals  $ROO^\bullet$  and predominates in food free from water. It is shown that the corresponding kinetic rate constants ( $k$ ) are strongly correlated to the BDEs (Fig. C.7). The phenols with the highest  $k$  (framed zone) are expected to be most reactive antioxidants in non-aqueous media.

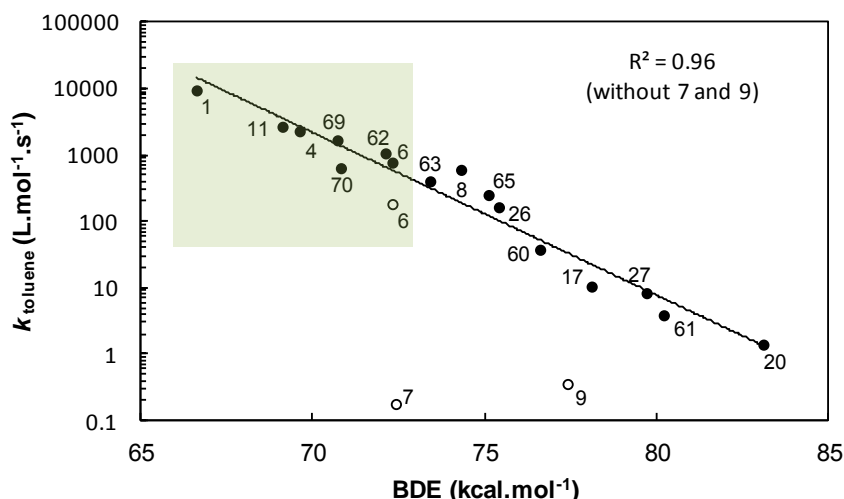


Figure C.7: Logarithm of the rate constants ( $\log k$ ) for the reaction of phenolic antioxidants with DPPH $^\bullet$  (○ hindered phenols and ● other phenols) in toluene vs their BDEs calculated with the DFT method in vacuum

Phenolic antioxidants were also characterized by the maximum number of radicals trapped by each antioxidant molecule ( $\sigma_{\text{exp}}$ ). The determination of the number of hydrogen radicals trapped by DPPH $^\bullet$  followed by the mass spectrometry analysis of the final medium provides crucial information on the mechanism and on the chemical structure of degradation products formed from antioxidants. The mechanism of interaction between DPPH $^\bullet$  and phenols takes place in two steps: **1**) abstraction of

the phenolic hydrogen and **2)** transfer of a second hydrogen from the phenoxyl radical  $\text{ArO}^\bullet$  or formation of dimers. The antioxidants with the highest  $\sigma_{\text{exp}}$  are expected to have good antioxidant power.

Finally, the global approach deals with the efficiency of antioxidants during the preservation of FAMES of linseed oil. Antioxidants react with lipid peroxy radicals  $\text{LOO}^\bullet$  before they react with other lipid molecules to produce further free radicals. The autoxidation of omega-3 FAMES in the presence of the different phenols has been kinetically investigated by measuring the oxygen consumption using the RapidOxy<sup>®</sup> apparatus which provides information on induction periods (IP) and oxidation rates ( $R_{\text{ox}}$ ). An exponential correlation is found between these two important parameters. Extended induction periods characterize effective phenolic antioxidants. Moreover, phenols are powerful antioxidants when the oxidation rate  $R_{\text{ox}}$  is low which means that they quickly inhibit peroxy radicals and reduce the consumption of oxygen (**Fig. C.8**).

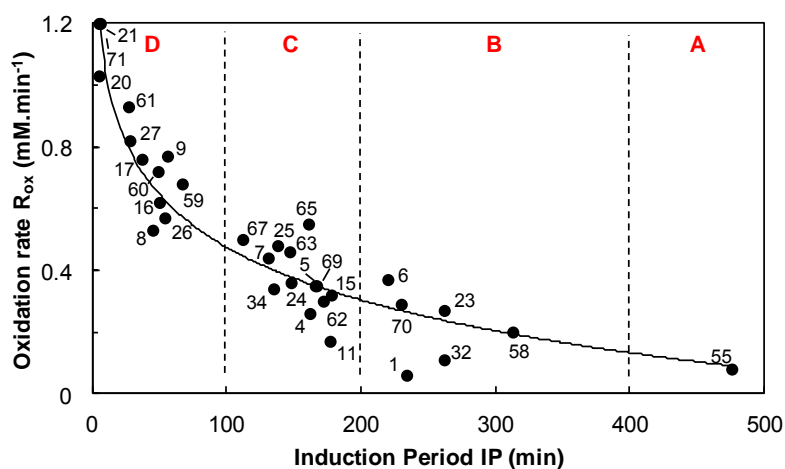
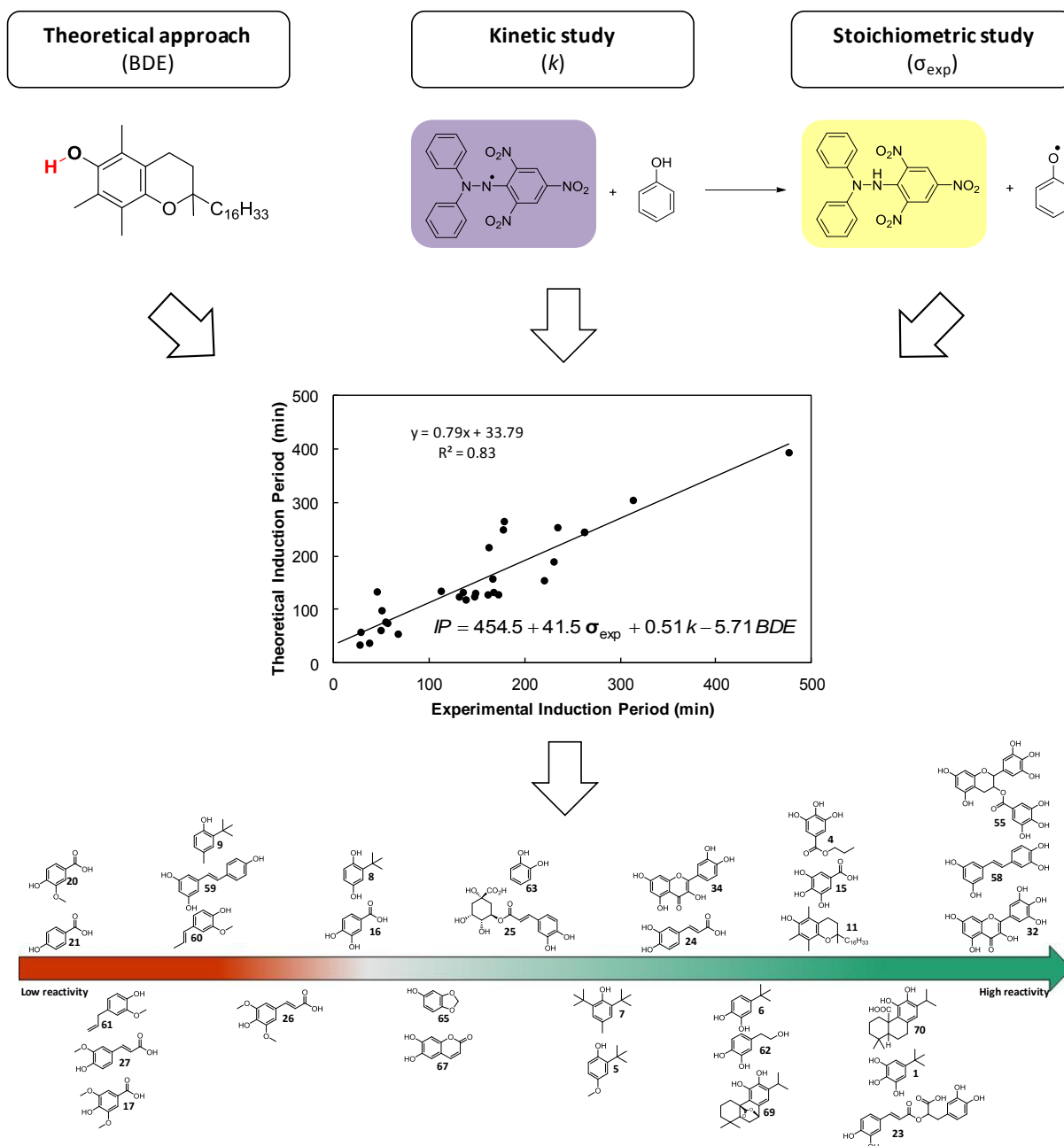


Figure C.8: Oxidation rate ( $R_{\text{ox}}$ ) vs Induction Period (IP) for the preservation of FAMES of linseed oil against oxidation

Surprisingly, the efficiency of phenolic antioxidants for the preservation of FAMES of linseed oil against oxidation is predicted by the use of thermodynamic (BDE), kinetic ( $k$ ) and stoichiometric ( $\sigma_{\text{exp}}$ ) parameters (**Fig. C.9**). *Tri*-hydroxyphenols are found to be more reactive than *di*-hydroxyphenols which are in turn more effective than monophenols. Natural phenols, *i.e.* rosmarinic acid **23**, myricetin **32**, epigallocatechin gallate **55**, piceatannol **58** and carnosic acid **70** are the best natural alternatives to  $\alpha$ -tocopherol **11** and synthetic antioxidants for the protection of edible oil rich in omega-3 from oxidation and sustain their physiological benefits.



**Figure C.9: Structures/properties relationships on phenolic antioxidants and prediction of the induction periods obtained during the protection of  $\omega$ -3 oils against oxygen by kinetic rate constants ( $k$ ), stoichiometric numbers (DPPH<sup>•</sup> test) and calculated BDEs.**

By bringing together all these findings, one can give the structural requirements for obtaining effective antioxidants for the protection of omega-3 oils: **1)** catechol or pyrogallol substructure, **2)** conjugated with a *para*-electron-donating group (EDG) and **3)** free *ortho* position. Actually, all phenolic antioxidants having those structural features exhibit *i)* very low BDEs, *ii)* high ionization potentials (IPs), *iii)* high kinetic rate constant of hydrogen transfer ( $k$ ) and *iv)* high number of radicals trapped by molecule of phenols ( $\sigma_{\text{exp}}$ ) through the formation of active dimers.

▪ *Synergy between antioxidants*

Whatever the antioxidant selected, it is advantageous to minimize its concentration while maintaining its effectiveness. However, scientists observed sometimes, without clear explanation, synergistic or antagonistic effects between antioxidants. From this point of view, one of the main goals of this PhD was to shed some light on the mechanism of synergies observed with some couples antioxidant/co-antioxidant since it is a potential profitable method to improve the preservation of oils. Therefore, the final challenge of this thesis was to highlight the required conditions for obtaining synergistic mixtures.

The initial reaction rates ( $V_i$ ) between mixtures of antioxidants composed by  $\alpha$ -tocopherol and co-phenolic antioxidants with  $\text{DPPH}^\bullet$  have been investigated. The radical HAT mechanism is always the driving force for the protection of oils thanks to the homolytic cleavage of the phenolic OH bond. The Bond Dissociation Enthalpy (BDE) of this bond (ArO-H) is the critical parameter governing the synergies (**Fig. C.10**). More precisely, a  $\Delta\text{BDE}$  variation of  $5.4 \text{ kcal.mol}^{-1}$  from co-antioxidants to  $\alpha$ -tocopherol allows the regeneration of the primary antioxidant. Conversely, higher  $\Delta\text{BDE}$  leads to additive profiles.

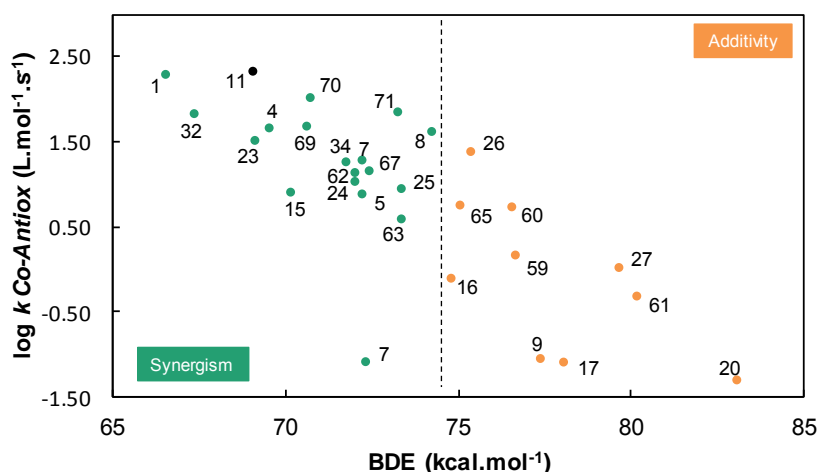


**Figure C.10:** Kinetic rate constants of hydrogen transfer ( $\log k_{\text{Co-Antiox}}$ ) obtained in ethyl acetate vs  $\text{BDE}_{\text{Co-Antiox}}$  calculated in vacuum by the DFT B3LYP/6-311++G(2d,2p)//B3LYP/6-311G(d,p) method, green (●) and orange (●) dots illustrate respectively co-antioxidants capable to regenerate  $\alpha$ -tocopherol 11 (synergism and super synergism) or not (additivity) respectively

Mechanisms of interactions have been proposed and discussed in terms of molecular structure of the co-antioxidants. Catechol and hydroquinone derivatives have stronger co-antioxidant properties compared to monophenols. This result may be explained by the easy transfer of a second phenolic hydrogen from the *ortho*- or *para*-semiquinone radicals to  $\text{DPPH}^\bullet$  or  $\text{ROO}^\bullet$  giving the *ortho*- or *para*-quinone derivatives.

Surprisingly, the same BDE threshold is found with the RapidOxy<sup>®</sup> measurements ( $\Delta\text{BDE} = 5.4 \text{ kcal.mol}^{-1}$ ) (**Fig. C.11**). Pyrogallol derivatives are more efficient in the regeneration of  $\alpha$ -tocopherol than catechol compounds which are themselves more active than monophenols. Gallic acid **15** and propyl gallate **4**, which are the co-antioxidants with the closest BDE to that of  $\alpha$ -tocopherol **11**, lead to the best synergistic effects. Other natural mixtures of antioxidants have been studied and the best synergistic effects are obtained for the combinations of two natural phenolic antioxidants with the lowest  $\Delta\text{BDE}$ .

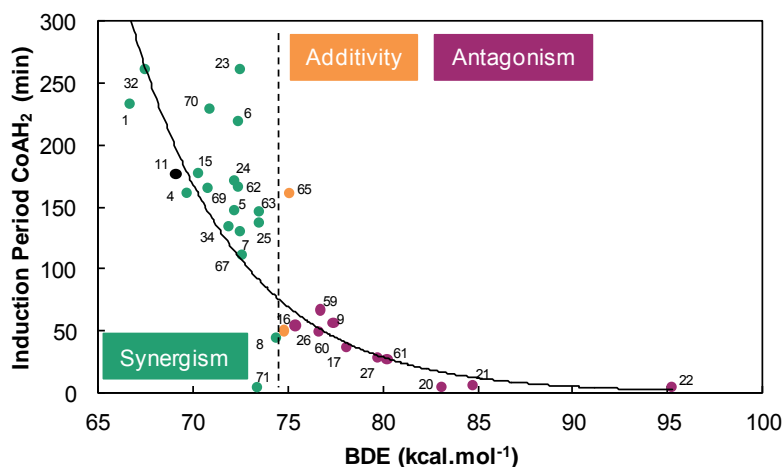


Figure C.11: Induction periods of co-antioxidants ( $IP_{CoAH_2}$ ) vs their respective BDEs, green (•), orange (•) and red (•) dots illustrate phenols capable to regenerate  $\alpha$ -tocopherol 11 (super synergism and synergism) or not (additivity and antagonism) respectively

The influence of the main thermodynamic and kinetic parameters on the synergies between the two antioxidants is summarized in **figure C.12**.

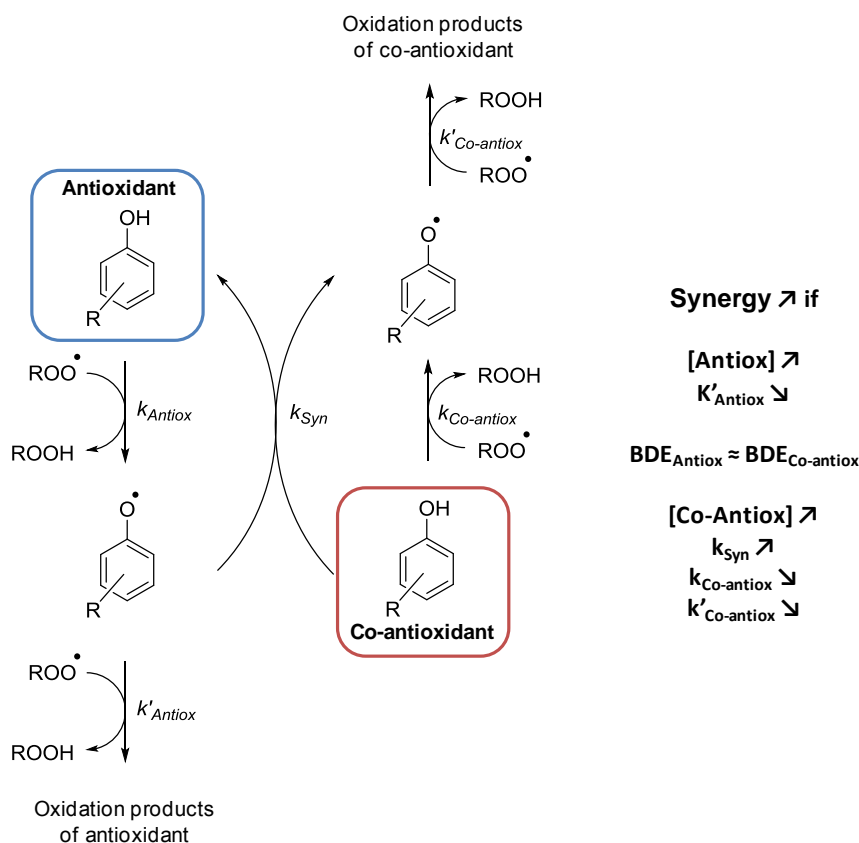


Figure C.12: Simplified scheme for the synergistic interaction between the primary antioxidant and co-antioxidants, synergies are influenced by kinetic, concentration and BDE parameters

The study of the solvent effect on synergies showed that the co-antioxidant mechanisms are complex and cannot be transposed to another matrix. The  $\alpha$ -tocopherol/co-antioxidants synergies highlighted in oils disappear when the polarity of the medium increases because new transient species appear (*i.e.* tocopheroxylum cation) and change the kinetics and mechanisms of reaction.

- *Prospects and new challenges*

This work shows the difficulties to selectively detect low peroxide content (< 1 %). LC-MS/MS is the most selective and sensitive method to separate and identify complex mixtures of non-degraded hydroperoxides. The method developed herein is based on the oxidized FAMES whereas oils are composed by triglycerides. Therefore, our method must be extended to oxidized oil systems. Moreover, as the detection of fatty acid peroxyhemiacetals could be a new crucial investigation in food, further studies on their effects on the stability of oils should be undertaken.

This work points out the extreme complexity of the mechanisms of reaction of antioxidants and combination of phenols. The scale of predictive reactivity established on BDEs could be extended to other phenolic antioxidants as there are numerous phenols in nature. Moreover, based on the requirements pointed out for the chemical structures of efficient antioxidants, the synthesis of new promising phenolic antioxidants deserves to be undertaken. Then, antioxidants and combinations of phenols must be tested under more realistic conditions of oxidation (atmospheric pressure, room temperature and under stirring) into an oil system to improve the relevance of our predictions. As metals play a crucial role in the triggering of the oxidation process, new associations of phenolic antioxidants combined with metal chelators could be tested during the protection of omega-3 oils. It may also be finally interesting to investigate the effects of phenols and combination of antioxidants into emulsified systems which are often the end-products delivered to consumers.

# REFERENCES

---

1. Poulnois, C. La grande histoire des Oméga-3.  
<http://fr.calameo.com/books/000358701e891443defe9>
2. Burr, G. O.; Burr, M. M., A new deficiency disease produced by the rigid exclusion of fat from the diet. *The Journal of Biological Chemistry* **1929**, *82*, 345-67.
3. Burr, G. O.; Burr, M. M., The nature and role of the fatty acids essential in nutrition. *The Journal of Biological Chemistry* **1930**, *86*, 587-621.
4. Sinclair, H. M., Deficiency of essential fatty acids and atherosclerosis, etcetera. *Lancet* **1956**, *270*, 381-3.
5. Dyerberg, J.; Bang, H. O.; Hjoerne, N., Fatty acid composition of the plasma lipids in Greenland Eskimos. *The American Journal of Clinical Nutrition* **1975**, *28*, 958-66.
6. Burr, M. L., Lessons from the story of n-3 fatty acids. *Am. J. Clin. Nutr.* **2000**, *71*, 397S-398S.
7. Kafatos, A. G., *Diet, antioxidants, and health - case study: the Cretan experience*. CRC1999; p 119-129.
8. Hirai, A.; Hamazaki, T.; Terano, T.; Nishikawa, T.; Tamura, Y.; Kumagai, A.; Sajiki, J., Eicosapentaenoic acid and platelet function in Japanese. *Lancet* **1980**, *2*, 1132-3.
9. Bergstrom, S.; Samuelsson, B., Prostaglandins. *Endeavour* **1968**, *27*, 109-13.
10. Hamberg, M.; Samuelsson, B., Mechanism of the biosynthesis of prostaglandins E1 and F1 $\alpha$ . *J. Biol. Chem.* **1967**, *242*, 5336-43.
11. Vane, J. R.; Sinzinger, H.; Samuelsson, B.; Paoletti, R.; Ramwell, P.; Wong, P. Y. K.; Editors, *Recent Advances in Prostaglandin, Thromboxane, and Leukotriene Research*. . Plenum1997; p 454 pp.
12. NobelMedia, The Nobel Prize in Physiology or Medicine 1982. *Nobelprize.org* **2014**.
13. Lorgèril, M.; Salen, P.; Martin, J. L.; Monjaud, I.; Delaye, J.; Mamelle, N., Mediterranean diet, traditional risk factors, and the rate of cardiovascular complications after myocardial infarction: final report of the Lyon Diet Heart Study. *Circulation* **1999**, *99*, 779-85.
14. Lorgèril, M.; Salen, P., Dietary prevention of coronary heart disease: the Lyon diet heart study and after. *World Rev. Nutr. Diet.* **2005**, *95*, 103-114.
15. Kryzhanovskii, S. A.; Vititnova, M. B.,  $\omega$ -3 polyunsaturated fatty acids and the cardiovascular system. *Hum Physiol* **2009**, *35*, 491-501.
16. Von Schacky, C.; Harris, W. S., Cardiovascular benefits of omega-3 fatty acids. *Cardiovascular Research* **2007**, *73*, 310-315.
17. Heinrichs, S. C., Dietary omega-3 fatty acid supplementation for optimizing neuronal structure and function. *Molecular Nutrition & Food Research* **2010**, *54*, 447-56.
18. Hibbelm, J. R., Depression, suicide and deficiencies of omega-3 essential fatty acids in modern diets. *World Review of Nutrition and Dietetics* **2009**, *99*, 17-30.
19. Balanza-Martinez, V.; Fries, G. R.; Colpo, G. D.; Silveira, P. P.; Portella, A. K.; Tabarees-Seisdedos, R.; Kapczinski, F., Therapeutic use of omega-3 fatty acids in bipolar disorder. *Expert Review of Neurotherapeutics* **2011**, *11*, 1029-1047.
20. Bernardi, J. R.; Ferreira, C. F.; Senter, G.; Krolow, R.; de, A. B. W.; Portella, A. K.; Kauer-Sant'anna, M.; Kapczinski, F.; Dalmaz, C.; Goldani, M. Z.; Silveira, P. P., Early life stress interacts with the diet deficiency of omega-3 fatty acids during the life course increasing the metabolic vulnerability in adult rats. *PLoS One* **2013**, *8*, e62031.
21. Almeida, I.; Fernandes, T. J. R.; Guimaraes, B. M. R.; Oliveira, M. B. P. P. In *Omega-3 dietary intake: review on supplementation, health benefits and resources sustainability*, 2014, Nova Science Publishers, Inc.2014; pp 191-211.
22. Ito, H., Omega-3 polyunsaturated fatty acids and coronary unstable plaque - hint to further reduce coronary events. *Circulation Journal* **2013**, *77*, 2473-2474.
23. Mozurkewich, E.; Berman, D. R.; Chilimigras, J., Role of omega-3 fatty acids in maternal, fetal, infant and child wellbeing. *Expert Review of Obstetric & Gynecology* **2010**, *5*, 125-138.
24. Ghesquier, E. Quatre médicaments anti-Alzheimer devraient être remboursés.  
<http://www.actusante.net/maladies/quatre-medicaments-anti-alzheimer-devraient-etre-derembourses-5629>

25. Comment faire face au stress ? <http://www.medecine-douce.net/comment-faire-face-au-stress/>
26. Center, T. O.-. Omega-3s, brain and mental health. <http://omega-3centre.com/newsletters/subscribers/2010-11-15-subscribers-newsletter.html>
27. Merritt, A. The heart of the matter: the cardiovascular system. <https://www.acefitness.org/blog/588/the-heart-of-the-matter-the-cardiovascular-system>
28. DeFilippis, A. P.; Sperling, L. S., Understanding omega-3's. *American Heart Journal* **2006**, *151*, 564-570.
29. AFSSA Acides gras de la famille Oméga-3 et système cardiovasculaire : intérêt nutritionnel et allégations. <http://www.afssa.fr>
30. Swanson, D.; Block, R.; Mousa, S. A., Omega-3 fatty acids EPA and DHA: health benefits throughout life. *Advances in Nutrition* **2012**, *3*, 1-7.
31. Czernichow, S. Les oméga 3 : origines et rôle métabolique. <http://www.institut-benjamin-delessert.net>
32. EurekaSanté Oméga-3 des huiles végétales. <http://www.eurekasante.fr>
33. Kris-Etherton, P. M.; Harris, W. S.; Appel, L. J.; Committee, f. t. N., Fish Consumption, Fish Oil, Omega-3 Fatty Acids, and Cardiovascular Disease. *Circulation* **2002**, *106*, 2747-2757.
34. Souccar, T. Les aliments riches en oméga-3. <http://www.thierrysouccar.com>
35. Choe, E.; Min, D. B., Mechanisms and factors for edible oil oxidation. *Comprehensive Reviews in Food Science and Food Safety* **2006**, *5*, 169-186.
36. Frankel, E. N., Lipid oxidation: Mechanisms, products and biological significance. *J Am Oil Chem Soc* **1984**, *61*, 1908-1917.
37. St. Angelo, A. J.; Editor, *Lipid Oxidation in Food*. ACS1992; p 364 pp.
38. Lallana, E.; Tirelli, N., Oxidation-Responsive Polymers: Which Groups to Use, How to Make Them, What to Expect From Them. *Macromolecular Chemistry and Physics* **2013**, *214*, 143-158.
39. Marteau, C.; Ruyffelaere, F.; Aubry, J. M.; Penverne, C.; Favier, D.; Nardello-Rataj, V., Oxidative degradation of fragrant aldehydes. Autoxidation by molecular oxygen. *Tetrahedron* **2013**, *69*, 2268-2275.
40. Miyamoto, S.; Martinez, G. R.; Medeiros, M. H. G.; Di Mascio, P., Singlet molecular oxygen generated from lipid Hydroperoxides by the Russell mechanism: studies using <sup>18</sup>O-labeled linoleic acid hydroperoxide and monomol light emission measurements. *J. Am. Chem. Soc.* **2003**, *125*, 6172-6179.
41. Kanner, J.; Rosenthal, I., An assessment of lipid oxidation in foods. *Pure Appl. Chem.* **1992**, *64*, 1959-64.
42. Neff, W. E.; Frankel, E. N., Photosensitized oxidation of methyl linolenate monohydroperoxides: hydroperoxy cyclic peroxides, dihydroperoxides and hydroperoxy bis(cyclic peroxide)s. *Lipids* **1984**, *19*, 952-7.
43. Frankel, E. N.; Neff, W. E.; Rohwedder, W. K.; Khambay, B. P. S.; Garwood, R. F.; Weedon, B. C. L., Analysis of autoxidized fats by gas chromatography-mass spectrometry. III. Methyl linolenate. *Lipids* **1977**, *12*, 1055-61.
44. Havrilla, C. M.; Hachey, D. L.; Porter, N. A., Coordination (Ag<sup>+</sup>) Ion Spray-Mass Spectrometry of Peroxidation Products of Cholesterol Linoleate and Cholesterol Arachidonate: High-Performance Liquid Chromatography-Mass Spectrometry Analysis of Peroxide Products from Polyunsaturated Lipid Autoxidation. *J. Am. Chem. Soc.* **2000**, *122*, 8042-8055.
45. Seal, J. R.; Havrilla, C. M.; Porter, N. A.; Hachey, D. L., Analysis of unsaturated compounds by Ag<sup>+</sup> coordination ionspray mass spectrometry studies of the formation of the Ag<sup>+</sup>/lipid complex. *J. Am. Soc. Mass Spectrom.* **2003**, *14*, 872-880.
46. Becker, E.; Nissen, L.; Skibsted, L., Antioxidant evaluation protocols: Food quality or health effects. *Eur Food Res Technol* **2004**, *219*, 561-571.
47. Cillard, J.; Cillard, P., Mécanismes de la peroxydation lipidique et des anti-oxydations. *Oléagineux, Corps gras, Lipides* **2006**, *13*, 24-29.
48. Denisov, E. T.; Afanas'ev, I. B.; Editors, *Oxidation and Antioxidants in Organic Chemistry and Biology*. 2005; p 1024 pp.
49. Ohkatsu, Y.; Suzuki, F., Synergism between phenolic antioxidants in autoxidation. *journal of the Japan Petroleum Institute* **2011**, *54*, 22-29.

50. Carr, A. C.; Zhu, B.-Z.; Frei, B., Potential antiatherogenic mechanisms of ascorbate (vitamin C) and  $\alpha$ -tocopherol (vitamin E). *Circulation Research* **2000**, *87*, 349-354.
51. McCay, P. B., Vitamin E: interactions with free radicals and ascorbate. *Annual Review of Nutrition* **1985**, *5*, 323-40.
52. Valgimigli, L.; Pratt, D. A. In *Antioxidants in chemistry and biology* 2012 John Wiley & Sons Ltd.; pp 1623-1677.
53. Saito, M.; Sakagami, H.; Fujisawa, S., Cytotoxicity and apoptosis induction by butylated hydroxyanisole (BHA) and butylated hydroxytoluene (BHT). *Anticancer Res.* **2003**, *23*, 4693-4701.
54. Lucarini, M.; Peduli, G. F. In *Overview of antioxidant activity of vitamin E* 2007 CABI Publishing; pp 3-10.
55. Foote, C. S., Mechanisms of photosensitized oxidation. *Science* **1968**, *162*, 963-70.
56. Min, D. B.; Boff, J. M., Chemistry and reaction of singlet oxygen in foods. *Compr. Rev. Food Sci. Food Saf.* **2002**, *1*, 58-72.
57. Nakagawa, Y., Initiation of apoptotic signal by the peroxidation of cardiolipin of mitochondria. *Ann. N. Y. Acad. Sci.* **2004**, *1011*, 177-184.
58. Labuza, T. P., Kinetics of lipid oxidation in foods. *Crit. Rev. Food Technol.* **1972**, *2*, 355-405.
59. Indarti, E.; Majid, M. I. A.; Hashim, R.; Chong, A., Direct FAME synthesis for rapid total lipid analysis from fish oil and cod liver oil. *J. Food Compos. Anal.* **2004**, *18*, 161-170.
60. Scharff, J. P.; Perrin, R., *Chimie Industrielle*. 1993.
61. Guillen, M. D.; Cabo, N., Fourier transform infrared spectra data versus peroxide and anisidine values to determine oxidative stability of edible oils. *Food Chem.* **2002**, *77*, 503-510.
62. Hamilton, R. J. In *The chemistry of rancidity in foods* 1983 Appl. Sci.; pp 1-20.
63. Halvorsen, B. L.; Blomhoff, R., Determination of lipid oxidation products in vegetable oils and marine omega-3 supplements. *Food & Nutrition Research* **2011**, *55*, 10.3402/fnr.v55i0.5792.
64. Seppanen, C. M.; Saari Csallany, A., Formation of 4-hydroxynonenal, a toxic aldehyde, in soybean oil at frying temperature. *J Amer Oil Chem Soc* **2002**, *79*, 1033-1038.
65. Ohfuji, T.; Kaneda, T., Characterization of toxic compound in thermally oxidized oil. *Lipids* **1973**, *8*, 353-9.
66. Chi, Y.-S.; Obendorf, S. K., Aging of oily soils on textile materials: a literature review. *J. Surfactants Deterg.* **1998**, *1*, 407-418.
67. Moore, J. H., Jr., Wigner spin rule in collisions of nitrogen(+) ions with helium, neon, argon, molecular nitrogen and molecular oxygen. *Phys. Rev. A* **1973**, *8*, 2359-62.
68. Schaich, K. M. In *Lipid oxidation: theoretical aspects* 2005 John Wiley & Sons, Inc.; pp 269-355.
69. Brown, R., Excited states and free radicals in biology and medicine by R. V. Bensasson, E. J. Land and T. G. Truscott. *J. Photochem. Photobiol., A* **1995**, *85*, 197.
70. Porter, N. A.; Caldwell, S. E.; Mills, K. A., Mechanisms of free radical oxidation of unsaturated lipids. *Lipids* **1995**, *30*, 277-90.
71. Frankel, E. N., Chemistry of free radical and singlet oxidation of lipids. *Prog. Lipid Res.* **1984**, *23*, 197-221.
72. Frankel, E. N.; Neff, W. E.; Rohwedder, W. K.; Khambay, B. P. S.; Garwood, R. F.; Weedon, B. C. L., Analysis of autoxidized fats by gas chromatography-mass spectrometry: I. Methyl oleate. *Lipids* **1977**, *12*, 901-7.
73. Frankel, E. N., Lipid oxidation. *Prog. Lipid Res.* **1980**, *19*, 1-22.
74. Neff, W. E.; Frankel, E. N., Quantitative analyses of hydroxystearate isomers from hydroperoxides by high-pressure liquid chromatography of autoxidized and photosensitized-oxidized fatty esters. *Lipids* **1980**, *15*, 587-90.
75. Brill, W. F., The isolation and rearrangement of pure acyclic allylic hydroperoxides. *J. Am. Chem. Soc.* **1965**, *87*, 3286-7.
76. Garwood, R. F.; Khambay, B. P. S.; Weedon, B. C. L.; Frankel, E. N., Allylic hydroperoxides from the autoxidation of methyl oleate. *J. Chem. Soc., Chem. Commun.* **1977**, 364-5.
77. Dolev, A.; Rohwedder, W. K.; Dutton, H. J., Mechanism of lipoxidase reaction. I. Specificity of hydroperoxidation of linoleic acid. *Lipids* **1967**, *2*, 28-32.
78. Brash, A. R., Autoxidation of methyl linoleate: identification of the bis-allylic 11-hydroperoxide. *Lipids* **2000**, *35*, 947-952.

79. Frankel, E. N., Chemistry of autoxidation: mechanism, products and flavor significance. *AOCS Monogr.* **1985**, *15*, 1-37.
80. Frankel, E. N.; Neff, W. E.; Rohwedder, W. K.; Khambay, B. P. S.; Garwood, R. F.; Weedon, B. C. L., Analysis of autoxidized fats by gas chromatography-mass spectrometry: II. Methyl linoleate. *Lipids* **1977**, *12*, 908-13.
81. Bergstrom, S., Autoxidation of linoleic acid. *Nature (London, U. K.)* **1945**, *156*, 717-18.
82. Pryor, W. A.; Stanley, J. P.; Blair, E., Autoxidation of polyunsaturated fatty acids: II. A suggested mechanism for the formation of TBA-reactive materials from prostaglandin-like endoperoxides. *Lipids* **1976**, *11*, 370-9.
83. Terao, J.; Matsushita, S., Further oxygenated compounds produced from methyl linoleate monohydroperoxides in the process of autoxidation. *Agric. Biol. Chem.* **1975**, *39*, 2027-33.
84. Schneider, C.; Porter, N. A.; Brash, A. R., Routes to 4-hydroxynonenal: Fundamental issues in the mechanisms of lipid peroxidation. *J. Biol. Chem.* **2008**, *283*, 15539-15543.
85. Frankel, E. N.; Evans, C. D.; McConnell, D. G.; Selke, E.; Dutton, H. J., Autoxidation of methyl linolenate. Isolation and characterization of hydroperoxides. *J. Org. Chem.* **1961**, *26*, 4663-9.
86. Begemann, P. H.; Woestenburg, W. J.; Leer, S., Structure of four methyl linolenate diperoxides. *Journal of Agricultural and Food Chemistry* **1968**, *16*, 679-684.
87. Coxon, D. T.; Price, K. R.; Chan, H. W. S., Formation, isolation and structure determination of methyl linolenate diperoxides. *Chem. Phys. Lipids* **1981**, *28*, 365-78.
88. Shahidi, F.; Zhong, Y., Lipid oxidation and improving the oxidative stability. *Chemical Society Reviews* **2010**, *39*, 4067-4079.
89. Neff, W. E.; Frankel, E. N.; Weisleder, D., High-pressure liquid chromatography of autoxidized lipids. II. Hydroperoxy-cyclic peroxides and other secondary products from methyl linolenate. *Lipids* **1981**, *16*, 439-48.
90. Porter, N. A.; Funk, M. O.; Gilmore, D.; Isaac, R.; Nixon, J., The formation of cyclic peroxides from unsaturated hydroperoxides: models for prostaglandin biosynthesis. *J. Am. Chem. Soc.* **1976**, *98*, 6000-5.
91. O'Connor, D. E.; Mihelich, E. D.; Coleman, M. C., Isolation and characterization of bicycloendoperoxides derived from methyl linolenate. *J. Am. Chem. Soc.* **1981**, *103*, 223-4.
92. Rawls, H. R.; Van Santen, P. J., Possible role for singlet oxygen in the initiation of fatty acid autoxidation. *J. Amer. Oil Chem. Soc.* **1970**, *47*, 121-5.
93. DeRosa, M. C.; Crutchley, R. J., Photosensitized singlet oxygen and its applications. *Coordination Chemistry Reviews* **2002**, *233-234*, 351-371.
94. Kim, H. L., Oxidation mechanism of riboflavin destruction and antioxidant mechanism of tocotrienols. *Ohio State University* **2007**.
95. Grossweiner, L. I., Singlet Oxygen: Generation and Properties.
96. Huang, R.; Choe, E.; Min, D. B., Effects of riboflavin photosensitized oxidation on the volatile compounds of soymilk. *J. Food Sci.* **2004**, *69*, C733-C738.
97. Nyman, E. S.; Hynninen, P. H., Research advances in the use of tetrapyrrolic photosensitizers for photodynamic therapy. *Journal of Photochemistry and Photobiology B: Biology* **2004**, *73*, 1-28.
98. Schweitzer, C.; Schmidt, R., Physical Mechanisms of Generation and Deactivation of Singlet Oxygen. *Chem. Rev. (Washington, DC, U. S.)* **2003**, *103*, 1685-1757.
99. Shimizu, N.; Bartlett, P. D., Photooxidation of olefins sensitized by  $\alpha$ -diketones and by benzophenone. A practical epoxidation method with biacetyl. *J. Am. Chem. Soc.* **1976**, *98*, 4193-200.
100. Aubry, J.-M.; Bouttemy, S., Preparative Oxidation of Organic Compounds in Microemulsions with Singlet Oxygen Generated Chemically by the Sodium Molybdate/Hydrogen Peroxide System. *J. Am. Chem. Soc.* **1997**, *119*, 5286-5294.
101. Aubry, J. M.; Nardello, V., Generation of singlet oxygen from the catalytic system H<sub>2</sub>O<sub>2</sub>/Ca(OH)<sub>2</sub> and applications to the selective oxidation of unsaturated compounds. *Stud. Surf. Sci. Catal.* **1997**, *110*, 883-892.
102. Aubry, J. M., Search for singlet oxygen in the decomposition of hydrogen peroxide by mineral compounds in aqueous solutions. *Journal of the American Chemical Society* **1985**, *107*, 5844-5849.

103. Nardello, V.; Marti, M.-J.; Pierlot, C.; Aubry, J.-M., Photochemistry without light: oxidation of rubrene in a microemulsion with a chemical source of singlet molecular oxygen, ( $^1O_2$ ,  $^1\Delta_g$ ). *J. Chem. Educ.* **1999**, *76*, 1285-1288.
104. Tanielian, C.; Mechin, R., Reactions of singlet oxygen with polyisoprene and model compounds. *Tetrahedron* **1985**, *41*, 2139-46.
105. Foote, C. S., Photosensitized oxygenations and the role of singlet oxygen. *Accounts Chem. Res.* **1968**, *1*, 104-10.
106. Merkel, P. B.; Kearns, D. R., Remarkable solvent effects on the lifetime of  $^1\Delta_g$  oxygen. *J. Amer. Chem. Soc.* **1972**, *94*, 1029-30.
107. Ogilby, P. R.; Foote, C. S., Chemistry of singlet oxygen. 42. Effect of solvent, solvent isotopic substitution, and temperature on the lifetime of singlet molecular oxygen ( $^1\Delta_g$ ). *J. Am. Chem. Soc.* **1983**, *105*, 3423-30.
108. Salokhiddinov, K. I.; Byteva, I. M.; Gurinovich, G. P., Lifetime of singlet oxygen in different solvents. *Zh. Prikl. Spektrosk.* **1981**, *34*, 892-7.
109. Stratakis, M.; Orfanopoulos, M., Regioselectivity in the ene reaction of singlet oxygen with alkenes. *Tetrahedron* **2000**, *56*, 1595-1615.
110. Harding, L. B.; Goddard, W. A., III, The mechanism of the ene reaction of singlet oxygen with olefins. *J. Am. Chem. Soc.* **1980**, *102*, 439-49.
111. Griesbeck, A. G.; Cho, M., Singlet oxygen addition to homoallylic substrates in solution and microemulsion: novel secondary reactions. *Tetrahedron Lett.* **2009**, *50*, 121-123.
112. Maranzana, A.; Ghigo, G.; Tonachini, G., Mechanistic Significance of Peroxide Trapping Experiments, with Epoxide Detection, in  $^1\Delta_g$  Dioxygen Reactions with Alkenes. *J. Org. Chem.* **2003**, *68*, 3125-3129.
113. Clennan, E. L., New Mechanistic and Synthetic Aspects of Singlet Oxygen Chemistry. *Tetrahedron* **2000**, *56*, 9151-9179.
114. Kohno, Y.; Egawa, Y.; Itoh, S.; Nagaoka, S.-i.; Takahashi, M.; Mukai, K., Kinetic study of quenching reaction of singlet oxygen and scavenging reaction of free radical by squalene in n-butanol. *Biochim. Biophys. Acta, Lipids Lipid Metab.* **1995**, *1256*, 52-6.
115. Greer, A., Christopher Foote's Discovery of the Role of Singlet Oxygen [ $^1O_2$  ( $^1\Delta_g$ )] in Photosensitized Oxidation Reactions. *Acc. Chem. Res.* **2006**, *39*, 797-804.
116. Nardello, V.; Caron, L.; Aubry, J.-M.; Bouttemy, S.; Wirth, T.; Chantou, R. S.-M.; Adam, W., Reactivity, Chemoselectivity, and Diastereoselectivity of the Oxyfunctionalization of Chiral Allylic Alcohols and Derivatives in Microemulsions: Comparison of the Chemical Oxidation by the Hydrogen Peroxide/Sodium Molybdate System with the Photooxygenation. *J. Am. Chem. Soc.* **2004**, *126*, 10692-10700.
117. Nakajima, A.; Hidaka, H., Photosensitized oxidation of oleic acid, methyl oleate, and olive oil using visible light. *J. Photochem. Photobiol., A* **1993**, *74*, 189-94.
118. Rawls, H. R.; Van Santen, P. J., Singlet oxygen: a possible source of the original hydroperoxides in fatty acids. *Ann. N. Y. Acad. Sci.* **1970**, *171*, 135-8.
119. Frankel, E. N.; Neff, W. E.; Weisleder, D., Formation of hydroperoxy bis-epidioxides in sensitized photooxidized methyl linolenate. *J. Chem. Soc., Chem. Commun.* **1982**, 599-600.
120. Frankel, E. N.; Neff, W. E.; Bessler, T. R., Analysis of autoxidized fats by gas chromatography-mass spectrometry: V. Photosensitized oxidation. *Lipids* **1979**, *14*, 961-7.
121. Chan, H. W. S., Photo-sensitized oxidation of unsaturated fatty acid methyl esters. The identification of different pathways. *J. Amer. Oil Chem. Soc.* **1977**, *54*, 100-4.
122. Fedeli, E.; Camurati, F.; Jacini, G., Structure of monohydroperoxides formed by chlorophyll-photosensitized oxidation of methyl linoleate. *J. Amer. Oil Chem. Soc.* **1971**, *48*, 787-9.
123. Cobern, D.; Hobbs, J. S.; Lucas, R. A.; Lucas, R. A., Location of hydroperoxide groups in monohydroperoxides formed by chlorophyll-photosensitized oxidation of unsaturated esters. *J. Chem. Soc. C* **1966**, 1897-902.
124. Mihelich, E. D., Structure and stereochemistry of novel endoperoxides isolated from the sensitized photooxidation of methyl linoleate. Implications for prostaglandin biosynthesis. *J. Am. Chem. Soc.* **1980**, *102*, 7141-3.
125. Frankel, E. N.; Neff, W. E.; Selke, E.; Weisleder, D., Photosensitized oxidation of methyl linoleate: secondary and volatile thermal decomposition products. *Lipids* **1982**, *17*, 11-18.

126. Neff, W. E.; Frankel, E. N.; Selke, E.; Weisleder, D., Photosensitized oxidation of methyl linolenate monohydroperoxides: hydroperoxy cyclic peroxides, dihydroperoxides, keto esters and volatile thermal decomposition products. *Lipids* **1983**, *18*, 868-76.
127. Yin, H.; Xu, L.; Porter, N. A., Free Radical Lipid Peroxidation: Mechanisms and Analysis. *Chem. Rev. (Washington, DC, U. S.)* **2011**, *111*, 5944-5972.
128. Neff, W. E.; Frankel, E. N.; Weisleder, D., Photosensitized oxidation of methyl linolenate. Secondary products. *Lipids* **1982**, *17*, 780-90.
129. Labuza, T. P.; Silver, M.; Cohn, M.; Heidelbaugh, N. D.; Karel, M., Metal-catalyzed oxidation in the presence of water in foods. *J. Amer. Oil Chem. Soc.* **1971**, *48*, 527-31.
130. Erben-Russ, M.; Michel, C.; Bors, W.; Saran, M., Absolute rate constants of alkoxy radical reactions in aqueous solution. *J. Phys. Chem.* **1987**, *91*, 2362-5.
131. Howard, J. A.; Ingold, K. U., Absolute rate constants for hydrocarbon autoxidation. VI. Alkyl aromatic and olefinic hydrocarbons. *Can. J. Chem.* **1967**, *45*, 793-802.
132. Kim, S. S.; Kim, S. Y.; Ryou, S. S.; Lee, C. S.; Yoo, K. H., Solvent effects in the hydrogen abstractions by tert-butoxy radical: veracity of the reactivity/selectivity principle. *J. Org. Chem.* **1993**, *58*, 192-6.
133. Walling, C.; Wagner, P. J., Positive halogen compounds. X. Solvent effects in the reactions of tert-butoxy radicals. *J. Am. Chem. Soc.* **1964**, *86*, 3368-75.
134. Tsentlovich, Y. P.; Kulik, L. V.; Gritsan, N. P.; Yurkovskaya, A. V., Solvent Effect on the Rate of  $\beta$ -Scission of the tert-Butoxyl Radical. *J. Phys. Chem. A* **1998**, *102*, 7975-7980.
135. Kochi, J. K., Chemistry of alkoxy radicals: cleavage reactions. *J. Am. Chem. Soc.* **1962**, *84*, 1193-7.
136. Walling, C.; Wagner, P., Effects of solvent on transition states in the reactions of tertbutoxy radicals. *J. Am. Chem. Soc.* **1963**, *85*, 2333-4.
137. Simic, M. G., Free radical mechanisms in autoxidation processes. *J. Chem. Educ.* **1981**, *58*, 125-31.
138. Ingold, K. U., Peroxy radicals. *Accounts Chem. Res.* **1969**, *2*, 1-9.
139. Avila, D. V.; Brown, C. E.; Ingold, K. U.; Luszyk, J., Solvent effects on the competitive  $\beta$ -scission and hydrogen atom abstraction reactions of the cumyloxyl radical. Resolution of a long-standing problem. *J. Am. Chem. Soc.* **1993**, *115*, 466-70.
140. Walling, C.; Padwa, A., Positive halogen compounds. VI. Effects of structure and medium on the  $\beta$ -scission of alkoxy radicals. *J. Am. Chem. Soc.* **1963**, *85*, 1593-7.
141. Mayo, F. R.; Miller, A. A.; Russell, G. A., The oxidation of unsaturated compounds. IX. The effects of structure on the rates and products of oxidation of unsaturated compounds. *J. Am. Chem. Soc.* **1958**, *80*, 2500-07.
142. Nawar, W. W., Thermal degradation of lipids. *J. Agr. Food Chem.* **1969**, *17*, 18-21.
143. Porter, N. A.; Lehman, L. S.; Weber, B. A.; Smith, K. J., Unified mechanism for polyunsaturated fatty acid autoxidation. Competition of peroxy radical hydrogen atom abstraction,  $\beta$ -scission, and cyclization. *J. Am. Chem. Soc.* **1981**, *103*, 6447-55.
144. Van Sickle, D. E.; Mayo, F. R.; Gould, E. S.; Arluck, R. M., Effects of experimental variables in oxidations of alkenes. *J. Am. Chem. Soc.* **1967**, *89*, 977-84.
145. Dix, T. A.; Marnett, L. J., Free radical epoxidation of 7,8-dihydroxy-7,8-dihydrobenzo[a]pyrene by hematin and polyunsaturated fatty acid hydroperoxides. *J. Am. Chem. Soc.* **1981**, *103*, 6744-6.
146. Wu, G.-S.; Stein, R. A.; Mead, J. F., Autoxidation of fatty acid monolayers adsorbed on silica gel: III. Effects of saturated fatty acids and cholesterol. *Lipids* **1978**, *13*, 517-24.
147. Wu, G.-S.; Stein, R. A.; Mead, J. F., Autoxidation of fatty acid monolayers adsorbed on silica gel: II. Rates and products. *Lipids* **1977**, *12*, 971-8.
148. Chan, H. W. S.; Matthew, J. A.; Coxon, D. T., A hydroperoxyepidioxide from the autoxidation of a hydroperoxide of methyl linolenate. *J. Chem. Soc., Chem. Commun.* **1980**, 235-6.
149. Hiatt, R.; McCarrick, T., Bimolecular initiation by hydroperoxides. *Journal of the American Chemical Society* **1975**, *97*, 5234-5237.
150. Elson, I. H.; Mao, S. W.; Kochi, J. K., Electron spin resonance study of addition of alkoxy radicals to olefins. *J. Am. Chem. Soc.* **1975**, *97*, 335-41.
151. Lewis, F. M.; Mayo, F. R., Copolymerization. IX. Comparison of some cis and trans isomers. *J. Am. Chem. Soc.* **1948**, *70*, 1533-6.

152. Frankel, E. N.; Neff, W. E.; Selke, E.; Brooks, D. D., Analysis of autoxidized fats by gas chromatography-mass spectrometry: X. Volatile thermal decomposition products of methyl linolenate dimers. *Lipids* **1988**, *23*, 295-8.
153. Parker, T. D.; Adams, D. A.; Zhou, K.; Harris, M.; Yu, L., Fatty acid composition and oxidative stability of cold-pressed edible seed oils. *J. Food Sci.* **2003**, *68*, 1240-1243.
154. Martin-Polvillo, M.; Marquez-Ruiz, G.; Dobarganes, M. C., Oxidative stability of sunflower oils differing in unsaturation degree during long-term storage at room temperature. *J. Am. Oil Chem. Soc.* **2004**, *81*, 577-583.
155. Velasco, J.; Andersen, M. L.; Skibsted, L. H., Evaluation of oxidative stability of vegetable oils by monitoring the tendency to radical formation. A comparison of electron spin resonance spectroscopy with the Rancimat method and differential scanning calorimetry. *Food Chem.* **2004**, *85*, 623-632.
156. Vever-Bizet, C.; Dellinger, M.; Brault, D.; Rougee, M.; Bensasson, R. V., Singlet molecular oxygen quenching by saturated and unsaturated fatty acids and by cholesterol. *Photochem. Photobiol.* **1989**, *50*, 321-5.
157. Shahidi, F.; Spurvey, S. A., Oxidative stability of fresh and heat-processed dark and light muscles of mackerel (*Scomber scombrus*). *J. Food Lipids* **1996**, *3*, 13-25.
158. Min, D. B.; Wen, J., Effects of dissolved free oxygen on the volatile compounds of oil. *J. Food Sci.* **1983**, *48*, 1429-30.
159. Mistry, B. S.; Min, D. B., Effects of fatty acids on the oxidative stability of soybean oil. *J. Food Sci.* **1987**, *52*, 831-2.
160. Uri, N., Physico-chemical aspects of autoxidation. *Autoxidation Antioxidants (W. O. Lundberg, Edtor. Interscience Publishers)* **1961**, *1*, 55-106.
161. Bray, W. C.; Gorin, M. H., Ferryl ion, a compound of quadrivalent iron. *J. Am. Chem. Soc.* **1932**, *54*, 2124-5.
162. Caspi, D., Enzymes in Organic Synthesis. Episode II: kinetic, acylative, and dynamic resolutions. 2003.
163. Abuzaytoun, R.; Shahidi, F., Oxidative Stability of Algal Oils As Affected by Their Minor Components. *J. Agric. Food Chem.* **2006**, *54*, 8253-8260.
164. Choe, E.; Min, D. B., Mechanisms of Antioxidants in the Oxidation of Foods. *Compr. Rev. Food Sci. Food Saf.* **2009**, *8*, 345-358.
165. Hopkins, C. Y.; Bernstein, H. J., Applications of proton magnetic resonance spectra in fatty acid chemistry. *Can. J. Phys.* **1959**, *37*, 775-82.
166. Guillen, M. D.; Ruiz, A., Edible oils: Discrimination by <sup>1</sup>H nuclear magnetic resonance. *J. Sci. Food Agric.* **2003**, *83*, 338-346.
167. Guillen, M. D.; Ruiz, A., High resolution <sup>1</sup>H nuclear magnetic resonance in the study of edible oils and fats. *Trends Food Sci. Technol.* **2002**, *12*, 328-338.
168. Johnson, L. F.; Shoolery, J. N., Determination of unsaturation and average molecular weight of natural fats by nuclear magnetic resonance (N.M.R.). *Anal. Chem.* **1962**, *34*, 1136-9.
169. Aursand, M.; Rainuzzo, J. R.; Grasdalen, H., Quantitative high-resolution carbon-13 and proton nuclear magnetic resonance of  $\omega$ 3 fatty acids from white muscle of Atlantic salmon (*Salmo salar*). *J. Am. Oil Chem. Soc.* **1993**, *70*, 971-81.
170. Sacchi, R.; Medina, I.; Aubourg, S. P.; Addeo, F.; Paolillo, L., Proton nuclear magnetic resonance rapid and structure-specific determination of  $\omega$ -3 polyunsaturated fatty acids in fish lipids. *J. Am. Oil Chem. Soc.* **1993**, *70*, 225-8.
171. Igarashi, T.; Aursand, M.; Hirata, Y.; Gribbestad, I. S.; Wada, S.; Nonaka, M., Nondestructive quantitative determination of docosahexaenoic acid and n-3 fatty acids in fish oils by high-resolution <sup>1</sup>H nuclear magnetic resonance spectroscopy. *J. Am. Oil Chem. Soc.* **2000**, *77*, 737-748.
172. Wollenberg, K., Quantitative triacylglycerol analysis of whole vegetable seeds by proton and carbon-13 magic angle sample spinning NMR spectroscopy. *J. Am. Oil Chem. Soc.* **1991**, *68*, 391-400.
173. Siddiqui, N.; Sim, J.; Silwood, C. J. L.; Toms, H.; Iles, R. A.; Grootveld, M., Multicomponent analysis of encapsulated marine oil supplements using high-resolution <sup>1</sup>H and <sup>13</sup>C NMR techniques. *J. Lipid Res.* **2003**, *44*, 2406-2427.

174. Carvalho, M. S.; Mendonca, M. A.; Pinho, D. M. M.; Resck, I. S.; Suarez, P. A. Z., Chromatographic analyses of fatty acid methyl esters by HPLC-UV and GC-FID. *J. Braz. Chem. Soc.* **2012**, *23*, 763-769.
175. Spitzer, V., Structure analysis of fatty acids by gas chromatography - low resolution electron impact mass spectrometry of their 4,4-dimethyloxazoline derivatives - a review. *Prog. Lipid Res.* **1997**, *35*, 387-408.
176. Dodds, E. D.; McCoy, M. R.; Rea, L. D.; Kennish, J. M., Gas chromatographic quantification of fatty acid methyl esters: Flame ionization detection vs. electron impact mass spectrometry. *Lipids* **2005**, *40*, 419-428.
177. Thurnhofer, S.; Vetter, W., A Gas Chromatography/Electron Ionization–Mass Spectrometry–Selected Ion Monitoring Method for Determining the Fatty Acid Pattern in Food after Formation of Fatty Acid Methyl Esters. *Journal of Agricultural and Food Chemistry* **2005**, *53*, 8896-8903.
178. Freedman, B.; Kwolek, W. F.; Pryde, E. H., Quantitation in the analysis of transesterified soybean oil by capillary gas chromatography. *JAOCS, J. Am. Oil Chem. Soc.* **1986**, *63*, 1370-5.
179. Nollet, L. M. L.; Editor, *Food Analysis by HPLC*. Dekker2000; p 1049 pp.
180. Di Nicola, G.; Pacetti, M.; Polonara, F.; Santori, G.; Stryjek, R., Development and optimization of a method for analyzing biodiesel mixtures with non-aqueous reversed phase liquid chromatography. *J. Chromatogr. A* **2008**, *1190*, 120-126.
181. Řezanka, T., Analysis of Polyunsaturated Fatty Acids Using High Performance Liquid Chromatography – Atmospheric Pressure Chemical Ionization Mass Spectrometry. *Journal of High Resolution Chromatography* **2000**, *23*, 338-342.
182. MASONACO Electrospray (ESI) and atmospheric Pressure Chemical Ionization (APCI). <https://sites.google.com/site/masonaco/Home/mass-spectrometry/sample-introduction-and-ionization/esi-apci>
183. Vrkoslav, V.; Cvacka, J., Identification of the double-bond position in fatty acid methyl esters by liquid chromatography/atmospheric pressure chemical ionisation mass spectrometry. *J. Chromatogr. A* **2012**, *1259*, 244-250.
184. Hodges, R. V.; Beauchamp, J. L., Application of alkali ions in chemical ionization mass spectrometry. *Anal. Chem.* **1976**, *48*, 825-9.
185. Staley, R. H.; Beauchamp, J. L., Intrinsic acid-base properties of molecules. Binding energies of lithium(1+) ion to  $\pi$ - and n-donor bases. *J. Am. Chem. Soc.* **1975**, *97*, 5920-1.
186. Teesch, L. M.; Adams, J., Metal ions as special reagents in analytical mass spectrometry. *Org. Mass Spectrom.* **1992**, *27*, 931-43.
187. Bayer, E.; Gfrörer, P.; Rentel, C., Coordination-Ionspray-MS (CIS-MS), a Universal Detection and Characterization Method for Direct Coupling with Separation Techniques. *Angewandte Chemie International Edition* **1999**, *38*, 992-995.
188. Jackson, A. U.; Shum, T.; Sokol, E.; Dill, A.; Cooks, R. G., Enhanced detection of olefins using ambient ionization mass spectrometry: Ag<sup>+</sup> adducts of biologically relevant alkenes. *Anal. Bioanal. Chem.* **2011**, *399*, 367-376.
189. Hayen, H.; Karst, U., Strategies for the liquid chromatographic-mass spectrometric analysis of non-polar compounds. *J. Chromatogr. A* **2003**, *1000*, 549-565.
190. Rentel, C.; Gfrörer, P.; Bayer, E., Coupling of capillary electrochromatography to coordination ion spray mass spectrometry, a novel detection method. *Electrophoresis* **1999**, *20*, 2329-2336.
191. Medvedovici, A.; Lazou, K.; D'Oosterlinck, A.; Zhao, Y.; Sandra, P., Analysis of jojoba oil by LC-coordination ion spray-MS (LC-CIS-MS). *J. Sep. Sci.* **2002**, *25*, 173-178.
192. Ruiz-Gutierrez, V.; Perez-Camino, M. C., Update on solid-phase extraction for the analysis of lipid classes and related compounds. *J. Chromatogr. A* **2000**, *885*, 321-341.
193. Flieger, J.; Szumilo, H., Optimizing chromatographic conditions for separation of fatty acid methyl esters by argentation thin-layer chromatography. *J. Planar Chromatogr.--Mod. TLC* **2000**, *13*, 426-431.
194. Scholfield, C. R., Argentation high performance liquid chromatography of methyl esters. *J. Am. Oil Chem. Soc.* **1980**, *57*, 331-4.

195. Ghebreyessus, K. Y.; Schiltz, H.; Angelici, R. J., Partial separation of polyunsaturated fatty acid esters from FAMES mixtures by adsorption on silver nitrate-impregnated silica gel. *J. Am. Oil Chem. Soc.* **2006**, *83*, 645-652.
196. INSTRUMENT, D., Peroxide Number of Edible oils - NFT 60-220 and ISO 3960. **1995 and 2001**.
197. Lenz, M. L.; Hughes, H.; Mitchell, J. R.; Via, D. P.; Guyton, J. R.; Taylor, A. A.; Gotto, A. M., Jr.; Smith, C. V., Lipid hydroperoxy and hydroxy derivatives in copper-catalyzed oxidation of low density lipoprotein. *J. Lipid Res.* **1990**, *31*, 1043-50.
198. Wolff, S. P., Ferrous ion oxidation in presence of ferric ion indicator xylenol orange for measurement of hydroperoxides. In *Methods in Enzymology*, Academic Press 1994; Vol. Volume 233, pp 182-189.
199. Gay, C.; Collins, J.; Gebicki, J. M., Hydroperoxide assay with the ferric-xylenol orange complex. *Anal Biochem* **1999**, *273*, 149-55.
200. Jiang, Z. Y.; Hunt, J. V.; Wolff, S. P., Ferrous ion oxidation in the presence of xylenol orange for detection of lipid hydroperoxide in low density lipoprotein. *Anal Biochem* **1992**, *202*, 384-9.
201. Nourooz-Zadeh, J.; Tajaddini-Sarmadi, J.; Ling, K. L.; Wolff, S. P., Low-density lipoprotein is the major carrier of lipid hydroperoxides in plasma. Relevance to determination of total plasma lipid hydroperoxide concentrations. *Biochem J* **1996**, *313* ( Pt 3), 781-6.
202. Nourooz-Zadeh, J.; Tajaddini-Sarmadi, J.; Wolff, S. P., Measurement of Hydroperoxides in Edible Oils Using the Ferrous Oxidation in Xylenol Orange Assay. *Journal of Agricultural and Food Chemistry* **1995**, *43*, 17-21.
203. Yin, H.; Porter, N. A., Specificity of the ferrous oxidation of xylenol orange assay: analysis of autoxidation products of cholesteryl arachidonate. *Analytical Biochemistry* **2003**, *313*, 319-326.
204. Association), I. I. F., IFRA Analytical Method: Determination of the Peroxide Value.
205. Jessup, W.; Dean, R. T.; Gebicki, J. M., Iodometric determination of hydroperoxides in lipids and proteins. *Methods Enzymol.* **1994**, *233*, 289-303.
206. van de Voort, F. R.; Ismail, A. A.; Sedman, J.; Emo, G., Monitoring the oxidation of edible oils by Fourier transform infrared spectroscopy. *J. Am. Oil Chem. Soc.* **1994**, *71*, 243-53.
207. Dugan, L. R., Jr.; Beadle, B. W.; Henick, A. S., An infrared absorption study of autoxidized methyl linoleate. *J. Am. Oil Chem. Soc.* **1949**, *26*, 681-5.
208. Martinez-Yusta, A.; Goicoechea, E.; Guillen, M. D., A review of thermo-oxidative degradation of food lipids studied by <sup>1</sup>H NMR spectroscopy: influence of degradative conditions and food lipid nature. *Compr. Rev. Food Sci. Food Saf.* **2014**, *13*, 838-859.
209. Sohde, K.; Ogawa, T.; Matsushita, S., Nuclear magnetic resonance spectrometric determinations of hydroperoxides of methyl linoleate and safflower oil. *Yukagaku* **1974**, *23*, 228-32.
210. Skiera, C.; Steliopoulos, P.; Kuballa, T.; Holzgrabe, U.; Diehl, B., <sup>1</sup>H-NMR Spectroscopy as a New Tool in the Assessment of the Oxidative State in Edible Oils. *J. Am. Oil Chem. Soc.* **2012**, *89*, 1383-1391.
211. Goicoechea, E.; Guillen, M. D., Analysis of Hydroperoxides, Aldehydes and Epoxides by <sup>1</sup>H Nuclear Magnetic Resonance in Sunflower Oil Oxidized at 70 and 100 °C. *J. Agric. Food Chem.* **2010**, *58*, 6234-6245.
212. Guillen, M. D.; Goicoechea, E., Detection of primary and secondary oxidation products by Fourier transform infrared spectroscopy (FTIR) and <sup>1</sup>H nuclear magnetic resonance (NMR) in sunflower oil during storage. *J. Agric. Food Chem.* **2007**, *55*, 10729-10736.
213. Saeed, S.; Howell, N. K., High-performance liquid chromatography and spectroscopic studies on fish oil oxidation products extracted from frozen Atlantic mackerel. *J. Am. Oil Chem. Soc.* **1999**, *76*, 391-397.
214. Pajunen, T. I.; Koskela, H.; Hase, T.; Hopia, A., NMR properties of conjugated linoleic acid (CLA) methyl ester hydroperoxides. *Chem. Phys. Lipids* **2008**, *154*, 105-114.
215. Liu, W.; Morrow, J. D.; Yin, H., Quantification of F2-isoprostanes as a reliable index of oxidative stress in vivo using gas chromatography-mass spectrometry (GC-MS) method. *Free Radical Biology and Medicine* **2009**, *47*, 1101-1107.
216. Frankel, E. N.; Neff, W. E.; Rohwedder, W. K.; Khambay, B. P. S.; Garwood, R. F.; Weedon, B. C. L., Analysis of autoxidized fats by gas chromatography-mass spectrometry. III. Methyl linolenate. *Lipids* **1977**, *12*, 1055-61.

217. Frankel, E. N.; Neff, W. E.; Selke, E., Analysis of autoxidized fats by gas chromatography-mass spectrometry: VII. Volatile thermal decomposition products of pure hydroperoxides from autoxidized and photosensitized oxidized methyl oleate, linoleate and linolenate. *Lipids* **1981**, *16*, 279-85.
218. Kenar, J. A.; Havrilla, C. M.; Porter, N. A.; Guyton, J. R.; Brown, S. A.; Klemp, K. F.; Selinger, E., Identification and Quantification of the Regioisomeric Cholesteryl Linoleate Hydroperoxides in Oxidized Human Low Density Lipoprotein and High Density Lipoprotein. *Chem. Res. Toxicol.* **1996**, *9*, 737-744.
219. Miyazawa, T.; Fujimoto, K.; Kaneda, T., Detection of Picomole Levels in Lipid Hydroperoxides by a Chemiluminescence Assay. *Agricultural and Biological Chemistry* **1987**, *51*, 2569-2573.
220. Miyazawa, T.; Yasuda, K.; Fujimoto, K.; Kaneda, T., Presence of phosphatidylcholine hydroperoxide in human plasma. *J Biochem* **1988**, *103*, 744-6.
221. Yin, H.; Brooks, J. D.; Gao, L.; Porter, N. A.; Morrow, J. D., Identification of Novel Autoxidation Products of the  $\omega$ -3 Fatty Acid Eicosapentaenoic Acid in Vitro and in Vivo. *Journal of Biological Chemistry* **2007**, *282*, 29890-29901.
222. Haefliger, O. P.; Sulzer, J. W., Rapid LC-UV-ESI-MS method to investigate the industrial preparation of polyunsaturated fatty acid hydroperoxides in real-time. *Chromatographia* **2007**, *65*, 435-442.
223. Schneider, C.; Schreier, P.; Herderich, M., Analysis of lipoxygenase-derived fatty acid hydroperoxides by electrospray ionization tandem mass spectrometry. *Lipids* **1997**, *32*, 331-6.
224. Frankel, E. N.; Neff, W. E.; Plattner, R. D., Chemical ionization-mass spectrometry of secondary oxidation products from methyl linoleate and linolenate. *Lipids* **1986**, *21*, 333-7.
225. Yin, H.; Hachey, D. L.; Porter, N. A., Structural analysis of diacyl peroxides by electrospray tandem mass spectrometry with ammonium acetate: bond homolysis of peroxide-ammonium and peroxide-proton adducts. *Rapid Commun Mass Spectrom* **2000**, *14*, 1248-54.
226. Ito, J.; Mizuochi, S.; Nakagawa, K.; Kato, S.; Miyazawa, T., Tandem Mass Spectrometry Analysis of Linoleic and Arachidonic Acid Hydroperoxides via Promotion of Alkali Metal Adduct Formation. *Anal. Chem. (Washington, DC, U. S.)* **2015**, *87*, 4980-4987.
227. Kohler, M.; Leary, J. A., LC/MS/MS of carbohydrates with postcolumn addition of metal chlorides using triaxial electrospray probe. *Anal. Chem.* **1995**, *67*, 3501-8.
228. Frankel, E. N.; Neff, W. E.; Selke, E.; Brooks, D. D., Thermal and metal-catalyzed decomposition of methyl linolenate hydroperoxides. *Lipids* **1987**, *22*, 322-7.
229. Frankel, E. N.; Neff, W. E.; Selke, E., Analysis of autoxidized fats by gas chromatography-mass spectrometry. IX. Homolytic vs. heterolytic cleavage of primary and secondary oxidation products. *Lipids* **1984**, *19*, 790-800.
230. Rezanka, T., Analysis of polyunsaturated fatty acids using high performance liquid chromatography - atmospheric pressure chemical ionization mass spectrometry. *J. High Resolut. Chromatogr.* **2000**, *23*, 338-342.
231. Wilson, R.; Lyall, K., Simultaneous determination by GC-MS of epoxy and hydroxy FA as their methoxy derivatives. *Lipids* **2002**, *37*, 917-24.
232. Tanielian, C.; Chaineaux, J., Singlet oxygen reactions with model compounds of cis- and trans-polyisoprene containing two units. *Journal of Photochemistry* **1978**, *9*, 19-32.
233. Tanielian, C.; Chaineaux, J., Singlet oxygen reactions with model compounds of cis- and trans-polyisoprene containing one unit. Kinetic aspects. *J. Polym. Sci., Polym. Chem. Ed.* **1979**, *17*, 715-29.
234. Monroe, B. M., Rates of reaction of singlet oxygen with olefins. *J. Phys. Chem.* **1978**, *82*, 15-18.
235. Caminade, A. M.; Khatib, F. E.; Koenig, M.; Aubry, J. M., Ozonides and phosphite source of singlet oxygen: yield and mechanism. *Can. J. Chem.* **1985**, *63*, 3203-9.
236. Nilsson, J.; Carlberg, J.; Abrahamsson, P.; Hulthe, G.; Persson, B. A.; Karlberg, A. T., Evaluation of ionization techniques for mass spectrometric detection of contact allergenic hydroperoxides formed by autoxidation of fragrance terpenes. *Rapid Commun. Mass Spectrom.* **2008**, *22*, 3593-3598.
237. Rudbaeck, J.; Islam, N.; Nilsson, U.; Karlberg, A.-T., A sensitive method for determination of allergenic fragrance terpene hydroperoxides using liquid chromatography coupled with tandem mass spectrometry. *J. Sep. Sci.* **2013**, *36*, 1370-1378.

238. Bou, R.; Codony, R.; Tres, A.; Decker, E. A.; Guardiola, F., Determination of hydroperoxides in foods and biological samples by the ferrous oxidation-xylenol orange method: A review of the factors that influence the method's performance. *Anal. Biochem.* **2008**, *377*, 1-15.
239. Rudbaeck, J.; Ramzy, A.; Karlberg, A.-T.; Nilsson, U., Determination of allergenic hydroperoxides in essential oils using gas chromatography with electron ionization mass spectrometry. *J. Sep. Sci.* **2014**, *37*, 982-989.
240. Frankel, E. N.; Neff, W. E.; Rohwedder, W. K.; Khambay, B. P. S.; Garwood, R. F.; Weedon, B. C. L., Analysis of autoxidized fats by gas chromatography-mass spectrometry: II. Methyl linoleate. *Lipids* **1977**, *12*, 908-13.
241. Tallman, K. A.; Roschek, B., Jr.; Porter, N. A., Factors Influencing the Autoxidation of Fatty Acids: Effect of Olefin Geometry of the Nonconjugated Diene. *J. Am. Chem. Soc.* **2004**, *126*, 9240-9247.
242. Rodgers, M. T.; Armentrout, P. B., Cationic Noncovalent Interactions: Energetics and Periodic Trends. *Chemical Reviews* **2016**, *116*, 5642-5687.
243. Bogan, M. J.; Agnes, G. R., Poly(ethylene glycol) doubly and singly cationized by different alkali metal ions: Relative cation affinities and cation-dependent resolution in a quadrupole ion trap mass spectrometer. *J. Am. Soc. Mass Spectrom.* **2002**, *13*, 177-186.
244. Kaufman, J. M.; Jaber, A. J.; Stump, M. J.; Simonsick Jr, W. J.; Wilkins, C. L., Interference from multiple cations in MALDI-MS spectra of copolymers. *International Journal of Mass Spectrometry* **2004**, *234*, 153-160.
245. Rogatsky, E.; Jayatilake, H.; Goswami, G.; Tomuta, V.; Stein, D., Sensitive LC MS Quantitative Analysis of Carbohydrates by Cs<sup>+</sup> Attachment. *J. Am. Soc. Mass Spectrom.* **2005**, *16*, 1805-1811.
246. Giuffrida, F.; Destailats, F.; Skibsted, L. H.; Dionisi, F., Structural analysis of hydroperoxy- and epoxy-triacylglycerols by liquid chromatography mass spectrometry. *Chemistry and Physics of Lipids* **2004**, *131*, 41-49.
247. Pulfer, M. K.; Harrison, K.; Murphy, R. C., Direct electrospray tandem mass spectrometry of the unstable hydroperoxy bishemiacetal product derived from cholesterol ozonolysis. *Journal of the American Society for Mass Spectrometry* **2004**, *15*, 194-202.
248. Calandra, M. J.; Wang, Y.; Impellizzeri, J.; Frank, S.; de Saint Laumer, J.-Y.; Leocata, S.; Chaintreau, A., Terpene hydroperoxide chemistry in citrus oils; reaction with endogenous aldehydes to form peroxyhemiacetals. *Flavour and Fragrance Journal* **2016**, n/a-n/a.
249. Guillén, M. D.; Uriarte, P. S., Aldehydes contained in edible oils of a very different nature after prolonged heating at frying temperature: Presence of toxic oxygenated  $\alpha,\beta$  unsaturated aldehydes. *Food Chemistry* **2012**, *131*, 915-926.
250. Mistry, J.; Kennedy, J. F., Antioxidants in Food: Practical Applications, edited by J. Pokorny. *Carbohydr. Polym.* **2003**, *52*, 88-89.
251. Tucker, J. M.; Townsend, D. M., Alpha-tocopherol: roles in prevention and therapy of human disease. *Biomed. Pharmacother.* **2005**, *59*, 380-387.
252. Alander, J.; Andersson, A.-C.; Lindstroem, C., Cosmetic emollients with high stability against photo-oxidation. *Lipid Technol.* **2006**, *18*, 226-230.
253. Antolovich, M.; Prenzler, P. D.; Patsalides, E.; McDonald, S.; Robards, K., Methods for testing antioxidant activity. *Analyst (Cambridge, U. K.)* **2002**, *127*, 183-198.
254. Dziedzic, S. Z.; Hudson, B. J. F., Phosphatidylethanolamine as a synergist for primary antioxidants in edible oils. *JAOCS, J. Am. Oil Chem. Soc.* **1984**, *61*, 1042-5.
255. Marinova, E. M.; Yanishlieva, N. V., Antioxidative activity of phenolic acids on triacylglycerols and fatty acid methyl esters from olive oil. *Food Chemistry* **1996**, *56*, 139-145.
256. Schwarz, K.; Bertelsen, G.; Nissen, L. R.; Gardner, P. T.; Heinonen, M. I.; Hopia, A.; Huynh-Ba, T.; Lambelet, P.; McPhail, D.; Skibsted, L. H.; Tijburg, L., Investigation of plant extracts for the protection of processed foods against lipid oxidation. Comparison of antioxidant assays based on radical scavenging, lipid oxidation and analysis of the principal antioxidant compounds. *Eur. Food Res. Technol.* **2001**, *212*, 319-328.
257. McDonald, S.; Prenzler, P. D.; Antolovich, M.; Robards, K., Phenolic content and antioxidant activity of olive extracts. *Food Chem.* **2001**, *73*, 73-84.
258. Bowry, V. W.; Stocker, R., Tocopherol-mediated peroxidation. The prooxidant effect of vitamin E on the radical-initiated oxidation of human low-density lipoprotein. *Journal of the American Chemical Society* **1993**, *115*, 6029-6044.

259. Chacon, J. N.; Gaggini, P.; Sinclair, R. S.; Smith, F. J., Photo- and thermal-oxidation studies on methyl and phenyl linoleate: anti-oxidant behaviour and rates of reaction. *Chem. Phys. Lipids* **2000**, *107*, 107-120.
260. Huang, D.; Ou, B.; Prior, R. L., The Chemistry behind Antioxidant Capacity Assays. *J. Agric. Food Chem.* **2005**, *53*, 1841-1856.
261. Burton, G. W.; Ingold, K. U., Autoxidation of biological molecules. 1. Antioxidant activity of vitamin E and related chain-breaking phenolic antioxidants in vitro. *Journal of the American Chemical Society* **1981**, *103*, 6472-6477.
262. Lucarini, M.; Pedulli, G. F., Free radical intermediates in the inhibition of the autoxidation reaction. *Chemical Society Reviews* **2010**, *39*, 2106-2119.
263. Howard, J. A.; Ingold, K. U., Inhibited autoxidation of styrene. IV. Solvent effects. *Can. J. Chem.* **1964**, *42*, 1044-56.
264. Amorati, R.; Fumo, M. G.; Menichetti, S.; Mugnaini, V.; Pedulli, G. F., Electronic and Hydrogen Bonding Effects on the Chain-Breaking Activity of Sulfur-Containing Phenolic Antioxidants. *The Journal of Organic Chemistry* **2006**, *71*, 6325-6332.
265. Howard, J. A.; Ingold, K. U., Absolute rate constants for hydrocarbon autoxidation. I. Styrene. *Can. J. Chem.* **1965**, *43*, 2729-36.
266. Pryor, W. A.; Strickland, T.; Church, D. F., Comparison of the efficiencies of several natural and synthetic antioxidants in aqueous SDS [sodium dodecyl sulfate] micelle solutions. *J. Am. Chem. Soc.* **1988**, *110*, 2224-9.
267. Pryor, W. A.; Cornicelli, J. A.; Devall, L. J.; Tait, B.; Trivedi, B. K.; Witiak, D. T.; Wu, M., A rapid screening test to determine the antioxidant potencies of natural and synthetic antioxidants. *J. Org. Chem.* **1993**, *58*, 3521-32.
268. Kleinveld, H. A.; Hak-Lemmers, H. L.; Stalenhoef, A. F.; Demacker, P. N., Improved measurement of low-density-lipoprotein susceptibility to copper-induced oxidation: application of a short procedure for isolating low-density lipoprotein. *Clin Chem* **1992**, *38*, 2066-72.
269. Frankel, E. N.; Meyer, A. S., The problems of using one-dimensional methods to evaluate multifunctional food and biological antioxidants. *J. Sci. Food Agric.* **2000**, *80*, 1925-1941.
270. Meyer, A. S.; Yi, O.-S.; Pearson, D. A.; Waterhouse, A. L.; Frankel, E. N., Inhibition of Human Low-Density Lipoprotein Oxidation in Relation to Composition of Phenolic Antioxidants in Grapes (*Vitis vinifera*). *J. Agric. Food Chem.* **1997**, *45*, 1638-1643.
271. Frankel, E. N.; German, J. B.; Davis, P. A., Headspace gas chromatography to determine human low density lipoprotein oxidation. *Lipids* **1992**, *27*, 1047-51.
272. Frankel, E. N.; Hu, M. L.; Tappel, A. L., Rapid headspace gas chromatography of hexanal as a measure of lipid peroxidation in biological samples. *Lipids* **1989**, *24*, 976-81.
273. Van de Voort, F. R.; Ismail, A. A.; Sedman, J.; Dubois, J.; Nicodemo, T., The determination of peroxide value by Fourier transform infrared spectroscopy. *J. Am. Oil Chem. Soc.* **1994**, *71*, 921-6.
274. Holley, A. E.; Cheeseman, K. H., Measuring free radical reactions in vivo. *Br. Med. Bull.* **1993**, *49*, 494-505.
275. Milic, B. L.; Djilas, S. M.; Canadanovic-Brunet, J. M., Antioxidative activity of phenolic compounds on the metal-ion breakdown of lipid peroxidation system. *Food Chem.* **1998**, *61*, 443-447.
276. Sharma, M. K.; Buettner, G. R., Interaction of vitamin C and vitamin E during free radical stress in plasma: an ESR study. *Free Radical Biol. Med.* **1993**, *14*, 649-53.
277. Simic, M. G. In *Kinetic and mechanistic studies of peroxy, vitamin E and antioxidant free radicals by pulse radiolysis* 1980 Plenum; pp 17-26.
278. Vicente, M. L.; Empis, J. A.; Deighton, N.; Glidewell, S. M.; Goodman, B. A.; Rowlands, C. C., Use of EPR and ENDOR spectroscopy in conjunction with the spin trapping technique to study the high-temperature oxidative degradation of fatty acid methyl esters. *J. Chem. Soc., Perkin Trans. 2* **1998**, 449-454.
279. Rosen, G. M.; Rauckman, E. J.; Finkelstein, E. In *Spin trapping of radical species involved in the propagation of lipid peroxidation* 1980 Plenum; pp 71-87.
280. Brigati, G.; Lucarini, M.; Mugnaini, V.; Pedulli, G. F., Determination of the Substituent Effect on the O-H Bond Dissociation Enthalpies of Phenolic Antioxidants by the EPR Radical Equilibration Technique. *J. Org. Chem.* **2002**, *67*, 4828-4832.

281. Lucarini, M.; Pedrielli, P.; Pedulli, G. F.; Cabiddu, S.; Fattuoni, C., Bond Dissociation Energies of O-H Bonds in Substituted Phenols from Equilibration Studies. *J. Org. Chem.* **1996**, *61*, 9259-9263.
282. Brand-Williams, W.; Cuvelier, M. E.; Berset, C., Use of a free radical method to evaluate antioxidant activity. *Food Sci. Technol.* **1995**, *28*, 25-30.
283. Mishra, K.; Ojha, H.; Chaudhury, N. K., Estimation of antiradical properties of antioxidants using DPPH[rad] assay: A critical review and results. *Food Chem.* **2012**, *130*, 1036-1043.
284. Foti, M. C.; Daquino, C.; Mackie, I. D.; DiLabio, G. A.; Ingold, K. U., Reaction of Phenols with the 2,2-Diphenyl-1-picrylhydrazyl Radical. Kinetics and DFT Calculations Applied To Determine ArO-H Bond Dissociation Enthalpies and Reaction Mechanism. *J. Org. Chem.* **2008**, *73*, 9270-9282.
285. Litwinienko, G.; Ingold, K. U., Abnormal Solvent Effects on Hydrogen Atom Abstractions. 1. The Reactions of Phenols with 2,2-Diphenyl-1-picrylhydrazyl (dpph•) in Alcohols. *The Journal of Organic Chemistry* **2003**, *68*, 3433-3438.
286. Gardes-Albert, M.; Bonnefont-Rousselot, D.; Abedinzadeh, Z.; Jore, D., Reactive oxygen species. How oxygen may become toxic? *Actual. Chim.* **2003**, 91-96.
287. Noguchi, N.; Niki, E., Phenolic antioxidants: A rationale for design and evaluation of novel antioxidant drug for atherosclerosis. *Free Radical Biol. Med.* **2000**, *28*, 1538-1546.
288. Halliwell, B.; Aeschbach, R.; Löliger, J.; Aruoma, O. I., The characterization of antioxidants. *Food Chem. Toxicol.* **1995**, *33*, 601-617.
289. Zhang, H.-Y.; Sun, Y.-M.; Wang, X.-L., Substituent effects on O-H bond dissociation enthalpies and ionization potentials of catechols: a DFT study and its implications in the rational design of phenolic antioxidants and elucidation of structure - activity relationships for flavonoid antioxidants. *Chem. - Eur. J.* **2003**, *9*, 502-508.
290. Wright, J. S.; Johnson, E. R.; DiLabio, G. A., Predicting the Activity of Phenolic Antioxidants: Theoretical Method, Analysis of Substituent Effects, and Application to Major Families of Antioxidants. *J. Am. Chem. Soc.* **2001**, *123*, 1173-1183.
291. van Acker, S. A. B. E.; Koymans, L. M. H.; Bast, A., Molecular pharmacology of vitamin E: structural aspects of antioxidant activity. *Free Radical Biol. Med.* **1993**, *15*, 311-28.
292. Zhang, H.-Y., On the O-H bond dissociation enthalpy of catechol. *New J. Chem.* **2003**, *27*, 453-454.
293. Zhang, H.-Y., Theoretical methods used in elucidating activity differences of phenolic antioxidants. *J. Am. Oil Chem. Soc.* **1999**, *76*, 745-748.
294. Zhang, H.-Y., Selection of theoretical parameter characterizing scavenging activity of antioxidants on free radicals. *J. Am. Oil Chem. Soc.* **1998**, *75*, 1705-1709.
295. Wright, J. S.; Carpenter, D. J.; McKay, D. J.; Ingold, K. U., Theoretical Calculation of Substituent Effects on the O-H Bond Strength of Phenolic Antioxidants Related to Vitamin E. *J. Am. Chem. Soc.* **1997**, *119*, 4245-4252.
296. Pratt, D. A.; DiLabio, G. A.; Brigati, G.; Pedulli, G. F.; Valgimigli, L., 5-Pyrimidinols: Novel Chain-Breaking Antioxidants More Effective than Phenols. *J. Am. Chem. Soc.* **2001**, *123*, 4625-4626.
297. Bowry, V. W.; Ingold, K. U., The Unexpected Role of Vitamin E ( $\alpha$ -Tocopherol) in the Peroxidation of Human Low-Density Lipoprotein. *Acc. Chem. Res.* **1999**, *32*, 27-34.
298. Klein, E.; Lukes, V.; Cibulkova, Z.; Polovkova, J., Study of N-H, O-H, and S-H bond dissociation enthalpies and ionization potentials of substituted anilines, phenols, and thiophenols. *J. Mol. Struct-Theochem* **2006**, *758*, 149-159.
299. Klein, E.; Lukes, V., Study of gas-phase O-H bond dissociation enthalpies and ionization potentials of substituted phenols - Applicability of ab initio and DFT/B3LYP methods. *Chem. Phys.* **2006**, *330*, 515-525.
300. Watanabe, A.; Noguchi, N.; Fujisawa, A.; Kodama, T.; Tamura, K.; Cynshi, O.; Niki, E., Stability and reactivity of aryloxy radicals derived from a novel antioxidant BO-653 and related compounds. Effects of substituent and side chain in solution and membranes. *J. Am. Chem. Soc.* **2000**, *122*, 5438-5442.
301. Gotoh, N.; Noguchi, N.; Tsuchiya, J.; Morita, K.; Sakai, H.; Shimasaki, H.; Niki, E., Inhibition of oxidation of low density lipoprotein by vitamin E and related compounds. *Free Radical Res.* **1996**, *24*, 123-134.
302. Noguchi, N.; Okimoto, Y.; Tsuchiya, J.; Cynshi, O.; Kodama, T.; Niki, E., Inhibition of oxidation of low-density lipoprotein by a novel antioxidant, BO-653, prepared by theoretical design. *Arch. Biochem. Biophys.* **1997**, *347*, 141-147.

303. Zhang, H. Y.; Sun, Y. M.; Chen, D. Z., O-H bond dissociation energies of phenolic compounds are determined by field/inductive effect or resonance effect? A DFT study and its implication. *Quantitative Structure-Activity Relationships* **2001**, *20*, 148-152.
304. Leopoldini, M.; Marino, T.; Russo, N.; Toscano, M., Antioxidant Properties of Phenolic Compounds: H-Atom versus Electron Transfer Mechanism. *J. Phys. Chem. A* **2004**, *108*, 4916-4922.
305. Klein, E.; Lukes, V.; Ilcin, M., DFT/B3LYP study of tocopherols and chromans antioxidant action energetics. *Chem. Phys.* **2007**, *336*, 51-57.
306. DiLabio, G. A.; Pratt, D. A.; Wright, J. S., Theoretical calculation of gas-phase ionization potentials for mono- and polysubstituted benzenes. *Chemical Physics Letters* **1999**, *311*, 215-220.
307. Bakalbassis, E. G.; Lithoxidou, A. T.; Vafiadis, A. P., Theoretical Calculation of Accurate Absolute and Relative Gas- and Liquid-Phase O-H Bond Dissociation Enthalpies of 2-Mono- and 2,6-Disubstituted Phenols, Using DFT/B3LYP. *J. Phys. Chem. A* **2003**, *107*, 8594-8606.
308. Anouar, E.; Kosinova, P.; Kozłowski, D.; Mokrini, R.; Duroux, J. L.; Trouillas, P., New aspects of the antioxidant properties of phenolic acids: a combined theoretical and experimental approach. *Phys. Chem. Chem. Phys.* **2009**, *11*, 7659-7668.
309. Bosque, R.; Sales, J., A QSPR Study of O-H Bond Dissociation Energy in Phenols. *Journal of Chemical Information and Computer Sciences* **2003**, *43*, 637-642.
310. Brinck, T.; Haerberlein, M.; Jonsson, M., A Computational Analysis of Substituent Effects on the O-H Bond Dissociation Energy in Phenols: Polar Versus Radical Effects. *Journal of the American Chemical Society* **1997**, *119*, 4239-4244.
311. Korth, H.-G.; de Heer, M. I.; Mulder, P., A DFT Study on Intramolecular Hydrogen Bonding in 2-Substituted Phenols: Conformations, Enthalpies, and Correlation with Solute Parameters. *The Journal of Physical Chemistry A* **2002**, *106*, 8779-8789.
312. Sun, Y.-M.; Zhang, H.-Y.; Chen, D.-Z.; Liu, C.-B., Theoretical Elucidation on the Antioxidant Mechanism of Curcumin: A DFT Study. *Org. Lett.* **2002**, *4*, 2909-2911.
313. Amorati, R.; Menichetti, S.; Mileo, E.; Pedulli, G. F.; Viglianisi, C., Hydrogen-Atom Transfer Reactions from ortho-Alkoxy-Substituted Phenols: An Experimental Approach. *Chem. - Eur. J.* **2009**, *15*, 4402-4410, S4402/1-S4402/7.
314. Guerra, M.; Amorati, R.; Pedulli, G. F., Water Effect on the O-H Dissociation Enthalpy of Para-Substituted Phenols: a DFT Study. *J. Org. Chem.* **2004**, *69*, 5460-5467.
315. Nazarpour, E.; Zahedi, M.; Klein, E., Density Functional Theory (B3LYP) Study of Substituent Effects on O-H Bond Dissociation Enthalpies of trans-Resveratrol Derivatives and the Role of Intramolecular Hydrogen Bonds. *The Journal of Organic Chemistry* **2012**, *77*, 10093-10104.
316. Mohajeri, A.; Asemani, S. S., Theoretical investigation on antioxidant activity of vitamins and phenolic acids for designing a novel antioxidant. *Journal of Molecular Structure* **2009**, *930*, 15-20.
317. Nagaoka, S.; Kuranaka, A.; Tsuboi, H.; Nagashima, U.; Mukai, K., Mechanism of antioxidant reaction of vitamin E: charge transfer and tunneling effect in proton-transfer reaction. *The Journal of Physical Chemistry* **1992**, *96*, 2754-2761.
318. Burton, G. W.; Doba, T.; Gabe, E.; Hughes, L.; Lee, F. L.; Prasad, L.; Ingold, K. U., Autoxidation of biological molecules. 4. Maximizing the antioxidant activity of phenols. *J. Am. Chem. Soc.* **1985**, *107*, 7053-65.
319. Litwinienko, G.; Ingold, K. U., Abnormal Solvent Effects on Hydrogen Atom Abstraction. 3. Novel Kinetics in Sequential Proton Loss Electron Transfer Chemistry. *The Journal of Organic Chemistry* **2005**, *70*, 8982-8990.
320. Litwinienko, G.; Ingold, K. U., Abnormal Solvent Effects on Hydrogen Atom Abstraction. 2. Resolution of the Curcumin Antioxidant Controversy. The Role of Sequential Proton Loss Electron Transfer. *J. Org. Chem.* **2004**, *69*, 5888-5896.
321. Gross, K. C.; Seybold, P. G., Substituent effects on the physical properties and pKa of phenol. *Int. J. Quantum Chem.* **2001**, *85*, 569-579.
322. Amorati, R.; Valgimigli, L., Modulation of the antioxidant activity of phenols by non-covalent interactions. *Organic and Biomolecular Chemistry* **2012**, *10*, 4147-4158.
323. Leopoldini, M.; Russo, N.; Toscano, M., The molecular basis of working mechanism of natural polyphenolic antioxidants. *Food Chem.* **2010**, *125*, 288-306.

324. Li, M.-J.; Liu, L.; Fu, Y.; Guo, Q.-X., Accurate bond dissociation enthalpies of popular antioxidants predicted by the ONIOM-G3B3 method. *J. Mol. Struct. THEOCHEM* **2007**, *815*, 1-9.
325. Perez-Gonzalez, A.; Rebollar-Zepeda, A. M.; Leon-Carmona, J. R.; Galano, A., Reactivity indexes and O-H bond dissociation energies of a large series of polyphenols: implications for their free radical scavenging activity. *J. Mex. Chem. Soc.* **2012**, *56*, 241-249.
326. Mulder, P.; Korth, H.-G.; Pratt, D. A.; DiLabio, G. A.; Valgimigli, L.; Pedulli, G. F.; Ingold, K. U., Critical Re-evaluation of the O-H Bond Dissociation Enthalpy in Phenol. *J. Phys. Chem. A* **2005**, *109*, 2647-2655.
327. Chandra, A. K.; Uchamaru, T., The O-H Bond dissociation energies of substituted phenols and proton affinities of substituted phenoxide ions. A DFT Study. *International Journal of Molecular Sciences* **2002**, *3*, 407-422.
328. Lucarini, M.; Mugnaini, V.; Pedulli, G. F.; Guerra, M., Hydrogen-Bonding Effects on the Properties of Phenoxy Radicals. An EPR, Kinetic, and Computational Study. *Journal of the American Chemical Society* **2003**, *125*, 8318-8329.
329. Lucarini, M.; Pedrielli, P.; Pedulli, G. F.; Cabiddu, S.; Fattuoni, C., Bond Dissociation Energies of O-H Bonds in Substituted Phenols from Equilibration Studies. *The Journal of Organic Chemistry* **1996**, *61*, 9259-9263.
330. Szymusiak, H.; Zielinski, R., Bond dissociation enthalpy of phenolic antioxidants. *Polish Journal Of Food And Nutrition Sciences* **2003**, *12*, 129-135.
331. Hoelz, L. V. B.; Horta, B. A. C.; Araujo, J. Q.; Albuquerque, M. G.; Bicca de Alencastro, R.; da Silva, J. F. M., Quantitative structure-activity relationships of antioxidant phenolic compounds. *J. Chem. Pharm. Res.* **2010**, *2*, 291-306.
332. Thavasi, V.; Leong, L. P.; Bettens, R. P. A., Investigation of the Influence of Hydroxy Groups on the Radical Scavenging Ability of Polyphenols. *J. Phys. Chem. A* **2006**, *110*, 4918-4923.
333. Amorati, R.; Ferroni, F.; Lucarini, M.; Pedulli, G. F.; Valgimigli, L., A Quantitative Approach to the Recycling of  $\alpha$ -Tocopherol by Coantioxidants. *J. Org. Chem.* **2002**, *67*, 9295-9303.
334. Marteau, C.; Nardello-Rataj, V.; Favier, D.; Aubry, J. M., Dual role of phenols as fragrances and antioxidants: mechanism, kinetics and drastic solvent effect. *Flavour Frag. J.* **2013**, *28*, 30-38.
335. Nehru, K.; Jang, Y.; Oh, S.; Dallemer, F.; Nam, W.; Kim, J., Oxidation of hydroquinones by a nonheme iron(IV)-oxo species. *Inorg. Chim. Acta* **2008**, *361*, 2557-2561.
336. Marteau, C.; Guitard, R.; Penverne, C.; Favier, D.; Nardello-Rataj, V.; Aubry, J. M., Boosting effect of ortho-propenyl substituent on the antioxidant activity of natural phenols. *Food Chem.* **2016**, *196*, 418-427.
337. Natella, F.; Nardini, M.; Di Felice, M.; Scaccini, C., Benzoic and Cinnamic Acid Derivatives as Antioxidants: Structure-Activity Relation. *J. Agric. Food Chem.* **1999**, *47*, 1453-1459.
338. Nenadis, N.; Tsimidou, M. Z., Contribution of DFT computed molecular descriptors in the study of radical scavenging activity trend of natural hydroxybenzaldehydes and corresponding acids. *Food Res. Int.* **2012**, *48*, 538-543.
339. Chen, Y.; Xiao, H.; Zheng, J.; Liang, G., Structure-thermodynamics-antioxidant activity relationships of selected natural phenolic acids and derivatives: an experimental and theoretical evaluation. *PLoS One* **2015**, *10*.
340. Amorati, R.; Pedulli, G. F.; Cabrini, L.; Zambonin, L.; Landi, L., Solvent and pH Effects on the Antioxidant Activity of Caffeic and Other Phenolic Acids. *Journal of Agricultural and Food Chemistry* **2006**, *54*, 2932-2937.
341. Pino, E.; Campos, A. M.; Lopez-Alarcon, C.; Aspee, A.; Lissi, E., Free radical scavenging capacity of hydroxycinnamic acids and related compounds. *J. Phys. Org. Chem.* **2006**, *19*, 759-764.
342. Musialik, M.; Kuzmicz, R.; Pawlowski, T. S.; Litwinienko, G., Acidity of Hydroxyl Groups: An Overlooked Influence on Antiradical Properties of Flavonoids. *J. Org. Chem.* **2009**, *74*, 2699-2709.
343. Bors, W.; Heller, W.; Michel, C.; Saran, M., Flavonoids as antioxidants: Determination of radical-scavenging efficiencies. In *Methods in Enzymology*, Academic Press 1990; Vol. Volume 186, pp 343-355.
344. Amic, D.; Lucic, B., Reliability of bond dissociation enthalpy calculated by the PM6 method and experimental TEAC values in antiradical QSAR of flavonoids. *Bioorg. Med. Chem.* **2010**, *18*, 28-35.
345. Garcia Aranzazu, M.; Ruiz-Mendez, V.; Romero, C.; Brenes, M., Effect of refining on the phenolic composition of crude olive oils. *J. Am. Oil Chem. Soc.* **2006**, *83*, 159-164.

346. Hsu, D.-Z.; Chu, P.-Y.; Chandrasekaran, V. R. M.; Liu, M.-Y., Sesame lignan sesamol protects against aspirin-induced gastric mucosal damage in rats. *J. Funct. Foods* **2009**, *1*, 349-355.
347. Zhang, H.-Y.; Wang, L.-F., Theoretical elucidation of structure-activity relationship for coumarins to scavenge peroxy radical. *J. Mol. Struct.: THEOCHEM* **2004**, *673*, 199-202.
348. Erkan, N.; Ayranci, G.; Ayranci, E., Antioxidant activities of rosemary (*Rosmarinus officinalis* L.) extract, blackseed (*Nigella sativa* L.) essential oil, carnosic acid, rosmarinic acid and sesamol. *Food Chem.* **2008**, *110*, 76-82.
349. Lucarini, M.; Pedulli, G. F., Free radical intermediates in the inhibition of the autoxidation reaction. *Chem. Soc. Rev.* **2010**, *39*, 2106-2119.
350. Wright, J. S.; Johnson, E. R.; DiLabio, G. A., Predicting the Activity of Phenolic Antioxidants: Theoretical Method, Analysis of Substituent Effects, and Application to Major Families of Antioxidants. *J. Am. Chem. Soc.* **2001**, *123*, 1173-1183.
351. Guitard, R.; Paul, J. F.; Nardello, V.; Aubry, J. M., Myricetin, rosmarinic and carnosic acid as superior natural antioxidant alternatives to  $\alpha$ -tocopherol for the preservation of omega-3 oils (unpublished work). *Food Chem.* **2016**.
352. de Heer, M. I.; Korth, H.-G.; Mulder, P., Poly Methoxy Phenols in Solution: O-H Bond Dissociation Enthalpies, Structures, and Hydrogen Bonding. *J. Org. Chem.* **1999**, *64*, 6969-6975.
353. Svobodova Varekova, R.; Geidl, S.; Ionescu, C.-M.; Skrehota, O.; Kudera, M.; Sehnal, D.; Bouchal, T.; Abagyan, R.; Huber, H. J.; Koca, J., Predicting pKa Values of Substituted Phenols from Atomic Charges: Comparison of Different Quantum Mechanical Methods and Charge Distribution Schemes. *J. Chem. Inf. Model.* **2011**, *51*, 1795-1806.
354. Perrin, D. D., *Dissociation Constants of Organic Bases in Aqueous Solution. (Pure and Applied Chemistry)*. Butterworths1965; p 473 pp.
355. Jover, J.; Bosque, R.; Sales, J., Neural Network based QSPR study for predicting pKa of phenols in different solvents. *QSAR Comb. Sci.* **2007**, *26*, 385-397.
356. Pietta, P.-G., Flavonoids as Antioxidants. *Journal of Natural Products* **2000**, *63*, 1035-1042.
357. Goupy, P.; Dufour, C.; Loonis, M.; Dangles, O., Quantitative Kinetic Analysis of Hydrogen Transfer Reactions from Dietary Polyphenols to the DPPH Radical. *J. Agric. Food Chem.* **2003**, *51*, 615-622.
358. Litwinienko, G.; Ingold, K. U., Solvent Effects on the Rates and Mechanisms of Reaction of Phenols with Free Radicals. *Accounts of Chemical Research* **2007**, *40*, 222-230.
359. Valgimigli, L.; Ingold, K. U.; Luszyk, J., Antioxidant Activities of Vitamin E Analogs in Water and a Kamlet-Taft  $\beta$ -Value for Water. *J. Am. Chem. Soc.* **1996**, *118*, 3545-9.
360. Bondet, V.; Brand-Williams, W.; Berset, C., Kinetics and mechanisms of antioxidant activity using the DPPH free radical method. *Food Science and Technology* **1997**, *30*, 772.
361. Hussain, H. H.; Babic, G.; Durst, T.; Wright, J. S.; Flueraru, M.; Chichirau, A.; Chepelev, L. L., Development of Novel Antioxidants: Design, Synthesis, and Reactivity. *The Journal of Organic Chemistry* **2003**, *68*, 7023-7032.
362. Tikhonov, I.; Roginsky, V.; Pliss, E., The chain-breaking antioxidant activity of phenolic compounds with different numbers of O-H groups as determined during the oxidation of styrene. *Int. J. Chem. Kinet.* **2009**, *41*, 92-100.
363. Foti, M. C.; Johnson, E. R.; Vinqvist, M. R.; Wright, J. S.; Barclay, L. R. C.; Ingold, K. U., Naphthalene Diols: A New Class of Antioxidants. Intramolecular Hydrogen Bonding in Catechols, Naphthalene Diols, and Their Aryloxy Radicals. *J. Org. Chem.* **2002**, *67*, 5190-5196.
364. Capitani, C. D.; Carvalho, A. C. L.; Rivelli, D. P.; Barros, S. B. M.; Castro, I. A., Evaluation of natural and synthetic compounds according to their antioxidant activity using a multivariate approach. *European Journal of Lipid Science and Technology* **2009**, *111*, 1090-1099.
365. Alamed, J.; Chaiyasit, W.; McClements, D. J.; Decker, E. A., Relationships between Free Radical Scavenging and Antioxidant Activity in Foods. *Journal of Agricultural and Food Chemistry* **2009**, *57*, 2969-2976.
366. Lagouri, V.; Nisteropoulou, E., Antioxidant properties of *O. onites*, *T. vulgaris* and *O. basilicum* species grown in Greece and their total phenol and rosmarinic acid content. *Journal of Food Lipids* **2009**, *16*, 484-498.
367. Abraham, M. H.; Grellier, P. L.; Prior, D. V.; Duce, P. P.; Morris, J. J.; Taylor, P. J., Hydrogen bonding. Part 7. A scale of solute hydrogen-bond acidity based on log K values for complexation in tetrachloromethane. *J. Chem. Soc., Perkin Trans. 2* **1989**, 699-711.

368. Abraham, M. H.; Grellier, P. L.; Prior, D. V.; Morris, J. J.; Taylor, P. J., Hydrogen bonding. Part 10. A scale of solute hydrogen-bond basicity using log K values for complexation in tetrachloromethane. *J. Chem. Soc., Perkin Trans. 2* **1990**, 521-9.
369. Marteau, C. *Activité antioxydante des phénols : mécanismes, cinétiques, effets de solvants et synergies*. Université Lille 1, Lille, 2013.
370. McClure, T. D.; Liebler, D. C., A Rapid Method for Profiling the Products of Antioxidant Reactions by Negative Ion Chemical Ionization Mass Spectrometry. *Chem. Res. Toxicol.* **1995**, *8*, 128-35.
371. Gates, P. J.; Lopes, N. P., Characterisation of flavonoid aglycones by negative ion chip-based nanospray tandem mass spectrometry. *Int. J. Anal. Chem.* **2012**, 259217, 7 pp.
372. Tkachev, V. V.; Aldoshin, S. M.; Shilov, G. V.; Komissarov, V. N.; Sayapin, Y. A.; Korobov, M. S.; Borodkin, G. S.; Minkin, V. I., Structure of the oxidative dimerization product of 4,6-di(tert-butyl)pyrogallol. *Russian Chemical Bulletin* **2007**, *56*, 276-280.
373. Saito, S.; Kawabata, J., DPPH (=2,2-diphenyl-1-picrylhydrazyl) radical-scavenging reaction of protocatechuic acid (=3,4-dihydroxybenzoic acid): difference in reactivity between acids and their esters. *Helvetica Chimica Acta* **2006**, *89*, 1395-1407.
374. Arakawa, R.; Yamaguchi, M.; Hotta, H.; Osakai, T.; Kimoto, T., Product analysis of caffeic acid oxidation by on-line electrochemistry/electrospray ionization mass spectrometry. *Journal of the American Society for Mass Spectrometry* **2004**, *15*, 1228-1236.
375. Pierpoint, W. S., The enzymic oxidation of chlorogenic acid and some reactions of the quinone produced. *Biochemical Journal* **1966**, *98*, 567-80.
376. Balla, J.; Kiss, T.; Jameson, R. F., Copper(II)-catalyzed oxidation of catechol by molecular oxygen in aqueous solution. *Inorganic Chemistry* **1992**, *31*, 58-62.
377. De Lucia, M.; Panzella, L.; Pezzella, A.; Napolitano, A.; D'Ischia, M., Oxidative chemistry of the natural antioxidant hydroxytyrosol: hydrogen peroxide-dependent hydroxylation and hydroxyquinone/o-quinone coupling pathways. *Tetrahedron* **2006**, *62*, 1273-1278.
378. McPhail, D. B.; Hartley, R. C.; Gardner, P. T.; Duthie, G. G., Kinetic and Stoichiometric Assessment of the Antioxidant Activity of Flavonoids by Electron Spin Resonance Spectroscopy. *Journal of Agricultural and Food Chemistry* **2003**, *51*, 1684-1690.
379. Masuda, T.; Kirikihira, T.; Takeda, Y., Recovery of antioxidant activity from carnosol quinone: Antioxidants obtained from a water-promoted conversion of carnosol quinone. *Journal of Agricultural and Food Chemistry* **2005**, *53*, 6831-6834.
380. Masuda, T.; Inaba, Y.; Takeda, Y., Antioxidant Mechanism of Carnosic Acid: Structural Identification of Two Oxidation Products. *Journal of Agricultural and Food Chemistry* **2001**, *49*, 5560-5565.
381. Castaldi, P.; Garau, G.; Palma, A.; Deiana, S., Formation of biopolymers owing to the oxidation of esculetine by Cu(II) ions in a Ca-polygalacturonate network. *J. Inorg. Biochem.* **2012**, *108*, 30-35.
382. Fujimoto, A.; Masuda, T., Antioxidation mechanism of rosmarinic acid, identification of an unstable quinone derivative by the addition of odourless thiol. *Food Chemistry* **2012**, *132*, 901-906.
383. Hamama, A. A.; Nawar, W. W., Thermal decomposition of some phenolic antioxidants. *Journal of Agricultural and Food Chemistry* **1991**, *39*, 1063-9.
384. Caregnato, P.; Gara, P. M. D.; Bosio, G. N.; Gonzalez, M. C.; Russo, N.; Michelini, M. d. C.; Martire, D. O., Theoretical and Experimental Investigation on the Oxidation of Gallic Acid by Sulfate Radical Anions. *The Journal of Physical Chemistry A* **2008**, *112*, 1188-1194.
385. Arab Chamjangali, M.; Bakherad, M.; Ameri, M., Electrochemical oxidation of catechol derivatives in the presence of 3-acetyldihydro-2(3H)-furanone: efficient and green method for synthesis of new butyrolactone derivatives. *Monatshefte für Chemie* **2015**, *146*, 111-117.
386. Imagawa, H.; Takino, Y., The oxidation of myricetin glycosides by tea oxidase. Formation of 2',2'''-biflavonol, a new biflavonoid. *Agricultural and Biological Chemistry* **1962**, *26*, 541-2.
387. Nematollahi, D.; Rafiee, M.; Samadi-Maybodi, A., Mechanistic study of electrochemical oxidation of 4-tert-butylcatechol. A facile electrochemical method for the synthesis of new trimer of 4-tert-butylcatechol. *Electrochim. Acta* **2004**, *49*, 2495-2502.
388. Kummer, S.; Ruth, W.; Kragl, U., Oxidation of Flavonols in an Electrochemical Flow Cell Coupled Online with ESI-MS. *Electroanalysis* **2015**, Ahead of Print.

389. Boehmdorfer, S.; Patel, A.; Netscher, T.; Gille, L.; Rosenau, T., On the dimers of  $\beta$ -tocopherol. *Tetrahedron* **2011**, *67*, 4858-4861.
390. Bolon, D. A., Generation of O-quinone methides in solution. Trimerization. *The Journal of Organic Chemistry* **1970**, *35*, 715-19.
391. Bowry, V. W.; Ingold, K. U., Extraordinary Kinetic Behavior of the  $\alpha$ -Tocopheroxyl (Vitamin E) Radical. *J. Org. Chem.* **1995**, *60*, 5456-67.
392. Omura, K., Electron Transfer between Protonated and Unprotonated Phenoxy Radicals. *The Journal of Organic Chemistry* **2008**, *73*, 858-867.
393. Zhang, N.; Kawakami, S.; Higaki, M.; Wee, V. T., New oxidation pathway of 3,5-di-tert-butyl-4-hydroxytoluene: an ionspray tandem mass spectrometric and gas chromatographic/mass spectrometric study. *J. Am. Oil Chem. Soc.* **1997**, *74*, 781-786.
394. Fujisawa, S.; Atsumi, T.; Kadoma, Y.; Ishihara, M.; Ito, S.; Yokoe, I., Kinetic radical scavenging activity and cytotoxicity of 2-methoxy- and 2-t-butyl-substituted phenols and their dimers. *Anticancer Res.* **2004**, *24*, 3019-3026.
395. Kadoma, Y.; Ito, S.; Yokoe, I.; Fujisawa, S., Comparative study of the alkyl and peroxy radical-scavenging activity of 2-t-Butyl-4-methoxyphenol (BHA) and its dimer, and their theoretical parameters. *In Vivo* **2008**, *22*, 289-296.
396. Omura, K., Antioxidant synergism between butylated hydroxyanisole and butylated hydroxytoluene. *J Amer Oil Chem Soc* **1995**, *72*, 1565-70.
397. Carunchio, F.; Crescenzi, C.; Girelli, A. M.; Messina, A.; Tarola, A. M., Oxidation of ferulic acid by laccase: identification of the products and inhibitory effects of some dipeptides. *Talanta* **2001**, *55*, 189-200.
398. Kaeding, W. W., Oxidation of phenols with cupric salts. *Talanta* **1963**, *28*, 1063-7.
399. Bortolomeazzi, R.; Verardo, G.; Liessi, A.; Callea, A., Formation of dehydrodiisoeugenol and dehydrodieugenol from the reaction of isoeugenol and eugenol with DPPH radical and their role in the radical scavenging activity. *Food Chemistry* **2009**, *118*, 256-265.
400. Shingai, Y.; Fujimoto, A.; Nakamura, M.; Masuda, T., Structure and Function of the Oxidation Products of Polyphenols and Identification of Potent Lipoxigenase Inhibitors from Fe-Catalyzed Oxidation of Resveratrol. *J. Agric. Food Chem.* **2011**, *59*, 8180-8186.
401. Constantin, M.-A.; Conrad, J.; Beifuss, U., An unprecedented oxidative trimerization of sesamol catalyzed by laccases. *Tetrahedron Letters* **2012**, *53*, 3254-3258.
402. Decker, E. A., Antioxidant mechanisms. *Food Science and Technology* **2002**, *117*, 517-542.
403. Zhang, Y.; Smuts, J. P.; Dodbiba, E.; Rangarajan, R.; Lang, J. C.; Armstrong, D. W., Degradation Study of Carnosic Acid, Carnosol, Rosmarinic Acid, and Rosemary Extract (*Rosmarinus officinalis* L.) Assessed Using HPLC. *Journal of Agricultural and Food Chemistry* **2012**, *60*, 9305-9314.
404. Kemin *Rosamox as natural antioxidant: the cascade effect of Rosamox*; 2013.
405. Li, J.; Bi, Y.; Liu, W.; Sun, S.; Liu, C.; Ma, S., Effect of acid value on TBHQ and BHT losses in heating oils: Identification of the esterification products of TBHQ and free fatty acids. *J. Am. Oil Chem. Soc.* **2014**, *91*, 1763-1771.
406. Valgimigli, L.; Amorati, R.; Fumo, M. G.; DiLabio, G. A.; Pedulli, G. F.; Ingold, K. U.; Pratt, D. A., The Unusual Reaction of Semiquinone Radicals with Molecular Oxygen. *The Journal of Organic Chemistry* **2008**, *73*, 1830-1841.
407. Cort, W. M., Antioxidant activity of tocopherols, ascorbyl palmitate, and ascorbic acid and their mode of action. *J. Amer. Oil Chem. Soc.* **1974**, *51*, 321-5.
408. Jerzykiewicz, M.; Cwiela-Piasecka, I.; Jezierski, A., Pro- and Antioxidative Effect of  $\alpha$ -Tocopherol on Edible Oils, Triglycerides and Fatty Acids. *J. Am. Oil Chem. Soc.* **2013**, *90*, 803-811.
409. Kim, H. J.; Lee, H. O.; Min, D. B., Effects and prooxidant mechanisms of oxidized  $\alpha$ -tocopherol on the oxidative stability of soybean oil. *J. Food Sci.* **2007**, *72*, C223-C230.
410. Mercier, S.; Mondor, M.; Villeneuve, S.; Marcos, B.; Moresoli, C., Assessment of the Oxidative Stability of Flaxseed-Enriched Lasagna Using the Rancimat Method. *J. Food Process. Preserv.* **2015**, *39*, 1729-1734.
411. Kurhade, A. H.; Waghmare, J. S., Effect of Banana Peel Oleoresin on Oxidative Stability of Sunflower and Soybean Oil. *J. Food Process. Preserv.* **2015**, *39*, 1788-1797.

412. Tavares, M. L. A.; Queiroz, N.; Santos, I. M. G.; Souza, A. L.; Cavalcanti, E. H. S.; Barros, A. K. D.; Rosenhaim, R.; Soledade, L. E. B.; Souza, A. G., Sunflower biodiesel. *J. Therm. Anal. Calorim.* **2011**, *106*, 575-579.
413. Liang, Y. C.; May, C. Y.; Foon, C. S.; Ngan, M. A.; Hock, C. C.; Basiron, Y., The effect of natural and synthetic antioxidants on the oxidative stability of palm diesel. *Fuel* **2006**, *85*, 867-870.
414. Hossain, M.; Sujan, S. M. A.; Jamal, M. S., Antioxidant effect on oxidation stability of blend fish oil biodiesel with vegetable oil biodiesel and petroleum diesel fuel. *Int. J. Renewable Energy Dev.* **2013**, *2*, 75-80, 6 pp.
415. Pinto, L. M.; de Souza, A. L.; Souza, A. G.; Santos, I. M. G.; Queiroz, N., Comparative evaluation of the effect of antioxidants added into peanut (*arachis hypogae* L.) oil biodiesel by P-DSC and rancimat. *J. Therm. Anal. Calorim.* **2015**, *120*, 277-282.
416. Jain, S.; Sharma, M. P., Stability of biodiesel and its blends: A review. *Renewable Sustainable Energy Rev.* **2010**, *14*, 667-678.
417. Botella, L.; Bimbela, F.; Martin, L.; Arauzo, J.; Sanchez, J. L., Oxidation stability of biodiesel fuels and blends using the Rancimat and PetroOXY methods. Effect of 4-allyl-2,6-dimethoxyphenol and catechol as biodiesel additives on oxidation stability. *Front. Chem. (Lausanne, Switz.)* **2014**, *2*, 1-9.
418. Atoui, A. K.; Mansouri, A.; Boskou, G.; Kefalas, P., Tea and herbal infusions: their antioxidant activity and phenolic profile. *Food Chem.* **2004**, *89*, 27-36.
419. Ju, J.; Lu, G.; Lambert, J. D.; Yang, C. S., Inhibition of carcinogenesis by tea constituents. *Semin. Cancer Biol.* **2007**, *17*, 395-402.
420. Kamal-Eldin, A.; Appelqvist, L.-A., The chemistry and antioxidant properties of tocopherols and tocotrienols. *Lipids* **1996**, *31*, 671-701.
421. Chan, A. C.; Tran, K.; Raynor, T.; Ganz, P. R.; Chow, C. K., Regeneration of vitamin E in human platelets. *J. Biol. Chem.* **1991**, *266*, 17290-5.
422. Roberts, W. G.; Gordon, M. H., Determination of the Total Antioxidant Activity of Fruits and Vegetables by a Liposome Assay. *J. Agric. Food Chem.* **2003**, *51*, 1486-1493.
423. Niki, E.; Saito, T.; Kawakami, A.; Kamiya, Y., Inhibition of oxidation of methyl linoleate in solution by vitamin E and vitamin C. *The Journal of Biological Chemistry* **1984**, *259*, 4177-82.
424. Golumbic, C.; Mattill, H. A., Antioxidants and the autoxidation of fats. XIII. The antioxygenic action of ascorbic acid in association with tocopherols, hydroquinones and related compounds. *J. Am. Chem. Soc.* **1941**, *63*, 1279-80.
425. Barclay, L. R. C.; Locke, S. J.; MacNeil, J. M., The autoxidation of unsaturated lipids in micelles. Synergism of inhibitors vitamins C and E. *Can. J. Chem.* **1983**, *61*, 1288-90.
426. Liao, K.-l.; Yin, M.-c., Individual and Combined Antioxidant Effects of Seven Phenolic Agents in Human Erythrocyte Membrane Ghosts and Phosphatidylcholine Liposome Systems: Importance of the Partition Coefficient. *J. Agric. Food Chem.* **2000**, *48*, 2266-2270.
427. Leung, H.-W.; Vang, M. J.; Mavis, R. D., The cooperative interaction between vitamin E and vitamin C in suppression of peroxidation of membrane phospholipids. *Biochim. Biophys. Acta, Lipids Lipid Metab.* **1981**, *664*, 266-72.
428. Bascetta, E.; Gunstone, F. D.; Walton, J. C., Electron spin resonance study of the role of vitamin E and vitamin C in the inhibition of fatty acid oxidation in a model membrane. *Chem. Phys. Lipids* **1983**, *33*, 207-10.
429. Scarpa, M.; Rigo, A.; Maiorino, M.; Ursini, F.; Gregolin, C., Formation of  $\alpha$ -tocopherol radical and recycling of  $\alpha$ -tocopherol by ascorbate during peroxidation of phosphatidylcholine liposomes. An electron paramagnetic resonance study. *Biochim. Biophys. Acta, Gen. Subj.* **1984**, *801*, 215-19.
430. Laranjinha, J.; Vierira, O.; Madeira, V.; Almeida, L., Two related phenolic antioxidants with opposite effects on vitamin E content in low density lipoproteins oxidized by ferrylmyoglobin: consumption vs regeneration. *Arch. Biochem. Biophys.* **1995**, *323*, 373-81.
431. Bisby, R. H.; Parker, A. W., Reaction of Ascorbate with the  $\alpha$ -Tocopheroxyl Radical in Micellar and Bilayer Membrane Systems. *Archives of Biochemistry and Biophysics* **1995**, *317*, 170-178.
432. Castro, I. A.; Rogero, M. M.; Junqueira, R. M.; Carrapeiro, M. M., 2,2-diphenyl-1-picrylhydrazil free radical scavenging activity of antioxidant mixtures evaluated by response surface methodology. *Int. J. Food Sci. Technol.* **2006**, *41*, 59-67.

433. Pazos, M.; Andersen, M. L.; Medina, I.; Skibsted, L. H., Efficiency of Natural Phenolic Compounds Regenerating  $\alpha$ -Tocopherol from  $\alpha$ -Tocopheroxyl Radical. *Journal of Agricultural and Food Chemistry* **2007**, *55*, 3661-3666.
434. Chen, C.-Y.; Milbury, P. E.; Lapsley, K.; Blumberg, J. B., Flavonoids from Almond Skins Are Bioavailable and Act Synergistically with Vitamins C and E to Enhance Hamster and Human LDL Resistance to Oxidation. *The Journal of Nutrition* **2005**, *135*, 1366-1373.
435. Jia, Z.-S.; Zhou, B.; Yang, L.; Wu, L.-M.; Liu, Z.-L., Antioxidant synergism of tea polyphenols and  $\alpha$ -tocopherol against free radical induced peroxidation of linoleic acid in solution. *J. Chem. Soc., Perkin Trans. 2* **1998**, 911-915.
436. Pedrielli, P.; Skibsted, L. H., Antioxidant Synergy and Regeneration Effect of Quercetin, (-)-Epicatechin, and (+)-Catechin on  $\alpha$ -Tocopherol in Homogeneous Solutions of Peroxidating Methyl Linoleate. *Journal of Agricultural and Food Chemistry* **2002**, *50*, 7138-7144.
437. Pekkarinen, S. S.; Heinonen, I. M.; Hopia, A. I., Flavonoids quercetin, myricetin, kaemferol and (+)-catechin as antioxidants in methyl linoleate. *Journal of the Science of Food and Agriculture* **1999**, *79*, 499-506.
438. Becker, E. M.; Ntouma, G.; Skibsted, L. H., Synergism and antagonism between quercetin and other chain-breaking antioxidants in lipid systems of increasing structural organisation. *Food Chemistry* **2007**, *103*, 1288-1296.
439. Marinova, E.; Toneva, A.; Yanishlieva, N., Synergistic antioxidant effect of  $\alpha$ -tocopherol and myricetin on the autoxidation of triacylglycerols of sunflower oil. *Food Chemistry* **2007**, *106*, 628-633.
440. Zhou, B.; Wu, L.-M.; Yang, L.; Liu, Z.-L., Evidence for  $\alpha$ -tocopherol regeneration reaction of green tea polyphenols in SDS micelles. *Free Radical Biol. Med.* **2005**, *38*, 78-84.
441. Zhu, Q. Y.; Huang, Y.; Tsang, D.; Chen, Z.-Y., Regeneration of  $\alpha$ -Tocopherol in Human Low-Density Lipoprotein by Green Tea Catechin. *Journal of Agricultural and Food Chemistry* **1999**, *47*, 2020-2025.
442. Cai, Y.-J.; Ma, L.-P.; Hou, L.-F.; Zhou, B.; Yang, L.; Liu, Z.-L., Antioxidant effects of green tea polyphenols on free radical initiated peroxidation of rat liver microsomes. *Chem. Phys. Lipids* **2002**, *120*, 109-117.
443. Cillard, J.; Cillard, P., Inhibitors of the prooxidant activity of  $\alpha$ -tocopherol. *JAOCS, J. Am. Oil Chem. Soc.* **1986**, *63*, 1165-9.
444. Amorati, R.; Ferroni, F.; Pedulli, G. F.; Valgimigli, L., Modeling the Co-Antioxidant Behavior of Monofunctional Phenols. Applications to Some Relevant Compounds. *The Journal of Organic Chemistry* **2003**, *68*, 9654-9658.
445. Kurechi, T.; Kikugawa, K.; Kato, T., Studies on the antioxidants. XIII. Hydrogen donating capability of antioxidants to 2,2-diphenyl-1-picrylhydrazyl. *Chem. Pharm. Bull.* **1980**, *28*, 2089-93.
446. Iglesias, J.; Pazos, M.; Andersen, M. L.; Skibsted, L. H.; Medina, I., Caffeic Acid as Antioxidant in Fish Muscle: Mechanism of Synergism with Endogenous Ascorbic Acid and  $\alpha$ -Tocopherol. *J. Agric. Food Chem.* **2009**, *57*, 675-681.
447. Peyrat-Maillard, M. N.; Cuvelier, M. E.; Berset, C., Antioxidant activity of phenolic compounds in 2,2'-azobis(2-amidinopropane) dihydrochloride (AAPH)-induced oxidation: Synergistic and antagonistic effects. *J. Am. Oil Chem. Soc.* **2003**, *80*, 1007-1012.
448. Mortensen, A.; Skibsted, L. H., Relative stability of carotenoid radical cations and homolog tocopheroxyl radicals. A real time kinetic study of antioxidant hierarchy. *FEBS Lett.* **1997**, *417*, 261-266.
449. Schroeder, M. T.; Becker, E. M.; Skibsted, L. H., Molecular Mechanism of Antioxidant Synergism of Tocotrienols and Carotenoids in Palm Oil. *Journal of Agricultural and Food Chemistry* **2006**, *54*, 3445-3453.
450. Liu, D.; Shi, J.; Colina, I. A.; Kakuda, Y.; Xue, S. J., The scavenging capacity and synergistic effects of lycopene, vitamin E, vitamin C, and  $\beta$ -carotene mixtures on the DPPH free radical. *LWT--Food Sci. Technol.* **2008**, *41*, 1344-1349.
451. Palozza, P.; Krinsky, N. I.,  $\beta$ -Carotene and  $\alpha$ -tocopherol are synergistic antioxidants. *Arch. Biochem. Biophys.* **1992**, *297*, 184-7.

452. Fang, J.-G.; Lu, M.; Chen, Z.-H.; Zhu, H.-H.; Li, Y.; Yang, L.; Wu, L.-M.; Liu, Z.-L., Antioxidant effects of resveratrol and its analogues against the free-radical-induced peroxidation of linoleic acid in micelles. *Chem. - Eur. J.* **2002**, *8*, 4191-4198.
453. Gardner, H. W.; Kleiman, R.; Weisleder, D.; Inglett, G. E., Cysteine adds to lipid hydroperoxide. *Lipids* **1977**, *12*, 655-60.
454. Sims, R. J.; Fioriti, J. A., Methional as an antioxidant for vegetable oils. *J. Am. Oil Chem. Soc.* **1977**, *54*, 4-7.
455. Koga, T.; Terao, J., Phospholipids Increase Radical-Scavenging Activity of Vitamin E in a Bulk Oil Model System. *J. Agric. Food Chem.* **1995**, *43*, 1450-4.
456. Bandarra, N.; Campos, R.; Batista, I.; Nunes, M. L.; Empis, J., Antioxidant synergy of  $\alpha$ -tocopherol and phospholipids. *J. Amer. Oil Chem. Soc.* **1999**, *76*, 905-913.
457. Kourimska, L.; Pokorny, J.; Reblova, Z., Phospholipids as inhibitors of oxidation during food storage and frying. *Prehrambeno-Tehnol. Biotehnol. Rev.* **1994**, *32*, 91-4.
458. Pokorny, J.; Reblova, Z.; Ranny, M.; Kanova, J.; Panek, J.; Davidek, J., Natural lecithins and phosphorylated acylglycerols as inhibitors of autoxidation of fats and oils. *Nahrung* **1992**, *36*, 461-5.
459. Pokorny, J.; Luan, N.; Svobodova, H.; Janicek, G., Stabilization of fats with natural antioxidants. Part 4. Antioxidative effect of soybean phospholipids. *Nahrung* **1976**, *20*, K3-4.
460. Yee, J. J.; Shipe, W. F., Using enzymatic proteolysis to reduce copper-protein catalysis of lipid oxidation. *J. Food Sci.* **1981**, *46*, 966-7, 969.
461. Riisom, T.; Sims, R. J.; Fioriti, J. A., Effect of amino acids on the autoxidation of safflower oil in emulsions. *J. Am. Oil Chem. Soc.* **1980**, *57*, 354-9.
462. Boots, A. W.; Kubben, N.; Haenen, G. R. M. M.; Bast, A., Oxidized quercetin reacts with thiols rather than with ascorbate: implication for quercetin supplementation. *Biochem. Biophys. Res. Commun.* **2003**, *308*, 560-565.
463. Marteau, C.; Favier, D.; Nardello-Rataj, V.; Aubry, J.-M., Dramatic solvent effect on the synergy between  $\alpha$ -tocopherol and BHT antioxidants. *Food Chem.* **2014**, *160*, 190-195.
464. Guzman, R.; Tang, H.; Salley, S.; Ng, K. Y. S., Synergistic effects of antioxidants on the oxidative stability of soybean oil- and poultry fat-based biodiesel. *J. Am. Oil Chem. Soc.* **2009**, *86*, 459-467.
465. Kurechi, T.; Kato, T., Studies on the antioxidants. XV. Combination effects of butylated hydroxyanisole, butylated hydroxytoluene and their analogs on hydrogen donation to 2,2-diphenyl-1-picrylhydrazyl. *Chem. Pharm. Bull.* **1981**, *29*, 3012-18.
466. Gearhart, W. M.; Stuckey, B. N., A comparison of commercially used phenolic antioxidants in edible animal fats. *J. Am. Oil Chem. Soc.* **1955**, *32*, 386-90.
467. Kadoma, Y.; Ishihara, M.; Fujisawa, S., A quantitative approach to the free radical interaction between  $\alpha$ -tocopherol and the coantioxidants eugenol, resveratrol or ascorbate. *In Vivo* **2006**, *20*, 61-67.
468. Dai, F.; Chen, W.-F.; Zhou, B., Antioxidant synergism of green tea polyphenols with  $\alpha$ -tocopherol and L-ascorbic acid in SDS micelles. *Biochimie* **2008**, *90*, 1499-1505.
469. Lucarini, M.; Pedulli, G. F.; Cipollone, M., Bond Dissociation Enthalpy of  $\alpha$ -Tocopherol and Other Phenolic Antioxidants. *J. Org. Chem.* **1994**, *59*, 5063-70.
470. Foti, M. C.; Daquino, C., Kinetic and thermodynamic parameters for the equilibrium reactions of phenols with the  $\text{dpph}\cdot$  radical. *Chem. Commun. (Cambridge, U. K.)* **2006**, 3252-3254.
471. Parnell, R. D.; Russell, K. E., Electron spin resonance study of the second-order decay of 4-alkyl-2,6-di-tert-butylphenoxyl radicals in solution. *J. Chem. Soc., Perkin Trans. 2* **1974**, 161-4.
472. Weiner, S. A.; Mahoney, L. R., Mechanistic study of the termination reactions of 2,4,6-trialkylphenoxy radicals carboxylic acids. *J. Amer. Chem. Soc.* **1972**, *94*, 5029-33.
473. Schultz, B. E.; Hansen, K. C.; Lin, C. C.; Chan, S. I., Rapid Photochemical Generation of Ubiquinol through a Radical Pathway: An Avenue for Probing Submillisecond Enzyme Kinetics. *J. Org. Chem.* **2000**, *65*, 3244-3247.
474. Uluata, S.; McClements, D. J.; Decker, E. A., How the Multiple Antioxidant Properties of Ascorbic Acid Affect Lipid Oxidation in Oil-in-Water Emulsions. *J. Agric. Food Chem.* **2015**, *63*, 1819-1824.
475. Suarna, C.; Baca, M.; Southwell-Keely, P. T., Oxidation of the  $\alpha$ -tocopherol model compound 2,2,5,7,8-pentamethyl-6-chromanol in the presence of alcohols. *Lipids* **1992**, *27*, 447-53.

476. Peng, H. M.; Webster, R. D., Investigation into Phenoxonium Cations Produced during the Electrochemical Oxidation of Chroman-6-ol and Dihydrobenzofuran-5-ol Substituted Compounds. *J. Org. Chem.* **2008**, *73*, 2169-2175.
477. Lee, S. B.; Lin, C. Y.; Gill, P. M. W.; Webster, R. D., Transformation of  $\alpha$ -Tocopherol (Vitamin E) and Related Chromanol Model Compounds into Their Phenoxonium Ions by Chemical Oxidation with the Nitrosonium Cation. *J. Org. Chem.* **2005**, *70*, 10466-10473.
478. Williams, L. L.; Webster, R. D., Electrochemically Controlled Chemically Reversible Transformation of  $\alpha$ -Tocopherol (Vitamin E) into Its Phenoxonium Cation. *J. Am. Chem. Soc.* **2004**, *126*, 12441-12450.
479. Rosenau, T.; Kloser, E.; Gille, L.; Mazzini, F.; Netscher, T., Vitamin E Chemistry. Studies into Initial Oxidation Intermediates of  $\alpha$ -Tocopherol: Disproving the Involvement of 5a-C-Centered "Chromanol Methide" Radicals. *J. Org. Chem.* **2007**, *72*, 3268-3281.
480. Suarna, C.; Southwell-Keely, P. T., Effect of alcohols on the oxidation of the vitamin E model compound, 2,2,5,7,8-pentamethyl-6-chromanol. *Lipids* **1989**, *24*, 56-60.